

University of Alberta

One-sided Steel Shear Connections in Column Removal Scenario

by

Hossein Daneshvar

A thesis submitted to the Faculty of Graduate Studies and Research in partial
fulfilment of the requirements for the degree of

Doctor of Philosophy

in

Structural Engineering

Department of Civil and Environmental Engineering

©Hossein Daneshvar
Fall 2013
Edmonton, Alberta

Permission is hereby granted to the University of Alberta Libraries to reproduce single copies of this thesis and to lend or sell such copies for private, scholarly or scientific research purposes only. Where the thesis is converted to, or otherwise made available in digital form, the University of Alberta will advise potential users of the thesis of these terms.

The author reserves all other publication and other rights in association with the copyright in the thesis and, except as herein before provided, neither the thesis nor any substantial portion thereof may be printed or otherwise reproduced in any material form whatsoever without the author's prior written permission.

DEDICATION

To my parents

ABSTRACT

There are many design methodologies and philosophies intended to provide structural integrity or increase structural robustness, thereby making structures resistant to progressive collapse. However, there is little information that reveals sources and levels of inherent robustness in structural steel members and systems. The present study seeks to begin the process of behaviour evaluation of components and assemblages initially designed for other purposes than progressive collapse, such as gravity loads, and make recommendations regarding their performance and possible methods for improvements for the new scenario. These recommendations can lead to more economical design and safer structural steel systems in the event of localised damage that has the potential to spread to a disproportionately large part of the structure.

Connections play a major role in ensuring general integrity of different types of steel structural systems. Hence, numerical investigations have been performed to extend the current body of knowledge on connections and, consequently, the structural response in the event of progressive collapse. This study is intended to examine the response of steel frames with simple shear connections in the aftermath of unusual and extreme localized loads. The main goal of this research is to evaluate the behaviour of some prevalent and economical one-sided (i.e., connected only on one side of the supported beam web) shear connection types—shear tab, tee (WT), and single angle—in buildings, and perform numerical analyses on those connection configurations under extreme loading scenarios represented generically by the so-called “column removal scenario”. Characteristic features of the connection response, such as the potential to develop a reliable alternative path load through catenary action and ultimate rotational capacities, are discussed to provide a solid foundation for assessing the performance of buildings with these types of connections. Observations regarding the analysis results are synthesized and conclusions are drawn with respect to the demands placed on the connections. The results of this research project should contribute to a better understanding of the resistance of steel structures with one-sided shear connections to progressive collapse.

ACKNOWLEDGEMENT

I express my gratitude to the creator of this world for providing me persistence, patience and courage to make this job accomplished.

I wish to express my deep gratitude to my parents for their unconditional love and inspiration. I am unable to find a word to express my appreciation to them. I must express my gratitude to my sister and brother for the love, support and constant encouragement.

The author is deeply indebted to his supervisor for his support, continuous guidance, and interest, Dr. Robert G. Driver. I learnt a lot from him not just academically but also personally and professionally. It was a great honour to do the PhD study under his supervision. His wise comments, valuable support and constructive advices throughout this project are greatly appreciated.

I would like to thank Dr. Christopher Raebel from Milwaukee School of Engineering and Dr. Christopher Foley from Marquette University for their support and generosity for providing me with the experimental data used for verification in this research and also serving as external committee member. The suggestions and recommendations of other committee members, Dr. Roger Cheng, Dr. Gary Faulkner, Dr. Marwan El-rich and Dr. Rick Chalaturnyk are also acknowledged.

I would like to thank all my fellow graduate students in our research group for their comments and help.

I acknowledge the support from my supervisor at work, Ayman Kamel, who was thoroughly supporting me since he had gone through the same journey as a graduate student. I also would like to thank my colleagues at Ghods-Niroo Consulting Engineers particularly Mr. Amir Hodayoun Fathi for all his support.

Last but not the least, I gratefully acknowledge my beloved Mahshid for her continuous support.

This page is intentionally left blank

TABLE OF CONTENTS

1 INTRODUCTION.....	1
1.1 Overview	1
1.2 Research Motivation.....	2
1.3 Progressive collapse definition	4
1.4 Progressive collapse – historic perspective.....	5
1.5 Research objectives and scope	6
1.6 Research methodology.....	7
1.7 Thesis organization.....	8
2 BEHAVIOUR OF SIMPLE SHEAR CONNECTIONS IN COLUMN REMOVAL SCENARIO.....	21
2.1 Introduction.....	21
2.2 Scope of the research and objective.....	24
2.3 Shear connections under conventional loading.....	25
2.4 Shear connections in progressive collapse scenario.....	27
2.4.1 Steel connection experiments simulating column removal scenario.....	31
2.4.2 Sub-structural idealization for column removal studies.....	31
2.5 Introduction of connection model assembly to investigate column removal scenario.....	32
2.6 Selected Experimental Study.....	33
2.7 Experimental result calculation.....	33
2.8 Possibility of existence of arch action	34
2.9 Modelling of steel connections using FEA.....	35
2.10 Summary and conclusions.....	36
3 BENCHMARK IN FINITE ELEMENT MODELLING OF STEEL SHEAR CONNECTIONS IN COLUMN REMOVAL SCENARIO.....	55

3.1 Introduction.....	55
3.2 Scope of the research and objectives.....	58
3.3 Literature review on finite element modelling of steel connections.....	59
3.4 Concept of convergence.....	62
3.5 Introduction of the case study model.....	63
3.5.1 Selected study program.....	63
3.5.2 Finite element modelling assembly.....	63
3.5.2.1 Parts geometry.....	64
3.5.2.2 Material definition.....	64
3.5.2.3 Loading steps.....	64
3.5.2.3.1 Bolt pre-tensioning.....	64
3.5.2.3.2 Push-down loading.....	65
3.5.2.4 Interaction properties.....	65
3.5.2.5 Constraints.....	65
3.5.2.6 Boundary condition.....	66
3.6 Element selection.....	66
3.7 Meshing.....	69
3.7.1 Mesh generation procedure.....	70
3.7.2 Mesh Convergence Study.....	71
3.8 Sources of nonlinearity.....	71
3.8.1 Material nonlinearity.....	72
3.8.1.1 Hot rolled sections and plates.....	73
3.8.1.2 High Strength Bolts.....	73
3.8.2 Geometric nonlinearity.....	73
3.8.3 Boundary nonlinearity.....	74
3.8.3.1 Introduction.....	74
3.8.3.2 Surface-based contact.....	75
3.8.3.2.1 General versus contact pairs.....	75
3.8.3.2.2 Contact discretization method (surface-to-surface versus node-to-surface)	76
3.8.3.2.2.1 Contact properties.....	77
3.8.3.2.2.1.1 Normal behaviour.....	77

3.8.3.2.2.1.1.1 Penalty contact stiffness.....	78
3.8.3.2.2.1.1.2 Linear versus nonlinear penalty contact.....	79
3.8.3.2.2.1.2 Tangential behaviour.....	80
3.8.3.2.3 Contact tracking (relative sliding)	81
3.8.3.3 Element-based contact.....	81
3.9 Solving techniques.....	82
3.9.1 Solving a nonlinear problem.....	83
3.9.1.1 Newton-Raphson technique.....	84
3.9.1.2 Quasi-Newton technique.....	86
3.9.1.3 Contact solution.....	87
3.9.2 Convergence Criteria.....	87
3.9.3 Stabilization of initial rigid body motion... ..	89
3.9.4 Time incrementation.....	90
3.9.5 Riks versus general static methods.....	91
3.10 Numerical failure criteria.....	91
3.10.1 Steel sections and plate.....	92
3.10.2 High strength bolts.....	93
3.11 Results extraction.....	94
3.12 Sensitivity analysis.....	94
3.12.1 Element Type.....	95
3.12.2 Coefficient of friction.....	96
3.12.3 Hole size.....	96
3.12.4 Contact stiffness.....	96
3.12.5 Pre-tensioning.....	97
3.12.6 Material definition.....	97
3.12.7 Mesh size.....	97
3.13 Final results.....	98
3.14 General tips for reaching converged solution.....	99
3.15 Summary and conclusions.....	100

4 COMPRESSIVE ARCHING AND TENSILE CATENARY ACTION IN STEEL SHEAR CONNECTIONS UNDER COLUMN REMOVAL SCENARIO.....	132
4.1 Introduction.....	132
4.2 Literature survey.....	133
4.3 Axial response of steel connection in column removal scenario.....	134
4.3.1 Numerical approach.....	135
4.3.2 Analytical approach.....	137
4.4 Results.....	139
4.5 Conclusion.....	139
5 BEHAVIOUR OF SHEAR TAB CONNECTIONS IN COLUMN REMOVAL SCENARIO.....	154
5.1 Introduction.....	154
5.2 Objectives and scope.....	155
5.3 Selected previous research on shear tab connections.....	156
5.4 Numerical study methods.....	163
5.4.1 Selected experimental program.....	163
5.4.2 Finite element models description.....	163
5.5 Verification results.....	164
5.5.1 Three bolt shear tab connections (3ST)	165
5.5.1.1 Deformed shapes and failure modes.....	165
5.5.1.2 Shear-tension and moment interaction graphs.....	166
5.5.2 Four bolt shear tab connections (4ST)	167
5.5.2.1 Deformed shapes and failure modes.....	167
5.5.2.2 Shear-tension and moment interaction graphs.....	168
5.5.3 Five bolt shear tab connections (5ST)	169
5.5.3.1 Deformed shapes and failure modes.....	169
5.5.3.2 Shear-tension and moment interaction graphs.....	169
5.6 Parametric study results.....	170

5.6.1 Three bolt shear tab connections (3ST)	170
5.6.2 Four bolt shear tab connections (4ST)	172
5.6.3 Five bolt shear tab connections (5ST)	175
5.7 Comparison of the results.....	177
5.7.1 Three bolt shear tab connections (3ST).....	177
5.7.1.1 Plate thickness.....	177
5.7.1.2 Bolt size.....	178
5.7.1.3 Bolt type.....	179
5.7.2 Four bolt shear tab connections (4ST)	179
5.7.2.1 Plate thickness.....	179
5.7.2.2 Bolt size.....	180
5.7.2.3 Bolt type.....	180
5.7.3 Five bolt shear tab connections (5ST)	180
5.7.3.1 Plate thickness.....	180
5.7.3.2 Bolt size.....	181
5.7.3.3 Bolt type.....	181
5.8 Rotational ductility of shear tab connections in column removal scenario.....	182
5.9 Summary and conclusion.....	183
6 BEHAVIOUR OF WT CONNECTIONS IN COLUMN REMOVAL SCENARIO.....	230
6.1 Introduction.....	230
6.2 Objective and scope.....	231
6.3 Selected previous research.....	232
6.4 Numerical study method.....	234
6.4.1 Selected experimental program.....	234
6.4.2 Finite element model description.....	235
6.5 Verification results.....	236
6.5.1 Three bolt WT connections (3WT)	236
6.5.1.1 Deformed shapes and failure modes	236
6.5.1.2 Shear, tension, and moment interaction.....	237
6.5.2 Four bolt WT connections (4WT)	238

6.5.2.1 Deformed shapes and failure modes.....	238
6.5.2.2 Shear, tension, and moment interaction.....	239
6.5.3 Five bolt WT connections (5WT)	240
6.5.3.1 Deformed shapes and failure modes.....	240
6.5.3.2 Shear, tension, and moment interaction.....	240
6.6 Parametric study results.....	241
6.6.1 Three bolt WT connections (3WT)	241
6.6.2 Four bolt WT connections (4WT)	244
6.6.3 Five bolt WT connections (5WT)	247
6.7 Comparison of the results.....	250
6.7.1 Three bolt WT connections (3WT)	250
6.7.1.1 WT size.....	250
6.7.1.2 Bolt size.....	251
6.7.1.3 Bolt type.....	251
6.7.2 Four bolt WT connections (4WT)	252
6.7.2.1 WT size.....	252
6.7.2.2 Bolt size.....	253
6.7.2.3 Bolt type.....	253
6.7.3 Five bolt WT connections (5WT)	254
6.7.3.1 WT size.....	254
6.7.3.2 Bolt type.....	254
6.7.3.3 Bolt type.....	255
6.8 Rotational ductility of WT connections in column removal scenario.....	255
6.9 Summary and conclusion.....	257
7 BEHAVIOUR OF SINGLE ANGLE CONNECTIONS UNDER COLUMN REMOVAL SCENARIO.....	303
7.1 Introduction.....	303
7.2 Objectives and scope.....	304
7.3 Selected previous research.....	304
7.4 Numerical study method.....	308
7.4.1 Selected experimental program.....	308

7.4.2 Finite element model description.....	308
7.5 Verification results.....	309
7.6 Parametric study results.....	310
7.6.1 Three bolt single angle connections (3SA)	310
7.6.2 Four bolt single angle connections (4SA)	313
7.6.3 Five bolt single angle connections (5SA)... ..	315
7.7 Comparison of the results.....	318
7.7.1 Three bolt single angle connections (3SA)	318
7.7.1.1 Plate thickness.....	318
7.7.1.2 Bolt size.....	319
7.7.1.3 Bolt type.....	319
7.7.2 Four bolt single angle connections (4SA)	320
7.7.2.1 Plate thickness.....	320
7.7.2.2 Bolt size.....	320
7.7.2.3 Bolt type.....	320
7.7.3 Five bolt single angle connections (5SA).....	321
7.7.3.1 Plate thickness.....	321
7.7.3.2 Bolt size.....	322
7.7.3.3 Bolt type.....	322
7.8 Rotational ductility of single angle connections in column removal scenario..	322
7.9 Conclusion.....	324
8 SUMMARY, CONCLUSIONS, AND RECOMMENDATIONS FOR FUTURE RESEARCH.....	357
8.1 Summary.....	357
8.2 Conclusions.....	358
8.3 Recommendations for future research.....	363
LIST OF REFERENCES.....	365
APPENDIX A: MATERIAL PROPERTIES.....	373

LIST OF TABLES

Table 1.1: Progressive collapse case studies.....	10
Table 2.1: Simple beam-to-column connections.....	38
Table 2.2: Types of material used in shear connections.....	38
Table 2.3: Selected column removal scenario experiments for steel structures.....	39
Table 3.1: Different phases in finite element analysis of bolted steel connections (Krishnamurthy 1980).....	102
Table 3.2: Finite element model summary.....	103
Table 3.3: Integration order of element available in Abaqus (Daneshvar and Driver 2012).....	104
Table 3.4: Full versus partial element integration available in Abaqus (Daneshvar and Driver 2012).....	104
Table 3.5: Mesh refinement analysis results; refinement across the thickn.....	105
Table 3.6: Master and slave surfaces in the shear tab connection.....	105
Table 3.7: Nonlinear penalty contact parameters (Dassault Systèmes 2009)	105
Table 3.8: Direct Lagrange Multiplier versus penalty method (Dassault Systèmes 2009).....	106
Table 3.9: Implicit versus explicit analysis method (Dassault Systèmes 2011c)	106
Table 3.10: Sensitivity analysis.....	107
Table 3.11: Benchmark results; verification with experimental work (Thompson 2009).....	108
Table 4.1: Geometric properties of ST test specimens (Thompson 2009)	141
Table 4.2: Geometric properties of WT test specimens (Friedman 2009)	141
Table 4.3: Geometric properties of SA test specimens (Johnson 2009)	141
Table 5.1: Typical materials used for shear tab connections.....	186
Table 5.2: Limitations of conventional shear tab connections (AISC 2010)	186
Table 5.3: Summary of characteristic features of FE models of ST connections.....	187
Table 5.4: Comparison of numerical and experimental (Thompson 2009) responses of shear tab connections with three bolts at initial failure.....	188
Table 5.5: Comparison of numerical and experimental (Thompson 2009) responses of shear tab connections with four bolts at initial failure.....	188

Table 5.7: Summary of numerical and experimental responses of shear tab connections at initial failure.....	190
Table 5.8: Comparison of plastic rotational capacities of shear tab connections based on ASCE 41 (2006), DoD (2009), and proposed equation.....	191
Table 6.1: Typical material used for WT connections.....	261
Table 6.2: Summary of shear strength tests by Astanceh and Nader (1990)	261
Table 6.3: Summary of characteristic features of FE models of WT connections.....	262
Table 6.4: Comparison of numerical and experimental (Friedman 2009) responses of shear tab connections with three bolts (3WT) at initial failure.....	263
Table 6.5: Comparison of numerical and experimental (Friedman 2009) responses of shear tab connections with four bolts (4WT) at initial failure.....	263
Table 6.6: Comparison of numerical and experimental (Friedman 2009) responses of shear tab connections with five bolts (5WT) at initial failure.....	264
Table 7.1: Advantages and disadvantages of single-sided connections (Murray 2013).....	327
Table 7.2: Typical material used for SA connections.....	327
Table 7.3: Summary of characteristic features of FE models of SA connections.....	328
Table 7.4: Summary of numerical responses of single angle connections at initial failure.....	329

LIST OF FIGURES

Figure 1.1: Frames with shear connections: (a) braced frame (b) moment resisting frame.....	13
Figure 1.2: Progressive collapse scenario: (a) in braced frame (b) in moment resisting frame.....	14
Figure 1.3: Ronan Point apartment tower in Newham, England (Nair 2003)	15
Figure 1.4: Skyline Plaza, Kansas City, USA (Crowder 2005)	15
Figure 1.5: Hyatt Regency Hotel Skywalks, Kansas City, USA.....	16
Figure 1.6: L’ambiance Plaza, Bridgeport, USA (NIST 2007)	16
Figure 1.7: Alfred P. Murrah Federal Building, Oklahoma City, USA (NIST 2005)	17
Figure 1.8: Khobar towers, Alkhobar, Saudi Arabia (NIST 2005)	17
Figure 1.9: WTC 1 and WTC 2, New York, USA (NIST 2005).....	18
Figure 1.10: WTC 7, New York, USA (NIST 2007)	18
Figure 1.11: Pentagon, Arlington, USA (NIST 2005)	19
Figure 1.12: Bankers Trust Building (Deutsche Bank), New York, USA (NIST 2007).....	19
Figure 1.13: Project objectives at a glance.....	20
Figure 2.1: Connection definition.....	40
Figure 2.2: Typical moment–rotation curves for different types of connection (Kameshki and Saka 2003)	40
Figure 2.3: Common types of single-sided shear connections (a) shear tab, (b) tee, (c) single angle.....	41
Figure 2.4: Frames with shear connections under conventional loads (a) frame under vertical loadings, (b) member response to vertical loading.....	42
Figure 2.5: Frames with shear connections under conventional loads (a) frame under lateral loadings, (b) member response to lateral loading (AISC 2010)	43
Figure 2.6: Moment–rotation behaviour of steel connections under conventional loading (AISC 2010)	44
Figure 2.7: Fully-restrained (FR), partially-restrained (PR) and shear connection definitions (AISC 2010)	44
Figure 2.8: Semi-rigid plane member with (a) rotational springs, (b) axial and rotational springs.....	45
Figure 2.9: (a) Generalized component force–deformation relations for depicting modelling and acceptance criteria (Fema 2000) (b) the effective force–deformation relationship for a	

typical component in an earthquake and progressive collapse scenario (Powell 2005)	45
Figure 2.10: (a) Frame with shear connections in column removal scenario (b) member response (c) simplified member response	46
Figure 2.11: Simultaneous presence of shear, tension and moment at connection location in column removal scenario	47
Figure 2.12: Formation of catenary behaviour in beams (a) isolated double span (b) deformed shape under gravity load (c) small rotation: flexural phase (d) large rotation: catenary phase	48
Figure 2.13: Generalized component force-deformation relations for depicting modelling for 152 mm, 228 mm and 304 mm shear tab connections	49
Figure 2.14: Possible sub-structuring options for column removal scenario	50
Figure 2.15: Common test setups for beam-to-column connection tests under column removal scenario, pertaining to (a) substructure 1 (b) substructure 2 (c) substructure 3 (d) substructure 4	51
Figure 2.16: Proposed connection assembly model under column removal scenario: (a) undeformed configuration (b) small rotation: flexural phase (c) large rotation: catenary phase (d) simplified model	52
Figure 2.17: Test setup assembly (Thompson 2009)	53
Figure 2.18: Possibility of formation of compressive arch action in column removal scenario	53
Figure 2.19: Finite element model of shear tab connections	54
Figure 3.1: Test setup of selected experimental program (Thompson 2009)	109
Figure 3.2: Part dimensions (a) shear tab (b) stub column (c) beam (Thompson 2009)	110
Figure 3.3: Finite element model of steel shear tab connection	111
Figure 3.4: Applying bolt pretension	111
Figure 3.5: Symmetry constraint at the centerline of the stub column; rigid surface and horizontal spring at far end	112
Figure 3.6: Structural elements in Abaqus/Standard (a) continuum solid element (b) shell element (c) membrane element (d) rigid element (e) beam element (f) truss element (g) spring/dashpot (Dassault Systèmes 2009)	112
Figure 3.7: Continuum solid elements in abaqus/standard (a) linear element (eight node brick, C3d8) (b) quadratic element (twenty node brick, C3D20)(c) modified second-order element (ten node tetrahedron, C3D10m) (d) linear element (four node tetrahedron, C3d4) (Dassault Systèmes 2009)	113
Figure 3.8: Mesh size in different segments of the beam	113

Figure 3.9: Mesh refinement across the thickness: (a) coarse: one element in thickness; (b) normal: two elements in thickness; (c) fine: three elements in thickness.....	114
Figure 3.10: ASTM A325 versus Astm A490 (Kulak et al. 2001)	114
Figure 3.11: Contact definition (a) constraint not active (b) constraint activated (Dassault Systèmes 2011b)	115
Figure 3.12: Bolt-hole interaction (Ashakul 2004) (a) before installation of gap elements (b) after installation of gap element.....	115
Figure 3.13: (A) Contact element (b) general contact (c) contact pair.....	116
Figure 3.14: Different types of surface-based contact (a) Node-to-Surface (b) Surface-to-Surface.....	117
Figure 3.15: Contact pressure versus penetration diagram for direct Lagrange Multiplier and penalty method.....	117
Figure 3.16: Penalty method diagram.....	117
Figure 3.17: Penalty contact pressure–overclosure diagram: linear versus nonlinear stiffness method.....	118
Figure 3.18: Contact pressure–penetration diagram: Lagrange Multiplier versus penalty method.....	118
Figure 3.19: Sources of nonlinearity in the implicit formulation.....	119
Figure 3.20: Step, increment and iteration definition in Newton–Raphson method.....	119
Figure 3.21: Newton–Raphson method diagram (Dassault Systèmes 2011c)	120
Figure 3.22: Severe discontinuity iteration (SDI) in the shank–hole interaction (a) undeformed (b) deformed (c) contact force versus displacement diagram.....	120
Figure 3.23: Solution flowchart for contact problem; severe discontinuity iterations (SDI) (Dassault Systèmes 2011c)	121
Figure 3.24: Solution flowchart for a nonlinear problem including contact (Dassault Systèmes 2011c)	121
Figure 3.25: Bolted connection subjected to simultaneous moment, tension and shear loads.....	122
Figure 3.26: Tension coupon test (a) geometry and meshing (b) loading and boundary conditions (c) stress distribution before failure (d) element removal at PEEQ=0.55 to simulate initiation of rupture.....	122
Figure 3.27: Numerical model of ASTM A325 bolts under shear loading (a) geometry and meshing (b) loading and boundary conditions (c) stress distribution before failure (d) element removal at PEEQ=0.55 to simulate initiation of rupture.....	123
Figure 3.28: Numerical and experimental response of ASTM A325 bolt under shear loading.....	124

Figure 3.29: Numerical and experimental response of ASTM A490 bolt under shear loading.....	124
Figure 3.30: Shear force versus chord rotation curves at the bolt line; Experimental (Thompson 2009) and finite element results for different types of elements.....	125
Figure 3.31: Shear force versus chord rotation curves at the bolt line; experimental (Thompson 2009) and finite element results for different coefficients of friction.....	125
Figure 3.32: Shear force versus chord rotation curves at the bolt line; Experimental (Thompson 2009) and finite element results for different hole sizes.....	126
Figure 3.33: Shear force versus chord rotation curves at the bolt line; experimental (Thompson 2009) and finite element results for different linear penalty stiffness scale factors.....	126
Figure 3.34: Shear force versus chord rotation curves at the bolt line; Experimental (Thompson 2009) and finite element results for different pretension displacement.....	127
Figure 3.35: Shear force versus chord rotation curves at the bolt line; experimental (Thompson 2009) and finite element results for different material properties.....	127
Figure 3.36: (a) Deformed shapes of assembly; (b) Shear tab from experiment (Thompson 2009); (c) Shear tab from finite element simulation.....	128
Figure 3.37: Shear force versus chord rotation curves at the bolt line; experimental (Thompson 2009) and finite element results.....	129
Figure 3.38: Axial force versus chord rotation curves at the bolt line; experimental (Thompson 2009) and finite element results.....	129
Figure 3.39: Moment versus chord rotation curves at the bolt line; experimental (Thompson 2009) and finite element results.....	130
Figure 3.40: Convergence difficulties at the corners (a) S-To-S (b) N-To-S.....	130
Figure 3.41: Actual geometry versus faceted geometry.....	131
Figure 4.1: Axial response of a gravity framing system after column removal.....	142
Figure 4.2: (a) Compressive arching action accompanied by (b) tensile catenary response of a gravity framing system after column removal.....	142
Figure 4.3: Double span analytical/experimental models and axial response of a connection in a column removal scenario (a) Girhammar (1980), (b) Izzuddin et al. (2008a), (c) Astaneh Asl (2007)	143
Figure 4.4: Development of compressive arching and catenary tension under column removal scenario (a) top and bottom seated angle connection (b) single angle connection with real hinges and axial springs at the ends (Daneshvar et al. 2012).....	144
Figure 4.5: Test setup of selected experimental program (Thompson 2009).....	145

Figure 4.6: Finite element models of (a) 3 bolt shear tab (3ST), (b) 4 bolt shear tab (4ST), (c) 5 bolt shear tab (5ST)	146
Figure 4.7: Comparison of numerical and experimental axial responses of connection 3ST	147
Figure 4.8: Comparison of numerical and experimental axial responses of connection 4ST	147
Figure 4.9: Comparison of numerical and experimental axial responses of connection 5ST	148
Figure 4.10: Comparison of numerical and experimental axial responses of connection 3WT	148
Figure 4.11: Comparison of numerical and experimental axial responses of connection 4WT	149
Figure 4.12: Comparison of numerical and experimental axial responses of connection 5WT	149
Figure 4.13: Comparison of numerical and experimental axial responses of connection 3SA	150
Figure 4.14: Comparison of numerical and experimental axial responses of connection 4SA	150
Figure 4.15: Comparison of numerical and experimental axial responses of connection 5SA	151
Figure 4.16: Axial deformation from (a) vertical deflection, and (b) eccentric connection rotation (Daneshvar et al. 2012)	152
Figure 4.17: Comparison of axial deformations of numerical and simplified analytical models for ST connections (Daneshvar et al. 2012)	153
Figure 4.18: Axial response of connection 3ST for different end spring stiffnesses (Daneshvar et al. 2012)	153
Figure 5.1: Types of shear tab connections: (a) welded-bolted (b) welded-welded.....	192
Figure 5.2: Different parameters of conventional shear tab.....	192
Figure 5.3: Finite element grid for the beam model.....	193
Figure 5.4: Moment-rotation relationship in the beam-line model (Richard et al. 1980).....	193
Figure 5.5: Test setup (Richard et al. 1980)	194
Figure 5.6: Eccentricity defined by Richard et al. (1980)	194
Figure 5.7: Off-axis shear tab connections Hormby et al. (1984)	195
Figure 5.8: Beam line definitions for $F_y=36$ and $F_y=50$ steel beams (Hormby et al. 1984).....	195

Figure 5.9: Directions of plate deformations at bolt holes after tests (Astaneh et al. 1989).....	196
Figure 5.10: Loading history applied to shear connections under gravity loads (Astaneh et al. 2002)	196
Figure 5.11: Hierarchy of failure modes: ductile and brittle (Astaneh et al. 2002).....	197
Figure 5.12: Typical moment–rotation curves (Astaneh et al. 2002)	197
Figure 5.13: Moment–rotation curves proposed for shear tabs in composite beams (Astaneh 2005)	198
Figure 5.14: Selected experimental program test setup (Thompson 2009)	198
Figure 5.15: FE models of: (a) full connection assembly, (b) 3 bolt ST connection (3ST), (c) 4 bolt ST connection (4ST), (d) 5 bolt ST connection (5ST)	199
Figure 5.16: Deformed shape of the connection assembly (a) experiment (Thompson 2009) (b) finite element.....	200
Figure 5.17: Main source of ductility: bottom hole deformation: (a) experimental (Thompson 2009) (b) numerical results (c) magnified view of bottom hole region.....	201
Figure 5.18: Failure of 3ST at the bottom hole by bearing deformation and rupture (a) experimental (Thompson 2009) and (b) numerical results (c) magnified view of bottom hole region.....	202
Figure 5.19: Failure of 4ST at the bottom hole by bearing deformation and rupture (a) experimental (Thompson 2009) and (b) numerical results (c) magnified view of bottom hole region.....	203
Figure 5.20: Failure of 5ST at the bottom hole by bearing deformation and rupture (a) experimental (Thompson 2009) and (b) numerical results (c) magnified view of bottom hole region.....	204
Figure 5.21: Typical bolt shear deformation and failure (a) experimental (Thompson 2009) and (b) numerical results.....	205
Figure 5.22: Comparison of numerical and experimental shear response of connection 3ST.....	205
Figure 5.23: Comparison of numerical and experimental tensile response of connection 3ST.....	206
Figure 5.24: Comparison of numerical and experimental flexural response of connection 3ST.....	206
Figure 5.25: Comparison of numerical and experimental shear response of connection 4ST.....	207
Figure 5.26: Comparison of numerical and experimental tensile response of connection 4ST.....	207
Figure 5.27: Comparison of numerical and experimental flexural response of connection 4ST.....	208

Figure 5.28: Comparison of numerical and experimental shear response of connection 5ST.....	208
Figure 5.29: Comparison of numerical and experimental tensile response of connection 5ST.....	209
Figure 5.30: Comparison of numerical and experimental flexural response of connection 5ST.....	209
Figure 5.31: Bolt line forces versus beam end rotation – Specimen 3ST-3/8-3/4.....	210
Figure 5.32: Bolt line forces versus beam end rotation – specimen 3ST-1/4-3/4.....	210
Figure 5.33: Bolt line forces versus beam end rotation – Specimen 3ST-1/2-3/4.....	211
Figure 5.34: Bolt line forces versus beam end rotation – specimen 3ST-3/8-5/8.....	211
Figure 5.35: Bolt line forces versus beam end rotation – Specimen 3ST-3/8-7/8.....	212
Figure 5.36: Bolt line forces versus beam end rotation – specimen 3ST-3/8-3/4-A490.....	212
Figure 5.37: Bolt line forces versus beam end rotation – specimen 4ST-3/8-3/4.....	213
Figure 5.38: Bolt line forces versus beam end rotation – Specimen 4ST-1/4-3/4.....	213
Figure 5.39: Bolt line forces versus beam end rotation – specimen 4ST-1/2-3/4.....	214
Figure 5.40: Bolt line forces versus beam end rotation – specimen 4ST-3/8-5/8.....	214
Figure 5.41: Bolt line forces versus beam end rotation – specimen 4ST-3/8-7/8.....	215
Figure 5.42: Bolt line forces versus beam end rotation – Specimen 4ST-3/8-3/4-A490.....	215
Figure 5.43: Bolt line forces versus beam end rotation – specimen 5ST-3/8-3/4.....	216
Figure 5.44: Bolt line forces versus beam end rotation – Specimen 5ST-1/4-3/4.....	216
Figure 5.45: Bolt line forces versus beam end rotation – specimen 5ST-1/2-3/4.....	217
Figure 5.46: Bolt line forces versus beam end rotation – Specimen 5ST-3/8-5/8.....	217
Figure 5.47: Bolt line forces versus beam end rotation – Specimen 5ST-3/8-7/8.....	218
Figure 5.48: Bolt line forces versus beam end rotation – SPECIMEN 5ST-3/8-3/4-A490.....	218
Figure 5.49: Comparison of shear response of 3ST connections with different plate thicknesses.....	219
Figure 5.50: Comparison of tensile response of 3ST connections with different plate thicknesses.....	219
Figure 5.51: Comparison of flexural response of 3ST connections with different plate thicknesses.....	220
Figure 5.52: Comparison of shear response of 3ST connections with different bolt sizes.....	220

Figure 5.53: Comparison of tensile response of 3ST connections with different bolt sizes.....	221
Figure 5.54: Comparison of flexural response of 3ST connections with different bolt sizes.....	221
Figure 5.55: Comparison of shear response of 4ST connections with different plate thicknesses.....	222
Figure 5.56: Comparison of tensile response of 4ST connections with different plate thicknesses.....	222
Figure 5.57: Comparison of flexural response of 4ST connections with different plate thicknesses.....	223
Figure 5.58: Comparison of shear response of 4ST connections with different bolt sizes.....	223
Figure 5.59: Comparison of tensile response of 4ST connections with different bolt sizes.....	224
Figure 5.60: Comparison of flexural response of 4ST connections with different bolt sizes.....	224
Figure 5.61: Comparison of shear response of 5ST connections with different plate thicknesses.....	225
Figure 5.62: Comparison of tensile response of 5ST connections with different plate thicknesses.....	225
Figure 5.63: Comparison of flexural response of 5ST connections with different plate thicknesses.....	226
Figure 5.64: Comparison of shear response of 5ST connections with different bolt sizes.....	226
Figure 5.65: Comparison of tensile response of 5ST connections with different bolt sizes.....	227
Figure 5.66: Comparison of flexural response of 5ST connections with different bolt sizes.....	227
Figure 5.67: Shear tab connection rotation capacities versus connection depth for all the experimental and numerical data.....	228
Figure 5.68: Proposed equation for shear tab connection rotation capacities versus connection depth.....	228
Figure 5.69: Comparison of plastic rotation capacities of shear tab connections based on ASCE 41 (2006), DoD (2009) and proposed equation.....	229
Figure 6.1: Types of WT shear connections: (a) welded-bolted (b) bolted-welded (c) welded-welded (d) bolted-bolted (Astaneh and Nader 1990)	266
Figure 6.2: Typical failure modes (Astaneh and Nader 1989)	266
Figure 6.3: Assumed induced force on WT and bolts (Thornton 1996).....	267
Figure 6.4: Yield lines in WT shear connection: (a) welded (b) bolted (Thornton 1996).....	267

Figure 6.5: Test setup (Friedman 2009)	268
Figure 6.6: FE models of: (a) full connection assembly, (b) 3 bolt WT connection (3WT), (c) 4 bolt WT connection (4WT), (d) 5 bolt WT connection (5WT)	268
Figure 6.7: Deformed shape of the connection assembly: (a) experiment (b) finite element.	269
Figure 6.8: Failure of 3WT, experimental (Friedman 2009) and numerical results: (a) deformed shape (b) bolt rupture (c) bottom hole bearing deformation.....	270
Figure 6.9: Failure of 4WT, experimental (Friedman 2009) and numerical results: (a) deformed shape (b) bolt rupture (c) bottom hole bearing deformation.....	271
Figure 6.10: Failure of 5WT, experimental (Friedman 2009) and numerical results: (a) deformed shape (b) bolt rupture (c) bottom hole bearing deformation.....	272
Figure 6.11: Comparison of numerical and experimental shear response of connection 3WT.....	273
Figure 6.12: Comparison of numerical and experimental tensile response of connection 3WT.....	273
Figure 6.13: Comparison of numerical and experimental flexural response of connection 3WT.....	274
Figure 6.14: Comparison of numerical and experimental shear response of connection 4WT.....	274
Figure 6.15: Comparison of numerical and experimental tensile response of connection 4WT.....	275
Figure 6.16: Comparison of numerical and experimental flexural response of connection 4WT.....	275
Figure 6.17: Comparison of numerical and experimental shear response of connection 5WT.....	276
Figure 6.18: Comparison of numerical and experimental tensile response of connection 5WT.....	276
Figure 6.19: Comparison of numerical and experimental flexural response of connection 5WT.....	277
Figure 6.20: Bolt line forces versus beam end rotation – specimen 3WT125X33.5-3/4.....	277
Figure 6.21: Bolt line forces versus beam end rotation – specimen 3WT100X26-3/4.....	278
Figure 6.22: Bolt line forces versus beam end rotation – specimen 3WT155X33.5-3/4.....	278
Figure 6.23: Bolt line forces versus beam end rotation – specimen 3WT125X33.5-5/8.....	279
Figure 6.24: Bolt line forces versus beam end rotation – specimen 3WT125X33.5-7/8.....	279

Figure 6.25: Bolt line forces versus beam end rotation – Specimen 3WT125X33.5-3/4-A490.....	280
Figure 6.26: Bolt line forces versus beam end rotation – specimen 4WT125X33.5-3/4.....	280
Figure 6.27: Bolt line forces versus beam end rotation – specimen 4WT100X26-3/4.....	281
Figure 6.28: Bolt line forces versus beam end rotation – specimen 4WT155X33.5-3/4.....	281
Figure 6.29: Bolt line forces versus beam end rotation – SPECIMEN 4WT125X33.5-5/8.....	282
Figure 6.30: Bolt line forces versus beam end rotation – specimen 4WT125X33.5-7/8.....	282
Figure 6.31: Bolt line forces versus beam end rotation – specimen 4WT125X33.5-3/4-A490.....	283
Figure 6.32: Bolt line forces versus beam end rotation – specimen 5WT125X33.5-3/4.....	283
Figure 6.33: Bolt line forces versus beam end rotation – specimen 5WT100X26-3/4.....	284
Figure 6.34: Bolt line forces versus beam end rotation – specimen 5WT155X33.5-3/4.....	284
Figure 6.35: Bolt line forces versus beam end rotation – specimen 5WT125X33.5-5/8.....	285
Figure 6.36: Bolt line forces versus beam end rotation – specimen 5WT125X33.5-7/8.....	285
Figure 6.37: Bolt line forces versus beam end rotation – specimen 5WT125X33.5-3/4-A490.....	286
Figure 6.38: Comparison of shear response of 3WT connections with different WT sections.....	286
Figure 6.39: Comparison of tensile response of 3WT connections with different WT sections.....	287
Figure 6.40: Comparison of flexural response of 3WT connections with different WT sections.....	287
Figure 6.41: Comparison of shear response of 3WT connections with different bolt sizes..	288
Figure 6.42: Comparison of tensile response of 3WT connections with different bolt sizes.....	288
Figure 6.43: Comparison of flexural response of 3WT connections with different bolt sizes.....	289
Figure 6.44: Comparison of shear response of 3WT connections with different bolt types.....	289
Figure 6.45: Comparison of tensile response of 3WT connections with different bolt types.....	290
Figure 6.46: Comparison of flexural response of 3WT connections with different bolt types.....	290

Figure 6.47: Comparison of shear response of 4WT connections with different WT sections.....	291
Figure 6.48: Comparison of tensile response of 4WT connections with different WT sections.....	291
Figure 6.49: Comparison of flexural response of 4WT connections with different WT sections.....	292
Figure 6.50: Comparison of shear response of 4WT connections with different bolt sizes.....	292
Figure 6.51: Comparison of tensile response of 4WT connections with different bolt sizes.....	293
Figure 6.52: Comparison of flexural response of 4WT connections with different bolt sizes.....	293
Figure 6.53: Comparison of shear response of 4WT connections with different bolt types.....	294
Figure 6.54: Comparison of tensile response of 4WT connections with different bolt types.....	294
Figure 6.55: Comparison of flexural response of 4WT connections with different bolt types.....	295
Figure 6.56: Comparison of shear response of 5WT connections with different WT sections.....	295
Figure 6.57: Comparison of tensile response of 5WT connections with different WT sections.....	296
Figure 6.58: Comparison of flexural response of 5WT connections with different WT sections.....	296
Figure 6.59: Comparison of shear response of 5WT connections with different bolt sizes.....	297
Figure 6.60: Comparison of tensile response of 5WT connections with different bolt sizes.....	297
Figure 6.61: Comparison of flexural response of 5WT connections with different bolt sizes.....	298
Figure 6.62: Comparison of shear response of 5WT connections with different bolt types.....	298
Figure 6.63: Comparison of tensile response of 5WT connections with different bolt types.....	299
Figure 6.64: Comparison of flexural response of 5WT connections with different bolt types.....	299
Figure 6.65: WT connection total rotation capacities versus connection depth.....	300

Figure 6.66: Proposed equation for WT connection total rotation capacities versus connection depth – bolt shear rupture limit state.....	300
Figure 6.67: Proposed equation for WT connection total rotation capacities versus connection depth – WT rupture limit state.....	301
Figure 6.68: Proposed equation for WT connection plastic rotation capacities versus connection depth – bolt shear rupture limit state.....	301
Figure 6.69: Proposed equation for WT connection plastic rotation capacities versus connection depth – WT rupture limit state.....	302
Figure 7.1: Types of SA shear connections: (a) welded-bolted (b) bolted-welded (c) welded-welded (d) bolted-bolted.....	330
Figure 7.2: Elastic-perfectly plastic moment-rotation curves (Kishi and Chen 1990).....	331
Figure 7.3: General deformation pattern of single angle connection (Kishi and Chen 1990).....	331
Figure 7.4: Modelling of angle performed by Kishi and Chen (1990).....	332
Figure 7.5: Application of yield line theory for single angle connection (Gong 2009).....	332
Figure 7.6: Finite element models of: (a) full connection assembly, (b) three bolt single angle connection (3SA), (c) four bolt single angle connection (4SA), (d) five bolt single angle connection (5SA).....	333
Figure 7.7: Deformed shape of finite element connection assembly.....	333
Figure 7.8: Failure of 3SA, numerical results: (a) deformed shape of connection assembly, (b) angle deformed shape – front view, (c) failure initiation – back view, (d) bolt shear deformation.....	334
Figure 7.9: Failure of 4SA, numerical results: (a) deformed shape of connection assembly, (b) angle deformed shape – front view, (c) failure initiation – back view, (d) bolt shear deformation.....	335
Figure 7.10: Failure of 5SA, numerical results: (a) deformed shape of connection assembly, (b) angle deformed shape – front view, (c) failure initiation – back view, (d) bolt shear deformation.....	336
Figure 7.11: Comparison of numerical and experimental shear response of connection 3SA.....	337
Figure 7.12: Comparison of numerical and experimental tensile response of connection 3SA.....	337
Figure 7.13: Comparison of numerical and experimental flexural response of connection 3SA.....	338
Figure 7.14: Bolt line forces versus beam end rotation – specimen 3SA-3/8-3/4.....	338
Figure 7.15: Bolt line forces versus beam end rotation – specimen 3SA-1/4-3/4.....	339

Figure 7.16: Bolt line forces versus beam end rotation – specimen 3SA-1/2-3/4.....	339
Figure 7.17: Bolt line forces versus beam end rotation – specimen 3SA-3/8-5/8.....	340
Figure 7.18: Bolt line forces versus beam end rotation – specimen 3SA-3/8-7/8.....	340
Figure 7.19: Bolt line forces versus beam end rotation – specimen 4SA-3/8-3/4.....	341
Figure 7.20: Bolt line forces versus beam end rotation – specimen 4SA-1/4-3/4.....	341
Figure 7.21: Bolt line forces versus beam end rotation – specimen 4SA-1/2-3/4.....	342
Figure 7.22: Bolt line forces versus beam end rotation – specimen 4SA-3/8-5/8.....	342
Figure 7.23: Bolt line forces versus beam end rotation – specimen 4SA-3/8-7/8.....	343
Figure 7.24: Bolt line forces versus beam end rotation – specimen 5SA-3/8-3/4.....	343
Figure 7.25: Bolt line forces versus beam end rotation – specimen 5SA-1/4-3/4.....	344
Figure 7.26: Bolt line forces versus beam end rotation – specimen 5SA-1/2-3/4.....	344
Figure 7.27: Bolt line forces versus beam end rotation – specimen 5SA-3/8-5/8.....	345
Figure 7.28: Bolt line forces versus beam end rotation – specimen 5SA-3/8-7/8.....	345
Figure 7.29: Comparison of shear response of 3SA connections with different angle thicknesses.....	346
Figure 7.30: Comparison of tensile response of 3SA connections with different angle thicknesses.....	346
Figure 7.31: Comparison of flexural response of 3SA connections with different angle thicknesses	347
Figure 7.32: Comparison of shear response of 3SA connections with different bolt sizes.....	347
Figure 7.33: Comparison of tensile response of 3SA connections with different bolt sizes.....	348
Figure 7.34: Comparison of tensile response of 3SA connections with different bolt sizes.....	348
Figure 7.35: Comparison of shear response of 4SA connections with different angle thicknesses.....	349
Figure 7.36: Comparison of tensile response of 4SA connections with different angle thicknesses.....	349
Figure 7.37: Comparison of flexural response of 4SA connections with different angle thicknesses.....	350
Figure 7.38: Comparison of shear response of 4SA connections with different bolt sizes.....	350
Figure 7.39: Comparison of tensile response of 4SA connections with different bolt sizes.....	351

Figure 7.40: Comparison of flexural response of 4SA connections with different bolt sizes.....	351
Figure 7.41: Comparison of shear response of 5SA connections with different angle thicknesses.....	352
Figure 7.42: Comparison of tensile response of 5SA connections with different angle thicknesses.....	352
Figure 7.43: Comparison of flexural response of 5SA connections with different angle thicknesses.....	353
Figure 7.44: Comparison of shear response of 5SA connections with different bolt sizes.....	353
Figure 7.45: Comparison of tensile response of 5SA connections with different bolt sizes.....	354
Figure 7.46: Comparison of flexural response of 5SA connections with different bolt sizes.....	354
Figure 7.47: Single angle connection total rotation capacities versus connection depth.....	355
Figure 7.48: Proposed equation for single angle connection total rotation capacities versus connection depth.....	355
Figure 7.49: Proposed equation for single angle connection plastic rotations versus connection depth.....	356
Figure 7.50: Comparison of proposed equations for plastic rotation of shear tab, single angle, and WT connections.....	356

LIST OF SYMBOLS

A	beam cross section area
a	distance from the bolt line to the weld line
\mathbf{B}	relationship between displacement and strain increments
C_0	clearance at which contact pressure is zero
c_{max}	maximum displacement correction
\mathbf{c}_u	correction to displacement vector
\mathbf{D}	relationship between stress and strain matrix
d	upper quadratic limit in nonlinear penalty stiffness
d_b	bolt diameter
d_{conn}	distance between the centres of the top and bottom bolts
E	modulus of elasticity for steel (200 GPa)
EI	bending rigidity of the beam
e	lower quadratic limit in nonlinear penalty stiffness; eccentricity of the load
e_{36}	eccentricity of the load using Grade 36 steel
e_{50}	eccentricity of the load using Grade 50 steel
e_b	eccentricity for designing bolts
e_{new}	relative error at current iteration
e_{old}	relative error at previous iteration
e_r	lower quadratic limit ratio in nonlinear penalty stiffness
e_w	eccentricity for designing welds
e_v	vertical distance between centres of rotation
F_y	minimum yield strength
f_{avg}	average force concept in Abaqus

h	the current clearance between two nodes of the gap element; depth of the bolt pattern
I	summation of internal loads
\mathbf{K}_0	stiffness matrix
K_{a-con}	axial stiffness of the connection
K_{a-str}	stiffness of the springs represent the stiffness of the test setup or surrounding structure
K_f	final stiffness in nonlinear penalty stiffness
K_i	connection initial stiffness; initial stiffness in nonlinear penalty stiffness
K_{lin}	linear stiffness in linear penalty contact
K_p	penalty contact
K_s	secant stiffness of the connection at service loads
$K_{\theta-con}$	flexural stiffness of the connection
L	length of the beam
L_b	horizontal distance from the true pin to the bolt line
L_c	horizontal distance from the true pin to the interior column flange
L_{eh}	horizontal edge distance in shear tab
L_{ev}	vertical edge distance in shear tab
L_{st}	the horizontal distance from the true pin to the strain guage location
L_{ST}	length of shear tab
M	moment at the connection location
M_{36}	moment at the connection location using Grade 36 steel plate
M_{50}	moment at the connection location using Grade 50 steel plate
M_b	moment at the bolt line
M_n	maximum flexural strength of connection

M_{ref}	reference moment based on a pure moment
M_s	moment at service load
M_{st}	moment at the strain gauge line
M_u	ultimate moment capacity of the connection
M_y	yield moment strength of the connection
M^*	intermediate non-dimensional moment
M_{slip}^+	positive moment causing slip in the shear tab connection
M_{max}^+	maximum positive moment of shear tab connection
M_{slip}^-	negative moment causing slip in the shear tab connection
M_{max}^-	maximum negative moment of shear tan connection
M_{drop}^+	bending moment of shear tab connection after failure of the slab
n	number of bolts; shape parameter
\mathbf{n}	direction of contact
P	applied concentrated force; axial force
p	external load
PT	bolt pretension displacement
\tilde{q}	time average force concept in Abaqus
R	general behaviour of springs
R_{a-str}	axial behaviour of the rest of the structure or test setup
R_{a-con}	axial behaviour of the connection
$R_{\theta-con}$	flexural behaviour of the connection
$\mathbf{R}(\mathbf{u})$	residual at displacement \mathbf{u}
R_{max}	maximum residual
R_{kp}	plastic connection stiffness
R_{ki}	initial connection stiffness

R_α	residual at iteration α
T	tension force at the connection location; distance between k area of wide flange section
t_p	plate thickness
t_w	weld size
U	displacement vector; total displacements at the first and second hole forming the GAPUNI element
U_s	vertical displacement of middle column in column removal scenario
V	shear force at the connection location
W	applied uniform load
Δ_1	beam axial deformation caused by vertical displacement of removed column
Δ_2	beam axial deformation caused by the eccentricity of the centres of rotation of the two connections
Δ_{axial}	total axial deformation accumulates between the beam supports
Δ_{beam}	axial deformation of the beam
$\Delta_{connection}$	total axial deformation of the connections at each end of the beam
$\Delta_{restraint}$	axial deformation of the surrounding structure
Δu_{max}	maximum displacement increment
ε_{nom}	nominal or engineering stress
ε_{true}	true strain
$\bar{\varepsilon}_p$	equivalent plastic strain
$\dot{\bar{\varepsilon}}_p$	Mises plastic strain
Θ	connection rotation; chord rotation
θ_0	reference plastic rotation
Θ_b	beam end rotation
Θ_s	rotation at service load

Θ_p	plastic rotational capacity
Θ_u	maximum connection rotation
Θ_{tot}	total rotational capacity
θ_{slip}^+	rotation when positive moment causing a slip in the shear tab is reached
θ_{drop}^+	rotation when the moment has dropped to the level of the bare shear tab moment
θ_{max}^+	rotation of shear tab when the maximum positive moment is reached
θ_{ult}^+	rotational ductility of shear tab in the positive moment direction
θ_{slip}^-	rotation of shear tab when negative moment causing a slip in the bolts is reached
θ_{max}^-	rotation of shear tab when the maximum negative moment is reached
θ_{ult}^-	rotational ductility of shear tab in the negative moment direction
Φ^*	free end rotation of the beam divided by a reference rotation
σ	stress in the model
σ_{nom}	nominal or engineering stress
σ_{true}	true stress

LIST OF ABBREVIATIONS

Abaqus/CAE	Complete Abaqus Environment
ACI	American Concrete Institute
AISC	American Institute of Steel Construction
ANSI	American National Standards Institute
ASCE	American Society of Civil Engineers
ASTM	American Society for Testing and Materials
CEN	European Committee for Standardization
CRS	Column removal scenario
CSA	Canadian Standard Association
DoD	Department of Defence
DWT	Draw Wire Transducer
EN	European Standard
EP	Expected Properties of steel
FEA	Finite Element Analysis
FEM	Finite Element Modeling
FEMA	Federal Emergency Management Agency
FR	Fully Restrained connections
GSA	General Service Administration
LB	Lower Bound for steel
MANS	Maximum Nominal Strength

MINS	Minimum Nominal Strength
NFORC	Element Force Nodal output in Abaqus
NSF	National Science Foundation
N-to-S	Node to Surface
PEEQ	Equivalent plastic strain
PEEQMAX	Maximum equivalent plastic strain
PR	Partially restrained connections
SA	Single Angle connection
SDI	Severe discontinuity iteration
ST	Shear Tab connection
S-to-S	Surface to Surface
UEL	User Element subroutine in Abaqus
UFC	Uniform Facilities Criteria
UMAT	User Material subroutine in Abaqus
WT	Tee Shear connection
WTC	World Trade Center

1 Introduction

1.1 Overview

There are many design methodologies and philosophies intended to provide structural integrity or increase structural robustness, i.e., make steel structures resistant to progressive collapse. However, there is little information that reveals sources and levels of inherent robustness in structural members and systems. Furthermore, in available codes and specifications, the level of structural system integrity has not been quantified precisely (Foley et al. 2007). The present study seeks to begin the process of behaviour evaluation of components and assemblages initially designed for other purposes than progressive collapse, such as gravity loads, and make recommendations on their performance and possible methods for improvements for the new scenario. These recommendations can lead to more economical design and safer structural steel systems in the event of localised damage that has the potential to progress to a disproportionately large part of the structure.

To meet the stated goals, an extended literature survey was conducted to gain insights from past experience all over the world. All available design code provisions for mitigating progressive collapse, as well as the current state-of-the-art related to modelling steel structural components against progressive collapse scenarios, were reviewed. Experimental efforts were also studied to create a solid foundation to validate design concepts and analytical methods. It is observed that connections play a significant role in general integrity of different types of steel structural systems. Hence, numerical investigations have been performed to extend the current body of knowledge on connections and, consequently, the structural response in the event of progressive collapse.

The study of connection behaviour is the main part of this research and is intended to examine the response of steel frames with simple shear connections in the aftermath

of unusual and extreme loads, regardless of their lateral load resisting systems. Figure 1.1 shows examples of braced and moment frames with shear connections. As can be seen, most of the connections in the steel frames are shear connections. As a result, the main goal of the research is to evaluate the behaviour of some prevalent connection types that are used as shear connections, e.g., shear tab (ST), tee (WT) and single angle (SA) in buildings today, and perform numerical analyses on those connection configurations under loading scenarios that could trigger progressive collapse. After that, characteristic features of the connection response, e.g., alternative catenary path load mechanism and ultimate rotational capacities, are discussed to provide a solid foundation for assessing the performance of buildings with these types of connections. Observations regarding the analysis results are synthesized and conclusions are drawn with respect to the demands placed on the connections. The results of this research project should contribute to a better understanding of the resistance of steel structures with one-sided shear connections to progressive collapse.

1.2 Research Motivation

Progressive collapse has been an important issue in building failure characterization since the Ronan Point collapse (Griffiths 1968). Unfortunately, progressive collapse had not received much attention between the early 1970s and 2001; however, it has been an interesting and increasing concern specifically after the terrorist attack of the World Trade Center Towers in 2001. This incident caught the attention of practitioners and researchers and focussed scrutiny on potential deficiencies in structural designs, and also the fact that there is an urgent need to move steadily forward on research in this area. Obviously, complexities exist in the responses of both individual components and assemblages of components that require a mix of empirical, analytical and numerical methods (Marchand and Alfawakhiri 2004).

Progressive collapse is a rare event in western nations; however, considerable casualties can occur when it happens. Besides terrorist attacks, potential progressive

collapse triggers include accidental explosions, vehicular impact, design and construction flaws, extreme environmental loading, etc. Based on this fact, there are many pressures arising from governmental and defence interests, particularly in the United States, but there has also been a widespread recognition among professionals that our understanding in this area is relatively weak. Some design criteria have been codified in the United States, but they are clearly in their infancy. Issues pertaining to structural integrity and inherent robustness are discussed in concrete codes such as ACI 318-10 (ACI 2010) and CSA A23.3 (CSA 2004), but the analogous steel codes, AISC (AISC 2010) and S16 (CSA 2009), do not discuss important structural integrity issues such as robustness of simple connections in depth.

Evaluation of connection behaviour during progressive collapse is a relatively new topic in steel structures research, and more study is needed. For instance, the U.S. General Services Administration, in its primer on progressive collapse, notes that limited test data exist for steel frame beam-to-column connections subjected to the type of loading conditions that accompany removal of a column (GSA 2003). Furthermore, the American Institute of Steel Construction has published a primer on blast and progressive collapse (Marchand and Alfawakhiri 2004) in which current research needs for progressive collapse have been highlighted. It states that steel connections should meet the ANSI/AISC 341-02 seismic provisions (AISC 2002) for inelastic rotational capacity until more tests and numerical studies have been conducted on the performance of steel connections, including the effects of moment and axial tension interaction.

Progressive collapse vulnerability is rarely considered explicitly in general design work. The main concern is that as the pressures to consider it mount, requirements will be put in place without a complete understanding of the behaviour of steel structures in this regard. This could have considerable adverse economic consequences to the steel industry, when a great deal of progressive collapse resistance may well exist from conventional construction methods. For instance, certain types of shear connections likely have substantial inherent tensile capacity, or

at least could have with minor modifications, and could be relied upon for collapse prevention in the event of the loss of a single column. Additionally, structures designed to prevent progressive collapse do not necessarily have a higher cost of construction. For example, well-detailed ductile joints that would have been used in a well-designed structure anyway, might help the general integrity of the structure significantly (Taylor 1975).

1.3 Progressive collapse definition

Progressive collapse is characterized by a cascading progression of damage that is not proportionate to the initial failure. When a member of a structure, usually a column, is removed or destroyed because of severe natural or manmade hazards, the internal forces in the neighbouring structural members change and increase in an attempt to redistribute the supported loads. If the additional internal forces as a result of local failure can't be redistributed, partial or total collapse of the structure happens (Song and Sezen 2009). The concept is illustrated in Figure 1.2.

There are different definitions for progressive collapse available in the literature. Foley et al. (2007) defines progressive collapse resisting structural design "as having a level of robustness such that an event that compromises (renders ineffective) a relatively small portion of the structural system cannot grow to encompass a portion of the structure much greater than the area involved in the initial event."

UFC 2009 (DoD 2009) defines progressive collapse as "a chain reaction of failures following damage to a relatively small portion of a structure. The damage resulting from progressive collapse is out of proportion to the damage that initiated the collapse."

GSA 2003 (GSA 2003) defines progressive collapse as a situation where local failure of a primary structural component leads to the collapse of adjoining members which,

in turn, leads to additional collapse. Hence, the total damage is disproportionate to the original cause.

ASCE 7-10 (ASCE 2010) defines progressive collapse as "the spread of an initial local failure from element to element, eventually resulting in the collapse of an entire structure or a disproportionately large part of it".

European standard (CEN 1990) EN 1990:2002 uses the term "disproportionate" collapse instead of "progressive" collapse, stated as: "A structure shall be designed and executed in such a way that it will not be damaged by events such as explosion, impact, and the consequences of human errors, to an extent disproportionate to the original cause."

Basically, progressive collapse can be proportionate or disproportionate to the initial damage based on the level of total damage and the acceptable limits assumed or chosen. However, in this research, the use of the term progressive implies disproportionate implicitly.

Based on ASCE's definition, two conditions are needed for occurrence of progressive collapse: first, an external cause such as abnormal loading to initiate damage and, second, inadequacy in structural continuity, redundancy, and/or ductility. Since connections play an important role in providing continuity and ductility, the response of steel connections under such abnormal situations has received renewed interest. (Marchand 2008).

1.4 Progressive collapse – historic perspective

In Table 1.1, some historic cases of progressive collapse are explained in order to provide insight into the importance of the issue under consideration. This historic summary re-emphasizes the fact that the topic selected for this research project is of primary concern, due to the fact that connections play an important role in providing robustness.

There are several lessons that could be learnt from the past cases of progressive collapse. However, the most important ones that are common in almost all cases are issues regarding structural integrity, redundancy and, more particularly, alternative paths for transferring loads. Structural integrity needs to be considered at the design level and also different stages of construction to prevent progressive collapse in case local damage happens. Providing redundancy and alternative load paths can mitigate the potential for progressive collapse significantly. Structures should be able to redistribute the loads and to remain stable after loss of a main load-bearing member, such as a wall or a column. Ductility in all components of the structure, but particularly in the connections, helps greatly to mitigate the progressive collapse effect.

1.5 Research objectives and scope

As mentioned previously, the main goal of this project is to provide the foundation to evaluate the behaviour of steel frames with shear connections subjected to progressive collapse scenarios more realistically. For this purpose, the key elements are to establish the behavioural characteristics of the connections initially designed for purposes other than progressive collapse for the new need. The main focus of the research is shear connections that are initially designed to transfer only shear force from the supported beam to the supporting column. Because of the single-purpose method generally used for designing such connections, some might think that they are prone to brittle failure under unanticipated loading, without providing alternative load paths, resulting in a progressive type of collapse.

To answer this question, three types of connections are considered: shear tab, WT and single angle. The main identical feature of the selected shear connections is that they are not symmetric about the vertical axis, and are thus referred to herein as "one-sided" shear connections. After determining the behaviour of all of these types of connections, characteristic behavioural features, such as rotational ductility, are

established and discussed. These results, in terms of force–rotation curves, can be assigned to the connection locations in the whole-structural model for simulating the column removal scenario. Catenary action is considered in connection behaviour determination as a key difference between traditional seismic and progressive collapse-type connection performance.

1.6 Research methodology

The flowchart illustrated in Figure 1.13 shows the proposed method to achieved the objectives of the project stated in section 1.5. The main research comprises a variety of numerical investigations, with validation of the results being achieved using available experimental data. For shear tab,WT and single angle connections, the test results of Thompson (2009), Friedman (2009) and Johnston (2009), respectively, as a part of an extensive experimental program performed at the Milwaukee School of Engineering, are used. Numerical studies performed were mainly aimed at providing the internal force–rotation characteristics of bolted shear connections that can be utilized in progressive collapse analysis of steel frames. Shear, axial force, and flexural responses are presented for different types of shear connections. Numerical and experimental results are compared, and conclusions are made.

Abaqus/CAE (Dassault Systèmes 2009) is used for all stages in the simulations. Although the Abaqus finite element program was used in this study, with correct definition of the models, as discussed in chapter 3, other commercially-available software with similar capabilities could also be used. A benchmark example is established, also with current state-of-the-art simulation techniques, for the sake of the current study goals and for use with any other numerical research intended to focus on the behaviour of shear connections in a column removal scenario.

Based on available references, there is a limited understanding of the concept of ductility demands placed on connections in steel structures and members subjected to abnormal loading events. Recent major advances in knowledge related to the ductile

design of structures for resisting earthquakes, e.g., ASCE 41 (ASCE 2006), have opened the door to important research on progressive collapse that can make use of many of the same principles. Similar methodology is adopted in two progressive collapse guidelines: *Progressive Collapse Analysis and Design Guidelines for New Federal Office Buildings and Major Modernization Projects* (GSA 2003) and *Design of Buildings to Resist Progressive Collapse* (DoD 2009). Both guidelines, GSA and DoD, propose the same approaches based on threat-independent methodology for new and existing buildings that has been accepted in this research. The focus of this project will be on the “alternate load path” methods in which loads that were resisted by damaged or removed elements must be transferred to undamaged elements, thereby preventing collapse. This method involves removing a vertical element and analyzing the remaining elements for their ability to “bridge” over. More discussion on these issues is presented in chapters 2 and 3.

1.7 Thesis organization

Chapter 1 is dedicated to a brief overview of the project, including the main motivations for the research. Progressive collapse, as the main impetus for looking at shear connections again, is defined. After that, the main objectives of the project are established and appropriate methodology is proposed to reach the objectives stated.

Chapter 2 contains the general introduction to shear connections and describes their behaviour under conventional and progressive collapse types of loading. A finite element model is proposed based on selected experimental data to accomplish the objectives stated in chapter 1.

Chapter 3 introduces a benchmark finite element example for modelling steel shear connections in the column removal scenario. All the numerical challenges to solve this highly nonlinear problem, including those related to the material, geometry and contact between surfaces, are discussed and solutions are proposed.

Chapter 4 takes a close look at the axial behaviour of shear connections during a column removal scenario, and particularly the possibility of formation of a compressive strut in the connection assembly.

Chapters 5, 6 and 7 contain the main results of the research, including the shear, tension, and moment response curves of the shear tab, WT and single angle connections, respectively. The effects of different parameters, such as the depth and thickness of the connecting part and bolt size and type, are investigated and observations are reported. The rotational capacity of each type is investigated in detail and equations are proposed as modelling parameters for use with the alternative load path method.

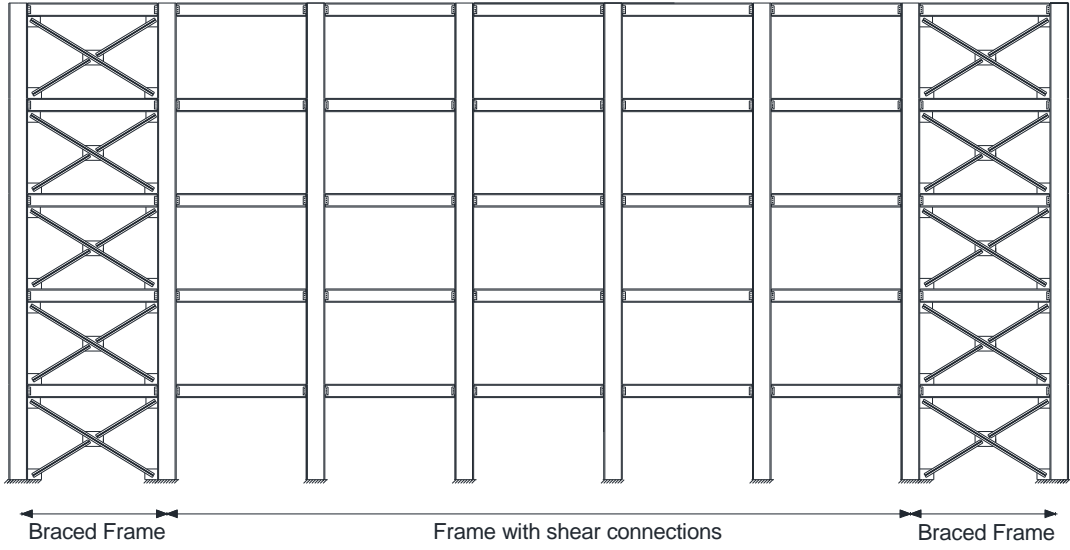
In chapter 8, a summary of the methodology and conclusions of the research are presented. Recommendations for future research are also included in this chapter.

Table 1.1: progressive collapse case studies

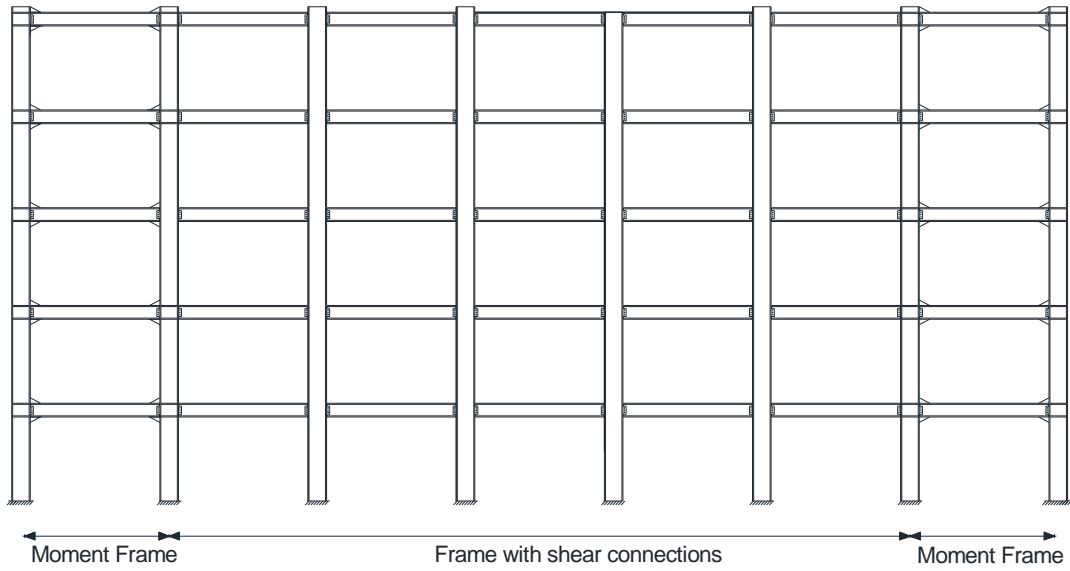
	Name of Building	Location	Structural system	Year	Picture	Threat	Initial Failure	Consequences
1	Ronan Point	Newham, England	precast concrete panel	1968	Figure 1.3	gas explosion	failure of precast exterior concrete wall at one upper storey	collapse of the entire corner of the building
2	Skyline Plaza	Kansas City, USA	reinforced concrete flat plate type	1973	Figure 1.4	construction defect	premature removal of the shoring on one of the floors	punching shear failure of the slab around the removed shore; consequently, full height collapse
3	Hyatt Regency Hotel Skywalks	Kansas City, USA	tower with atrium floor and three pedestrian walkways constructed of structural steel suspended overhead by steel rods	1981	Figure 1.5	crowd	failure of single connection	4th floor walkway collapsed onto the 2nd floor walkway

4	L'Ambiance Plaza	Bridgeport, Connecticut	post-tensioned concrete slab supported on steel columns	1987	Figure 1.6	construction defect	sudden loss of support for one or more slabs	entire collapse of both wings of the building
5	Alfred P. Murrah Federal Building	Oklahoma City, Oklahoma	reinforced concrete OMRF one way slab system	1995	Figure 1.7	bomb explosion	failure of columns supporting the transfer girder	progressive collapse of all the floors above the transfer girder
6	Khobar Towers	Alkhobar, Saudi Arabia	precast concrete wall and floor	1996	Figure 1.8	bomb explosion	the facade wall of the closest building and some interior floor and wall components were destroyed	collapse did not spread out much beyond the affected area
7	WTC 1 and WTC 2	New York, USA	an innovative frame-tube concept including exterior wall, the core, the floor system and the hat truss	2001	Figure 1.9	airplane crash	structural members are severely damaged on several upper floors of the buildings	fire ensued and consequently, the whole structures collapsed

8	WTC 7	New York, USA	braced frames with transfer truss and transfer girders	2001	Figure 1.10	flaming debris	failure of some columns due to impact of debris or exposing to fire	global collapse
9	Pentagon	Arlington, Virginia, USA	cast-in-place reinforced concrete	2001	Figure 1.11	airplane crash	about fifty columns on the first floor were removed	relatively small portion of the affected area collapsed but only after sufficient time for excavating
10	Bankers Trust Building (Deutsche Bank)	New York, USA	steel structure - ordinary moment frame in both directions	2001	Figure 1.12	debris shedding	debris from South WTC tower impact the 23 rd floor of the building	although the vertical column destroyed between 18 th and 9 th floors, no further damage greater than what was caused by debris collision reported

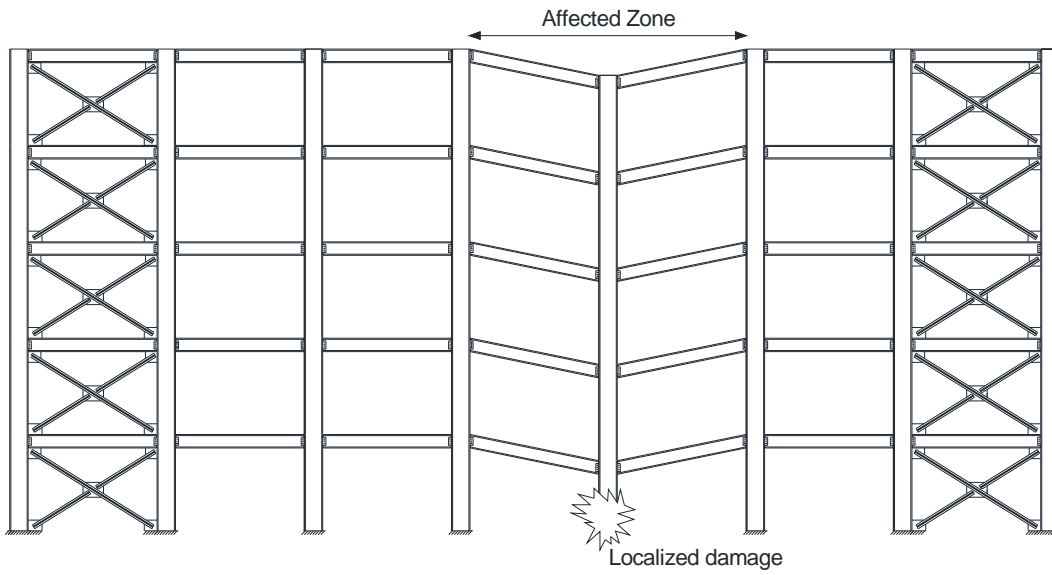


(a)

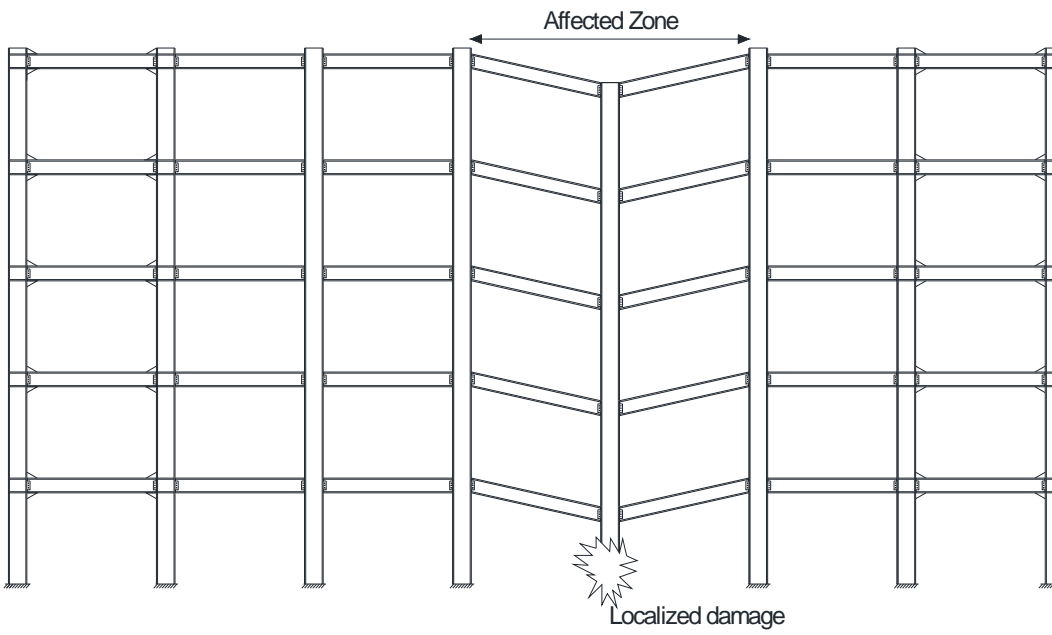


(b)

Figure 1.1: Frames with shear connections: (a) braced frame (b) moment resisting frame



(a)



(b)

Figure 1.2: Progressive collapse scenario: (a) in braced frame (b) in moment resisting frame



Figure 1.3: Ronan Point apartment tower in Newham, England (Nair 2003)



Figure 1.4: Skyline Plaza, Kansas City, USA (Crowder 2005)

Source: https://pdc.usace.army.mil/library/ufc/4-023-03/pc_historical_perspective.pdf



Figure 1.5: Hyatt Regency Hotel Skywalks, Kansas City, USA

Source: <http://www.nytimes.com/2008/07/27/us/27hyatt.html>



Figure 1.6: L'Ambyance Plaza, Bridgeport, USA (NIST 2007)



Figure 1.7: Alfred P. Murrah Federal Building, Oklahoma City, USA (NIST 2005)

Source: http://en.wikipedia.org/wiki/Alfred_P._Murrah_Federal_Building



Figure 1.8: Khobar Towers, Alkhobar, Saudi Arabia (NIST 2005)



Figure 1.9: WTC 1 and WTC 2, New York, USA (NIST 2005)



Figure 1.10: WTC 7, New York, USA (NIST 2007)



Figure 1.11: Pentagon, Arlington, USA (NIST 2005)

Source: <http://www.loc.gov/rr/frd/Pentagon.htm>



Figure 1.12: Bankers Trust Building (Deutsche Bank), New York, USA (NIST 2007)

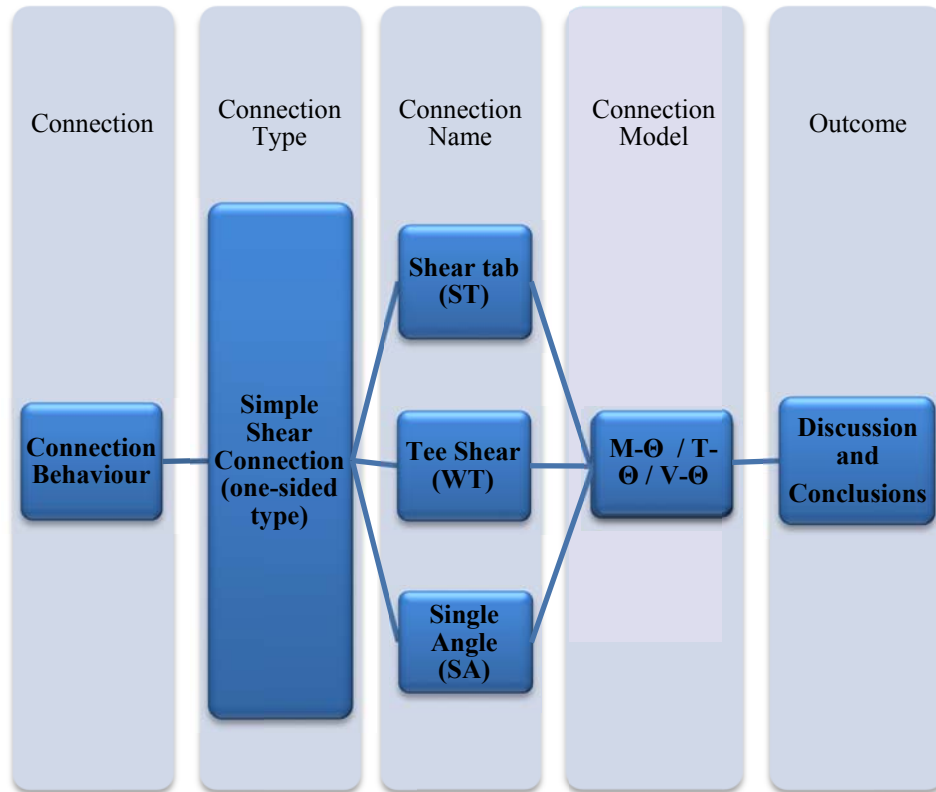


Figure 1.13: Project objectives at a glance

2 Behaviour of Simple Shear Connections in Column Removal Scenario

2.1 Introduction

Shear connections in beams are conventionally designed to transfer shear forces only. It is assumed that there is no substantial moment transfer due to the fact that beam end rotation is allowable. Additionally, the amount of axial force applied to the shear connections subjected to vertical loads is typically negligible. There are different types of shear connections, such as shear tab, WT, single angle and double angle connections. Although the behaviour of these connections under gravity load and, to some extent, in cyclic loading has been established during the past several decades, their response to the column removal scenario that is commonly considered for progressive collapse analysis is still relatively unknown. In this case, the connection is exposed to the simultaneous presence of shear, tension and moment.

In this study, the behaviour of shear connections under conventional loading is introduced and discussed. After that, the new double span scenario, and the demands it imposes on the connections, are established. Subsequently, a rational procedure is proposed to investigate the behaviour of steel shear connections when a column is compromised, through the process of numerical modelling. It is concluded that the numerical models, verified by appropriately-selected experimental data, are accurate tools to determine the desired behaviour of shear connections in a column-loss event. A general nonlinear finite element model is suggested to conduct the connection analyses. The experimental program used for verification of the results is described, and the results-extraction process is discussed.

A connection is defined herein as a region joining a column and a beam using a connecting element such as an angle or a plate and also fasteners (welds or bolts), as shown in Figure 2.1. It is customary in conventional structural analysis to assume fixed or pinned connections at the intersection of beams and columns in steel structures. The assumption might be acceptable in terms of conventional design methods, but when it comes to performance evaluation and performance-based design concepts, more realistic modelling techniques may be required.

Based on existing experiments, the actual behaviour of a connection is somewhere between these two idealized conditions (Kameshki and Saka 2003). Beam-to-column joint deformation is complicated due to local distortions, giving rise to mechanical and geometrical nonlinearities, and also the influence of interaction among different elements.

Figure 2.2 shows typical moment–rotation curves of different types of connections. Nonlinearities in

Figure 2.2 are also the results of yielding of connection components or slip of the fasteners (William 1988).

There are several forms of shear connection used in steel structures, with common examples shown in Table 2.1. Although beams with shear connections are often assumed to rotate freely, they do possess rotational restraint (AISC 2010). This small amount of restraint can be neglected and the connection idealized as a hinge when subjected to the gravity load. Based on the definition generally accepted in the literature, connections with moment capacities less than 20 % of the plastic moment capacity of the connected beams can be called shear connections (Astaneh-Asl 2005).

From a structural integrity point of view, behaviour of shear connections might be different from what is normally assumed. DeStefano (2006) suggested utilizing ductile connections with high axial load resistance, such as symmetric two-sided connections (e.g., double angle rather than single-sided connections such as shear

tab, WT or single angle) to increase the structural robustness against progressive collapse. This was one of the main motivations for focusing on the performance of three types of all-bolted connections, shown in Figure 2.3, that are all single-sided. One of the main advantages of one-sided, bolted connections is the reduced labour on-site. Table 2.2 summarizes the materials usually utilized in these types of connection.

Based on the definition of progressive collapse in chapter 1, two conditions are required for occurrence of progressive collapse: first, an external cause such as abnormal loading to initiate damage and, second, inadequacy of structural continuity, redundancy and ductility. Since connections play an important role in providing continuity and also ductility, the response of steel connections under such an abnormal situation has received renewed interest (Marchand 2008). Shear connections are deemed to be the most vulnerable regions in a steel frame because they are normally designed to resist shear forces only. However, it is believed that a properly-designed bolted shear connection is capable of transferring tension and moment in addition to shear forces.

Due to the fact that progressive collapse is a relatively new topic faced by structural engineers and researchers, few experiments have been completed on connections loaded under the so-called “column removal” scenario, which is commonly used for progressive collapse analysis and design. Connection behaviour is a significant portion of the whole performance evaluation procedure in order to characterize the performance of framed buildings against progressive collapse. After modelling the real behaviour of each component, structural evaluation can be achieved with a fully nonlinear analysis for the damaged structure subjected to the column removal scenario. The main focus of this research is on the former part because without the accurate behaviour of the components, performing the system analysis is based on simplifying assumptions that might lead to inaccurate and, in some cases, misleading results.

In this chapter, after establishing the scope and objectives of the chapter, the shear connection behaviour subjected to conventional loading is discussed in section 2.3. To provide a solid background for the current study, the applicable research regarding the behaviour of shear connections in progressive collapse conditions—including the available physical tests, the structural idealization and the selected experimental programs—are discussed in section 2.4. In section 2.5, a connection subassembly model is proposed to investigate the behaviour of different types of shear connections in the future chapters. The possibility of the formation of arching forces is acknowledged in section 2.8 to provide a basis for a more elaborate discussion in chapter 4. At the end, a general finite element model is proposed to be used for shear tab, WT and single angle types of connections in chapters 5, 6 and 7 respectively.

2.2 Scope of the research and objective

This research is focused upon three types of shear connections, but the modelling procedures outlined can be applied to other types as well. The intents of this chapter are to:

- establish the key differences between the behaviour of shear connections in conventional loading and in a double-span event;
- select an appropriate substructure to investigate the behaviour of shear connection assemblies that can mimic the behaviour and failure modes in a progressive collapse event;
- develop a model for shear connections subjected to a column loss event;
- gain insight into the response of steel shear connections subjected to combined bending, shear and tension.

Since the main interest in this research is the connection performance in progressive collapse type of loading, the effect of the floor slab has been ignored.

The column and the beam remain elastic in this extreme load-effect simulation and the focus is on the connection itself.

2.3 Shear connections under conventional loading

Figure 2.4(a) shows a frame with shear connections under vertical gravity loads. One specific member with shear connections at both ends is isolated and shown with its responses in Figure 2.4(b). As observed, axial force in the beam is negligible when the structure is subjected just to the gravity loads. The amount of shear at the beam ends is substantial. This shear is the force that the shear connections are designed for in conventional design. Nonetheless, shear connections are not designed to resist moment under gravity loads. However, as can be seen from the figure, there are some flexural demands at the location of the connections that depend on the rotational stiffness of the connection.

Figure 2.5(a) shows a frame with shear connections under lateral loads (seismic or wind). One specific member with shear connections at both ends is isolated and its responses are shown in Figure 2.5(b). Depending on the nature of the braced frames and the loads themselves, axial forces in the beam may be significant. However, the amount of shear is small. There are some flexural demands at the locations of the connections as well. Nevertheless, shear connections are not normally considered part of lateral load bearing system.

It is generally assumed that the most important behavioural characteristics of the connection under conventional loads can be modelled by the moment–rotation ($M-\Theta$) curve. Various components of these characteristics, including stiffness, strength and ductility of a connection, are demonstrated in the $M-\Theta$ curve. The nonlinear behaviour of the connection begins at low moment–rotation levels; the initial stiffness of the connection, represented by K_i in Figure 2.6, does not

adequately characterize connection response at the service load. Furthermore, many connection types do not exhibit a reliable initial stiffness. The secant stiffness, K_s , at service loads is taken as an index property of the connection stiffness (AISC 2010), as follows:

$$K_s = \frac{M_s}{\Theta_s} \quad (2-1)$$

where M_s is the moment at the service load and Θ_s is the rotation at the same point. If $\frac{K_s L}{EI} \geq 20$, the connection is called a “moment” or “fully-restrained” (FR) connection. In cases where $\frac{K_s L}{EI} \leq 2$, the connection is considered a “simple” shear connection. Anything between these two limits is considered a “partially-restrained” (PR) connection. In the above terms, L and EI are the length and bending rigidity of the beam, respectively. The concept is illustrated in Figure 2.7.

The strength of a connection, M_n , is the maximum moment that the connection is capable of carrying. It can be determined based on the principles of ultimate limit state design of the connection or on the basis of physical experiments or high fidelity numerical modelling with well-defined failure criteria. AISC (2010) suggests that if the moment–rotation response does not have a peak load then the strength at the rotation of 0.02 radians may be taken as M_n . Fully-restrained connections may have strength less than the beam strength. However, partially-restrained connections might exhibit strength greater than the beam's (AISC 2010). In case of shear connections, the possibility of M_n exceeding the beam strength is almost zero.

Generally the strength of the connection must be adequate to resist the moment demand induced by the combination of gravity and lateral load. In the case of shear connections, since the strength of the beam exceeds the strength of the connection most of the inelastic deformation is concentrated in the connection (AISC 2010). In seismic applications, rotational springs are often used to simulate

nonlinear behaviour of the connection, as shown in Figure 2.8(a). This simulation is based on assuming that the moment–curvature relationship dominates its behaviour (Krauthammer 2006). Determination of such a spring's definition is of primary importance.

In order to approach the real behaviour of the structure under seismic loading, consideration of joint behaviour, including the connection itself, is mandatory. There are many seismic design codes and guidelines available, but when it comes to performance-based design and evaluation of seismic behaviour of structures, the number of the key documents and guidelines decreases substantially. One of the most influential documents on this issue is “ASCE 41-06: Seismic Rehabilitation of Existing Buildings” (ASCE 2007) that is a revised version of “FEMA 356: Prestandard and Commentary for the Seismic Rehabilitation of Buildings” (FEMA 2000). In their proposed nonlinear analysis procedures, including static and dynamic, one concentrated plasticity method, called the plastic hinge method, is used. Plastic hinges are the locations where a structure absorbs kinematic energy of an earthquake (Marchand 2008). ASCE 41-06 and FEMA 356 define the plastic hinge model as a linearized force–deformation curve, as shown in Figure 2.9(a). The curves are the definitions of the rotational springs at the connections that were discussed earlier. Therefore, the connections can be substituted by rotational springs with appropriately-selected moment–rotation relationships for evaluating the performance of buildings under seismic loading.

AISC 41-06 and FEMA 356 propose identical values for a , b and c (Figure 2.9(a)) for both fully- and partially-restrained moment connections. This information comes from various research programs on cyclic behaviour of steel connections over several decades. This large database is worth examining to learn if and how it is possible to apply the data for new needs such as progressive collapse mitigation (Daneshvar and Driver 2010).

2.4 Shear connections in progressive collapse scenario

Progressive collapse evaluation is conducted based on two major available guidelines that were published by GSA (2003) and DoD (2009). For instance, the DoD (2009) guideline proposes three approaches based on threat-independent methodology for both new and existing buildings: tie forces, alternative load path analysis and enhanced local resistance. Alternative load path is a widely accepted method in which the loads resisted by damaged or removed elements must be transferred to the undamaged elements. It involves removing a vertical element and analyzing the remaining elements for their ability to “bridge” over. The loss of a member can be modelled either by abrupt dynamic or quasi-static removal, depending on the method. This method is the origin of the column removal scenario for progressive collapse evaluation.

The deformed shape of the frame with shear connections after removal of a column is shown in Figure 2.10(a). In order to simplify the problem, the double span is isolated with a concentrated load at the middle column as shown in Figure 2.10(b). Figure 2.10(c) illustrates the response of double-span beams. As can be seen from Figure 2.10, a substantial amount of shear, axial force and moment are present at the location of the connection, which distinguishes the column removal event from traditional connection design methods. This simultaneous presence of internal forces is illustrated in Figure 2.11. The responses of the member shown in Figure 2.12 are rotation-dependent since the problem is a nonlinear large-deformation one. It means that catenary axial force will become significant after a certain amount of rotation. In other words, there is a specific mechanics sequence by which a simple shear connection devolves from a flexure-dominant connection, as shown in the Figure 2.12(c), into a catenary-dominant subassembly, depicted in Figure 2.12(d). The rotational demand on connections at this devolution point is difficult to define. Also, the maximum rotational capacity of the connections in this scenario is another issue that needs to be determined to establish the performance of connections.

Similar to the seismic evaluation codes discussed in section 2.3, the localized plastic hinge concept is adopted in the alternative load path method as well. Evaluation of collapse behavior of buildings that include frames with shear connections requires considering the shear connections with well-defined responses in a column loss event. The GSA (2003) guidelines neglect the frames with shear connections in progressive collapse evaluation of the structure. DoD (2009) recognizes the frames with shear connections as a vertical collapse resistance system. It provides a table that includes the moment–rotation behaviour of shear tab and double angle shear connections. DoD’s connection table is very similar to the one in ASCE 41-06. Both seismic and progressive collapse codes and guidelines quantify and linearize the real moment–rotation curve as shown in Figure 2.9(a).

Based on the available references, there is a limited understanding of the concept of ductility demands placed on connections in steel structures and members subjected to abnormal loading events (Foley et al. 2007). Figure 2.13 compares the response of shear tab connections with different depths based on a progressive collapse guideline, DoD, and a seismic code, ASCE 41. As depicted, the DoD model predicts considerably lower connection ductility in comparison with ASCE 41 for all the connections considered. Nevertheless, Powell (2005) believes that less ductility is expected under earthquake loads, where there are several deformation cycles and hence more degradation. For progressive collapse loads there is only one half-cycle. Hence, it can be expected that the ductility limits for progressive collapse loads will be larger than those given by ASCE 41, as observed in Figure 2.9(b), and that the amounts of strength loss will be smaller (Powell 2005). Figure 2.13 does not confirm Powell's idea. Another important issue is the presence of tension in the DoD curves, although it is hidden. This tension might reduce the ductility of connection in the push-down type of progressive collapse analysis. In the ASCE 41 definition, there is no effect of tension. These issues are investigated in chapter 5 for shear tabs and in chapters 6 and 7 for WT and single angle connections, respectively.

GSA (2003) notes that limited test data exist for steel frame beam-to-column connections subjected to the type of loading conditions that accompany removal of a column, and this remains true today. Furthermore, the American (Powell 2005) Institute of Steel Construction has published a primer on blast and progressive collapse (Marchand and Alfawakhiri 2004) in which research needs for progressive collapse have been highlighted. It states that steel connections should meet the ANSI/AISC 341-02 seismic provisions (AISC 2002) for inelastic rotational capacity until more tests and numerical studies have been conducted on the performance of steel connections, including the effects of moment and axial tension interaction. DoD specifies that the tables available in ASCE 41 be used in order to model the behaviour of the connections if not available in DoD's tables.

Furthermore, in progressive collapse analysis, plastic hinges or rotational springs, as well as axial springs, should be adopted, as illustrated in Figure 2.8(b), since catenary action is important. However, it needs to be investigated if catenary action is achievable in shear connections and if that is reliable to be considered as an alternative load path. Determination of the behaviour of these two springs that represents the connections' behaviour is one of the primary tasks. Axial springs should also be adopted to represent the presence of the rest of the structure, too. It is believed that none of the available test data and numerical studies on this topic comprehensively address the effect of external restraint on member behaviour.

It is inferred that steel shear connections in column removal scenarios need a number of experimental and numerical studies to establish accurate connection models. Besides, more variable and economic designs can be achieved by considering the real behaviour of the steel shear connection. In addition, other inelastic behaviour associated with progressive collapse mitigation should be considered, such as connection axial tension and moment interaction due to large displacements, as discussed by (Daneshvar and Driver 2010).

2.4.1 Steel connection experiments simulating column removal scenario

The number of tests on steel shear connections simulating double-span scenario is limited. Hence, more experimental work is required in order to assess the behavior of the connections for this scenario. Unfortunately, there is no protocol or guideline about experimentation of components of steel structures for the column removal scenario. A few tests have been performed by different universities and other organizations; however, the lack of a standard protocol creates difficulty in assessing and interpreting data and coming to unified solutions, as happened for seismic evaluation of connections.

Table 2.3 summarizes some of the available beam-to-column connection tests simulating a progressive collapse type of loading.

2.4.2 Sub-structural idealization for column removal studies

In order to investigate the response of steel connections when an adjacent column has been compromised, the connection needs to be isolated from the rest of the structure, which is replaced by appropriate boundary conditions.

Figure 2.14 depicts possible substructures that could be used for connection evaluation in a column removal scenario. Each substructure requires special considerations for the loading protocol. For example, for substructure A (a stub column attached to a connection and a cantilever beam), appropriate proportions of shear, axial force and moment should be imposed on the subassembly in order to simulate the double-span scenario correctly (Daneshvar et al. 2012).

Based on the selected substructure, a different test setup could be used. Figure 2.15 shows the schematic test outlines for the four cases shown in Figure 2.14. In Figure 2.15(b), the far ends of the beams are usually designed to act as a hinge; however, the middle stub column specimen is the main case-study connection. The main difference between Figure 2.15(c) and Figure 2.15(d) is in the exterior

columns and their boundary conditions. In Figure 2.15(a) and (c), the effect of the rest of the structure has been neglected implicitly, albeit Figure 2.15(b) and (d) possess more control on boundary conditions to simulate the effect of the rest of the structure on the connection behaviour.

2.5 Introduction of connection model assembly to investigate column removal scenario

Based on the structural idealization discussed in section 2.4.2, a connection assembly model has been proposed to simulate the column removal scenario, as illustrated in Figure 2.16(a). The model is a refined version of the model by Astaneh (Astaneh-Asl 2007), which consists of a middle stub column, two beams with axial and rotational springs at each end, and two springs at far ends to simulate the surrounding structure. R_{a-con} and $R_{\theta-con}$ are the axial and flexural response of the connection, respectively, and R_{a-str} represents axial behaviour of the rest of the structure or test setup. In this model, connection performance is evaluated by a push down test in which vertical load/displacement is applied to the connection assembly. Unlike Astaneh's model, the constitutive laws that govern the behaviour of R_{a-str} , R_{a-con} and $R_{\theta-con}$ are not just the stiffness values. These R values represent the general behaviour of springs, including an elastic stage, ductile inelastic stage and degrading or softening branch. The model is developed based on the assumption that at small rotations, the connection assembly takes load through flexural behaviour, as illustrated in Figure 2.16(b). As the rotation increases, the connection subassembly develops catenary action, as shown in Figure 2.16(c). Since numerical analysis of two connections with all details is time-consuming and tedious, the model in Figure 2.16(a) was simplified to the model shown in Figure 2.16(d) to focus on the middle connections.

2.6 Selected Experimental Study

Three test programs were conducted in conjunction with each other on shear tab, WT and single angle connections by Thompson (2009), Friedman (2009) and Johnston (2009) at the Milwaukee School of Engineering. These tests have been used to verify the numerical study. Figure 2.17 shows the test setup according to all three sets of tests performed.

The test specimens consisted of a planar two-span beam, with the beams attached to a central column stub by a plate, angle or WT and to “true pin” connections at the far ends of the beams. A vertical displacement was applied to the central stub column in order to simulate a controlled collapse of an interior column. The main reasons that these suites of experiments are selected for the current research are:

- the test setup simulates a double-span scenario, as described in available progressive collapse design guidelines; it is also compatible with the proposed connection model in section 2.5;
- the destructive nature of the test: the assembly is pushed down to its ultimate capacity. The connection goes through large rotations, in contrast to many previous tests on the shear connections;
- the reporting of catenary force (axial force): catenary resistance is recognized as one of the main distinguishing factors in the characterization of a connection's robustness for progressive collapse prevention. It is also an alternative path for transferring loads for resisting against collapse after a column has been compromised. Catenary action is explicitly reported in the test reports, which is contrary to most previous tests on shear connections.

2.7 Experimental result calculation

The procedure taken by Thompson (2009) and Friedman (2009) are used to achieve the internal forces from the experiment. It is noted that the same procedure was applied to the single angle data to produce the internal force versus rotation curves (Johnson 2009). Solving a system of simultaneous equations using the stress values on opposite sides of the beam neutral axis, will lead to the determination of axial and flexural force at the location of strain gauges.

It is noted that strain gauge 2 and 3 on the left beam and 5 and 8 on the right beam are selected for the purpose of load calculation. As it is shown in Figure 2.10 (c), the axial tensile force is constant within the length of the beam. In order to calculate the moment at the bolt line, linear moment distribution is assumed, considering a zero moment location at the points of simulated true pin. Hence, the moment at the bolt line can be determined based on Equation (2-2) using linear interpolation:

$$M_b = \frac{L_b}{L_{st}} M_{st} \quad (2-2)$$

where L_b is the horizontal distance from the true pin to the bolt line; L_{st} is the horizontal distance from the true pin to the strain gauge location; M_b is the moment at the bolt line; and M_{st} is the moment at the strain gauge location. Hereinafter, whenever moment is mentioned, M_b is the main purpose (Thompson 2009).

2.8 Possibility of existence of arch action

Formation of catenary action in the connection is highly dependent on the boundary condition of the test assembly. In other words, the external axial restraint provided by the test setup is very influential on the axial response of the

connection, as the system goes through large displacements. The precise amount of this external restraint is unknown, but due to the small span-to-depth ratio of the beam utilized in the experiments, there is a high probability that a compressive arch action would form as the middle column is pushed down. This phenomenon is shown in Figure 2.18. In this research, the external restraint provided to the beam by the surrounding frame is simulated by axial springs at the far ends of the beams. Further study is needed to characterise the influence of support flexibility on the catenary behaviour of shear connections under the column removal scenario. Moreover, non-linear springs or springs with different behaviour in compression and tension may be required to achieve an accurate axial response.

2.9 Modelling of steel connections using FEA

There are several unknowns in the model shown in Figure 2.16(c) that makes analysing the system with certainty impossible. For instance, it is necessary to establish the ultimate value of the angle θ in Figure 2.10(b), called θ_u when referring to the maximum rotation that the shear connection can tolerate before failure. The commonly assumed beam end rotation for simply-supported framing under gravity loads, 0.03 radians, underestimates the connection rotational capacity considerably. Besides, there is an interaction among the three mentioned springs, e.g., the moment and axial responses of the connection have mutual effects on each other. Furthermore, the axial response of the rest of the structure influences the axial behaviour of the connection considerably. However, it is not yet clear how the effect of the rest of the structure can influence the connection behaviour and to what extent the external spring may have played role in the connection behaviour.

Numerical simulation is deemed to be an appropriate tool to solve the model proposed in section 2.5. The finite element models consist of the central column and adjacent beams, as well as the connections with complete detailing, as shown

for shear tabs in Figure 2.19. Shear connections might be welded or bolted to the column flange and beam web. Since the connection is the point of interest, all characteristic features of the connections need to be included in the model. The central column is pushed down, while the connection performance is monitored. Beams are extended only to the point of zero moment and a true pin was simulated at each end of the assembly by applying a rigid plate to the cross-section, connected to a horizontal axial spring to approximate the flexibility of the test setup and any bolt slippage or local hole deformation. This spring is representative of the restraint from the surrounding structure in the building. All other characteristic features of the finite element model are discussed in chapter 3.

2.10 Summary and conclusions

- In keeping with the current trend towards the robustness evaluation of steel structures, specific methods need to be considered to determine the behaviour of steel shear connections and extreme demands.
- Shear connection behaviour subjected to conventional loading and progressive collapse conditions, including the available physical tests, structural idealization and the selected experimental program, are discussed.
- A connection subassembly model is proposed to investigate the behaviour of different types of shear connections when a column is compromised.
- Although the effect of axial catenary behaviour is implicitly considered in the flexural response of the connection in the current progressive collapse guidelines, it is important to monitor axial response of the connection in a column removal scenario due to its significant role as an alternative path load.
- In a column removal scenario, large deflections are acceptable without collapse. It is possible to take advantage of catenary action so that the

connections can be detailed for this new need, but to do this the amount of reserve axial strength available in conventional shear connections must be determined.

- The possibility of formation of arch forces at small beam rotations is acknowledged.
- A general finite element model is proposed as a tool for investigating the behaviour of shear connections under the column removal scenario. Finite element modelling techniques can be utilized to simulate the ability of a design to withstand extreme loading conditions that are not considered in the regular design process.

Table 2.1: Simple beam-to-column connections

Category	Type
Double angle beam connection	bolted - bolted
	bolted - welded
	welded - bolted
	welded - welded
End plate connection	bolted
	welded
Single angle beam connection	bolted - bolted
	bolted - welded
	welded - bolted
	welded - welded
Shear tab beam connection	bolted
	welded
WT beam connection	bolted - bolted
	bolted - welded
	welded - bolted
	welded - welded
Seated beam connection	welded unstiffened angle seats
	bolted unstiffened angle seats
	stiffened seated

Table 2.2: Types of material used in shear connections

Connection Type	Abbreviation	Component	Material	Description
Shear tab	ST	plate	ASTM A36/300W	-
		bolts	ASTM A325, A490	standard/slotted hole
		welds	E70XX electrode	fillet welds
WT	WT	WT section	ASTM A992/350W	-
		bolts	ASTM A325, A490	standard/slotted hole
Single angle	SA	angle	ASTM A36/300W	-
		bolts	ASTM A325, A490	standard/slotted hole

Table 2.3: Selected column removal scenario experiments for steel structures

No	Summarized test description	Organization	Reference
1	Behavior of bolted beam-column connections under catenary action in damaged steel structures	Swedish Council for Building	(Girhammar 1980)
2	Progressive collapse resistance of steel building floors	University of California, Berkeley	(Astaneh-Asl et al. 2002)
3	Behaviour of simple shear connections under combined effect of shear and tension	University of New Brunswick	(Guravich and Dawe 2006)
4	Performance of seismic moment resisting connections under column removal scenario	National Institute of Standards and Technology	(NIST 2010)
5	Recommended performance levels for alternate path analysis of blast-damaged steel connections	Protection Engineering Consultants	(Marchand 2008)
6	Axial, shear and moment interaction of WT connections	Milwaukee School of Engineering	(Friedman 2009)
7	Axial, shear and moment interaction of single plate “shear tab” connections	Milwaukee School of Engineering	(Thompson 2009)
8	Axial, shear and moment interaction of single plate “shear tab” connections	Milwaukee School of Engineering	(Johnson 2009)
9	Performance of steel shear connections under combined moment, shear, and tension	University of Alberta	(Oosterhof and Driver 2012)
10	Overview of AISC/NSF structural integrity research and preliminary results	AISC/NSF	(Weigand et al. 2012)

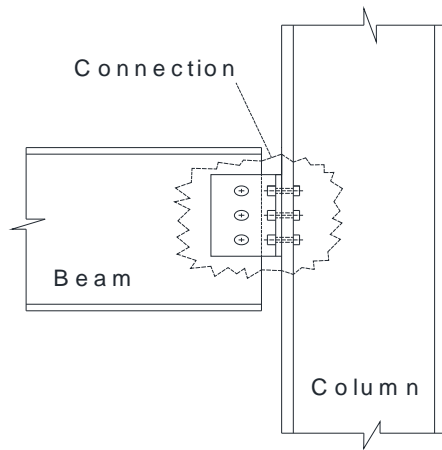


Figure 2.1: Connection definition

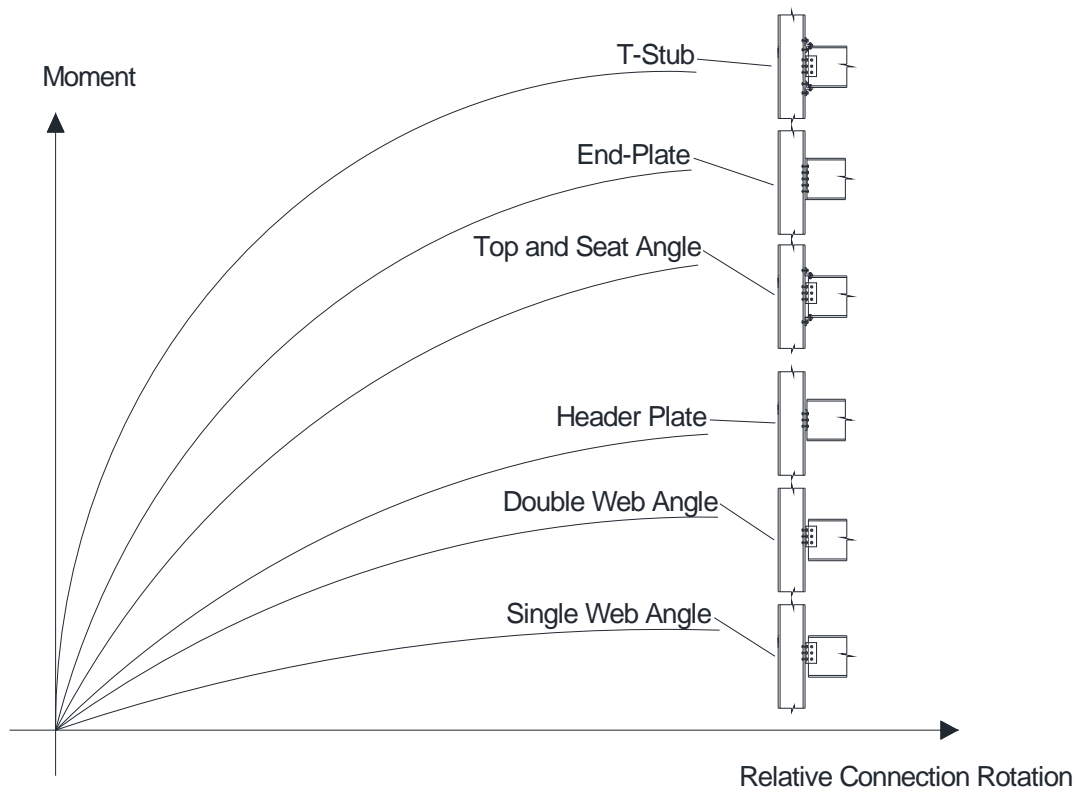


Figure 2.2: Typical moment–rotation curves for different types of connection
(Kameshki and Saka 2003)

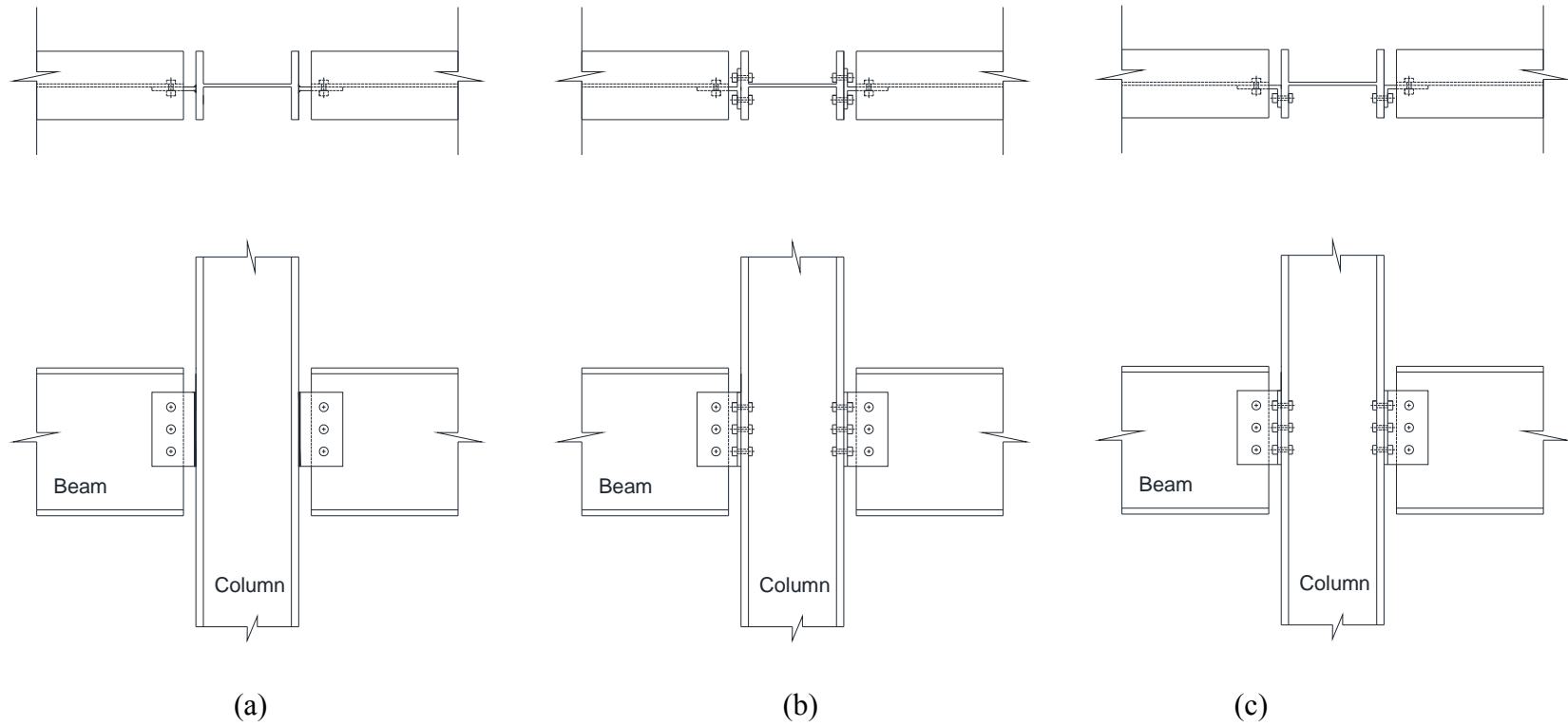
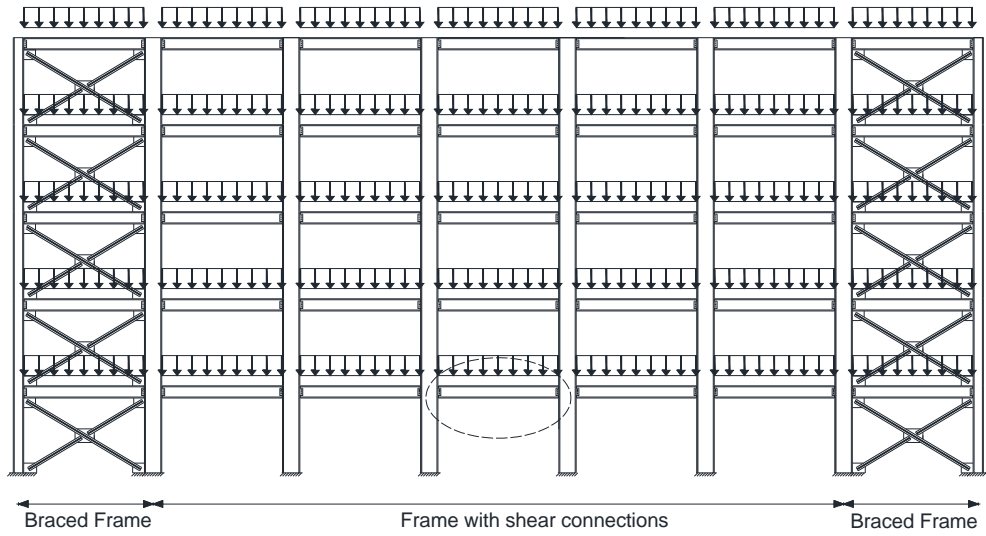
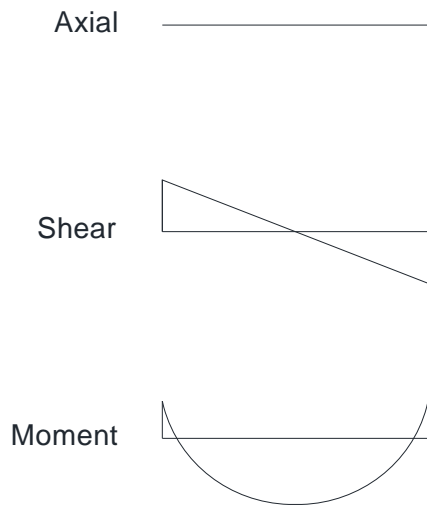


Figure 2.3: Common types of single-sided shear connections (a) shear tab, (b) tee, (c) single angle

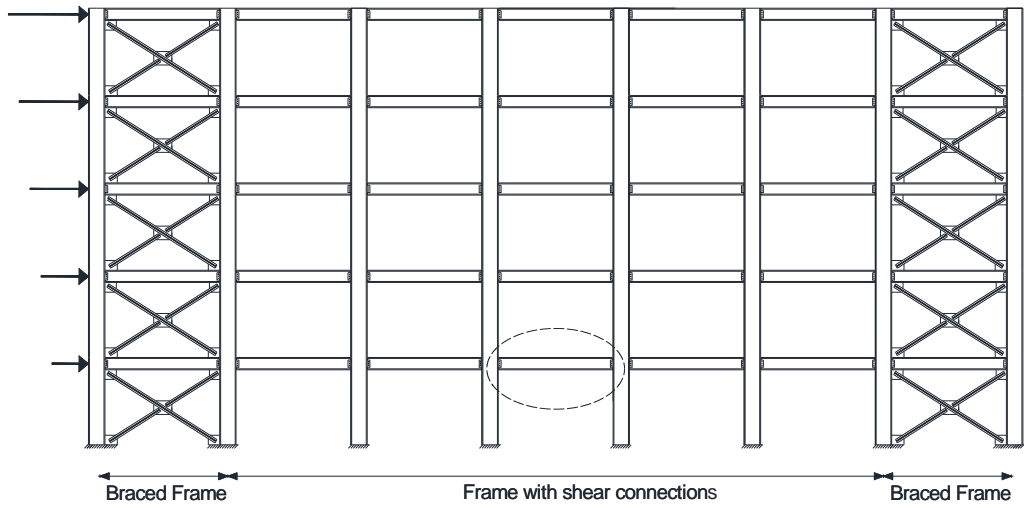


(a)



(b)

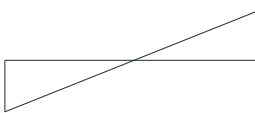
Figure 2.4: Frames with shear connections under conventional loads (a) frame under vertical loadings, (b) member response to vertical loading



(a)

Axial 

Shear 

Moment 

(b)

Figure 2.5: Frames with shear connections under conventional loads (a) frame under lateral loadings, (b) member response to lateral loading (AISC 2010)

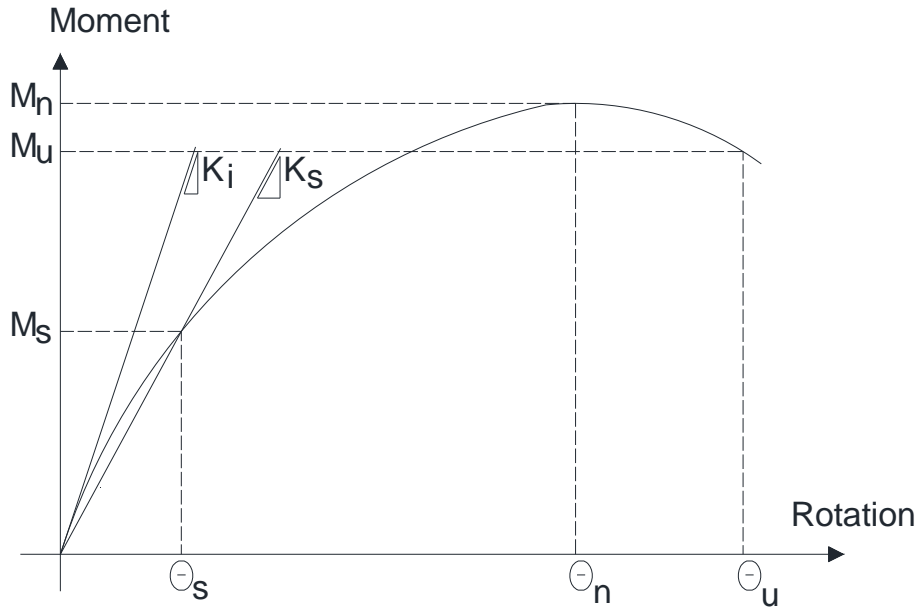


Figure 2.6: Moment–rotation behaviour of steel connections under conventional loading (AISC 2010)

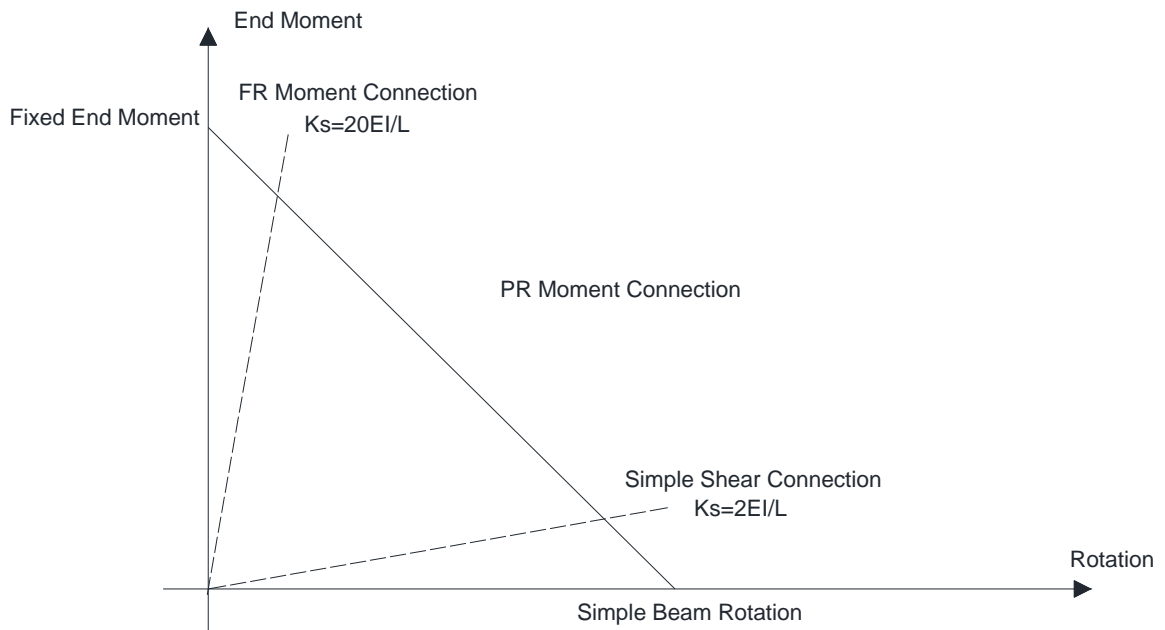


Figure 2.7: Fully-restrained (FR), partially-restrained (PR) and shear connection definitions (AISC 2010)

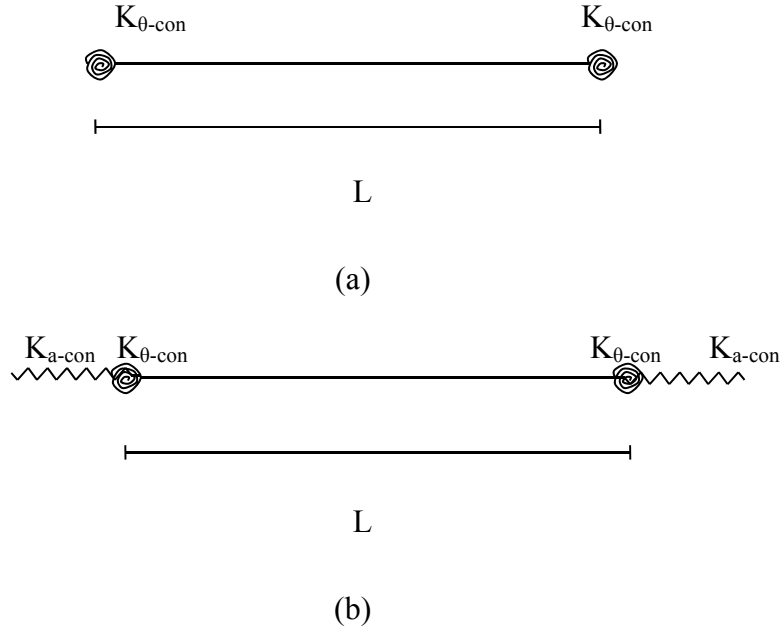


Figure 2.8: Semi-rigid plane member with (a) rotational springs, (b) axial and rotational springs

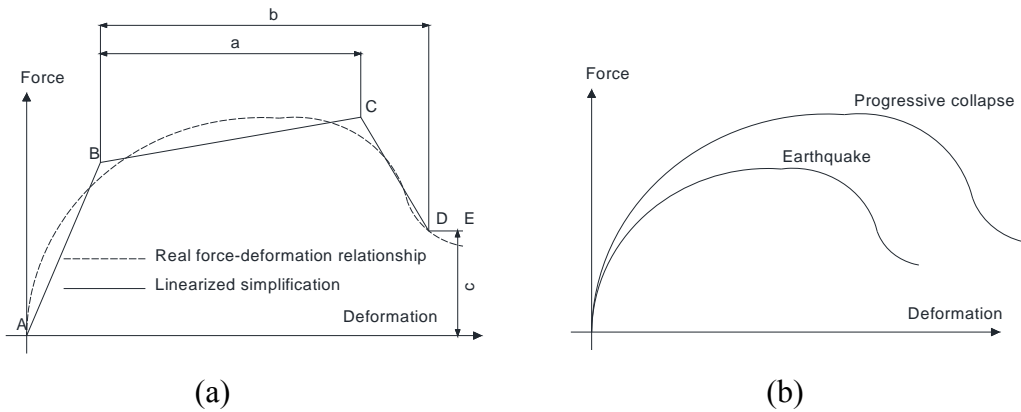
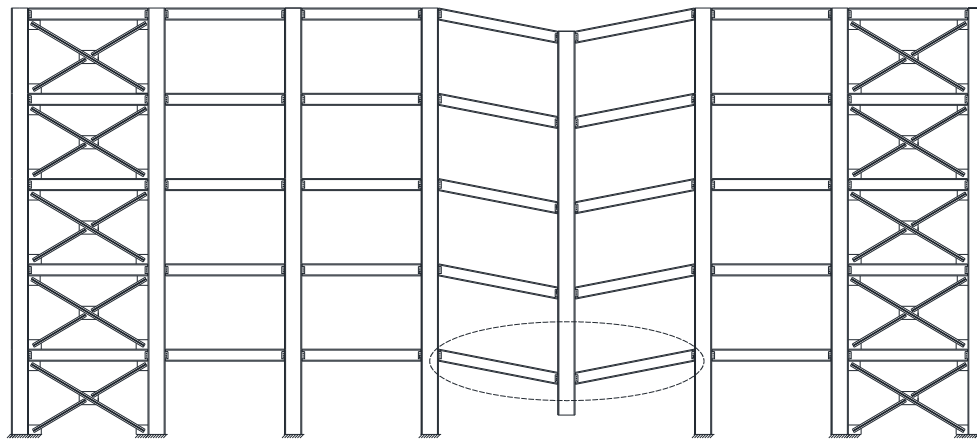
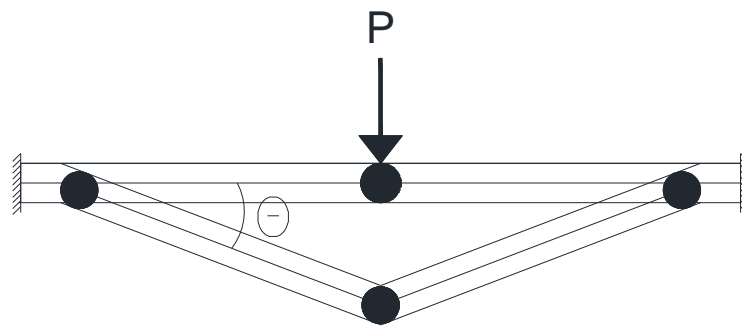


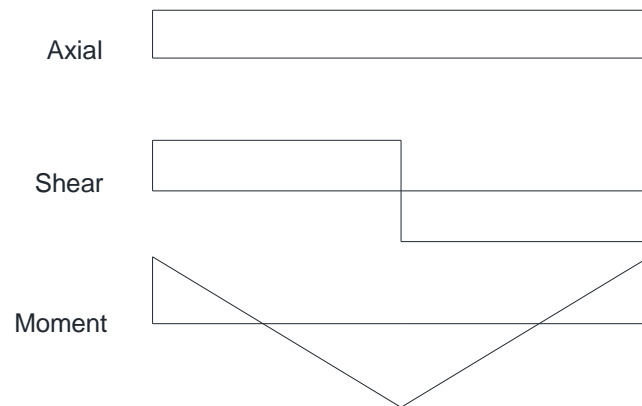
Figure 2.9: (a) Generalized component force–deformation relations for depicting modelling and acceptance criteria (FEMA 2000) (b) The effective force–deformation relationship for a typical component in an earthquake and progressive collapse scenario (Powell 2005)



(a)



(b)



(c)

Figure 2.10: (a) Frame with shear connections in column removal scenario (b) member response (c) simplified member response

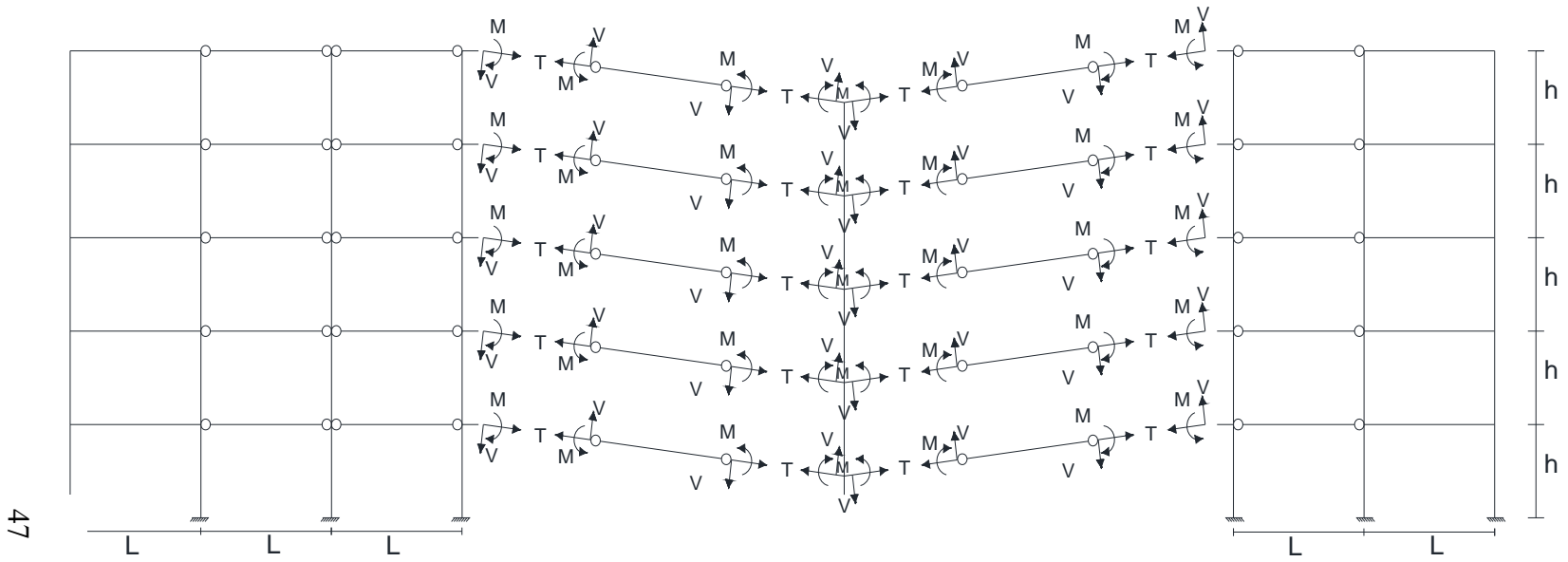


Figure 2.11: Simultaneous presence of shear, tension and moment at connection location in column removal scenario

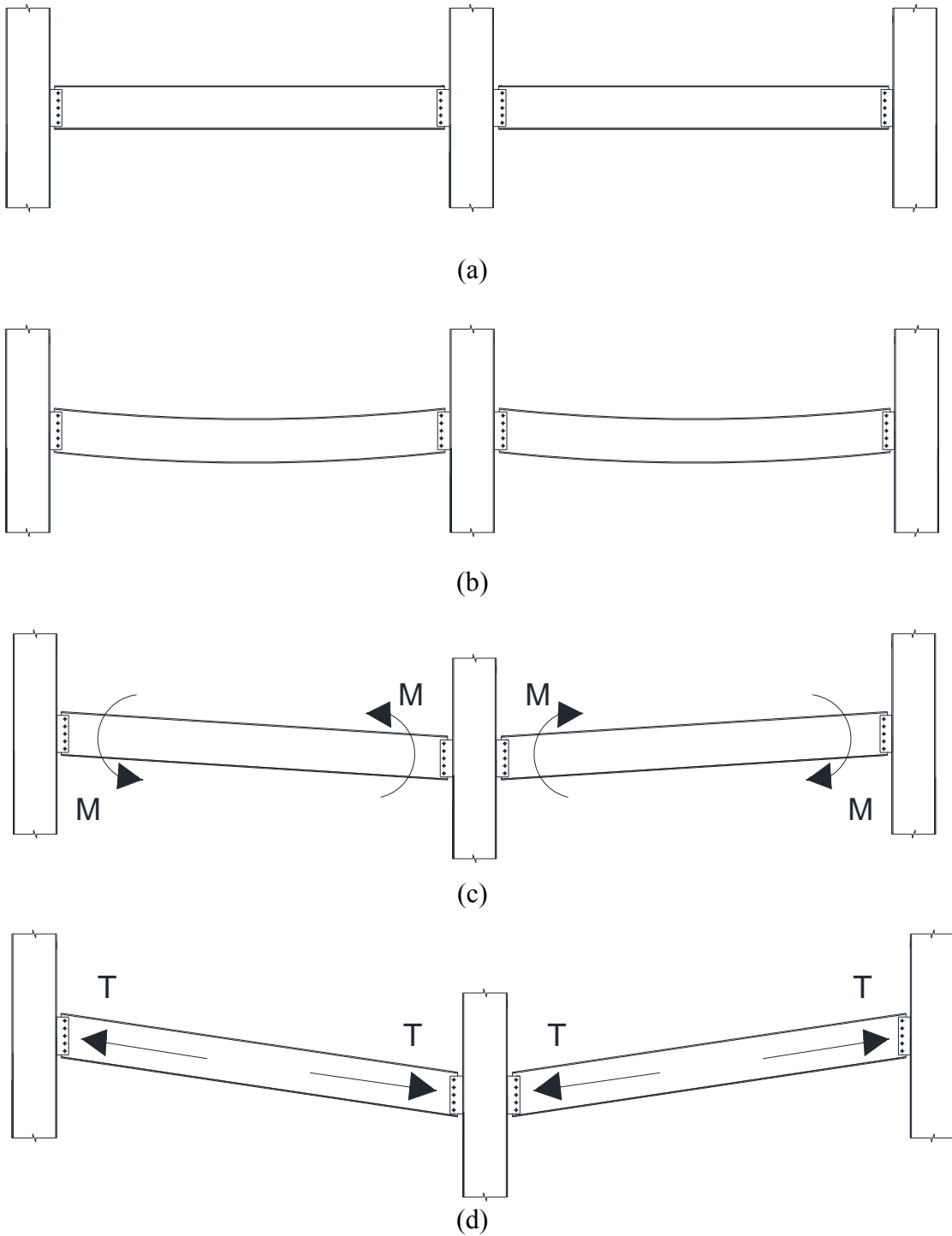
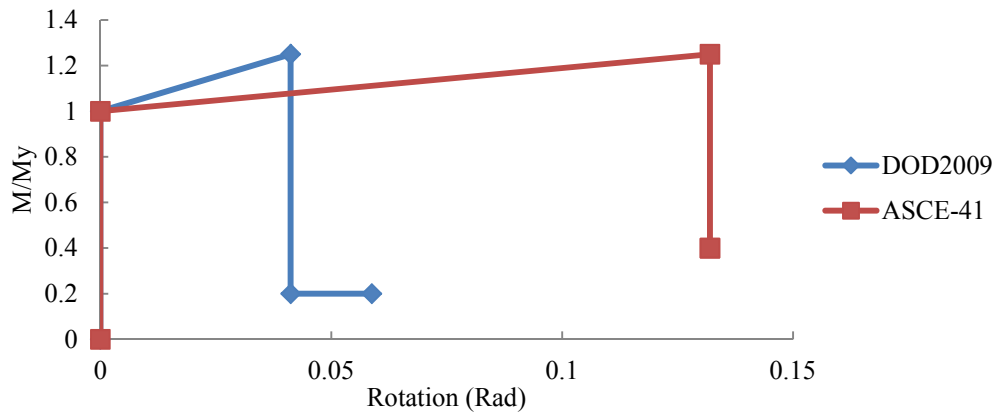
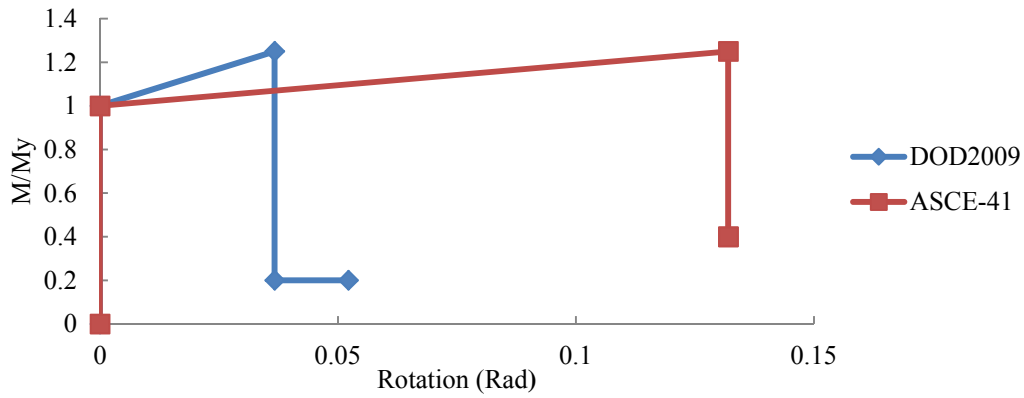


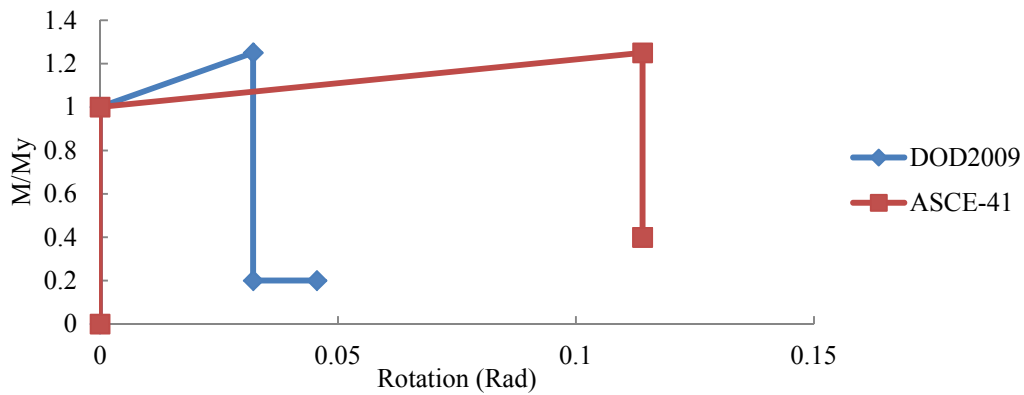
Figure 2.12: Formation of catenary behaviour in beams (a) isolated double span (b) deformed shape under gravity load (c) small rotation: flexural phase (d) large rotation: catenary phase



(a)



(b)



(c)

Figure 2.13: Generalized component force-deformation relations for depicting modelling for 152 mm, 228 mm and 304 mm shear tab connections

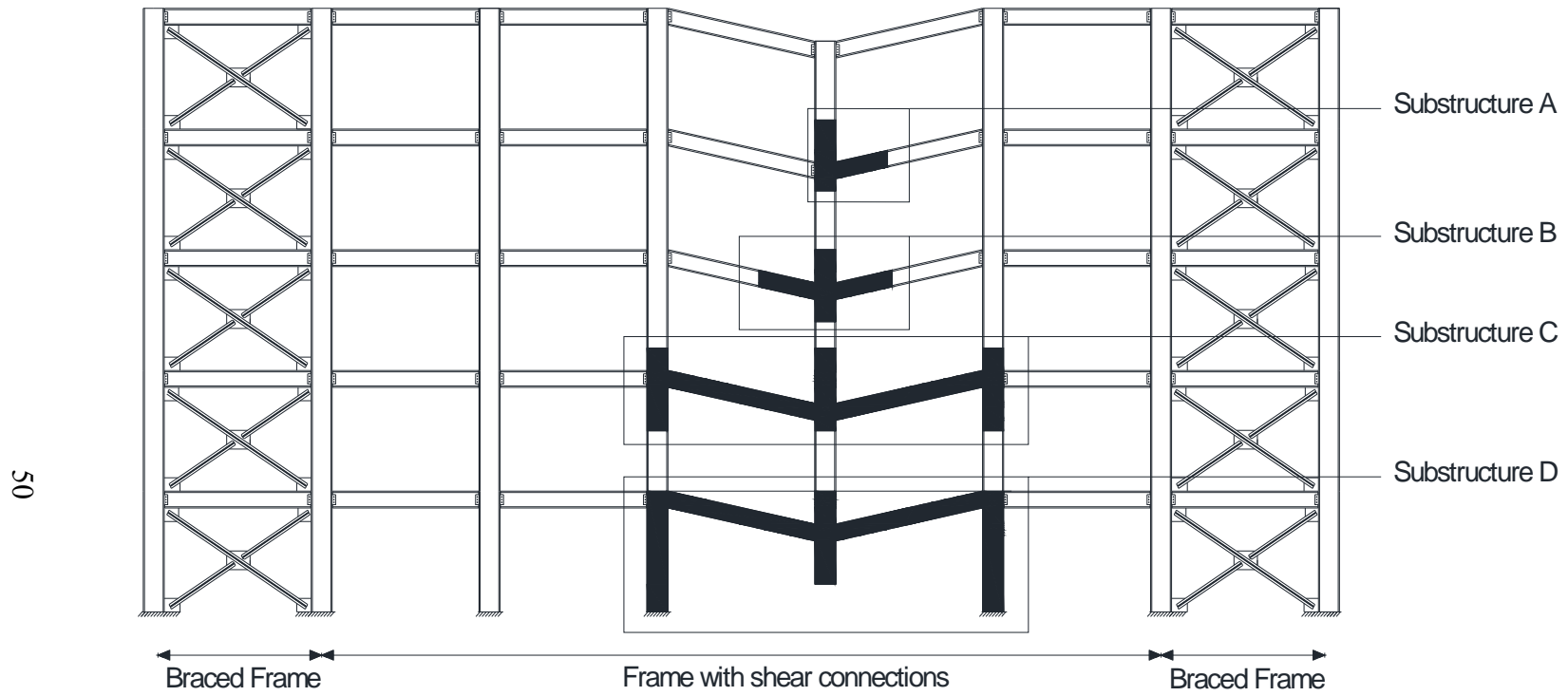
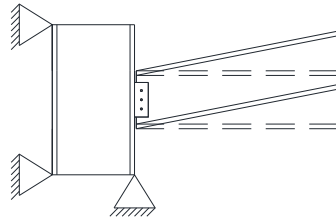
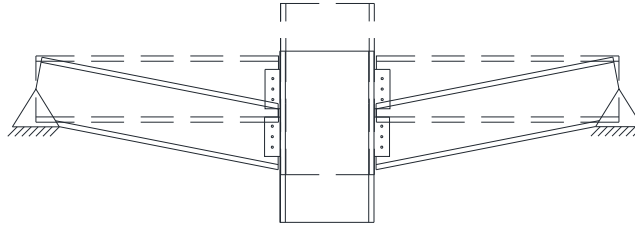


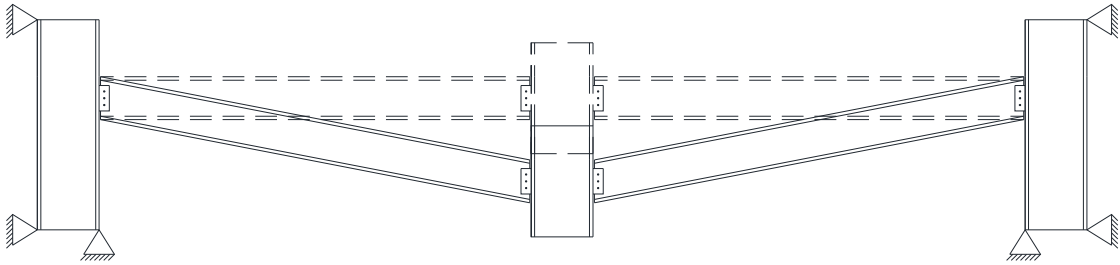
Figure 2.14: Possible sub-structuring options for column removal scenario



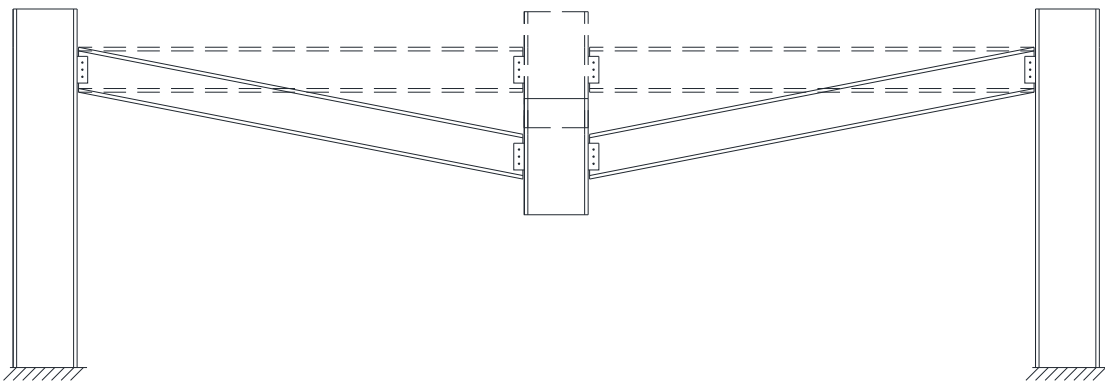
(a)



(b)

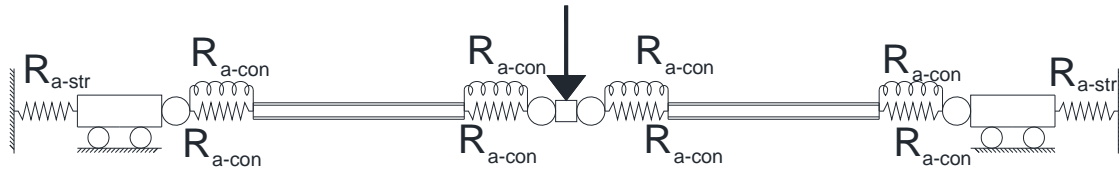


(c)

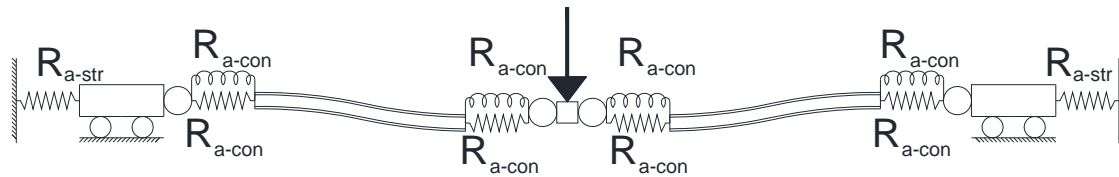


(d)

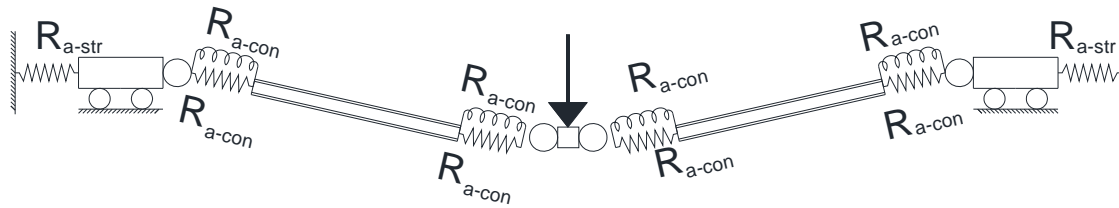
Figure 2.15: Common test setups for beam-to-column connection tests under column removal scenario, pertaining to (a) substructure 1 (b) substructure 2 (c) substructure 3 (d) substructure 4



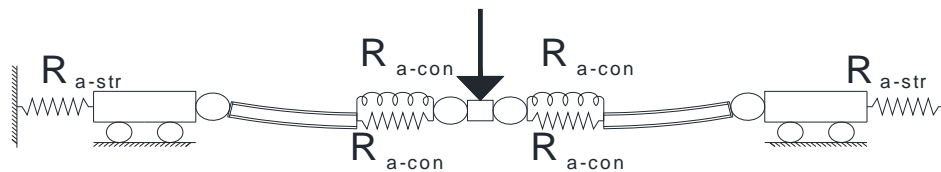
(a)



(b)



(c)



(d)

Figure 2.16: Proposed connection assembly model under column removal scenario:
 (a) undeformed configuration (b) small rotation: flexural phase (c) large rotation:
 catenary phase (d) simplified model

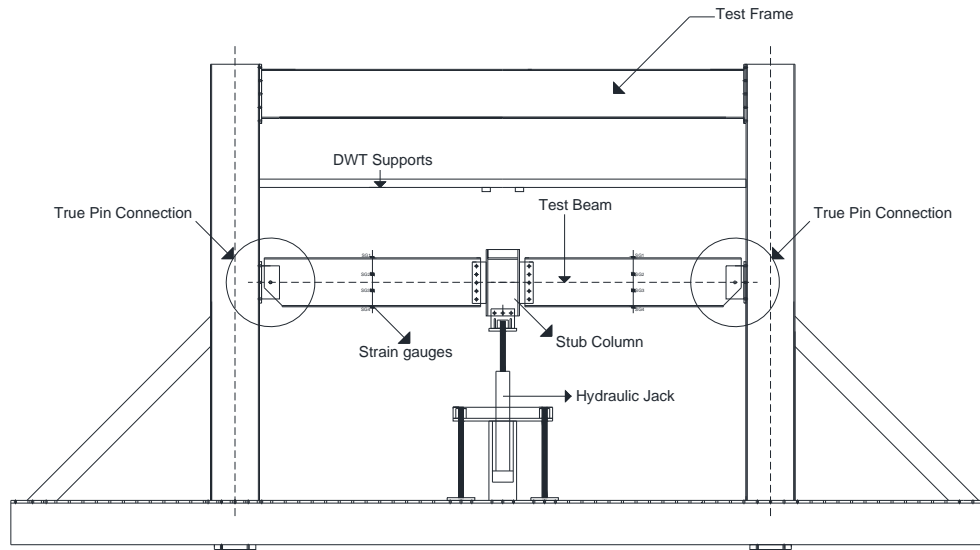


Figure 2.17: Test setup assembly (Thompson 2009)

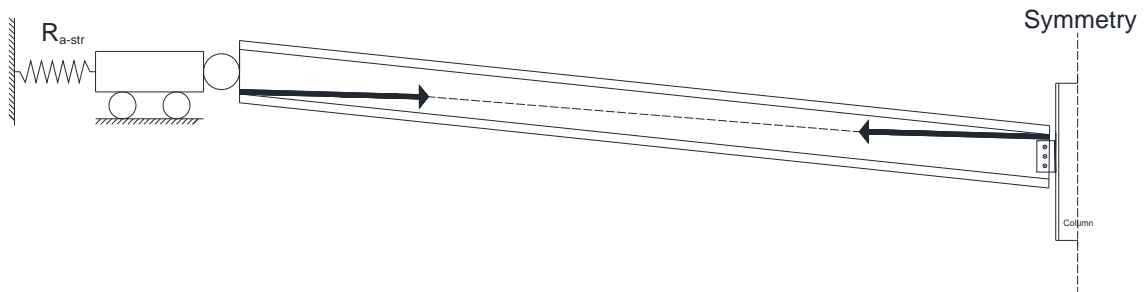


Figure 2.18: Possibility of formation of compressive arch action in column removal scenario

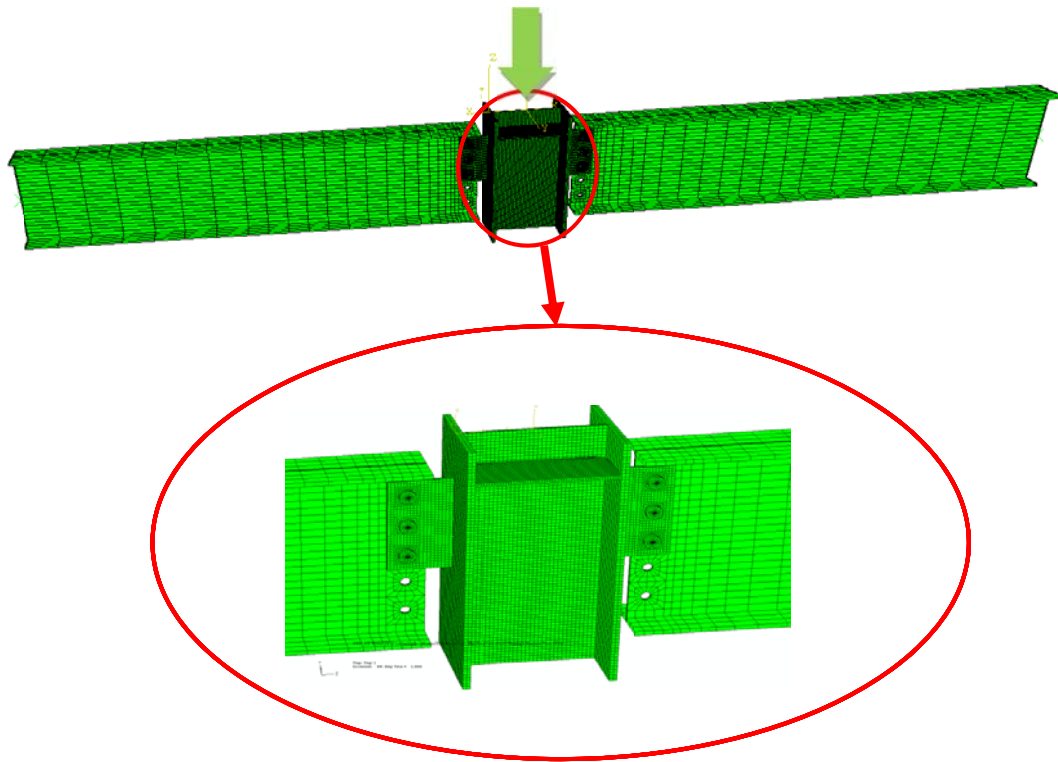


Figure 2.19: Finite element model of shear tab connections

3 Benchmark in Finite Element Modelling of Steel Shear Connections in Column Removal Scenario

3.1 Introduction

As a general fact, knowledge of connection behaviour and how it affects the overall frame performance is a prerequisite to the evaluation of steel structures against conventional loads such as gravity loads or wind/earthquake lateral loads. The importance of connection behaviour is even more significant when it comes to extreme loading scenarios such as progressive collapse. Due to the fact that progressive collapse is a relatively new topic faced by structural engineers and researchers, few experiments were conducted on connections loaded under the so-called “column removal” scenario, which is commonly used for progressive collapse analysis and design. Experimental programs are also difficult and expensive to conduct. Therefore, numerical studies are needed to extend the database on different connection behaviour in the new scenario. Besides, modelling techniques for steel connections cannot be directly transferred between different loading situations, thus raising the need for more research on this issue.

The finite element modelling technique is one of the most attractive and powerful methods in determining the response of steel connection assemblies. Finite element analysis of steel connections is challenging due to complex geometry, unknown boundary conditions, sequence of loading and nonlinearities. Nowadays, there are substantial improvements in the sophisticated commercial finite element analysis software such as Abaqus (Dassault Systèmes 2009) that makes it possible to simulate highly nonlinear complex behaviours. Although Abaqus software was used in this study, any other commercially available software with similar capabilities could have obtained the same results with correct definition of the models. However, some challenges exist that need to be resolved in order to reach acceptable results.

Previously, some researchers such as Bursi and Jaspart (1997) and also Selamet and Garlock (2010) tried to come up with some benchmark examples for finite element modelling of bolted steel connections. Although the models they proposed in their research, such as those of tee connections or lap joints in direct tension, can provide insight on contact simulation and nonlinearity definitions, they cannot act as a benchmark for finite element models in the column removal scenario due to the differences in how the connection is loaded. The simultaneous presence of shear, tension and moments at large rotations with the specific load proportions that the column loss event has imposed, makes the problem complex and unique in its own fashion that requires verification in its own way.

Modelling the detailed steel connection in the column removal scenario requires knowledge of solid mechanics, contact mechanics, simulation techniques and convergence algorithms (Selamet and Garlock 2010). Mainly, there are some convergence difficulties that need to be solved in order to reach a validated and verified finite element model using an implicit analysis method. Most of the convergence issues are derived from the discontinuous nonlinear contact and also localized yielding that are the main focuses of this chapter. It is necessary to understand the logic for solving nonlinear problems—and more particularly contact problems—in steel connection modelling in order to reduce convergence difficulties and obtain an accurate response.

In this chapter, after discussing the scope and motivations of the research, a brief literature review is provided to give insight on the previous numerical efforts to model steel connections. After establishing the definition of convergence in nonlinear finite element problems, a benchmark example is introduced and discussed in section 3.5, including the geometry, material definition, loading steps, interaction, constraints and boundary conditions. The process of element selection, mesh generation and mesh sensitivity studies are discussed in sections 3.6 and 3.7.

It is believed that the challenges involved in numerical studies for simulating the performance of connections when a column has been compromised are derived chiefly from nonlinearity sources. Therefore, a significant part of the chapter is dedicated to nonlinearity definitions, and especially highly nonlinear behaviour of contact, that are discussed in section 3.8.

In section 3.9, the solution technique is discussed to provide a rigid foundation for the validity of all the numerical models utilized in this research. It is shown that a general static implicit analysis is an appropriate tool to achieve the objectives of the research.

It is also necessary to present the failure criterion to predict the failure loads and modes using finite element analysis. Rupture, either in structural members or fasteners, is one of the common limit states that play an important role in failure of steel bolted connections. Traditional fracture mechanics techniques rely on the response of a crack in the model, although in bolted steel connections, there are no pre-existing sharp cracks or flaws. Therefore, applying the traditional fracture technique could have some issues (Kanvinde and Deierlein 2004). In section 3.10, the global failure criteria that have been used throughout the research are established.

A brief explanation of the process of extracting results of the experimental and numerical models is provided in section 3.11. After that, sensitivity analyses performed for this research are reported in section 3.12, considering some of the selected parameters in the selected range.

After ensuring the validity of the numerical models, the final results are reported in section 3.13. The outcome of the research is not only helpful to estimate the failure load, but also to trace the entire internal load versus rotation path. This force–rotation behaviour of shear connections in a column loss event is required in order to perform progressive collapse analysis of a whole building. In summary, this study can help in the prediction, development and interpretation of the performance of steel shear connections in a column removal scenario.

In section 3.14, some fundamental recommendations are made regarding how to obtain a converged solution. The guidelines and recommendations provided in this chapter are applicable not only to shear tab connections, but also to all other types of bolted steel shear connections.

In chapters 4, 5, 6 and 7, the established procedures are applied to other geometries and different types of shear connections including WT and single angle, and comparisons with experimental results are performed. The additional verifications confirm the correctness and accuracy of the proposed numerical modelling procedure.

3.2 Scope of the research and objectives

The main objectives of this chapter are:

- to present a rational approach to establish and calibrate a finite element model for simple shear connections;
- to introduce a simple shear tab connection model that can be used as a benchmark to validate finite element models of simple shear connections subjected to extreme loading effects such as a column removal scenario; and
- to discuss and provide recommendations on how to achieve a converged solution in steel shear connections using state-of-the-art simulation techniques.

The welds are not considered explicitly in the models based on the assumption of flawless welding processes and material. Besides, no weld failure was reported in the pertaining experimental program that was used for the verification. The dynamic and/or cyclic nature of the column removal scenario is out of the scope of this research. Residual stresses and initial geometric imperfections were

ignored in the analyses due to the fact that the actual residual stress distribution or size and distribution of geometric imperfections are unknown.

3.3 Literature review on finite element modelling of steel connections

There are different numerical studies on various types of connections during the last few decades. These studies utilized two- or three-dimensional (3D) models with various levels of simplifying assumptions. Many simplifications were assumed in early studies of bolted connections using the finite element method since the computational power was limited. Avoidance of detailed modelling and reducing the computational cost were the main reasons for these simplifying assumptions. The following literature survey is focused on the highlights of finite element modelling assumptions for steel beam-to-column connections under a monotonic loading regime. Research on seismic (cyclic/dynamic) performance of steel connection models and modelling of steel connections in a fire scenario are beyond the scope of this research.

It is believed that Krishnamurthy (1980) took the first steps in applying finite element simulations in steel bolted connection modelling. He established the sources of complex highly nonlinear response of the connection and, based on that, he concluded that the traditional concepts of elastic continuum mechanics, analytical approaches based on structural theory and yield line theories are not the appropriate tools for assessing the response of bolted connections due to the presence of highly nonlinear behaviours. He developed a methodology to predict the behaviour of different types of moment connections, including seat and top angle, tee-stub and end plate connections. Table 3.1 summarizes his proposed phases for finite element analysis of steel connections.

Due to the limitations of computational capabilities, three-dimensional analyses of large models were not feasible at that time. Krishnamurthy (1980) assumed linear elastic material for 3D analyses and bilinear elastic-perfectly plastic or tri-linear

stress-strain curves, for 2D analyses. The clearance between the bolt shank and the hole was ignored in his models. He assumed that the supporting members are rigid. His models contain pretension in the bolts as well. A series of cycles of nodal releases, reattachments and displacements and reaction calculations were repeated in order to simulate contact interaction. Each analysis was terminated if the capacity of the component is reached or divergence occurred because of local yielding. He used a constant strain triangle for two-dimensional and sub-parametric eight node brick elements for three-dimensional models. He also established the correlation between two-dimensional and three dimensional finite element models of bolted steel connections (Krishnamurthy and Graddy 1976). He defined "correlation factor" as the ratio of three-dimensional to two-dimensional result variable and proposed the correlation factor of 1.4 for displacement and rotation, 1.2 for average stress and 1.8 for maximum stress for the studied particular configurations. However, due to the three-dimensional nature of the problem, they are incapable of reproducing some characteristic features such as three-dimensional failure modes.

Bursi and Jaspart (1997) introduced benchmarks for finite element connection model validation. They modelled two tee stub connections, pre-loaded and non-preloaded, with different failure modes by brick elements in the large deformation regime using LAGAMINE software. They simulated the interaction between different components via contact elements using a penalty technique. However, they stated that the Lagrange multiplier approach is superior to the penalty method, which needs an arbitrary penalty stiffness number that may have significant effects on the accuracy of the results and the convergence rate (Bursi and Jaspart 1998). They noted that shell elements, no matter how thin or thick, are not suitable for modelling the connection components and especially the bolts and concluded that at least three layers of brick elements should be used for bending-dominated problems to capture the stiffness and strength of the component accurately. In bolt discretization, they used three-dimensional brick elements assuming the washers were attached to the bolt head. In order to account for this assumption, which imposes additional flexibility because of the nuts and the

threaded part of the shank, they used Agerskov's model (1976) to utilize an effective bolt length. In the follow-up paper (Bursi and Jaspart 1998), they used Abaqus code to simulate end plate connections and their failure modes. By comparing the results of element performance for different formulations, Bursi and Jaspart concluded that incompatible brick elements, called C3D8I element in Abaqus (Dassault Systèmes 2009), predict better results for bending-dominated problems with relatively small thickness.

There are numerous numerical studies on end-plate connections. As an example, Kukreti et al. (1987) established a methodology to develop moment–rotation relationships for end plate connections by following the same procedure as Krishnamurthy (Krishnamurthy and Graddy 1976). They used a nonlinear material model and imposed a strain limit as the failure criteria criterion (0.02 for plate elements and 0.006 for the bolt shank). Another numerical study was carried out by Yang et al. (2000) on double web angles, bolted to the column flange and welded to beam web. Although they included contact between the bolt head and angle, they ignored the interaction between the bolt shank and the hole.

Citipitioglu et al. (2002) used available experimental programs to examine the ability of 3D models to mimic the overall test results. They use imposed deformation as a calibration procedure for applying a pretension force in the bolts' shanks. They included the effects of slip by recognizing interaction between all the components in Abaqus. Nonlinear 3D continuum elements were used for all parts of the connections except the bolts that were modelled as elastic components in order to ease the convergence problems. The results of their studies showed that the response of finite element bolted partially-restrained connections are highly dependent on bolt pretension and slip definition of contact, since the forces are transferred through friction due to clamping between the members caused by the pre-tensioning of the bolts. The connection model is discretized using C3D8I eight-node brick elements with full integration and incompatible modes. C3D6 six-node wedge elements were used to model the core of the bolts.

Barth et al. (2002) conducted finite element analyses of the WT connections. They monitored the entire load versus deflection path of the connection in addition to estimating the failure load. They assumed that the bolts are rigid and modelled just the flange of the supporting column assuming that column's stiffness makes a rigid part. The bolts were modelled as elastic components in order to ease the convergence problems.

Ju et al. (2004) used finite element modelling to analyze butt-type bolted connections. They used a node-to-Hermit-surface contact element and found similarity between the capacities of the finite element models of bolted connections and those calculated using the AISC specification (1986), despite the complexity of the stress and strain fields during loading. They observed that thinner plate causes a minor bending effect on the bolt. However, the locations of the maximum bolt plastic strains are different because of the bolt bending effect and shear force. As a result, although plate thickness dominates the amount of bending effect, it does not affect the bolt failure.

Although improvements in computational power and advanced finite element technology have enabled the researchers to simulate elaborate and sophisticated tasks such as connection assembly modelling, some issues such as convergence problems, justification with the experimental results and modelling the failure modes remain challenging and to some extent unknown. This chapter deals with all the mentioned difficulties in order to provide a solid base for the next chapters.

3.4 Concept of convergence

"Convergence" can imply different meanings in finite element analysis, including mesh convergence, nonlinear solution convergence and also convergence to the accurate solution. For transient loading of the connection, accuracy of the time integration method might be an issue but not for quasi-static loading. (Dassault Systèmes 2011c). In implicit solution techniques of finite element analysis of steel

connection modelling, obtaining the converged solution in the nonlinear region is the main obstacle due to the presence of all types of nonlinearity, including material, geometric and contact nonlinearities. Satisfying all the convergence issues in addition to good engineering judgment in creating a finite element model will lead to an accurate solution.

3.5 Introduction of the case study model

In order to propose a benchmark example in numerical modelling of the behaviour of steel shear connections in progressive collapse, an adaptive experimental program is needed.

3.5.1 Selected study program

In this research, the experiments conducted by Thompson (2009) are utilized to verify the numerical study as discussed in chapter 2. The full-depth shear connection with one column of five bolts is selected as a benchmark example. The test setup is shown in Figure 3.1. A detailed sketch of all components of the test assembly is illustrated in Figure 3.2.

3.5.2 Finite element modelling assembly

The finite element models consist of the central column, the adjacent beams, as well as the connections with complete detailing; all modelled with three-dimensional solid elements as shown in Figure 3.3. Since the connection is the point of interest, all the characteristic features of the connections are included in the model. Model information is summarized in Table 3.2 and the details are explained in the following sections.

3.5.2.1 Parts geometry

All the parts are modelled exactly based on the dimensions shown in Figure 3.2. The dimensions of the bolt head and nut are taken from the AISC Handbook (AISC 2010). The head and the nut are simplified to cylinders, since their geometry does not have any effect on the analysis results. Since in the experimental program, the bolts were assembled with the threads excluded from shear planes, the finite element bolt models are assumed to be smooth cylinder. No fillet was modelled on the hot-rolled sections as well.

3.5.2.2 Material definition

All hot-rolled sections are made of ASTM A992 (2011) . The shear tab and the bolts are made of ASTM A36 (2008) and ASTM A325 (2009) steel, respectively. The material behaviour is discussed in Appendix A.

3.5.2.3 Loading steps

The whole loading sequence is performed in two separate steps: first applying the bolt pre-tension and then the push-down vertical load.

3.5.2.3.1 Bolt pre-tensioning

Based on the experiment reports, the bolts are installed to a “snug-tight” condition (Thompson 2009). “Snug-tight” condition requires that the holes be properly aligned, the bolt to be inserted and then the nuts to be turned on until all the plies in the joint are in firm contact. It can be attained by the ordinary attempt of a worker using a spud wrench. As such, the amount of any initial tension in the bolt can be expected to be both small and variable. This can affect the load transfer mechanism.

In the numerical model, a small amount of pre-tensioning is required not only to simulate the snug-tight condition but also to prevent the rigid body motion of the bolts in the standard size holes. There are several methods to apply pre-tensioning to the bolts such as applying a temperature gradient in order to impose a pre-

determined amount of axial force directly. In this research, the bolt pretension has been incorporated by applying displacement to one end on the shank surface, as illustrated in Figure 3.4. The application of this displacement considerably improves the convergence as well. It is noted that the main purpose of applying pretension is that the connected parts be in firm contact with each other. It is not intended to use “pre-tensioned” bolts in the model. However, the effect of pre-tensioning is investigated in the section 3.12.

3.5.2.3.2 Push-down loading

The central column is pushed down, while the connection performance is monitored. This is performed by a hydraulic jack located at the bottom of the central stub column. Two load cells measured the applied load. In the numerical model, the middle stub column was loaded via displacement control, which is much more stable than force control during contact simulation. In order to produce the quasi-static behaviour, displacements are increased at a slow rate.

3.5.2.4 Interaction properties

Interaction properties play an important role in connection modelling. Contact should be defined between each two surfaces that might come to touch, such as bolt shank–beam hole contact, etc. The properties can be divided into normal and tangential behaviour. Because of the importance of the issue, it is discussed thoroughly in section 3.8.3.

3.5.2.5 Constraints

Different constraints are applied to the model in order to simulate the desirable response. First of all, a symmetry constraint is imposed to take advantage of axial symmetry in the connection assembly. Only one-half of the subassembly is modelled and the symmetry condition is applied at the centerline of the stub column web as shown in Figure 3.5.

Fully constrained contact behaviour (tie constraint) is used for modelling welds to bond the shear tab to the column flange. Tie constraint uses a master–slave formulation. The constraint prevents slave nodes from separating or sliding relative to the master surface. Slave nodes can be moved on to the master surface in the initial configuration strain free. In order to avoid out-of-plane displacement of the test assembly, out-of-plane displacement of one joint in the beam is restricted.

3.5.2.6 Boundary condition

In common connection modelling for either cyclic or monotonic loading, elaborate support models are not considered due to the relative insensitivity of the subassembly response to the variation in the support condition. However, in connection modelling subjected to extreme loading such as the column removal scenario, the boundary condition is deemed to be of significant importance. As shown in Figure 3.1, the true pin connection is designed so that the whole assembly can rotate freely. In the experiment, it is achieved by 1-1/4 inch diameter ASTM A490 bolts in the standard size hole, reinforced by 3/8 inch thick a ASTM A36 doubler plate on one side of the web. The main purpose of such a connection is to provide a zero-moment location that can resist unidirectional tensile force in the line of the beam centroid. In order to simulate the same condition in the numerical model, a thin rigid plate (Figure 3.5) with two axial springs at the far ends of the beams is applied. The springs are representative of the flexibility of the test setup and the rest of the structure adjacent to the double-span scenario in the experiments and the real structure, respectively. More description is available in chapter 4.

3.6 Element selection

It is possible to simplify the process of simulation of steel connections by accepting the two-dimensional simulation assumption. Some studies have

established the correlation between two-dimensional and three-dimensional modelling of steel connections (Krishnamurthy and Graddy 1976). However, bolted connections are three dimensional problems in nature. Hence, it is highly recommended to use three-dimensional elements in order to capture the physical features of connections as much as possible.

Different types of element in Abaqus are shown in Figure 3.6. Each element is characterized by five phenomena, including family, degrees of freedom, number of nodes, formulation and integration. For stress–displacement analysis, translations and rotations at each node are the degrees of freedom. Shell elements possess both translational and rotational degrees of freedom; however, in solid element, the nodes just have translational degrees of freedom (Dassault Systèmes 2009). This could imply some restriction on the minimum number of elements through the thickness for bending-dominated components in order to assure that the through-thickness deformation has been captured.

There are different types of three-dimensional elements in Abaqus, including quadratic, tetrahedron and wedge, as shown in Figure 3.7 (Dassault Systèmes 2009). Tetrahedron elements will add to the analysis cost significantly as more elements are required to reach an acceptable refined mesh. Basically, there can be considerable reduction in the analysis cost by using quadratic elements. Consequently, it is recommended to generally use quadratic elements for modelling steel connections. It is difficult to utilize quadratic or quadratic-dominated elements everywhere in bolted connections such as the hole regions. It is suggested to use the partition technique in order to overcome this challenge. There are some situations that require wedge shape elements, such as the core of the shanks of the bolts.

Different factors affect the process of element selection in steel connection modelling. For instance, the incompressibility of plastic deformation in metals imposes some limitations on the types of element suitable for elastic–plastic analysis. This phenomenon may make some elements over-constrained and cause volumetric locking. Volumetric locking results in a stiff response (Dassault

Systèmes 2009). Table 3.3 and Table 3.4 summarize the properties of different types of continuum elements available in Abaqus that might be considered in steel connection modelling; focusing on order and integration method of elements, respectively. Based on the information that Table 3.3 provides, the order of element for the application under consideration is implied. Because of large plastic deformation and also high strain gradients in bolt hole regions of connection models, and also the presence of contact, it is suggested to use first order elements.

Reduced integration elements are efficient and no less accurate than fully integrated elements, although they possess fewer integration points. As a result, incompressibility constraints are satisfied with ease. Therefore, they are not over-constrained in the steel connection simulations. The primary difficulty with first order reduced integration elements is that they are vulnerable to hourglassing, which is the possibility of zero strains at integration points. Abaqus's hourglass control feature accompanied with fine mesh controls this behaviour (Dassault Systèmes 2009).

Regular first-order displacement elements are usually too stiff in bending-dominated problems. In order to eliminate the parasitic shear stresses and also the Poisson's effect that stiffens the response of such models, additional incompatible deformation modes might be defined for the elements. These incompatible modes increase the internal degrees of freedom of the element (13 for C3D8I), while enhancing the bending behaviour. Although the computational cost increases, they are still less expensive than second-order elements. The incompatible mode elements do not suffer from hourglassing since they utilize full integration (Dassault Systèmes 2009).

Considering the issues mentioned in Table 3.3 and Table 3.4, and taking into account different factors involved in the connection assembly model (e.g., presence of large strain and complex contact definition), it is recommended to adopt the first-order reduced-integration (C3D8R) type of element for the

majority of the model that stress-strain accuracy is not required. The C3D8R element uses one integration point to represent the element. Generally the incompatible mode elements should be used in the regions where bending response must be modeled accurately, and they should be of rectangular shape to provide the most accuracy. Hence, the main connecting part of the connection, here the shear tab, is modeled with the C3D8I element. The bolts also require sufficient accuracy in stress values to predict the failure mode and behaviour. Therefore, using the reduced integrated element for them is not suggested. On the other hand, their behaviour is not dominated by bending. As a result, a full-integration type of element is suggested for all types of bolts. The effect of using different types of elements in the connecting parts is investigated in section 3.12.1.

3.7 Meshing

In order to make sure that the result of finite element simulation is adequately precise, a mesh refinement study is necessary. Increasing the mesh density leads to a unique value that represents the response of the model. Basically, if the same results are produced with different meshes, it is confirmed that the solution is mathematically accurate. This solution is an approximation of the physical response of the model. Potential sources of difference in the response include the geometry of model, material model, boundary conditions, and loads. This concept is applied to h-based element technology used in Abaqus (Dassault Systèmes 2009).

There are some exceptions to the mesh convergence rule, such as fracture or localization problem (Dassault Systèmes 2011c). Obviously, determination of bolted connection behaviour to failure in a progressive collapse analysis is a localization problem because the damage is accumulated at certain parts of the connection assembly, such as the bolt shank or around the bolt hole. Therefore, the principle of mesh convergence is not applied. Additionally, due to the

presence of contacts, all parts are mesh dependent in terms of acceptable proportionality of element size in different parts. Master and slave surfaces should be defined with respect to the associated mesh density. This will prevent excessive penetration of surfaces and consequently, inaccurate results. Therefore, the size of the mesh should be determined in the assembly. However, in order to approach the real behaviour of the physical model, a decent mesh size is necessary. Based on this fact, the approximate size of the elements is selected as 6.25 mm x 6.5 mm in the connecting part, the shear tab. This size gets smaller as we approach the hole due to the presence of a radial mesh. Nevertheless, a mesh study needs to be done to realize the number of the elements within the part thickness in order to capture the out-of-plane deformation as is discussed in section 3.7.2.

3.7.1 Mesh generation procedure

Since the problem is three-dimensional in nature, continuum solid elements were used in a hexahedral shape mesh. The only elements that were not hexahedral in shape were in the core areas of the bolts. Triangular prisms (wedges) are used in such areas by applying hex-dominated meshing techniques to the bolts. For modelling of shear tabs, three elements through the thickness is used as is investigated in section 3.7.2. In the beams, the mesh was fine around the bolt hole and gradually got coarser moving towards the far ends of the beam. The average size of element in the different segments of the beam is shown in .

It is recommended to use mapped mesh in the connection modelling. It has several advantages, such as complete control of the size and shape of the elements. Definitely, densely packed elements are desirable around the bolt hole with high stress concentration. Using radial mesh around the bolt hole makes the smallest elements around the hole, which is the area where the highest values and variations of stresses are expected. Furthermore, high strain concentration observed near the bolt holes requires a reasonably fine mesh to reach convergence.

3.7.2 Mesh Convergence Study

For the purpose of mesh refinement analysis, the shear tab plate with five holes is isolated from the assembly, since the main goal of the research is to determine the behaviour of the shear tab. Bolt mesh size is investigated separately. Besides, preliminary analyses and experimental evidence show that most of the nonlinear behaviour is accumulated in the shear tab region and the bolt shank. Instead of including complex bolt–plate interactions, distributed pressure over the bottom half of the holes is considered in order to load the model. In reality, the pressure magnitude varies around the hole circumference, but it is assumed to be uniform. In this study, the influences of mesh density across the thickness of the plate (Figure 3.9) are investigated for two particular results: the maximum von Mises stress and the vertical displacement of the bottom of the top hole. The results for these three mesh refinement studies are summarized in Table 3.5.

It is observed that the mesh density with two elements across the thickness is adequate. There is no considerable advantage in terms of more accurate results using more elements through the thickness. Although the "two element through the thickness" mesh is deemed to be sufficient, in order to capture out-of-plane deformation in the shear tab, it is suggested to use a minimum of three elements through the thickness. For the sake of consistency, the three element rule within the thickness at the connecting part is respected in the whole research program.

3.8 Sources of nonlinearity

The behaviour of steel connections cannot be approximated adequately as linear due to the presence of types of nonlinearities. It is necessary to perform a nonlinear analysis, since the behaviour of each component of the connection individually is highly nonlinear, as is the behaviour of the whole assembly as a system. All three sources of nonlinearity that are common in structural simulations exist in connection modelling for progressive collapse, including

material nonlinearity, geometric nonlinearity, and boundary nonlinearity, as discussed in the sections 3.8.1 to 3.8.3.

3.8.1 Material nonlinearity

Steel is modelled differently in various literatures on finite element modelling of steel bolted connections. Since the capacity of the connection is of interest, post-yield behaviour is important in defining material behaviour. Material properties can be idealized as bilinear, trilinear or piecewise linear stress-strain diagrams. It is believed that dislocation motion is the main micromechanical mechanism for ductile behaviour of steel as a polycrystalline material. The mechanism driving dislocation motion is the force associated with the dislocation mechanism. Thus, microscopically, the main stress measure is the force per unit of current area, called the true (or Cauchy) stress in the steel material (Dassault Systèmes 2011a). Therefore, true strain and true stress must be used when plasticity data are being defined in Abaqus. However, most available generic material behaviour is in the form of nominal, or engineering, stress versus strain. In order to convert nominal values to true ones, the incompressibility of plastic deformations is taken into account. The conversions are shown in Equation (3-1) and Equation (3-2):

$$\sigma_{true} = \sigma_{nom} (1 + \epsilon_{nom}) \quad (3-1)$$

$$\epsilon_{true} = \ln(1 + \epsilon_{nom}) \quad (3-2)$$

These equations are valid prior to necking. The strains provided in material test data are the total strains. In order to define the plastic strains, it is necessary to decompose these values into elastic and plastic strain components. Linear interpolation is used between the provided data points in order to obtain the overall material response. Abaqus assumes a constant stress response outside the range of data provided (Dassault Systèmes 2009).

3.8.1.1 Hot rolled sections and plates

Due to the variation of steel mechanical properties, it is good to perform tension coupon tests for the sake of accuracy of numerical modelling. In lieu of tension coupon tests results, generic material curves should be used for all components. The approaches to develop the material model for each steel type are summarized in Appendix A. All types of steel used in this study are assumed to be homogenous and isotropic with an elastic modulus of 200 GPa and Poisson's ratio of 0.3 and, hence, a shear modulus of 77.2 GPa. Due to the fact that material definition could contribute to the accuracy of the results, sensitivity analyses are performed to investigate this issue, as discussed in section 3.12.6.

3.8.1.2 High Strength Bolts

High strength bolts are used in structural steel most frequently. They are made from heat-treated steel—either high-strength bolt (ASTM A325 bolts) or quenched and tempered alloy steel (ASTM A490 bolts) (Kulak et al. 2001). The response of single ASTM A325 and A490 bolts to a loading producing shear on two planes are shown in Figure 3.10. As illustrated, the A490 bolt is a higher strength bolt than the ASTM A3235 bolt, with slightly lower ductility. All the details regarding the bolt material property calculations used in this thesis are discussed in Appendix A. Furthermore, the behaviour of individual bolts was verified versus the available shear load versus deformation relationship curves reported by Kulak et al. (2001), as discussed in section 3.10.

3.8.2 Geometric nonlinearity

Large displacements may cause a nonlinear relationship between displacement and strain increments. For many structural applications, it is necessary to write the equilibrium equations based on the deformed structure. If loading on the structure causes large deformations, nonlinearity in geometry is involved and superposition cannot be applied. Due to the presence of large deformation in the model under

investigation, geometric nonlinearity must be included. In Abaqus, the effect of nonlinear geometry is included when the loading step is defined.

3.8.3 Boundary nonlinearity

3.8.3.1 Introduction

Steel bolted connection modelling involves contact simulations of different components, allowing transmission of force from one part to another. The force could be in the form of normal stress or, in the presence of friction, a limited amount of shear stress. In the numerical modelling, the mere physical proximity of two surfaces in the connection assembly model is not enough for contact definition. The analysis engine should detect when the surfaces are separated or are in contact, as simplified in Figure 3.11, and also when they slip or stick in order to apply appropriate contact constraint correctly. Numerically, contact behaviour is highly nonlinear and causes large and instantaneous changes in the behaviour of the assembly (severely discontinuous form of nonlinearity). Consequently, convergence difficulties that occasionally cause inaccurate results are inevitable. The user is responsible for all physical and the majority of the numerical aspects of the models. It is also necessary to understand the logic for solving contact problems in steel connection modelling in order to reduce convergence problems. The solving procedure will be discussed in section 3.9.

Previously, interaction between different parts of the connection assembly was modeled by a contact element. For instance, in order to capture the interaction between the hole and the bolt shank, gap elements were modeled in the probable contact zones of the finite element model.

Figure 3.12 shows a schematic view of such a contact modelling. A schematic view of one type of contact element is shown in Figure 3.13(a). A brief discussion on element-based contact is provided in section 3.8.3.3 as well. After that, element-based contact evolved to a surface-based contact simulation method

which is more representative of the physics of contact simulation. Abaqus/Standard supports both surface-based and element-based approaches in contact modelling. In this research, the surface-based method is utilized. All the basic theory of surface-based contact is discussed in section 3.8.3.2.

3.8.3.2 Surface-based contact

Due to greater flexibility and ease of use of surface-based contact approach, compared to the element-based method, it is recommended to use this method in connection modelling. Abaqus/Standard offers two surface-based contact approaches called general contact and contact pairs.

3.8.3.2.1 General versus contact pairs

General contact definitions are highly automated, and all contact surfaces of parts can interact in one single domain, as shown in Figure 3.13(b). Any exterior surface can interact with any other exterior surface. Nevertheless, contact pairs allow contact between two designated surfaces, shown in Figure 3.13(c). In contact pairs, all potential contact pairs must be defined separately. In this method, one surface is called the master surface and another the slave surface. Each of these surfaces possesses some characteristic features. The master surface can penetrate the slave surface but not vice versa. The stiffer, less-refined region should be the master. The active contact region should change more rapidly on the master surface in order to minimize contact status changes. Besides, the master surface normal should point toward the slave surface; all the elements underlying a surface should be compatible in terms of dimension and order of interpolation (first or second order). If the mentioned criteria are not respected in the finite element simulation, a convergence problem is highly probable in the connection simulation.

Contact pairs are more efficient, since the surfaces are limited in scope. Utilizing general contact is a trade-off between the ease of defining the contact and the analysis performance. Although general contact is suitable for complex topology,

it is not highly efficient in models like connections that are complex in terms of the number of interactions; and consequently, it often does not lead to a converged solution. The general contact was initially developed for Abaqus/Explicit. It is robust and high-performance (Dassault Systèmes 2009). However, there is some lag in its performance in Abaqus/Standard. Therefore, the contact-pair algorithm is recommended in steel connection simulation, although it requires more effort in terms of pre-processing. It is noted that both methods can be used in the same model together.

There are totally six contact pairs in the shear tab connection model: bottom surface of bolt head and shear tab, bolt shank and shear tab, bolt shank and beam web, bolt nut and beam web, shear tab and beam web, and beam end and column flange. The last one is the potential contact that might occur in case of a small gap between the beam end and column flange. In this research, this gap is selected in a fashion that “prying” of the connection due to contact of the beam flange on the column flange may not occur. Table 3.6 shows which surface is selected as master or slave in the analysis.

3.8.3.2.2 Contact discretization method (surface-to-surface versus node-to-surface)

In terms of contact discretization methods, two methods of "Surface-to-Surface" versus "Node-to-Surface" exist in Abaqus. In the traditional Node-to-Surface method, contact is enforced between a node and its neighboring surface facet. In the Surface-to-Surface method, contact is enforced between a node in the slave surface and a larger number of master surface facets local to it. In other words, contact enforcement has an average weighted sense. The concept is shown at Figure 3.14 for the bolt-hole interaction definition.

For steel connection modelling, it is recommended to use Surface-to-Surface methods due to considerable advantages such as reduction in snagging of surfaces, surface penetration, and contact stress inaccuracy. The most important issue is that the Surface-to-Surface reduces the possibility of penetration of master

nodes into the slave surface in comparison with the Node-to-Surface method. It is noted that the Surface-to-Surface contact discretization generates asymmetric terms in the system of equations. These terms have a strong influence on convergence in regions where the master and slave surface are not parallel to each other. Therefore, an asymmetric solver is recommended for all finite-sliding Surface-to-Surface contact problems, including steel connection simulation.

Snagging is one of the main problems with the Node-to-Surface method. Abaqus/Standard automatically applies a smoothing procedure for Node-to-Surface. However, there is no smoothing problem with the Surface-to-Surface discretization method. The Surface-to-Surface discretization method possesses an inherent smoothing which leads to a better convergence rate. Although the Surface-to-Surface contact formulation has no special issues for any quadratic elements, first-order type of elements are preferred for the model, as discussed in section 3.6.

3.8.3.2.2.1 Contact properties

The concept of contact modelling can be split into normal and tangential contact.

3.8.3.2.2.1.1 Normal behaviour

There are two primary methods in Abaqus to enforce normal direction contact constraints: the "direct Lagrange multiplier" method and a "penalty" method. The fundamental difference between the two methods is that the Lagrange multiplier method exactly enforces the contact constraint by adding degrees of freedom to the problem, while the penalty method approximately enforces the contact constraint without applying additional degrees of freedom by using axial springs. This approximation leads to a small amount of penetration in the penalty method, comparing to the direct Lagrange multiplier, as illustrated in Figure 3.15. The penalty method is depicted schematically in Figure 3.16. The upper surface is the master, and the lower surface is the slave. While the over-closure has been exaggerated, it is clear that the stiffness of the spring resists the penetration of the master node into the master surface in proportion to its degree of penetration.

It is believed that, in problems such as steel connection modelling, adequately capturing the load transfer through the contacting interfaces is more important than the precise enforcement of the zero penetration condition. The penalty method is attractive in such applications because it is usually possible to trade off some small amount of penetration for improved convergence rates. Advantages and disadvantages of each method are summarized in Table 3.8. Author experience has also shown that in simulation of steel shear connections in large deformation, the default penalty stiffness chosen by Abaqus produces results that are not comparable in accuracy to results produced by experiments. Experience has also shown that the direct Lagrange multiplier method is not appropriate due to convergence difficulties.

3.8.3.2.2.1.1.1 Penalty contact stiffness

The state-of-the-art knowledge about the contact stiffness and its methods of calculation is quite inadequate in the face of current and fast growing needs in the field of simulation techniques. Correct modelling of contact increases the precision of contact calculation and makes it possible to conduct a simulation of different types of connection with the same procedure. Based on the available literature, the normal contact stiffness is dependent on mean pressures and touching surface characteristics, such as surface hardness, roughness and additives, e.g., lubrication or painting.

The penalty method implementation in Abaqus attempts to choose a reasonable penalty stiffness based on the underlying element stiffness. However, the default penalty stiffness is not suitable for the structural steel interaction. It is required to calibrate the quantities in order to capture accurate behaviour. In Abaqus, there are some options to scale the penalty stiffness or prescribe the penalty stiffness directly. In the case of very large scaled or user-prescribed penalty stiffness, Abaqus automatically invokes special logic that minimizes the possibility of ill-conditioning. If the scale factor is greater than 100, Abaqus will automatically switch to the Lagrange multiplier method to avoid ill-conditioning issues.

In this research, the penalty stiffness has been calibrated and estimated based on the available experimental results. It is observed that the penalty stiffness varies for different type of steel, e.g., ASTM A36 and ASTM A992. The reason is related to the difference in the casting and rolling procedure and also the difference in the material properties such as roughness and hardness. However, exact determination of this issue is out of the scope of this research. Based on experience, a value for the scale factor between 0.001 and 0.003 is recommended for structural steel. ASTM A36, with a lower yield and ultimate strength, is close to the lower margin (0.001) and ASTM A992 is approaching the upper bound of the proposed range (0.003). Sensitivity of the results to the penalty stiffness factor is discussed in section 3.12.4.

3.8.3.2.2.1.1.2 Linear versus nonlinear penalty contact

The penalty stiffness used for enforcing contact constraints can be constant or variable. Hence, the contact pressure–overclosure relationship can be linear or nonlinear. In the nonlinear approach, the penalty stiffness has constant initial and final values; these values serve as bounds for an intermediate overclosure regime in which the stiffness varies quadratically. A schematic comparison of the pressure–overclosure relationships for the linear and nonlinear penalty methods is given in Figure 3.17. The various parameters used for defining the nonlinear pressure–overclosure relationship with the default values are summarized in Table 3.7 based on the characteristics of the underlying elements of the slave surface. User control for changing the default values is provided, but the nonlinear penalty possesses a large number of parameters to set before applying. These parameters are not defined in the existing literature for structural steel and there are too many parameters to calibrate for each model. However, the nonlinear penalty method has some characteristics that make it appropriate for steel connection modelling. For instance, relatively low penalty stiffness is used while the contact pressure is small. This serves to reduce the severity of the discontinuity in contact stiffness when the contact status changes. Besides, the smooth increase of the penalty

stiffness with overclosure helps to avoid inaccuracies associated with significant penetrations, without introducing additional discontinuities.

The low initial penalty stiffness typically results in better convergence for steel connection problems that are prone to divergence with linear penalty contact, and the higher final stiffness keeps the overclosure at an acceptable level. Nonlinear penalty contact tends to reduce the number of severe discontinuity iterations due to a smaller initial stiffness; however, it will increase the number of equilibrium iterations due to the nonlinear pressure–overclosure behaviour significantly. Hence, application of nonlinear penalty contact will not result in a reduction of the total iteration count compared to linear penalty contact. As a result, for normal behaviour, it is suggested to apply a hard-contact formulation with a penalty constraint enforcement method considering linear stiffness. The related parameters should be calibrated with experimental data.

3.8.3.2.2.1.2 Tangential behaviour

Friction between contact interfaces produces shear stresses. The response in the tangential direction can be divided into two phases of stick and slip. If the shear stress reaches a critical value, one surface slides on the other one. In the stick phase, there is no tangential displacement. Friction is highly nonlinear and nonconservative. Therefore, it produces unsymmetrical terms in the system of equations.

There are several formulations available in Abaqus for friction, including frictionless, rough, penalty and Lagrange Multiplier. In the first method, surfaces slide freely without friction; however, the rough formulation assumes an infinite coefficient of friction. The penalty method permits some relative motion of the surfaces, called "elastic slip", when they should be sticking. Lagrange multiplier enforces exact sticking constraints at an interface between two surfaces with no relative motion. Figure 3.18 compares the last two methods that represent friction more realistically (Dassault Systèmes 2009).

For steel connections, it is recommended to use the penalty formulation with the Isotropic Coulomb friction model. It is also suggested to use a coefficient of friction equal to 0.3 for steel material. The Lagrange multiplier formulation prevents convergence of the solution since there are many points that are iterating between sticking and slipping conditions. Furthermore, there is a strong interaction between local slipping/sticking conditions and contact stresses in the steel connections that increase the computational cost of the analysis due to adding more degrees of freedom to the model.

3.8.3.2.3 Contact tracking (relative sliding)

Relative sliding of the connection components interacting with each other is another important phenomenon that needs to be included in the model. Abaqus uses two different analysis methods to deal with this phenomenon: "small sliding" and "finite sliding". Small sliding is less computationally expensive, but sliding must not exceed a fraction of a typical element dimension (Dassault Systèmes 2009). In the column removal connection modelling scenario, sliding in the connection assembly can be much more than what is assumed to be acceptable for "small sliding"; therefore, it is recommended to apply the "finite sliding" method in this case.

3.8.3.3 Element-based contact

There are certain types of modelling problems in which the element-based contact approach has some advantages over a surface-based definition, such as contact between two pipelines. Steel connection modelling is not one of them due to large number of contact points. As mentioned in section 3.8.3.1, it is recommended to use surface-based contact in the steel connection modelling due to its simplicity and ease of use. However, for the sake of completeness, this section provides a brief discussion on element-based contact applicable to the steel connection modelling.

Most concepts that have already been discussed in the earlier sections for surface-based contacts are valid also for contact elements. The Lagrange multiplier formulation approach for normal behaviour and penalty and Lagrange approaches for friction modelling are available. The solving algorithm for contact elements is the severe discontinuity iterations method, similar to surface-based contact. There are different types of contact-type elements available in commercial finite element software such as Abaqus. Among them, GAP elements are an appropriate option for connection modelling. GAPUNI elements, one type of GAP elements in Abaqus, monitor small-sliding node-to-node contact based on Equation (3-3):

$$h = d + \mathbf{n} \cdot (\mathbf{U}^2 - \mathbf{U}^1) \geq 0 \quad (3-3)$$

in which h is the current clearance between two nodes of the gap, d is the initial gap and \mathbf{n} is the direction of contact. \mathbf{U}^2 and \mathbf{U}^1 are the total displacements at the first and second node forming the GAPUNI element. When h becomes negative, the gap contact element is closed and the constraint $h = 0$ is imposed. Figure 3.13(a) illustrates a schematic view of such an element.

3.9 Solving techniques

There are two distinctive methods to solve finite element problems: implicit and explicit. The implicit method solves for static or dynamic equilibrium, while the explicit method solves transient dynamic response using explicit direct-integration procedures. In the implicit method, each increment must reach convergence. Due to the presence of a large number of contact surfaces in the connection model assembly, convergence difficulties may occur in this method, while the explicit solver might exhibit fewer convergence difficulties (DassaultSystèmes 2011b). It is inferred that convergence is not an issue in the explicit numerical integration solution scheme; however, the results might be less reliable than using the implicit solver. Therefore, the results of the explicit solver should be verified closely.

Table 3.9 summarizes the key differences between the implicit and explicit methods. Based on the mentioned logic, the implicit method has been selected for the research.

3.9.1 Solving a nonlinear problem

As mentioned before, connection modelling is a highly nonlinear problem in nature. To solve the convergence problems associated with nonlinearity, the software solving techniques must be understood. For static nonlinear problems, the system of governing equations needed to be solved is shown in Equation (3-4) to satisfy equilibrium:

$$\mathbf{P} - \mathbf{I} = \mathbf{0} \quad (3-4)$$

where \mathbf{P} is the external load and \mathbf{I} is the summation of the internal loads, determined according to Equation (3-5):

$$\mathbf{I} = \int_v \mathbf{B}^T \boldsymbol{\sigma} dv \quad (3-5)$$

where \mathbf{B} is the relationship between displacement and strain increments and $\boldsymbol{\sigma}$ is the stress in the model.

Figure 3.19 shows how each parameter in Equation (3-5) presents different types of nonlinearities. The equilibrium Equation (3-4) could be linearized by expanding the Taylor series and canceling the higher order terms, as stated in Equation (3-6):

$$\mathbf{K}_0 \mathbf{U} = \mathbf{P} \quad (3-6)$$

in which:

$$\mathbf{K}_0 = \int_{v_0} \mathbf{B}^T \mathbf{D} \mathbf{B} dv \quad (3-7)$$

where v_0 represents the undeformed shape of the model under investigation and D is defined in Equation (3-8):

$$6 = D P \quad (3-8)$$

There are different techniques to solve such a nonlinear system of equations. In all of the methods, the total applied load or displacement is broken into small increments. Then, an approximate solution is obtained for each load increment. Several iterations might be needed to obtain a sufficiently accurate approximate solution. Two robust incremental/iterative methods for solving the nonlinear problems are Newton-Raphson and Quasi-Newton techniques (Dassault Systèmes 2011c). These methods are discussed in the section 3.9.1.1 and 3.9.1.2.

3.9.1.1 Newton-Raphson technique

The Newton-Raphson method is the most robust method to solve nonlinear systems. As discussed earlier, in this method each step is made up of several increments and the total load history is divided into several load steps based on the loading nature. The total load/displacement applied in each step is broken into smaller increment in order to capture the nonlinear solution path. Each increment needs several iterations (Figure 3.20). In order to solve Newton-Raphson iteration, a linear equation in c_u is being solved using Equation (3-9):

$$K_{tangent} c_u = P - I \quad (3-9)$$

where c_u is the correction to \mathbf{u} , called the displacement correction. To obtain the linear system of equations, Equation (3-9) can be rewritten as Equation (3-10):

$$R(\mathbf{u}) = P - I \quad (3-10)$$

where $R(\mathbf{u})$ is the residual at \mathbf{u} . Residual represents the out-of-balance force at \mathbf{u} . When $R(\mathbf{u})=0$, it means that the system reaches equilibrium. Physically, residuals represent the magnitude and distribution of extra external force at each degree needed to bring the structure into equilibrium at \mathbf{u} . It is noted that \mathbf{u} is an

equilibrium position for $\mathbf{P}-\mathbf{R}(\mathbf{u})$, not \mathbf{P} ; hence, $\mathbf{R}(\mathbf{u}) \neq 0$. It is intended to find \mathbf{c}_u , so that $\mathbf{u} + \mathbf{c}_u$ is in equilibrium or, in other words, Equation (3-11) is satisfied:

$$\mathbf{R}(\mathbf{u} + \mathbf{c}_u) = \mathbf{0} \quad (3-11)$$

Expanding the Taylor series for the Equation (3-11) leads to Equation (3-12):

$$\mathbf{R}_u(\mathbf{u} + \mathbf{c}_u) = \mathbf{R}_u + \frac{\partial \mathbf{R}}{\partial \mathbf{u}} \mathbf{c}_u + \dots = \mathbf{0} \quad (3-12)$$

Ignoring the higher-order terms in the Equation (3-13) results in Equation (3-14):

$$\left. \frac{\partial \mathbf{R}}{\partial \mathbf{u}} \right|_{\mathbf{u}} \mathbf{c}_u = -\mathbf{R}_u \quad (3-13)$$

Substituting (3-13) into (3-9) leads to an equation that is known at \mathbf{u} and linear in \mathbf{c}_u . Once \mathbf{c}_u is calculated using the Newton-Raphson formula, \mathbf{u} will be updated using Equation (3-14):

$$\mathbf{u}_{i+1} = \mathbf{u}_i + \mathbf{c}_u \quad (3-14)$$

Figure 3.21 is an illustration of the method. Two criteria should be satisfied for the convergence test to see if \mathbf{u}_{i+1} is an equilibrium position. The first one is the sum of all the forces acting on each node and the other one is the displacement correction. In order to achieve convergence in each load increment, the load magnitude should be reduced. The main goal is to limit the number of iterations to five at each load increment. If there are too many attempts in a single increment, Abaqus fails to converge and terminates. Each iteration in the Newton-Raphson technique includes the formulation (building the stiffness matrix) and solution of linearized equilibrium equations. Each iteration is assumed to be correct if the error of the equations is smaller than certain user-defined tolerances:

$$\mathbf{P} - \mathbf{I} = \mathbf{R}_\alpha < \textit{Tolerance} \quad (3-15)$$

The magnitude of accepted tolerances in the Newton-Raphson method is defined in section 3.9.2. It is noted that this method is unconditionally stable for any increment size. However, there are some cases in which finding a converged solution is not possible.

By default, Abaqus/Standard will extrapolate the $\Delta\mathbf{u}$ calculated in the previous increment and use it as the estimate for $\Delta\mathbf{u}$ in the current increment. This method usually helps to improve the rate of convergence in the analysis and speeds up the simulation. Newton-Raphson exhibits quadratic convergence. Relative error, e , between successive iterations decreased by relative error itself:

$$e_{new} \propto e_{old}^2 \quad (3-16)$$

3.9.1.2 Quasi-Newton technique

The Quasi-Newton technique is also an incremental–iterative solution for nonlinear problems. The main difference between this method and the conventional Newton-Raphson method is how frequently the stiffness matrix is recalculated. In the full Newton-Raphson technique, the stiffness matrix is recalculated at each iteration. However, when utilizing the quasi-Newton technique the stiffness matrix reforms after a certain number of iterations. It may save substantial computational effort, particularly in problems with a large system of equations in which the stiffness matrix is not changing much from one iteration to the next.

The quasi-Newton method is not recommended in steel connection analysis due to alteration in the contact status and, as a result, in the stiffness matrix from one iteration to another. Additionally, the current version of Abaqus/Standard does not support the quasi-Newton method with asymmetric problems, e.g., problems with high friction coefficients. This is another reason to use the full Newton-Raphson method.

3.9.1.3 Contact solution

Discontinuous nonlinearities such as contact typically have an adverse impact on convergence behaviour. In connection modelling, the most significant contacts in terms of importance and quantity are the bolt shank–hole interaction, as shown in Figure 3.22(a). It is assumed that the bolt is initially located at the center of the hole. After applying load, the bolt shank comes into contact with the edge of the hole, as illustrated in Figure 3.22(b). Contact causes kinks in the load versus displacement curve. There is a slope discontinuity upon any changes in contact status. This alteration interrupts the overall convergence rate of the model. "Severe discontinuity iteration" (SDI) is used to filter out contact from convergence rate tracking. An SDI is an iteration during which contact constraints change state (open, close, stick, slip). Abaqus/Standard treats SDIs and equilibrium iterations separately. The logic to adjust the increment size treats SDIs separately as well. Figure 3.23 shows the flowchart that explains how Abaqus /standard solves a contact problem by utilizing the SDI method. The general solution for a nonlinear problem in the presence of contact is summarized in the flowchart shown in Figure 3.24 (Dassault Systèmes 2011c).

3.9.2 Convergence Criteria

Abaqus/Standard uses local load convergence criteria versus global criteria to ascertain convergence. In local methods, every node in the model should meet pertinent convergence criteria at each iteration. Nonetheless, the global criteria, such as energy balance, apply to the entire model. Local methods are more stringent and accurate. Abaqus/standard uses the concept of "average force", f_{avg} , and "time average force", \tilde{q} , in addition to maximum displacement correction check. There are also other convergence checks for contact and different types of elements.

The average of all of the nodal force components in all the elements of the model is called the average force, as calculated by Equation (3-17) (Dassault Systèmes 2011c):

$$f_{avg} = \frac{\left\{ \sum_{e=1}^{N_{element}} \sum_{n=1}^{N_{nodes}} \sum_{i=1}^{N_{dof}} |f_i^n| + \sum_{i=1}^{N_{loads}} f_i^{external} \right\}}{N_{sum}} \quad (3-17)$$

An average nodal force, \bar{q} , for the whole model at each iteration is calculated based on (3-18) (Dassault Systèmes 2011c) :

$$\bar{q} = \frac{(Sum\ of\ internal\ forces) + (Sum\ of\ external\ forces)}{(No.\ of\ active\ dofs\ in\ model) + (No.\ of\ active\ external\ forces)} \quad (3-18)$$

Applying the definition of \bar{q} , the "time average force", \tilde{q} , is determined as shown in Equation (3-19) (Dassault Systèmes 2011c):

$$\tilde{q} = \frac{(Sum\ of\ prior\ \bar{q}\ for\ converged\ iterations\ in\ this\ step\ plus\ \bar{q}\ for\ current\ iteration)}{(No.\ of\ increments\ in\ this\ step,\ including\ the\ current\ one)} \quad (3-19)$$

The parameter \tilde{q} is calculated for the model throughout each step at each iteration of the current increment.

It is also crucial to set an acceptable residual tolerance. In Abaqus/standard, the iteration is accepted as converged when R_{max} is reached, as shown in Equation (3-20):

$$R_{max} = 0.005 \tilde{q} \quad (3-20)$$

R_{max} is the maximum residual (out-of-balance force) and \tilde{q} is time average force for every node in the model. The 0.005 value is selected based on previous experience and engineering judgment, and is considered to provide a reasonable trade-off between accuracy and efficiency for quadratic convergence.

There are other convergence criteria that Abaqus/Standard uses in order to ascertain the accuracy of the implicit analysis results. Another convergence criterion is the "maximum displacement correction" check. This criterion limits the maximum displacement correction to less than or equal to 1% of the maximum displacement increment, as shown in the Equation (3-21):

$$c_{max} = 0.01 \Delta u_{max} \quad (3-21)$$

where c_{max} is the maximum displacement correction and Δu_{max} is the maximum displacement increment. In addition to all the mentioned convergence controls, there are other convergence criteria for contact problems.

All of these criteria can be altered by the user in case of convergence difficulties. However, for steel connection simulations, it is recommended to look for modelling issues rather than changing the default parameters for convergence. It is noted that relaxing the default convergence criteria may lead to divergent or inaccurate results. In certain cases of connection modelling, user intervention might be useful, such as when a model contains a crack or includes fracture, or the models contain user elements (UEL) or user material subroutines (UMAT). If the final behaviour of a specific type of connection is important, relaxing convergence criteria during initial analysis stages might help the cost; however, if the history of the connection performance is important, this is not recommended. Based on what was mentioned, no alteration has been applied to the default convergence rules in this research.

3.9.3 Stabilization of initial rigid body motion

Bolted connection assemblies rely on contact between bolts and different components to prevent unconstrained rigid body motion. Due to uncertainty of the location of the bolt shank in the hole, it is often impractical to model such systems with initially established contact. The initial play between the bolt and the other components causes initial unconstrained rigid body motion. Displacement-

controlled loading prior to establishing contact will lead to a non-singular solution. However, after establishment of contact, the system of equations is also stable for force-controlled loading. Pre-tensioning the bolts helps to establish contact and prevent rigid body motion, before applying the actual load step.

Abaqus/standard can also automatically control rigid body motions in static problems before contact closure and friction restrains such motions. This stabilization is based on the stiffness of the underlying elements. In this automated stabilization contact method, additional forces are imposed to all contact pairs equally in the normal tangential direction that will influence the solution during the step. At the end of the step, these newly introduced forces are ramped down to zero. The method is applicable only when the distance between the contact surfaces is smaller than a characteristic surface dimension. This method helps the convergence significantly, even though no true rigid body modes exist in the model. In the sample bolted connection without stabilization, the analysis requires a special analysis sequence, many SDIs, and non-default contact controls.

3.9.4 Time incrementation

Abaqus uses a sequence of steps, increments and iterations for defining the load history by applying an empirical algorithm automatically to control the increment size. Although there are many logical principles applied in these algorithms, the basics include two simple rules: first, the increment size is increased by a factor of 1.5 after obtaining convergence in four iterations and, second, the increment size is decreased by a factor of 0.25 after not obtaining convergence in more than 10 iterations.

The user provides an initial increment size for every step in nonlinear analysis. It is suggested to use a small fraction of the total step size (0.1-0.01). Maximum and minimum increment sizes should be specified by the user as well. Selection of approximate values for maximum and minimum increment size is also important. Abaqus requires input of the maximum number of increments allowed per step. If

the increment size is reduced due to cutbacks to a value below this minimum value, the analysis will terminate. In order to avoid termination, it is suggested to use a value between 10^{-15} to 10^{-10} for highly nonlinear connection models. Although there is no restriction on maximum allowable increment size—i.e., the entire load can be applied in a single increment—a reasonable value can lead to efficient solution and avoids cutbacks.

3.9.5 Riks versus general static methods

The Riks method (Riks 1979) is recommended for globally unstable problems. This method works well with contact as long as the contact itself is stable. Riks runs into problems where there is a loss of contact, such as a contact-driven snap-through problem, where the structure moves away from the contact. In this case, the Riks algorithm can't scale the load up or down to keep the model in contact and convergence failure will occur. The arc length method proposed by Riks generally cannot be applied to connection models due to the large number of contact surfaces and contact status changes. Figure 3.25 illustrates how contact status is changing due to the presence of different loads in the connection model in a column removal scenario. The general-static method implemented in Abaqus is therefore used in this study.

3.10 Numerical Failure Criteria

Failure in the experimental program is considered a situation at which the assembly has lost a considerable load carrying capacity or a rupture mechanism occurs. In the numerical model, the implicit analysis will continue until the model cannot find the solution due to excessive yielding, which is far beyond the failure point in the experiment. In order to capture the correct failure load and mode, it is necessary to establish numerical failure criteria. These criteria could be global, which include all the possible limit states of the connection, or could be more case-specific, and varied for each particular limit state. Each method has its pros

and cons, but the global failure criteria are more versatile and complete, although difficult to set effectively for general use. This criterion should be satisfied when some elements or nodes reach a certain stress or strain value. Stress criteria could be principal stress, in a specific direction, von Mises, Tresca, etc. Strain criteria could be also the principal strain or the equivalent strain. In this research, the equivalent plastic strain, PEEQ in Abaqus, has been selected as a variable upon which to impose a failure criterion. PEEQ is defined in Equation (3-22):

$$PEEQ = \bar{\varepsilon}_p|_0 + \int_0^t \dot{\bar{\varepsilon}}_p dt \quad (3-22)$$

where $\bar{\varepsilon}_p|_0$ is the initial equivalent plastic strain. The definition of $\dot{\bar{\varepsilon}}_p$ depends on the material model. For classical (Mises) plasticity $\dot{\bar{\varepsilon}}_p$ is defined in Equation (3-23):

$$\dot{\bar{\varepsilon}}_p = \sqrt{\frac{2}{3} \dot{\varepsilon}_p : \dot{\varepsilon}_p} \quad (3-23)$$

PEEQMAX is the maximum of the equivalent plastic strains among all of the section points. For a solid element, it represents the maximum PEEQ at the integration points. As mentioned in section 3.7.2, since the problem is mesh-dependent, an appropriate mesh size should be selected in order to capture the failure modes and loads accurately. PEEQ failure values for steel sections/plates and high strength bolts are introduced in sections 3.10.1 and 3.10.2, respectively.

3.10.1 Steel sections and plate

Rupture strain is very mesh-dependent and different researchers have proposed different values. For instance, for structural-grade steel, Khoo et al. (2002) showed that the localized rupture strain is approximately 80% to 120%. Huns et al. (2002) used tension coupon test in order to measure the localized rupture strain. Huns et al. considered a rupture strain of 100%, which was a lower bound

of their material test and an average of the range of values reported by Khoo et al. (2002). Epstein and Chamarajanagar (1996) proposed a rupture strain equal to five times the yield strain.

Unfortunately, there was no material tension coupon test performed for the selected experimental program; hence, it is hard to establish a failure value. However, the verified finite element model with available experimental results show that the shear tab starts to fail at approximate PEEQ equal to 0.55. This value is valid for the applied mesh size. As the mesh gets finer, a larger value for strain should be selected as a rupture point for the material. The proposed rupture strain criterion is observed in other experiments for other types of connections, such as WT. Hence, it is selected for all the other models in the subsequent chapters.

In order to make sure that the defined material model with the selected mesh size can capture necking and the required localized strain, a tension coupon with the same mesh size of the shear tab in the connection assembly is modeled, as shown in Figure 3.26. When the strain reaches the rupture point, the element is removed from the mesh in order to simulate the initiation of steel rupture. It is noted that in the current research, rupture initiation is of main interest due to the fact that rupture propagation is rapid and unstable with lots of uncertainties, and is beyond the point of maximum capacity of the localized connected part. Rupture propagation is therefore outside the scope of the research.

3.10.2 High strength bolts

In order to calibrate the ASTM A325 and ASTM A490 bolt types used in this research, and also establish a rupture strain value, a solid element model of the bolt in a double shear test is developed, as shown in Figure 3.27. The behaviour of the finite element model is compared to the typical result of the shear tests reported by Kulak et al (2001). As can be seen in Figure 3.28 and Figure 3.28, there is good correlation between the experimental and numerical results. These

figures also establish the rupture strain equal to 0.55 for this type of bolt with the mentioned mesh size. A mesh with the same size elements is used in the connection assembly.

3.11 Results extraction

Axial and moment forces in each step were obtained through strain measurements using strain gauges in the experiments (Thompson 2009). These data are used to determine the forces at the bolt line of the connections. The strains are converted to stress using Hooke's law, which assumes that the beam material at the strain gauge locations remains elastic. Numerical simulation confirmed the validity of this assumption. The measured strains are combinations of axial and flexural stress at the location of the strain gauges. The axial force at any section through the length of the beam remains unchanged. Assuming a triangular moment distribution, the flexural force at the bolt line was determined from extrapolation of flexural forces at the strain gauge location. The procedure is explained in chapter 2.

The same procedure was applied to determine the internal forces at the bolt line location of the simulated models. The toolset called "Free Body toolset" was used to record the resultant forces and moments at the location of the strain gauges on the test specimens. This toolset simply adds the forces at the nodes corresponding to the defined section. Hence, the element force nodal output (NFORC) is needed in order to create a free body cut. Since free body cuts cannot be saved in the output database file, a Macro (a set of Abaqus Scripting Interface commands) has been managed.

3.12 Sensitivity analysis

In order to gain confidence in the correctness and accuracy of the proposed finite element model, detailed sensitivity analyses are performed. Table 3.10

summarizes the variables on which the analyses are performed. For the sake of brevity, just the shear response of the connection is plotted. In sections 3.12.1 to 3.12.7, observations regarding different variables are discussed. Three tests were carried out on each configuration of shear tab connection (Thompson 2009) and each test produced results for two identical shear tabs, although their responses might be different. Therefore, six different responses from the experiments are available for comparison. The results of the third experiments on 5ST (five-bolt) connections are shown in Figure 3.30 to Figure 3.35 for the purpose of comparing with numerical results. The dashed lines and solid lines represent the results of the experiments and simulations, respectively. The termination point of the numerical simulation curves is based on the selected failure criterion, as discussed in section 3.10.

3.12.1 Element Type

It is observed that the global response of the connection assembly including shear, axial and flexural responses is not sensitive to the type of element for different components in terms of load path. However, different types of elements have different capabilities in capturing localized strain. Figure 3.30 shows the shear force versus rotation of the shear tab connection assembly for shear tabs consisting of element types C3D8R, C3D8, and C3D8I. The model with C3D8R elements reaches the established failure criterion far from the models with C3D8 and C3D8I elements, as well as initial failure observed in the experiments. It can be inferred that reduced integration elements (C3D8R) cannot capture the highly localized strain values precisely. Although the difference between C3D8 and C3D8I is small, C3D8I illustrates a better match with the experimental results. Based on what was discussed in section 3.6, it is recommended to use an incompatible type of element in regions where bending is dominant and the failure mode is of interest.

3.12.2 Coefficient of friction

The behaviour of the connection assembly is not significantly varied with the coefficient of friction between different components, and particularly the axial response. However, the closest response to the experimental results belongs to the model with the coefficient of friction equal to 0.3, as shown in Figure 3.31. Physical evidence for steel material shows that the selected value is reasonable.

3.12.3 Hole size

Figure 3.32 shows the shear response of the connection with different hole diameters. When the diameter of the hole is exactly equal to bolt diameter, the connection starts to capture load from the beginning. For the standard hole, a drop is observed in the load path until the contacts are established. For the oversized hole, the drop region is even larger. It can be concluded that any kind of variation in the relative bolt-to-hole size, including construction tolerances, will affect the load path. Slippage in the bolts results in a drop in the moment as well until bearing is achieved between the bolt shank and the hole in the plate. Furthermore, the location of the bolt in the hole is also important, since it determines when the contact is established. Due to the unknown nature of the problem and its variability, it is assumed that the bolts are located at the centers of the holes. This assumption is expected to affect only the initial part of the response curve.

3.12.4 Contact stiffness

illustrates the shear response of the connection with different penalty scale factors. Both load path and the convergence of the model are sensitive to this parameter. As a result, a model with an appropriately-selected parameter needs to be established for developing the benchmark example. Herein, the penalty scale factor of 0.0012 produced the best agreement with the experimental results, along with an acceptable convergence rate. Extensive research on different models leads

to the proposed range given in section 3.8.3.2.2.1.1.1, which are appropriate for all types of structural steel used in this research.

3.12.5 Pre-tensioning

Figure 3.34 depicts the shear–rotation curves for the models with different pretension forces in the bolts. Pre-tensioning, in terms of displacement applied to the bolt shanks, does not affect the overall load path significantly. However, it does influence the load path at early stages; e.g., the model with PT=0.5 mm produces better agreement with the experimental load path at the beginning of the load transfer. However, based on the argument in section 3.5.2.3.1, the connections in the selected experimental program are considered snug-tight, not pre-tensioned. As a result, the model with PT=0.1 mm is deemed to produce results with acceptable accuracy. It is noted that the PT equal to 0.02, 0.1 and 0.5 mm impose 12, 59 and 294 MPa initial stress in the bolts, respectively.

3.12.6 Material definition

illustrates the shear response of the connection with different material definitions discussed in section 3.5.2.2 and Appendix A. As can be seen in , the difference in the definition of material used in this research affects the load curves slightly. Selecting "minimum nominal strength" (MINS) and "maximum nominal strength" (MANS) material properties underestimates and overestimates, respectively, the response slightly. "Lower-bound" (LBS) and "expected-strength" (EPS) are appropriate properties to get acceptable results. The expected-strength (EPS) definition is utilized for all types of steel, including the bolts, in the finite element studies, as discussed in Appendix A.

3.12.7 Mesh size

The failure criterion definition utilized in this research is mesh sensitive. Besides, appropriate relative mesh densities of different parts in the assembly is a

challenge when contact exists. As mentioned in section 3.7, the principle of classical mesh convergence study does not apply due to the localized nature of the stress fields in the connection model. As a result, an appropriate mesh size is established as discussed in section 3.7. The effect of mesh size is investigated and it is observed that the model is not sensitive to the refinement of the mesh size in either the connecting part or the bolts. Moreover, convergence difficulties may occur if very refined meshing is used in the assembly.

3.13 Final results

The deformed shape of the overall test assembly and a direct comparison of the shear tab deformations and tearing observed in the model and the experiment are shown in Figure 3.36. It can be seen that there is close similarity between the experiment and the numerical simulation results. The numerical model can predict the location of failure initiation accurately. Plastic deformation is mostly accumulated around the bottom hole where the failure begins. Besides, the ductility of the system is mostly provided by bearing deformation developed around the holes, based on both numerical and experimental results.

Table 3.11 compares the experimental and finite element model results. Errors are calculated based on the assumption that the experimental results are the correct values. Final results show that different modelling assumptions, e.g., the location of the bolts at the center of the holes, are valid due to good agreement with the experimental results. As observed, the errors are all less than 7%, which is acceptable in such a complex model with numerous physical and numerical features and variables. The agreement for shear and rotation is particularly close. The internal forces—including shear, axial force, and moment—at the bolt line location versus chord rotation of the connection assembly are shown in Figure 3.37 to Figure 3.39. These curves verify the simulated model based on the acceptable agreement with the associated experimental results and the variability within the experimental results of nominally-identical specimens themselves.

3.14 General tips for reaching converged solution

As mentioned earlier, there are several causes for convergence problems, including allowing rigid body motion, conflicting constraints between boundary conditions, contacts, inadequate material data, inappropriate element types, and instability of the physical model such as development of load instabilities or severe localized plastic strain. Hence, the correct element type, appropriate boundary conditions and constraints, sufficient material data and an appropriate analysis technique should be utilized. In addition to all mentioned suggestions and recommendations to assist in model development of shear connections under a column removal scenario, to reach a converged solution some basic notes are provided in this section. Although basic, they are fundamental and help to reach convergence in the numerical modelling of steel connections:

- Most of the convergence problems arise from inappropriate definition of various aspects of the model, such as constraints, boundary conditions, material and element types. Although achieving a converged solution using implicit analysis with all different types of nonlinearity is a difficult task, the majority of convergence problems can be explained and corrected.
- It is suggested to add complexity to the model step by step, not simultaneously. Start with a simple connection model without plasticity, friction, and even contact (use tie constraint instead) in the geometry. After getting insight into the behaviour, add complexity as needed to achieve the modelling goals.
- As a general comment, avoid sharp corners in numerical models of connections. Particularly, when the physical connection surface is reasonably smooth, the numerical model should be smooth as well. However, in places that they are inevitable, it is recommended to use Surface-to-Surface formulation at corners because two constraints are applied, as shown in Figure 3.40, which is accurate and stable. Node-to-Surface applies just a single constraint in an "average" normal direction at

the corner, which is not stable and may cause a large penetration and snagging. The corner should be approximated by an adequately fine mesh to help convergence considerably. In modelling round corners, mesh refinement will tend to help convergence.

- Another source of convergence difficulties is the difference between the actual geometry and faceted geometry. Faceted geometry may cause a “noisy” solution; nevertheless, by geometric corrections an accurate solution can be obtained. It must be noted that geometric corrections might not be helpful in large deformation models. The shank section of bolts should be adjusted to conform to hole facets, as shown in Figure 3.41.
- Friction is an issue that could produce unsymmetrical terms in the stiffness matrix. The unsymmetrical solver is recommended for all finite-sliding Surface-to-Surface contact problems. It is noted that the unsymmetrical solver of Abaqus is automatically activated for friction coefficients greater than 0.2.
- It is recommended to select the stiffer surface as the master surface, although it has a coarser mesh. The master surface normal should point toward the slave surface; otherwise, convergence difficulties will occur.
- Since Abaqus does not have any specific built-in system of units, all the input data must be in consistency. SI (N-mm) is recommended to be the consistent units in all models. Make sure that the units and material properties are consistent.
- Providing reasonable values for the minimum and maximum increment size will help the convergence considerably.

3.15 Summary and conclusions

The following conclusions can be drawn from the finite element study presented in this chapter:

- The present study is aimed at proposing an efficient and unified methodology for finite element modelling of steel shear connections in a column removal scenario. The main goal of this chapter is establishing confidence in the proposed modelling approach by verifying simple shear tab connections subjected to extreme loading conditions caused by the loss of a primary supporting column.
- The finite element analysis user has to decide on several issues such as mesh discretization, element types and the solving algorithm. These selections may have tremendous effects on the model response and can lead to inaccurate results. Nonlinearity definitions, including material, geometric, and boundary (contact) nonlinearities, are the most challenging part of finite element modelling of connections, and recommendations have been established and verified.
- In connection modelling, obtaining the converged nonlinear solution is the main obstacle. Satisfying all the mentioned convergence issues in addition to good engineering judgment to create a finite element model leads to an accurate solution. Although experimental results are needed for model validation, it is not necessary to have them for each specific type of connection to verify the response. Following the same procedure that was previously verified can lead to “converged” (accurate) response. The example can be taken as a benchmark for validating the finite element modelling of shear connections in the column removal scenario.

Table 3.1: Different phases in finite element analysis of bolted steel connections
(Krishnamurthy 1980)

Phase	Description	Goal
Feasibility studies	trial, development and modification of different models	build a model with satisfactory physical attributes
Sensitivity studies	vary one quantity at a time while the other characteristics of the model are kept constant	understand the effect of modelling variables on overall behaviour of connection assembly
Correlation studies	validate the model using benchmark cases or pertinent experimental results	ascertain that the results are correct and accurate enough
Convergence studies	model three or more progressively finer meshes of connection to evaluate the accuracy of the solution	determine the appropriate element sizes considering the accuracy and cost
Parametric studies	vary the most significant variables to accomplish the desired task	investigate the effect of design variables by producing statistically valid results

Table 3.2: Finite element model summary

Model Summary	No.	Description
Parts	6	<ul style="list-style-type: none"> • W460X52 beam (W18X35) • W310X79 stub column (W12X53) • shear tab (381X127X9.525) with five standard size hole (15"X5"X3/8") • 19.05 mm bolt - (3/4") • stiffener plate between stub column flange • rigid plane
Materials	3	<ul style="list-style-type: none"> • ASTM A36 (shear tab and the stiffener) • ASTM A325 (bolts) • ASTM A992 (stub column)
Analysis steps	2	<ul style="list-style-type: none"> • Applying pretension • Applying vertical displacement
Interactions	6	<ul style="list-style-type: none"> • bolt shank-beam/shear tab hole • bolt head-shear tab • bolt nut-beam web • shear tab-beam web • beam end-column flange (potential)
Interaction properties	1	<ul style="list-style-type: none"> • tangential behaviour • normal behaviour
Interaction	3	<ul style="list-style-type: none"> • controls • initializations • stabilization
Constraints	4	<ul style="list-style-type: none"> • tying shear tab to column flange to simulate the weld • tying the stiffeners to the stub column • tying rigid surfaces to beam end • applying out-of-plane constrain
Boundary conditions	2	<ul style="list-style-type: none"> • symmetry constrain • two axial springs at far ends of the beams to simulate flexibility of the test setup

Table 3.3: Integration order of element available in Abaqus (Daneshvar and Driver 2012)

Element Type	Description
First order elements	<ul style="list-style-type: none"> constant strain throughout the element that prevents mesh locking when the material is approximately incompressible e.g. steel
	<ul style="list-style-type: none"> accuracy achieved with full integration versus reduced integration depends on the nature of the problem
	<ul style="list-style-type: none"> recommended in cases of large strains or high strain gradients
	<ul style="list-style-type: none"> Works well with contact
Second order elements	<ul style="list-style-type: none"> provide higher accuracy for problems not containing contact simulations or element distortion
	<ul style="list-style-type: none"> better modelling geometric features, e.g., modelling a curved surface with fewer elements
	<ul style="list-style-type: none"> effective in bending-dominated analysis
	<ul style="list-style-type: none"> the second-order reduced-integration elements may suffer from volumetric locking when strains exceed 20– 40%.

Table 3.4: Full versus partial element integration available in Abaqus (Daneshvar and Driver 2012)

Element Type	Description
Reduced-integration Elements	<ul style="list-style-type: none"> use lower-order integration just for the element matrix, not mass and loading – No locking concern
	<ul style="list-style-type: none"> reduces the time of analysis, especially in three-dimensional analysis
	<ul style="list-style-type: none"> less accuracy in the area of stress concentration
Full-integration Elements	<ul style="list-style-type: none"> may suffer from locking behaviour, including both shear and volumetric locking
	<ul style="list-style-type: none"> volumetric locking happens when the material behaviour is almost incompressible

Table 3.5: Mesh refinement analysis results; refinement across the thickness

Mesh density (No. of elements in thickness)	Displacement at the bottom of the top hole (mm)	Stress at the bottom of the top hole (MPa)	Stress at the top corner of shear tab (MPa)	Relative CPU time (Sec)
1 (Coarse)	0.37	279.5	250.3	4.3
2 (Normal)	0.56	276.7	253.0	8.5
3 (Fine)	0.58	277.0	253.3	12.9

Table 3.6: Master and slave surfaces in the shear tab connection

No.	Label	Master	Slave
1	Head-ST	bolt head	shear tab
2	Nut-Bm	bolt's nut	beam's web
3	ST-Bm	beam's web	shear tab
4	Shk-Hol-Bm	bolt's shank	beam's web hole
5	Shk-Hol-ST	bolt's shank	shear tab
6	Bm-Clm	beam cross section	column flange

Table 3.7: Nonlinear penalty contact parameters (Dassault Systèmes 2009)

Parameter	Symbol	Default value
Linear stiffness used for linear penalty contact	K_{lin}	10 times the representative underlying element stiffness
Initial stiffness	K_i	1/10 of the linear penalty stiffness
Final stiffness	K_f	10 times the linear penalty stiffness
Clearance at which contact pressure is zero	C_0	zero
Upper quadratic limit	d	3% of the characteristic length ¹
Lower quadratic limit	e	1% of the characteristic length ¹
Lower quadratic limit ratio	e_r	0.3333 ²

¹ computed by Abaqus/Standard to represent a typical facet size

² From the default values of the parameters d and e

Table 3.8: Direct Lagrange multiplier versus penalty method (Dassault Systèmes 2009)

Direct Lagrange multiplier contact		Penalty contact	
Advantages	Disadvantages	Advantages	Disadvantages
<ul style="list-style-type: none"> • exact constraint enforcement (zero penetration) • no need to define contact stiffness 	<ul style="list-style-type: none"> • larger system of equations • slow convergence rate 	<ul style="list-style-type: none"> • number of equations does not increase • improved convergence rate 	<ul style="list-style-type: none"> • approximate constraint enforcement (finite amount of penetration) • difficult to choose proper stiffness

Table 3.9: Implicit versus explicit analysis method (Dassault Systèmes 2011c)

	Explicit	Implicit
Convergence	not an issue	must be obtained at each increment
Stability	conditionally stable	unconditionally stable
Time increment	limited	large ones can be used
Result Reliability	need to verify more precisely	high

Table 3.10: Sensitivity analysis

Parameter	Variable
Element type	C3D8
	C3D8R
	C3D8I
Coefficient of friction	$\mu = 0.15$
	$\mu = 0.3$
	$\mu = 0.5$
Hole size	bolt size
	standard
	oversize
Linear penalty contact: scale factor	0.0012
	0.001
	0.005
	0.01
	0.1
	1
Pretension - Adjust length	0.02 mm
	0.1 mm
	0.5 mm
Material- shear tab - ASTM A36	EPS
	LBS
	MANS
	MINS

Table 3.11: Benchmark results; verification with experimental work (Thompson 2009)

Spec. Label	Side	Moment, M (kN.m)	Shear, V (kN)	Axial, P (kN)	Rotation, Θ (radians)	Failure Mode
5ST1	Left	-	-	-	-	-
	Right	55.90	47.11	147.73	0.073	Block Shear Rupture
5ST2	Left	-	-	-	-	-
	Right	60.54	52.00	202.13	0.069	Block Shear Rupture
5ST3	Left	68.49	45.46	151.42	0.071	Tension Rupture
	Right	-	-	-	-	-
5ST-Mean		61.64	48.19	167.09	0.071	
5ST-FEA		65.85	47.31	177.48	0.069	Shear tab bottom hole rupture
Deviation %		6.83	1.82	6.22	2.82	

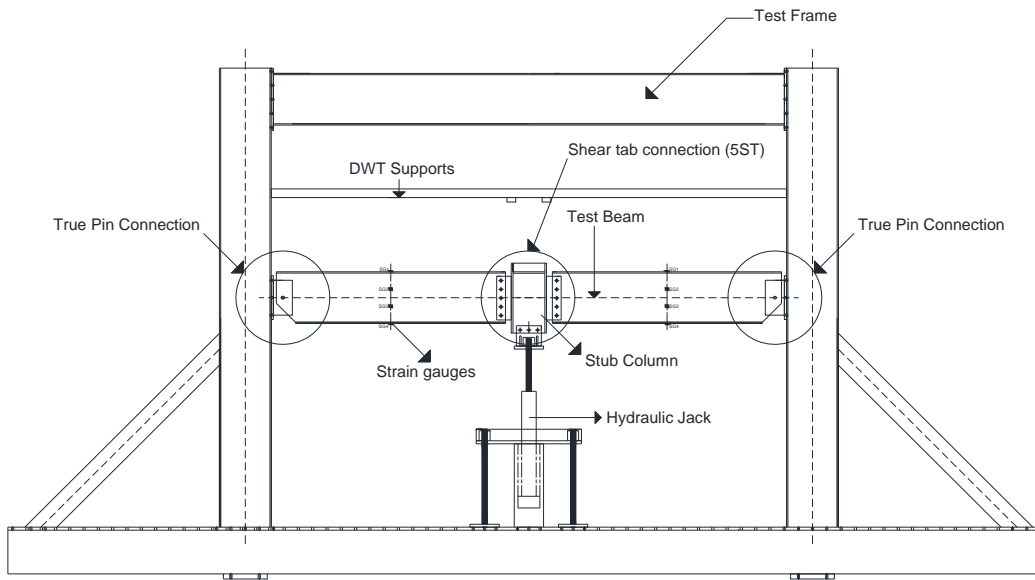
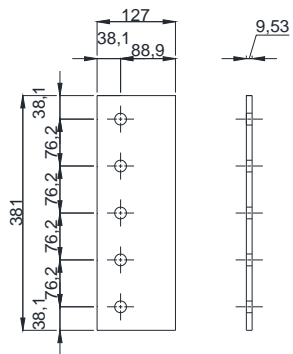
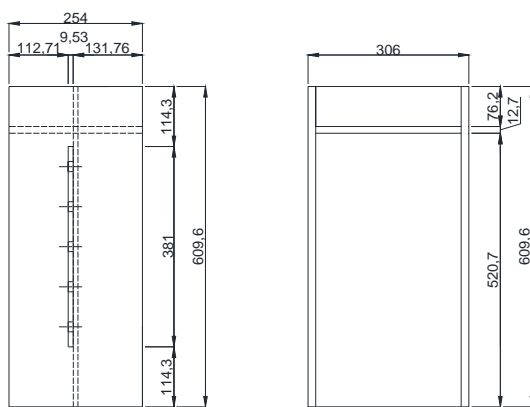


Figure 3.1: Test setup of selected experimental program (Thompson 2009)



(a)



(b)



(c)

Figure 3.2: Part dimensions (a) shear tab (b) stub column (c) beam (Thompson 2009)

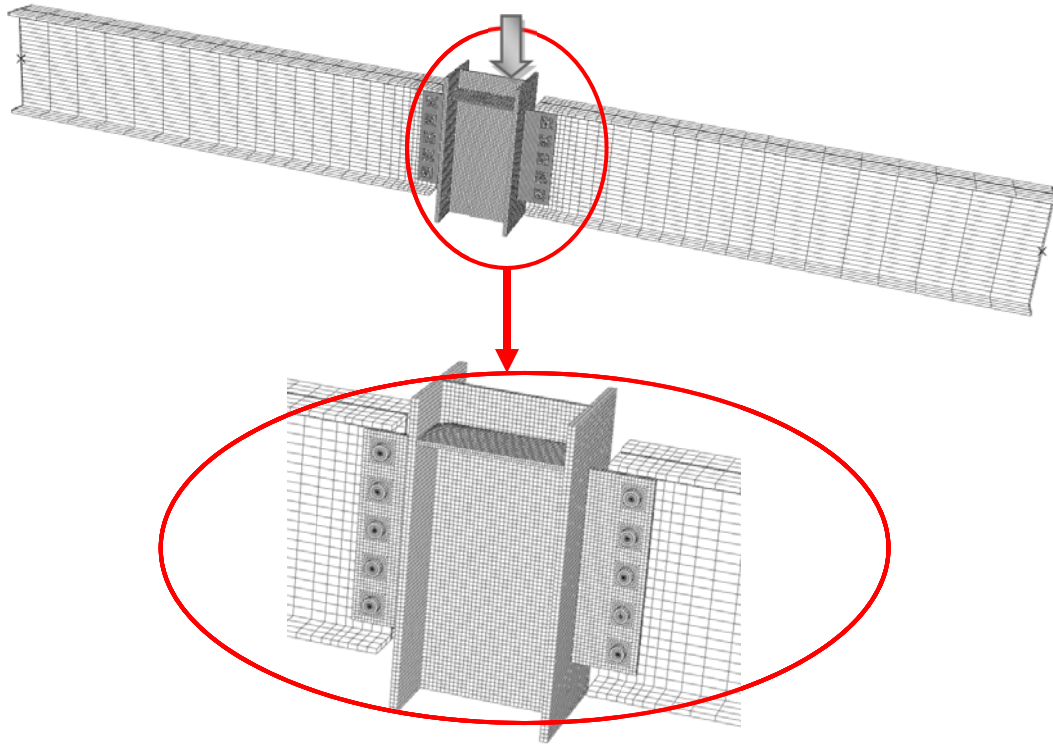


Figure 3.3: Finite element model of steel shear tab connection

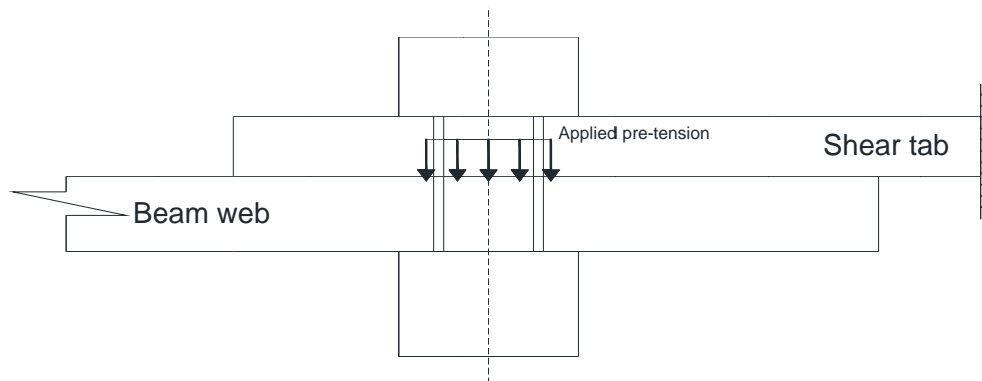


Figure 3.4: Applying bolt pretension

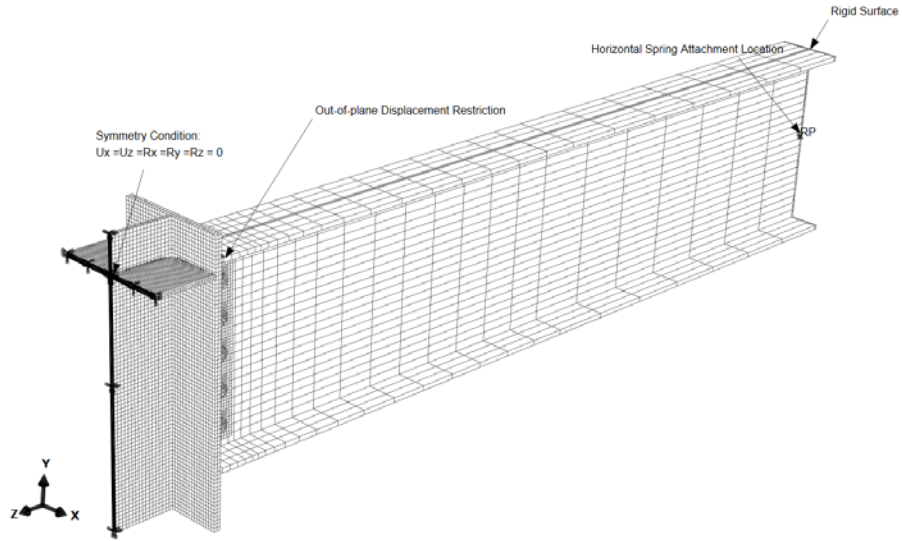


Figure 3.5: Symmetry constraint at the centerline of the stub column; rigid surface and horizontal spring at far end

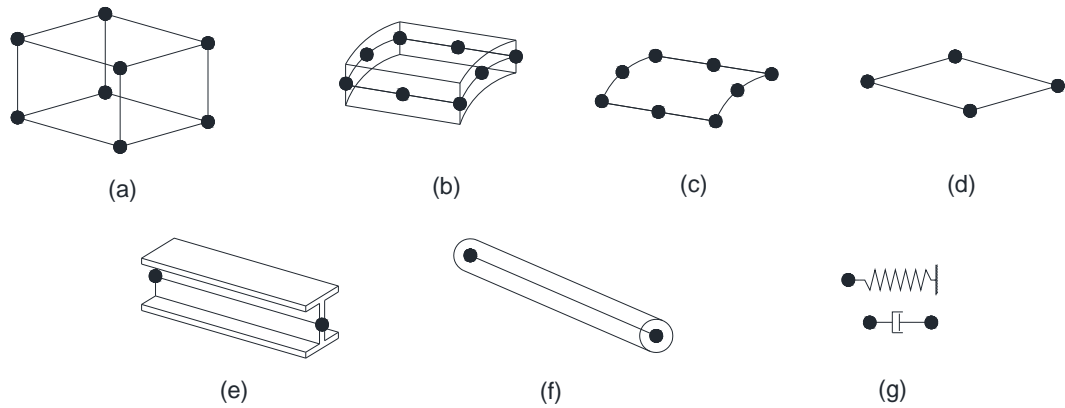


Figure 3.6: Structural elements in Abaqus/Standard (a) Continuum solid element (b) Shell element (c) Membrane element (d) Rigid element (e) Beam element (f) Truss element (g) Spring/dashpot (Dassault Systèmes 2009)

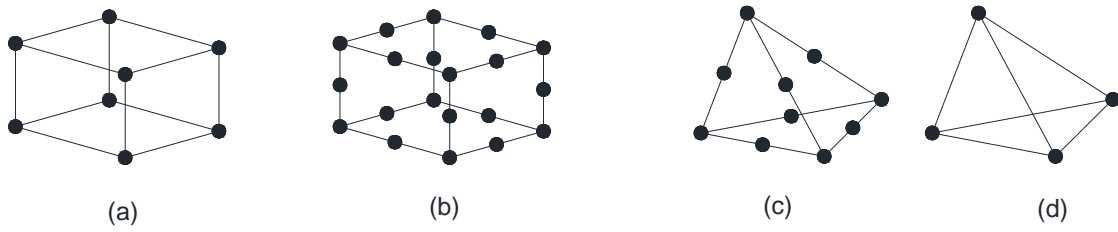


Figure 3.7: Continuum solid elements in Abaqus/Standard (a) Linear element (eight node brick, C3D8) (b) Quadratic element (twenty node brick, C3D20)(c) Modified second-order element (ten node tetrahedron, C3D10M) (d) Linear element (four node tetrahedron, C3D4) (Dassault Systèmes 2009)

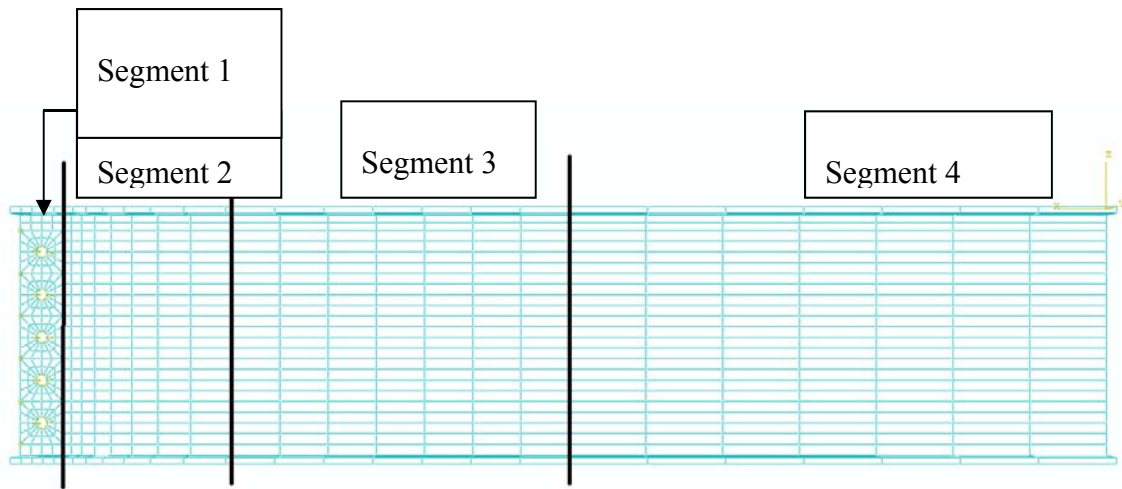


Figure 3.8: Mesh size in different segments of the beam

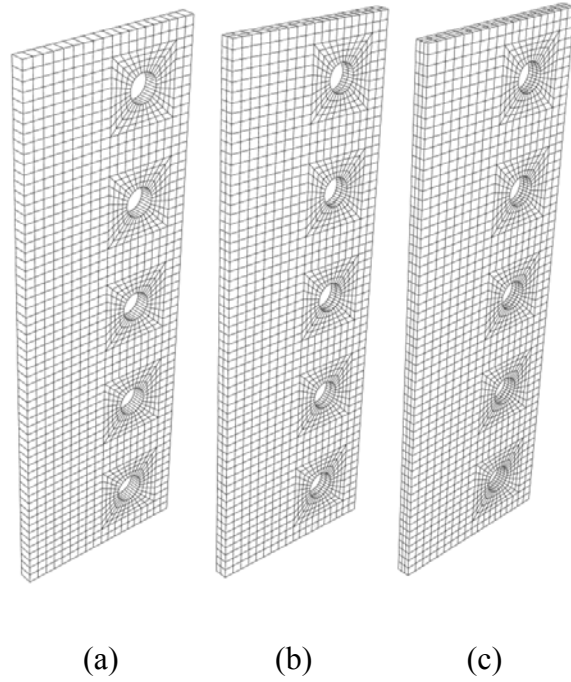


Figure 3.9: Mesh refinement across the thickness: (a) Coarse: one element in thickness; (b) Normal: two elements in thickness; (c) Fine: three elements in thickness

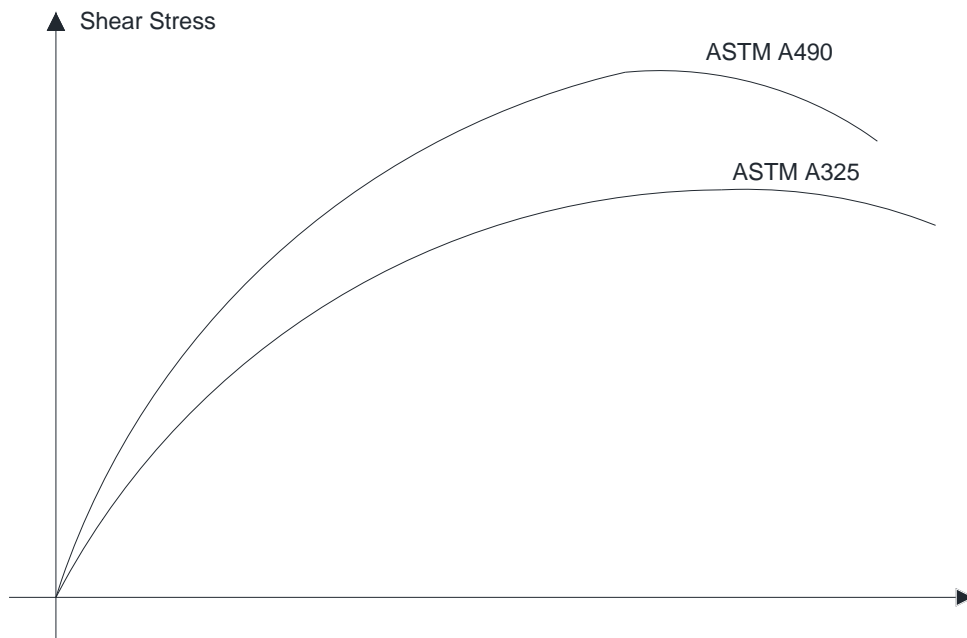


Figure 3.10: ASTM A325 versus ASTM A490 (Kulak et al. 2001)

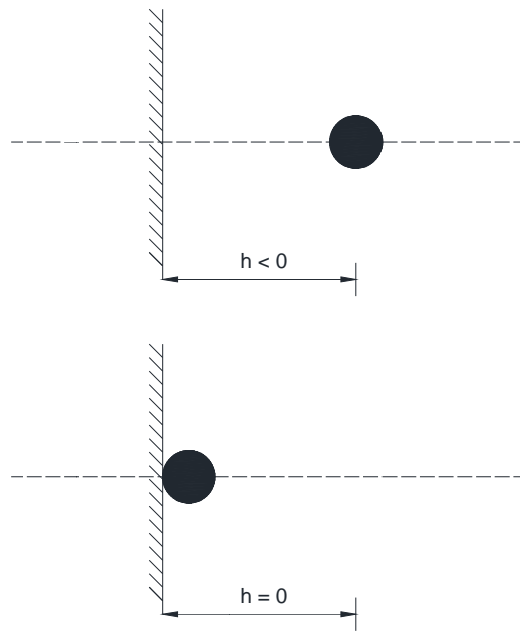


Figure 3.11: Contact definition (a) constraint not active (b) constraint activated (Dassault Systèmes 2011b)

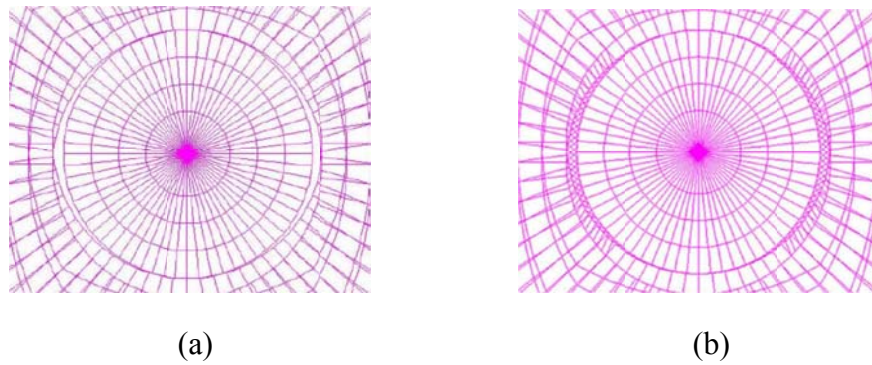
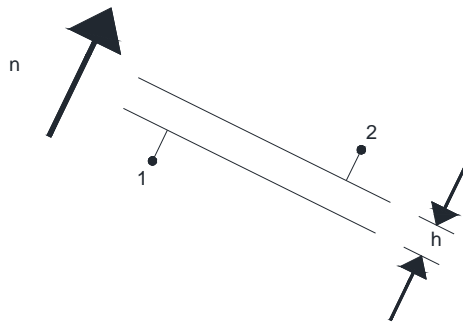
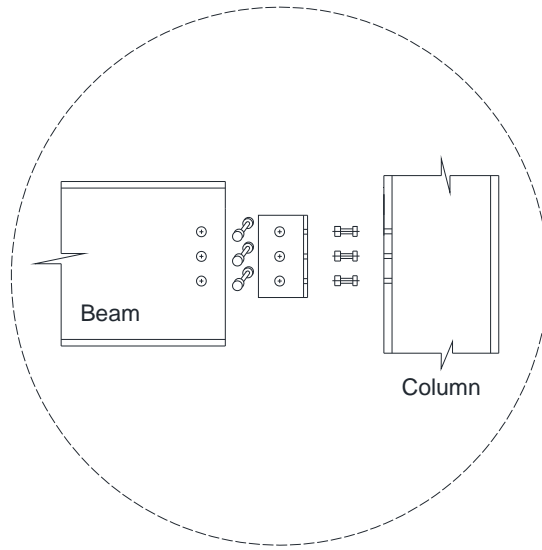


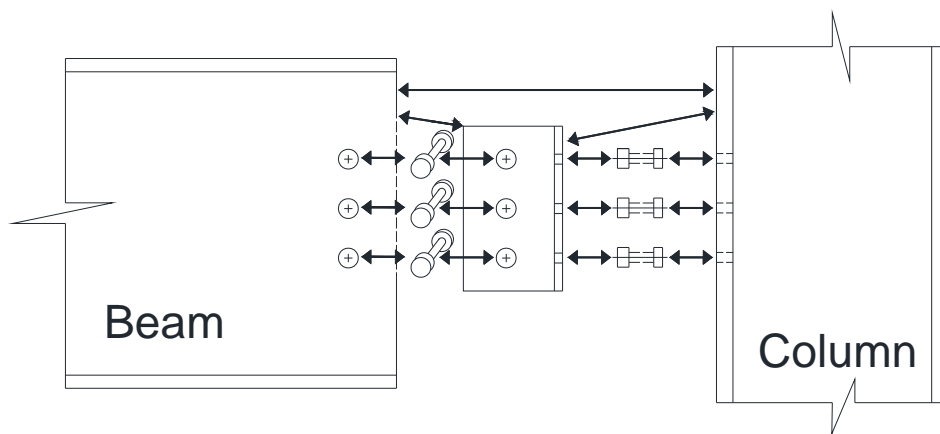
Figure 3.12: Bolt-hole interaction (Ashakul 2004) (a) before installation of GAP elements (b) after installation of GAP element



(a)



(b)



(c)

Figure 3.13: (a) Contact element (b) general contact (c) contact pair

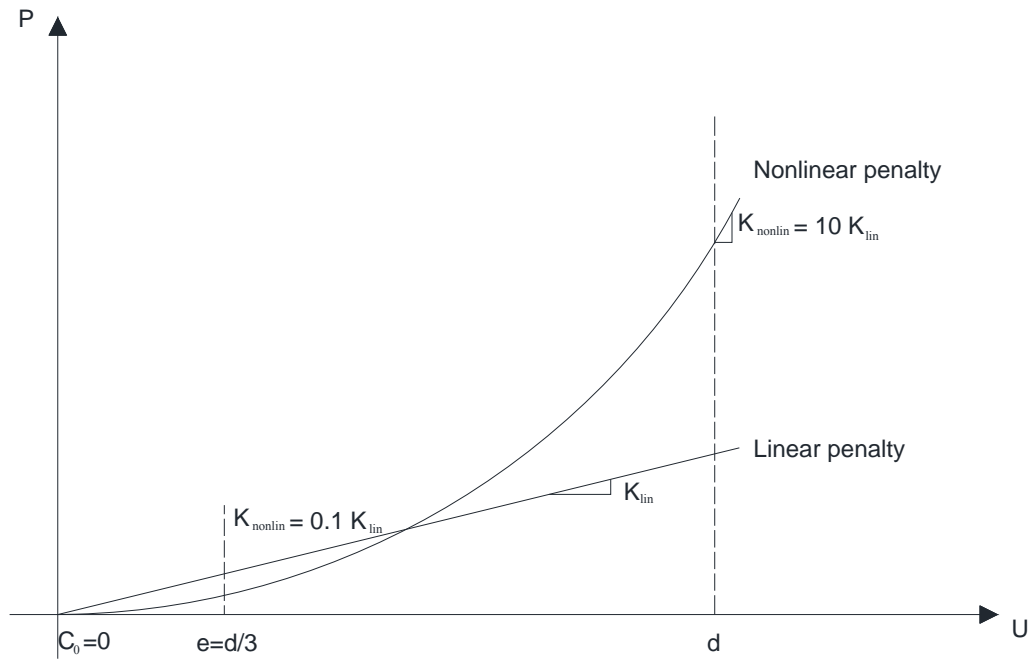


Figure 3.17: Penalty contact pressure–overclosure diagram: Linear versus nonlinear stiffness method

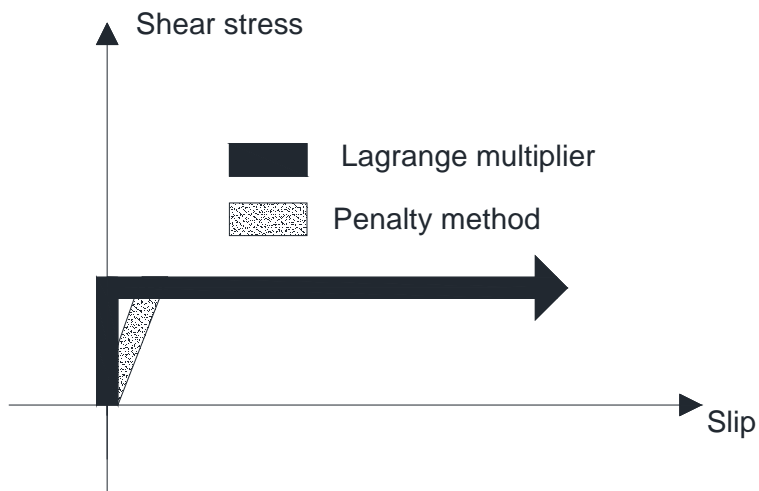


Figure 3.18: Contact pressure–penetration diagram: Lagrange multiplier versus penalty method (Dassault Systèmes 2011c)

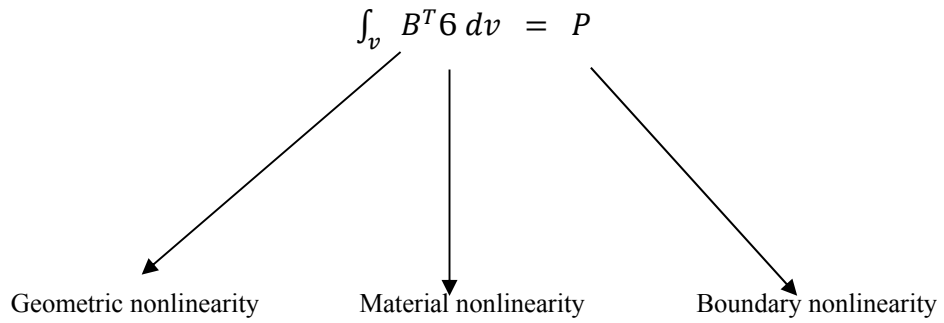


Figure 3.19: Sources of nonlinearity in the implicit formulation (Dassault Systèmes 2011c)

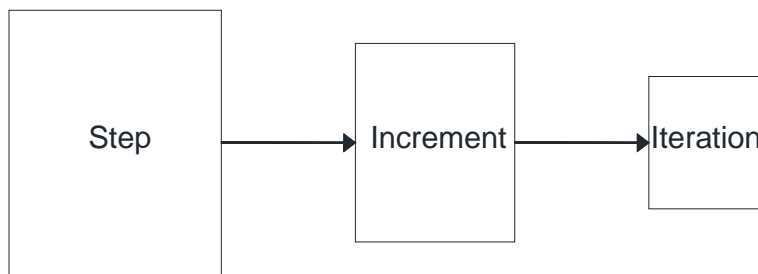


Figure 3.20: Step, increment and iteration definition in Newton–Raphson method

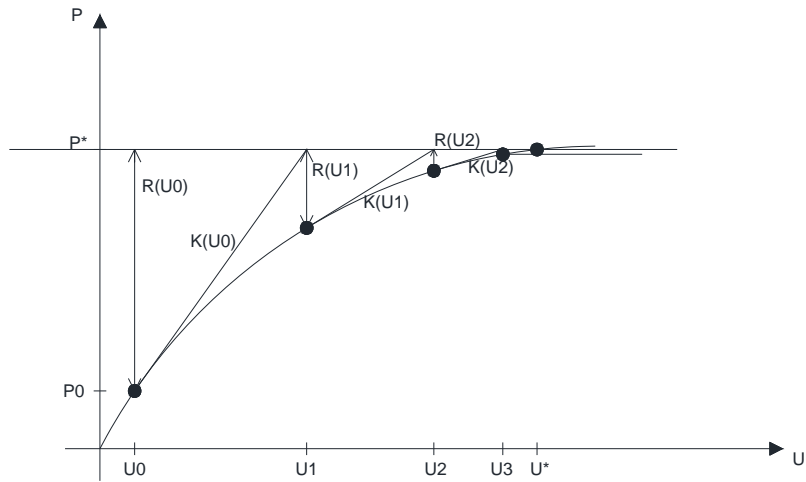


Figure 3.21: Newton–Raphson method diagram (Dassault Systèmes 2011c)

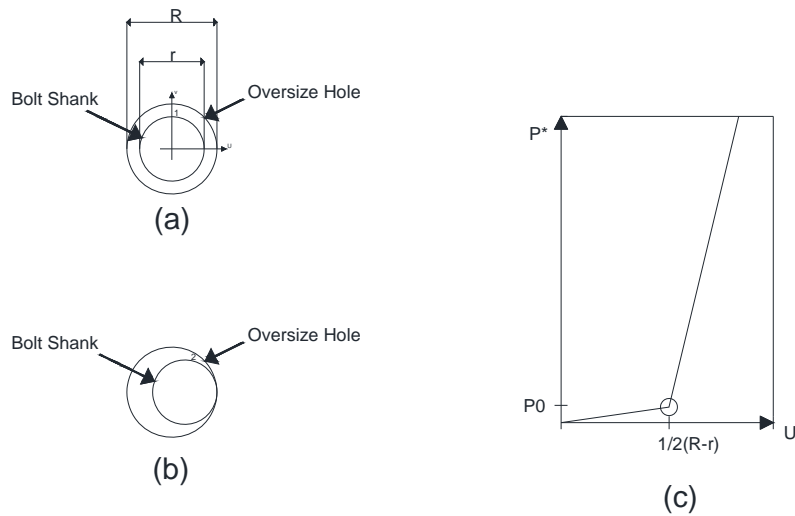


Figure 3.22: Severe discontinuity iteration (SDI) in the shank–hole interaction (a) undeformed (b) deformed (c) contact force versus displacement diagram

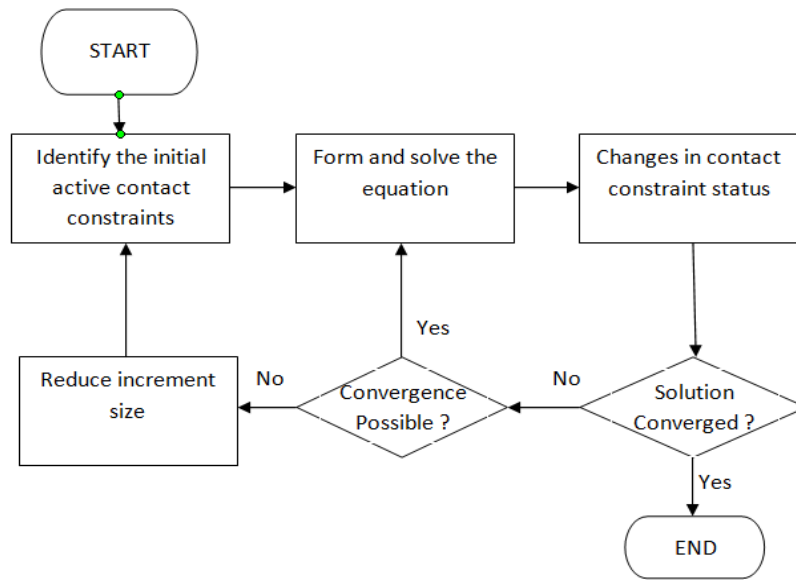


Figure 3.23: Solution flowchart for contact problem; severe discontinuity iterations (SDI) (Dassault Systèmes 2011c)

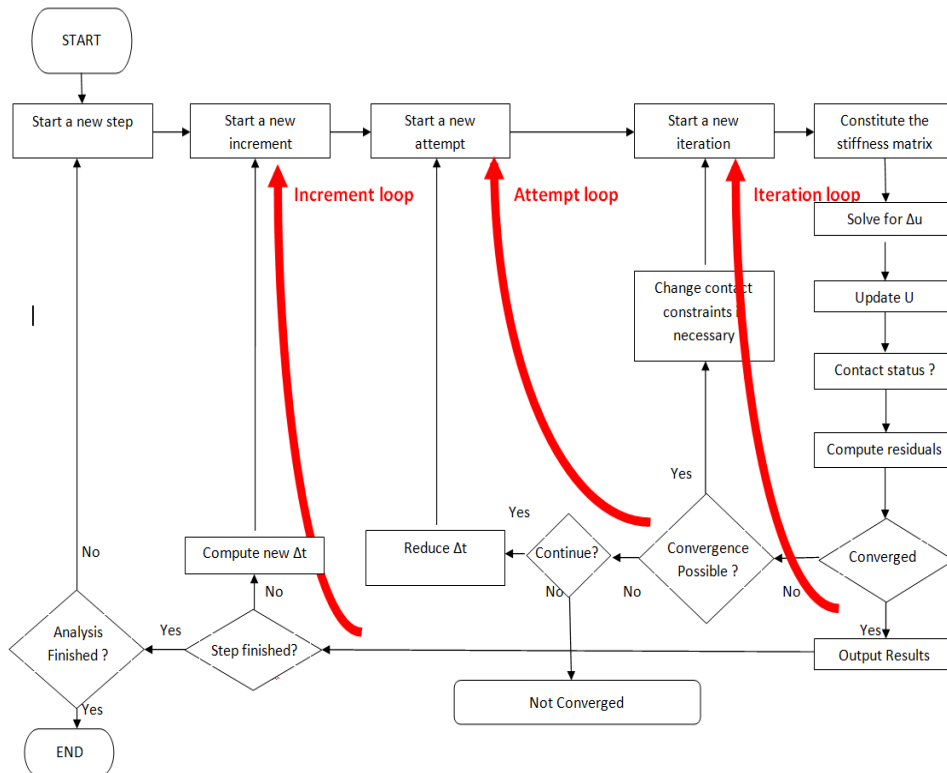


Figure 3.24: Solution flowchart for a nonlinear problem including contact (Dassault Systèmes 2011c)

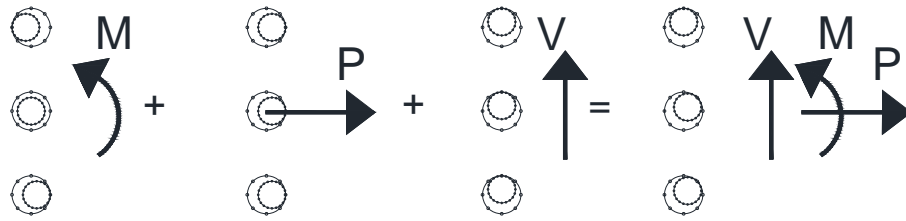


Figure 3.25: Bolted connection subjected to simultaneous moment, tension and shear loads

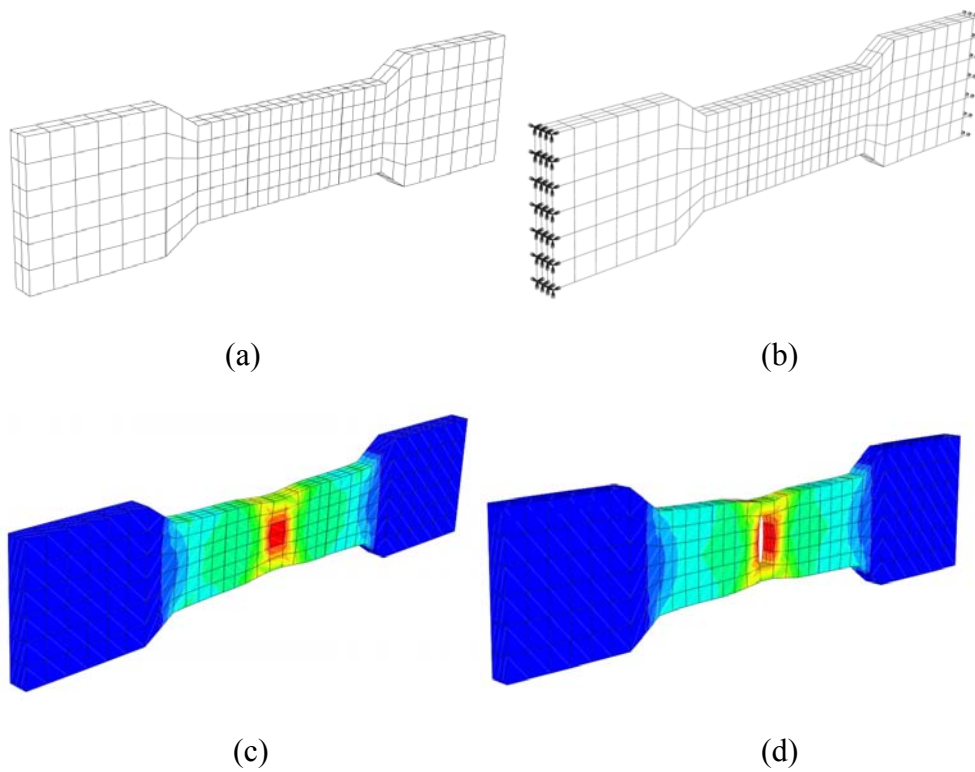


Figure 3.26: Tension coupon test (a) geometry and meshing (b) loading and boundary conditions (c) stress distribution before failure (d) element removal at $PEEQ=0.55$ to simulate initiation of rupture

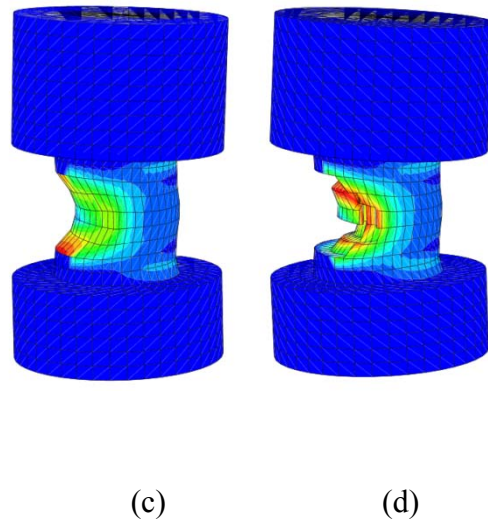
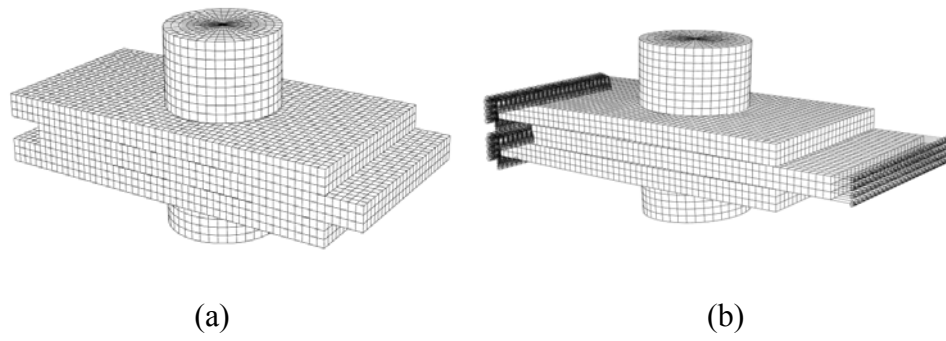


Figure 3.27: Numerical model of ASTM A325 bolts under shear loading (a) geometry and meshing (b) loading and boundary conditions (c) stress distribution before failure (d) element removal at $PEEQ=0.55$ to simulate initiation of rupture

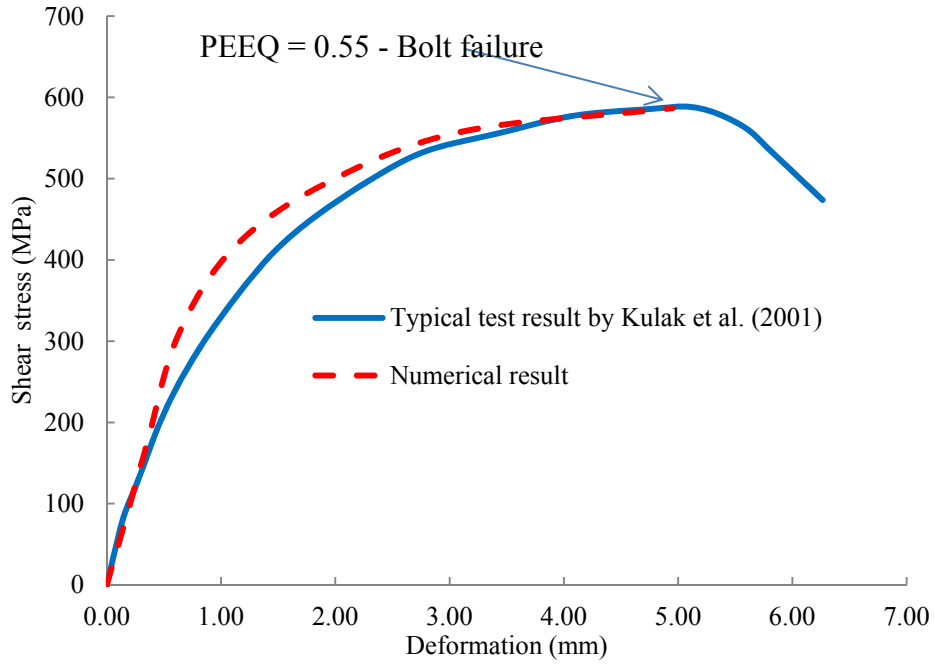


Figure 3.28: Numerical and experimental response of ASTM A325 bolt under shear loading

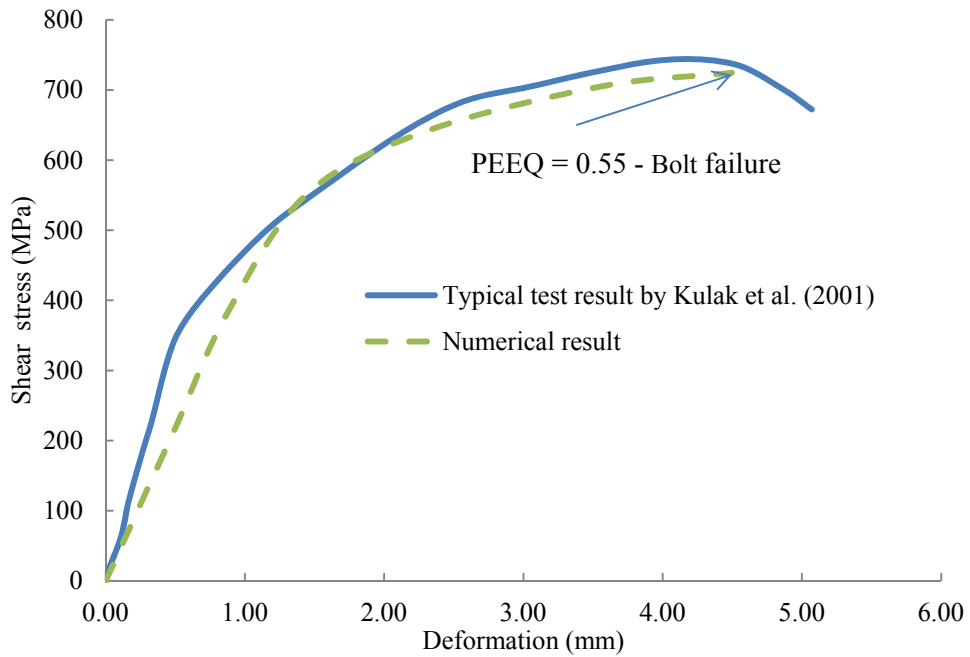


Figure 3.29: Numerical and experimental response of ASTM A490 bolt under shear loading

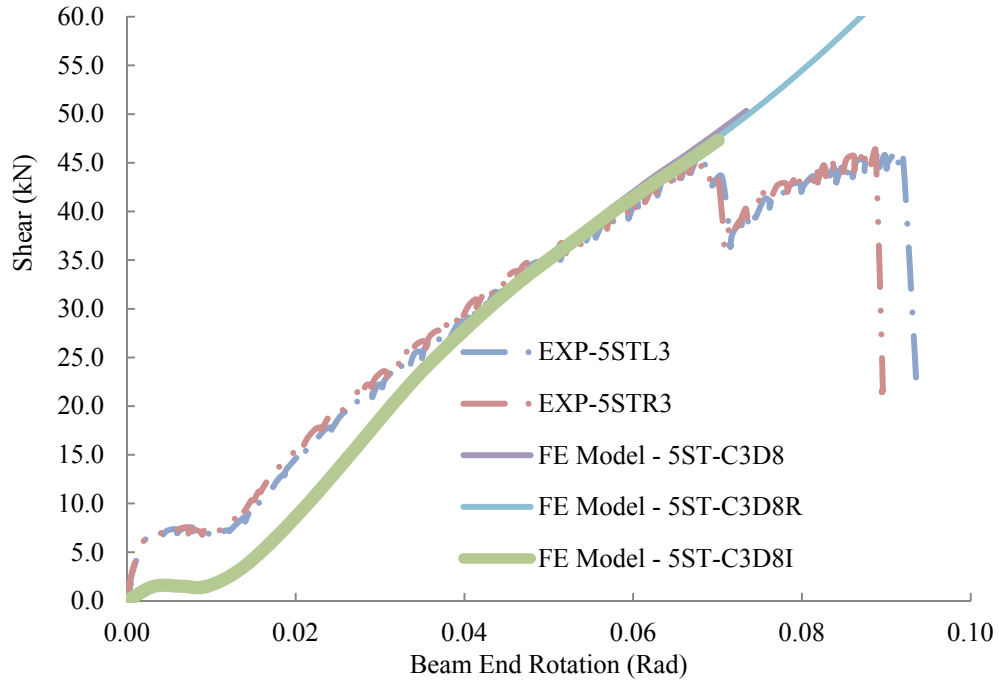


Figure 3.30: Shear force versus chord rotation curves at the bolt line; Experimental (Thompson 2009) and finite element results for different types of elements

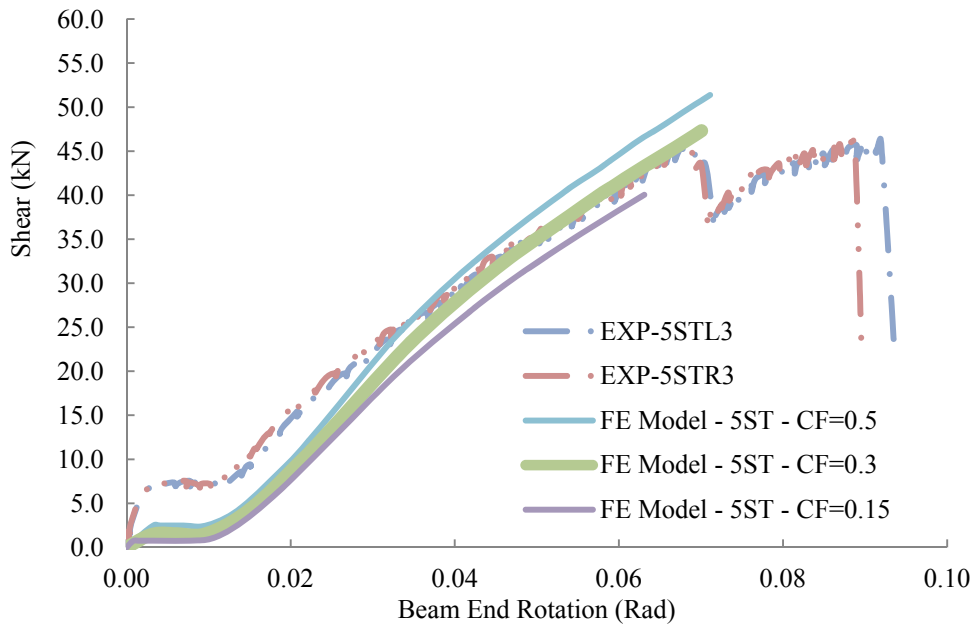


Figure 3.31: Shear force versus chord rotation curves at the bolt line; Experimental (Thompson 2009) and finite element results for different coefficients of friction

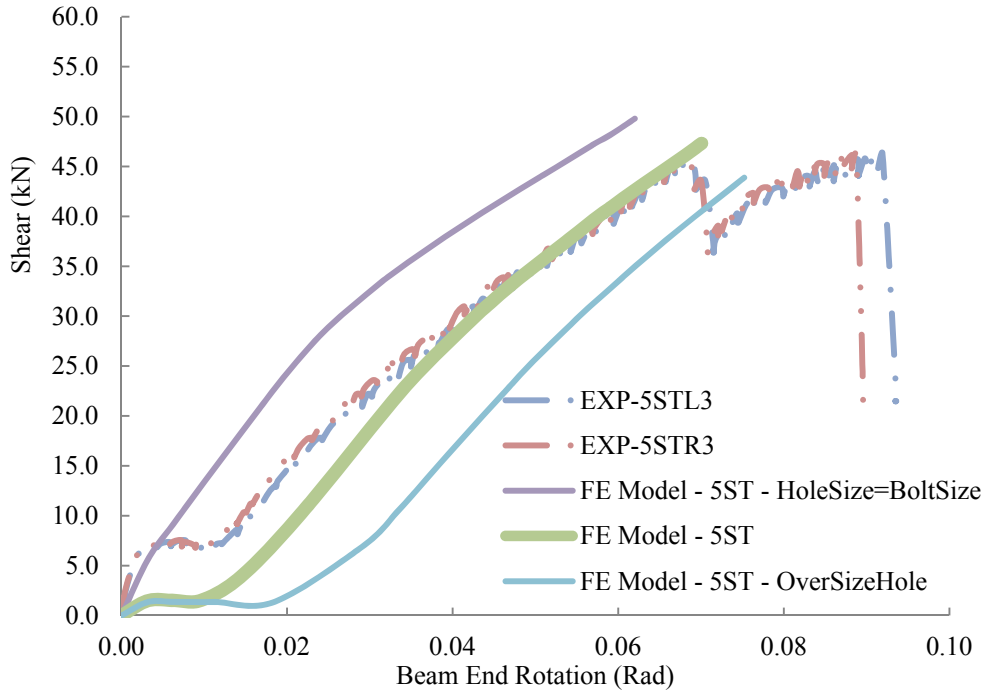


Figure 3.32: Shear force versus chord rotation curves at the bolt line; Experimental (Thompson 2009) and finite element results for different hole sizes

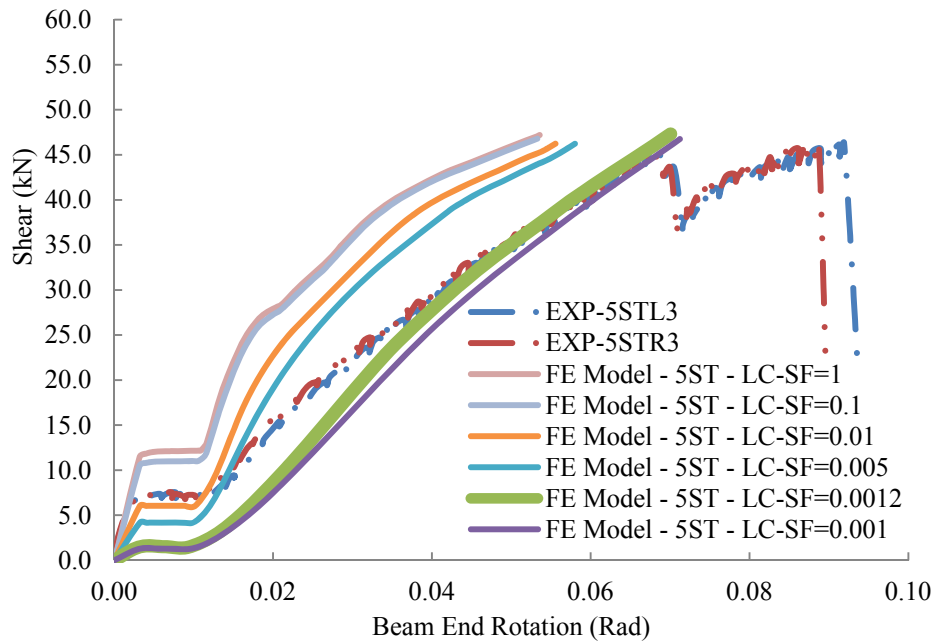


Figure 3.33: Shear force versus chord rotation curves at the bolt line; Experimental (Thompson 2009) and finite element results for different linear penalty stiffness scale factors

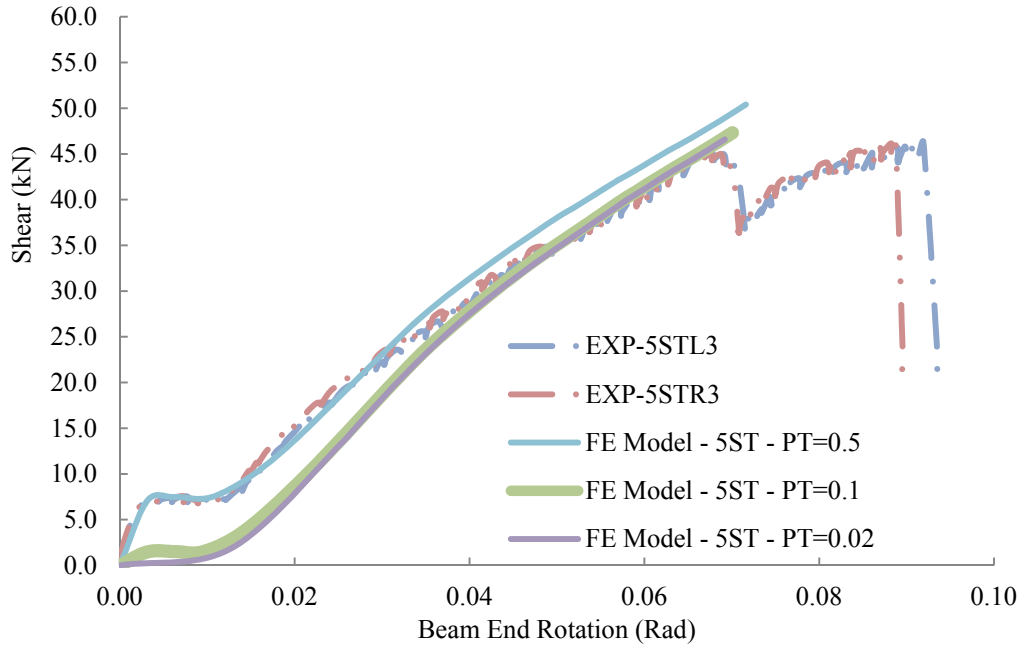


Figure 3.34: Shear force versus chord rotation curves at the bolt line; Experimental (Thompson 2009) and finite element results for different pretension displacement

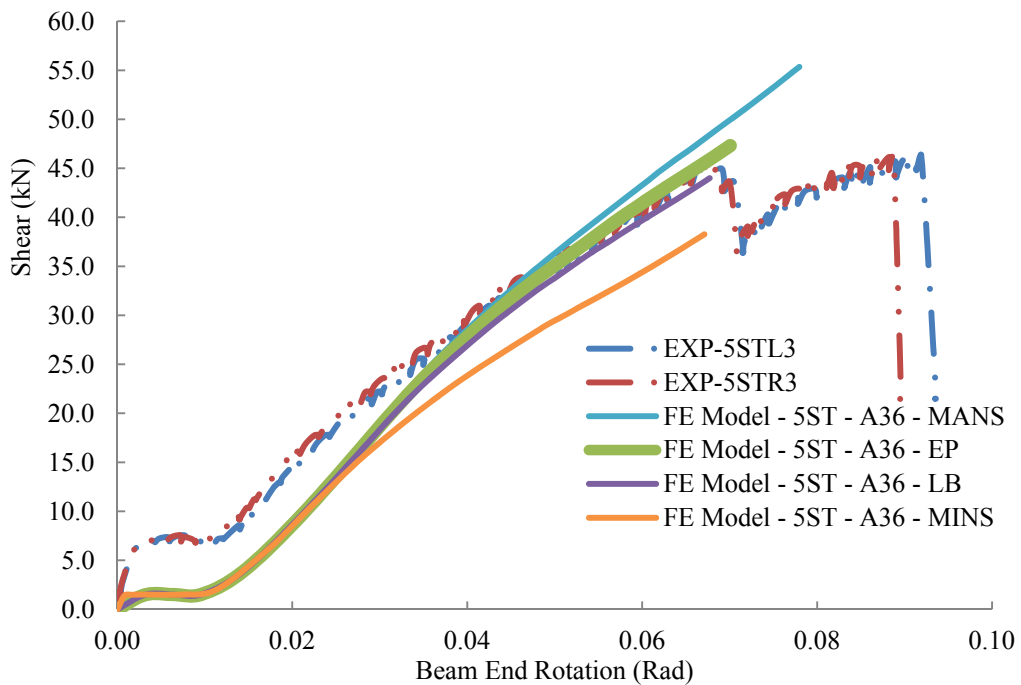


Figure 3.35: Shear force versus chord rotation curves at the bolt line; Experimental (Thompson 2009) and finite element results for different material properties

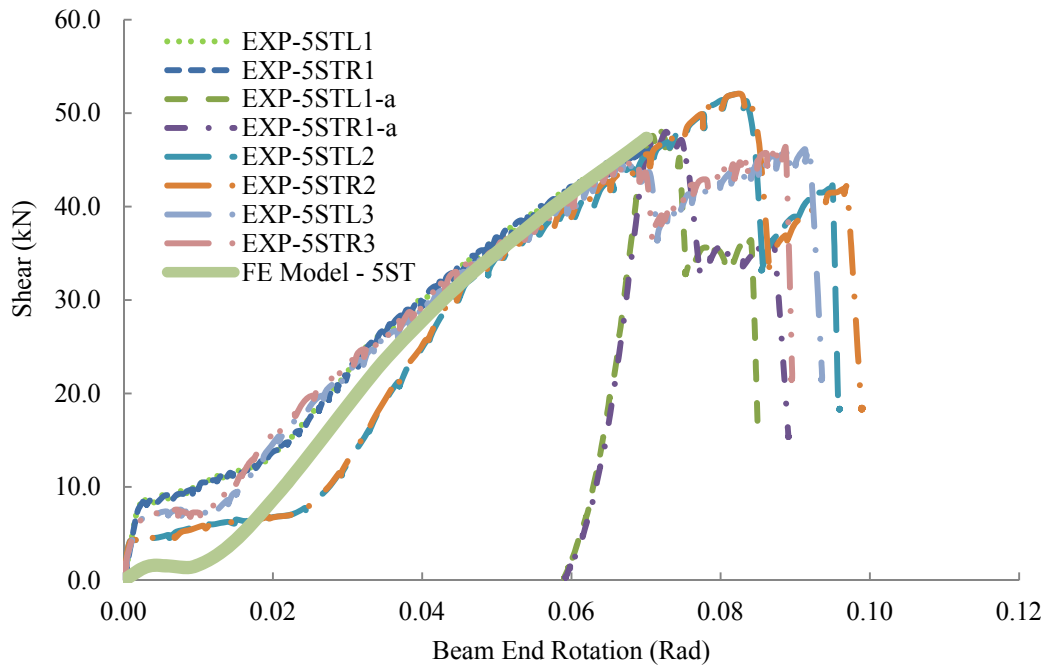


Figure 3.37: Shear force versus chord rotation curves at the bolt line; Experimental (Thompson 2009) and finite element results

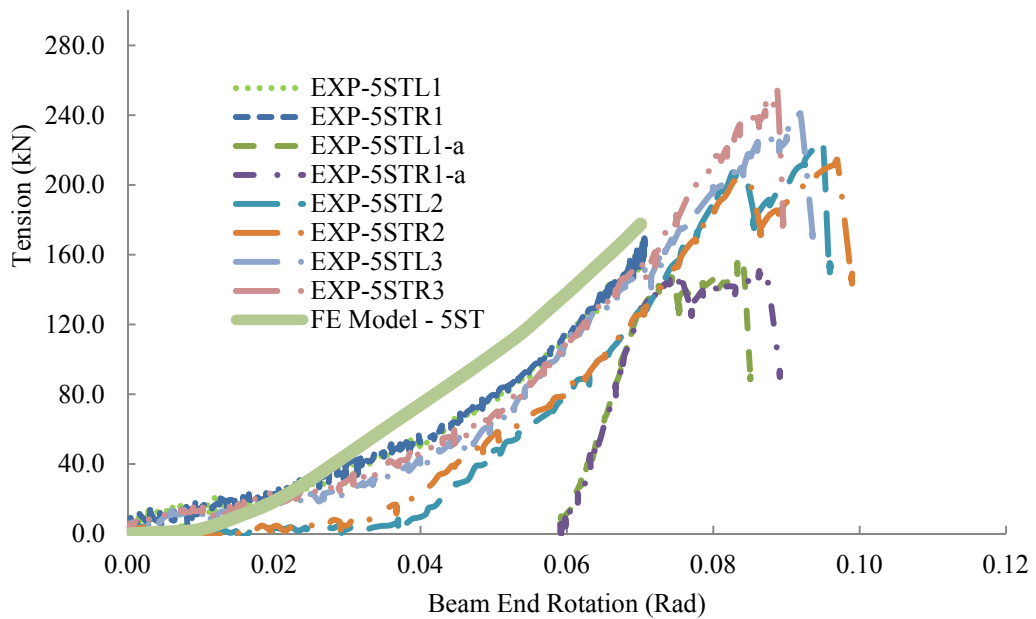


Figure 3.38: Axial force versus chord rotation curves at the bolt line; Experimental (Thompson 2009) and finite element results

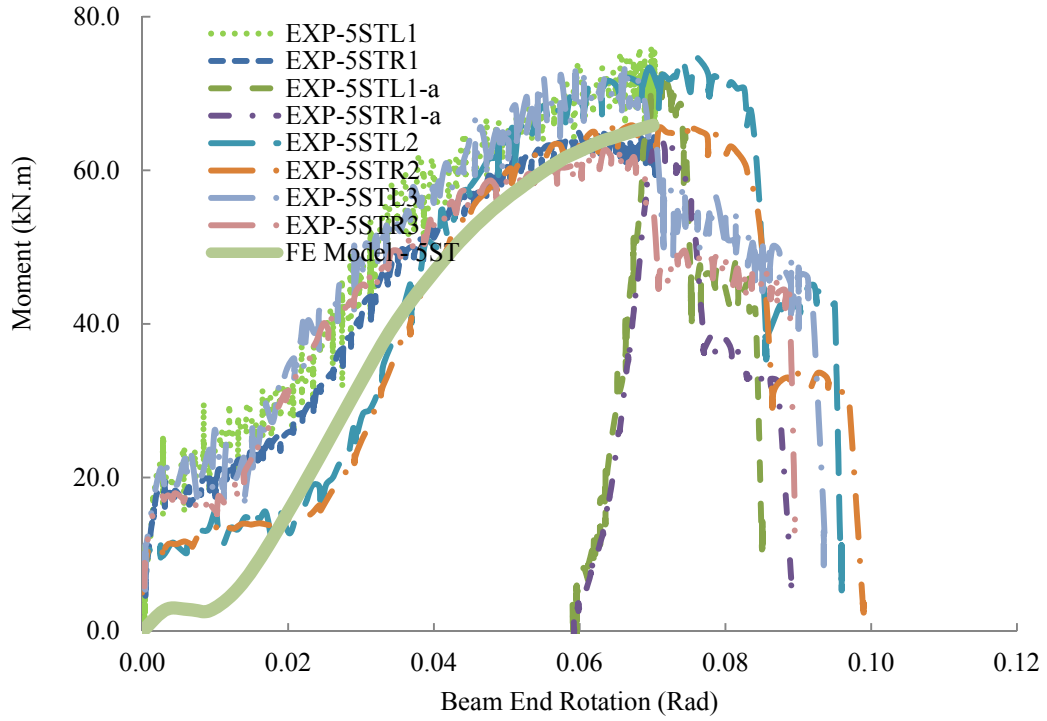


Figure 3.39: Moment versus chord rotation curves at the bolt line; Experimental (Thompson 2009) and finite element results

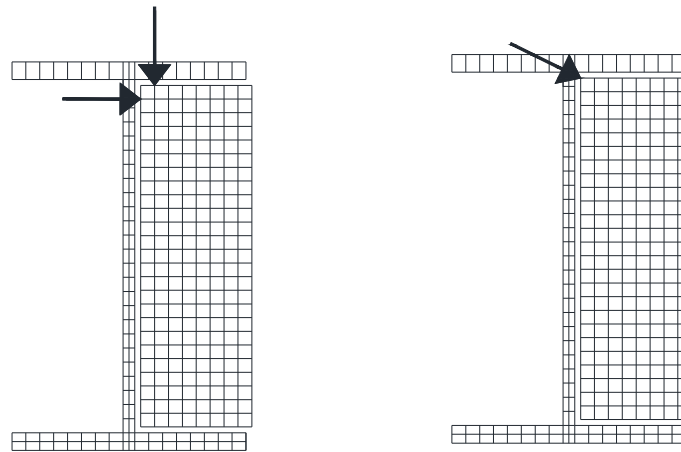


Figure 3.40: Convergence difficulties at the corners (a) S-to-S (b) N-to-S

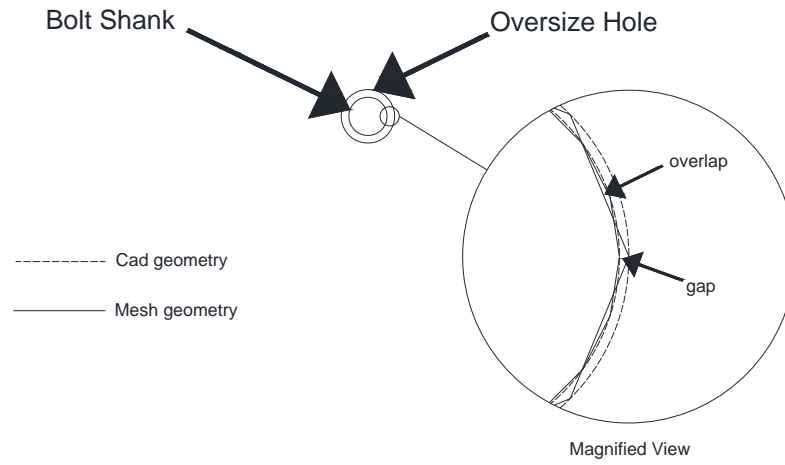


Figure 3.41: Actual geometry versus faceted geometry

4 Compressive Arching and Tensile Catenary Action in Steel Shear Connections under Column Removal Scenario

4.1 Introduction

Although the behaviour of many types of shear connection under conventional gravity loading has been established through research, their response to a column removal scenario is still relatively unknown. It is widely believed that beams adjacent to a lost column will develop cable-like tensile action, as illustrated schematically in Figure 4.1. In frames with shear connections, this requires the connections to continue to transfer shear forces, in addition to developing tensile catenary forces under large rotations. This tensile resistance can provide an alternative load path in a column removal scenario. In essence, structural collapse can be arrested following localized damage to a column if the adjacent shear connections can sustain sufficiently large rotations and tensile forces through catenary action.

In this research, the development of compressive arching action followed by tensile catenary action is investigated. It is shown that in a column removal scenario the connection may develop a considerable axial compressive force at small beam rotations before catenary action develops, as shown in Figure 4.2. This compressive force has typically been neglected in previous assessments of connection robustness.

After a brief review of the literature related to the axial response of steel shear connections in a column removal scenario, finite element analysis results of bolted steel connection assemblies, considering material, geometric and contact nonlinearities are presented. The models were verified using the available column

loss experiments performed on shear connections. A simplified analytical model is presented and compared to the observed axial response of the connections.

4.2 Literature survey

Girhammar (1980) appears to be the first researcher to acknowledge the presence of compressive arching action in steel assemblies in a column removal scenario. He conducted column-loss experiments on two types of bolted beam-to-column connections: seated “heel” connections and end-plate connections. Figure 4.3(a) shows a schematic view of the test assembly and the idealized axial response of the connection. Based on this study, end plate connections, as an example of a semi-rigid connection, exhibited three distinct response phases in a column removal scenario: arching, bending, and catenary actions. An equation was proposed for the compressive arching force based on the beam section properties, the moments at the ends, the connection eccentricity (discussed in section 4.3), and the horizontal play in the connection assembly (Girhammar 1980).

Izzuddin et al. (2008) proposed a simplified model for nonlinear static response of a beam, applicable to a column removal scenario, including connection response and external axial restraint (Figure 4.3(b)). For partially-restrained connections, special attention was drawn to the centre of rotation of the connection, which influenced the development of compressive arching (Izzuddin et al. 2008). The authors concluded that although this arching action was not of primary importance to connection design, it could enhance the nonlinear response of the beam assembly in a column loss event, especially with respect to dynamic load carrying capacity (Izzuddin et al. 2008).

Astaneh (2007) also discussed the progressive collapse resistance of steel frames with simple shear connections. An analogy of a three-hinged beam subjected to a concentrated load at mid-span—a classical problem discussed by Timoshenko (1955)—was used in order to simplify the problem of the loss of the middle column. Figure 4.3(c) shows the conceptual model and the idealized axial response of the connection. He also suggested a method to determine the catenary force and ultimate rotational capacity of the connection that can be utilized for design. However, the possibility of an axial compressive force developing in the shear connection was not discussed.

4.3 Axial response of steel connection in column removal scenario

The overall geometry of a symmetric two-bay frame with the central column removed is shown in Figure 4.4. The case considered includes flexible shear connections made up of seat and top angles. These connections tend to rotate about points at different elevations at the two beam ends, separated by an eccentricity, e_v . The “unrestrained path of motion” in the figure shows that if rotation were to occur about the points at the remaining columns, the points at the removed column (if unrestrained) would initially move towards each other at small beam rotations because of this eccentricity. Since the condition of symmetry restrains the central column to move vertically, a compressive “arch” (two compressive struts) forms. At larger beam rotations, catenary tension is developed as the unrestrained paths of motion of the two beams diverge (Daneshvar et al. 2012).

As seen in Figure 4.4, the axial shortening of the beam and connection at the early stage of the column removal scenario, which causes the compressive force, is very small in comparison with the vertical displacement of the severed column. In a

real structure or test assembly, this small deformation may be accommodated by bolt slippage or flexibility of the surrounding structure. In order to simplify the problem and focus on just one detailed connection, the test setup shown in Figure 4.5 is selected. In this connection assembly, the beams are cut at the inflection point; and far ends are substituted by true pin connections. A verified high-fidelity finite element model is used as a tool to monitor the response of shear connection assemblies in a column removal scenario as arching action forms. The model development is discussed in section 4.3.1. The analytical approach used to study arching behaviour in a column removal scenario is explained in section 4.3.2.

4.3.1 Numerical approach

Shear tab, WT and single angle connections have been selected for the finite element modelling due to the availability of suitable experimental data. The procedure and results can be extended to other types of shear connection, such as seated angle connections. Pre- and post-processing procedures were completed using Abaqus/CAE, and Abaqus/standard was used as the analysis engine (Systèmes Dassault 2009). Experiments performed by Thompson (2009), Friedman (2009) and Johnston (2009) were used to verify the results of the numerical models. A total of nine full-scale tests were carried out, keeping the connection depth (number of bolts) as the sole variable. The geometric properties of the test specimens are summarized in Table 4.1 to Table 4.3.

Three, four and five bolt shear tab, WT and single angle connections were modelled. Models consist of the central column and the adjacent beams, as well as the connections with complete detailing. Figure 4.6 shows the finite element models of shear tab connections, as an example. Shear tabs are welded to the column flange and bolted to the beam web. The central column is pushed down, while the connection performance is monitored. It is assumed that the welds are

flawless and of greater strength than the base material; therefore, the shear tab was tied directly to the flange of the column stub. This idealization was confirmed to be appropriate, since the strain in the vicinity of the weld line did not exceed the weld's rupture strain. (In addition, no weld rupture was reported from the experiments.)

Steel properties were not reported for the test specimens, so based on the identified steel grades (ASTM A36 for the shear tabs and ASTM A992 for the rolled sections), the material strengths were estimated using the nominal values multiplied by industry-established strength increase factors (GSA 2003). For the ASTM A325 bolts, an appropriate value of the strength increase factor was selected based on previous tests on bolts of the same grade. Pins at the inflection points were simulated by applying a rigid plate across the beam cross-section that is permitted to rotate about the beam's bending axis, and invoking a horizontal linear axial spring with a stiffness of 100 kN/mm to approximate the combined effects of the flexibility of the test setup and any slippage or deformation at the far-end pin supports. All other characteristic features of the numerical models, including contact behaviour, element types, and failure criteria, are presented in chapter 3. The 5ST connection used in this chapter is the same connection detail discussed in chapter 3 as a benchmark example. Good agreement of the numerical simulation and experimental results provides confidence to use the same principles for other types of shear connections.

Figure 4.7 to Figure 4.9 show the axial responses of connections 3ST, 4ST and 5ST, respectively, in the column removal scenario. Axial responses of 3WT, 4WT and 5WT are illustrated in Figure 4.10 to Figure 4.12. Figure 4.13 to Figure 4.15 show the same curves for 3SA, 4SA and 5SA. The figures show that the numerical model predicts the ultimate axial capacity of the connections well; however, there are some discrepancies in the axial load path. The magnitude of

arching action that formed during the experiments is less than what was observed in the simulation. The reason is that the accumulation of axial compression is sensitive to the axial restraint provided to the beams at the ends away from the lost column support, so any inaccuracies in the stiffness of the spring used in the model to represent the flexibility of the reaction frame and bolt slippage could cause the magnitudes of the compressive forces measured in the laboratory experiments to be different from those observed in the finite element results.

Connections with three bolts (3ST, 3WT and 3SA), which have the greatest vertical eccentricity because the connecting parts are positioned farthest from the central beam axis where the far-end pin was located in the tests, exhibit the greatest compressive arching forces. As the connection eccentricity decreases, the arching action decreases as well, which leads to almost no compressive force in connections 5ST and 5WT (which have no eccentricity because the shear tab and WT are centered on the beam axis), as shown in Figure 4.9 and Figure 4.12. The behaviour of the SA connections is a little different due to more flexibility of the angle in comparison with the plate and WT. The center of rotation of 5SA tends to move up towards the top of the connection. As a result, even in 5SA, vertical eccentricity exists and arching action forms, as shown in Figure 4.15.

4.3.2 Analytical approach

Simplified analytical calculations based on compatibility of displacements can be used to estimate the total axial deformation, Δ_{Axial} , that accumulates between the beam supports as a function of the chord rotation, θ , in a column removal scenario. If the horizontal restraint at the “remaining” column is not infinitely stiff due to the flexibility of the surrounding structure, displacement of the support point is included in this total deformation (Daneshvar et al. 2012).

The magnitude of Δ_{Axial} (measured along the axis of the beam between horizontally fixed reference points at the original column face locations) can be decomposed into two components: Δ_1 (resulting from the vertical motion downwards at the removed column), and Δ_2 (resulting from the eccentricity of the centres of rotation of the two connections). The geometries of these two components for the case of a seat and top angle are shown in Figure 4.16(a) and (b), and the combined effect is solved in Equation (4-1). At small rotations, the second (compressive) term, Δ_2 , tends to be dominant; at larger rotations, the first (tensile) term, Δ_1 , dominates the total axial deformation and leads to catenary action. Short span lengths and large centre of rotation eccentricities increase the dominance of arching action at small rotations. In the absence of such an eccentricity, catenary tension develops immediately following the column removal (Daneshvar et al. 2012).

shows potential components of the total axial deformation, Δ_{Axial} , where deformation contributing to the elongation of the system is taken as positive. The first term, $\Delta_{Connection}$, includes the total axial deformation of the connections at each end of the beam due to bolt slip, bolt deformation, and deformation of the connecting elements (typically, a plate or angles). Axial deformation of the beam, Δ_{Beam} , is typically much smaller than the connection deformation, since the beam tends to remain elastic for the case of shear connections. The deformation of the surrounding structure, $\Delta_{Restraint}$, also contributes to the total axial deformation in the system (Daneshvar et al. 2012).

$$\Delta_{Axial} = \Delta_1 - \Delta_2 = L \left(\frac{1}{\cos \theta} - 1 \right) - e_v \tan \theta \quad (4-1)$$

$$\Delta_{Axial} = \Delta_{Connection} + \Delta_{Beam} + \Delta_{Restraint} \quad (4-2)$$

Applying Equation (4-1) and to the shear tab connection models in Figure 4.6 leads to the results presented in section 4.4.

4.4 Results

Figure 4.17 demonstrates good agreement between the axial deformations from the finite element models of the test assemblies shown in Figure 4.6 and those calculated using Equation (4-1) and Equation (4-2). Figure 4.18 shows the effect of the boundary condition on the axial response of the connection assembly based on the finite element model. K_{a-str} is the stiffness of the springs at the far ends of the beam assembly that represents the stiffness of the test setup or surrounding structure in the experiment or the real structure, respectively. As demonstrated in Figure 4.18, the axial response of the shear connection, in the phases of both arch and catenary action, are highly dependent on the stiffness of surrounding structure. In this research, K_{a-str} is assumed equals to 100 kN/mm to be a realistic value based on the approximate dimensions and section sizes of the test setup. For comparison, a one-bay portal frame with W610X217 columns, a W460X52 beam and 3 m in height possesses an approximate lateral stiffness of 100 kN/mm. K_{a-str} equal to 10 kN/mm and 1000 kN/mm represent two extremes for lateral stiffness of stories in elastic frames, manifesting flexible and stiff storeys, respectively.

4.5 Conclusion

The following conclusions can be drawn from the discussion in chapter 4:

- In a column removal scenario, considerable axial compressive force may develop via arching action before catenary action begins. This phenomenon has been simulated numerically and the results show that the

vertical eccentricity between the centres of rotations of the connections at the ends of a beam is a primary parameter leading to the presence of this compressive force.

- Another important factor that affects the development of arching action is the stiffness of the surrounding structure. Whether the arching action forms in the connection assembly or not, the catenary resistance of the connection can act as an alternative load path in a column loss event.
- Since the arching action might occur at an early stage of connection response, it will not affect the ultimate capacity of the frame. Therefore, tensile catenary action is still the reliable alternative load path in response to a column removal scenario, and therefore the connection must be designed to resist these tensile loads.
- Good correlation of force–rotation curves obtained from the finite element model was achieved with those obtained from the tests in the tensile regime. However, there are some discrepancies in the magnitude of compression experienced during arching action. Finite element modelling could capture the arching action phase more precisely if the restraint at the beam's far ends in the experiments were known accurately. Good agreement between the results of analytical and numerical methods is also observed.
- Although the acknowledgement of the presence of compressive arching action as a part of axial response of shear connections in the column removal scenario is important, it is unlikely to enhance the connection performance to assist in bridging over the localized damage. As a result, its magnitude is not the point of concern in this research. Hence, the tensile part of axial behaviour of shear connections as an active alternative path load is reported in the remaining chapters.

Table 4.1: Geometric properties of ST test specimens (Thompson 2009)

No.	Specimen Label	Plate Type	Plate thickness (mm)	Bolt Type	Bolt diameter (mm)	Beam size	Column size
1	3ST	ASTM A36	9.5	ASTM A325	19.1	W460X52	W310X79
2	4ST	ASTM A36	9.5	ASTM A325	19.1	W460X52	W310X79
3	5ST	ASTM A36	9.5	ASTM A325	19.1	W460X52	W310X79

Table 4.2: Geometric properties of WT test specimens (Friedman 2009)

No.	Specimen Label	WT Type	WT Section	Bolt Type	Bolt diameter (mm)	Beam size	Column size
1	3WT	ASTM A992	WT125X33.5	ASTM A325	19.1	W460X52	W310X79
2	4WT	ASTM A992	WT125X33.5	ASTM A325	19.1	W460X52	W310X79
3	5WT	ASTM A992	WT125X33.5	ASTM A325	19.1	W460X52	W310X79

Table 4.3: Geometric properties of SA test specimens (Johnson 2009)

No.	Specimen Label	Angle Type	Angle Section	Bolt Type	Bolt diameter (mm)	Beam size	Column size
1	3SA	ASTM A36	L152X89X9.5	ASTM A325	19.1	W460X52	W310X79
7	4SA	ASTM A36	L152X89X9.5	ASTM A325	19.1	W460X52	W310X79
13	5SA	ASTM A36	L152X89X9.5	ASTM A325	19.1	W460X52	W310X79

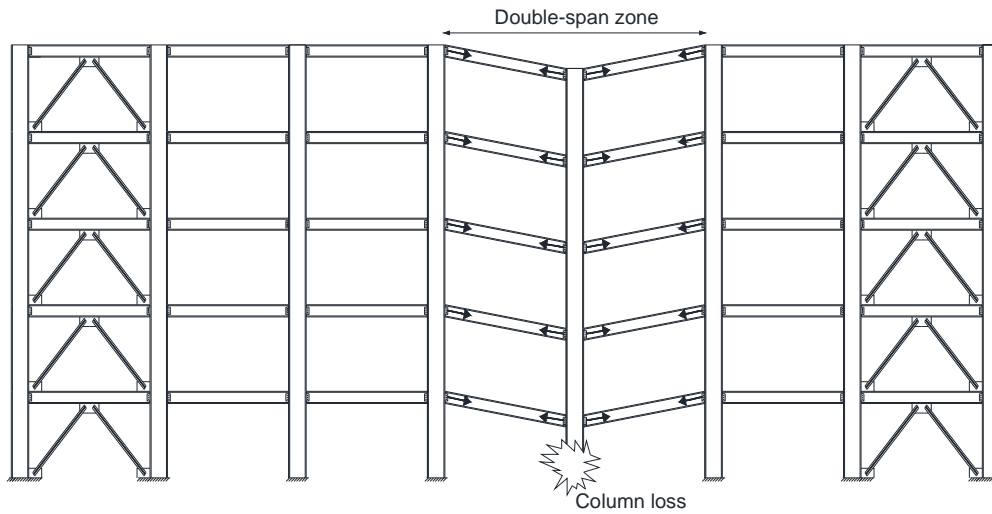
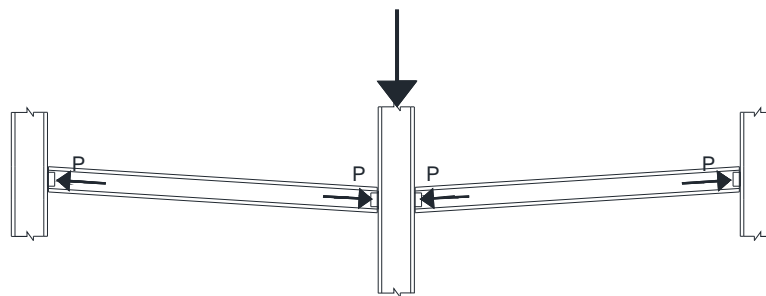
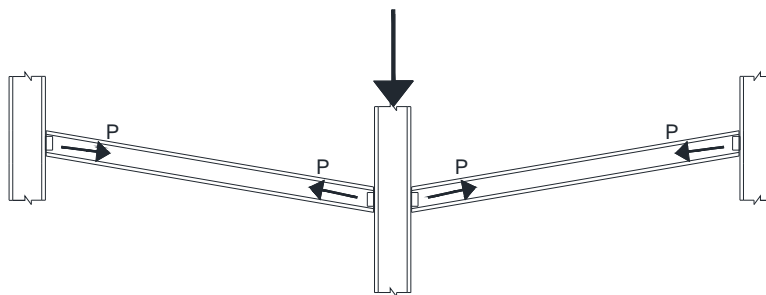


Figure 4.1: Axial response of a gravity framing system after column removal



(a)



(b)

Figure 4.2: (a) Compressive arching action accompanied by (b) tensile catenary response of a gravity framing system after column removal

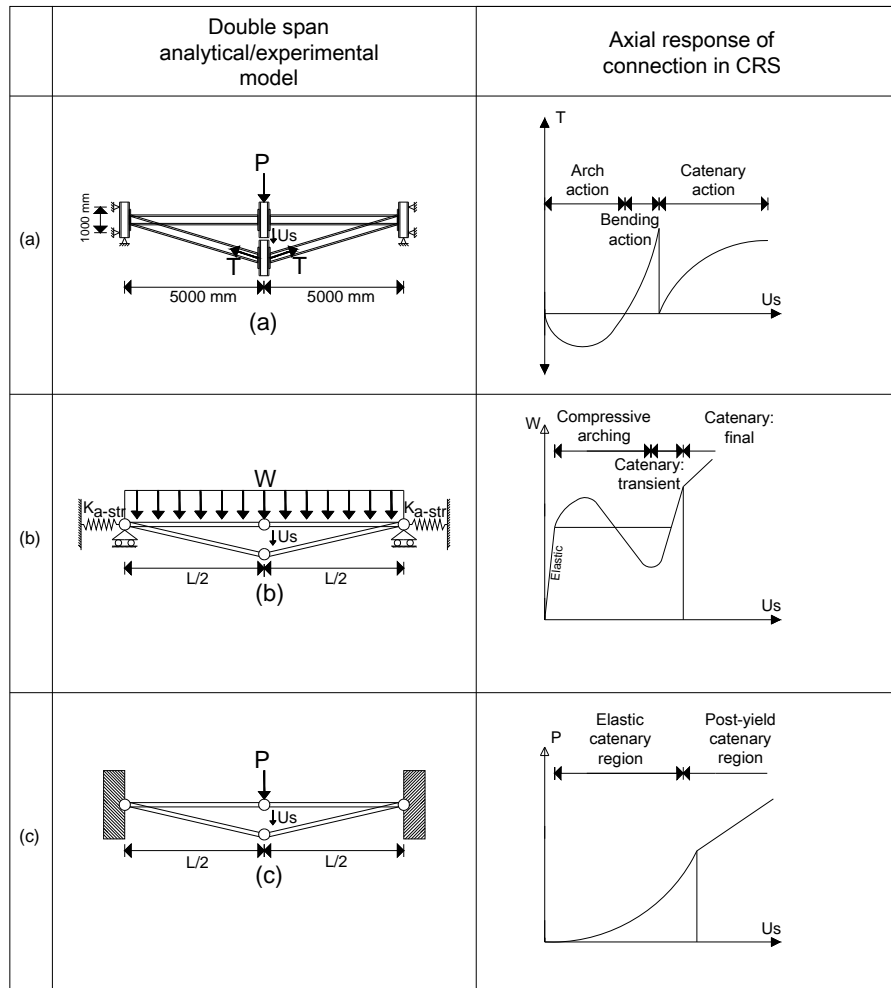
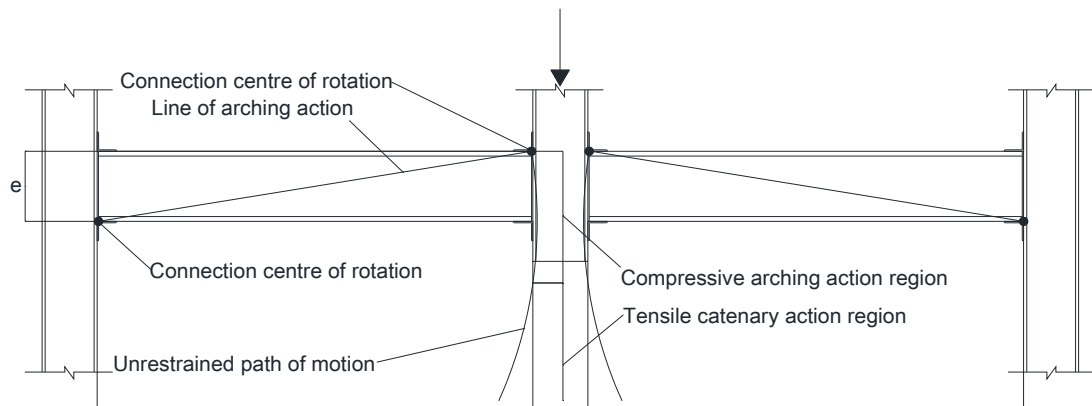
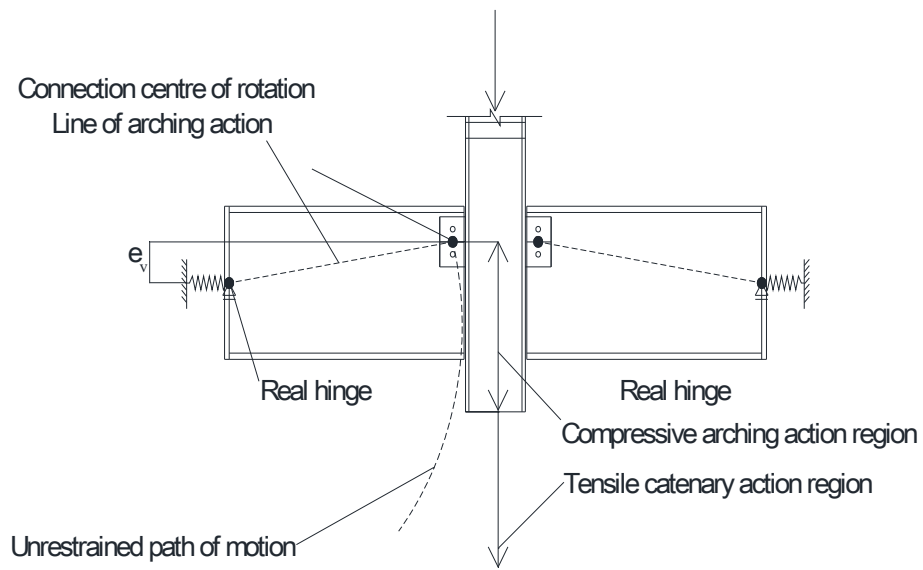


Figure 4.3: Double span analytical/experimental models and axial response of a connection in a column removal scenario (a) Girhammar (1980), (b) Izzuddin et al. (2008a), (c) Astaneh-Asl (2007)



(a)



(b)

Figure 4.4: Development of compressive arching and catenary tension under column removal scenario (a) top and bottom seated angle connection (b) single angle connection with real hinges and axial springs at the ends (Daneshvar et al. 2012)

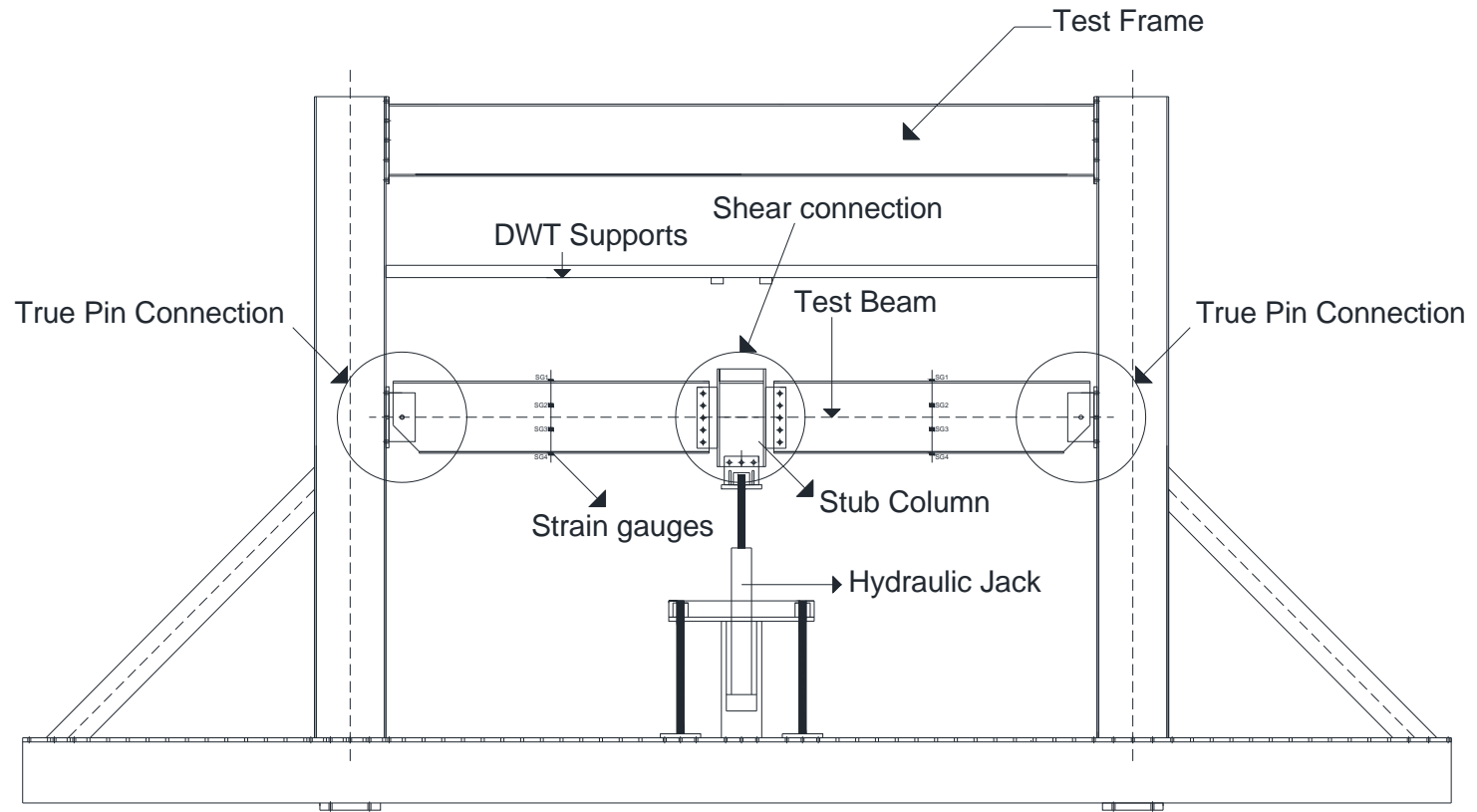
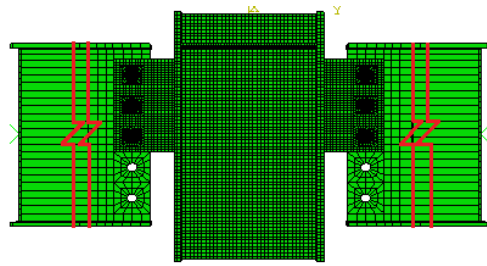
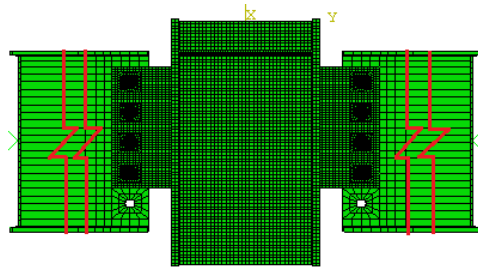


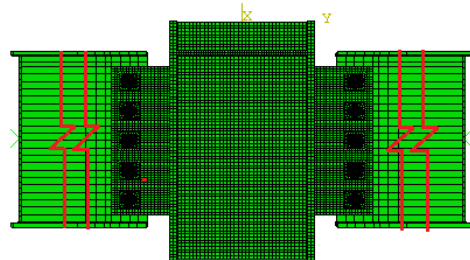
Figure 4.5: Test setup of selected experimental program (Thompson 2009)



(a)



(b)



(c)

Figure 4.6: Finite element models of (a) 3-bolt shear tab (3ST), (b) 4-bolt shear tab (4ST), (c) 5-bolt shear tab (5ST)

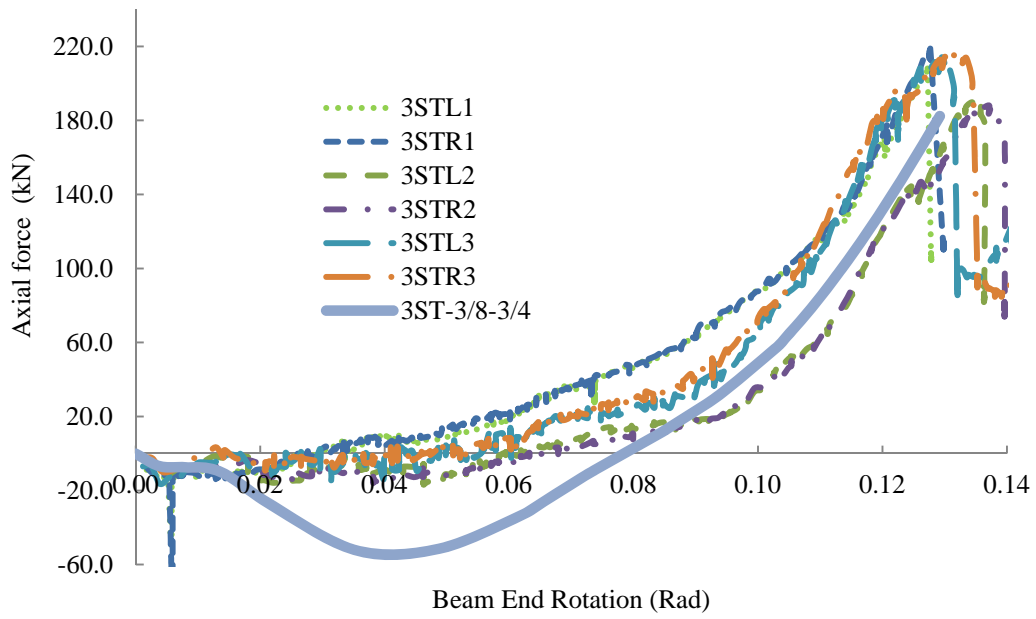


Figure 4.7: Comparison of numerical and experimental axial responses of connection 3ST

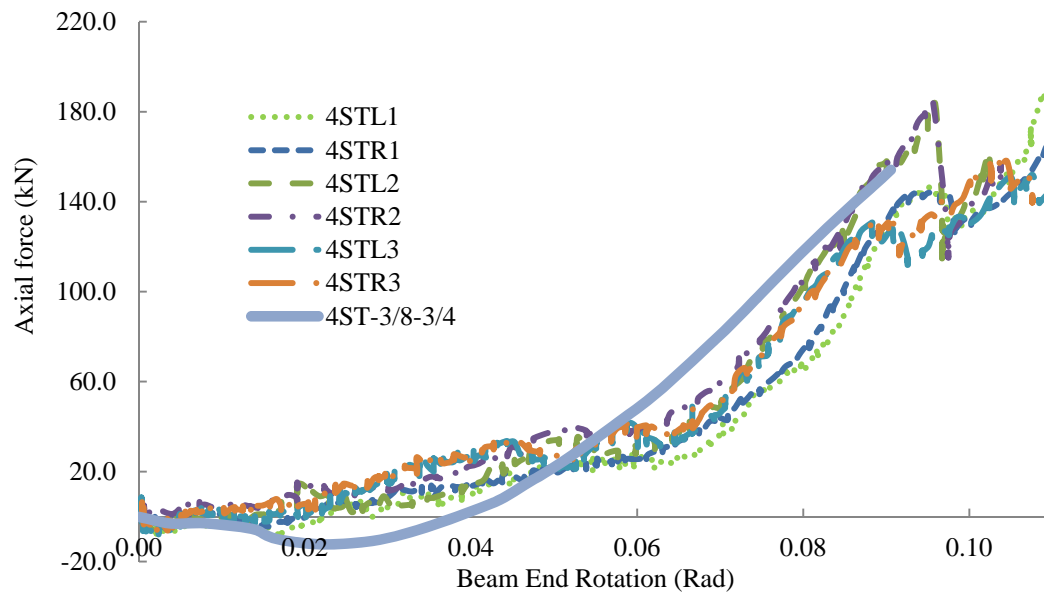


Figure 4.8: Comparison of numerical and experimental axial responses of connection 4ST

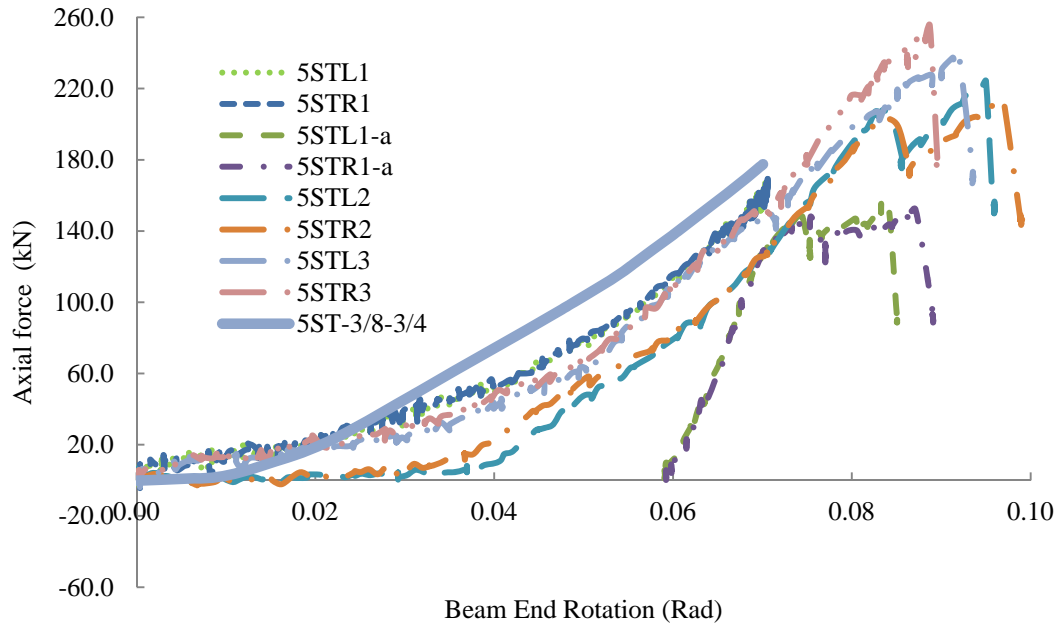


Figure 4.9: Comparison of numerical and experimental axial responses of connection 5ST

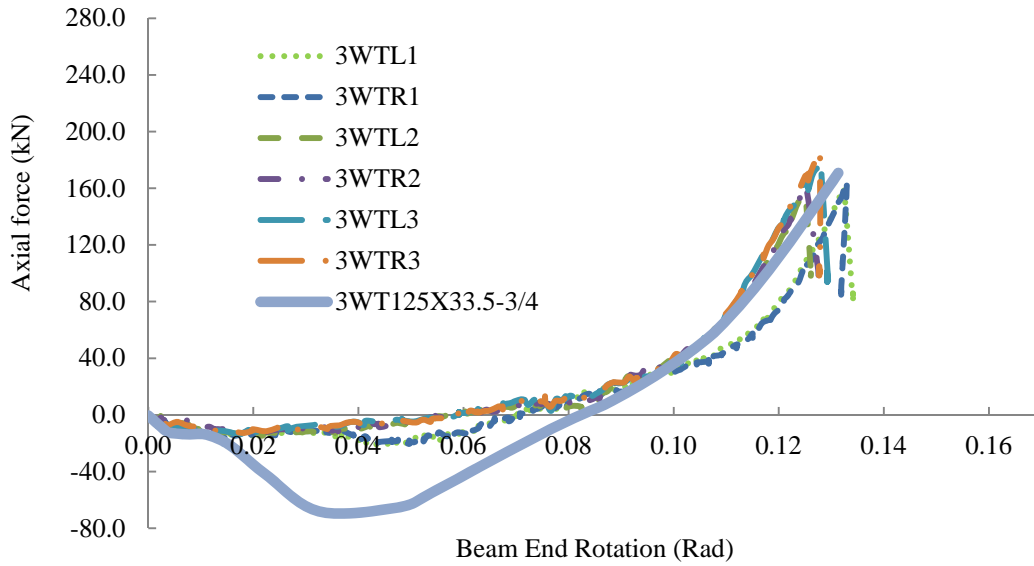


Figure 4.10: Comparison of numerical and experimental axial responses of connection 3WT

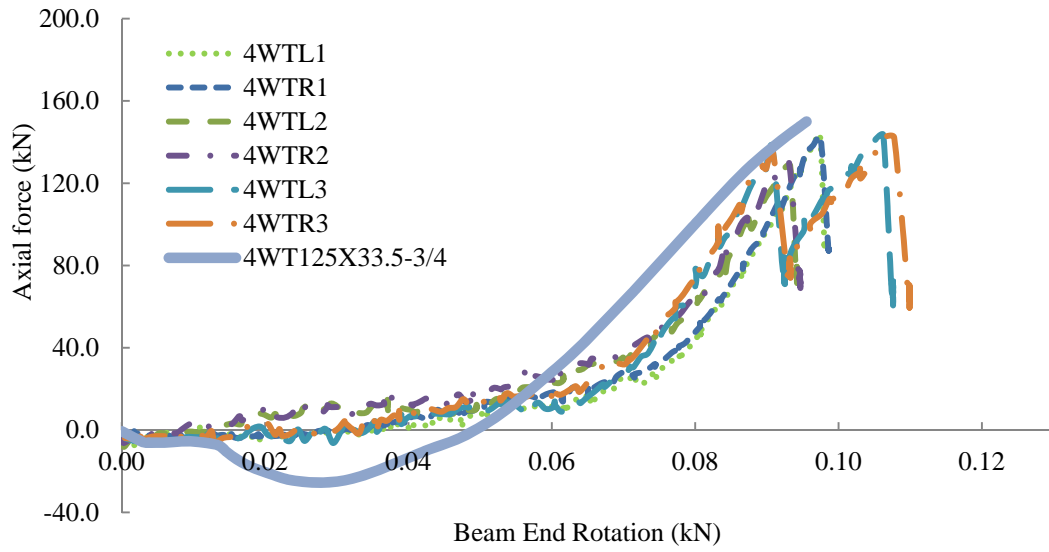


Figure 4.11: Comparison of numerical and experimental axial responses of connection 4WT

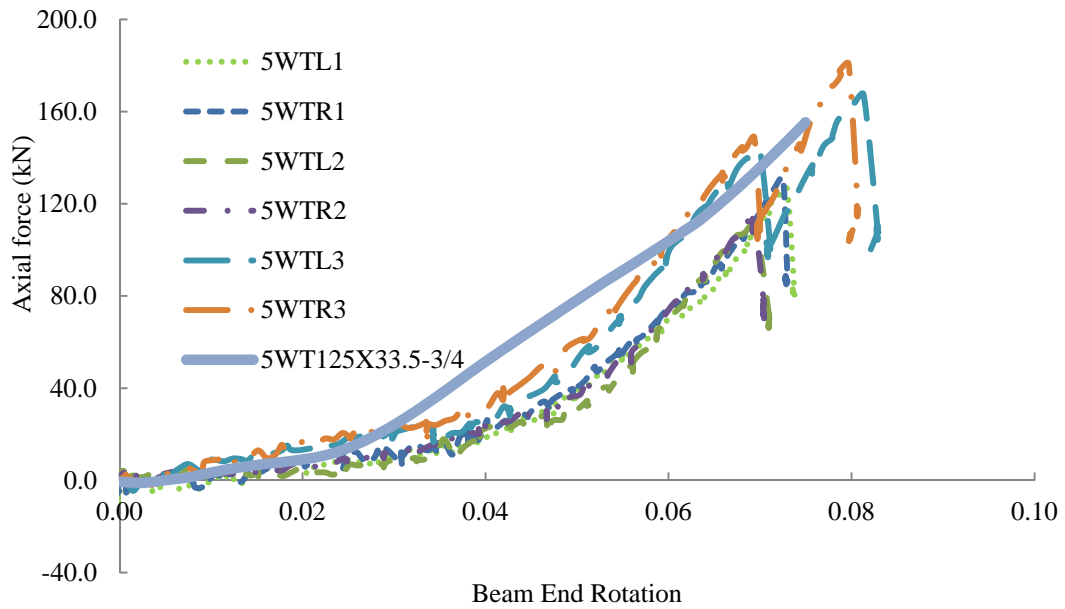


Figure 4.12: Comparison of numerical and experimental axial responses of connection 5WT

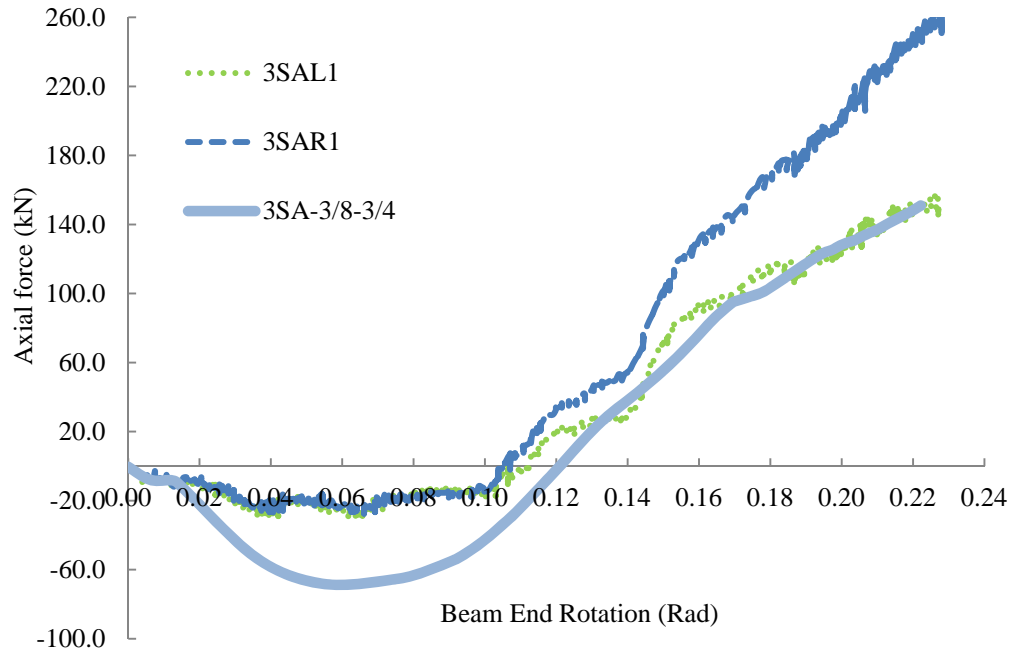


Figure 4.13: Comparison of numerical and experimental axial responses of connection 3SA

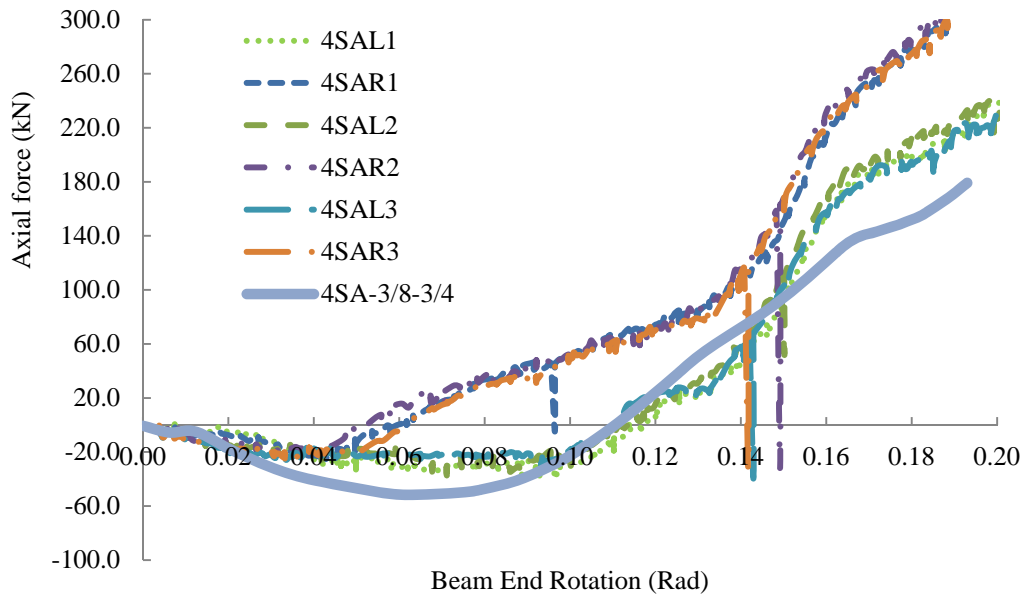


Figure 4.14: Comparison of numerical and experimental axial responses of connection 4SA

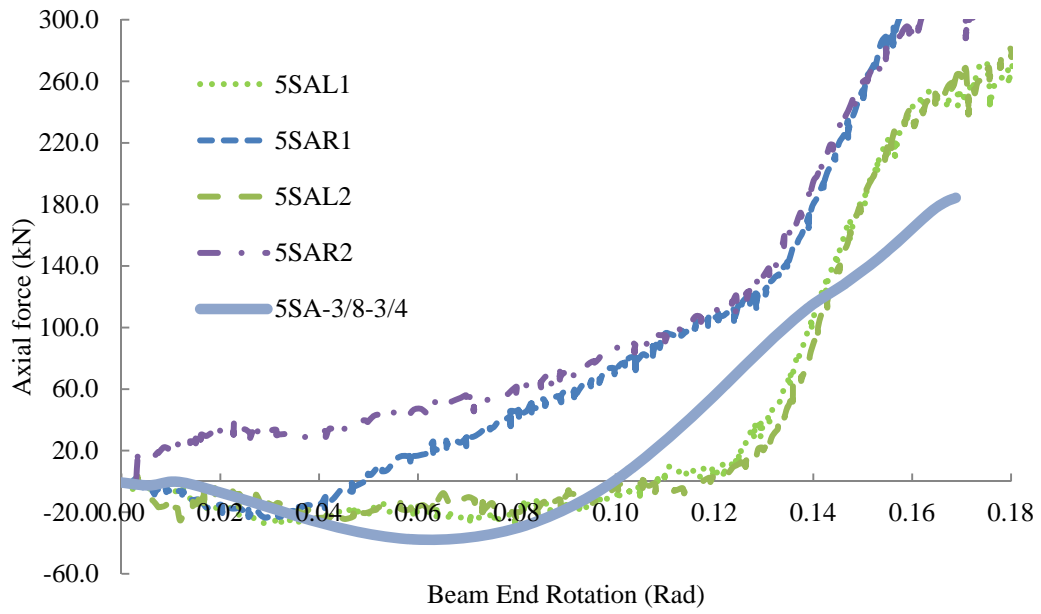
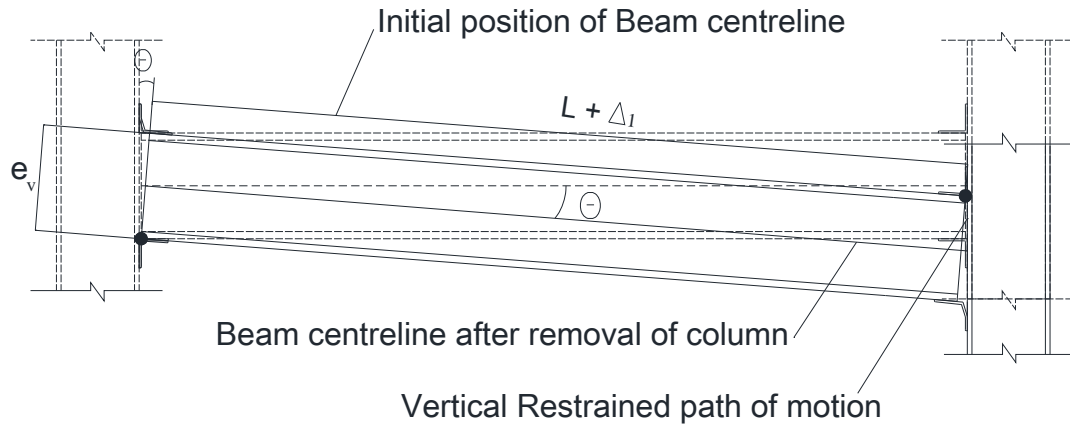
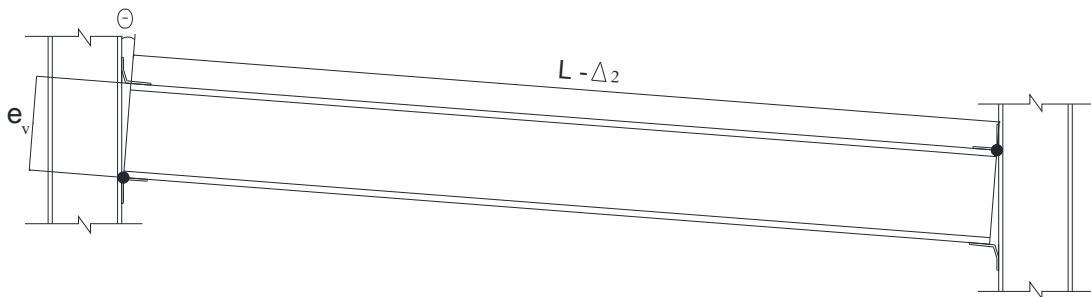


Figure 4.15: Comparison of numerical and experimental axial responses of connection 5SA



(a)



(b)

Figure 4.16: Axial deformation from (a) vertical deflection, and (b) eccentric connection rotation (Daneshvar et al. 2012)

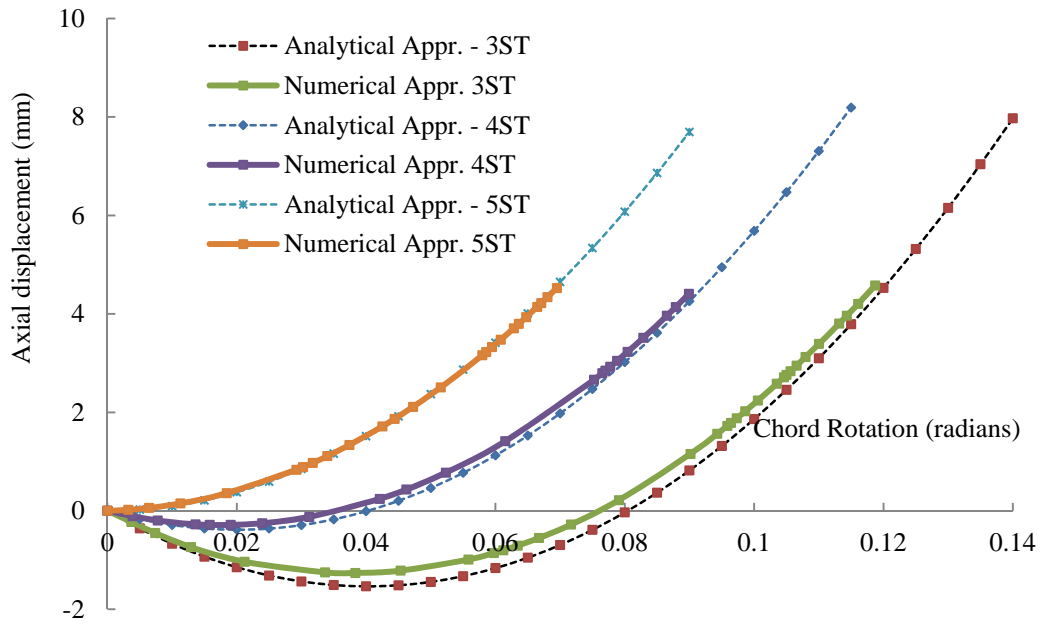


Figure 4.17: Comparison of axial deformations of numerical and simplified analytical models for ST connections (Daneshvar et al. 2012)

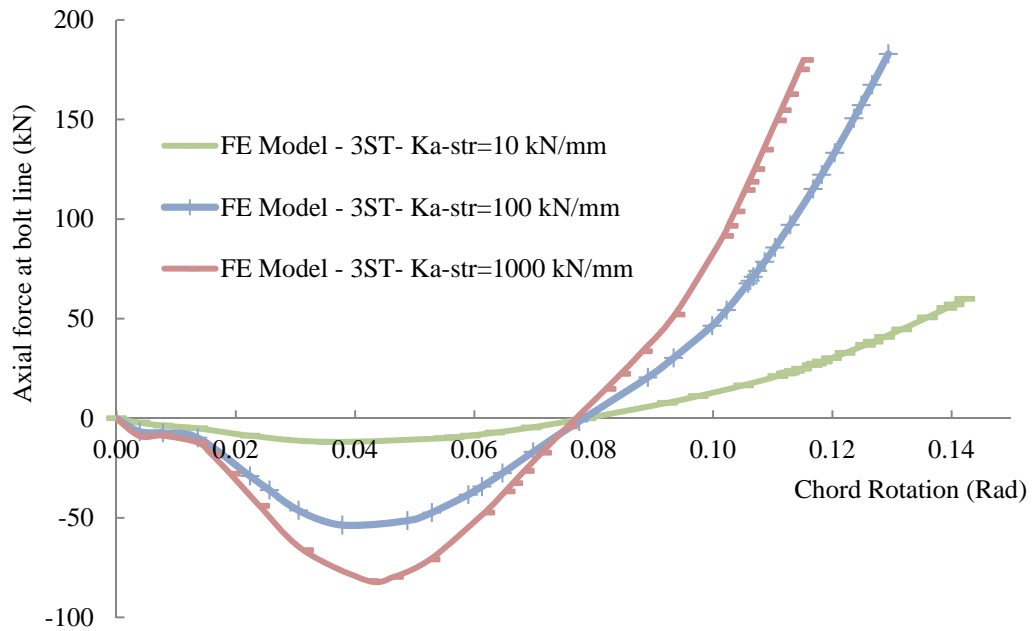


Figure 4.18: Axial response of connection 3ST for different end spring stiffnesses (Daneshvar et al. 2012)

5 Behaviour of Shear Tab Connections in Column Removal Scenario

5.1 Introduction

The shear tab, fin plate, or single plate connection is one of the simplest and most cost-effective shear connection types. It can either be bolted or welded to the beam web and welded to the column flange, as shown in . Common types of material used in shear tab connections are stated in Table 5.1. Shear tabs in beam-to-column connections are conventionally designed to transfer shear forces only. It is assumed that there is no substantial moment transfer due to the fact that beam end rotation occurs when the beam is loaded. Research on the strength and ductility of shear tab connections in conventional design is extensive. Although its behaviour under gravity and cyclic loading has been established, its response to the column removal scenario is still relatively unknown. In order to model the behaviour of such a connection in progressive collapse analyses, the DoD (2009) guideline provides a table that includes models for shear tab connections. However, as discussed in chapter 2, more research is required to shed light on the characteristic features of such connections to improve the current modelling definitions. The actual load path and stress distributions should be well-understood to propose modelling parameters in the column loss event.

In this chapter, numerical methods are applied to simulate the response of shear tab connections when a column is compromised. The finite element models are verified by available experimental data following the same loading regime. Verified models are then utilized to expand the database of the test results. Shear, axial force, and moment versus chord rotation diagrams are presented for both numerical and experimental results and conclusions are made. A parametric study is performed to extend the database on the behaviour of shear tab connections in column loss event. The results are utilized to develop the modelling parameters that can predict the rotational behaviour of shear tab connections in the new

scenario. At the end, the results are compared with the available codes and guidelines for earthquake and progressive collapse.

5.2 Objectives and scope

The main goal of this chapter is to investigate the behaviour of shear tab connections in the column removal scenario. The research study is intended to verify the results of high-fidelity finite element models of shear tab connections in terms of both load path and failure modes. These models can shed more light on the performance and the sources of ductility in shear tab connections. The results can be used to select suitable connection modeling parameters for progressive collapse evaluations of steel frames with similar shear connections.

The focus of the research is on bolted shear tab connections, shown in Figure 5.1(a). Numerically, this type of shear tab connection is perhaps the more challenging one in terms of analysis cost due to the presence of bolts, which leads to many contact surfaces and, consequently, potential convergence problems. Connection depth is the sole variable in the experimental models discussed herein. However, extensive parametric study is performed to expand the database on the behaviour of such connections by changing factors such as the plate thickness, bolt grade and diameter.

The *Steel Construction Manual* (2010) discusses two types of single plate beam-to-column connections called "conventional configuration" versus "extended configuration". The former, also referred to as "shear tab" or "fin plate" connections, has one vertical row of bolts at the supported beam web. There are several conditions—Table 5.2 summarizes the limitations and defines several of the parameters utilized in Table 5.1 (the others can be found in the list of symbols)—that need to be met to categorize a single plate in the conventional group. The "extended configuration" of single plate beam-to-column connection, utilizes one or more vertical rows of bolts. There have been several research programs on the behaviour of extended shear tabs, such as those performed by

Sherman and Ghorbanpour (2002) and Goodrich (2005). The focus of this research is on the "conventional configuration" definition, hereinafter called simply "shear tab". Moreover, this research is focused on the behaviour of shear connections in a subassembly, rather than on isolated shear connections. The process of subassembly selection is discussed in chapter 2.

5.3 Selected previous research on shear tab connections

In this section, a selective chronological progression of work related to research on shear tab connections is presented as background to the current research. Lipson (1968) initiated the investigation and attempted to establish characteristic features of these connections, including the behaviour of the connection under working loads and maximum rotational capacity by performing several tests. Nonetheless, the main purpose of Lipson's research was to determine if shear tab connections can qualify as "flexible" connections. Three types of connections were investigated including "welded-bolted" shear tab connections. All plates were ASTM A36 type and bolts were ASTM A325 and the bolt diameter was confined to 19.1 mm (3/4 in). The welding was made with the E70 series of electrodes. He tested the specimens under pure bending moment and also a combination of shear and moment, with or without rotation. Lipson observed three failure modes including weld rupture, vertical bolt tear-out of the bottom bolt and tensile yielding of the plate. He also observed a significant deformation of the bolt holes. He showed that the magnitude of the slip value for the bolts varied substantially for shear tab specimens. Besides, the effect of changing the gauge distance has only a small effect on the slip value. His experiments could not develop the full plastic moment of the connection because of small beam rotation. The connection was determined to be partially-restrained, with characteristics of both flexible and rigid connections.

Caccavale (1975) verified Lipson's experimental results using finite element analysis. He also performed several single shear tests on individual bolts to

determine the load–deformation response. He observed that the main source of shear tab connection ductility is distortion of the bolt holes providing that bolts have the necessary strength.

Richard et al. (1980) distinguished ductility sources in single plate connections: (1) bolt shear deformation (2) plate and/or beam web hole distortion (3) out-of-plane bending of the plate and/or beam web (4) bolt slippage. Based on his tests and the ones performed by Lipson (1968), he concluded that the amount of end moment transferred to the supporting member could be significant and depend on five factors: (1) number, size, and configuration of bolt pattern (2) thickness of the plate and/or beam web (3) beam span/depth ratio (4) beam loading pattern (concentrated or uniform force) (5) relative flexibility of supporting member. He acknowledged the effect of the flexibility of the supporting elements on the flexural response of one-sided connections. However, he assumed full restraint at the welded edge of the plate in his analytical models and physical tests.

Richard et al. (1980) also performed a series of "single bolt–single shear" experimental and numerical studies for various bolt sizes and plate thicknesses typically used in shear tab connections. Figure 5.3 shows a sample mesh grid they used for their finite element models. They developed the moment–rotation curves for two, three, five and seven bolt connections for different eccentricities by constructing the non-dimensional relationship demonstrated in Equation (5-1). In their work, eccentricity, e , was defined as the distance between the bolt line and the point of inflection in the beam. They proposed Equation (5-1) for defining the moment–rotation relationship of the studied connections.

$$M = M^* \left(1 - \left(1 - \frac{e}{h} \right)^{3.9} \right) M_{ref} \quad (5-1)$$

In the Equation (5-1), M is the connection moment; M_{ref} is the reference moment based on a pure moment assuming all bolts at their maximum capacities; M^* is the intermediate non-dimensional moment determined by Equation (5-2); Φ^* is the free end rotation of the beam divided by a reference rotation; Φ_{ref} is the reference

rotation calculated by Equation (5-3); n is the number of bolts; e is the eccentricity of the load; and h is the depth of the bolt pattern.

$$M^* = \frac{60\Phi^*}{\left(1 + \left(\frac{60\Phi^*}{1.1}\right)^2\right)^{3/2}} \quad (5-2)$$

$$\Phi_{ref} = \frac{0.3 \text{ in}}{\frac{(n-1)(3 \text{ in})}{2}} \quad (5-3)$$

Figure 5.4 illustrates the concept of beam line method—construction of a linear action of a beam on a nonlinear moment–rotation relationship of a connection—applied. The intersections of the beam line and the vertical and horizontal axes are the beam fixed-end moment and simple span end rotation, respectively. Full scale beam tests, shown in Figure 5.5 were performed to establish the validity of the applied models and methods. ASTM A325 bolts with 19.1 mm (3/4 in) and 22.2 mm (7/8 in) diameter were utilized. Plate material was ASTM A36 and ASTM A575 Grade 50 steel. Based on all the studies, Richard et al. (1980) proposed a design procedure for shear tab connections. The bolts were designed with an eccentricity, e , determined from Equation (5-4):

$$\frac{e}{h} = \left(\frac{e}{h}\right)_{ref} \left(\frac{n}{N}\right) \left(\frac{S_{ref}}{S}\right)^{0.4} \quad (5-4)$$

where h is the connection depth; n is number of bolts; N is 5 for 19.1 mm (3/4 in) and 22.2 mm (7/8 in) bolts, and 7 for 25.4 mm (1 in) ones; S_{ref} is 100 for 19.1 mm (3/4 in) bolts, 175 for 22.2 mm (7/8 in) bolts, and 450 for 25.4 mm (1 in) ones; and S is the section modulus of beam. $\left(\frac{e}{h}\right)_{ref}$ is determined by Equation (5-5) and Equation (5-6):

$$\left(\frac{e}{h}\right)_{ref} = 0.06 L/d - 0.15 \quad \text{for} \quad L/d \geq 6 \quad (5-5)$$

$$\left(\frac{e}{h}\right)_{ref} = 0.035 L/d \quad \text{for} \quad L/d < 6 \quad (5-6)$$

L/d is the length-to-depth ratio.

The welds in the procedure were also designed to resist moment, determined by Equation (5-7) :

$$M = V (e + a) \quad (5-7)$$

where V is the beam shear force; and a is the distance from the bolt line to the weld line. The concept is shown in Figure 5.6. Young and Disque (1981) developed tabular design aids based on Richard's proposed procedure that can significantly reduce the time required to design such connections.

In a later study, Richard et al. (1982) examined the application of ASTM A307 bolts in shear tab connections considering slotted holes. This connection was desirable because of more ductility and also less connection moment due to bolt movement in the slotted holes. Use of short-slotted holes avoids the large bolt diameter to plate thickness ratio providing ductility by preventing the bolt shear mode of failure.

Hornby et al. (1984) expanded the previous research by including connections with (1) slotted holes, (2) off-axis bolt groups, (3) Grade 50 steel beams, and (4) composite beams. An off-axis bolt group is defined as one whose center of gravity does not line up with the neutral axis of the beam, as shown in Figure 5.7. They observed that high strength A325 and A490 bolts behave similarly in round and slotted holes. The center of rotation for all the off-axis bolt group connections is at the center of the bolt group. The eccentricity of the connections with off-axis bolt groups varied, at most, $\pm 9\%$ of the symmetric concentric connection eccentricity. In the experiments using ASTM A572 Grade 50 steel beams, it was suggested that the eccentricity be modified as shown in Equation (5-8):

$$e_{50} = e_{36} \left(\frac{36}{50} \right) \quad (5-8)$$

The beam line method was also modified to be used with different types of steel, as shown in Figure 5.8 .

Astaneh (1889) investigated the demand and supply of ductility—the latter being defined as "the amount of rotation that a connection can tolerate before failure occurs"—in steel shear connections and proposed a refined beam line where both inelastic properties of the beam and the connection were considered to be applied in both service and ultimate load conditions. He (Astaneh et al. 1989) also performed a suite of experimental studies on shear tab connections and observed considerable shear and bearing yielding before failure, which caused a reduction of the rotational stiffness and also a release of end moment. Figure 5.9 shows a schematic view of bolt hole deformations after his tests. The tested beams showed ductile behaviour, tolerating rotations of 0.026 to 0.061 radians at the point of maximum shear. An increase in the number of bolts led to a decrease in rotational flexibility and ductility. Based on these experiments, five limit states were identified: (1) plate yielding (2) net section fracture of plate (3) bolt fracture (4) weld fracture (5) bolt hole bearing failure. Based on the test results, he proposed more realistic empirical values for the eccentricity definitions for designing bolts and weld, calculated by Equation (5-9) to Equation (5-11). Equation (5-9) and Equation (5-10) assume rigid and rotationally-flexible supports for the shear tab, respectively, although no experimental tests were completed on flexible supports:

$$e_b = (n - 1)(1.0) - a \quad (5-9)$$

$$e_b = \text{Max} \{(n - 1)(1.0) - a, a\} \quad (5-10)$$

$$e_w = \text{Max} \{(n)(1.0), a\} \quad (5-11)$$

where n and a were defined previously.

Astaneh (Astaneh et al. 1989) also developed a strength-based design procedure taking into account the required shear capacity as well as the necessary connection rotation. He recommended providing vertical and horizontal edge distances of at least 1.5 times the bolt diameter in order to avoid bearing fracture. Ductile yielding of the plate was ensured to be reached prior to brittle failure, by

limiting the plate thickness to less than $d_b/2 + 1/16$ in, where d_b is the bolt diameter. He limited the weld size to $3/4$ of the plate thickness to make sure that the plate would yield prior to weld yielding. It is noted that the 14th edition of the *Steel Construction Manual* (AISC 2010) recommends using $5/8$ instead of $3/4$.

Astaneh et al. (2002) examined more single plate shear connections subjected to gravity loading under the loading regime shown in . The researchers identified similar limit states to those found in the previous work (Astaneh et al. 1989), separating the bearing failure of the beam web or plate into bearing on bolt holes in the plate and the beam web (ductile limit state) and fracture of edge distances of bolt holes (brittle limit state). They observed that the contribution of shear deformations and distortions are significant above service loading. A design procedure was developed such that, first, ductile failure modes would happen, followed by brittle limit states, as shown in Figure 5.11. It was also observed that shear connections under gravity loads could tolerate rotations varying from 0.026 to 0.103 radians. Typical moment–rotation curves of the test specimens are illustrated in Figure 5.12.

Tests of beam-to-column-flange shear tab connections with floor slabs under combined gravity and cyclic lateral loading were also included in this study. These connections showed the same hierarchy of limit states as those with gravity loading alone. Typically, the composite action was lost after reaching a drift of approximately 0.04 radians. Then, a significant drop in the load capacity was observed, almost to that of the equivalent bare steel connections. Generally, the rotation capacity of shear tab connections is decreased by an increase in the depth of connection. Based on the test results, he proposed a simplified model for the moment–rotation response of shear tab connections shown in Figure 5.13 (Astaneh 2005).

Ashakul (2004) created a series of finite element models to evaluate the experimental work performed by Astaneh (1989c) and Sarkar (1992). The models were used to investigate several connection parameters such the a -distance—defined as the distance between the bolt line and the weld line—plate material and

thickness, and the connection position with respect to the beam neutral axis. He also studied single plate connections with two columns of bolts, which are not considered as “conventional” configuration as discussed in section 5.2. The results show that the a-distance will not affect the bolt shear rupture strength of a connection. He observed significant induced horizontal forces at the bolts if the plate materials and thicknesses do not satisfy the ductility criterion for the plate thickness shown in Equation (5-12):

$$t_p = 0.7 d_b \left(\frac{36}{F_y} \right) \quad (5-12)$$

where t_p is the plate thickness; d_b is the bolt diameter; and F_y is the minimum yield strength of the plate. This horizontal force reduces the shear strength of a bolt group and creates a moment that must be considered in design. A new design model for shear tab connections with single-column bolt pattern (“conventional” configuration) is proposed in his work.

There is very little research published on shear tab connections subjected to shear, moment and tension. Guravich et al. (2006) investigated the behaviour of simple beam-to-column connections subjected to combined shear and tension by performing experiments on different types of connections, including the shear tab configuration. Specimens were rotated to 0.03 radians and then a shear between zero and the design shear resistance was applied and held constant while the tensile load was applied until failure. They observed significant differences in interactions, ductility, and ultimate tensile strength. The main sources of the ductility were yielding due to bearing at bolt holes and shear yielding of the gross section of the components of the connections. They concluded that that most shear connections can take significant amounts of tensile force accompanied by the design shear capacity.

As discussed, there is extensive research performed on shear tab connections, attempting to characterize their behaviour, including the limit states and rotational capacity, under vertical shear load. However, the interaction of shear, tension and moment occurring in the event of column removal has been largely neglected. The

above review illustrates that there have been limited studies on the performance of shear connections subjected to progressive collapse type of loading scenarios.

5.4 Numerical study methods

The behaviour of shear tab connections subjected to the simultaneous presence of shear, moment, and tension is investigated using high-fidelity finite element models. All stages of simulation, including pre- and post-processing procedures, were performed using Abaqus/CAE, with Abaqus/standard used as the analysis engine (Dassault Systèmes 2009), as discussed in chapter 2.

5.4.1 Selected experimental program

Experiments performed by Thompson (2009) were utilized to verify the results of the numerical models. Figure 5.14 demonstrates the connection subassembly and the test setup. A total of nine full-scale tests were carried out, with the connection depth as the sole varying factor. The procedure of results extraction is discussed in chapter two. Although some of the tests were continued after the initial failure, the results up to this point are of interest in this research.

5.4.2 Finite element models description

Three-dimensional solid elements were used for all the components of the model due to the nature of the connection modeling problem. The models consist of the central column stub and the adjacent beams, as well as the connections with complete detailing, as shown in Figure 5.15(a). Three, four and five bolt shear tab connections were modeled, as illustrated in Figure 5.15(b) to Figure 5.15(d). The central stub column is pushed down, while the connection performance is monitored.

Since the connection is the point of interest, all characteristic features of the connections are included in the models. Strain-based fracture criteria were established and verified in chapter 3 for both the plate and the bolts in order to predict the failure modes. All other characteristic features of the models, including bolt pre-tensioning, material properties, contact calibration and element types are also discussed in chapter 3. The complete list including characteristic features of all the connections numerically studied is summarized in Table 5.3. A sample of the deformed shape of the connection assembly after the experiment is compared with its corresponding result from the finite element analysis in Figure 5.16.

The models are labeled based on the following method: first the number of the bolts, then ST, which is the abbreviation for shear tab connections utilized in this research, then the plate thickness and the bolt diameter, in imperial units. For example, 3ST-3/8-3/4 refers to the shear tab with three bolts; 3/8 in (9.5mm) plate thickness and 3/4 in (19.1 mm) diameter bolts. The bolts are all ASTM A325, unless at the end of label A490 is added. Material properties for all the plates correspond to ASTM A36. For the ones where experimental data is available, verification as well as comprehensive comparison of experimental and numerical results are performed.

5.5 Verification results

Although based on the benchmark example provided in chapter 2, following the procedure outlined is expected to produce valid results for all types of shear connections in the column loss event; however, the verification process is performed for all other shear tab connections with three and four bolts since the experimental results are available. It is noted that the benchmark example provided in chapter 2 was for a five-bolt shear tab connection. For the purpose of verification, deformed shapes, failure modes and internal force diagrams are compared with the experimental results.

Figure 5.17 to Figure 5.21 compare the experimental versus numerical deformed shape of shear tab connection components for all the experiments utilized in this study. Although there are similarities in the behaviour of each type, there are some differences that are discussed in the following sections. To ensure that a shear tab connection will survive the column removal scenario, it should be capable of carrying the combined effects of shear and moment, as well as a large catenary tensile force. The internal forces at the bolt line versus the chord rotation of connection assemblies 3ST, 4ST and 5ST are shown in Figure 5.22 to Figure 5-30. The dashed and solid lines represent the results of the experiments and simulations, respectively. While the general trends in all force responses of the connections correlate well, some discrepancies between the experimental and numerical results exist which are discussed in section 5.5.1 to 5.5.3:

5.5.1 Three bolt shear tab connections (3ST)

The comparison of the test results is performed based on the deformed shapes and the internal force interaction.

5.5.1.1 Deformed shapes and failure modes

Figure 5.17 shows the numerical versus experimental deformed shape of the 3ST connections before failure. The distribution of bearing stress at the bottom hole at thirty degree angle from the horizontal line is recorded in both the test report (Thompson 2009) and numerical results, as depicted in Figure 5.17. The trend of 30 degrees in the suite of experiments as well as the numerical model is illustrated in a magnified view of bottom hole region comparing with plastic strain distribution obtained by finite element model in Figure 5.17(c). The numerical stress distribution around the holes in the shear tab confirms a similar stress distribution to that in the experimental program by comparing to the flaking of mill scale. 4ST and 5ST connections are similar to 3ST to some extent in terms of distribution of stress at the bottom hole.

Figure 5.18 depicts the numerical versus experimental deformed shape of the 3ST connection after failure. As can be seen, most of the plastic deformation occurred around the bottom hole of the shear plate in which the rupture occurred, ultimately. No visible distortion occurred around the second hole. Presence of force couple is obvious in both the numerical model and experimental results, imposing compressive and tensile forces to the top and bottom hole, respectively. Figure 5.21 shows a typical bolt shear deformation obtained from the tests and finite element simulation. A substantial amount of shear deformation happens at the bottom bolt before failure.

Basically, the governing failure mode for all the 3ST experiments was shear tab failure. The numerical model predicts the shear tab bottom hole failure well with removed elements, as shown in Figure 5.18(b) and (c). Bolt shear rupture observed just in one of the test specimen. Based on the test record, there was an initial misalignment at the second hole location that had to be manually reamed to provide proper fit-up. Based on the test report, this might affect the failure mode due to interference in the bearing surface (Thompson 2009).

5.5.1.2 Shear-tension and moment interaction graphs

The internal forces at the bolt line versus the chord rotation of connection assemblies 3ST are shown in Figure 5.22 to Figure 5.24. The shear response of the connections (Figure 5.22), tensile behaviour (Figure 5.23) and moment response (Figure 5.24) serve to verify the models based on acceptable correlation with the associated experimental results.

There are some differences at the beginning of the experimental response of the 3ST connections, mostly tension and moment, in comparison with the numerical results. This difference is directly related to the location of the bolts in the holes in the experimental program. It is assumed that bolts are located exactly at the center of the holes in the finite element models. However, determination of the precise location of the bolts' shanks inside the holes is impracticable. As a result, some discrepancies at the early stage of loading are inevitable. Furthermore, some of

the holes are reamed in order to make them fit during erection of the test setup. This will add more complication to the problem in terms of variability and unknown issues embedded. Discrepancies observed in the tensile behaviour also can be assigned to the sensitivity of these responses to the unknown axial boundary conditions. However, it is also necessary to note that this matter does not influence the accuracy of desired result significantly.

Table 5.4 summarizes the test and finite element analysis values of the shear, moment, and tension at the initial failure—as discussed in chapter 3—for 3ST connection. Internal forces and chord rotations determined from the numerical models are in acceptable agreement with the experimental results. The largest deviation is related to the axial tensile force—about 12% deviation from experimental results—due to the sensitivity of the axial response to axial restraint provided to the beam and to possible inaccuracies in the stiffness of the springs. As seen in Table 5.4, the failure mode for the majority of the tests is tension rupture or block shear rupture at the bottom hole, and the finite element results portray the same type of ultimate limit state.

5.5.2 Four bolt shear tab connections (4ST)

Similar to shear tab connections with three bolts, a comparison of the test results is performed based on the deformed shapes and the internal force interaction.

5.5.2.1 Deformed shapes and failure modes

Figure 5.19 shows the numerical versus experimental deformed shape of the 4ST connection after failure. Similar to 3ST connection, most of the plastic deformation occurred around the bottom hole of the shear plate in which finally the rupture occurred. No distortion occurred around the second hole from top. The top and bottom bolts provided a greater percentage of flexural resistance. Presence of a force couple is obvious in both the numerical model and experimental results about the approximate location of the centroid of the bolt

group, closer to the second top bolt, imposing compressive force to the top hole and tensile force to the two bottom ones. Shear deformation occurred at the bottom bolt shank before failure, similar to what is shown in Figure 5.21. The stress distribution around the holes in the shear tab confirms the stress distribution happening in the experimental program following the 30 degree trend observed in the 3ST connections.

5.5.2.2 Shear-tension and moment interaction graphs

The internal forces at the bolt line versus the chord rotation of connection assemblies 4ST are shown in Figure 5.25 to Figure 5.27. The shear response of the connections (Figure 5.25), tensile behaviour (Figure 5.26) and moment response (Figure 5.27) serve to verify the models based on acceptable agreement with the associated experimental results. Similar to the 3ST connections, some differences exist in the load paths, particularly at the beginning of the experimental response of 4ST connections in comparison with the numerical results. The same reason mentioned for 3ST connection can be stated, including the location of the bolts in the holes in the experimental program and also the unknown axial stiffness of the test setup.

Table 5.5 summarizes the test and finite element analysis values of the shear, moment, and tension at the initial failure of the 4ST connections. As can be observed, shear and tensile forces, as well as chord rotations, determined from the numerical models are in acceptable agreement with the experimental results. The largest difference is related to the moment, which is about a 30% deviation from the mean of the experimental results. This difference comes from the small difference in the average experimental chord rotation and corresponding numerical value. In the experiments, just before failure, the flexural resistance of all specimens reduced drastically. The failure of the finite element model happens slightly sooner before experiencing the huge reduction in bending resistance. However, the flexural load path is similar to the experimental curves as shown in Figure 5.27, so this deviation is not considered as a disagreement between the

finite element model and experiments. As can be seen in Table 5.5, the failure mode for the tests is tension rupture or the block shear rupture at the bottom hole, and the finite element results convey the same type of ultimate limit state.

5.5.3 Five bolt shear tab connections (5ST)

Similar to the shear tab connections with three and four bolts, discussed in sections 5.5.1 and 5.5.2, respectively, the comparison of the test results is performed based on the deformed shapes and the internal forces. It is noted that this connection simulation is proposed as a benchmark in finite element modelling of shear connections in the column removal scenario in chapter 2. Because of initial error in the instrumentation of test 5ST1, the measured data was skewed (Thompson 2009).

5.5.3.1 Deformed shapes and failure modes

Figure 5.20 illustrates the numerical versus experimental deformed shape of the 5ST connection after failure. Similar to the 4ST connection, most of the plastic deformation occurred around the bottom hole of the shear plate in which the rupture occurred, ultimately. There is no distortion around the second and third hole from the top. The top and bottom two bolts provided a greater percentage of flexural resistance by forming a couple force about the approximate location of the centroid of the bolt group. Shear deformation accompanied by substantial plastic deformation of the bottom hole provides the ductility of the connection.

5.5.3.2 Shear-tension and moment interaction graphs

The internal forces at the bolt line versus the chord rotation of connection assemblies 5ST are shown in Figure 5.28 to Figure 5.30. Table 5.6 summarizes the experimental and finite element analysis values of the shear, moment, and tension at the initial failure for 5ST connections. Since this is the benchmark example, all quantities including shear, tension and moment, as well as chord rotations, determined from the numerical models are in acceptable agreement with

the experimental results. As observed in Table 5.6, the failure mode for the tests is tension rupture or the block shear rupture at the bottom hole, and the finite element results portray the same type of ultimate limit state.

5.6 Parametric study results

After verifying the finite element models with the test results, a parametric study is performed in order to investigate the effects of different design parameters such as plate thickness, bolt size and type, and also connection depth according to Table 5.3.

5.6.1 Three bolt shear tab connections (3ST)

Figure 5.31 to shows the interactions of shear, tension and moment for the shear tab connections with three bolts (3ST). The behaviour of 3ST-3/8-3/4 was discussed in section 5.5.1 since experimental results were available. Its response without the test curves is shown again in Figure 5.31 for the sake of completeness of the report. As labeled in Figure 5.31, the point that the flexural phase domination ends and catenary force begins to provide the major resistance is named the “devolution point”. For the 3ST-3/8-3/4 connection, the devolution point is located at the rotation corresponding to the maximum moment. The main reason for this is the fact that in 3-bolt connections the bottom and top bolts resist the moment demand through bearing resistance of the bolt–hole interaction. As soon as localized yielding happens around the contact surface, the flexural resistance starts to vanish and the connection finds another load path to take more load until failure. The failure will be in the catenary phase.

Figure 5.32 shows the interaction of internal forces at the bolt line for the model 3ST-1/4-3/4. In this model, the failure is initiated in the shear tab bottom hole region, as expected. A slight reduction in the ductility of the connection is observed in comparison with 3ST-3/8-3/4 due to the thinner plate and

consequently earlier failure. There are no significant plastic shear deformations observed in the bolts—even the bottom bolt—since most of the bearing deformation happens in the thin plate. The tensile force starts to come into existence exactly at the point of maximum moment. Shear force increases almost linearly up to the point of failure, interacting with tension and moment, especially at high rotations.

Figure 5.33 shows the interaction of internal forces at the bolt line for the model 3ST-1/2-3/4. In this model, the failure mode is shifted from the shear tab plate to the bottom bolt due to the increase in the thickness of the plate. However, the ductility of the connection is not increased significantly in comparison with 3ST-3/8-3/4. There is a significant plastic deformation in the bottom bolt shank prior to failure, although the other bolts remained nearly elastic. The tensile force starts to come into existence slightly before the point of maximum moment. This could be attributed to the thicker plate that still possesses additional flexural resistance when tensile catenary force starts to exist.

Figure 5.34 shows the interaction of internal forces at the bolt line for the model 3ST-3/8-5/8. In this model, both the bottom bolt and bottom hole region of the shear tab were close to failure. The rupture is initiated in the shear tab bottom hole region, followed closely by plate tearing behind the bolt. A substantial amount of plastic deformation developed in the bolt shank, which could have caused the bolt shear failure instead of plate rupture. Any variation in the material properties of the bolt or plate could cause the alteration in the failure mode of this connection. The ductility of the connection is slightly lower, but still comparable to the 3ST-3/8-3/4 model. There are significant plastic deformations around the bottom bolt hole area and also at the bottom bolt shank before failure. The tensile force starts to come into existence exactly at the point of maximum moment again.

Figure 5.35 shows the interaction of internal forces at the bolt line for the model 3ST-3/8-7/8. In this model, the failure is initiated in the shear tab bottom hole region as expected. Due to the larger bolt diameter compared to the previously-described models, only a slight amount of plastic deformation occurred in the bolt

shank, which is considered negligible. There are significant plastic deformations around the bottom bolt hole area. The tensile force starts to come into existence almost at the point of maximum moment again.

shows the interaction of internal forces at the bolt line for the model 3ST-3/8-3/4-A490. The behaviour of model 3ST-3/8-3/4-A490 is very similar to the 3ST-3/8-3/4 with ASTM A325 bolts. The dominated limit state of the connection is plate failure, as expected. However, unlike the similar model with A325 bolts, there is no substantial shear deformation in the bottom bolt shank observed. Since the dominant failure mode of 3ST-3/8-3/4 was bottom hole rupture, substituting the ASTM A325 bolts with ASTM A490 bolts has little effect on the connection performance. Changing the bolt type might vary the connection response in the models that fail due to bolt shear rupture, such as 3ST-3/8-5/8.

As observed in 3ST connections, regardless of the plate thickness, bolt size and type, as the flexural stiffness of the connection become zero and subsequently negative, the tensile catenary forces increased rapidly until the failure of the connection. Tensile catenary resistance starts to grow at the approximate chord rotation angle of 0.08, at which time the maximum flexural strength is reached. Basically, the amount of moment at failure of the connection is about or less than 10 kN.m, which for practical purposes could be considered negligible. Therefore, it can be inferred that the 3ST connections fail mainly because of catenary actions. The dominant failure mode of 3ST connections is shear tab rupture at the bottom bolt hole, although bolt shear rupture is also possible.

5.6.2 Four bolt shear tab connections (4ST)

Figure 5.37 to show the interactions of shear, tension and moment for the shear tab connections with four bolts (4ST). The behaviour of 4ST-3/8-3/4 was discussed in section 5.5.2. Its response without the test result curves is shown again in the Figure 5.37 for the sake of completeness of the report. The

“devolution point” in this connection is not as clear as was the case for the 3ST connections. A point might be distinguished as a devolution point in which a substantial decrease in flexural stiffness and an increase in axial stiffness occur, as shown in Figure 5.37. However, since the moment is still growing, for the 4ST connections this point is considered the onset of the “flexural–catenary phase”.

Figure 5.38 shows the interaction of internal forces at the bolt line for the model 4ST-1/4-3/4. The general behaviour of 4ST-1/4-3/4 is similar to the 3ST-1/4-3/4 model due to the same geometric and mechanical properties. The failure is initiated in the shear tab bottom hole region, as expected. A slight reduction in the ductility of the connection is observed in comparison with 4ST-3/8-3/4 because of the earlier failure of the thinner plate. No significant plastic shear deformation is observed in the bolts—even the bottom one—since most of the bearing deformations happen in the thin plate. The tensile force starts to grow at the rotation of 0.04. The rate of increase of the resisting moment diminishes gradually at this point as well. However, a range could be recognized that substantial amount of shear, tension and moment are interacting until failure of the connection happens.

Figure 5.39 shows the interaction of internal forces at the bolt line for the model 4ST-1/2-3/4. Similar to 3ST-1/2-3/4, in the 4ST-1/2-3/4 connection model assembly, the failure mode is shifted to the bottom bolt due to the increase in the thickness of shear tab plate over the previously-mentioned models. There is a slight increase in the rotational ductility of the connection in comparison with 4ST-3/8-3/4, but it is not significant. There are also substantial amounts of plastic deformations in the bottom bolt shank prior to failure. The top bolt also experienced some plastic deformation, but the other ones remained almost elastic. The devolution from flexural behaviour to the catenary phase is more obvious in this connection assembly. At the rotation of about 0.05, the tensile force starts to increase more rapidly as the slope of the flexural response reduced abruptly, making the “devolution point” more obvious in this connection.

shows the interaction of internal forces at the bolt line for the model 4ST-3/8-5/8. In the 4ST-3/8-5/8 model, the failures at the shear tab bottom hole and bottom bolt shank region happen at the same time. A substantial amount of plastic deformation happens in the bolt shank, accompanied by considerable bearing deformation at the bottom hole before failure. Any variation in the material properties of the bolt or plate could cause the domination of one over the other. The ductility of the connection is almost the same as the 4ST-3/8-3/4 model. The tensile force starts to become significant at the approximate chord rotation of 0.042. At the same rotation angle, the slope of flexural behaviour reduces drastically, which shows the switch from flexural behaviour to the flexural–catenary phase.

Figure 5.41 shows the interaction of internal forces at the bolt line for the model 4ST-3/8-7/8. In this model, the failure is initiated in the shear tab bottom hole region. A slight amount of plastic deformation developed in the bolt shank, which can be ignored. There are significant plastic deformations around the bottom bolt hole area. The devolution from flexural behaviour to the catenary phase occurs at the rotation of about 0.04. At this point, the tensile force starts to increase more rapidly as the slope of the flexural response reduces gradually. Similar to the other curves, shear force increases linearly after the approximate rotation of 0.02, interacting with tension and moment.

shows the interaction of internal forces at the bolt line for the model 3ST-3/8-3/4-A490. The behaviour of this model is very similar to 3ST-3/8-3/4 with ASTM A325 bolts. The dominated limit state of the connection is plate failure as expected. However, unlike the similar model with A325 bolts, there is no substantial shear deformation in the bolt shank observed.

The “devolution point” in 4ST connections is not clear, as was the case for 3ST connections, but still definable. A point might be distinguished as a devolution point in which a substantial decrease in flexural stiffness and an increase in axial stiffness occur simultaneously. After this point, the tensile catenary forces increase rapidly until the failure of the connection, in the presence of shear and

moment. Tensile catenary resistance starts to grow at the approximate chord rotation angle of 0.04, at which point the flexural response starts to degrade. Basically, the amount of moment at the failure is substantial and should not be ignored. Therefore, it can be inferred that the 4ST connections fail mainly because of flexural-catenary actions. The dominated failure mode of 4ST connections is shear tab rupture, although bolt shear rupture is also possible for smaller bolts.

5.6.3 Five bolt shear tab connections (5ST)

to Figure 5.48 depict the simultaneous presence of shear, tension and moment for the shear tab connections with five bolts (5ST). The behaviour of 5ST-3/8-3/4 was discussed in section 5.5.3. Its response without the test curves is shown again in the Figure 5.43 for the sake of completeness of the report. Similar to 4ST connections, the “devolution” point in this connection is not as clear as for the 3ST connections. A point might be distinguished as a devolution point in which a substantial decrease in flexural stiffness occurs. After that, tensile force and moment interact until the connection failure.

shows the interaction of internal forces at the bolt line for the model 5ST-1/4-3/4. Its behaviour is similar to the 4ST-1/4-3/4 and 3ST-1/4-3/4 models due to the same geometric and mechanical properties. The failure is initiated in the shear tab bottom hole region similarly. A slight reduction in the ductility of the connection is observed in comparison with 5ST-3/8-3/4 because of the earlier failure of the thinner plate. There is no significant plastic shear deformation observed in the bolts—even the bottom bolt—since most of the bearing deformations happen in the thin plate. In the five bolt connections the interaction of shear, tension and moment starts at the early stages of loading, after the establishment of contacts, which is about 0.01 radian of rotation. As a result, the devolution from flexural to the catenary phase happens in the range, not at a point. However, a point that the flexural stiffness reduced drastically is still noticeable at the approximate rotation of 0.03 radians.

Figure 5.45 shows the interaction of internal forces at the bolt line for model 5ST-1/2-3/4. Similar to 3ST-1/2-3/4 and 4ST-1/2-3/4, in the 5ST-1/2-3/4 connection model assembly, the failure mode is shifted to the bottom bolt due to the increase in the thickness of shear tab plate. There is a slight increase in the rotational ductility of the connection in comparison with 5ST-3/8-3/4. There is also a substantial amount of plastic deformation in the two bottom bolts and the one at the top prior to failure. The other two bolts remained essentially elastic. The devolution from flexural behaviour to the catenary phase is more obvious in this connection assembly. At the rotation of about 0.045 a small increase in the rate of tensile development of the connection occurs, which causes a reduction in the slope of the flexural response.

Figure 5.46 shows the interaction of internal forces at the bolt line for the model 5ST-3/8-5/8. In this model, the failure at the shear tab bottom hole and bottom bolt shank region occurs simultaneously, similar to 4ST-3/8-5/8. A substantial amount of plastic deformation was happening in the bolt shank accompanied by considerable bearing deformation at the bottom hole. Any variation in the material properties of the bolt or plate could cause the failure of one to dominate the overall behaviour. The ductility of the connection is almost the same as the 5ST-3/8-3/4 model. Similar to other five bolt shear tabs, it is hard to distinguish a devolution point to the tensile behaviour; however, the chord rotation of 0.035 might be considered as a point where the reduction in the flexural response starts more rapidly.

Figure 5.47 shows the interaction of shear, tension and moment at the bolt line for the model 5ST-3/8-7/8, in which the failure is initiated in the shear tab bottom hole region. A slight amount of plastic deformation happened in the bolt shank, which can be ignored. There are significant plastic deformations around the bottom bolt hole area. The devolution from flexural behaviour to the flexural-catenary phase occurs at the rotation of about 0.04. After 0.04 radians, although the rate of increase in moment is reduced, there is still a substantial moment at the

connection; as a result, the connection fails because of flexural and tensile demand at its ultimate limit state.

Figure 5.48 shows the interaction of internal forces at the bolt line for the model 5ST-3/8-3/4-A490. The behaviour of model 5ST-3/8-3/4-A490 is very similar to the 5ST-3/8-3/4 with ASTM A325 bolts. The dominant limit state of the connection is plate failure, as expected. However, unlike the similar model with A325 bolts, no substantial shear deformation in the bottom bolt shank was observed.

Unlike 3ST connections, the “devolution point” in 5ST connections is not clear. A point might be distinguished as a devolution point at which a substantial decrease in flexural stiffness happens. The tensile catenary forces increased rapidly, interacting with moment, until the failure of the connection. Tensile catenary resistance starts to grow from the beginning, after establishment of contact at the approximate chord rotation angle of 0.01 when flexural response starts to increase rapidly. The amount of moment and tension at the failure is substantial. Therefore, it can be inferred that the 5ST connections fail mainly because of flexural–catenary actions. The dominated failure mode of 5ST connections is shear tab rupture and bolt shear rupture in some cases, similar to 3ST and 4ST connections.

5.7 Comparison of the results

In this section, the effect of plate thickness, bolt size and bolt type are discussed separately for three, four and five bolt connections.

5.7.1 Three bolt shear tab connections (3ST)

5.7.1.1 Plate thickness

Figure 5.49 to Figure 5.51 illustrate the shear, tensile and flexural responses of 3ST connections with different plate thicknesses and 3/4 in. bolts. Generally, an

increase in plate thickness causes an increase in shear, tensile and flexural strengths of 3ST connections. The difference at small rotations is negligible, and as the rotation increases, the difference becomes more substantial. In terms of axial load path response, the difference among the curves is minimal, although the increase is still noticeable. In terms of load path, the axial response of the connection does not change by altering the shear tab thickness significantly. However, the maximum tensile catenary force they can develop is highly dependent on the plate thickness. The shear strength of connections with 6 mm (1/4 in) thickness is about half of the one with the 9.5 mm (3/8 in) shear tab plate. In terms of axial strength, this value is reduced to even less than 45%. Model 3ST-1/2-3/8, with the thickest plate, shows higher ductility due to postponing failure to higher rotations, which eventually occurred by bolt shear rupture. The maximum moment happens at approximately the same rotation for all thicknesses. All the flexural responses possess a descending branch after the peak moment until failure, as observed in Figure 5.51.

5.7.1.2 Bolt size

Figure 5.52 to Figure 5.54 illustrate the shear, tensile and flexural response of the 3ST connections with different bolt sizes. Similar to the effect of plate thickness, an increase in bolt diameter causes an increase in the flexural and shear responses of 3ST connections. However, in terms of axial response, the behaviours are almost the same, as shown in Figure 5.53, although the smaller bolt size, 5/8 in diameter, fails sooner than the other two. The change in the rotational capacity of 3ST connections due to a change in bolt diameter is very small and considered negligible. The shear and tensile strength of the 3ST-3/8-5/8 connection is approximately 70% of the other comparable two connections. The maximum moment happens at approximately the same rotation (0.08 radians) for all bolt sizes. All the flexural responses possess a descending branch after the peak moment until failure, as observed in Figure 5.54. In general, since the deformation capacity of bolts is relatively small, the use of larger bolts could

improve connection ductility by changing the failure mode from bolt rupture to infill plate bearing failure at the bolt hole.

5.7.1.3 Bolt type

The effect of the bolt grade—ASTM A325 versus ASTM A490—is also investigated for the 3ST-3/8-3/4 model. It is observed that the shear, axial and flexural response of the connection assembly with two different types of bolts are almost the same, with a minor difference in the rotational ductility. The connection with ASTM A325 bolts shows more ductility. As can be seen, there is no benefit in utilizing ASTM A490 bolts in terms of improved performance in the studied type of loading.

5.7.2 Four bolt shear tab connections (4ST)

5.7.2.1 Plate thickness

Figure 5.55 to Figure 5.57 illustrate the shear, tensile and flexural responses of 4ST connections with different plate thicknesses. The effect of plate thickness is almost the same as for the 3ST connections. It can be inferred that axial response of the connection does not change significantly by altering the shear tab thickness. The shear strength of connections with 6 mm (1/4 in) thickness is about 60% of the one with 9.5 mm (3/8 in) shear tab plate. In terms of axial strength, this value is reduced to less than 55%. The maximum moment happens at the approximate same rotation (0.09 radians) for the models with 9.5 mm (3/8 in) and 12.7 mm (1/2 in) that differs for the 6 mm (1/4 in) model. The limit state of the two thinner plates was plate rupture; nonetheless, the thicker plate shows more ductile behaviour and ultimately fails due to bolt shear rupture. 4ST-1/2-3/4 possesses the only flexural response with small descending branch after the peak moment until failure, as observed in Figure 5.56.

5.7.2.2 Bolt size

Figure 5.58 to Figure 5.60 illustrate the shear, tensile and flexural response of the 3ST connection with different bolt sizes. An increase in bolt diameter causes an increase in the flexural and shear response of 4ST connections. However, in terms of axial response, the behaviours are almost the same, as shown in Figure 5.59. The rotational ductility of 4ST connections with different bolt diameters is almost the same. The shear and tensile strengths of 4ST-3/8-5/8 are almost 85% of the 4ST-3/8-3/4 connections. The maximum moment happens at the approximate same rotation (0.08 radians) for all bolt size, which happens to be the moments at failure. None of the flexural responses possess a descending branch after the peak moment, as observed in Figure 5.60.

5.7.2.3 Bolt type

Similar to 3ST connection explanation, the effect of different bolt type—ASTM A325 versus ASTM A490—is also investigated for the 3ST-3/8-3/4 model. It is observed that the shears, axial and flexural response of connection assembly with two different types of bolts are almost the same, with a minor difference in the rotational ductility.

5.7.3 Five bolt shear tab connections (5ST)

5.7.3.1 Plate thickness

Figure 5.61 to Figure 5.63 illustrate the shear, tensile and flexural responses of 5ST connections with different plate thickness. The effect of plate thickness is almost the same as for the 3ST and 4ST connections. Generally, increase in plate thickness causes an increase in shear, tensile and flexural strength of 3ST connections. The difference at small rotations (up to 0.02 radians) is small; and as the rotation increases, the difference becomes more substantial. 5ST-3/8-3/4 behaviour is closer to the thicker plate model, 5ST-1/2-3/4, than the thinner one. In terms of load path, the axial response of the connection does not change

significantly by altering the shear tab thickness. However, the maximum tensile catenary force they can develop is highly dependent on the plate thickness, as observed in Figure 5.62. All the models start to go through tensile catenary force at the same rotation. It can be inferred that axial response of the connection does not change significantly by altering the shear tab thickness. The shear and tensile strength of connections with 6 mm (1/4 in) thickness is about 60% of the one with 9.5 mm (3/8 in) shear tab plate. The maximum moment corresponds to the failure moment for all the thicknesses. The limit state of the thicker plates was bolt shear rupture and that of the thinner plates is plate rupture. None of the curves possess a descending branch after the peak moment, as observed in Figure 5.63.

5.7.3.2 Bolt size

Figure 5.64 to Figure 5.66 illustrate the shear, tensile and flexural response of the 5ST connection with different bolt sizes. An increase in bolt diameter causes an increase in the flexural and shear response of 5ST connections. However, in terms of axial response, the behaviours are almost the same, as shown in Figure 5.65. The rotational ductility of 5ST connections with different bolt diameter is almost the same. The shear and tensile strength of 5ST-3/8-5/8 is about 80% of the 3ST-3/8-3/4 connections. The maximum moment happens at the approximate same rotation (0.065 radians) for all bolt size, which is the moment at failure. 5ST-3/8-3/4 is slightly more ductile than the other two connection models. None of the flexural responses possess a descending branch after the peak moment, as observed in Figure 5.66.

5.7.3.3 Bolt type

Similar to the 3ST and 4ST connection explanation, the effect of different bolt types—ASTM A325 versus ASTM A490—is also investigated for 3ST-3/8-3/4 model. It is observed that the shears, axial and flexural response of connection assembly with two different types of bolts are almost the same, with a minor difference in the rotational ductility.

Table 5.7 summarizes the results of the numerical models in addition to the experimental specimens at the initial failure of the connections.

5.8 Rotational ductility of shear tab connections in column removal scenario

Rotational capacity of shear tab connections is not affected greatly by variables such as plate thickness, bolt size and type. Within the scope of what has been studied in this research, the change in the failure mode does not significantly affect the rotational ductility either. However, the number of rows of bolts (depth of the connection) does have an effect. Rotational capacity is estimated based on the depth of the connection in current codes and guidelines. Figure 5.67 illustrates the distribution of rotational capacity of shear tab connections studied in this research versus connection depth. Experimental values (EXP) are the average values observed in the tests obtained from Table 5.4 to Table 5.6, producing totally three points in Figure 5.67. Finite element (FE) models add eighteen other points in order to increase the number of data points and, hence, making the regression analysis more accurate.

Figure 5.68 shows the best-fit regression line considering all of the data. As a result, Equation (5-13) in imperial and Equation (5-14) in SI units is proposed to determine rotational capacity of shear tabs in the column removal scenario.

$$\theta_{tot} = -0.0094 d_{conn} + 0.179 \quad (d_{conn} \text{ in inches}) \quad (5-13)$$

$$\theta_{tot} = -0.00037 d_{conn} + 0.179 \quad (d_{conn} \text{ in millimetres}) \quad (5-14)$$

where d_{conn} is the distance between the centres of the top and bottom bolts, and θ_{tot} is the total rotational capacity of the shear tab connection in radians.

θ_{tot} consists of elastic and plastic components. The plastic rotation is the rotation that guidelines such as ASCE 41 (2006) and DoD (2009) utilize to define the connection behaviour. By aid of finite element models, plastic rotation can be

separated from the elastic part and, through a regression analysis of the data for all cases considered, is reported as in Equation (5-15) and Equation (5-16):

$$\theta_p = -0.0066 d_{conn} + 0.125 \quad (d_{conn} \text{ in inches}) \quad (5-15)$$

$$\theta_p = -0.00026 d_{conn} + 0.125 \quad (d_{conn} \text{ in millimetres}) \quad (5-16)$$

It is noted that the average elastic rotations observed in the studied three, four and five bolt shear tab connections are 0.035, 0.03 and 0.02, respectively. Table 5.8 and Figure 5.69 compare the results for plastic rotational capacities of all shear connections based on ASCE 41 (2006) and shear tab connections according to DoD (2009) to the results of Equation (5-15). As can be seen, the amount of ultimate rotation that can be resisted by shear tab connections in the column removal scenario is generally less than what is proposed by the seismic guideline, ASCE 41 (2006). This is directly related to presence of tension in the column loss event at large rotations, which does not exist in a seismic scenario. However, the proposed methods gives rotational ductilities that tend to be slightly larger than what is proposed by DoD (2009) for deep connections and significantly larger for shallow ones. As expected, the DoD values are more conservative than what is proposed based on the current research.

5.9 Summary and Conclusion

In this research, the simultaneous presence of shear, moment and tension in shear tab connections was investigated. The comparison between the experimental and the numerical quantities emphasized the effectiveness and correctness of the proposed finite element models. Tensile catenary force as the alternative load path mechanism in a column removal scenario is observed interacting with flexural response at the connection location. Ductility of shear tab connections is derived largely from the local deformation of bolt holes, especially bottom holes, and to a lesser degree the bolt slippage and bolt shear deformation before failure. Tension rupture of the bottom hole was the governing failure mode in most of the cases;

however, bolt shear rupture was also observed. Other conclusions that can be drawn are:

- It cannot be assumed that all of the fasteners in a line share equally in carrying the load. In fact, the fasteners towards the bottom of the joint carry the largest portion of the load. This unequal loading of the fasteners is accentuated as the rotation increases.
- The maximum rotational capacity of the shear tab connections studied was between 0.06 and 0.13 for five to three bolts. For comparison, based on previous research the maximum value of rotational demand on a shear connection under gravity load is about 0.03 radians. The maximum rotational demand due to seismic loading is approximately 0.05 radians (Astaneh 2005). Even the accumulative effect of both gravity and seismic forces is approximately 0.08 radians, which is generally smaller than the rotational demand in the column removal scenario. The pattern of bolt hole deformation in conventional loading is different than in the column removal scenario.
- The point that the flexural phase domination ends and catenary force begins to provide the major resistance is named the “devolution point”. For 3ST connections, this point is located at the maximum moment. The main reason for this is the fact that in 3-bolt connections the bottom and top bolts are resisting the moment through bearing resistance of the bolt–hole interaction. As soon as localized yielding occurs around the contact surface, the flexural resistance starts to vanish and the connection attempts to find another load path to take more load until failure. The failure will be in the catenary phase. Generally, the switch between flexural behaviour and the tensile phase in 3ST connections can be distinguished more precisely than in 4ST and 5ST connections. In the latter types, after local yielding at the location of the top and bottom hole, the contact of the other bolts with holes may resist additional moment. As a result, part of the connection will go through tension, although there is a substantial amount of flexural resistance remaining in the connection. A point might be distinguished as a "devolution point" in which a substantial decrease in flexural stiffness happens. This decrease might be

accompanied by an increase in tensile response rate (4ST connections) or not (5ST connections). After this point, tension and moment will interact with each other until failure occurs. Therefore, it can be inferred that the 4ST and 5ST connections fail mainly because of flexural–catenary actions.

- The resulting response curves can be used as input for shear tab connection models in full-building progressive collapse analyses. Continuing research in this area has resulted in a better understanding of connection performance and more economical design of joints with shear tab connections in the column loss event.

Table 5.1: Typical materials used for shear tab connections

Component	Material	Description
Plate	A36, A572, 300W, 350W	-
Bolts	ASTM A325, A490	standard/slotted hole
Welds	E70XX electrode	fillet welds

Table 5.2: Limitations of conventional shear tab connections (AISC 2010)

No.	Limitation
1	t_p or $t_w \leq \text{limits}$
2	$L_{eh} \geq 2d_b$ for the plate or beam web
3	$L_{ev} \geq \text{limits}$
4	$a \leq 3 \frac{1}{2}$ in
5	$2 \leq n \leq 12$
6	$L_{ST} \geq T/2$
7	fillet weld size = $5/8 t_p$

Table 5.3: Summary of characteristic features of FE models of ST connections

No.	Specimen Label ¹	Plate Type	Plate thickness	Bolt Type	Bolt diameter	Remarks
1	3ST-3/8-3/4	ASTM A36	9.5mm (3/8 in)	ASTM A325	19.1 mm (3/4 in)	Used for verification ²
2	3ST-1/4-3/4	ASTM A36	6.4 mm (1/4" in)	ASTM A325	19.1 mm (3/4 in)	-
3	3ST-1/2-3/4	ASTM A36	12.7 mm (1/2 in)	ASTM A325	19.1 mm (3/4 in)	-
4	3ST-3/8-5/8	ASTM A36	9.5 mm (3/8 in)	ASTM A325	15.9 mm (5/8 in)	-
5	3ST-3/8-7/8	ASTM A36	9.5 mm (3/8 in)	ASTM A325	22.2 mm (7/8 in)	-
6	3ST-3/8-3/4	ASTM A36	9.5 mm (3/8 in)	ASTM A490	19.1 mm (3/4 in)	-
7	4ST-3/8-3/4	ASTM A36	9.5mm (3/8 in)	ASTM A325	19.1 mm (3/4 in)	Used for verification ²
8	4ST-1/4-3/4	ASTM A36	6.4 mm (1/4" in)	ASTM A325	19.1 mm (3/4 in)	-
9	4ST-1/2-3/4	ASTM A36	12.7 mm (1/2 in)	ASTM A325	19.1 mm (3/4 in)	-
10	4ST-3/8-5/8	ASTM A36	9.5 mm (3/8 in)	ASTM A325	15.9 mm (5/8 in)	-
11	4ST-3/8-7/8	ASTM A36	9.5 mm (3/8 in)	ASTM A325	22.2 mm (7/8 in)	-
12	4ST-3/8-3/4	ASTM A36	9.5 mm (3/8 in)	ASTM A490	19.1 mm (3/4 in)	-
13	5ST-3/8-3/4	ASTM A36	9.5mm (3/8 in)	ASTM A325	19.1 mm (3/4 in)	Used for verification ²
14	5ST-1/4-3/4	ASTM A36	6.4 mm (1/4" in)	ASTM A325	19.1 mm (3/4 in)	-
15	5ST-1/2-3/4	ASTM A36	12.7 mm (1/2 in)	ASTM A325	19.1 mm (3/4 in)	-
16	5ST-3/8-5/8	ASTM A36	9.5 mm (3/8 in)	ASTM A325	15.9 mm (5/8 in)	-
17	5ST-3/8-7/8	ASTM A36	9.5 mm (3/8 in)	ASTM A325	22.2 mm (7/8 in)	-
18	5ST-3/8-3/4	ASTM A36	9.5 mm (3/8 in)	ASTM A490	19.1 mm (3/4 in)	-

¹ Imperial units are utilized in labelling the models since the experimental program was designed based on imperial unit.

² Test results are available for these models.

Table 5.4: Comparison of numerical and experimental (Thompson 2009) responses of shear tab connections with three bolts at initial failure

Spec. Label	Side	Moment, M (kN.m)	Shear, V (kN)	Axial, P (kN)	Rotation, Θ (radians)	Failure Mode
3ST1	Left	-	-	-	-	-
	Right	Negligible	30.07	217.74	0.128	Bolt Shear Rupture
3ST2	Left	-	-	-	-	-
	Right	Negligible	28.60	188.12	0.125	Tension Rupture
3ST3	Left	-	-	-	-	-
	Right	Negligible	24.06	217.47	0.128	Tension Rupture
3ST-Mean			27.58	207.78	0.127	
3ST-FEA			27.24	182.31	0.129	Shear tab bottom hole rupture
Deviation %			1.23	12.26	1.57	

188

Table 5.5: Comparison of numerical and experimental (Thompson 2009) responses of shear tab connections with four bolts at initial failure

Spec. Label	Side	Moment, M (kN.m)	Shear, V (kN)	Axial, P (kN)	Rotation, Θ (radians)	Failure Mode
4ST1	Left	-	-	-	-	-
	Right	30.32	31.23	142.97	0.097	Block Shear Rupture
4ST2	Left	-	-	-	-	-
	Right	31.53	38.34	185.22	0.093	Bolt Shear Rupture
4ST3	Left	25.32	28.20	126.51	0.091	Tension Rupture
	Right	-	-	-	-	-
4ST-Mean		29.06	32.59	151.57	0.094	
4ST-FEA		37.66	33.86	154.14	0.090	Shear tab bottom hole rupture
Deviation %		29.61	3.89	1.70	3.91	

Table 5.6: Comparison of numerical and experimental (Thompson 2009) responses of shear tab connections with five bolts at initial failure

Spec. Label	Side	Moment, M (kN.m)	Shear, V (kN)	Axial, P (kN)	Rotation, Θ (radians)	Failure Mode
5ST1	Left	-	-	-	-	-
	Right	55.90	47.11	147.73	0.073	Block Shear Rupture
5ST2	Left	-	-	-	-	-
	Right	60.54	52.00	202.13	0.069	Block Shear Rupture
5ST3	Left	68.49	45.46	151.42	0.071	Tension Rupture
	Right	-	-	-	-	-
5ST-Mean		61.64	48.19	167.09	0.071	
5ST-FEA		65.85	47.31	177.48	0.069	Shear tab bottom hole rupture
Deviation %		6.83	1.82	6.22	2.82	

Table 5.7: Summary of numerical and experimental responses of shear tab connections at initial failure

No.	Specimen/Model Label	Connection Depth (mm)	Rotation (Rad)	V (kN)	T (kN)	M (kN.m)	Failure Mode
1	3ST-3/8-3/4-EXP	152.4	0.127	27.6	207.8	Negligible	Bolt shear rupture and ST bottom hole rupture
2	3ST-3/8-3/4	152.4	0.129	27.2	182.3	7.1	ST bottom hole rupture
3	3ST-1/4-3/4	152.4	0.112	13.7	78.9	9.2	ST bottom hole rupture
4	3ST-1/2-3/4	152.4	0.136	34.6	233.8	5.8	Bolt shear failure
5	3ST-3/8-5/8	152.4	0.121	20.1	131.0	8.2	ST bottom hole rupture (Bolt close to shear rupture)
6	3ST-3/8-7/8	152.4	0.129	28.9	180.7	10.9	ST bottom hole rupture
7	3ST-3/8-3/4-A490	152.4	0.122	23.3	144.4	10.8	ST bottom hole rupture
8	4ST-3/8-3/4-EXP	228.6	0.094	32.6	151.6	29.1	Block shear rupture; ST bottom hole rupture
9	4ST-3/8-3/4	228.6	0.091	33.9	154.1	37.7	ST bottom hole rupture
10	4ST-1/4-3/4	228.6	0.077	20.6	84.7	26.6	ST bottom hole rupture
11	4ST-1/2-3/4	228.6	0.103	43.9	214.8	41.5	Bolt shear failure
12	4ST-3/8-5/8	228.6	0.087	28.2	134.4	31.3	ST bottom hole rupture and bolt shear rupture
13	4ST-3/8-7/8	228.6	0.088	35.7	141.5	44.0	ST bottom hole rupture
14	4ST-3/8-3/4-A490	228.6	0.091	34.0	151.6	38.3	ST bottom hole rupture
15	5ST-3/8-3/4-EXP	304.8	0.071	48.2	167.1	61.6	Block shear rupture; ST bottom hole rupture
16	5ST-3/8-3/4	304.8	0.070	47.3	177.5	65.9	ST bottom hole rupture
17	5ST-1/4-3/4	304.8	0.059	30.0	107.9	44.6	ST bottom hole rupture
18	5ST-1/2-3/4	304.8	0.081	61.0	247.8	77.3	Bolt shear rupture
19	5ST-3/8-5/8	304.8	0.065	38.4	148.4	54.3	ST bottom hole rupture and bolt shear rupture
20	5ST-3/8-7/8	304.8	0.066	49.7	156.9	74.0	ST bottom hole rupture
21	5ST-3/8-3/4-A490	304.8	0.070	47.5	174.6	66.7	ST bottom hole rupture

Table 5.8: Comparison of plastic rotational capacities of shear tab connections based on ASCE 41 (2006), DoD (2009), and proposed equation

Connection depth	Connection rotation (rad)		
	ASCE 41	DoD 2009	Proposed
3 in (76.2 mm)	0.139	0.046	0.105
6 in (152.4 mm)	0.128	0.041	0.085
9 in (228.6 mm)	0.118	0.037	0.065
12 in (304.8 mm)	0.107	0.032	0.045
15 in (381 mm)	0.096	0.028	0.026

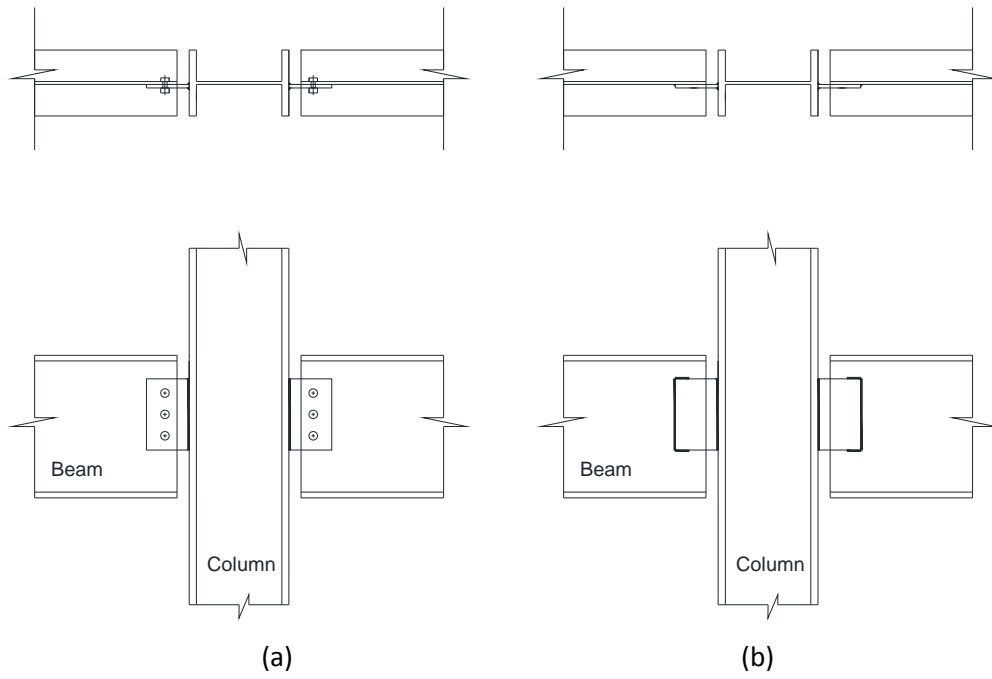


Figure 5.1: Types of shear tab connections: (a) welded-bolted (b) welded-welded

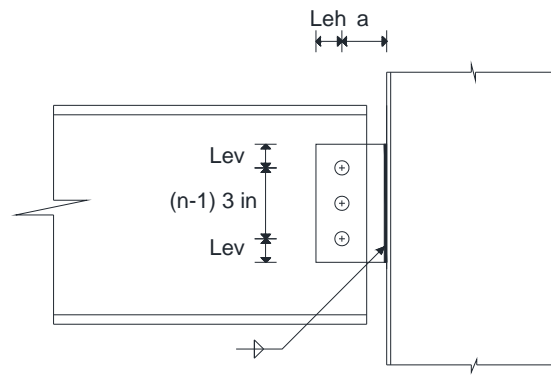


Figure 5.2: Different parameters of conventional shear tab



Figure 5.3: Finite element grid for the beam model

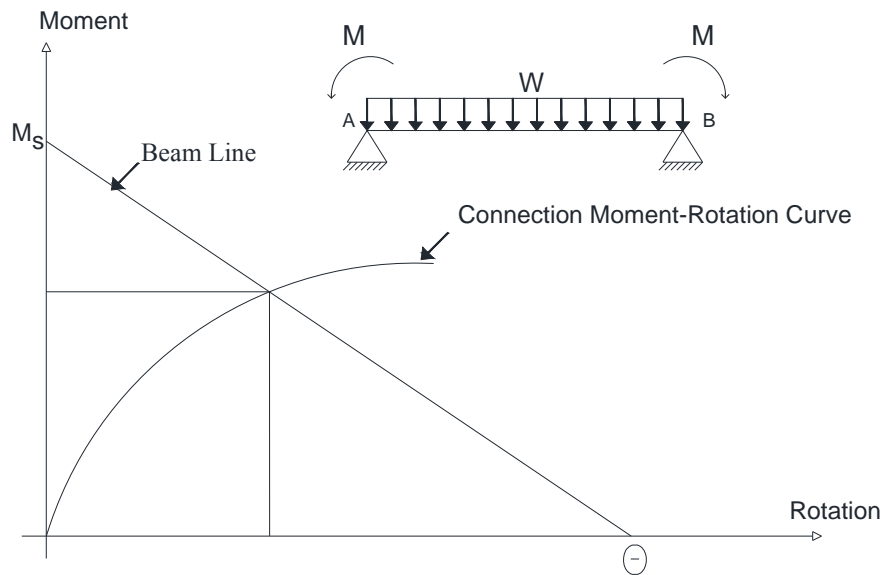


Figure 5.4: Moment-rotation relationship in the beam-line model (Richard et al. 1980)

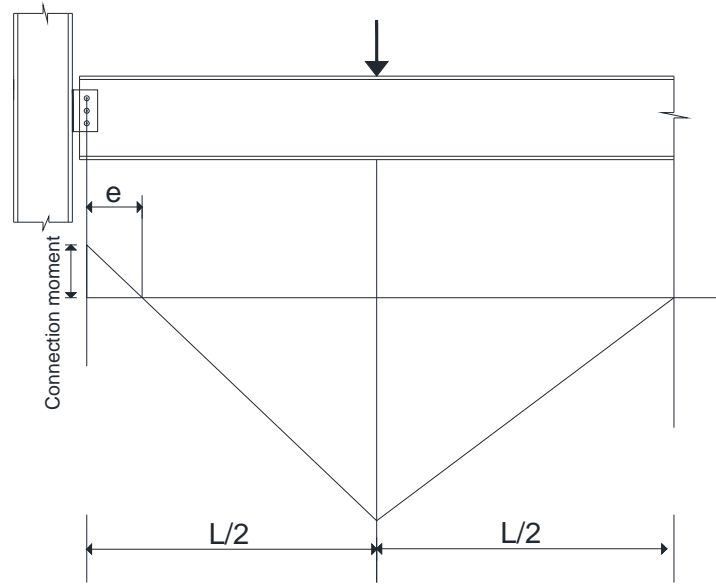


Figure 5.5: Test setup (Richard et al. 1980)

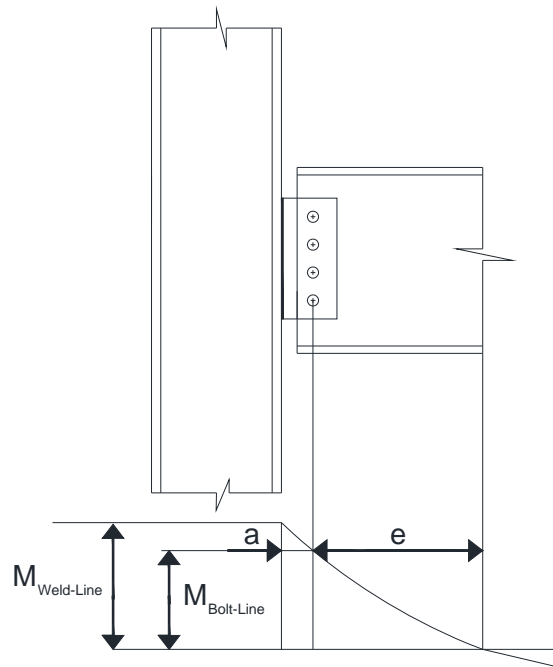


Figure 5.6: Eccentricity defined by Richard et al. (1980)

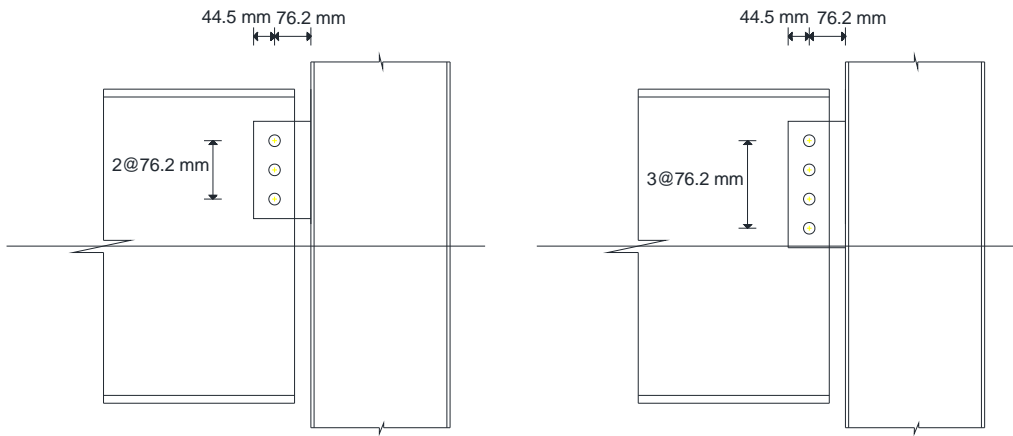


Figure 5.7: Off-axis shear tab connections Hormby et al. (1984)

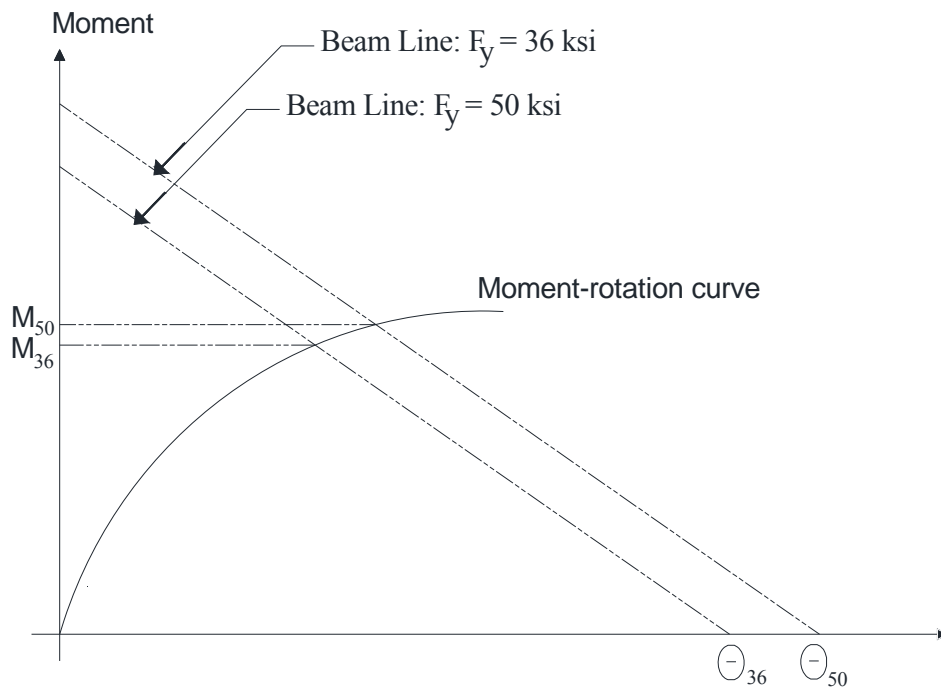


Figure 5.8: Beam line definitions for $F_y=36$ and $F_y=50$ steel beams (Hormby et al. 1984)

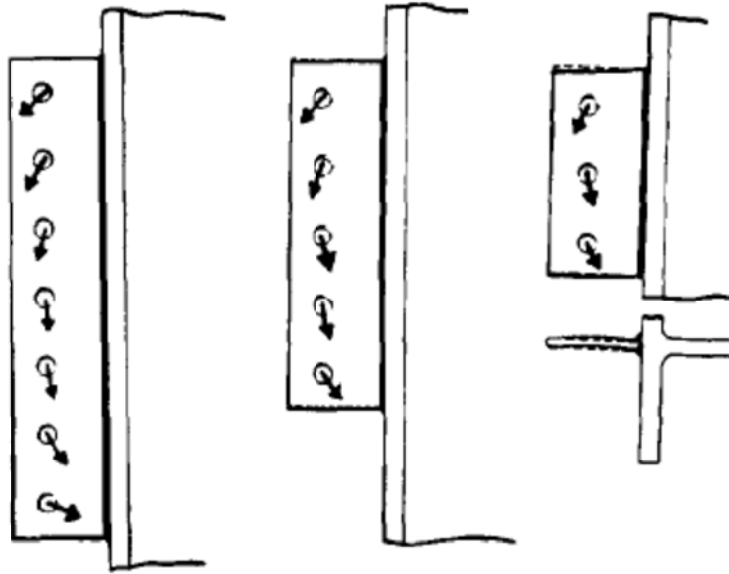


Figure 5.9: Directions of plate deformations at bolt holes after tests (Astaneh et al. 1989)

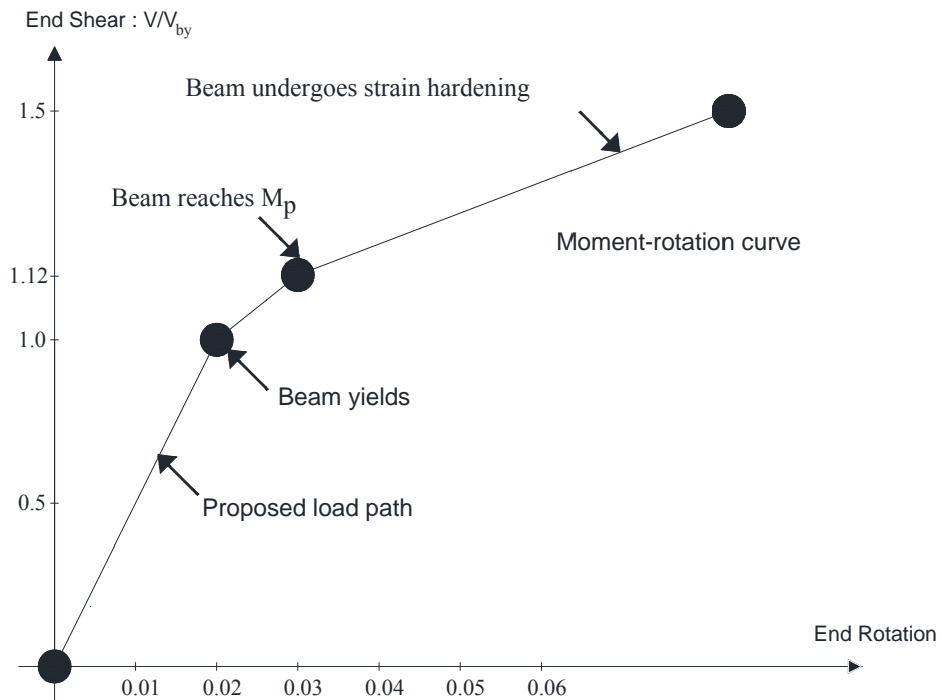


Figure 5.10: Loading history applied to shear connections under gravity loads (Astaneh et al. 2002)

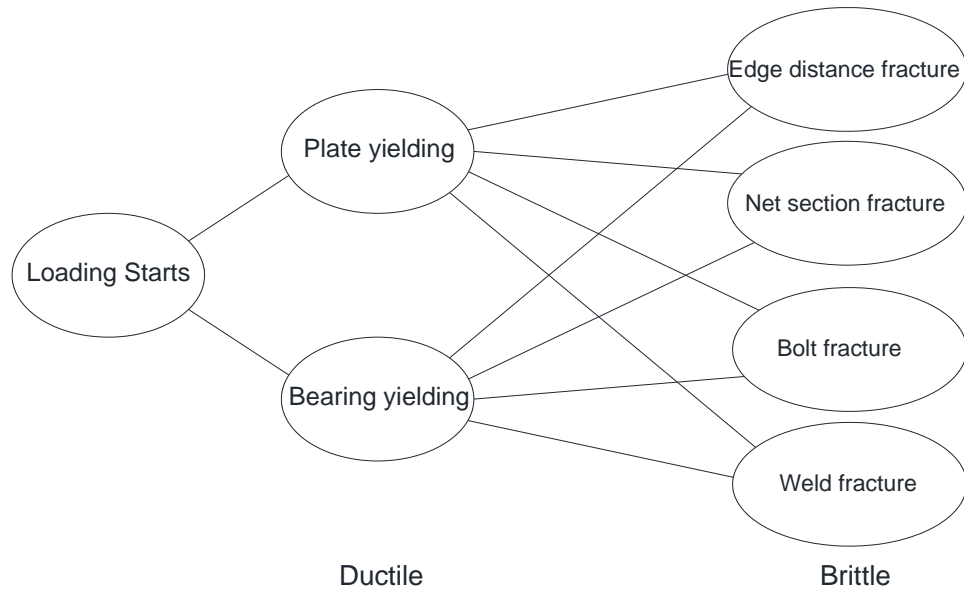


Figure 5.11: Hierarchy of failure modes: ductile and brittle (Astaneh et al. 2002)

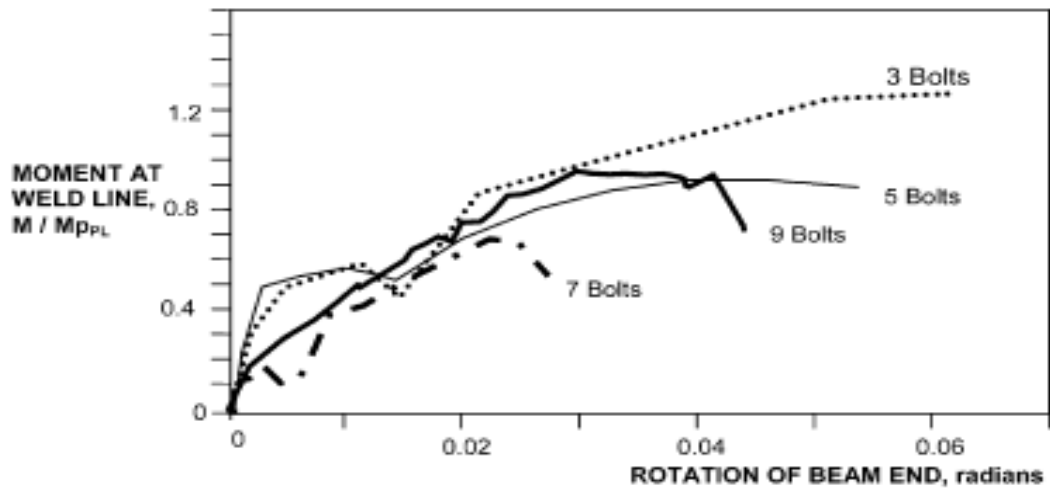


Figure 5.12: Typical moment–rotation curves (Astaneh et al. 2002)

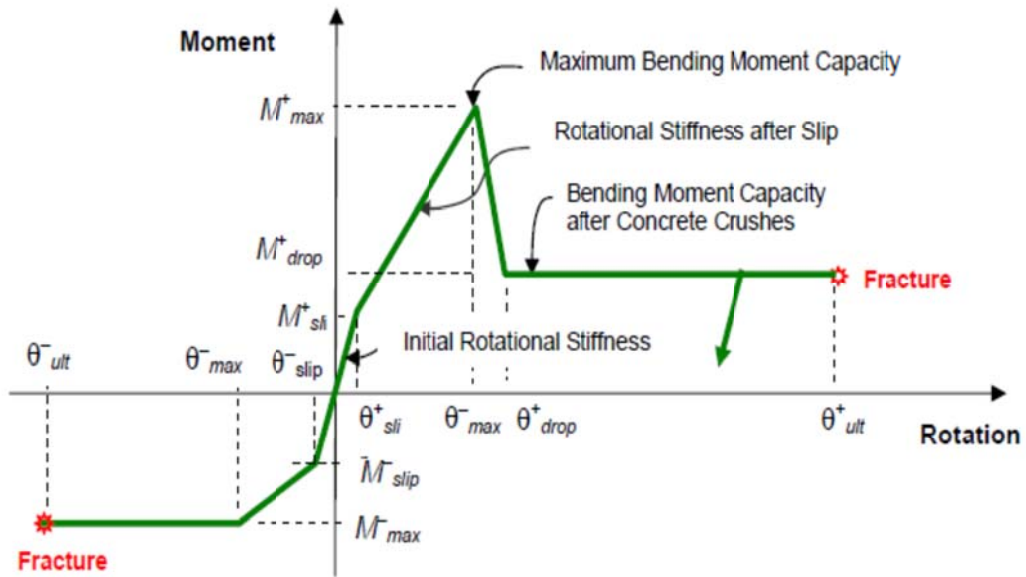


Figure 5.13: Moment–rotation curves proposed for shear tabs in composite beams (Astaneh 2005)

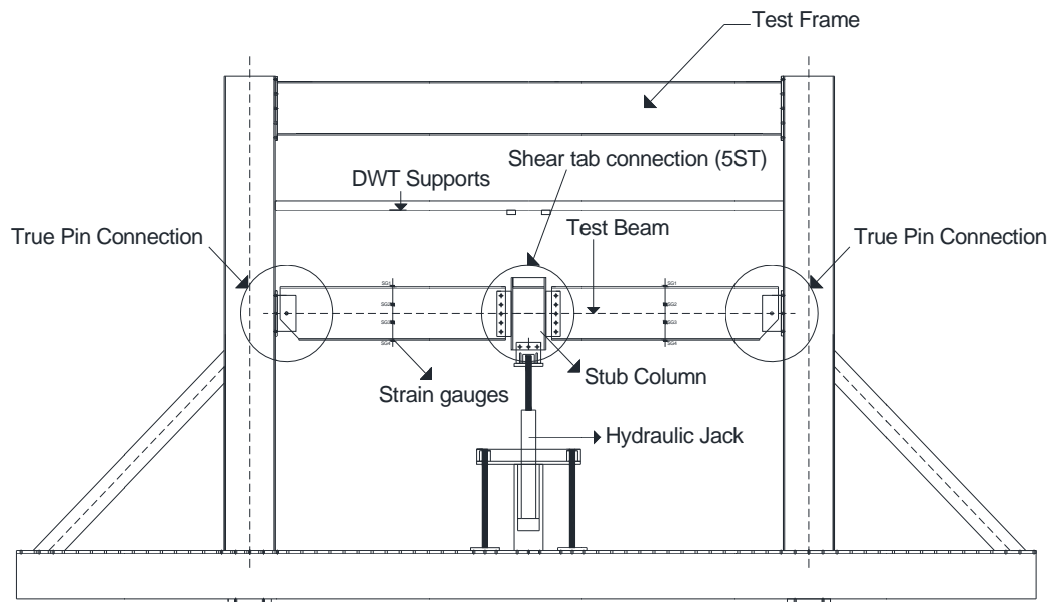
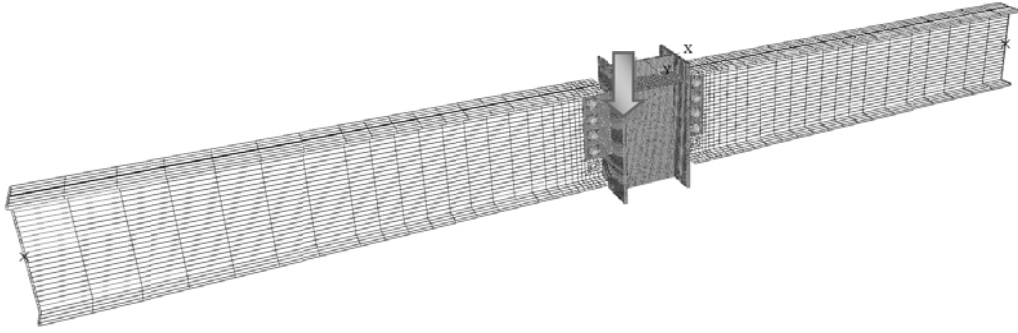
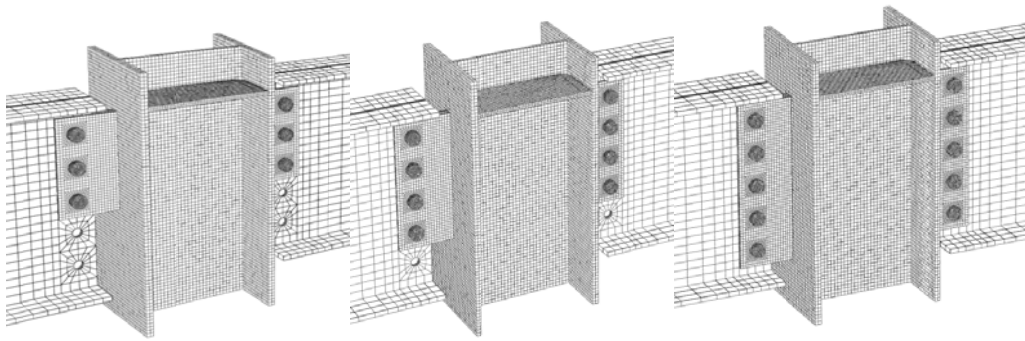


Figure 5.14: Selected experimental program test setup (Thompson 2009)



(a)



(b)

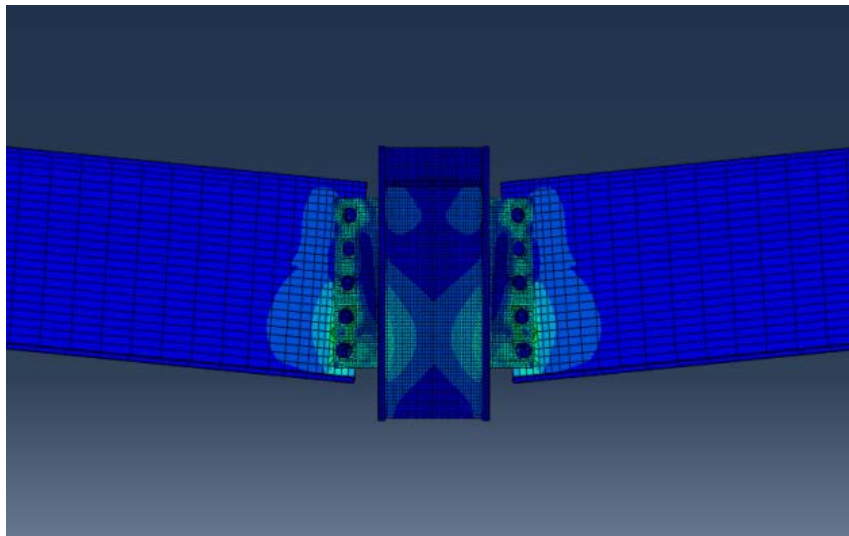
(c)

(d)

Figure 5.15: FE models of: (a) full connection assembly, (b) 3 bolt ST connection (3ST), (c) 4 bolt ST connection (4ST), (d) 5 bolt ST connection (5ST)



(a)

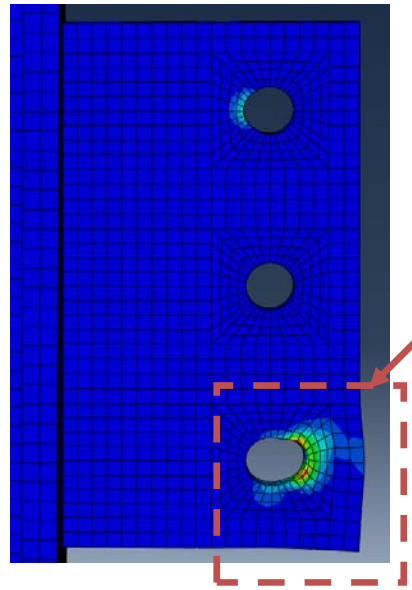


(b)

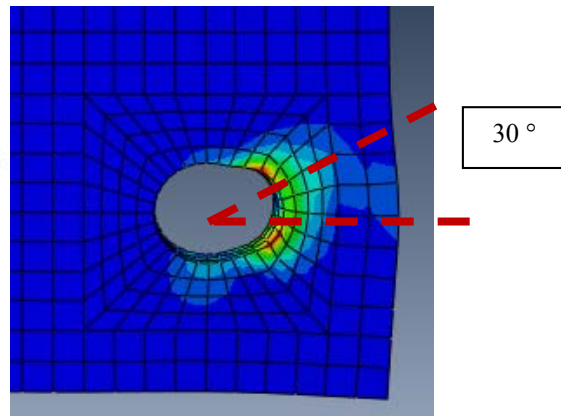
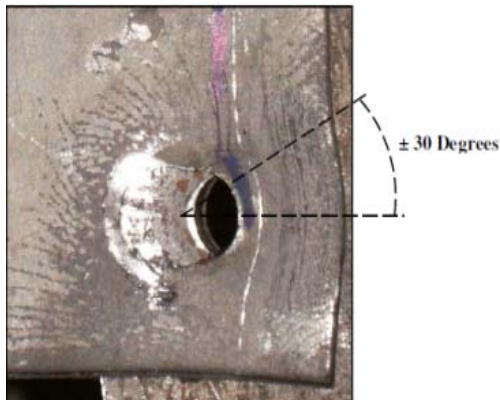
Figure 5.16: Deformed shape of the connection assembly (a) experiment (Thompson 2009) (b) finite element



(a)



(b)



(c)

Figure 5.17: Main source of ductility: bottom hole deformation: (a) experimental (Thompson 2009) (b) numerical results (c) magnified view of bottom hole region

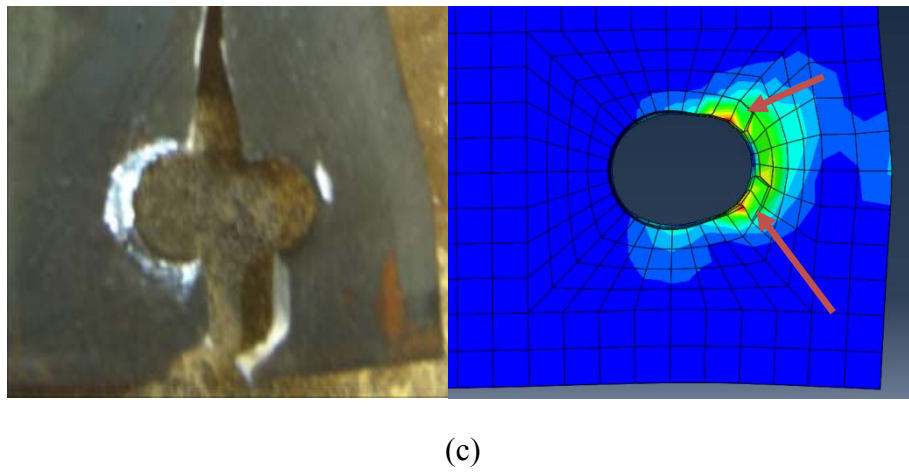
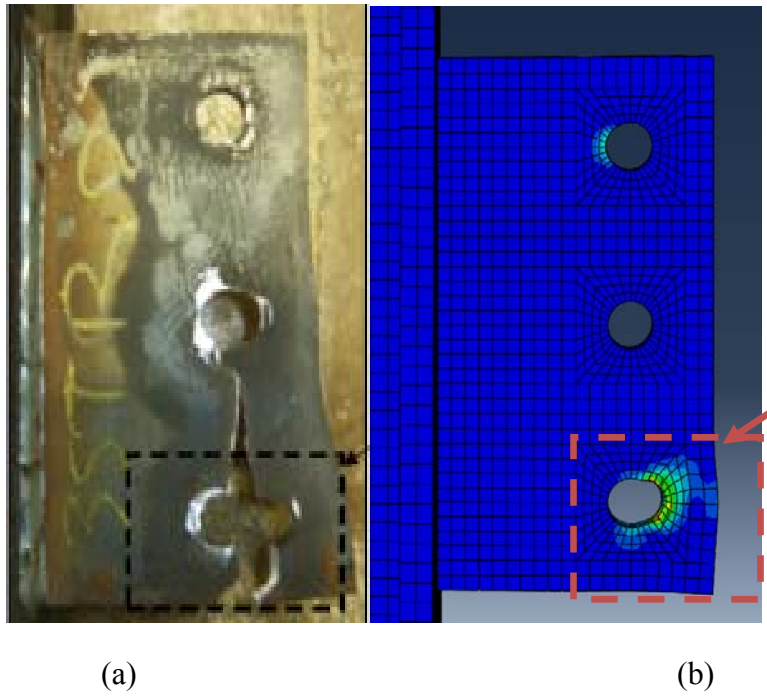


Figure 5.18: Failure of 3ST at the bottom hole by bearing deformation and rupture
(a) experimental (Thompson 2009) and (b) numerical results (c) magnified view
of bottom hole region

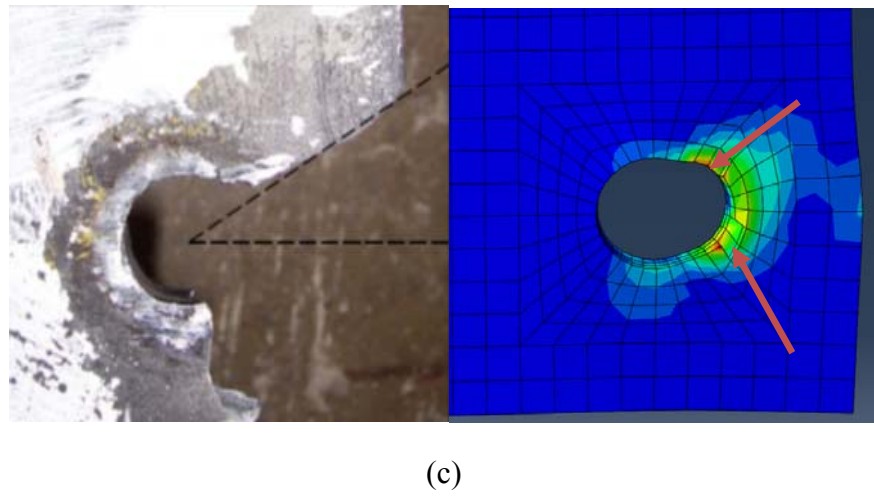
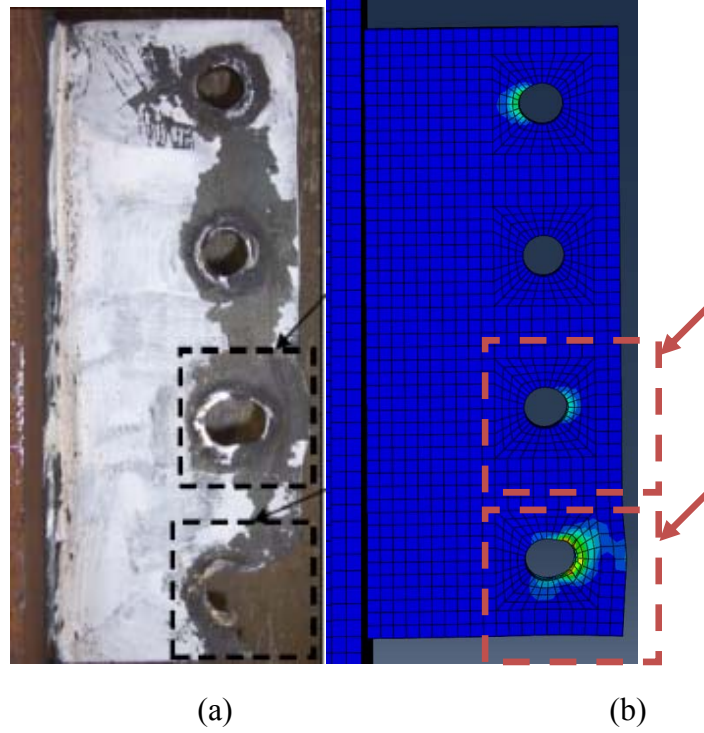
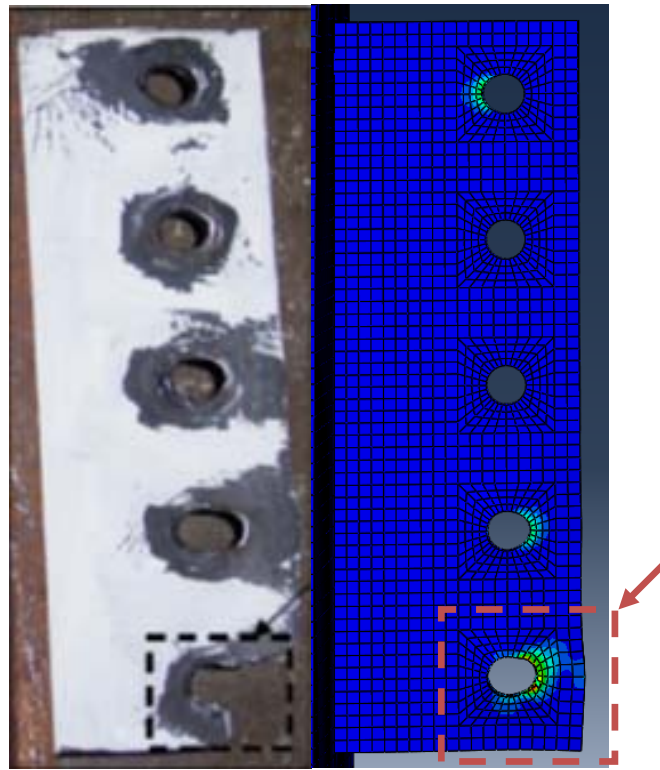
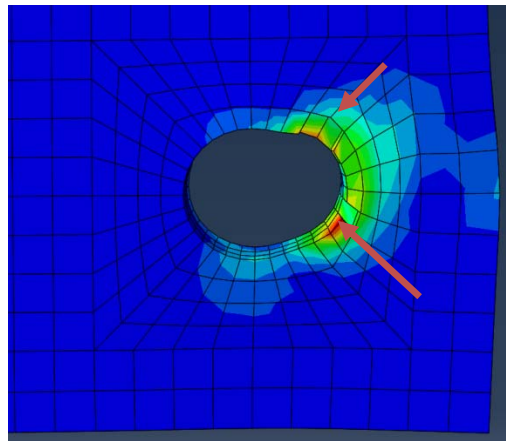


Figure 5.19: Failure of 4ST at the bottom hole by bearing deformation and rupture
 (a) experimental (Thompson 2009) and (b) numerical results (c) magnified view
 of bottom hole region



(a)

(b)

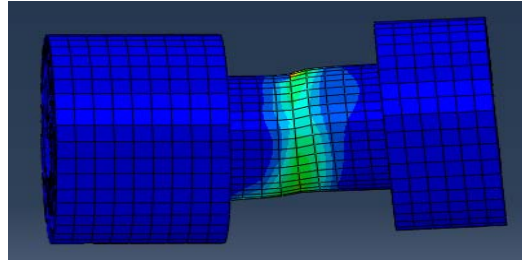


(c)

Figure 5.20: Failure of 5ST at the bottom hole by bearing deformation and rupture
(a) experimental (Thompson 2009) and (b) numerical results (c) magnified view
of bottom hole region



(a)



(b)

Figure 5.21: Typical bolt shear deformation and failure (a) experimental (Thompson 2009) and (b) numerical results

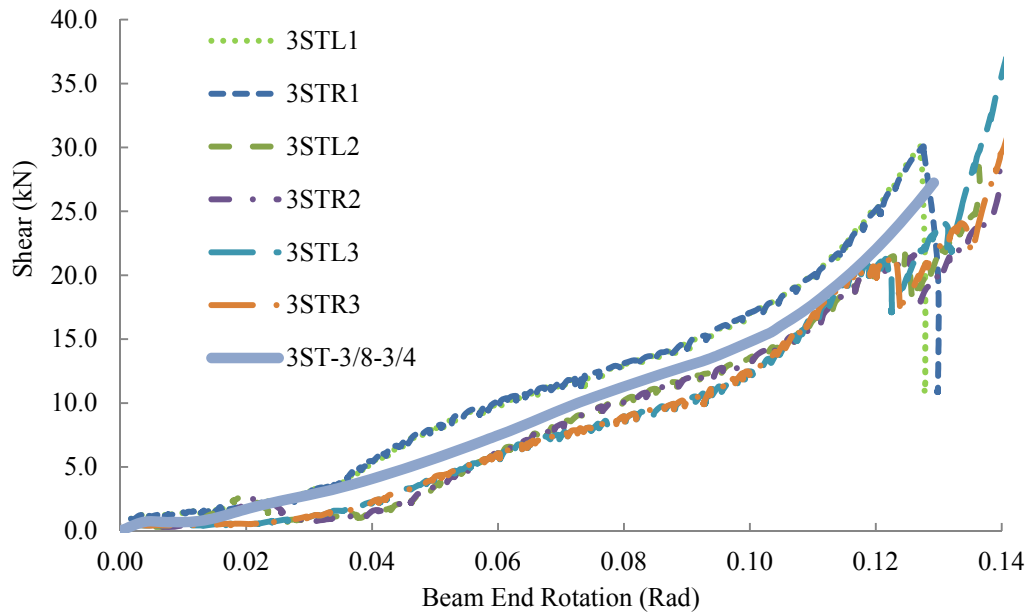


Figure 5.22: Comparison of numerical and experimental shear response of connection 3ST

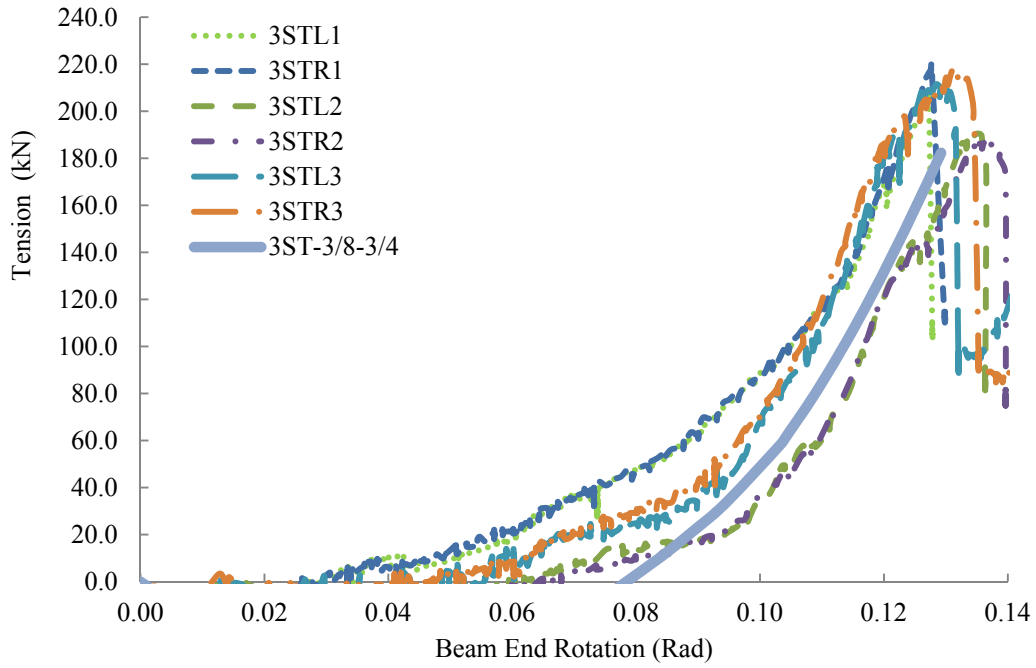


Figure 5.23: Comparison of numerical and experimental tensile response of connection 3ST

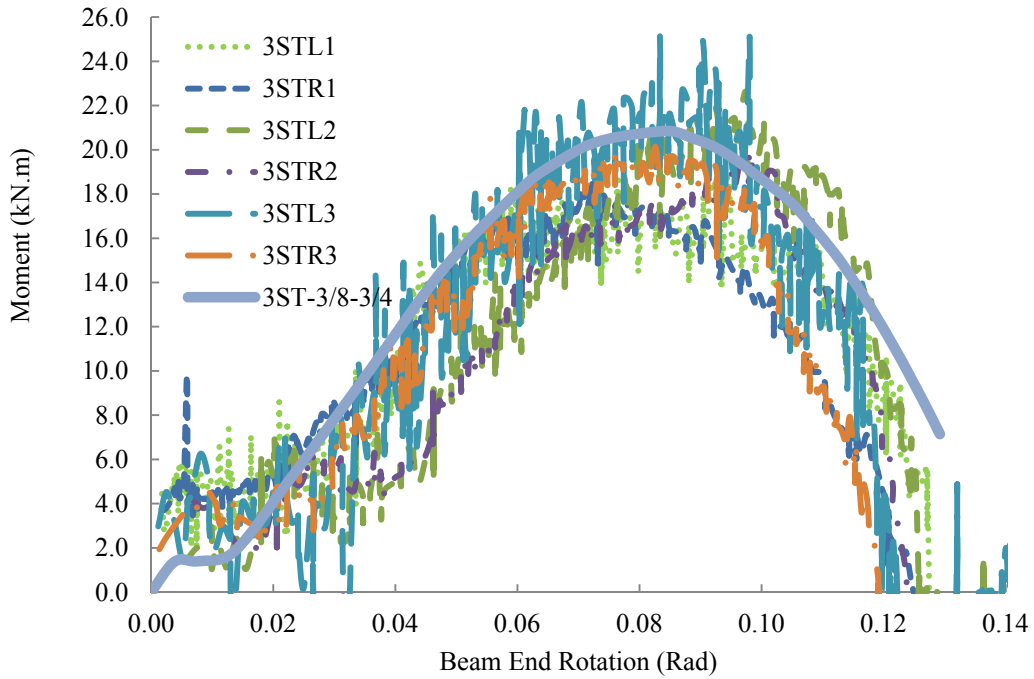


Figure 5.24: Comparison of numerical and experimental flexural response of connection 3ST

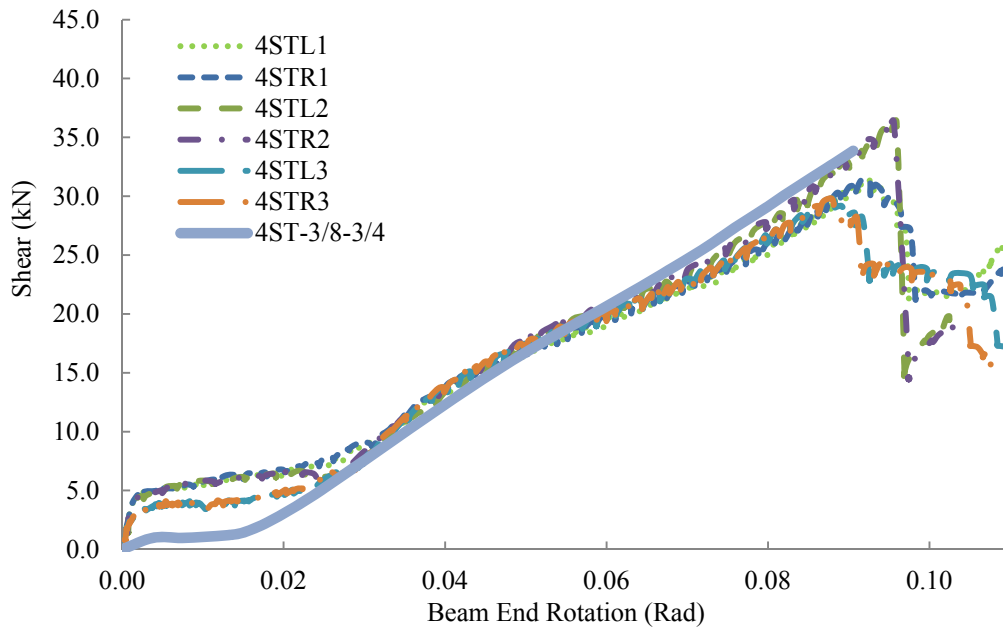


Figure 5.25: Comparison of numerical and experimental shear response of connection 4ST

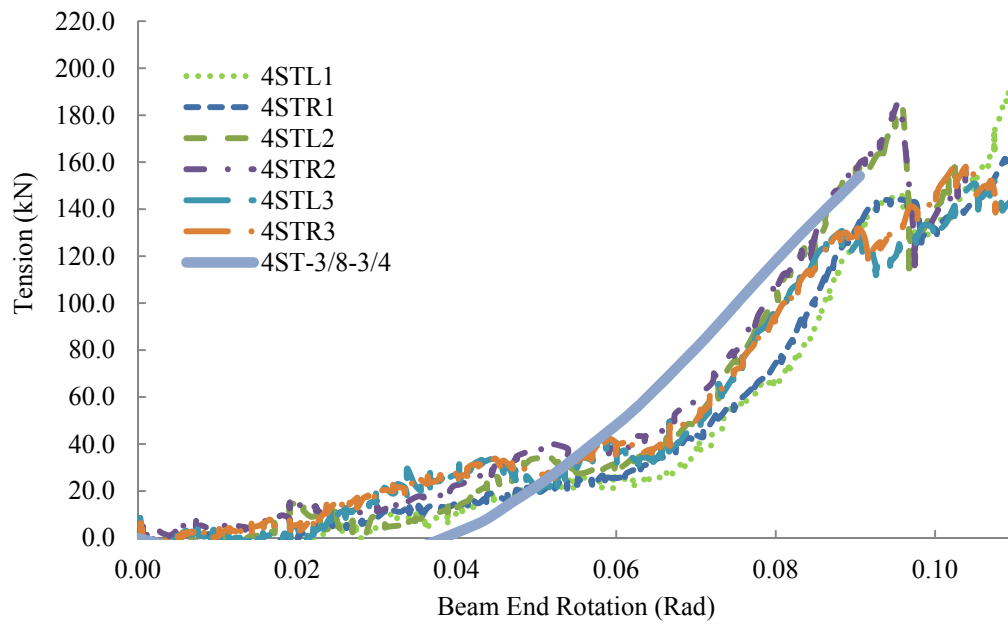


Figure 5.26: Comparison of numerical and experimental tensile response of connection 4ST

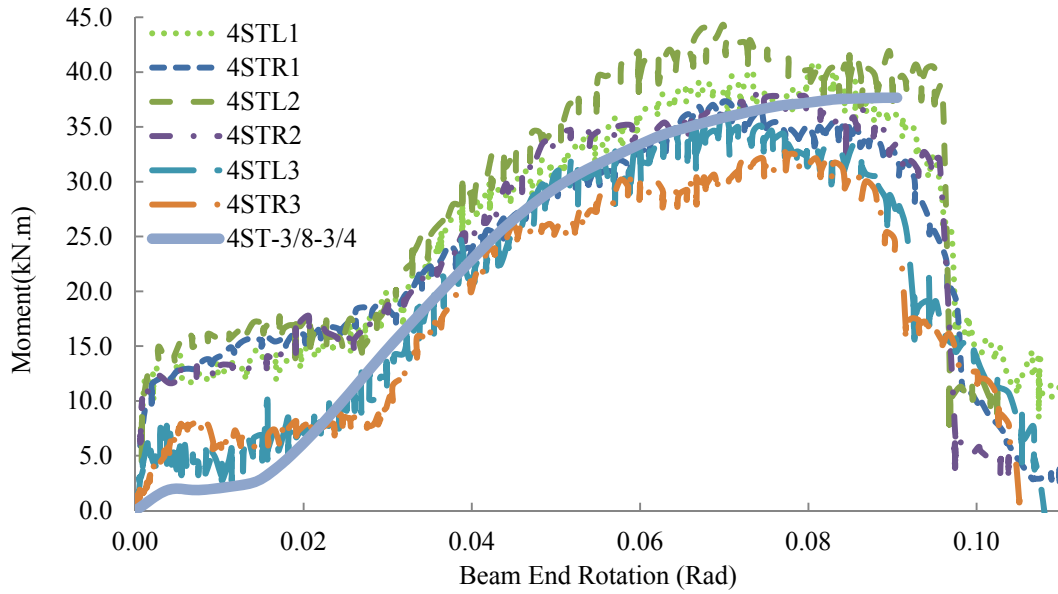


Figure 5.27: Comparison of numerical and experimental flexural response of connection 4ST

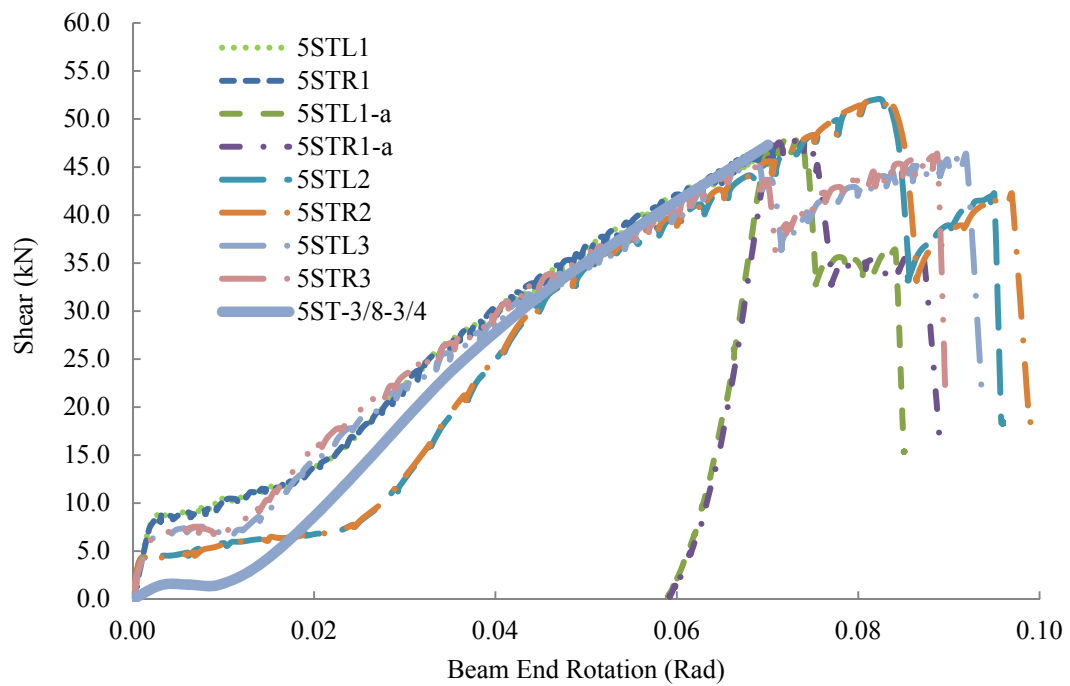


Figure 5.28: Comparison of numerical and experimental shear response of connection 5ST

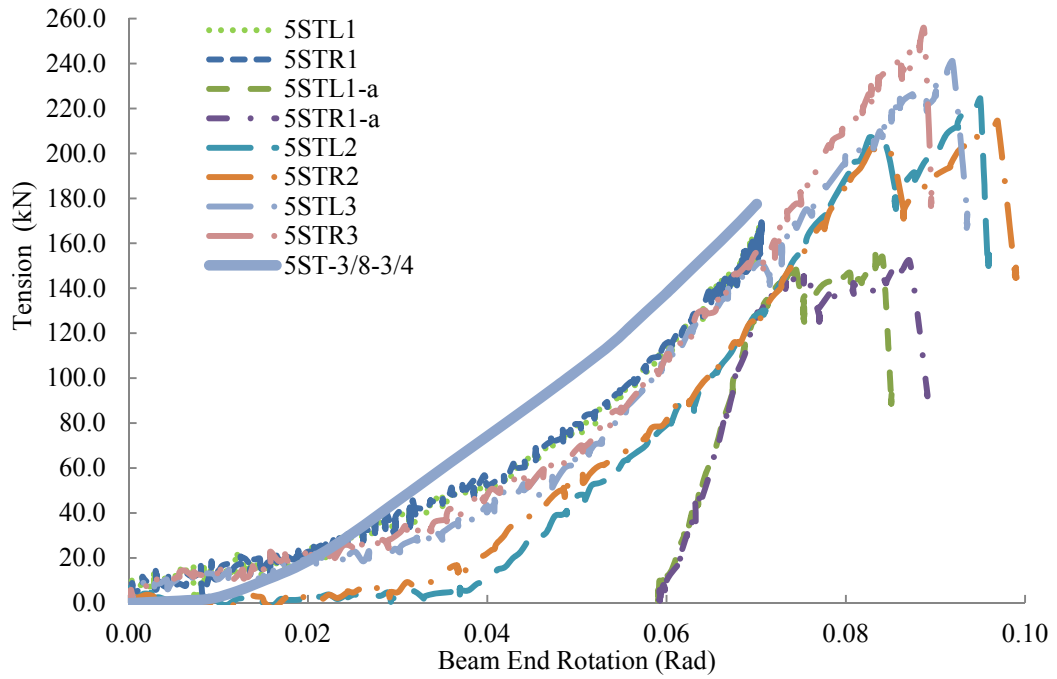


Figure 5.29: Comparison of numerical and experimental tensile response of connection 5ST

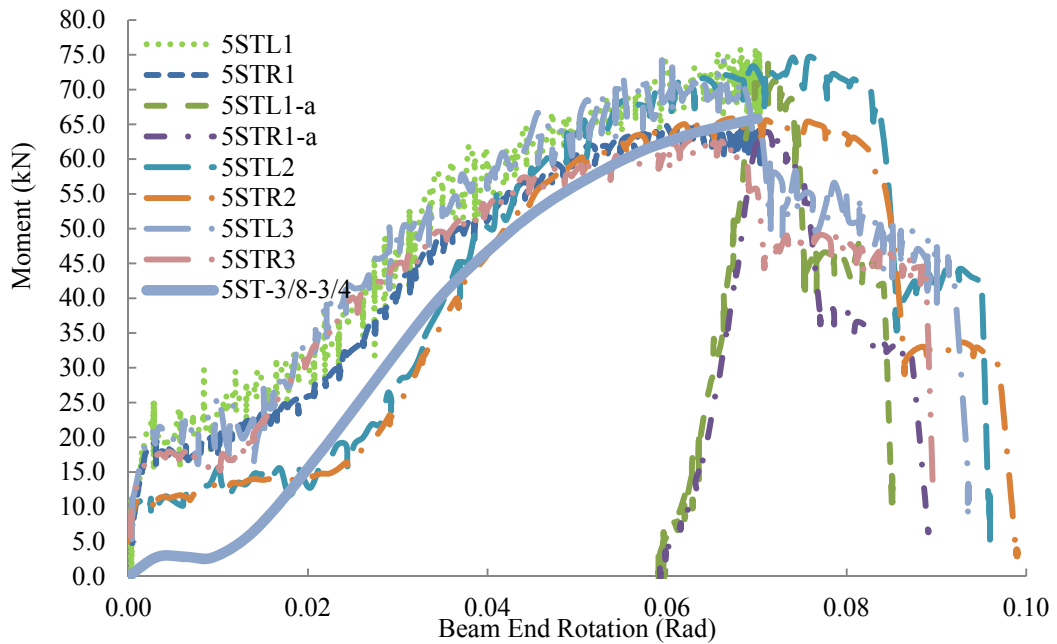


Figure 5.30: Comparison of numerical and experimental flexural response of connection 5ST

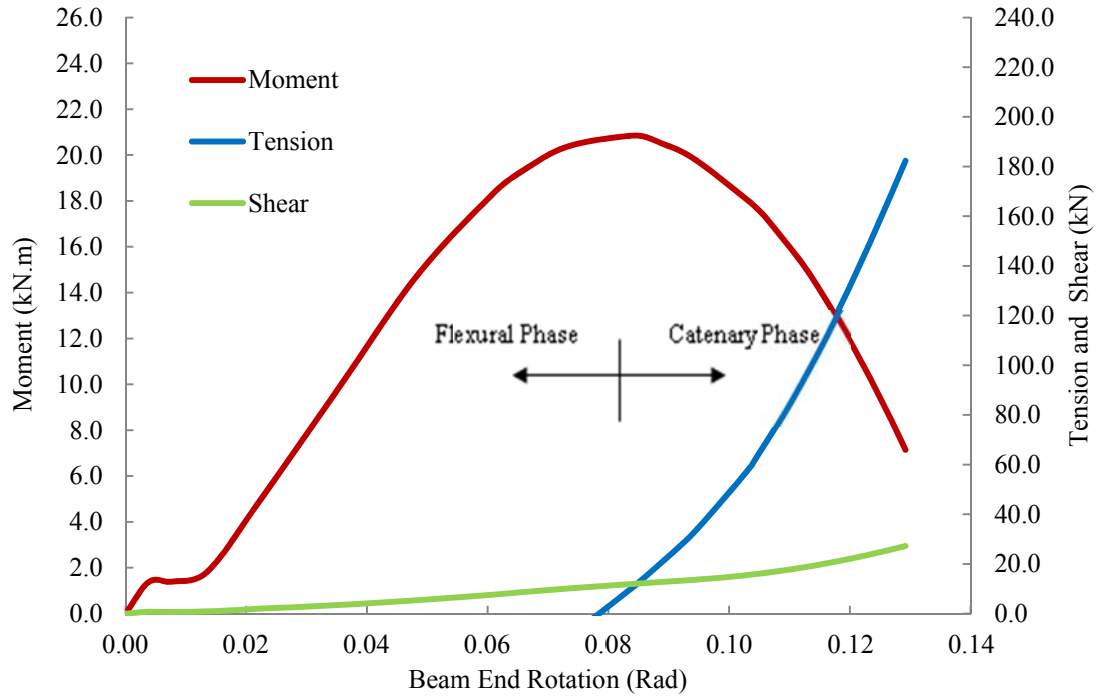


Figure 5.31: Bolt line forces versus beam end rotation – Specimen 3ST-3/8-3/4

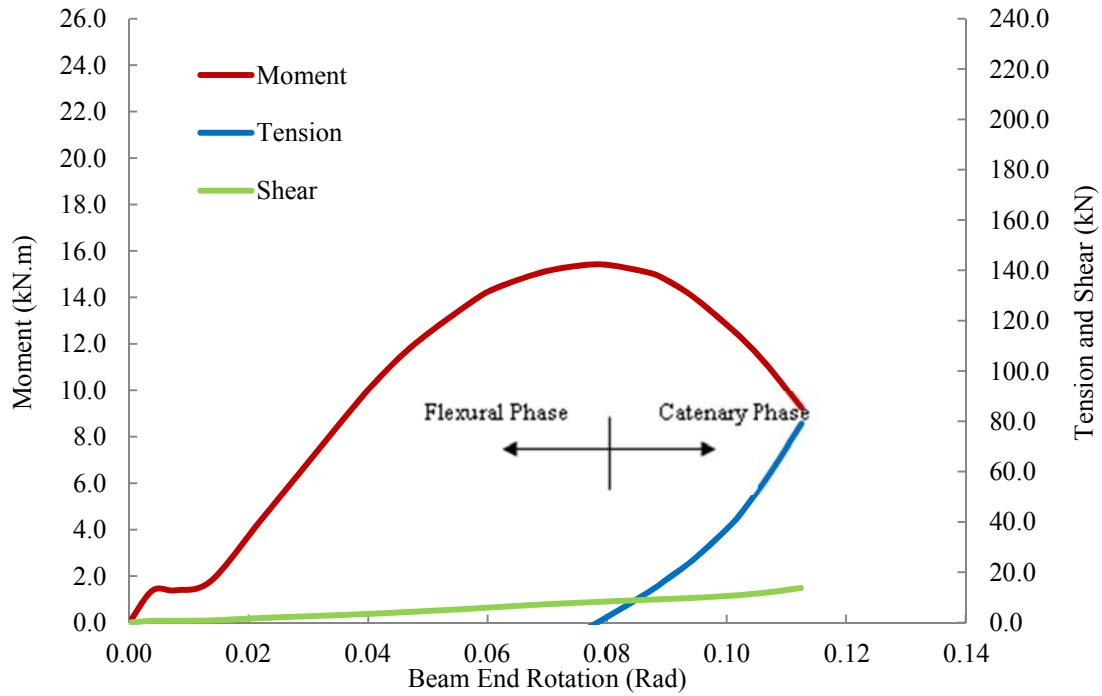


Figure 5.32: Bolt line forces versus beam end rotation – Specimen 3ST-1/4-3/4

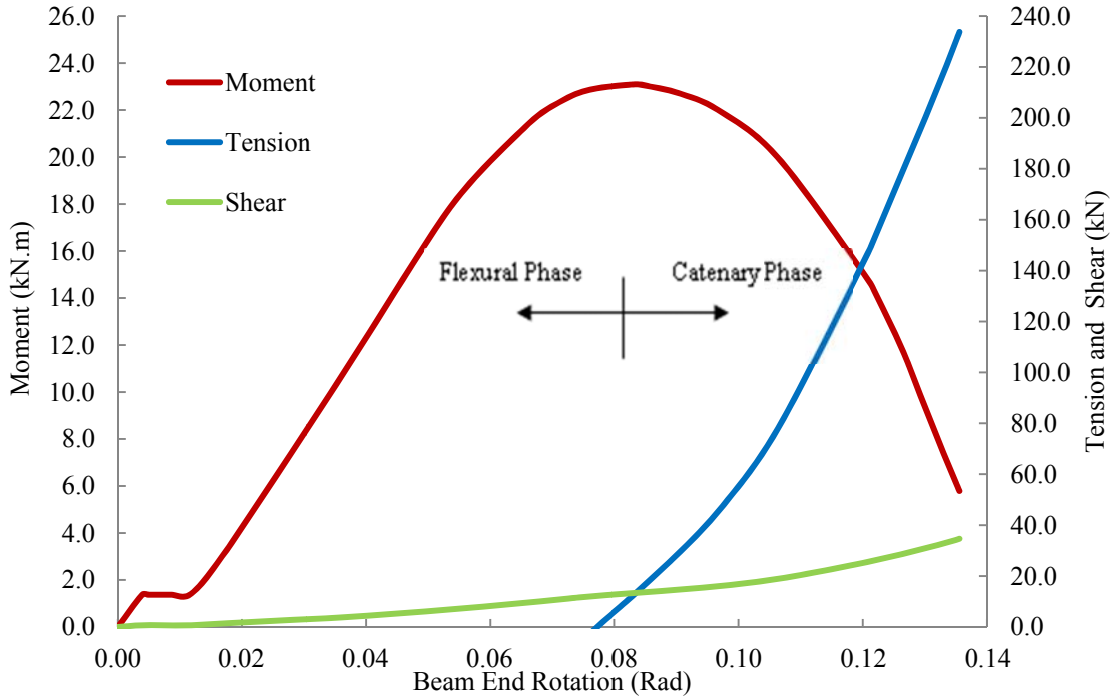


Figure 5.33: Bolt line forces versus beam end rotation – Specimen 3ST-1/2-3/4

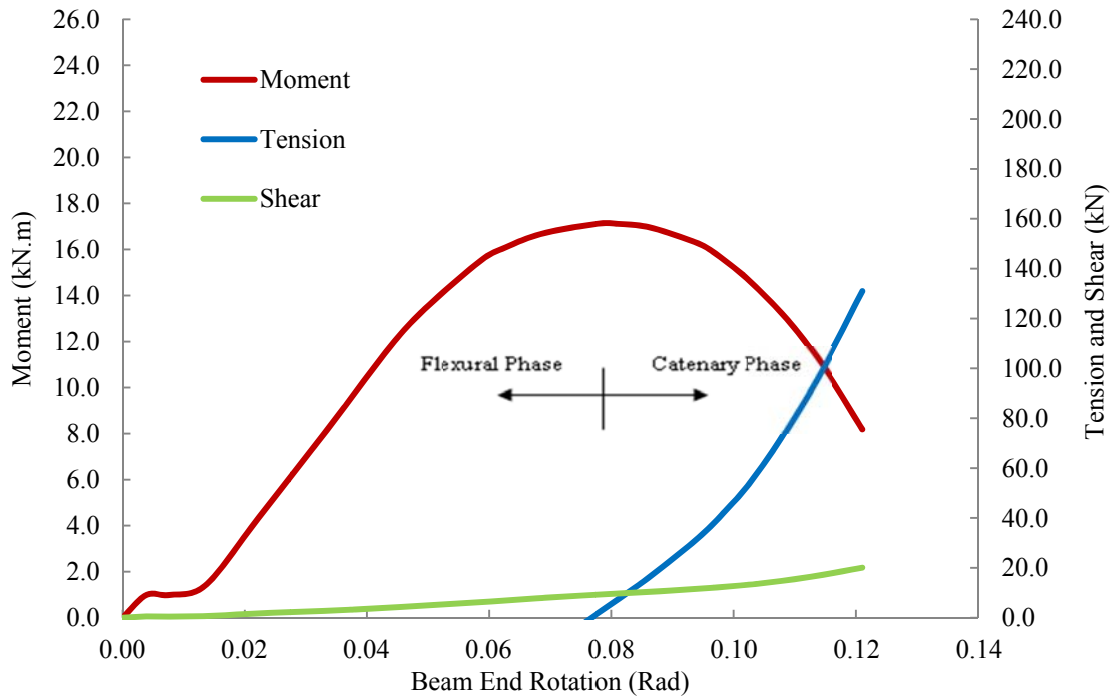


Figure 5.34: Bolt line forces versus beam end rotation – Specimen 3ST-3/8-5/8

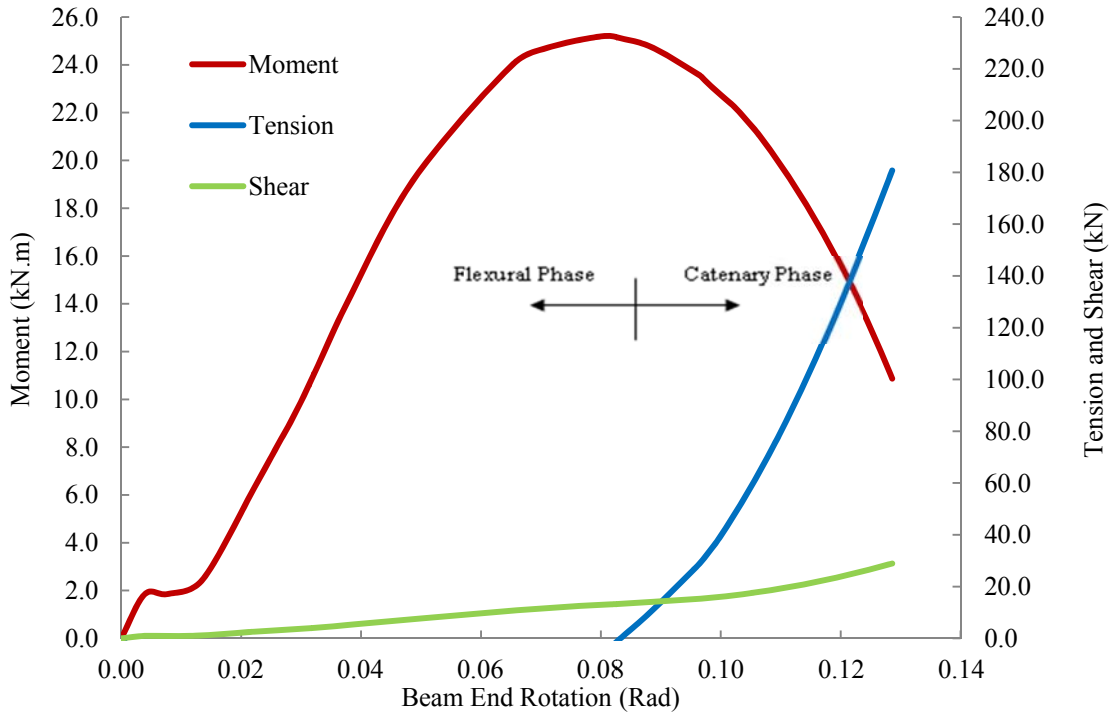


Figure 5.35: Bolt line forces versus beam end rotation – Specimen 3ST-3/8-7/8

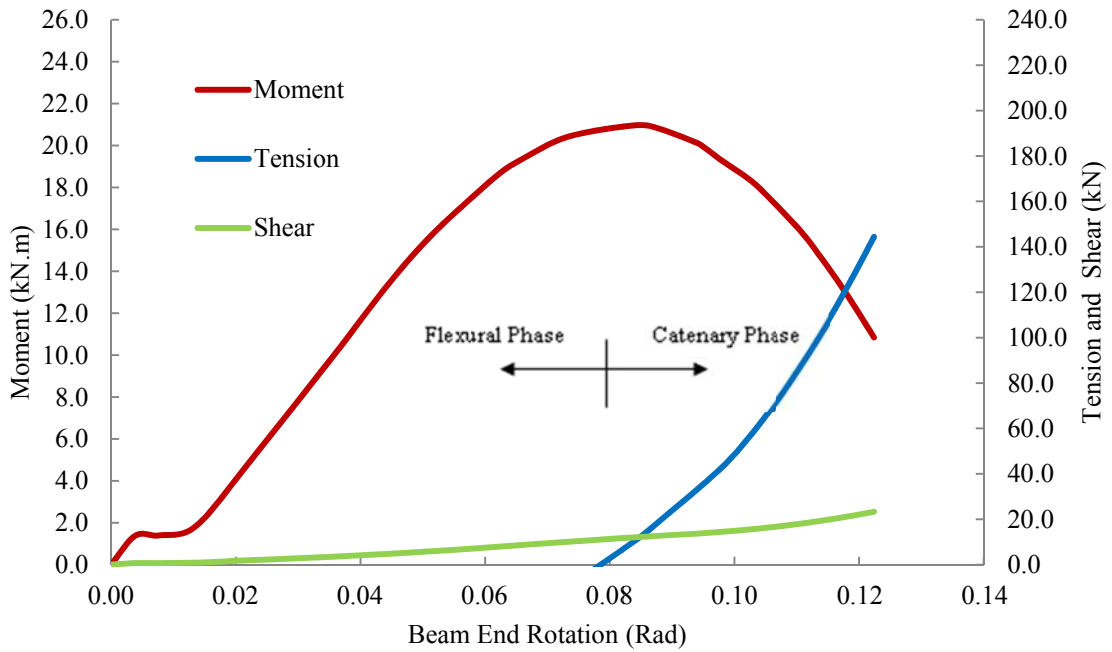


Figure 5.36: Bolt line forces versus beam end rotation – Specimen 3ST-3/8-3/4-A490

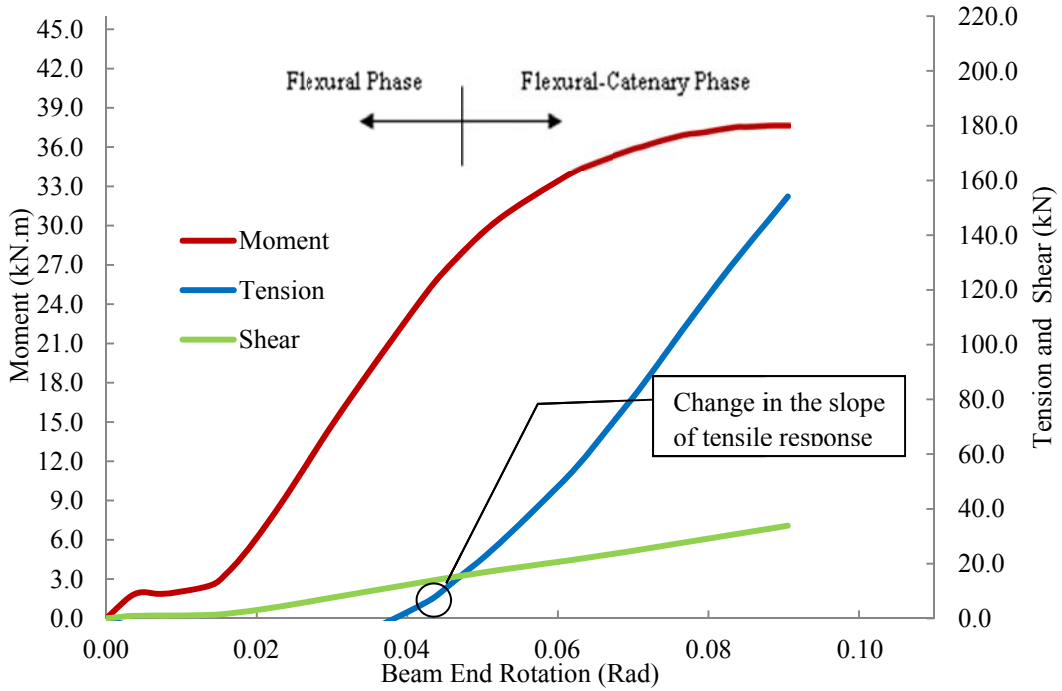


Figure 5.37: Bolt line forces versus beam end rotation – Specimen 4ST-3/8-3/4

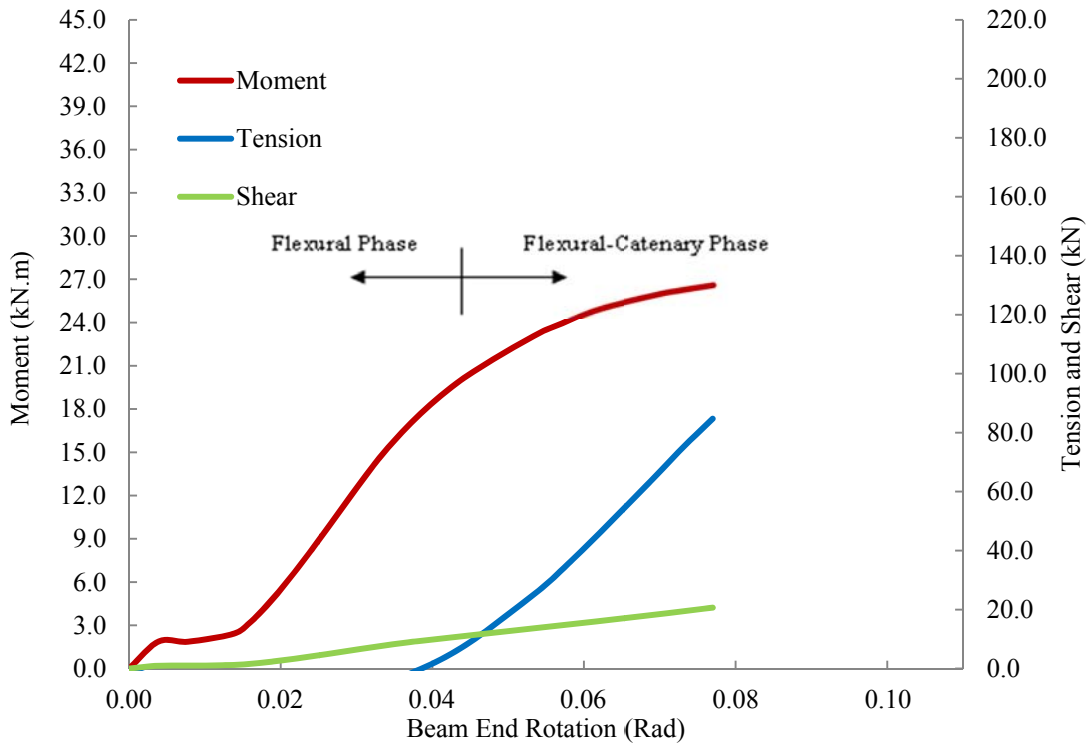


Figure 5.38: Bolt line forces versus beam end rotation – Specimen 4ST-1/4-3/4

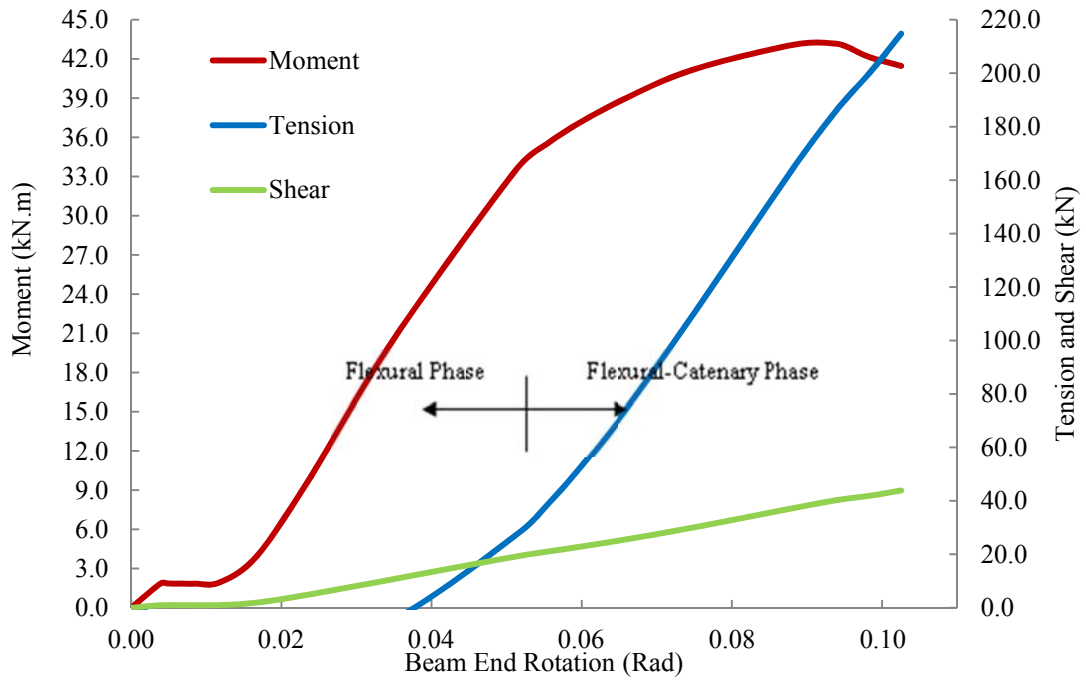


Figure 5.39: Bolt line forces versus beam end rotation – Specimen 4ST-1/2-3/4

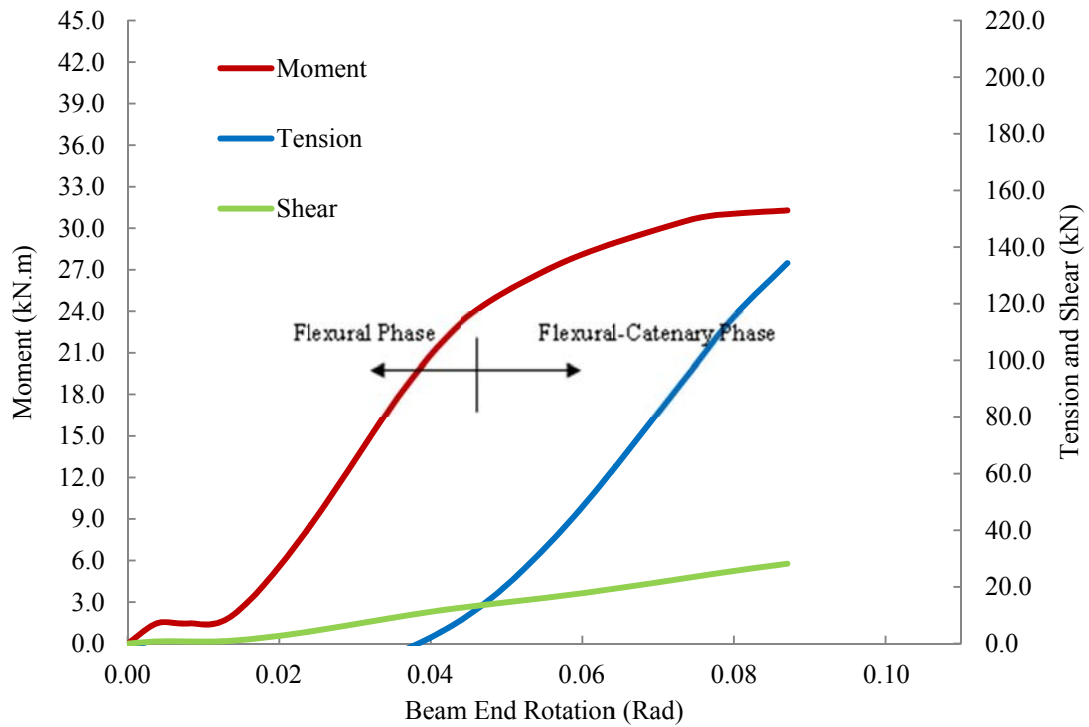


Figure 5.40: Bolt line forces versus beam end rotation – Specimen 4ST-3/8-5/8

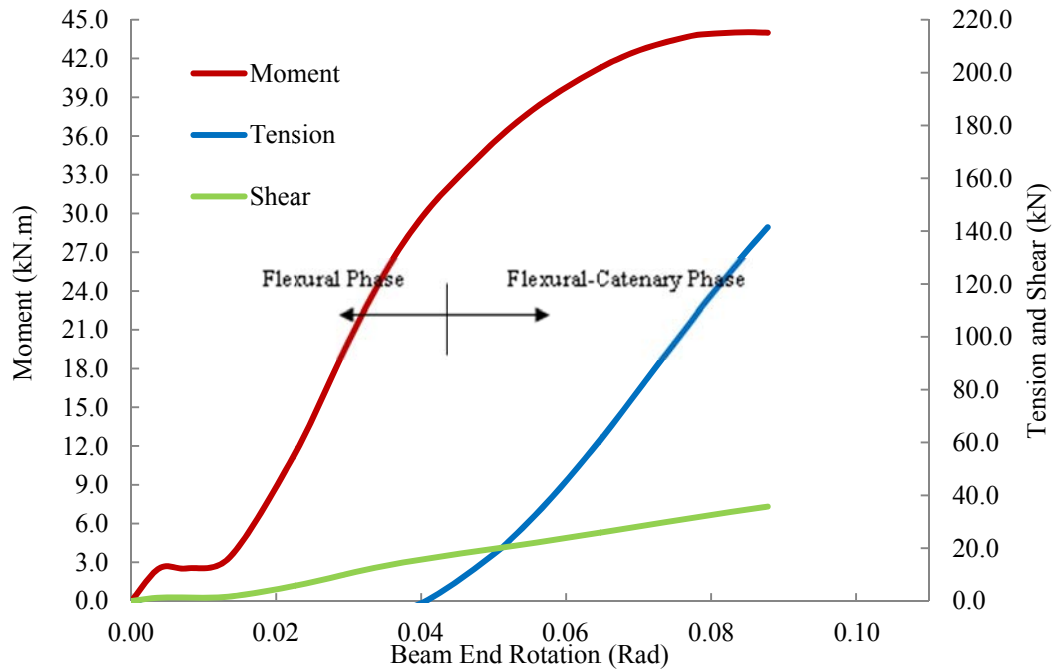


Figure 5.41: Bolt line forces versus beam end rotation – Specimen 4ST-3/8-7/8

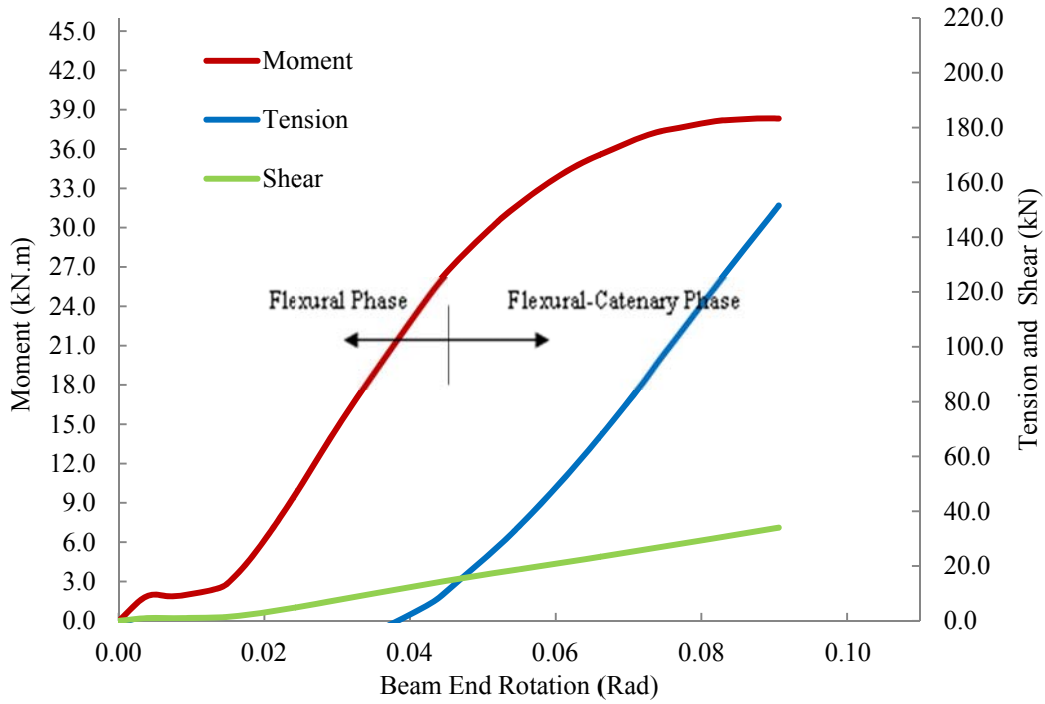


Figure 5.42: Bolt line forces versus beam end rotation – Specimen 4ST-3/8-3/4-A490

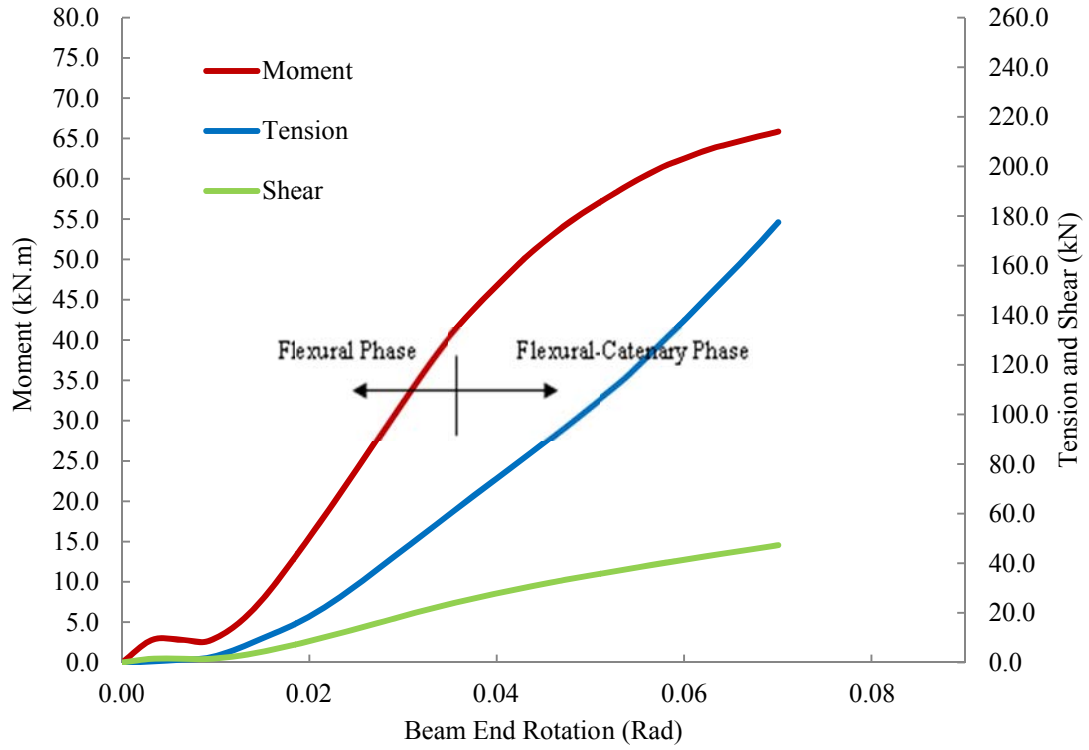


Figure 5.43: Bolt line forces versus beam end rotation – Specimen 5ST-3/8-3/4

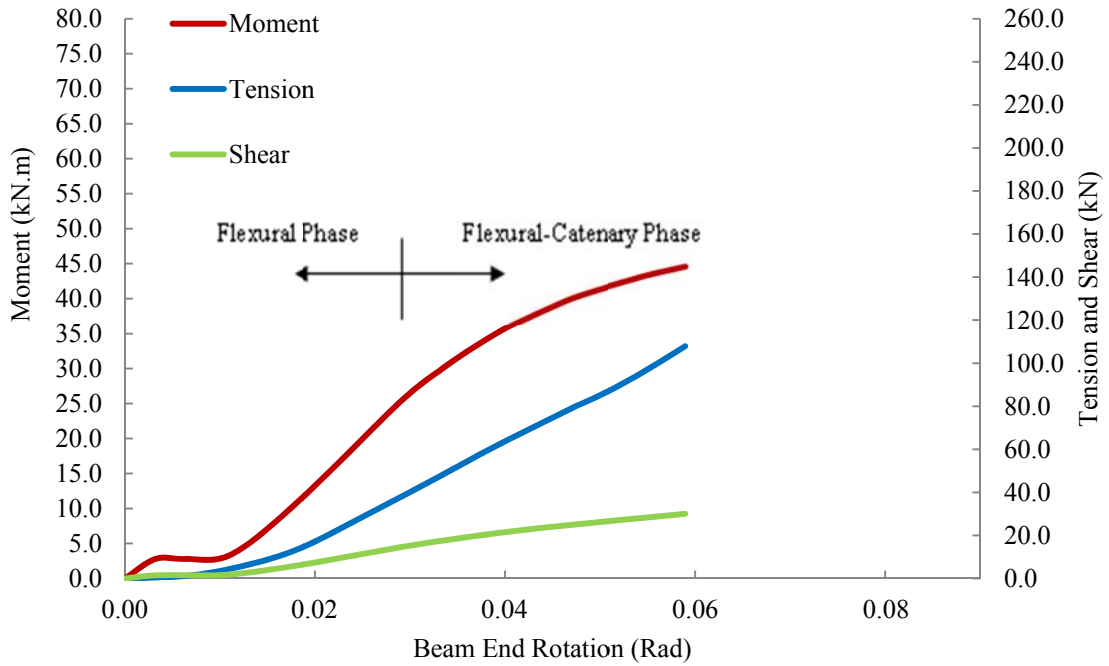


Figure 5.44: Bolt line forces versus beam end rotation – Specimen 5ST-1/4-3/4

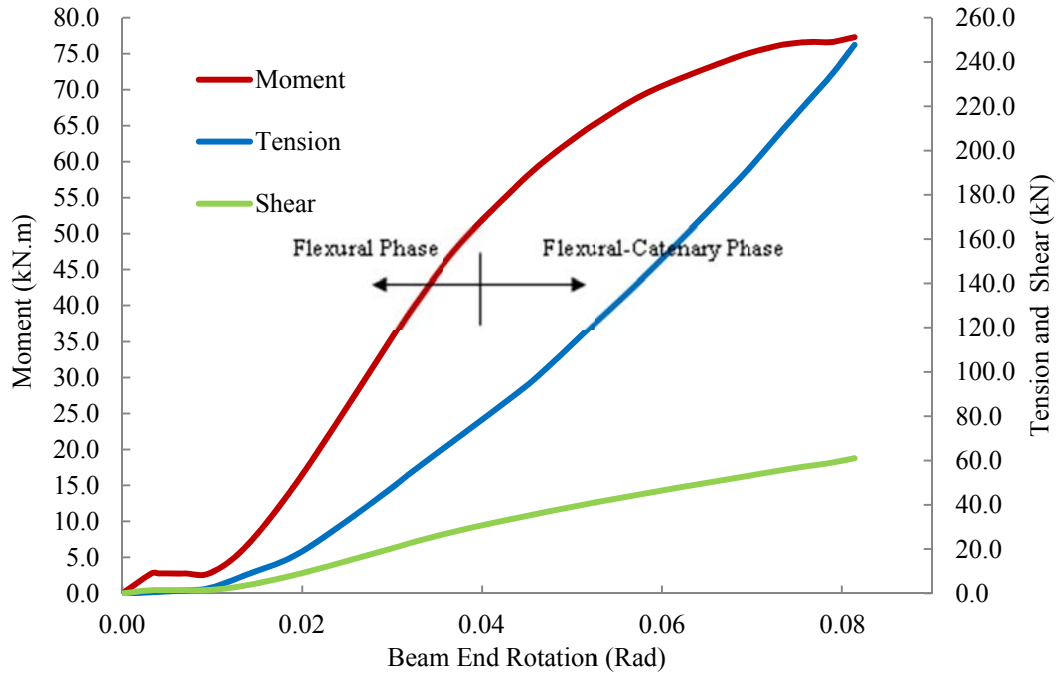


Figure 5.45: Bolt line forces versus beam end rotation – Specimen 5ST-1/2-3/4

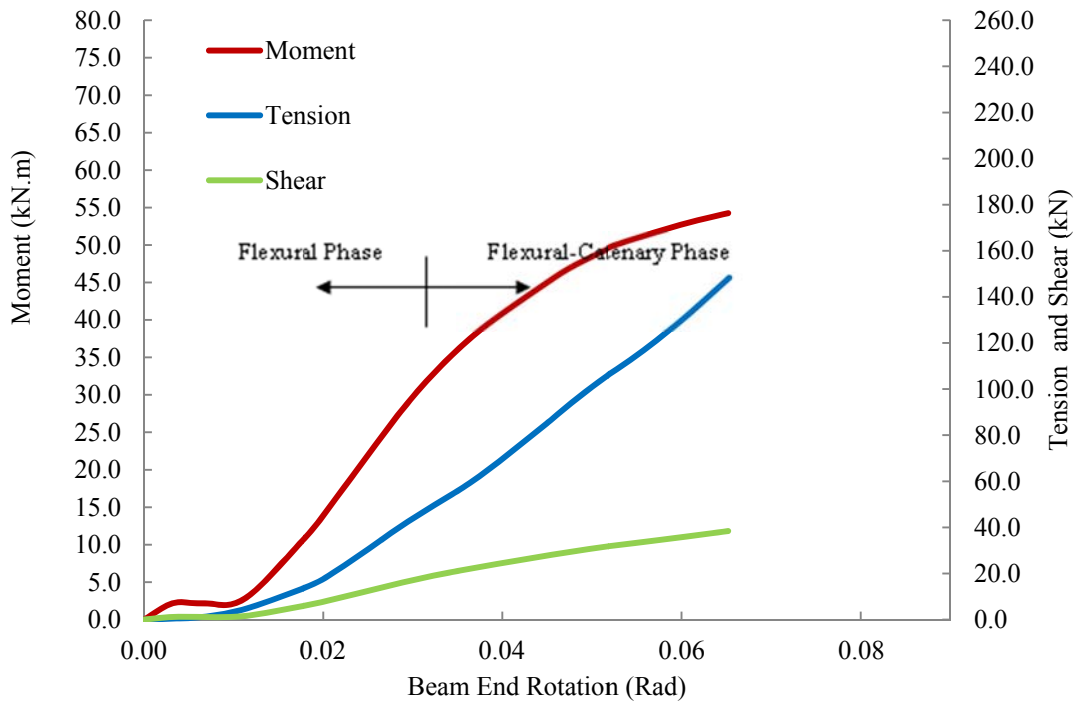


Figure 5.46: Bolt line forces versus beam end rotation – Specimen 5ST-3/8-5/8

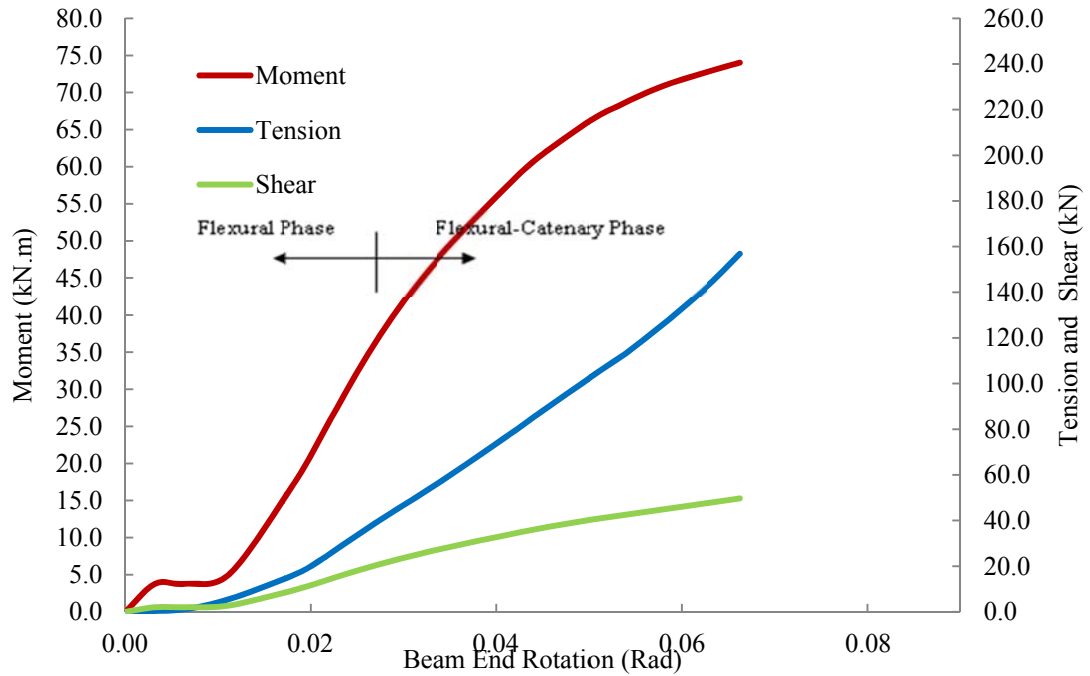


Figure 5.47: Bolt line forces versus beam end rotation – Specimen 5ST-3/8-7/8

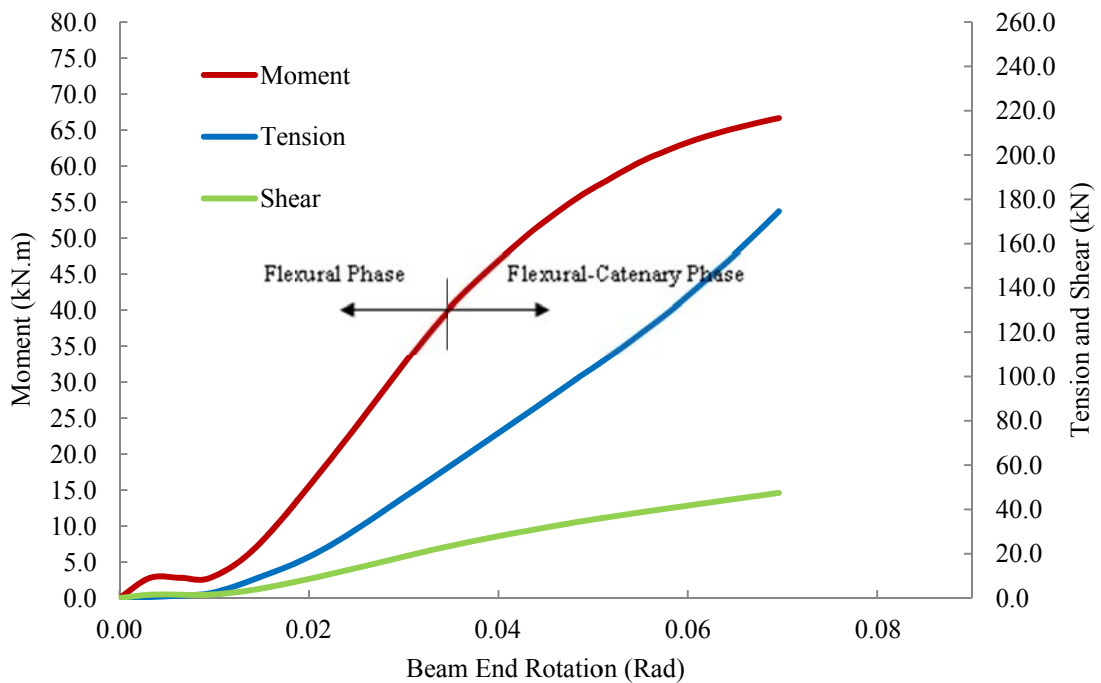


Figure 5.48: Bolt line forces versus beam end rotation – Specimen ST-3/8-3/4-A490

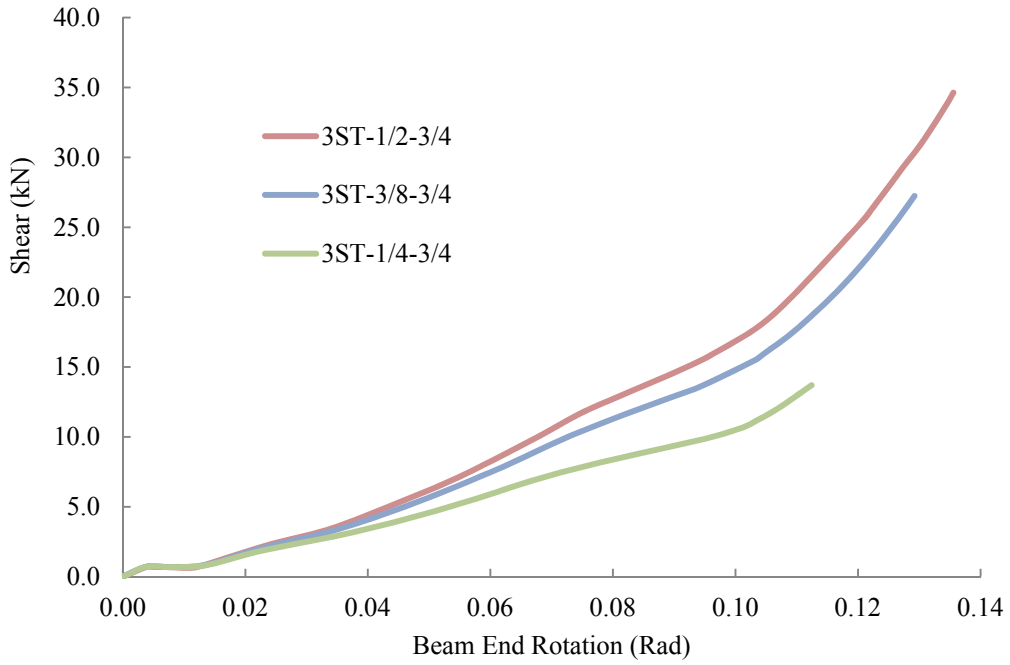


Figure 5.49: Comparison of shear response of 3ST connections with different plate thicknesses

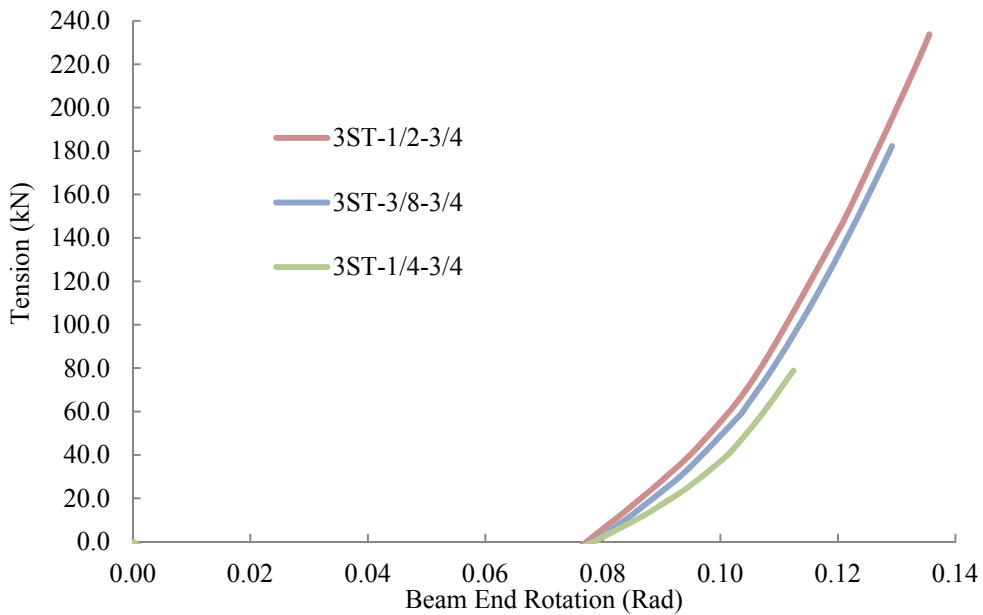


Figure 5.50: Comparison of tensile response of 3ST connections with different plate thicknesses

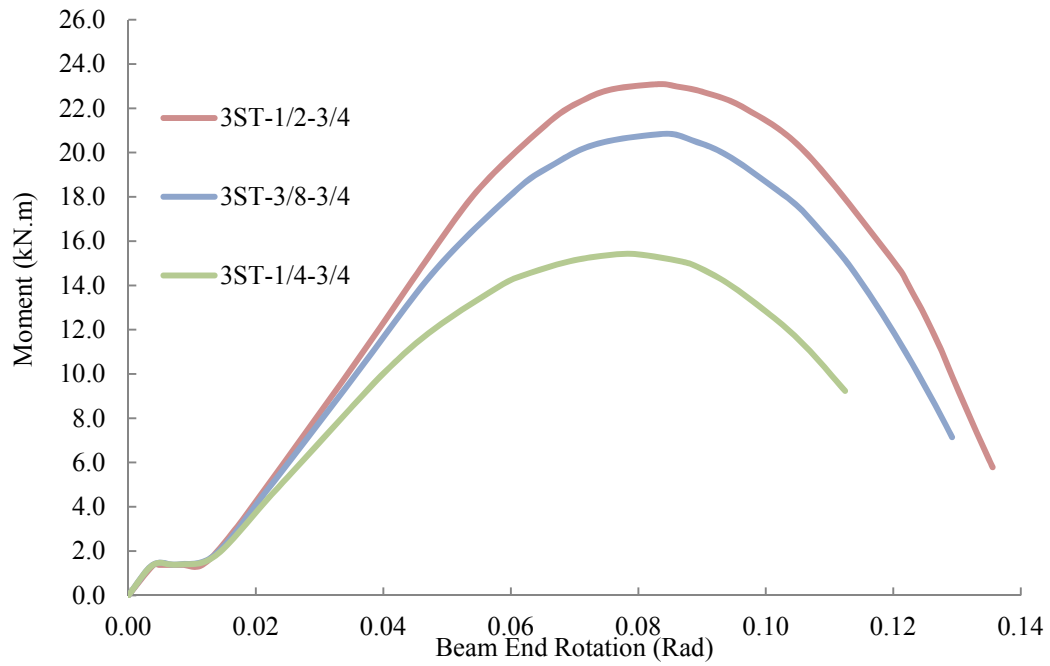


Figure 5.51: Comparison of flexural response of 3ST connections with different plate thicknesses

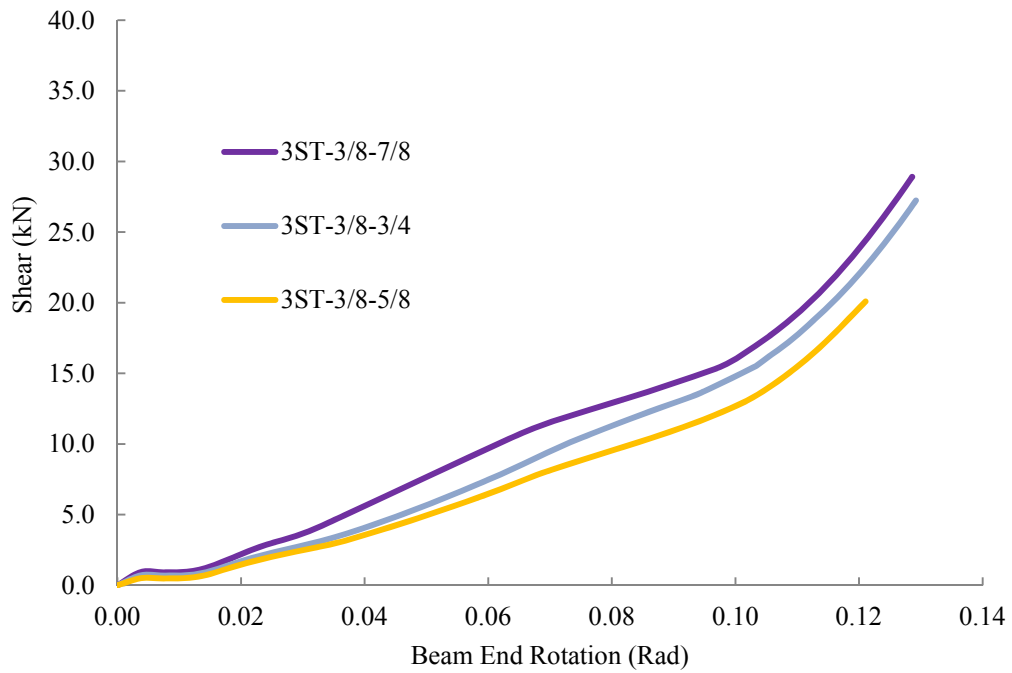


Figure 5.52: Comparison of shear response of 3ST connections with different bolt sizes

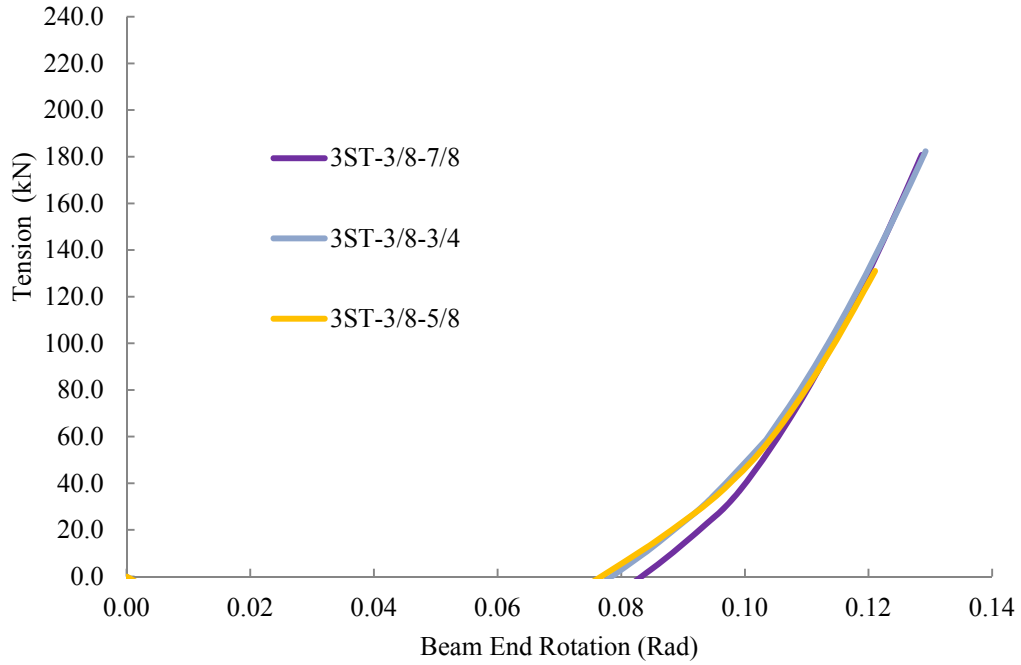


Figure 5.53: Comparison of tensile response of 3ST connections with different bolt sizes

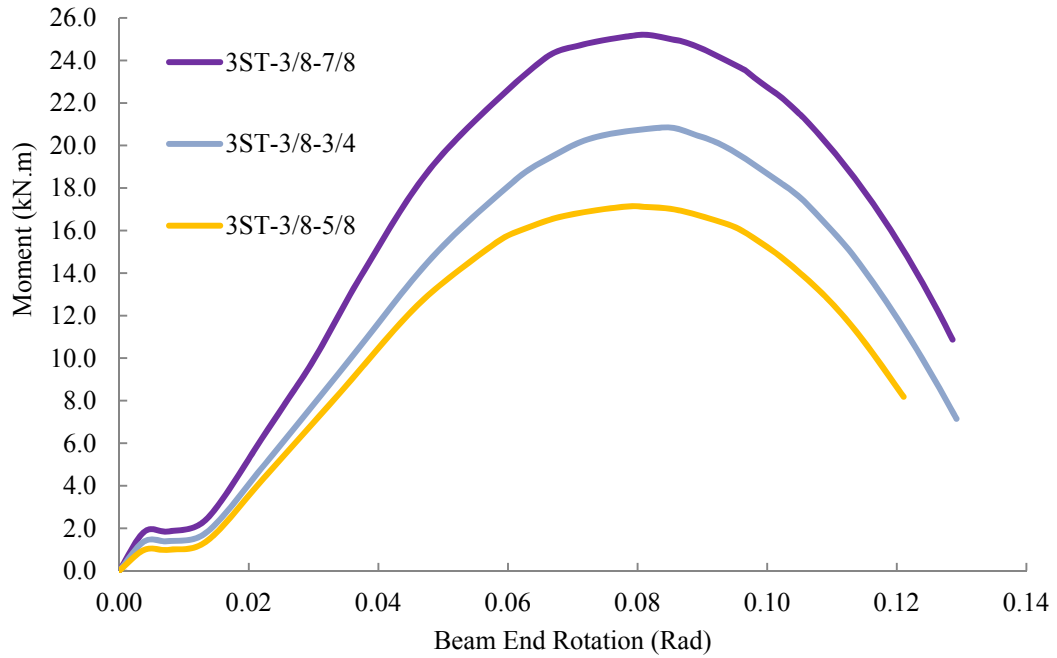


Figure 5.54: Comparison of flexural response of 3ST connections with different bolt sizes

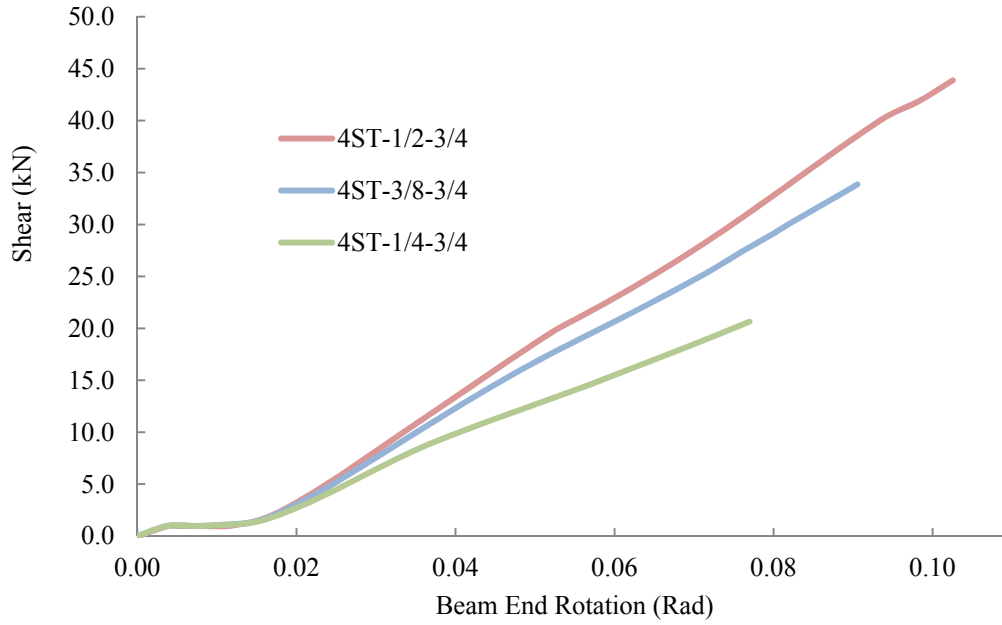


Figure 5.55: Comparison of shear response of 4ST connections with different plate thicknesses

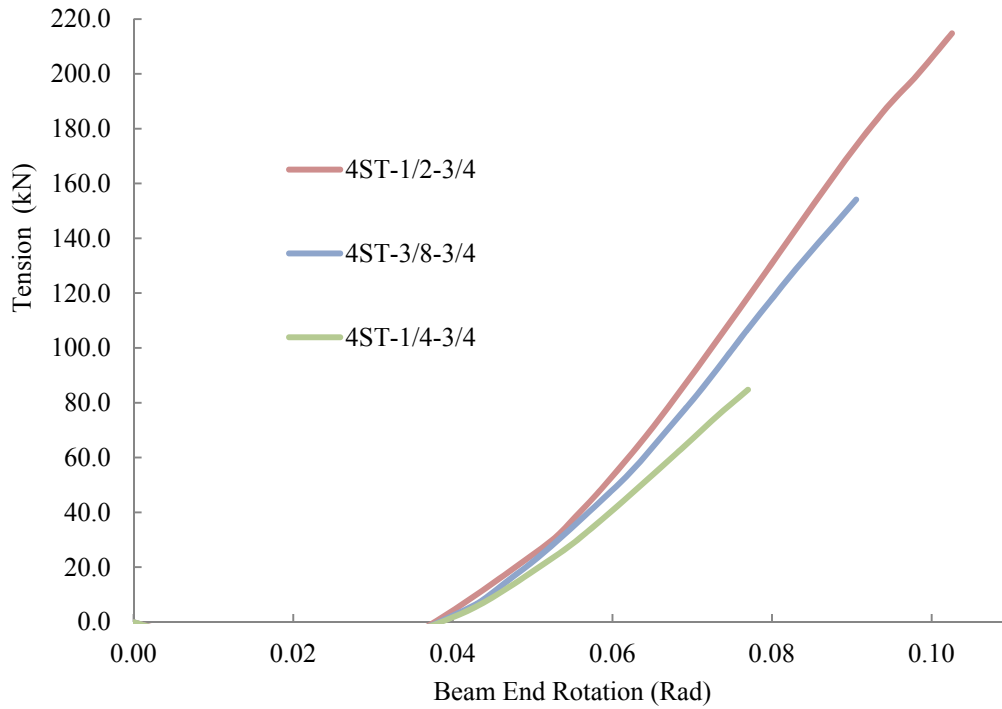


Figure 5.56: Comparison of tensile response of 4ST connections with different plate thicknesses

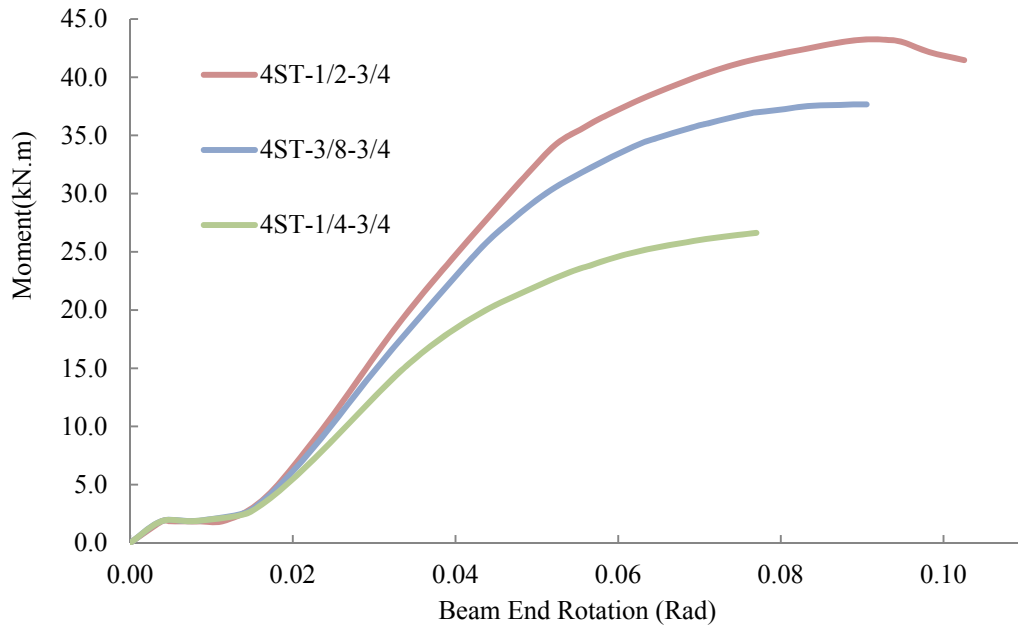


Figure 5.57: Comparison of flexural response of 4ST connections with different plate thicknesses

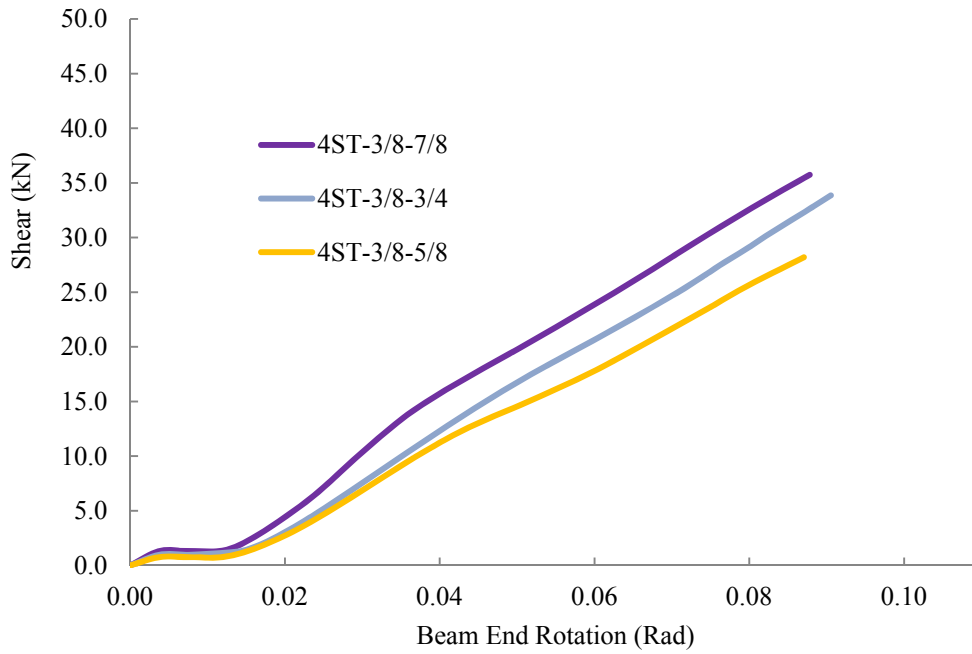


Figure 5.58: Comparison of shear response of 4ST connections with different bolt sizes

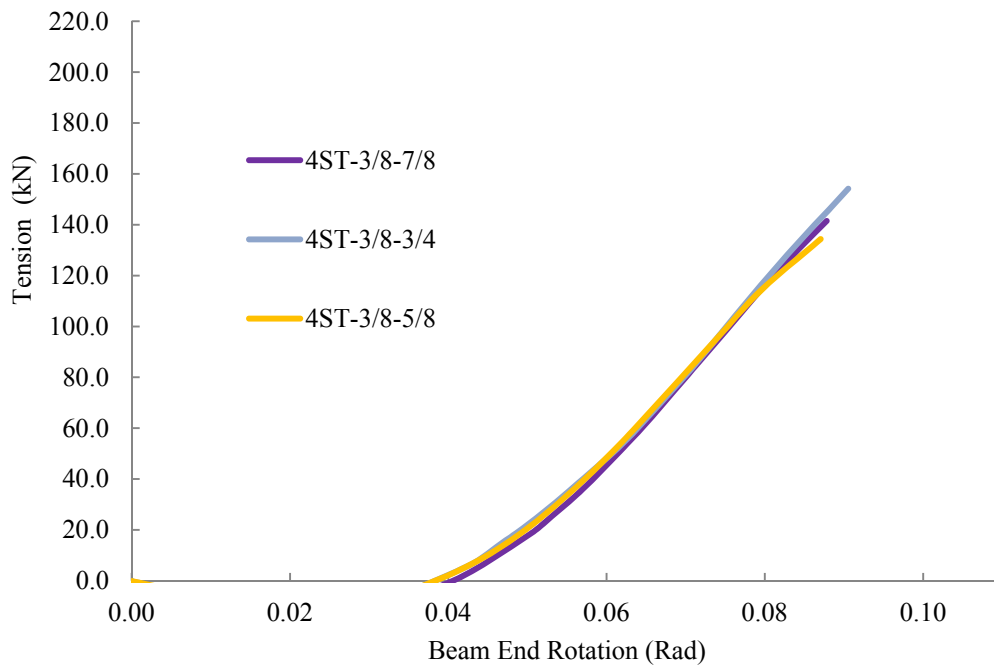


Figure 5.59: Comparison of tensile response of 4ST connections with different bolt sizes

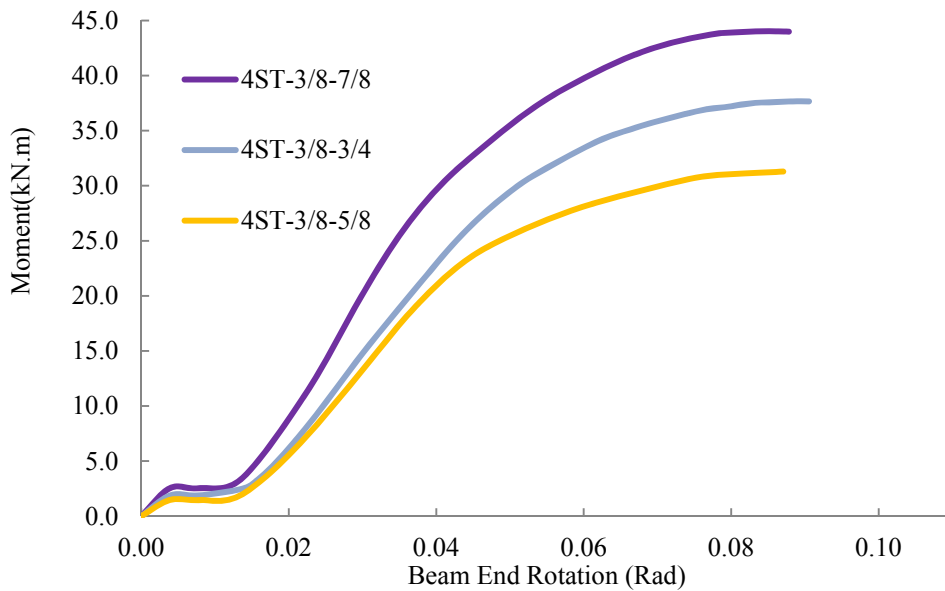


Figure 5.60: Comparison of flexural response of 4ST connections with different bolt sizes

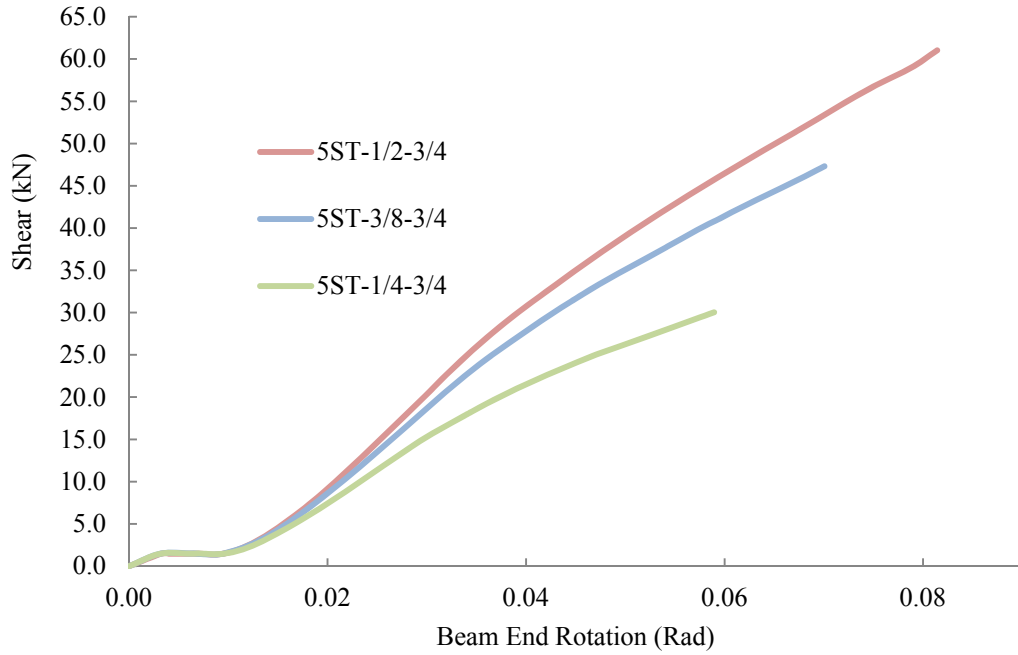


Figure 5.61: Comparison of shear response of 5ST connections with different plate thicknesses

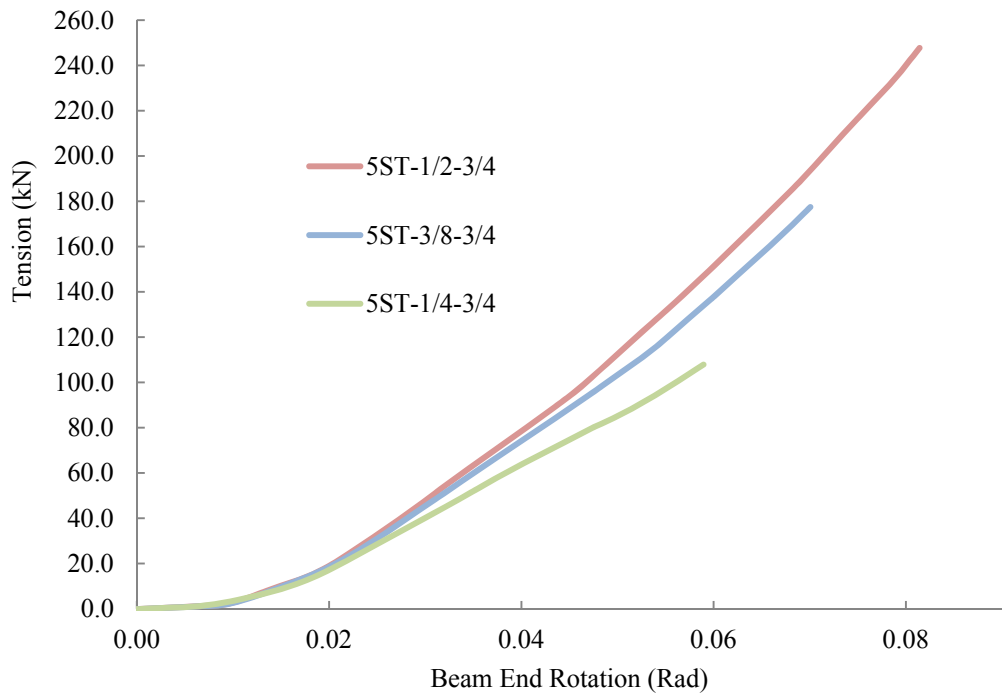


Figure 5.62: Comparison of tensile response of 5ST connections with different plate thicknesses

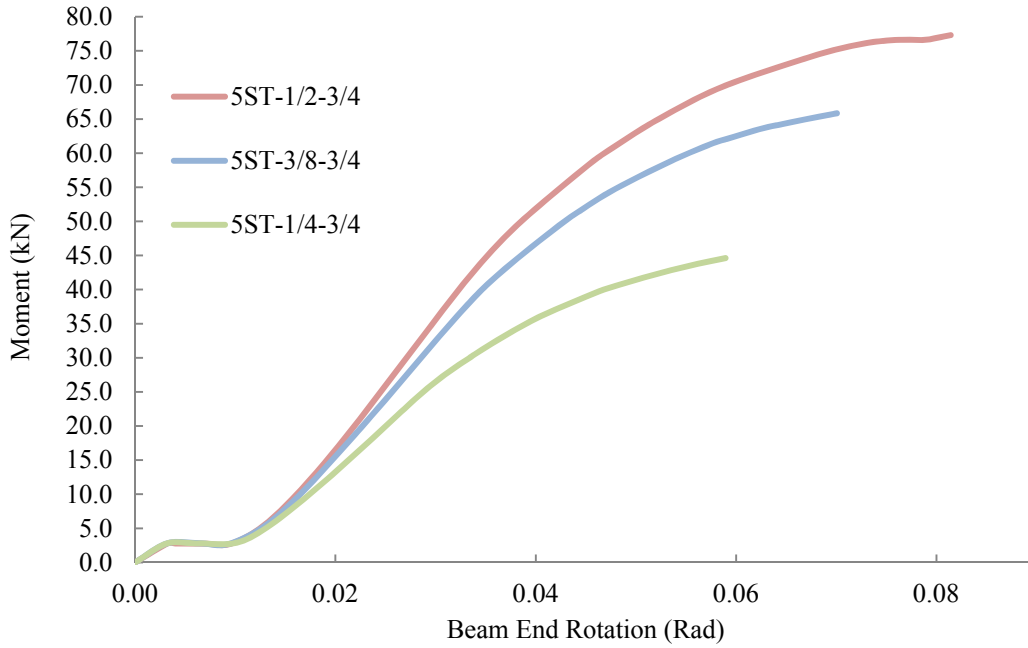


Figure 5.63: Comparison of flexural response of 5ST connections with different plate thicknesses

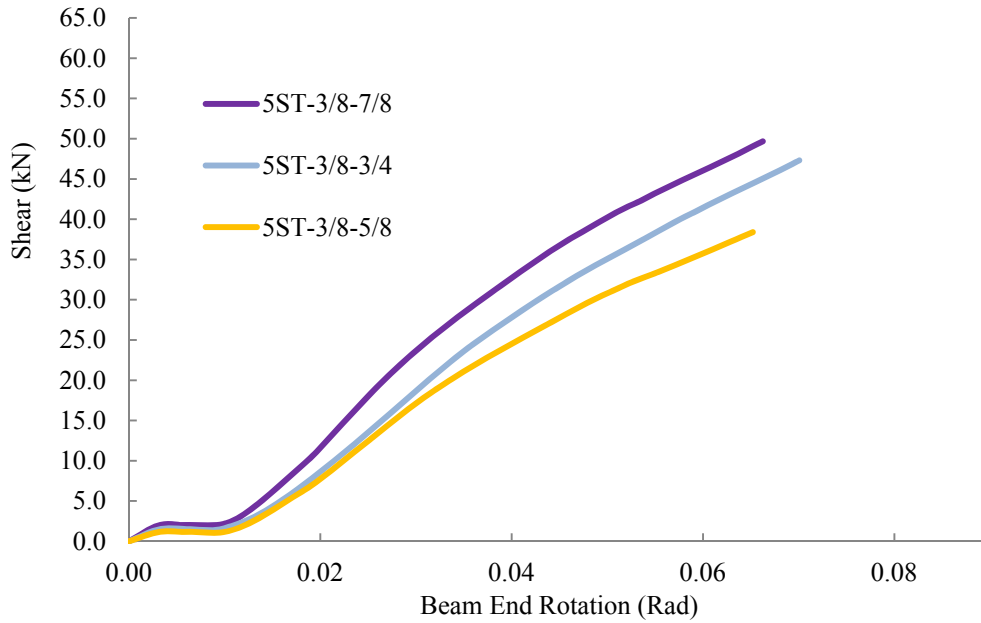


Figure 5.64: Comparison of shear response of 5ST connections with different bolt sizes

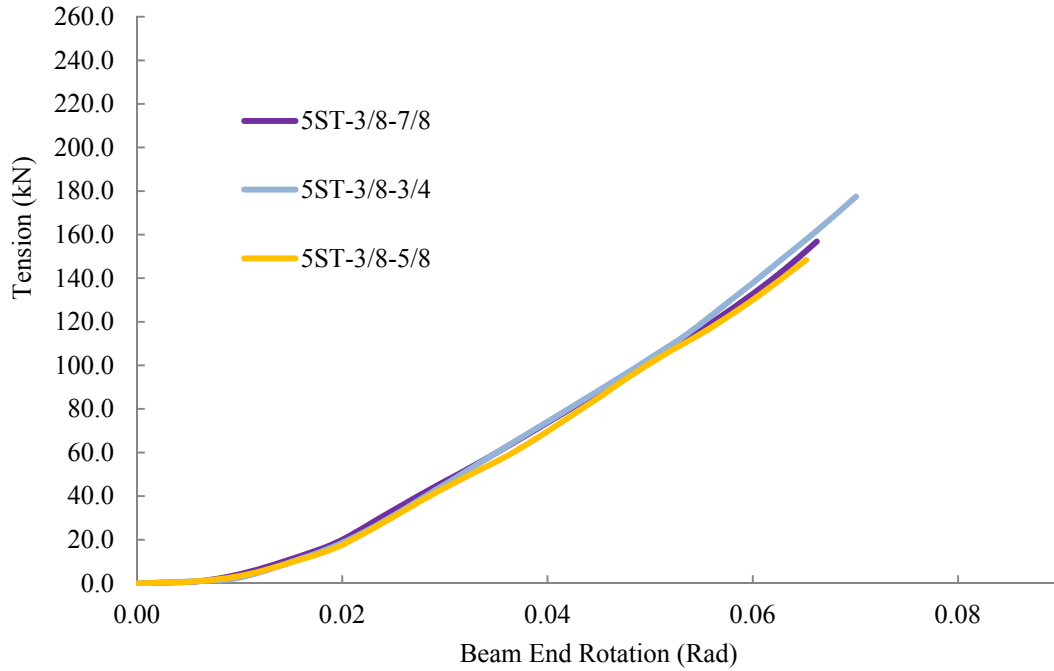


Figure 5.65: Comparison of tensile response of 5ST connections with different bolt sizes

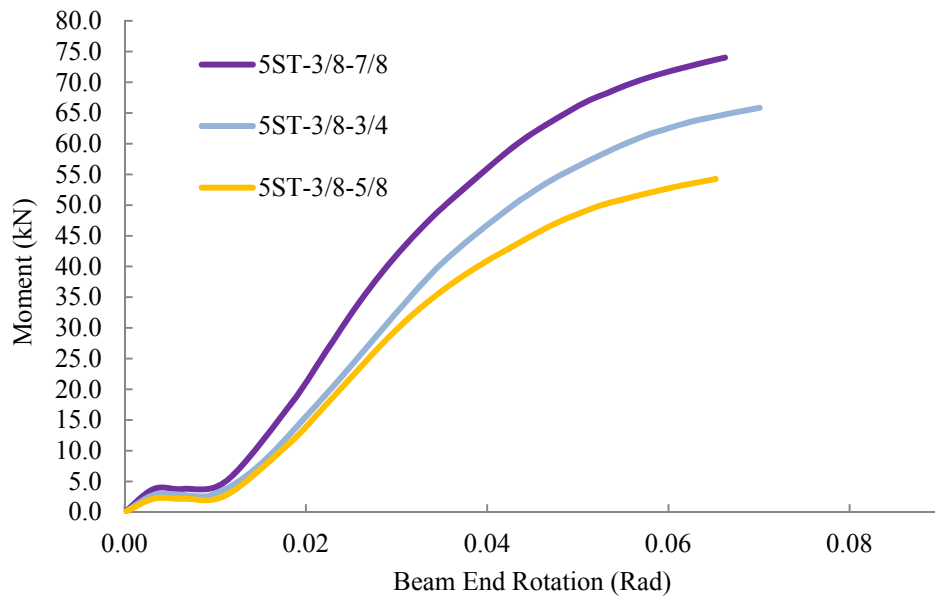


Figure 5.66: Comparison of flexural response of 5ST connections with different bolt sizes

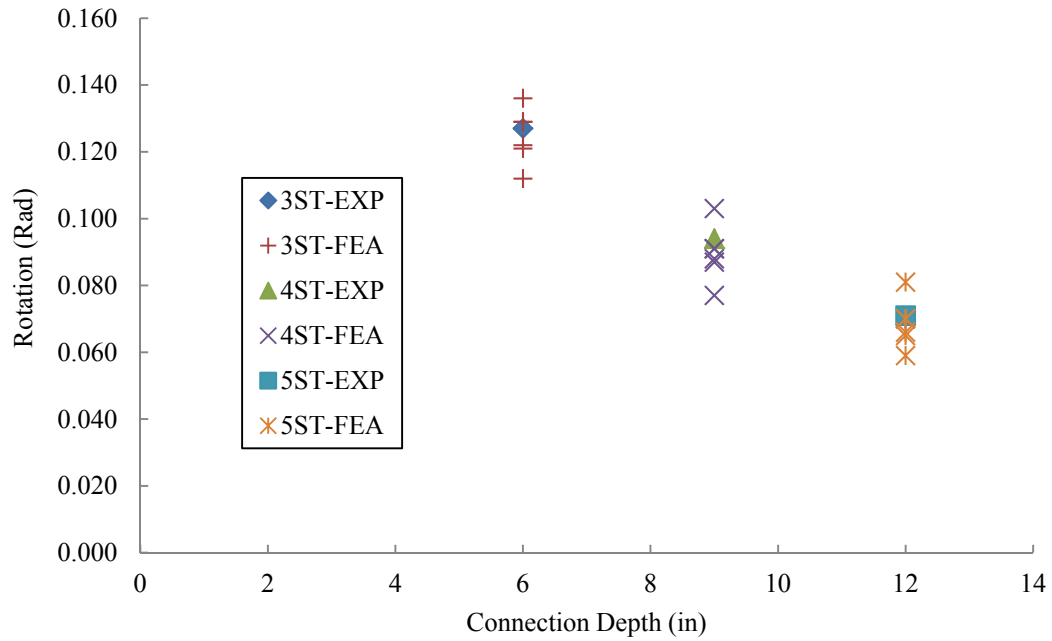


Figure 5.67: Shear tab connection rotation capacities versus connection depth for all the experimental and numerical data

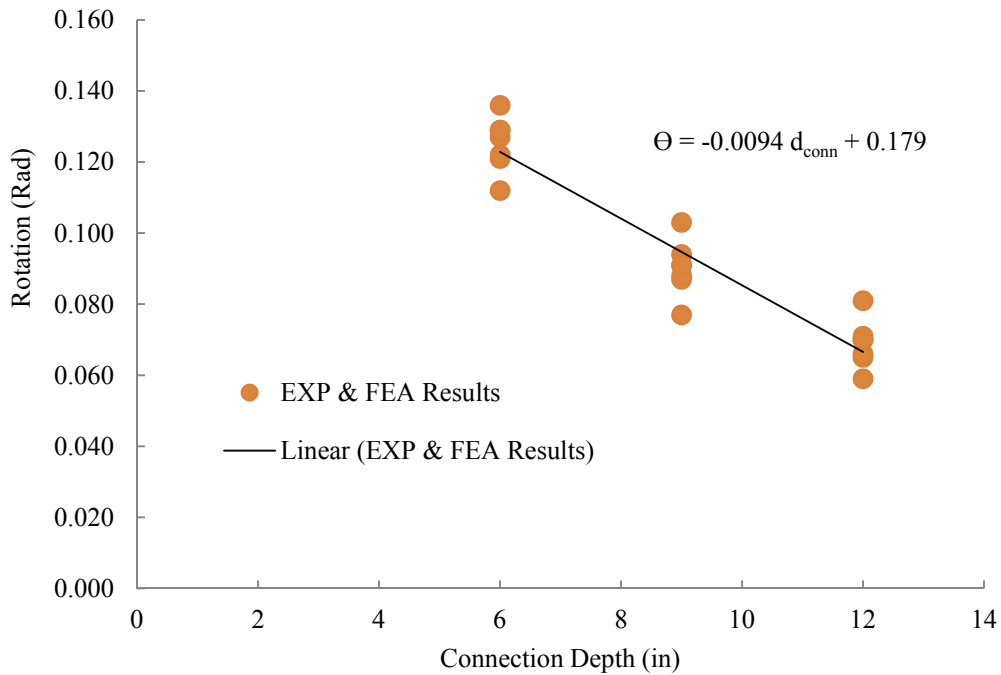


Figure 5.68: Proposed equation for shear tab connection rotation capacities versus connection depth

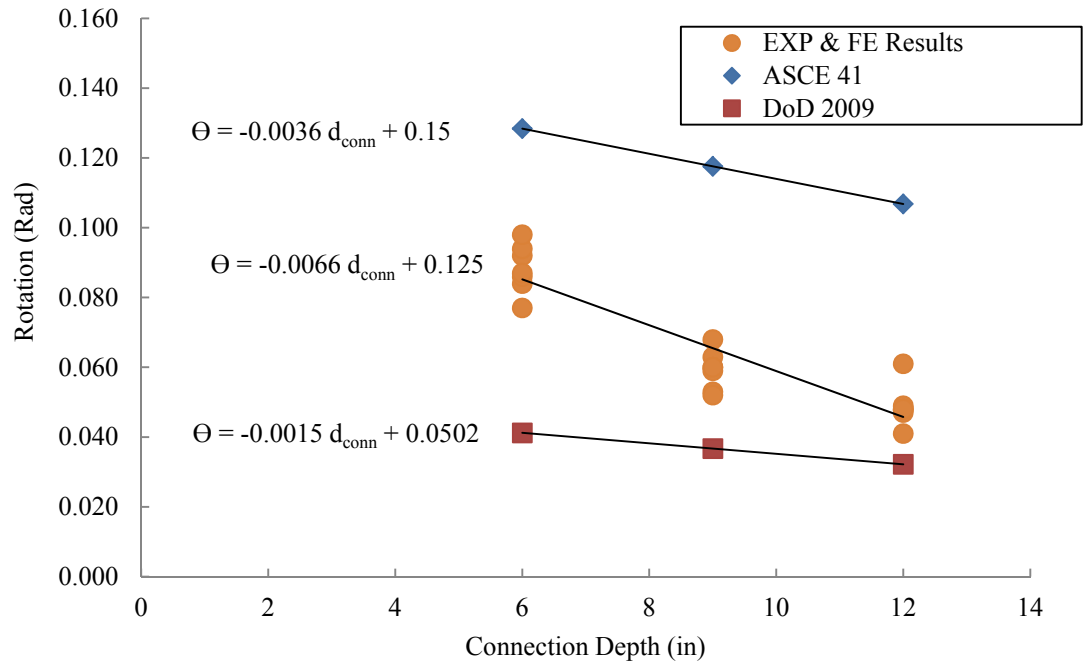


Figure 5.69: Comparison of plastic rotation capacities of shear tab connections based on ASCE 41 (2006), DoD (2009) and proposed equation

6 Behaviour of WT Connections in Column Removal Scenario

6.1 Introduction

WT connections are another relatively common option for steel gravity frames with simple shear connections. They can either be bolted or welded to the column flange and the beam web, as shown in Figure 6.1. Common types of material used in WT connections are mentioned in Table 6.1. A properly-designed WT shear connection is able to transfer shear force from a simply supported beam to an adjacent supporting column without developing significant moment. Sustaining tensile force is not generally considered in the common practice of designing shear connections. Meanwhile, since current progressive collapse design guidelines, such as those by the DoD (2009) and GSA (2003), ask designers to specify robust connections that maintain their integrity in a double-span “column removal” scenario, there is a necessity to investigate anticipated shear connection performance under the simultaneous presence of shear, moment, and tension. Currently, little is known about how WT connections would perform under these conditions.

In order to model the behaviour of steel connections in progressive collapse analyses, the DoD (2009) guidelines provide a table that includes models for double angle and shear tab connections. However, some important types of shear connections, such as WTs, are excluded. For these cases, engineers are directed to tables available in seismic design codes and guidelines, such as ASCE 41 (2006), although there are substantial differences between connection performances when subjected to seismic loading as opposed to a column loss event as discussed in chapter 2. Therefore, the behaviour of WT connections needs to be characterized in the new scenario. Behaviour characterization in this study of WT connections includes the investigation of the possible failure modes and the shear, axial and

moment interaction response of the connection when an adjacent column is compromised.

In this chapter, the finite element method is adopted to simulate the response of WT connections when a column is lost, regardless of the cause. The finite element models are verified by available experimental data following the same loading regime. Verified models are utilized to expand the database of the test results. Simultaneous presence of shear, axial force, and moment versus chord rotation diagrams are presented for both the numerical and experimental results. Effects of changes in WT size, bolt size and type are also investigated and conclusions are made. The results are utilized to develop the modelling parameters that can predict the rotational behaviour of WT connections in the new scenario.

6.2 Objective and scope

This chapter is focused on the behaviour of WT shear connections under simultaneous presence of shear, tension and moment. High-fidelity finite element models of WT shear connections in the column removal scenario are developed and verified in terms of both load path and failure modes. These models can shed more light on the performance and the sources of ductility in WT connections. The results can be used to select suitable connection modelling parameters for progressive collapse evaluations of steel frames with similar WT shear connections.

The focus of the research is on bolted-bolted WT shear connections, shown in Figure 6.1(d). This type of WT connection is perhaps the most challenging one in the whole research in terms of analysis cost due to the presence of numerous bolts, which leads to many contact surfaces and consequently potential convergence problems. Connection depth (and the resulting number of bolts) is the sole variable in the experimental specimens discussed herein. However,

extensive parametric study is performed to expand the database on the behaviour of such connections by changing factors such as the WT cross-sectional size, bolt grade and diameter.

6.3 Selected previous research

Astaneh (1989) investigated the demand and supply of ductility in steel shear connections, which became a basis for his later work on different types of shear connections including WT connections. Astaneh acknowledged shear, axial and moment as the major forces present in simple shear connections. While axial forces often also exist in industrial structures, shear is the most prevalent one. Among the associated displacements, including shear and axial displacements and also rotation, he concluded that rotation is the major component. He stated that there were no records of effects of axial loading on the behaviour of simple connections at that time. As a result, the main characteristic features he focused on were: (1) shear–moment interaction; (2) moment–rotation response; (3) shear force–shear displacement behaviour; (4) failure modes; and (5) shear force–rotation interaction. Due to the presence of irregularities, discontinuities, constraints, inelasticity and material hardening and softening that complicate the stress and strain fields in a shear connections, Astaneh recommended that experiments be conducted to measure mechanical features and sources of strength and ductility.

Astaneh and Nader (1989) studied the behaviour of WT connections by performing nine full-scale tests on WT connections that were welded to the column flange and bolted to the beam web with either three or five bolts (Figure 6.1(a)). Table 6.2 summarizes the results of the tests performed. The materials were ASTM A36 for the WT and ASTM A325 or ASTM A490 for the bolts. The connections were subjected to: (1) moments to measure the rotational ductility, and (2) combinations of shear and rotation—representative of a typical simply

supported beam—to measure the shear strength. Based on the experimental results, the authors concluded that WT connections subjected to shear are quite flexible and able to accommodate rotational demands as large as 0.07 radians. They observed a substantial amount of shear yielding in the stem and flange of the WT before failure happened. The failure limit states were: (1) WT stem yielding, (2) WT stem fracture, (3) bolt shear fracture, (4) weld fracture, (5) WT flange yielding, or (6) bolt hole bearing failure, all shown in Figure 6.2. The failure mode possible in thin-flange WTs is shear yielding of the WT flange, which was not observed during the tests. They suggested using at least a minimum of 1.5 times the diameter of the bolts as the horizontal and vertical edge distances. Their test results indicated that one of the major factors that provided ductility to the WT connections was the WT flange out-of-plane bending.

In a later work, Astaneh (2005) discussed three sources of rotational ductility in WT connections subjected to simultaneously applied shear and rotation: (a) out-of-plane bending of the WT flange; (b) yielding of the WT stem; (c) bolt slippage; and (d) bolt hole bearing deformation. The location of the inflection point in a WT connection of a simply supported beam is between the bolt and weld lines, similar to double angle connections. Hence, double angle and WT connections develop a relatively small moment.

Thornton (1996) applied an analytical approach to propose a design algorithm for WT connections bolted to the beam web and either welded or bolted to the support (Figure 6.1(a) and (d)). He used the results of Astaneh's experiments to verify the method for the welded-bolted connections; however, for the bolted-bolted connections he used the results of bolted double angle connections due to the lack of more appropriate experimental data. He assumed that WT connections under shear loading rotate about their lower edge, which produces the load distribution shown in Figure 6.3, where V is the net transverse shear distribution in the WT flange considering both sides of the stem at the vertical yield lines. He ignored the reduction effect of the shear force on the plastic moment capacity.

Based on yield line theory, the moment and shear capacity of the connection can be evaluated as shown in Figure 6.4. The equations derived in his research are used to analytically compare with the experimental research by Astaneh and Nader (1989). The same procedure is applied for the bolted connections, although there were no experiments for comparison. He proposed equations for minimum weld size and bolt diameter to ensure the required ductility.

In supplementary research, Thornton (1997) considered shear connections subjected to axial forces in addition to shear force. He concluded that the additional axial load tends to make shear connections less flexible. He developed equations that can be used to distinguish if this reduced flexibility will lead to progressive fracture of the connection. He also provided a design method that provides adequate strength with maximum flexibility for three types of shear connections including WTs.

6.4 Numerical study method

The behaviour of WT connections subjected to simultaneous shear, moment, and tension is investigated using high-fidelity finite element models. All stages of simulation, including pre- and post-processing procedures, were performed using Abaqus/CAE, with Abaqus/standard used as the analysis engine (Dassault Systèmes 2009).

6.4.1 Selected experimental program

Experiments performed by Friedman (2009) were used to verify the results of the numerical models. Figure 6.5 demonstrates the connection subassembly and the test setup. A total of nine full-scale tests were carried out, with the connection depth as the sole varying factor. Some of the tests were continued after the initial failure; however, only the results up to this point are of interest in this research.

6.4.2 Finite element model description

Three-dimensional solid elements were used for all the components of the model due to the nature of the connection modelling problem. The models consist of the central column stub and the adjacent beams, as well as the connections with complete detailing, as shown in Figure 6.6(a). Three, four and five bolt shear tab connections were modelled, as illustrated in Figure 6.6(b) to Figure 6.6(d). The plates are welded to the column flange and bolted to the beam web. The central stub column is pushed down, while the connection performance is monitored.

Since the connection is the point of interest, all characteristic features of the connections are included in the models. Strain-based fracture criteria established in chapter 3 were utilized for the WT connections after verification in order to predict the failure modes. All other characteristic features of the models, including bolt pre-tensioning, material properties, contact calibration and element types are discussed in chapter 3. Characteristic features of all the connections numerically studied are summarized in Table 6.3. A sample of the deformed shape of the connection assembly after the experiment is compared with its corresponding finite element analysis result in Figure 6.7.

The models are labelled based on the following method: first the number of bolts in a vertical line, then WT, which is the abbreviation for tee connections utilized in this research, then the WT section size in SI units and the bolt diameter in imperial units. For example, 3WT125X33.5-3/4 refers to the WT connection with three bolts; WT125X33.5 tee size, and 3/4 in (19.1 mm) diameter bolts. The bolts are all ASTM A325; unless at the end of label, “A490” is added. All the WT sections are made of ASTM A992 steel. For the ones for which experimental data is available (see Table 6.3), verification—as well as comprehensive comparisons of experimental and numerical results—is performed.

6.5 Verification results

Although based on the benchmark example provided in chapter 2 (following the procedure outlined is expected to produce valid results for all types of shear connections, including WT type, in the column loss event), the verification process is performed for WT connections with three, four, and five bolts since experimental results are available. For the purpose of verification, deformed shapes, failure modes, and internal force diagrams are compared with the experimental results.

Figure 6.8 to Figure 6.10 compare the experimental versus numerical deformed shape of WT connection components for all the experiments utilized in this study. Although there are similarities in the behaviour of each connection depth (i.e., three, four or five bolt), there are some differences that are discussed in the following sections. To ensure that a WT connection will survive the column removal scenario, it should be capable of carrying the combined effects of shear and moment, as well as a large catenary tensile force. The internal forces (i.e., shear, tension, and moment) at the bolt line versus the chord rotation of connection assemblies 3WT, 4WT and 5WT are shown in Figure 6.11 to Figure 6.19. The dashed and solid lines represent the results of the experiments and simulations, respectively. While the general trends in all force responses of the connections correlate well, some discrepancies between the experimental and numerical results exist, which are discussed in section 6.5.1 to 6.5.3:

6.5.1 Three bolt WT connections (3WT)

6.5.1.1 Deformed shapes and failure modes

Figure 6.8(a) shows the numerical and experimental deformed shapes of the 3WT connections before failure.

Figure 6.8(b) shows a typical bolt shear deformation and rupture obtained from the tests and finite element deformed shapes of the WT-to-beam bolts. Shear deformation in the bottom bolt leads to bolt shear rupture, which was the governing failure mode for all the 3WT experiments. The middle bolt remains almost elastic throughout the loading; meanwhile, the top bolt starts to experience plastic deformation due to compressive action from the force couple at early stages of loading, which is released after catenary action is developed in the connection. The numerical model predicts the bottom bolt shear rupture very well with removed elements, as shown in

Figure 6.8(b). Bolts connecting the WT flange to the stub column flange remain almost elastic (not shown in Figure 6.8(b)). The distribution of bearing stress at the bottom hole at a 15-to-30 degree angle from the horizontal line is recorded in both the test report (Friedman 2009) and the numerical results, as depicted in Figure 6.8(c) accompanied by a magnified view of the bottom hole region comparing with the plastic strain distribution obtained by the finite element model. Most of the plastic deformation occurred around the bottom hole of the WT section. No distortion occurred around the second hole. Presence of the force couple is obvious in both the numerical model and experimental results, imposing compressive and tensile forces to the top and bottom holes, respectively.

6.5.1.2 Shear, tension, and moment interaction

Internal forces at the bolt line versus the chord rotation of connection assemblies 3WT are shown in Figure 6.11 to Figure 6.13. The shear response of the connections (Figure 6.11), tensile behaviour (Figure 6.12) and moment response (Figure 6.13) serve to verify the models based on acceptable correlation with the associated experimental results.

There are some differences at the beginning of the experimental response of 3WT connections, mostly shear and moment, in comparison with numerical results. This difference is directly related to the location of the bolts in the holes in the

experimental program. It is assumed that the bolts are located exactly at the centre of the holes in the finite element models. However, determination of the precise locations of the bolts' shanks inside the holes is unfeasible. As a result, this discrepancy at the early stage of loading is inevitable. Furthermore, some of the holes were reamed due to minor misalignment in order to make them fit during erection of the test setup. This will add complication to the problem in terms of variability and unknown issues embedded. Table 6.4 summarizes the test and finite element analysis values of the shear, moment, and tension at the initial failure for the 3WT connections. Internal forces and chord rotations determined from the numerical models are in acceptable agreement with the experimental results, with less than a 9% deviation. Rotation at the initial failure, as one of the main studied parameters, has a deviation of less than 2%. As observed in Table 6.4, the failure mode for all of the tests is bolt shear rupture at the bottom hole, and the finite element results portray the same type of ultimate limit state.

6.5.2 Four bolt WT connections (4WT)

6.5.2.1 Deformed shapes and failure modes

Figure 6.9(a) shows the numerical and experimental deformed shapes of the 4WT connections at failure. Shear deformation at the bottom bolt shank led to a failure similar to what is shown in Figure 6.9(b). The top bolt and the third from the top experienced some plastic deformation; nevertheless, the rest of the bolts, including the WT-to-column-flange ones remained elastic. Similar to the 3WT connections, most of the plastic deformation occurred around the bottom hole of the WT and the bottom bolt, in which finally the rupture occurred. No distortion occurred around the second hole from the top. The top and bottom bolts provided a greater percentage of flexural resistance than the middle two. Presence of a force couple is obvious in both the numerical model and experimental results about the approximate location of the centroid of the bolt group, closer to the second top

bolt, imposing compressive force to the top hole and tensile force to the two bottom ones. Illustrated in Figure 6.9(c), the stress distribution around the bottom hole in the 4WT confirms the stress distribution happening in the experimental program following the 15-to-30 degree trend observed in the 3WT connections.

6.5.2.2 Shear, tension, and moment interaction

The internal forces at the bolt line versus the chord rotation of connection assemblies 4WT are shown in Figure 6.14 to Figure 6.16. The shear response of the connections (Figure 6.14), tensile behaviour (Figure 6.15), and moment response (Figure 6.16) serve to verify the models based on acceptable agreement with the associated experimental results. Similar to the 3WT connections, some differences exist in the load paths, particularly at the beginning of the experimental response of 4WT connections, in comparison with numerical result. The same reasons mentioned for 3WT connection can be stated, including the location of the bolts in the holes in the experimental program. Unknown horizontal stiffness of the test setup causes the difference observed in the Figure 6.15.

Table 6.5 summarizes the test and finite element analysis values of the shear, moment, and tension at the initial failure of the 4WT connections. As can be observed, shear and tension forces, as well as the chord rotations, determined from the numerical models are in acceptable agreement with the experimental results. The largest difference is related to the tension, which is about a 10% deviation from the experimental results, which is still considered acceptable. As can be seen in Table 6.5, the failure mode for the tests is bolt shear rupture at the bottom hole, and the finite element results convey the same type of ultimate limit state.

6.5.3 Five bolt WT connections (5WT)

6.5.3.1 Deformed shapes and failure modes

Figure 6.10(a) illustrates the numerical versus experimental deformed shapes of the 5WT connections. Similar to the 3WT and 4WT connections, most of the plastic deformation occurred around the bottom hole of the WT and the bottom bolt shank in which the rupture ultimately occurred, as shown in Figure 6.10(b). The top and the two bottom bolts connecting the WT to the beam web are the ones that experienced plastic deformation. The rest of the bolts, including the ones that connect the WT flange to the column, remained elastic. No distortion occurred around the second and third hole from the top, as shown in Figure 6.10(c). The top and bottom two bolts provided a greater percentage of flexural resistance than the other bolts by forming a force couple about the approximate location of the centroid of the bolt group. Shear deformation of the bolts accompanied by substantial plastic deformation of the bottom hole provides the ductility of the connection, along with flexural deformation of the WT flange. Similar to the 3WT and 4WT connections, the stress distribution around the bottom hole in the 5WT (15-to-30 degree trend) is in agreement with the stress distribution observed in the experimental program.

6.5.3.2 Shear, tension, and moment interaction

The internal forces at the bolt line versus the chord rotation of connection assemblies 5WT are shown in Figure 6.17 to Figure 6.19. Table 6.6 summarizes the experimental and finite element analysis values of the shear, moment, and tension at the initial failure for the 5WT connections. As observed, all quantities—including shear, tension, and moment, as well as chord rotations—determined from the numerical models are in acceptable agreement with the experimental results, with less than 10% deviation from the experimental results.

The failure mode for the tests is bolt shear rupture at the bottom hole, confirmed by the finite element results.

6.6 Parametric study results

After verifying the finite element models with the test results, a parametric study is performed in order to investigate the effects of different design parameters such as WT size, bolt size and type, and also connection depth, according to Table 6.3.

6.6.1 Three bolt WT connections (3WT)

Figure 6.20 to Figure 6.25 show the interactions of shear, tension and moment for the WT connections with three bolts (3WT). The behaviour of 3WT125X33.5-3/4 was discussed in section 6.5.1 since experimental results were available. Its response without the test curves is shown again in Figure 6.20 for the sake of completeness of the report. As labelled in Figure 6.20, the point that the flexural phase domination ends and catenary force begins to provide the major resistance is distinguished. This point is called the “devolution point”, similar to the shear tab connections discussed in chapter 5. For 3WT125X33.5-3/4, the devolution point occurs when the flexural response starts to degrade after the maximum moment is reached. The main reason for this is the fact that in three bolt connections the bottom and top bolts resist the moment through bearing resistance and out-of-plane bending of the WT’s flange. As soon as the localized yielding around the contact surface accompanied by out-of-plane bending deformation of the bottom of the WT’s flange happen, the flexural resistance starts to vanish and the connection attempts to find another path to take additional load. The eventual failure will be in the catenary phase. It is noted that for shear tab connections with three bolts (3ST), the devolution point was located almost at the maximum moment. In the 3WT connections, this point is shifted to after the maximum

moment due to out-of-plane bending of the WT, which does not exist in shear tab connections. Although this out-of-plane deformation is small in a WT125X33.5 section (with 15.7 mm and 8.9 mm flange and stem thickness, respectively), it exists particularly at the bottom of the connection and can act as one source of providing ductility.

Figure 6.21 shows the interaction of internal forces at the bolt line for the model 3WT100X26-3/4. In this model, the failure is initiated in the WT stem bottom hole region. An increase in the ductility of the connection is observed in comparison with 3WT125X33.5-3/4 due to the thinner stem and flange (12.6 mm and 7.9 mm flange and stem thickness, respectively). At the same time, thickness of the web is not so low that it causes premature failure. There are no significant plastic shear deformations observed in the bolts connecting the WT flange to the column. However, the top and bottom bolt connecting the WT stem to the beam web experience major shear deformations prior to failure. Most of the bearing deformation happens in the WT stem. Similar to 3WT125X33.5-3/4, the tensile force starts to come into existence after the point of maximum moment, when the flexural resistance starts to degrade. Shear force increases almost linearly up to the rotation of 0.11 and after that with an increased rate up to the failure, interacting with tension and moment especially at high rotations.

Figure 6.22 shows the interaction of internal forces at the bolt line for the model 3WT155X33.5-3/4. The flange and stem thickness of 3WT155X33.5 are 14.6 mm and 8.5 mm, respectively. This model fails due to WT bottom hole rupture, similar to 3WT100X26-3/4. However, the ductility of the connection is not increased significantly in comparison with 3WT125X33.5-3/4. It can be inferred that the reduction in the thickness causes the change in the failure mode of connection, but cannot increase the ductility of the connection significantly. There is a significant plastic deformation in the top and bottom bolt shank (WT-to-beam web bolts), particularly the bottom one, prior to failure, although the other bolts (WT-to-column bolts) remain almost elastic. The tensile force starts to come into

existence slightly after the point of maximum moment. This could be assigned to the contribution of out-of-plane deformation of WT flange that contributes to the flexural resistance of the WT connection after local yielding around the bolt holes, similar to what is discussed for 3WT125X33.5-3/4.

Figure 6.23 shows the interaction of internal forces at the bolt line for the model 3WT125X33.5-5/8. In this model, the failure happens in the bottom bolt. The amount of plastic deformation due to bearing is small around the top and bottom holes. The connection does not show significant tensile resistance due to premature failure of the bottom bolt. As a result, the ductility of the connection is also reduced in comparison with 3WT125X33.5-3/4, but is still comparable. There are significant plastic deformations at the top and bottom bolt shank before failure, which were the main source of ductility of the connection. Contribution of out-of-plane deformation of the WT flange is negligible. Although the devolution from flexural to catenary is obvious in the connection response, it could not go through the catenary phase significantly (about 0.02 radians).

Figure 6.24 shows the interaction of internal forces at the bolt line for the model 3WT125X33.5-7/8. In this model, the failure is initiated in the WT bottom hole region. Due to a larger bolt diameter, the amount of plastic deformation happening in the bolt shank is small but distinguishable. There are significant plastic deformations around the bottom bolt hole area in the WT stem. The tensile force starts to come into existence after the point of maximum moment, similar to the other 3WT connections.

Figure 6.25 shows the interaction of internal forces at the bolt line for the model 3WT125X33.5-3/4-A490. The behaviour of this model is similar to that of 3WT125X33.5-3/4 with ASTM A325 bolts. However, the dominant limit state of the connection is different. Using ASTM A490 bolts shifted the failure mode from the bottom bolt to the WT bottom hole region. The ductility of the connection is also reduced, which results in a reduction of the shear and tensile strength of the connection in comparison with the one with ASTM A325 bolts.

As observed in the foregoing discussion, in 3WT connections, regardless of the WT section, bolt size and type, as the flexural stiffness of the connection approaches zero and then starts to degrade subsequently, the tensile catenary force increases rapidly until the failure of the connection occurs. Tensile catenary resistance starts to grow at the approximate chord rotation angle of 0.085, at which time flexural response starts to reduce. The amount of moment present immediately prior to failure of the connection is variable, and in some cases substantial. However, it can be inferred that the 3WT connections fail mainly because of catenary action. The dominant failure mode of 3WT connections is the WT bottom hole rupture and bolt shear rupture.

6.6.2 Four bolt WT connections (4WT)

Figure 6.26 to Figure 6.31 show the interactions of shear, tension, and moment for WT shear connections with four bolts (4WT). The behaviour of 4WT125X33.5-3/4 was discussed in section 6.5.2, but its response without the test result curves is shown again in the Figure 6.26 for the sake of completeness of the report. The “devolution point” for this connection is not as clear as for the 3WT connections. Actually, there is a point that can be assigned as the “devolution point” in which after substantial decrease in flexural stiffness, the tensile force starts to ramp up, as shown in Figure 6.26. At the approximate rotation of 0.03 radians, yielding starts to happen around the top and bottom holes; however, the system still can capture more plastic deformation around the holes and also through out-of-plane bending of the WT flange. As a result, the moment increases further, but with reduced stiffness. Gradually, the amount of tensile force exceeds the compressive value and the whole section goes through catenary action, after the rotation of about 0.05. However, the connection fails in the flexural-catenary phase due to the presence of a significant amount of moment and tension at the time of failure.

Figure 6.27 shows the interaction of internal forces at the bolt line for the model 4WT100X26-3/4. In this model, the failure is initiated in the WT bottom hole

region. An increase in the ductility of the connection is observed in comparison with 3WT125X33.5-3/4 due to the thinner web and flange. At the same time, thickness of the web is not so low that it causes premature failure. The amount of out-of-plane deformation of the flange is significantly higher than for the 4WT125X33.5-3/4 model. There are no significant plastic shear deformations observed in the bolts connecting the WT flange to the column. However, the top and bottom bolt connecting the WT stem to the beam web experience significant shear deformation. Most of the bearing deformation happens around the top and bottom hole in the WT stem. Similar to 4WT125X33.5-3/4, the tensile force starts to come into existence after the devolution point (0.05 radians). This connection possesses the highest ductility, and, consequently, the highest tensile resistance. Shear force increases almost linearly after the 0.02 radians rotation, up to the point of failure.

Figure 6.28 shows the interaction of internal forces at the bolt line for the model 4WT155X33.5-3/4. This model fails due to WT bottom hole rupture, similar to 4WT100X26-3/4. However, the ductility of the connection is not increased significantly in comparison with 3WT125X33.5-3/4. There is a significant plastic deformation in the top and bottom bolt shank (WT-to-beam bolts), particularly the bottom one, prior to the failure, although the other bolts (WT-to-column) remain almost elastic. The tensile force starts to come into existence after the devolution point (0.03), similar to 4WT125X33.5-3/4 and 4WT100X26-3/4. The tensile catenary resistance of this model is slightly more than for the 4WT125X33.5-3/4 connection due to higher ductility. Shear force increases almost linearly after the 0.02 radians rotation, up to the point of failure, interacting with tension and moment especially at high rotations.

Figure 6.29 shows the interaction of internal forces at the bolt line for the model 4WT125X33.5-5/8. In this model, due to the reduction of bolt diameter comparing with 4WT125X33.5-3/4, the failure happens in the bottom bolt, as expected. The amount of plastic deformation due to bearing is small around the

top and bottom holes. The tensile capacity of the connection drops significantly due to premature failure of the bolts. As a result, the ductility of the connection is also reduced comparing to the 4WT125X33.5-3/4 model. There are significant plastic deformations at the top and bottom bolt shank before failure, which are the main source of ductility of the connection. Contribution of out-of-plane deformation of the WT flange is negligible in this case. Similar to the 3WT125X33.5-5/8 model, the flexural-catenary phase does not last (about 0.03 radians) due to early shear rupture of a 5/8 in (15.9 mm) bolt.

Figure 6.30 shows the interaction of internal forces at the bolt line for the model 4WT125X33.5-7/8. In this model, the failure is initiated in the WT bottom hole region. Due to the larger bolt size, only a small amount of plastic deformation happens in the bottom bolt shank. Top and bottom bolts of the WT-to-beam connection are the only bolts which deformed significantly; the rest of the bolts are almost elastic. There are significant plastic deformations around the bottom bolt hole area at the WT stem. Devolution from one phase to another is similar to other 4WT connections.

Figure 6.31 shows the interaction of internal forces at the bolt line for the model 4WT125X33.5-3/4-A490. The behaviour of model 4WT125X33.5-3/4-A490 is similar to that of 4WT125X33.5-3/4 with ASTM A325 bolts; however, the dominant limit state is changed due to the change in the bolt grade. Using ASTM A490 bolts shifts the failure mode from the bottom bolt to the WT bottom hole region, similar to what was observed in the 3WT connections. The ductilities of the connections are almost the same. The shear and flexural resistance of 4WT125X33.5-3/4-A490 is slightly higher than the similar connection with the ASTM A325 bolts.

The “devolution” point between load-carrying mechanisms for 4WT connections is not as clear as for 3WT connections, but still definable as a point. There is a point in which the tensile force starts to ramp up after a substantial decrease in flexural stiffness occurs. After this devolution point, the tensile catenary force

begins to play a role and grows rapidly until the failure of the connection, in the presence of shear and moment. Tensile catenary resistance starts to grow at the approximate chord rotation angle of 0.05 radians. The amount of moment at failure is substantial and cannot be ignored. Besides, where the tensile force starts to increase rapidly, the moment is still rising. Therefore, it can be inferred that the 4WT connections fail mainly because of flexural-catenary actions. The dominated failure mode of 4WT connections is the WT bottom hole rupture and bolt shear rupture, similar to 3WT connections.

6.6.3 Five bolt WT connections (5WT)

Figure 6.32 to Figure 6.37 depict simultaneous presence of shear, tension, and moment for the WT connections with five bolts (5WT). The behaviour of 5WT125X33.5-3/4 was discussed in section 6.5.3, but its response without the test curves is shown again in the Figure 6.32 for the sake of completeness of the report. A point is distinguished as a devolution point (at about the rotation of 0.025 radians) in which a substantial decrease in flexural stiffness occurs accompanied by an increase in the rate of tensile response of the connection until the failure.

Figure 6.33 shows the interaction of internal forces at the bolt line for the model 5WT100X26-3/4. Its behaviour is similar to the 4WT100X26-3/4 and 3WT100X26-3/4 models due to the same geometric and mechanical properties. The failure is initiated in the WT bottom hole region similarly. An increase in the ductility of the connection is observed in comparison with 5WT125X33.5-3/4 due to thinner web and flange. Out-of-plane deformation of the WT flange contributes to the ductility of the connection, particularly at the bottom part, which makes the connection more ductile than the other ones with different WT sections. There is no significant plastic shear deformation observed in the bolts—even the bottom bolt—since most of the bearing deformations happen in the thin plate. In the five bolt connections, the interaction of shear, tension, and moment starts at the early

stages of loading, after the establishment of contacts, which is about 0.01 radians of rotation. However, the devolution from the flexural to the catenary phase happens at a point of about 0.025 radians, at which point the flexural stiffness reduces drastically and the tension rate increases noticeably.

Figure 6.34 shows the interaction of internal forces at the bolt line for the model 5WT155X33.5-3/4. Similar to 3WT155X33.5-3/4 and 4WT155X33.5-3/4, in the 5WT155X33.5-3/4 connection model assembly, the failure mode is shifted to the bottom bolt due to the decrease in the thickness of WT stem. There is a slight increase in the rotational ductility of the connection in comparison with 5WT125X33.5-3/4. There is also a substantial amount of plastic deformation in the two bottom bolts and the one at the top prior to the failure. The other two bolts are almost elastic. The devolution from flexural behaviour to the flexural-catenary phase is obvious in Figure 6.34. At the rotation of about 0.022, a change happens at the rate of tensile response of the connection which causes a reduction in the slope of the flexural response.

Figure 6.35 shows the interaction of internal forces at the bolt line for the model 5WT125X33.5-5/8. In this model, due to the reduction of bolt diameter comparing with 4WT125X33.5-3/4 the failure happens in the bottom bolt, similar to 3WT and 4WT connections with same configuration. The amount of plastic deformation due to bearing is small around the top and bottom holes. The tensile capacity of the connection drops significantly due to premature failure of the bolts. As a result, the ductility of the connection is also reduced compared to the 5WT125X33.5-3/4 model. There are significant plastic deformations at the top and bottom bolt shank before failure, which are the main source of ductility of the connection. Contribution of out-of-plane deformation of the WT flange is negligible. Due to early shear rupture of a 5/8 in (15.9 mm) diameter bolt, the flexural-catenary phase does not have a large extent. However, at an approximate rotation of 0.022 radians a change happens in the rate of increase of tensile force, accompanied by a reduction in the slope of the flexural response.

Figure 6.36 shows the interaction of internal forces at the bolt line for the model 5WT125X33.5-7/8. In this model, the failure is initiated in the WT bottom hole region. Due to the larger bolt diameter, the amount of plastic deformation in the bottom bolt shank is small, but still distinguishable. The top and the two bottom bolts of the WT-to-beam connection are the only bolts that deformed slightly; the rest of the bolts are elastic. There are significant plastic deformations around the bottom bolt hole area. The devolution from flexural behaviour to the flexural-catenary phase is obvious. Similar to all the other 5WT models, 0.022 radians of rotation can be distinguished as a transition point in which the rate of tensile response of the connection increases accompanied by a reduction in the slope of the flexural response.

Figure 6.37 shows the interaction of internal forces at the bolt line for the model 5WT125X33.5-3/4-A490. The behaviour of this model is similar to that of 5WT125X33.5-3/4 with ASTM A325 bolts. However, the dominant limit state of the connection is different. Using ASTM A490 bolts shifted the failure mode from the bottom bolt to the WT bottom hole region. The ductility of the 5WT125X33.5-3/4-A490 connection is slightly less than that of 5WT125X33.5-3/4 with A325 bolts.

It is noted that 5WT connections go into catenary tension from the beginning, as discussed in chapter 4. Since the depth of the connection was almost the same as that of the beam, there is no vertical eccentricity in the 5WT connections comparing with 4WT ones (see chapter 4 for further explanation). As a result, tension does not need to cancel the compressive arching force in the connection, unlike for the 4WT connections. Consequently, a reduction in the flexural stiffness happens where the tensile response starts to ramp up rapidly where the devolution “point” can be distinguished in 5WT connections. Regardless of the WT section, bolt size and type, at the approximate rotation of 0.022 radians, a significant decrease and increase in the slope of the flexural and tensile responses, respectively, of the 5WT connections are observable. The amount of moment at

failure is significant. As a result, it can be inferred that the 5WT connections fail mainly because of flexural-catenary actions. The dominant failure mode of 5WT connections is the WT bottom hole rupture and bolt shear rupture, similar to what was observed for WT connections with three (3WT) and four (4WT) bolts.

Table 6.7 summarizes the results of the numerical models in addition to the experimental specimens at the initial failure of the connections.

6.7 Comparison of the results

In this section, the effect of WT size, bolt size and bolt type are discussed separately for three, four and five bolt connections.

6.7.1 Three bolt WT connections (3WT)

6.7.1.1 WT size

Figure 6.38 to Figure 6.40 illustrate the shear, tensile, and flexural responses of 3WT connections with different WT section sizes. Generally, the model 3WT100X26-3/4 behaves in a more ductile manner than the other two WT connections. As can be seen, the thinner stem and flange causes an increase in shear and tensile strengths of 3WT100X26-3/4 connections at the initial failure rotation. At small rotations, the difference of shear and flexural response is negligible, but as the rotation increases, the difference increases. In terms of tensile response, the difference among the curves is minimal for a given rotation, although the 3WT100X26-3/4 possesses more tensile capacity due to more ductility. In terms of load path, the tensile response of the connection does not change significantly by altering the WT section size. However, the maximum tensile catenary force they can develop is highly dependent on the WT geometry. The shear strengths of the 3WT125X33.5-3/4 and 3WT155X33.5-3/4 connections

are almost the same, but are smaller than that of 3WT100X26-3/4 (about 70%) at the initiation of failure. In terms of axial strength, this value reduces to about 67%. Model 3WT100X26-3/4, with thinner cross-sectional elements, shows higher ductility due to postponing failure to higher rotations; eventually it fails by WT bottom hole rupture. The maximum moment happens at approximately the same rotation for all the WT sizes. All the flexural responses possess a descending branch after the peak moment until failure, as observed in Figure 6.40. 3WT100X26-3/4 is the only connection among the three that possesses no flexural resistance at the time of failure due to tensile catenary behaviour.

6.7.1.2 Bolt size

Figure 6.41 to Figure 6.43 illustrate the shear, tensile, and flexural responses of the 3WT connections with different bolt sizes. An increase in bolt diameter causes an increase in the flexural and shear response of 3WT connections. However, in terms of axial response, the behaviours are almost the same, as shown in Figure 6.42, although the smaller bolt size—5/8 in diameter—fails earlier than the other two since large plastic strains occur in its bottom bolt shank. 3WT125X33.5-3/4 is more ductile than the connections with the larger and smaller bolt sizes because of the lower shear deformation in the bolts of 3WT125X33.5-7/8 and the early shear failure of the bolts in 3WT125X33.5-5/8. Therefore, the change in the rotational capacity of the 3WT connections due to a change in bolt diameter is dependent on the governing failure mode. The maximum moment happens at approximately the same rotation (0.065 radians) for all sizes. All the flexural responses possess a descending branch after the peak moment until failure, as observed in Figure 6.42.

6.7.1.3 Bolt type

Figure 6.44 to Figure 6.46 illustrate the shear, tensile, and flexural responses of the 3WT connections with different bolt types, ASTM A325 versus ASTM A490, for the 3WT125X33.5-3/4 model. It is observed that using A490 bolts changes the

connection failure mode from bolt shear failure to WT bottom hole rupture. In terms of load path, the shear, axial, and flexural responses of the connection assemblies with two different types of bolts are almost the same. There is an increase in the flexural curve due to usage of ASTM A490 bolts. However, the rotational ductility of 3WT125X33.5-3/4 with ASTM A325 bolts is slightly higher than the 3WT125X33.5-3/4-A490 model.

6.7.2 Four bolt WT connections (4WT)

6.7.2.1 WT size

Figure 6.47 to Figure 6.49 illustrates the shear, tensile, and flexural responses of 4WT connections with different WT section sizes. Generally, the model 4WT100X26-3/4 behaves in a more ductile manner than the other two WT connections. As can be seen, the thinner stem and flange cause an increase in shear and tensile strengths and also the rotational ductility. The difference in shear and flexural response at small rotations is small, and as the rotation increases, the difference increases. In terms of axial load path response, the difference among the curves is minimal, although 3WT100X26-3/4 possesses more tensile capacity due to more ductility. It can be inferred that the axial response of the connection does not change significantly by altering the WT section size for a given rotation. However, the maximum tensile catenary force they can develop is highly dependent on the WT geometry. The shear and tensile capacity of the connection increase with the reduction in the thickness of the WT stem and flange. Model 4WT100X26-3/4, with thinner cross-sectional element thicknesses, shows higher ductility due to postponing failure to higher rotations; it eventually fails by WT bottom hole rupture. The maximum moment happens at approximately the same rotation for all the WT sizes (0.08 radians). All the flexural responses possess a descending branch after the peak moment until failure, as observed in the Figure 6.49.

6.7.2.2 Bolt size

Figure 6.50 to Figure 6.52 illustrate the shear, tensile, and flexural responses of the 4WT connections with different bolt sizes. Generally, an increase in bolt diameter causes an increase in the flexural and shear response of 4WT connections. However, in terms of axial response, the behaviours are almost the same, as shown in Figure 6.51, although the smaller bolt size, 5/8 in (15.9 mm) diameter, fails sooner than the other two due to an excessive amount of plastic strain in the bottom bolt shank. Ductility of the 4WT125X33.5-3/4 and 4WT125X33.5-7/8 is almost the same. Change in the rotational capacity of 4WT connections due to a change in bolt diameter is dependent on the failure mode, similar to the 3WT connections. The maximum moment happens at the approximate same rotation (0.08 radians) for the 3WT125X33.5-3/4 and 3WT125X33.5-7/8 models. All the flexural responses possess a small descending branch after the peak moment until failure, as observed in Figure 6.52.

6.7.2.3 Bolt type

Figure 6.53 to Figure 6.55 illustrate the shear, tensile, and flexural responses of the 4WT connection with different bolt type. It is observed that using ASTM A490 bolts changes the connection failure mode from bolt shear failure to WT bottom hole rupture. In terms of load path, the shear, axial, and flexural responses of the connection assemblies with two different types of bolts are almost the same, with a slight increase in the shear and flexural strength after the rotation of 0.03 radians. However, the rotational ductility of the connections with different types of bolts is nearly identical.

6.7.3 Five bolt WT connections (5WT)

6.7.3.1 WT size

Figure 6.56 to Figure 6.58 illustrate the shear, tensile, and flexural responses of 5WT connections with different WT section sizes. Generally, the model 5WT100X26-3/4 behaves in a more ductile manner than the other two WT connections. As can be seen, a decrease in stem and flange thickness causes a slight increase in shear and tensile strength and also in rotational ductility. The difference in shear and flexural response at small rotations is negligible, but and as the rotation increases, the difference becomes more significant. In terms of axial tensile load path response, the difference among the curves is minimal, although the 5WT100X26-3/4 possesses more tensile capacity due to more ductility. The axial response of the connection does not change significantly by altering the WT section size. However, the maximum tensile catenary force it can develop is dependent on the WT geometry. The shear and tensile capacity of the connection increases with a reduction in the thickness of the WT stem and flange. Model 5WT100X26-3/4, with thinner cross-sectional element thicknesses, shows higher ductility due to postponing failure to higher rotations; eventually it fails by WT bottom hole rupture. The maximum moment happens at the approximate same rotation for all the WT sizes (about 0.08 radians). 5WT125X33.5-3/4 and 5WT155X33.5-3/4 possess almost the same flexural behaviour. The flexural response of 5WT100X26-3/4 is almost flat at the peak until failure, as observed in Figure 6.58.

6.7.3.2 Bolt type

Figure 6.59 to Figure 6.61 illustrate the shear, tensile, and flexural response of the 5WT connections with different bolt sizes. An increase in bolt diameter causes an increase in the flexural and shear responses of 5WT connections. However, in terms of axial response, the behaviours are almost the same, as shown in Figure

6.60, although the connection with the smallest bolt size, 5/8 in (15.9 mm) diameter, fails sooner than the other two due to the development of an excessive amount of plastic strains in the bottom bolt shank. The ductilities of 5WT125X33.5-3/4 and 5WT125X33.5-7/8 are almost the same. The change in rotational capacity of 5WT connections due to the change in bolt diameter is dependent on the failure mode, similar to 3WT and 4WT connections. The maximum moment happens at the approximate same rotation (0.08 radians) for the 5WT125X33.5-3/4 and 5WT125X33.5-7/8 models. None of the flexural responses possess a descending branch after the peak moment, as shown in Figure 6.61.

6.7.3.3 Bolt type

Figure 6.62 to Figure 6.64 illustrate the shear, tensile, and flexural responses of the 5WT connections with different bolt type. The effect of different bolt types, ASTM A325 versus ASTM A490, is similar to what was discussed for 3WT and 4WT connections in sections 6.7.1.3 and 6.7.2.3, respectively.

6.8 Rotational ductility of WT connections in column removal scenario

Based on what was discussed earlier in the chapter, the rotational capacity of WT connections is not significantly affected by variables such as WT section size, bolt size and type. However, a change in the failure mode does affect the rotational ductility of the connection. Moreover, the number of rows of bolts is making a difference, as well. As a result, rotational capacity can be estimated based on the depth of the connection, similar to common practice in current codes and guidelines. Figure 6.65 illustrates the distribution of rotational capacity of shear tab connections studied in this research versus connection depth. Experimental

values (EXP) are the average values observed in the tests, obtained from Table 6.4 to Table 6.6, producing totally three points in Figure 6.65. Finite element (FE) models add eighteen other points in order to increase the number of data and, hence, making the regression analysis more accurate. Figure 6.66 and Figure 6.67 show the best-fit line for specimens that failed by bolt shear rupture and WT rupture limit states, respectively. As can be seen in Figure 6.66, one set of three points is far below the rest. These data are related to the connection assembly with 5/8 in (15.9 mm) bolts, which fail prematurely due to small bolt size. As a result, Equation (6-1) (bolt shear rupture limit state) and Equation (6-2) (WT rupture) are proposed to determine rotational capacity of WT connections in the column removal scenario:

$$\theta_{tot} = -0.0088 d_{conn} + 0.170 \quad (d_{conn} \text{ in inches}) \quad (6-1)$$

$$\theta_{tot} = -0.0088 d_{conn} + 0.186 \quad (d_{conn} \text{ in inches}) \quad (6-2)$$

where d_{conn} is the distance between the centres of the top and bottom bolts, and θ_{tot} is the total rotational capacity of the shear tab connection in radians. It is interesting to note that the best-fit lines have the same slope and, as expected, the line for the bolt shear failure limit state predicts a lower rotational capacity. Equation (6-1) and Equation (6-2) are converted to SI units in Equation (6-3) and Equation (6-4):

$$\theta_{tot} = -0.00035 d_{conn} + 0.170 \quad (d_{conn} \text{ in millimetres}) \quad (6-3)$$

$$\theta_{tot} = -0.00035 d_{conn} + 0.186 \quad (d_{conn} \text{ in millimetres}) \quad (6-4)$$

θ_{tot} consists of both elastic and plastic components. The plastic rotation is the rotation that guidelines such as ASCE 41 (2006) and DoD (2009) utilize to define the connection behaviour. By aid of finite element models, plastic rotation can be separated from the elastic part and, through a regression analysis of the data for all

cases considered (see Figure 6.68 and Figure 6.69), is reported as Equation (6-5) for the bolt shear rupture limit state and Equation (6-6) for WT rupture:

$$\theta_p = -0.0078 d_{conn} + 0.141 \quad (d_{conn} \text{ in inches}) \quad (6-5)$$

$$\theta_p = -0.0076 d_{conn} + 0.152 \quad (d_{conn} \text{ in inches}) \quad (6-6)$$

As observable in Figure 6.69, one set of points plots higher than the others. These are the data related to connections WT100X26-3/4 with three, four, and five bolts. As discussed earlier, these connections possess higher ductility because they have a thinner WT flange and, consequently, receive a higher contribution to rotational capacity from out-of-plane flange bending.

Converting Equation (6-5) and Equation (6-6) to SI units produces Equation (6-7) and Equation (6-8):

$$\theta_p = -0.00031 d_{conn} + 0.141 \quad (d_{conn} \text{ in millimetres}) \quad (6-7)$$

$$\theta_p = -0.00030 d_{conn} + 0.152 \quad (d_{conn} \text{ in millimetres}) \quad (6-8)$$

Elastic rotation ends when the first sign of plastic strain starts to appear in the connection assembly. It is noted that the average elastic rotations observed in the three, four and five bolt WT connections studied are 0.024, 0.023 and 0.017 radians, respectively. Therefore, in the absence of appropriate tools to determine the elastic rotation limit for a WT connection, a value of 0.02 radians is a reasonable assumption for connections resembling those considered in this study.

6.9 Summary and Conclusion

In this chapter, the simultaneous presence of shear, moment and tension in WT connections was researched. Tensile catenary action is acknowledged as the load

transfer mechanism in a column removal scenario. Ductility of WT connections is derived largely from the local deformation in the stem adjacent to the bottom holes and the bolt slippage and deformation before failure. Out-of-plane bending of the WT flange between the bolt lines is another source; however, it was not significant in the connections with a thick flange. Either shear failure of the bottom bolt or WT bottom hole rupture was the governing failure mode in all cases. The response curves can be used as input for WT connection models in full-building progressive collapse analyses. Other conclusions that can be drawn are:

- It cannot be assumed that all of the fasteners in a line share equally in carrying the load. In fact, the fasteners towards the bottom of the joint carry the largest portion of the load. This unequal loading of the fasteners is accentuated as the rotation increased.
- The maximum rotation of these WT connections was between 0.075 and 0.127 radians for three to five bolts. Based on Astaneh's experiments (Astaneh and Nader 1990), the shear deformation and distortion of the WT section are the main sources of ductile behaviour for a simply supported beam under gravity loading. For the column removal scenario, on the other hand, the contribution of bolt hole bearing deformation, especially the one at the bottom, is also significant. Out-of-plane bending of the WT's flange, as another source of ductility, is not uniformly distributed over the length of the WT in the column removal scenario. Based on the results of the numerical analyses, out-of-plane flange deformation is at a maximum at the bottom of all three connections considered and is almost zero at the top.
- Most of the plastic deformation occurred around the bottom hole of the WT section and also in the bottom bolt shank, in which the rupture occurred. Plastic deformation in the other bolts is small in comparison with the bottom bolt. The numerical model predicts the bolt failure very well with removed elements.

- The point that the flexural phase domination ends and catenary force begins to provide the major resistance is named the “devolution point”. For 3WT connections, the devolution point happens after the maximum moment rotation. The main reason for this is the fact that in three bolt connections the bottom and top bolts resist the demanded moment through bearing resistance of the bolt-hole interaction. As soon as the localized yielding around the contact surface accompanied by out-of-plane bending deformation of the bottom of the WT’s flange occur, the flexural resistance starts to vanish and the connection tries to find another load path. The failure will take place in the catenary phase. Generally, the switch between flexural behaviour and the tensile phase in 3WT connections can be distinguished more accurately than for 4WT connections. In this case, there is a point that can be assigned as the devolution point, in which a tensile response starts to ramp up rapidly. Before the devolution point, yielding starts to happen around the top and bottom holes; however, the system still can capture more plastic deformation around the holes and also through out-of-plane bending of WT flange. As a result, more moment is captured, but with reduced stiffness. Gradually, the amount of tensile force exceeds the compression value and the whole section develops catenary action. However, the connection fails in the flexural-catenary phase due to the presence of a significant amount of moment and tension at the time of failure. It is noted that the 5WT connections go into catenary tension from the beginning. Tension does not need to cancel the compressive force at the connection, unlike for the 4WT connections. At the devolution point, a significant decrease in the slope of the flexural response and an increase in the tensile response of the 5WT connections are observable. Basically, the amount of moment at the failure is significant. As a result, it can be inferred that the 5WT connections fail mainly because of flexural-catenary action.

- The resulting response curves can be used as input for WT connection models in full-building progressive collapse analyses. Equations are proposed for determination of WT connection total rotational capacity and also plastic rotational capacity based on regression analyses of the cases studied.

Table 6.1: Typical material used for WT connections

Component	Material	Description
WT	ASTM A992, 350W	-
Bolts	ASTM A325, A490	standard/slotted hole

Table 6.2: Summary of shear strength tests by Astaneh and Nader (1990)

Test No.	WT section	No. Bolts	Bolt diameter [in (mm)]	Type of bolts	Rotation (radians)	Test shear capacity [kips (kN)]	Moment at bolt line [kip.in (kN.m)]	Observed failure mode
1	WT4X7.5	3	7/8 (22)	A325	0.034	55 (245)	143 (16.1)	Yielding of gross area of tee stem
2	WT7X19	5	7/8 (22)	A325	0.032	160 (712)	281 (31.7)	Yielding of gross area of tee stem
3	WT7X19	3	7/8 (22)	A325	0.067	107 (476)	14 (1.6)	Fracture of net area of tee stem
4	WT4X7.5	5	7/8 (22)	A325	-	-	-	Specimen failed during first phase
5	WT4X20	5	7/8 (22)	A325	0.035	183 (814)	300 (33.9)	Fracture of gross area of tee stem
6	WT4X20	3	7/8 (22)	A325	0.034	111 (494)	128 (14.5)	Fracture of gross area of tee stem
7	WT7X19 + 0.5-in web (13 mm)	5	7/8 (22)	A325	0.038	238 (1059)	37 (4.2)	Shear fracture of bolts
8	WT4X20 + 0.5-in web (13 mm) ¹	3	7/8 (22)	A490	0.039	141 (627)	393 (44.4)	Fracture of welds
9	WT4X20 + 0.5-in web (13 mm) ¹	5	7/8 (22)	A490	0.033	209 (930)	270 (30.5)	Shear fracture of bolts

¹ Web of WT was cut and replaced by ½ in thick (12.7 mm) ASTM A36 plate.

Table 6.3: Summary of characteristic features of FE models of WT connections

No.	Specimen Label ¹	WT Type	WT Section	Bolt Type	Bolt diameter	Remarks
1	3WT125X33.5-3/4	ASTM A992	WT125X33.5	ASTM A325	19.1 mm (3/4 in)	Used for verification ²
2	3WT100X26-3/4	ASTM A992	WT100X26	ASTM A325	19.1 mm (3/4 in)	-
3	3WT155X33.5-3/4	ASTM A992	WT155X33.5	ASTM A325	19.1 mm (3/4 in)	-
4	3WT125X33.5-5/8	ASTM A992	WT125X33.5	ASTM A325	15.9 mm (5/8 in)	-
5	3WT125X33.5-7/8	ASTM A992	WT125X33.5	ASTM A325	22.2 mm (7/8 in)	-
6	3WT125X33.5-3/4-A490	ASTM A992	WT125X33.5	ASTM A490	19.1 mm (3/4 in)	-
7	4WT125X33.5-3/4	ASTM A992	WT125X33.5	ASTM A325	19.1 mm (3/4 in)	Used for verification ²
8	4WT100X26-3/4	ASTM A992	WT100X26	ASTM A325	19.1 mm (3/4 in)	-
9	4WT155X33.5-3/4	ASTM A992	WT155X33.5	ASTM A325	19.1 mm (3/4 in)	-
10	4WT125X33.5-5/8	ASTM A992	WT125X33.5	ASTM A325	15.9 mm (5/8 in)	-
11	4WT125X33.5-7/8	ASTM A992	WT125X33.5	ASTM A325	22.2 mm (7/8 in)	-
12	4WT125X33.5-3/4-A490	ASTM A992	WT125X33.5	ASTM A490	19.1 mm (3/4 in)	-
13	5WT125X33.5-3/4	ASTM A992	WT125X33.5	ASTM A325	19.1 mm (3/4 in)	Used for verification ²
14	5WT100X26-3/4	ASTM A992	WT100X26	ASTM A325	19.1 mm (3/4 in)	-
15	5WT155X33.5-3/4	ASTM A992	WT155X33.5	ASTM A325	19.1 mm (3/4 in)	-
16	5WT125X33.5-5/8	ASTM A992	WT125X33.5	ASTM A325	15.9 mm (5/8 in)	-
17	5WT125X33.5-7/8	ASTM A992	WT125X33.5	ASTM A325	22.2 mm (7/8 in)	-
18	5WT125X33.5-3/4-A490	ASTM A992	WT125X33.5	ASTM A490	19.1 mm (3/4 in)	-

¹ Imperial units are utilized in labelling the bolts since the experimental program utilized imperial bolts.

² Test results are available for these models.

Table 6.4: Comparison of numerical and experimental (Friedman 2009) responses of shear tab connections with three bolts (3WT) at initial failure

Spec. Label	Side	Moment, M (kN.m)	Shear, V (kN)	Axial, P (kN)	Rotation, Θ (radians)	Failure Mode
3WT1	Left	9.30	23.66	158.89	0.13	Bottom bolt shear rupture
	Right	4.77	23.66	162.76	0.133	-
3WT2	Left	9.19	23.22	155.95	0.13	-
	Right	7.12	23.22	160.71	0.125	Bottom bolt shear rupture
3WT3	Left	3.34	24.24	179.44	0.13	Bottom bolt shear rupture
	Right	1.69	24.24	184.29	0.128	-
3WT-Mean		5.90	23.71	167.01	0.129	-
3WT-FEA		6.43	25.71	170.81	0.131	Bottom bolt shear rupture
Deviation %		8.94	8.44	2.28	1.95	-

Table 6.5: Comparison of numerical and experimental (Friedman 2009) responses of shear tab connections with four bolts (4WT) at initial failure

Spec. Label	Side	Moment, M (kN.m)	Shear, V (kN)	Axial, P (kN)	Rotation, Θ (radians)	Failure Mode
4WT1	Left	41.07	33.09	143.41	0.10	-
	Right	35.03	33.09	142.25	0.097	Bottom bolt shear rupture
4WT2	Left	38.25	31.58	128.38	0.093	-
	Right	33.62	31.58	129.93	0.09	Bottom bolt shear rupture
4WT3	Left	36.99	31.09	137.32	0.091	-
	Right	33.58	31.09	135.31	0.091	Bottom bolt shear rupture
4WT-Mean		36.42	31.92	136.10	0.094	-
4WT-FEA		35.05	32.76	149.95	0.096	Bottom bolt shear rupture
Deviation %		3.77	2.62	10.18	2.49	-

Table 6.6: Comparison of numerical and experimental (Friedman 2009) responses of shear tab connections with five bolts (5WT) at initial failure

Spec. Label	Side	Moment, M (kN.m)	Shear, V (kN)	Axial, P (kN)	Rotation, Θ (radians)	Failure Mode
5WT1	Left	68.63	44.35	126.55	0.073	Bottom bolt shear rupture
	Right	61.04	44.35	130.78	0.073	-
5WT2	Left	71.09	43.55	109.03	0.070	Bottom bolt shear rupture
	Right	63.17	43.55	112.81	0.069	-
5WT3	Left	69.99	47.28	142.48	0.071	Bottom bolt shear rupture
	Right	63.90	47.28	148.57	0.069	-
5WT-Mean		69.99	47.28	142.48	0.071	-
5WT-FEA		63.34	45.1	155.35	0.075	Bottom bolt shear rupture
Deviation %		9.50	4.62	9.04	5.63	-

Table 6.7: Summary of characteristic features of experimental and numerical models of WT connections

No.	Specimen/Model Label	Connection Depth (mm)	Rotation (Rad)	V (kN)	T (kN)	M (kN.m)	Failure Mode
1	3WT125X33.5-3/4-EXP	152.4	0.129	23.7	167.0	5.9	Bottom bolt shear rupture
2	3WT125X33.5-3/4	152.4	0.131	25.7	170.8	6.4	Bottom bolt shear rupture
3	3WT100X26-3/4	152.4	0.163	36.5	260.3	-	WT bottom hole rupture
4	3WT155X33.5-3/4	152.4	0.135	26.6	180.8	4.5	WT bottom hole rupture
5	3WT125X33.5-5/8	152.4	0.098	10.0	26.1	14.0	Bottom bolt shear rupture
6	3WT125X33.5-7/8	152.4	0.117	22.8	98.7	17.3	WT bottom hole rupture
7	3WT125X33.5-3/4-A490	152.4	0.120	20.4	104.3	15.2	WT bottom hole rupture
8	4WT125X33.5-3/4-EXP	228.6	0.094	31.9	136.1	36.4	Bottom bolt shear rupture
9	4WT125X33.5-3/4	228.6	0.096	32.8	150.0	35.1	Bottom bolt shear rupture
10	4WT100X26-3/4	228.6	0.120	38.7	195.0	24.9	WT bottom hole rupture
11	4WT155X33.5-3/4	228.6	0.107	35.7	176.6	32.1	WT bottom hole rupture
12	4WT125X33.5-5/8	228.6	0.073	13.8	71.1	26.9	Bottom bolt shear rupture
13	4WT125X33.5-7/8	228.6	0.094	35.7	146.6	41.7	WT bottom hole rupture
14	4WT125X33.5-3/4-A490	228.6	0.095	34.4	143.3	39.6	WT bottom hole rupture
15	5WT125X33.5-3/4-EXP	304.8	0.071	45.1	128.4	66.3	Bottom bolt shear rupture
16	5WT125X33.5-3/4	304.8	0.075	45.1	155.4	63.3	Bottom bolt shear rupture
17	5WT100X26-3/4	304.8	0.096	47.4	186.8	54.5	WT bottom hole rupture
18	5WT155X33.5-3/4	304.8	0.080	46.3	166.3	64.0	WT bottom hole rupture
19	5WT125X33.5-5/8	304.8	0.054	27.9	75.8	45.0	Bottom bolt shear rupture
20	5WT125X33.5-7/8	304.8	0.076	49.0	143.9	72.0	WT bottom hole rupture
21	5WT125X33.5-3/4-A490	304.8	0.071	45.9	135.9	68.6	WT bottom hole rupture

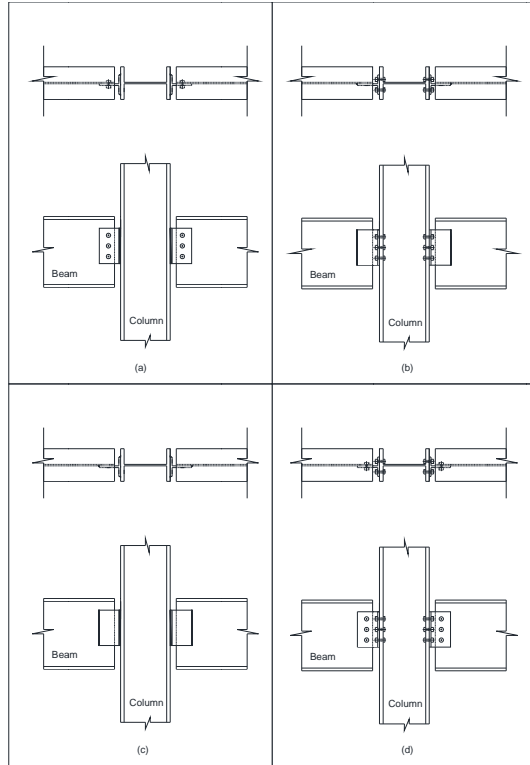


Figure 6.1: Types of WT shear connections: (a) welded-bolted (b) bolted-welded (c) welded-welded (d) bolted-bolted (Astaneh and Nader 1990)

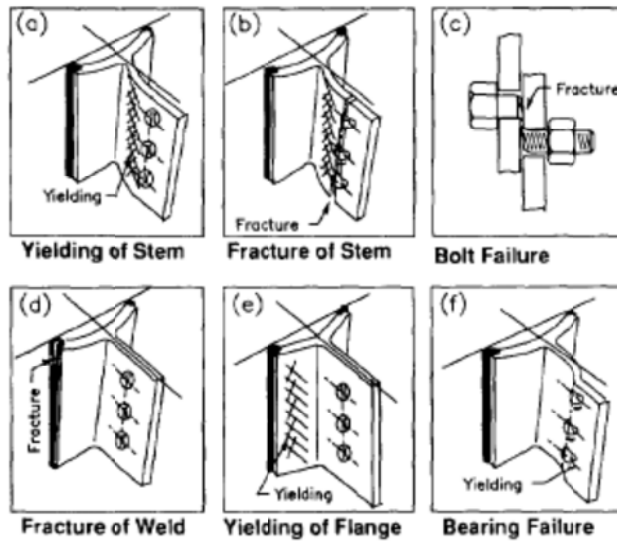


Figure 6.2: Typical failure modes (Astaneh and Nader 1989)

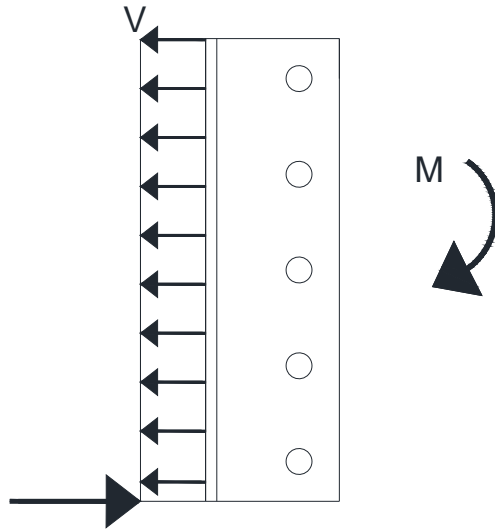


Figure 6.3: Assumed induced force on WT and bolts (Thornton 1996)

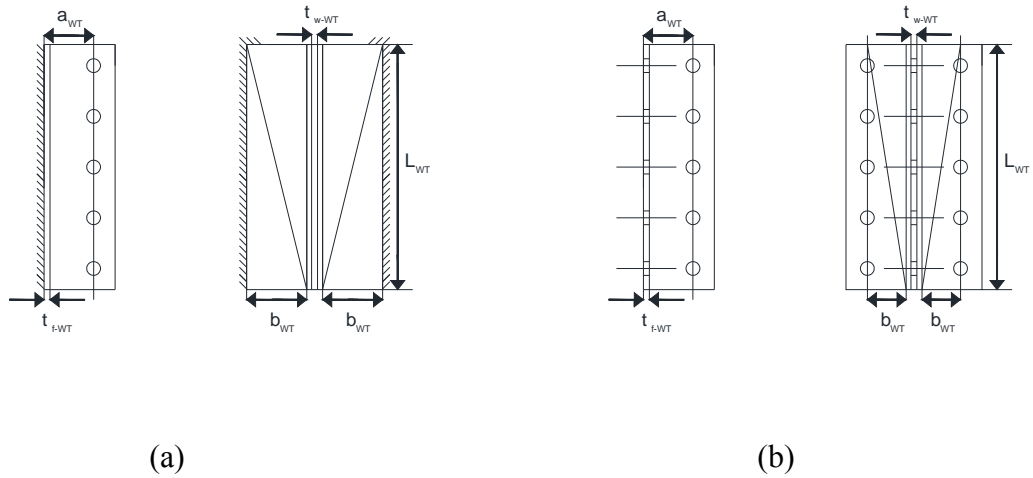


Figure 6.4: Yield lines in WT shear connection: (a) welded (b) bolted (Thornton 1996)

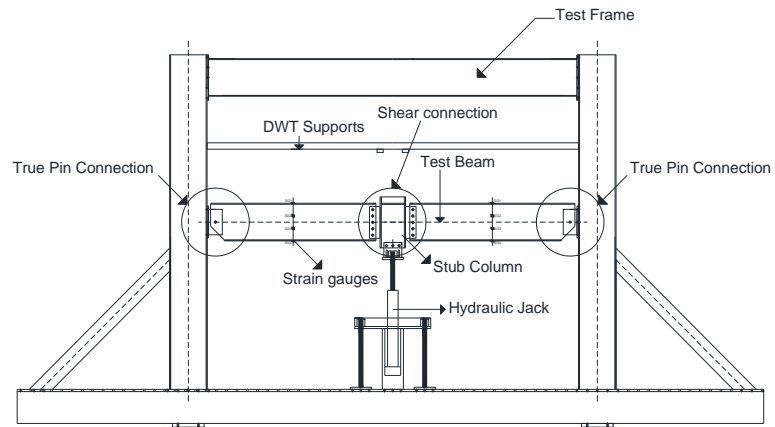
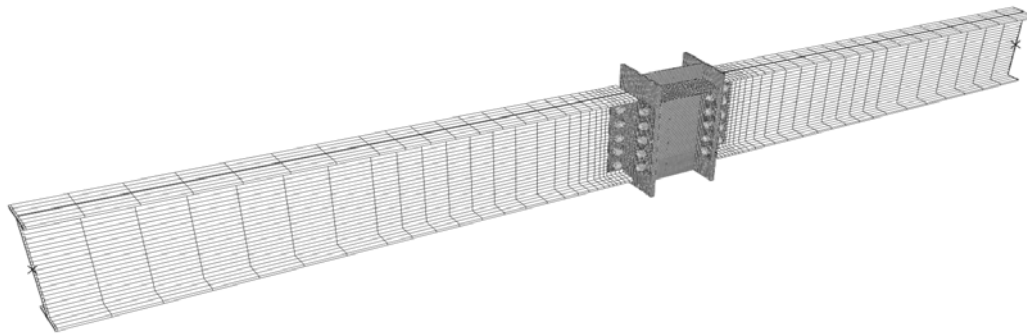
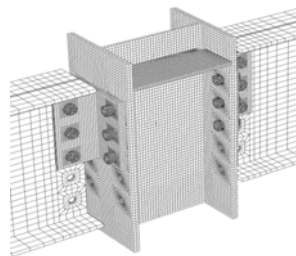


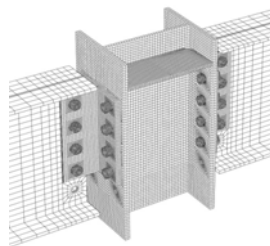
Figure 6.5: Test setup (Friedman 2009)



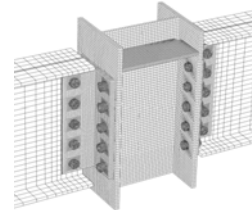
(a)



(b)



(c)

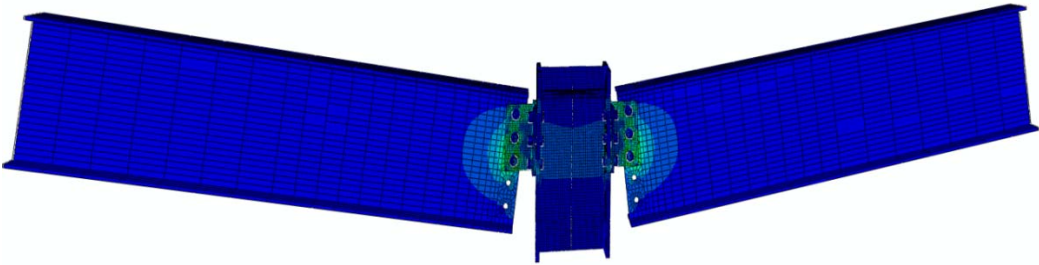


(d)

Figure 6.6: FE models of: (a) full connection assembly, (b) 3 bolt WT connection (3WT), (c) 4 bolt WT connection (4WT), (d) 5 bolt WT connection (5WT)



(a)



(b)

Figure 6.7: Deformed shape of the connection assembly: (a) experiment (b) finite element

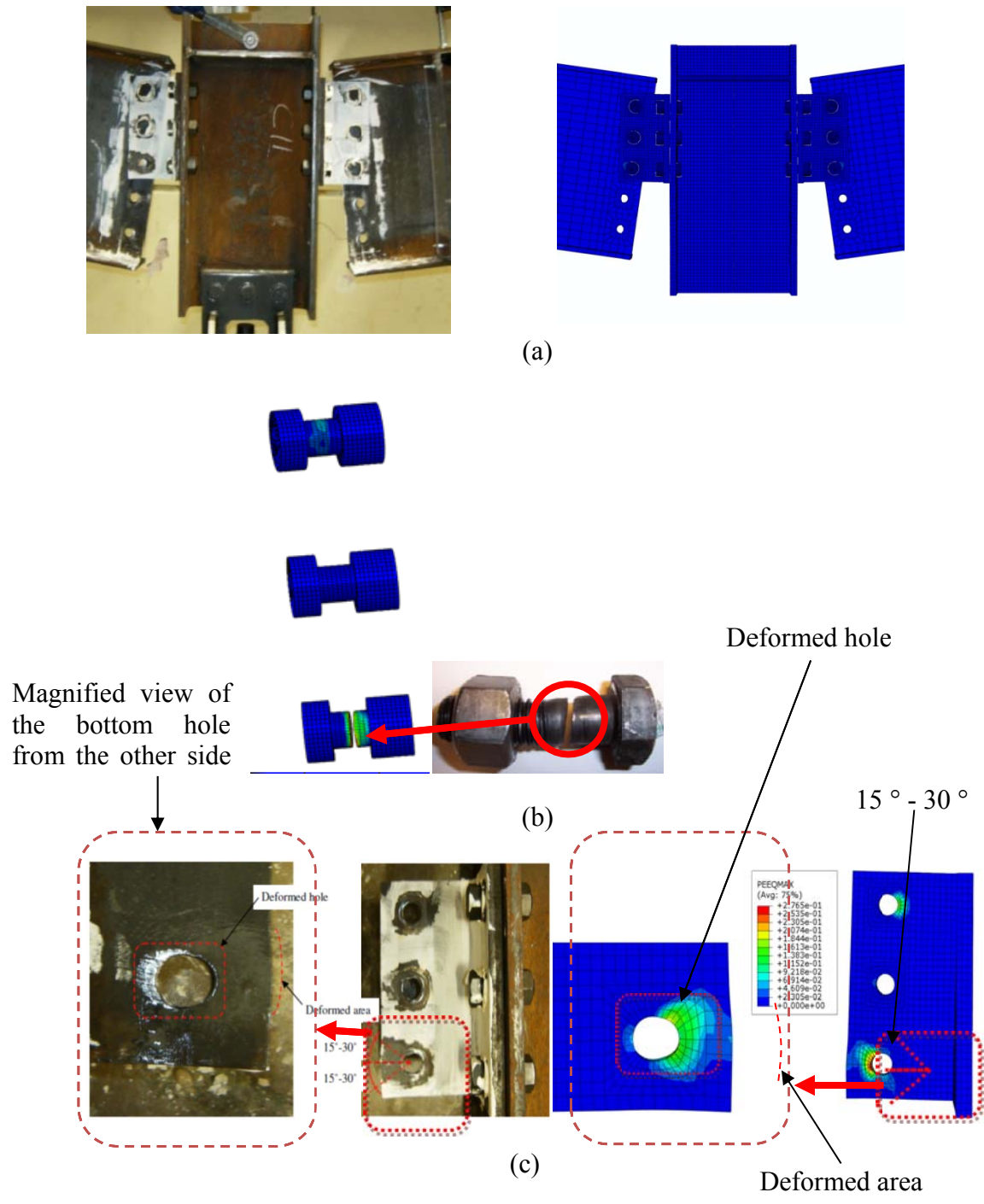


Figure 6.8: Failure of 3WT, experimental (Friedman 2009) and numerical results: (a) deformed shape (b) bolt rupture (c) bottom hole bearing deformation

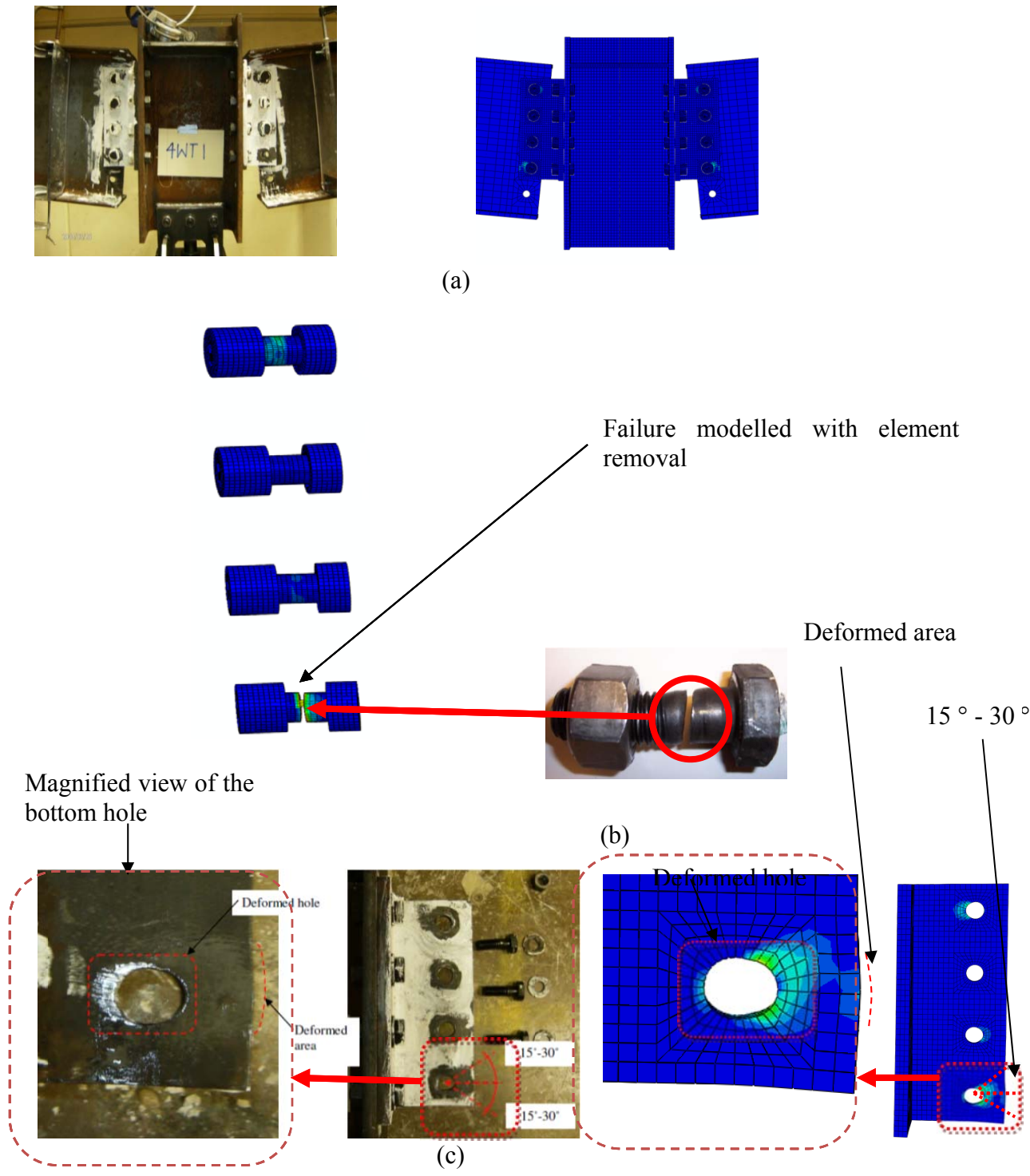
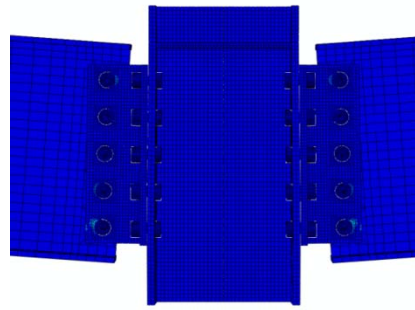


Figure 6.9: Failure of 4WT, experimental (Friedman 2009) and numerical results: (a) deformed shape (b) bolt rupture (c) bottom hole bearing deformation



(a)

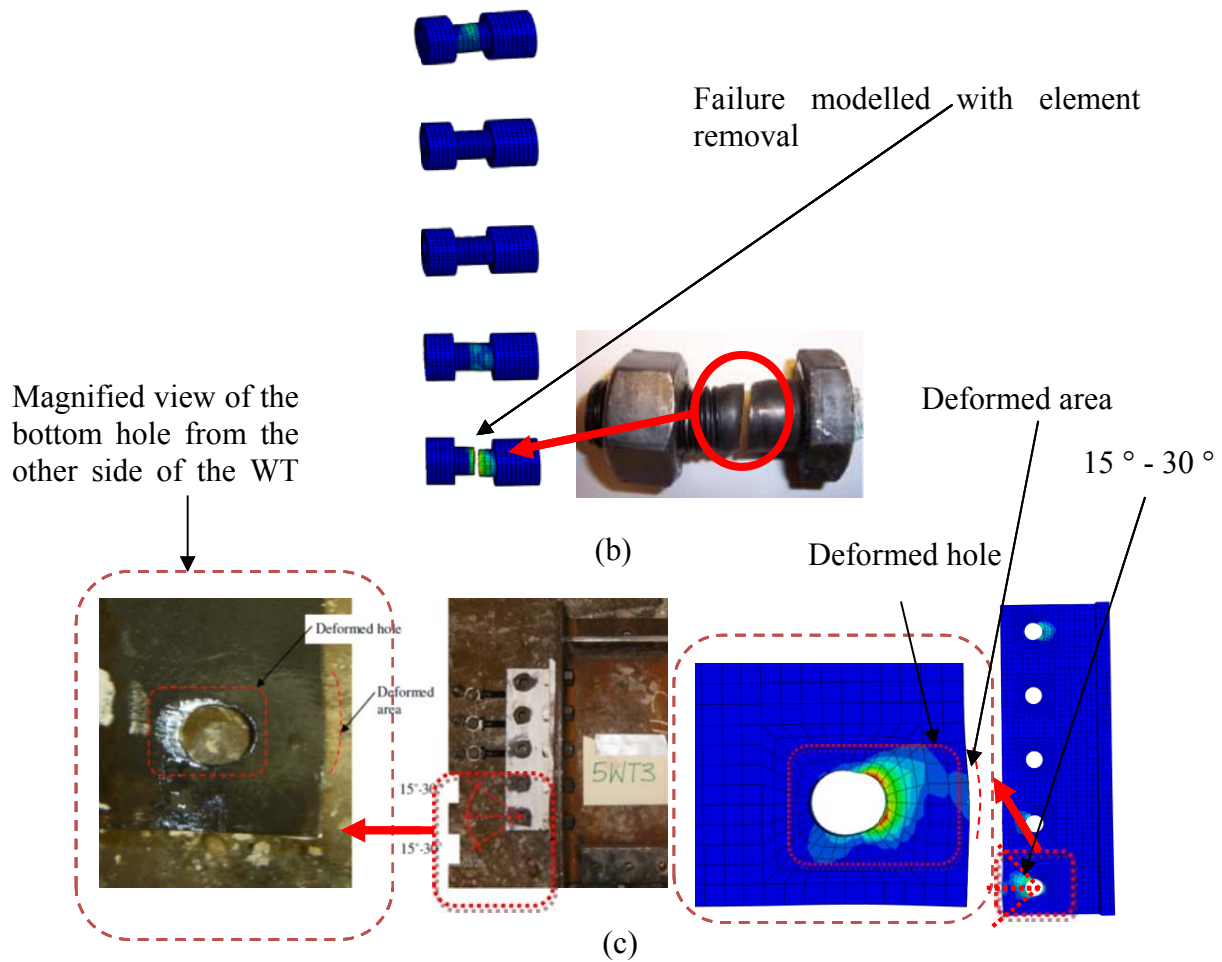


Figure 6.10: Failure of 5WT, experimental (Friedman 2009) and numerical results: (a) deformed shape (b) bolt rupture (c) bottom hole bearing deformation

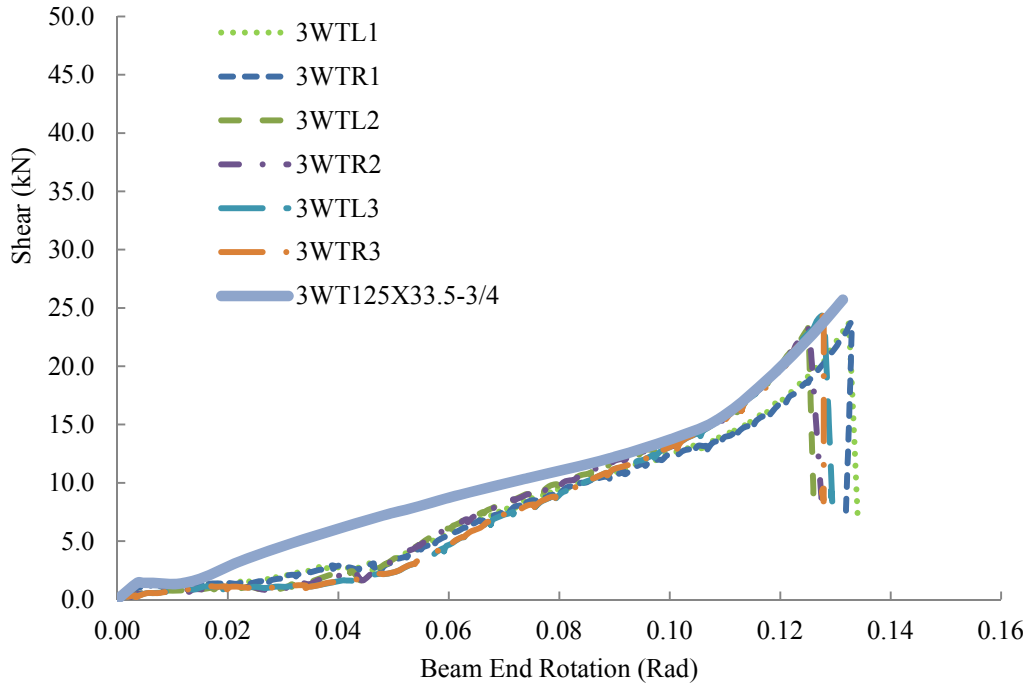


Figure 6.11: Comparison of numerical and experimental shear response of connection 3WT

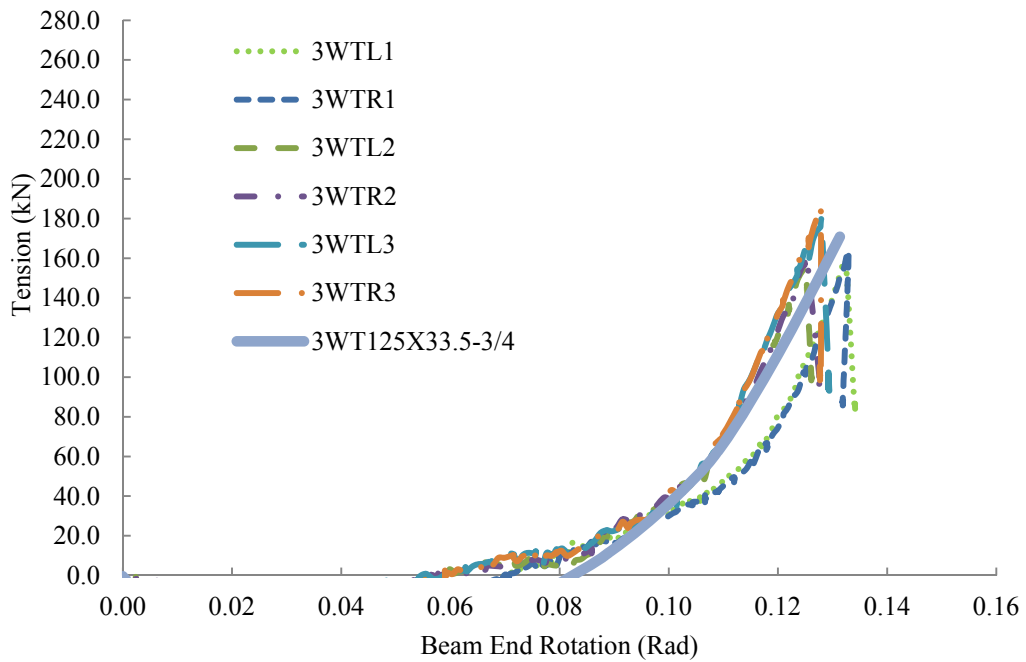


Figure 6.12: Comparison of numerical and experimental tensile response of connection 3WT

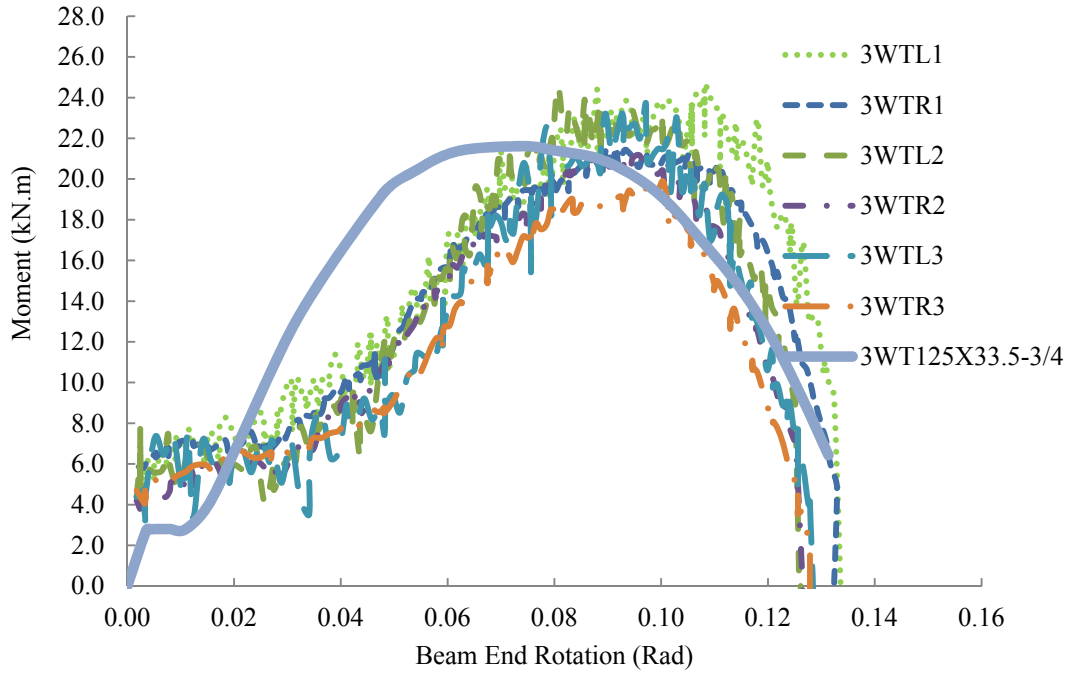


Figure 6.13: Comparison of numerical and experimental flexural response of connection 3WT

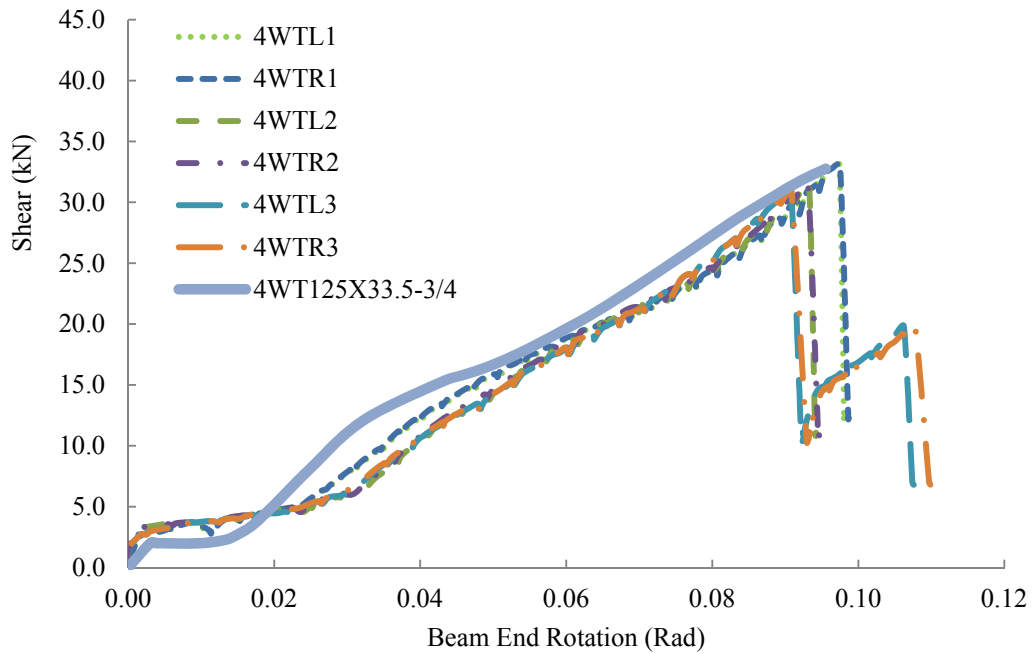


Figure 6.14: Comparison of numerical and experimental shear response of connection 4WT

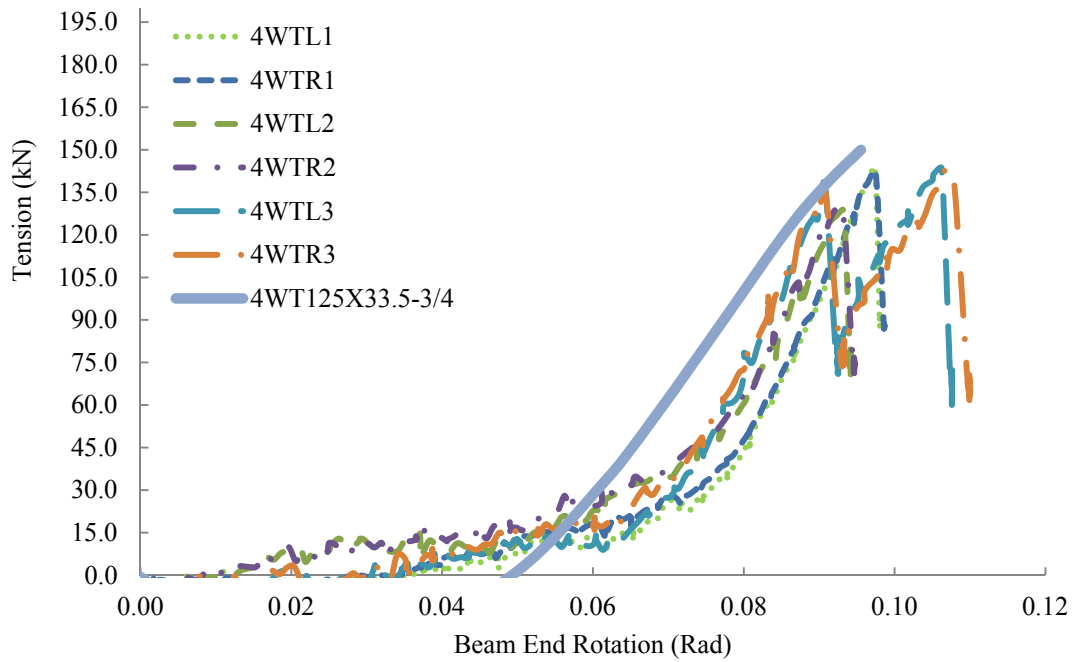


Figure 6.15: Comparison of numerical and experimental tensile response of connection 4WT

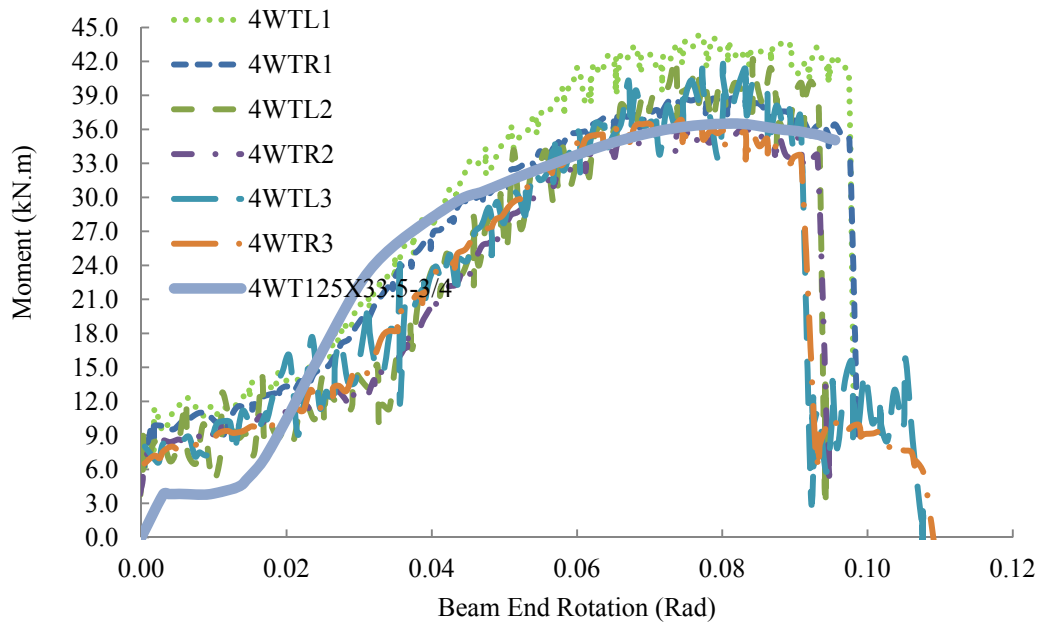


Figure 6.16: Comparison of numerical and experimental flexural response of connection 4WT

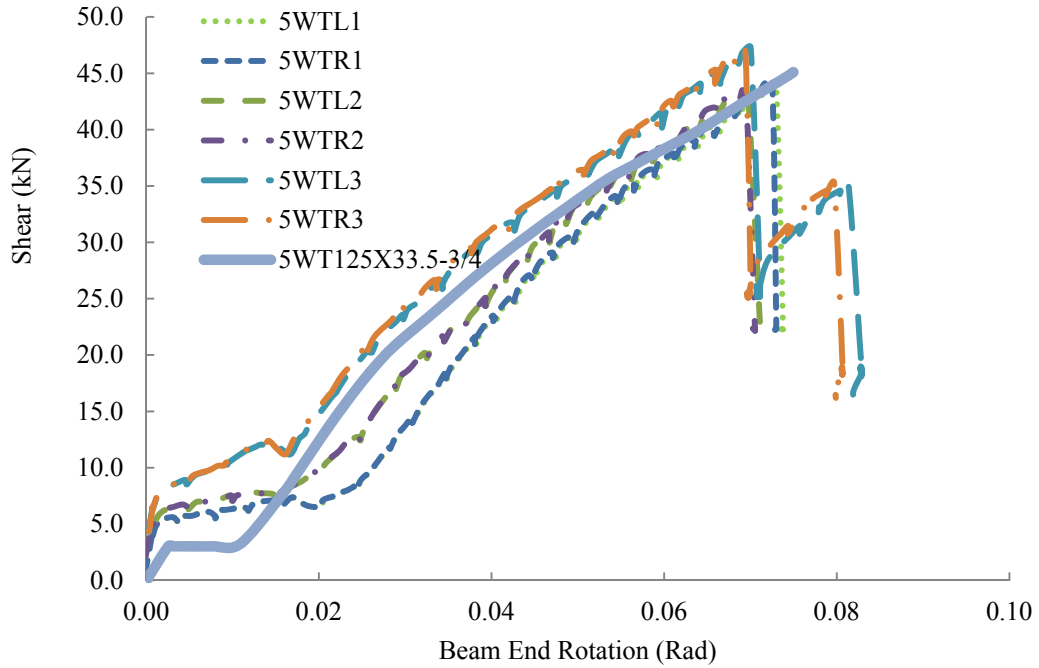


Figure 6.17: Comparison of numerical and experimental shear response of connection 5WT

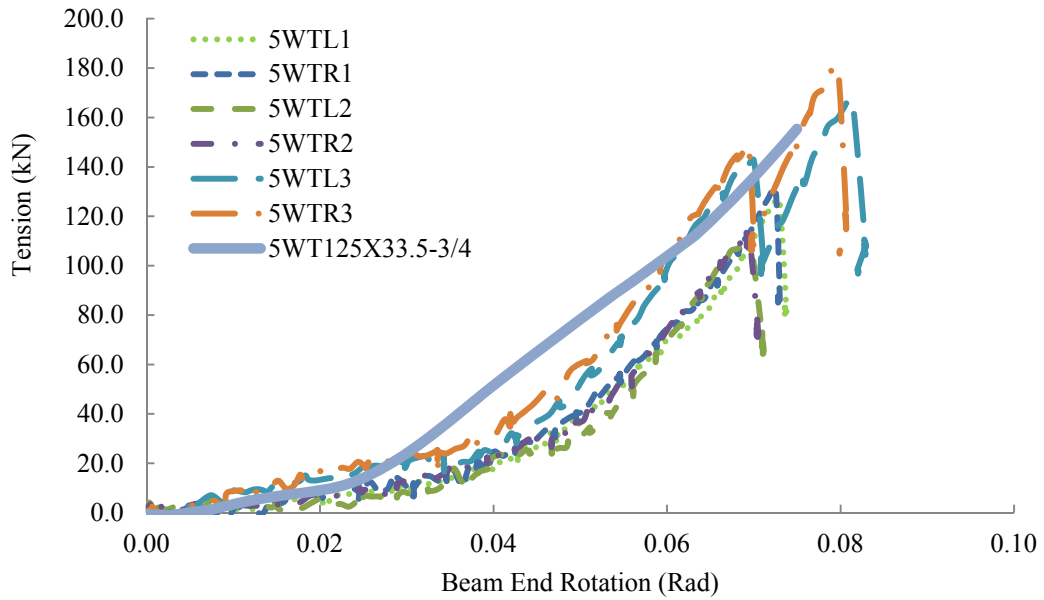


Figure 6.18: Comparison of numerical and experimental tensile response of connection 5WT

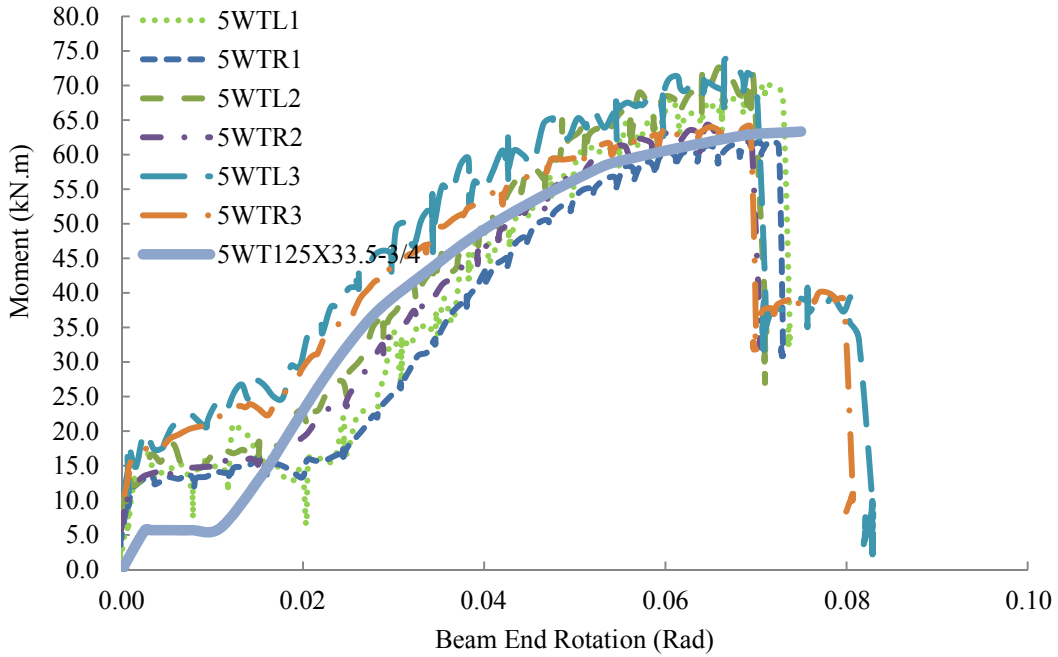


Figure 6.19: Comparison of numerical and experimental flexural response of connection 5WT

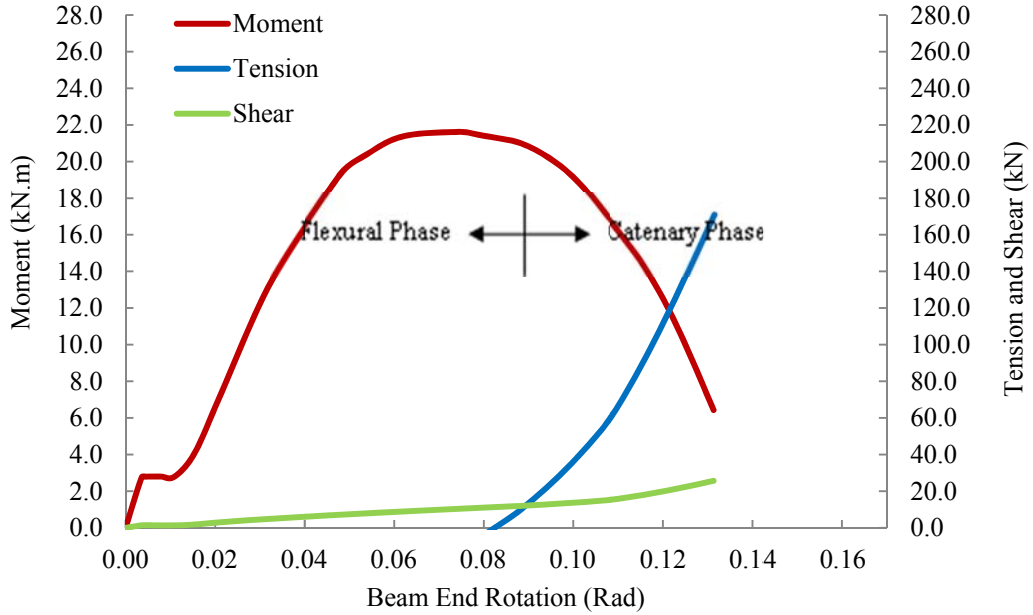


Figure 6.20: Bolt line forces versus beam end rotation – Specimen 3WT125X33.5-3/4

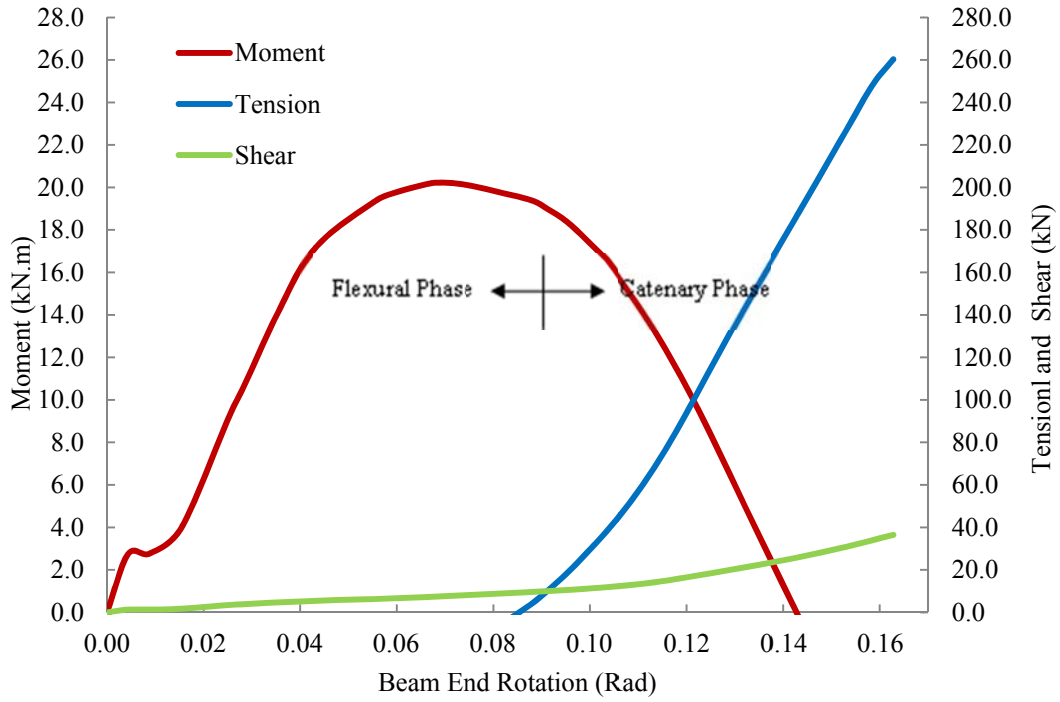


Figure 6.21: Bolt line forces versus beam end rotation – Specimen 3WT100X26-3/4

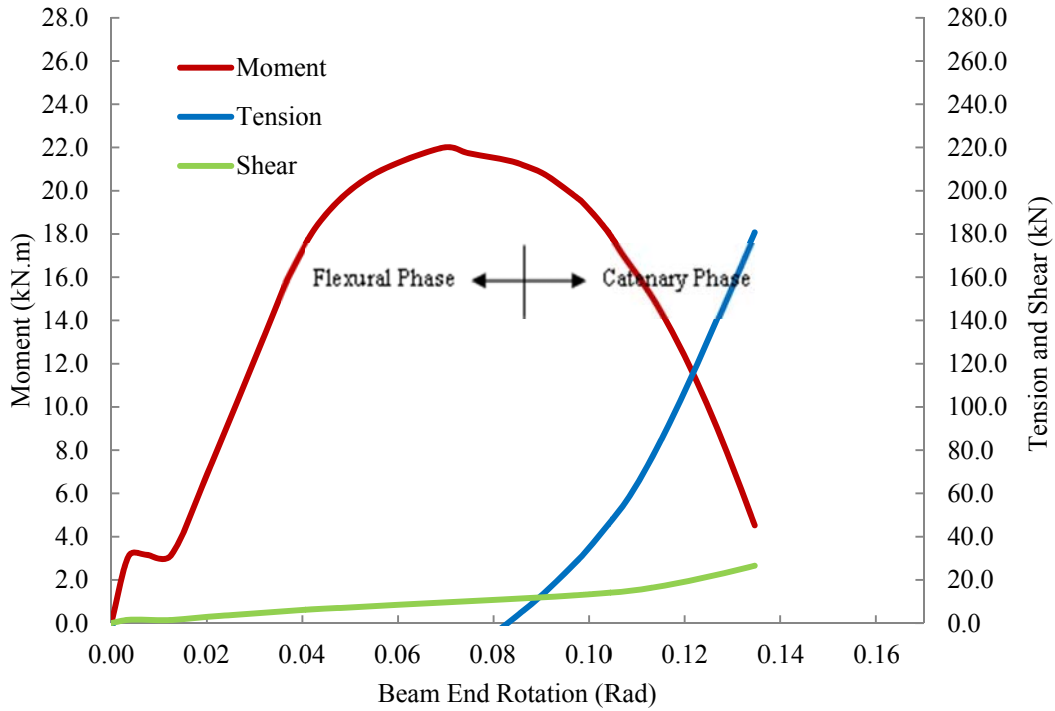


Figure 6.22: Bolt line forces versus beam end rotation – Specimen 3WT155X33.5-3/4

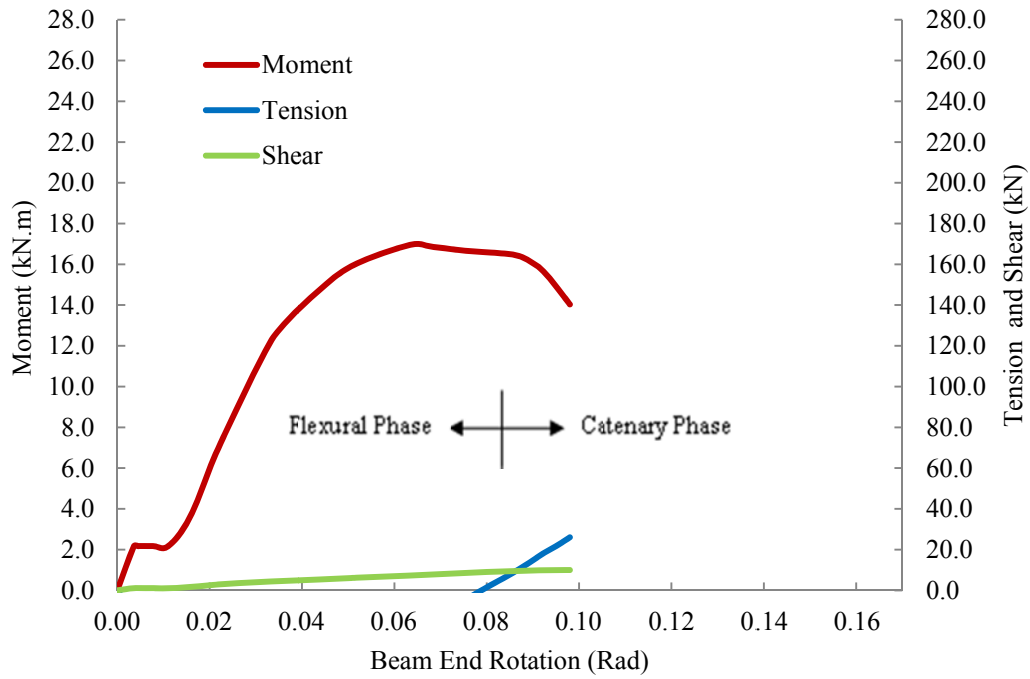


Figure 6.23: Bolt line forces versus beam end rotation – Specimen 3WT125X33.5-5/8

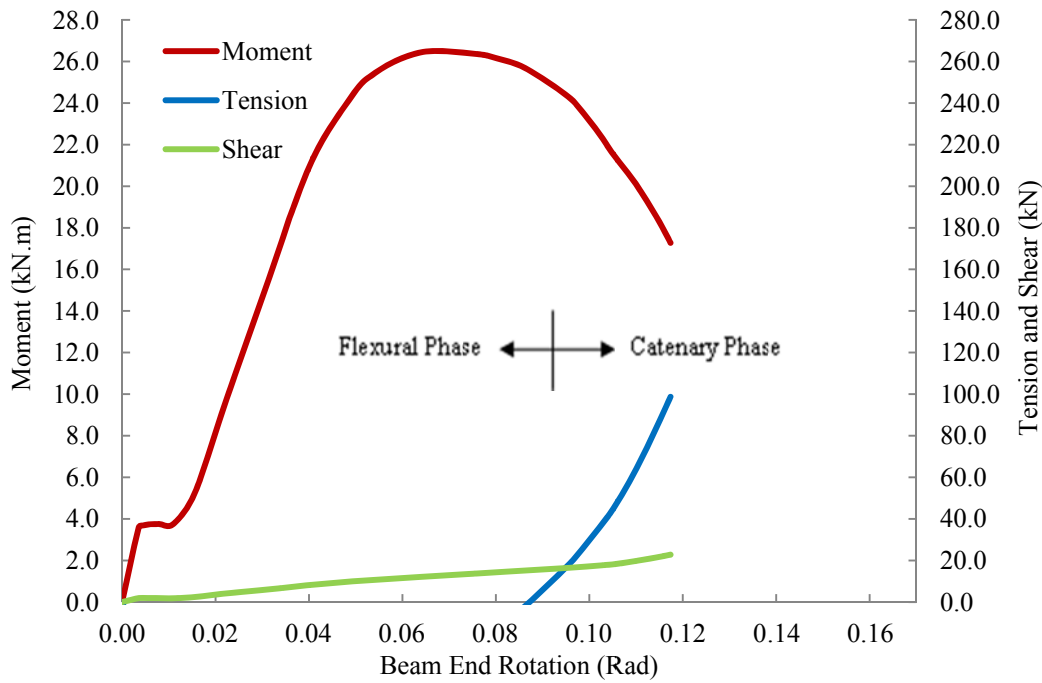


Figure 6.24: Bolt line forces versus beam end rotation – Specimen 3WT125X33.5-7/8

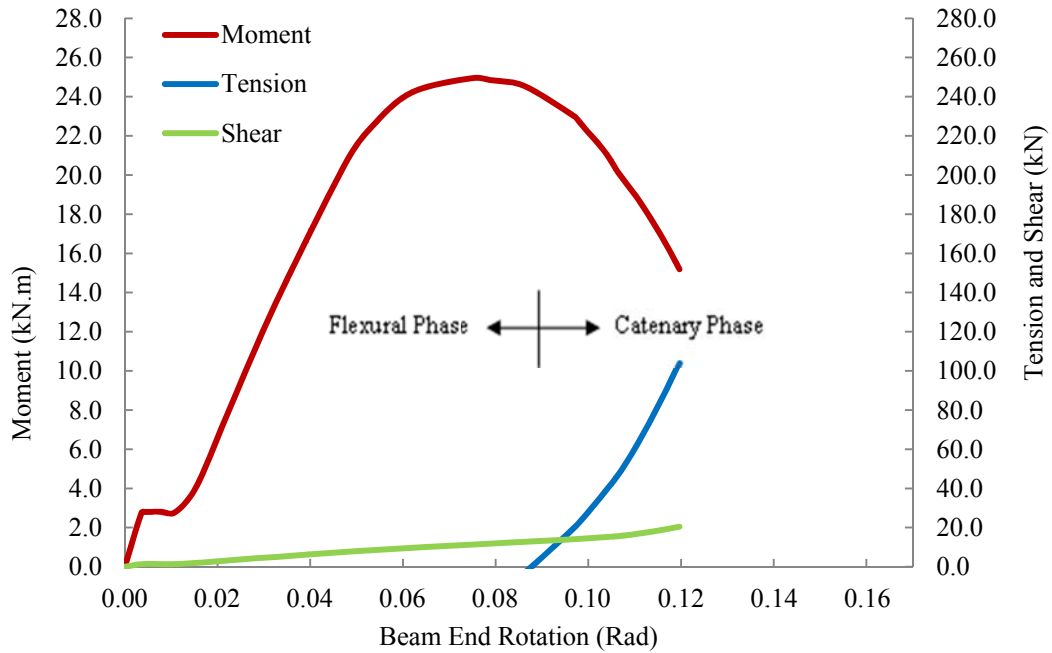


Figure 6.25: Bolt line forces versus beam end rotation – Specimen 3WT125X33.5-3/4-A490

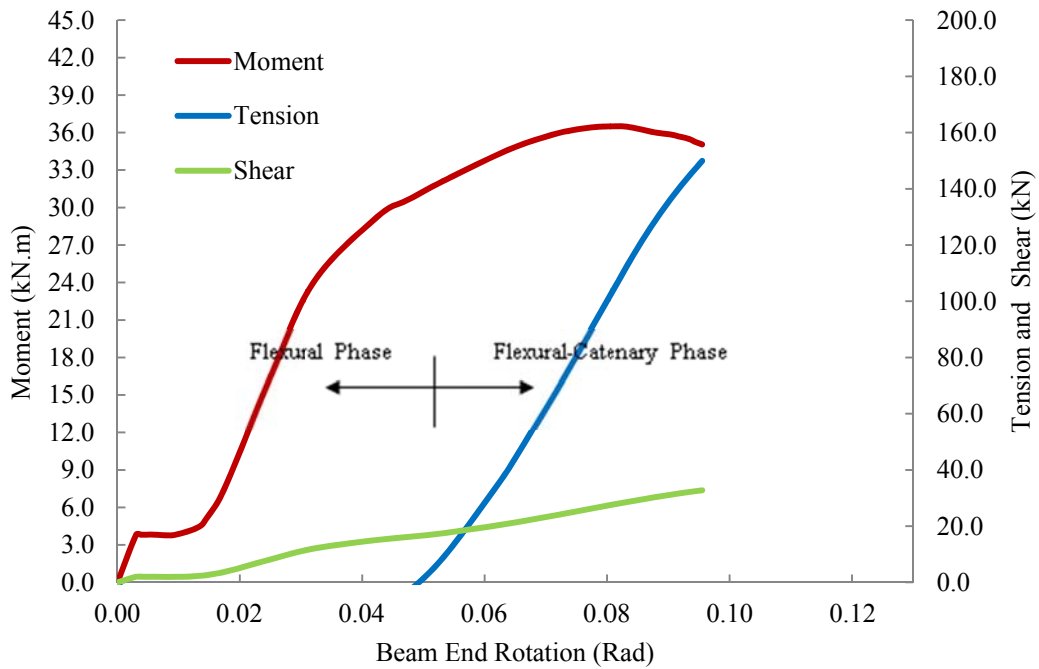


Figure 6.26: Bolt line forces versus beam end rotation – Specimen 4WT125X33.5-3/4

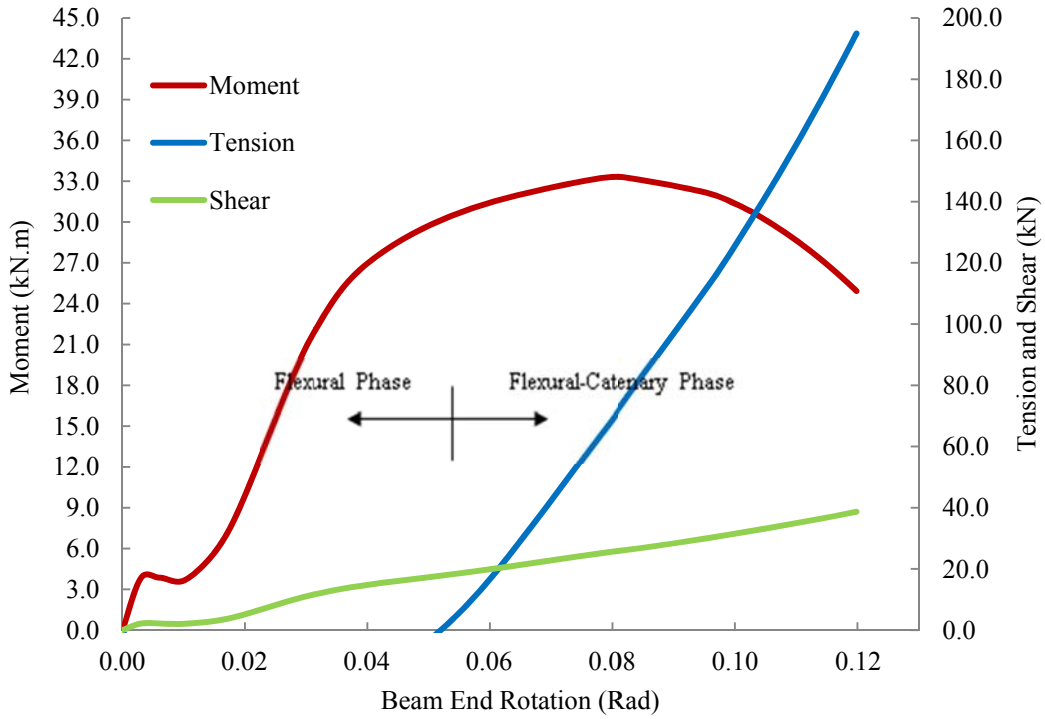


Figure 6.27: Bolt line forces versus beam end rotation – Specimen 4WT100X26-3/4

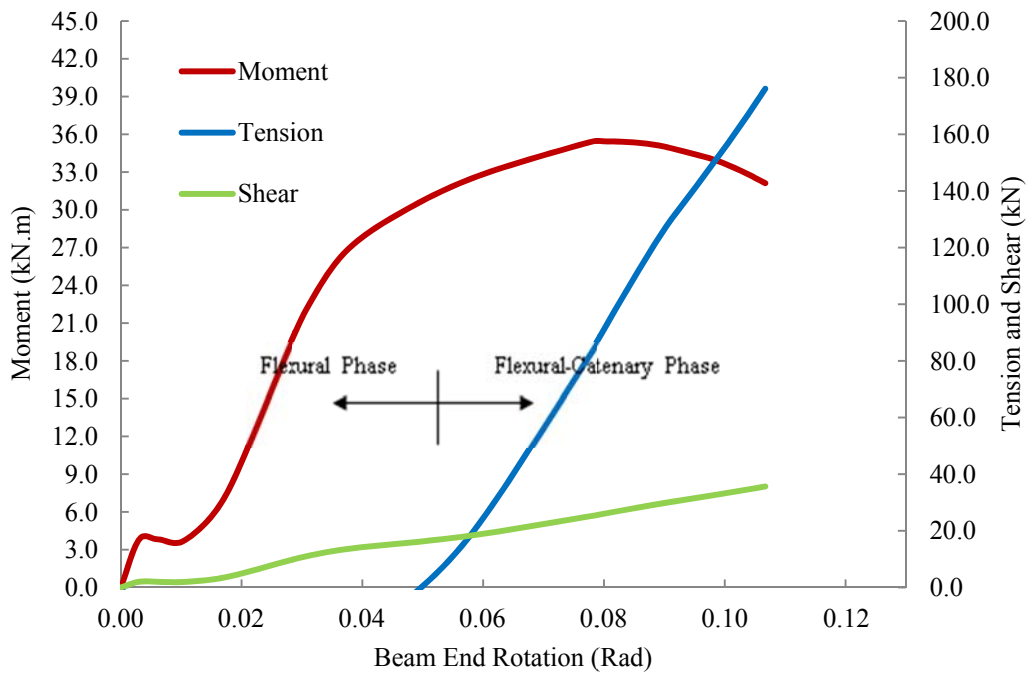


Figure 6.28: Bolt line forces versus beam end rotation – Specimen 4WT155X33.5-3/4

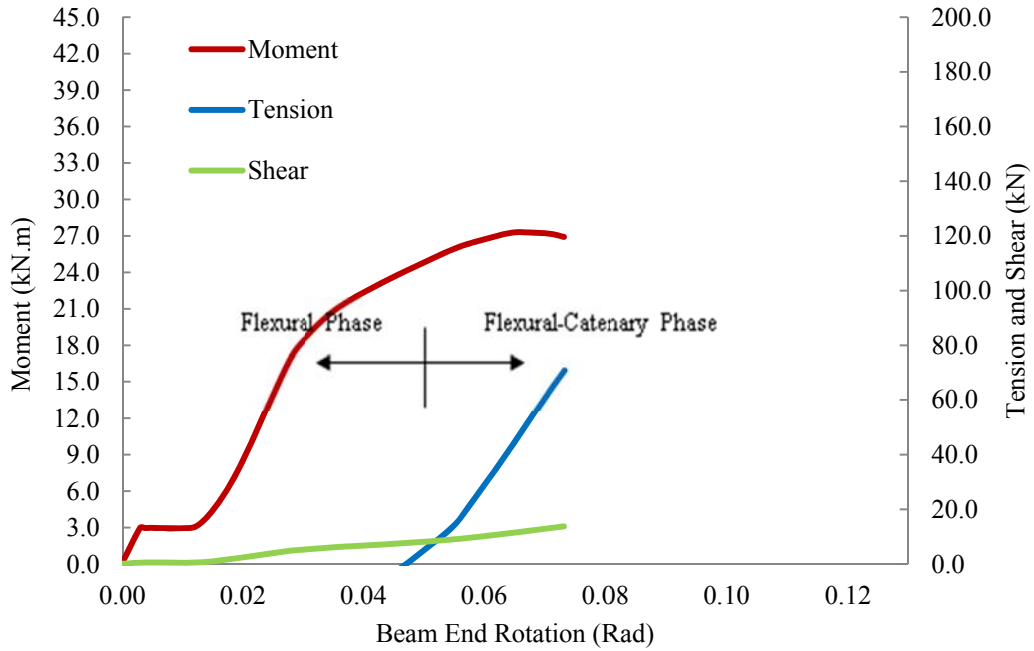


Figure 6.29: Bolt line forces versus beam end rotation – Specimen 4WT125X33.5-5/8

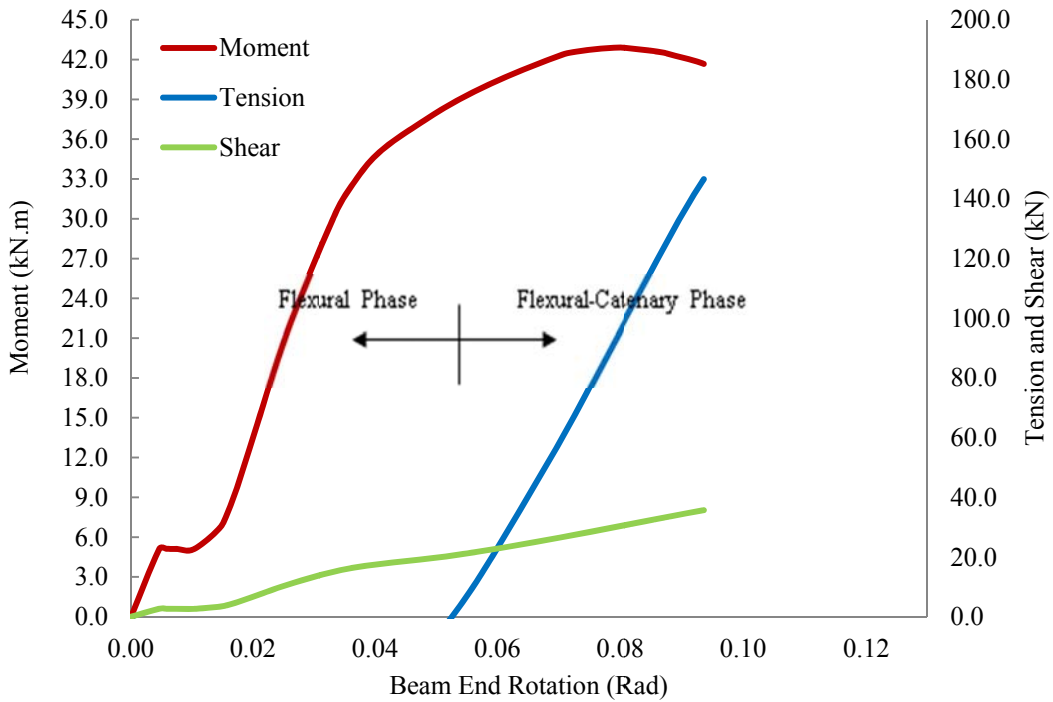


Figure 6.30: Bolt line forces versus beam end rotation – Specimen 4WT125X33.5-7/8

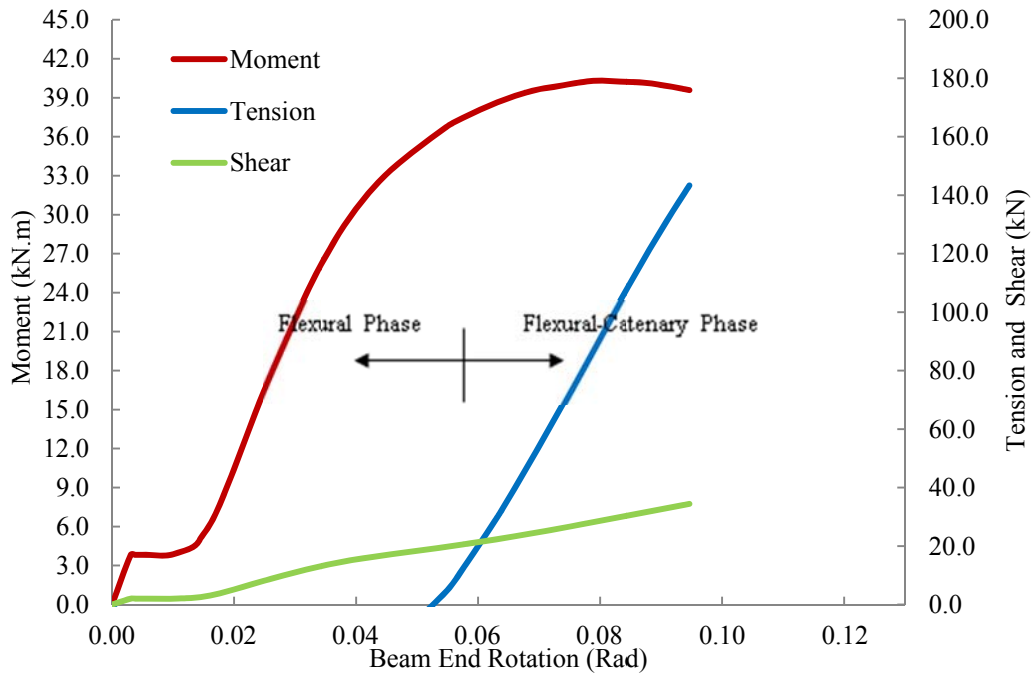


Figure 6.31: Bolt line forces versus beam end rotation – Specimen 4WT125X33.5-3/4-A490

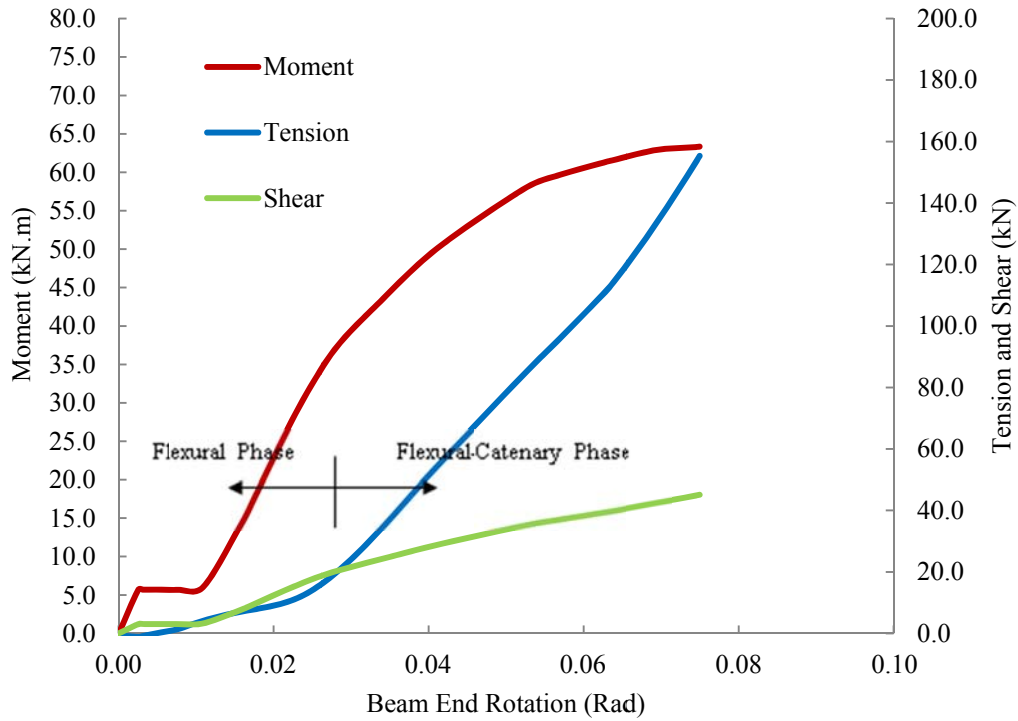


Figure 6.32: Bolt line forces versus beam end rotation – Specimen 5WT125X33.5-3/4

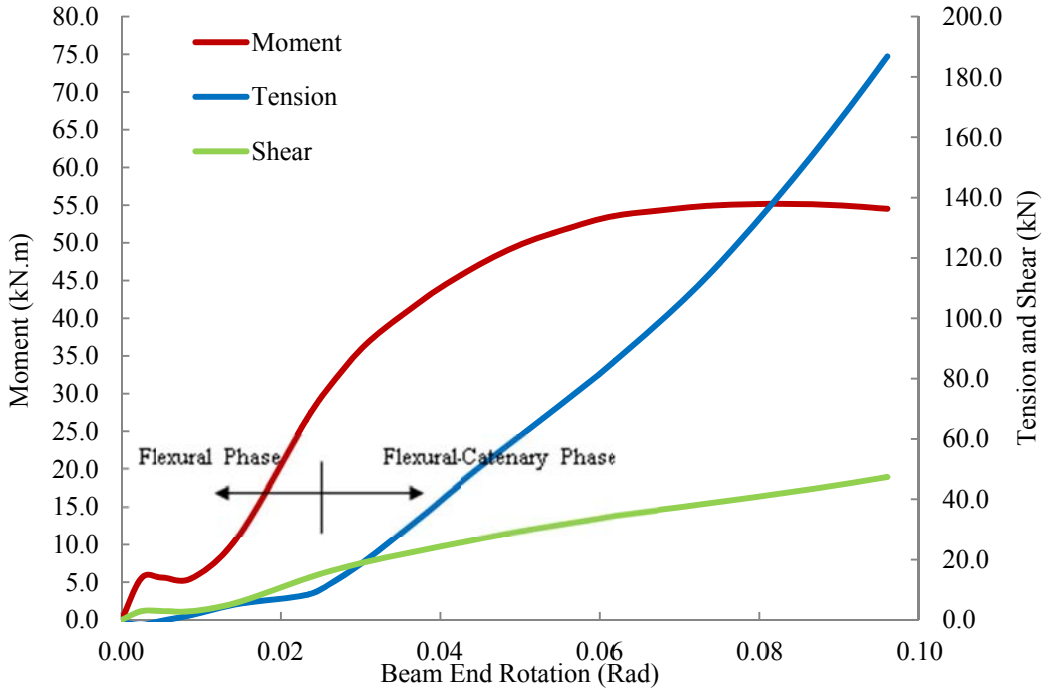


Figure 6.33: Bolt line forces versus beam end rotation – Specimen 5WT100X26-3/4

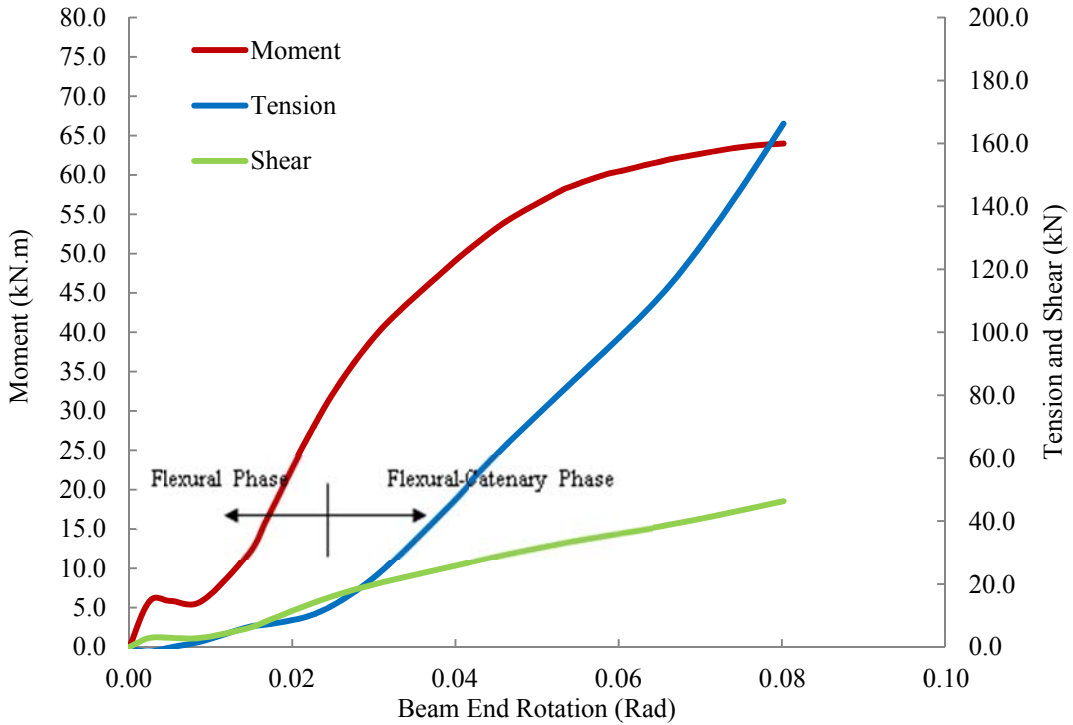


Figure 6.34: Bolt line forces versus beam end rotation – Specimen 5WT155X33.5-3/4

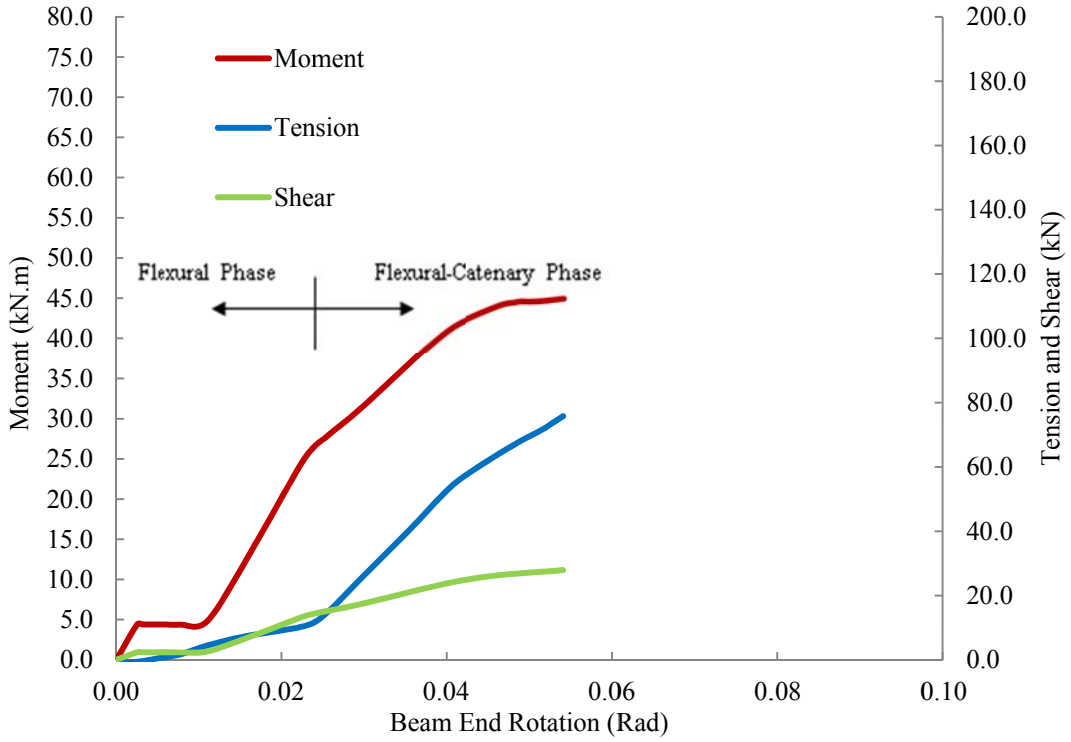


Figure 6.35: Bolt line forces versus beam end rotation – Specimen 5WT125X33.5-5/8

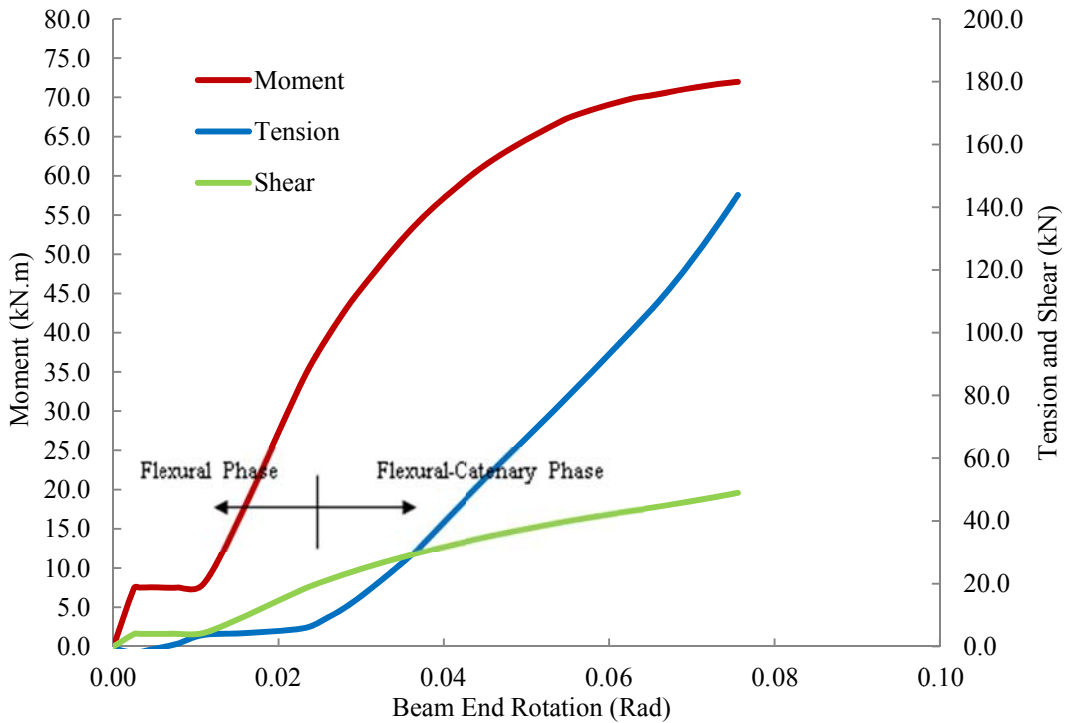


Figure 6.36: Bolt line forces versus beam end rotation – Specimen 5WT125X33.5-7/8

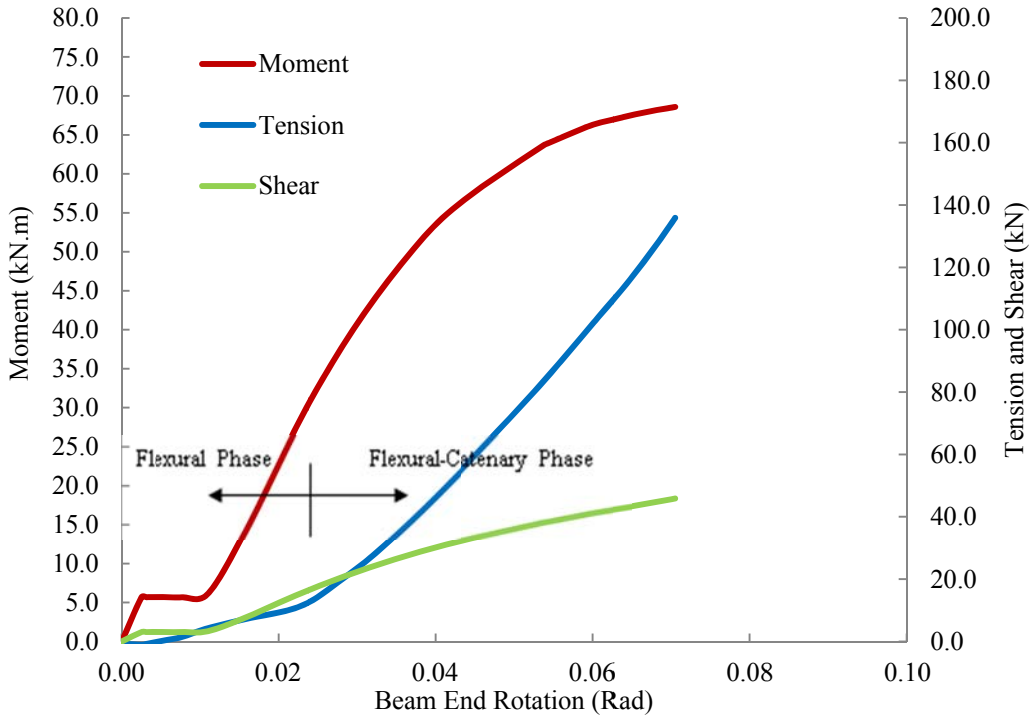


Figure 6.37: Bolt line forces versus beam end rotation – Specimen 5WT125X33.5-3/4-A490

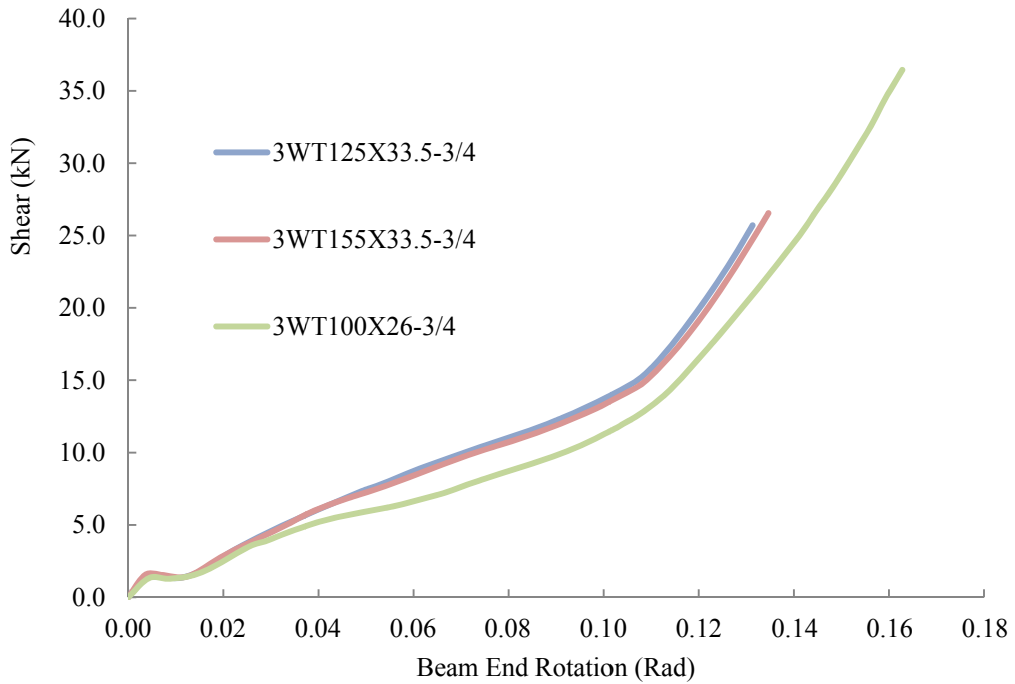


Figure 6.38: Comparison of shear response of 3WT connections with different WT sections

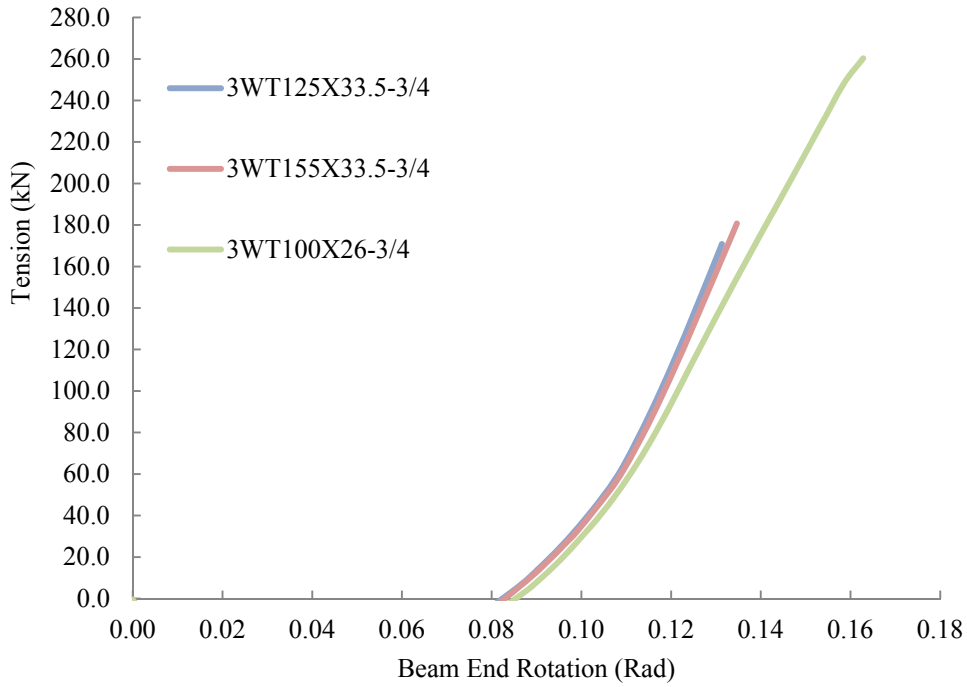


Figure 6.39: Comparison of tensile response of 3WT connections with different WT sections

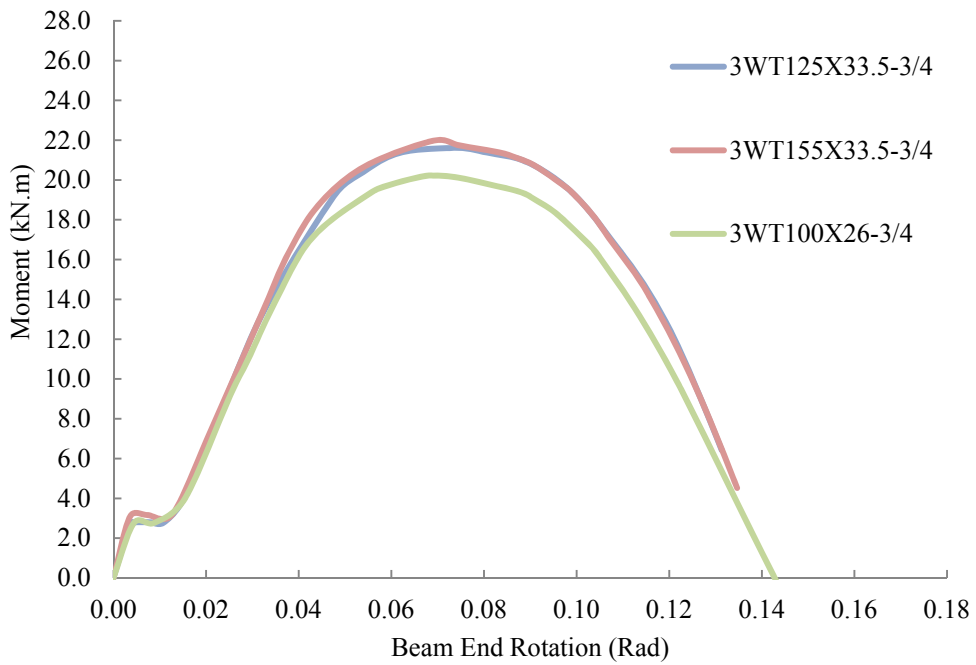


Figure 6.40: Comparison of flexural response of 3WT connections with different WT sections

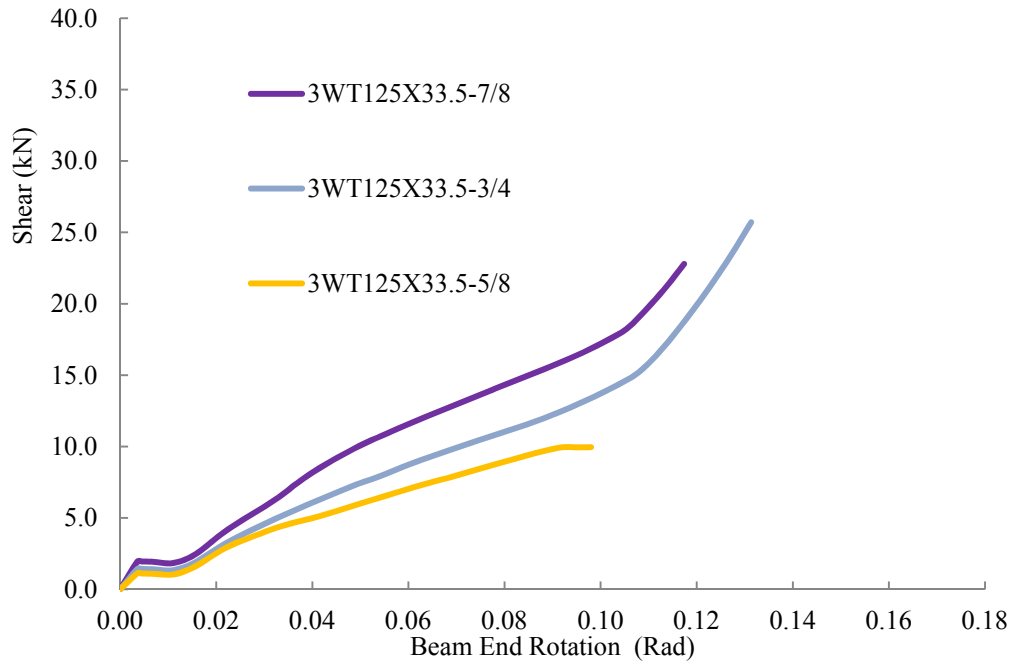


Figure 6.41: Comparison of shear response of 3WT connections with different bolt sizes

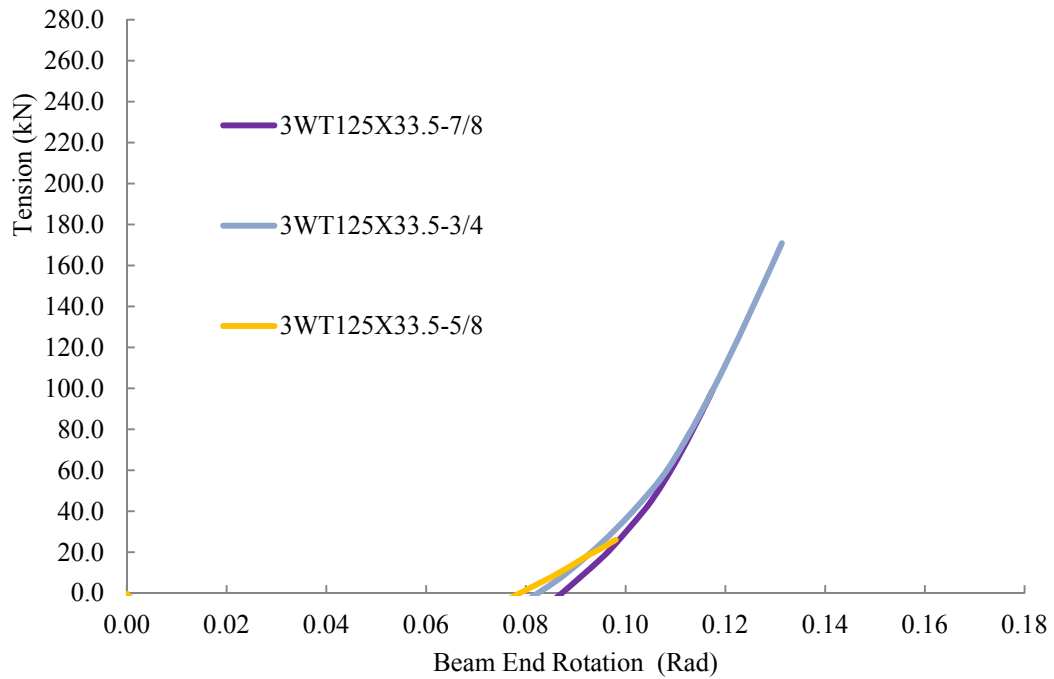


Figure 6.42: Comparison of tensile response of 3WT connections with different bolt sizes

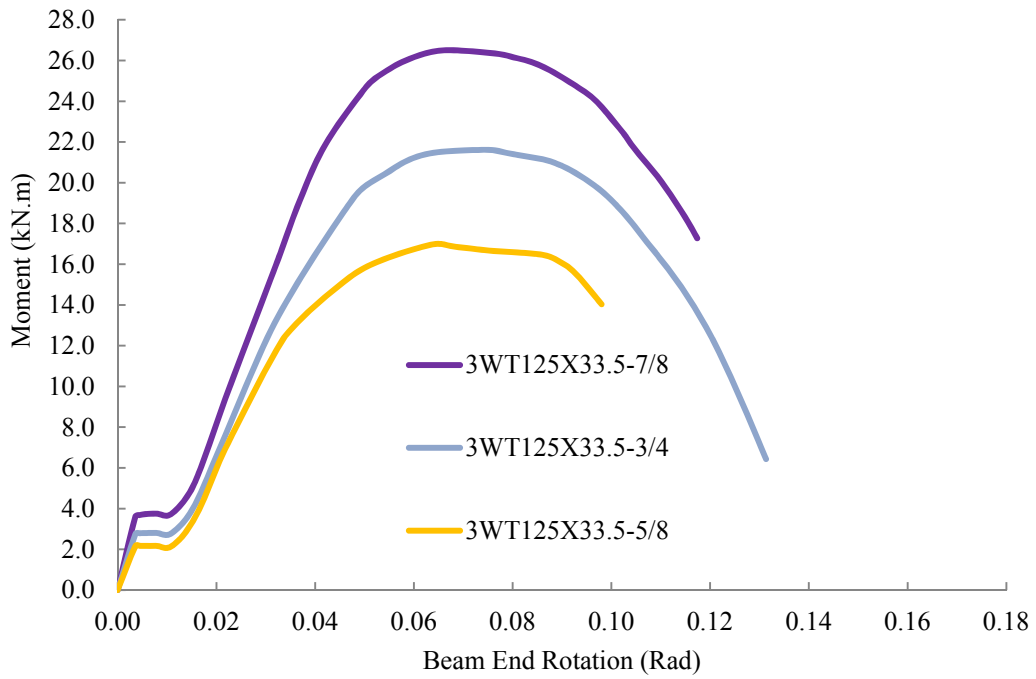


Figure 6.43: Comparison of flexural response of 3WT connections with different bolt sizes

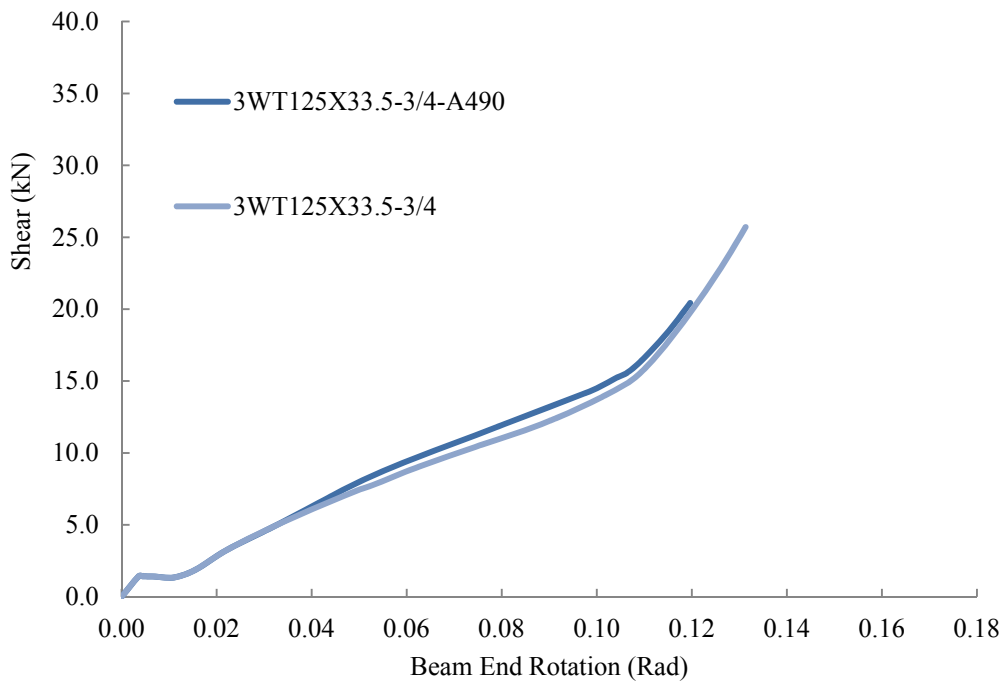


Figure 6.44: Comparison of shear response of 3WT connections with different bolt types

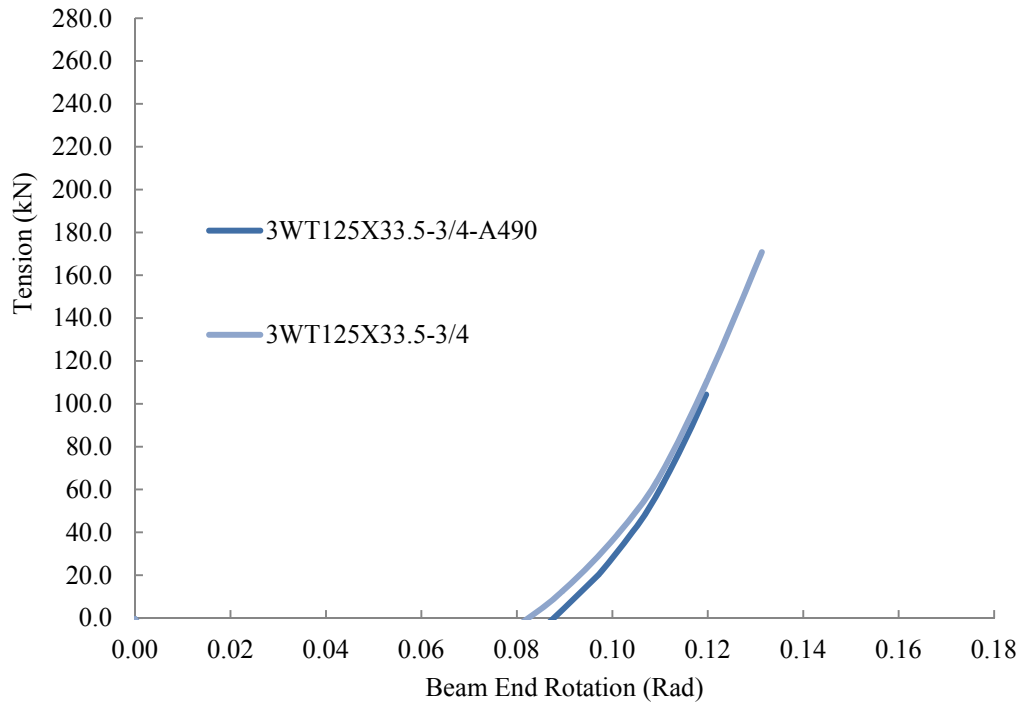


Figure 6.45: Comparison of tensile response of 3WT connections with different bolt types

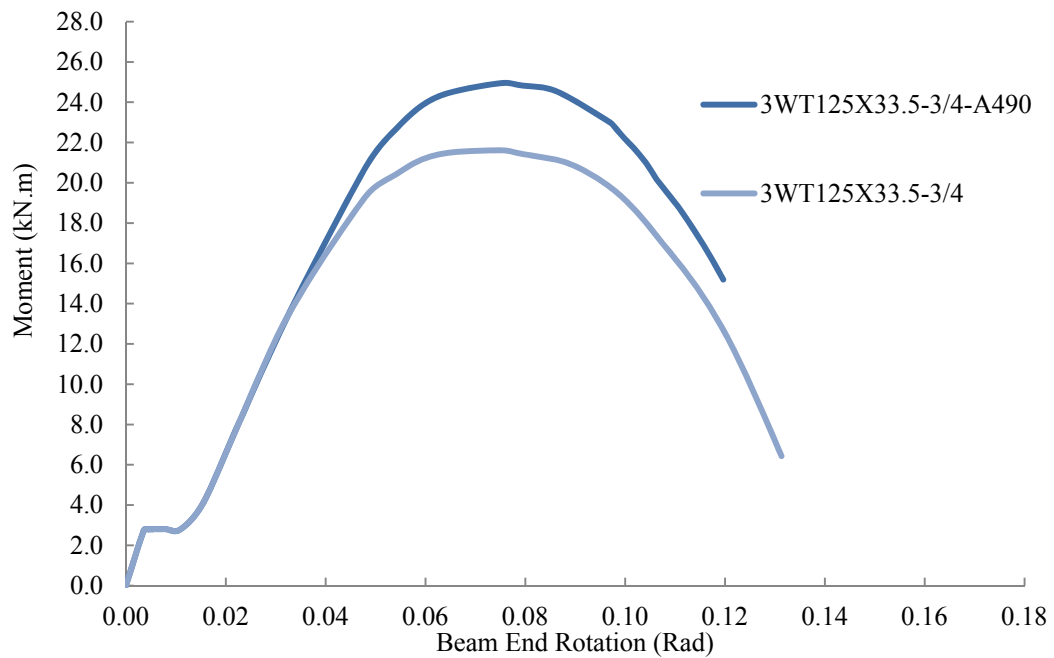


Figure 6.46: Comparison of flexural response of 3WT connections with different bolt types

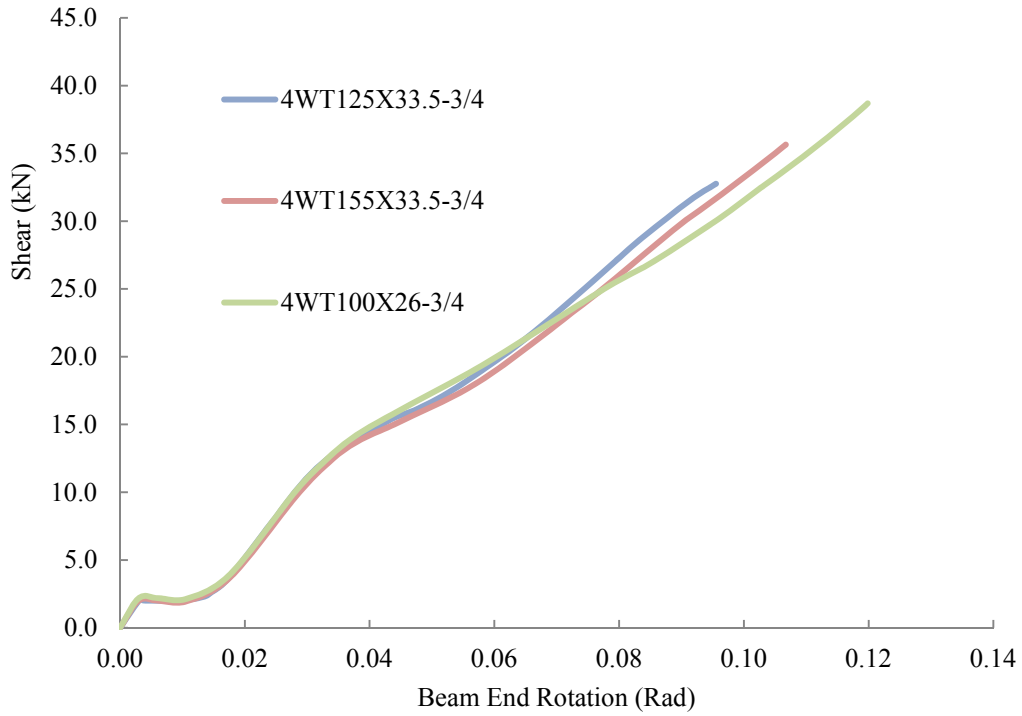


Figure 6.47: Comparison of shear response of 4WT connections with different WT sections

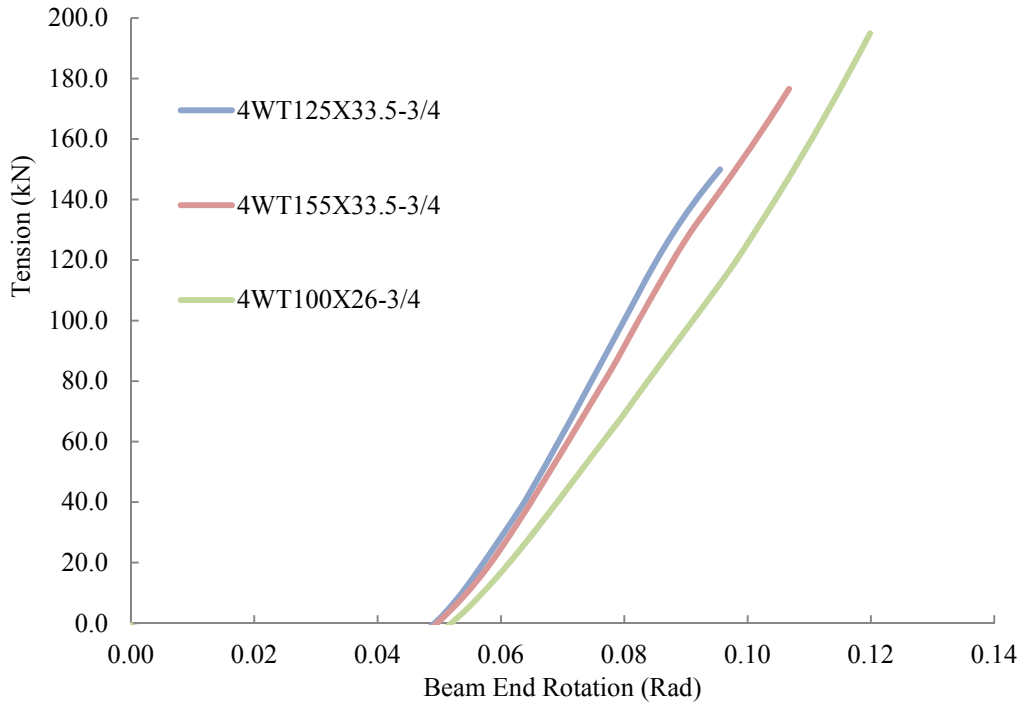


Figure 6.48: Comparison of tensile response of 4WT connections with different WT sections

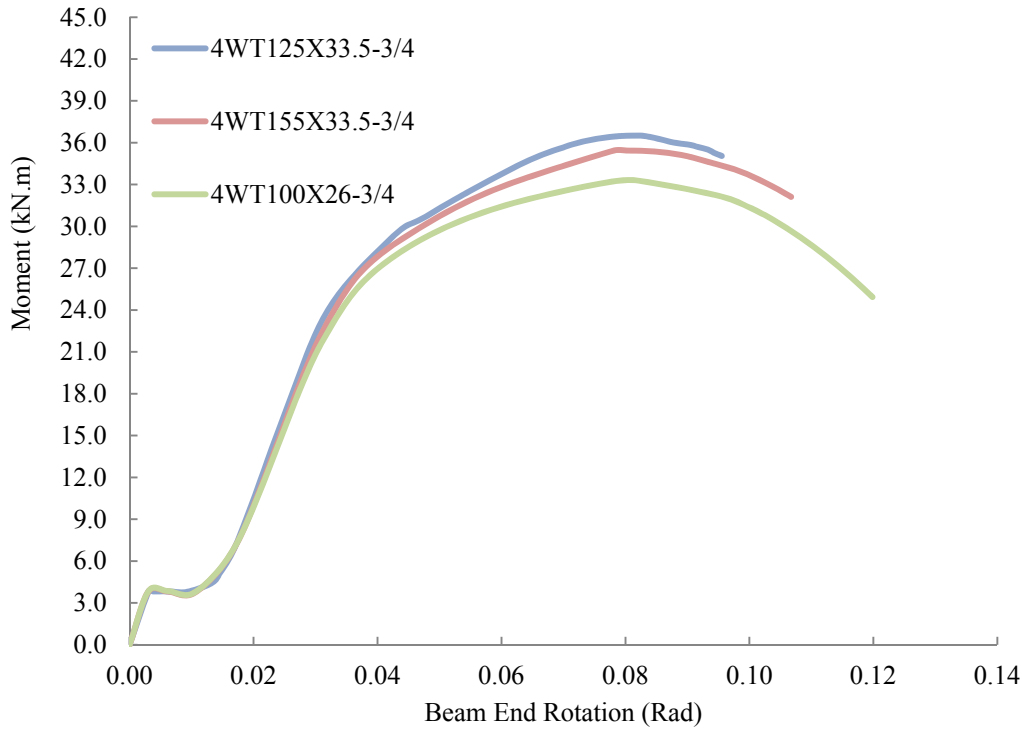


Figure 6.49: Comparison of flexural response of 4WT connections with different WT sections

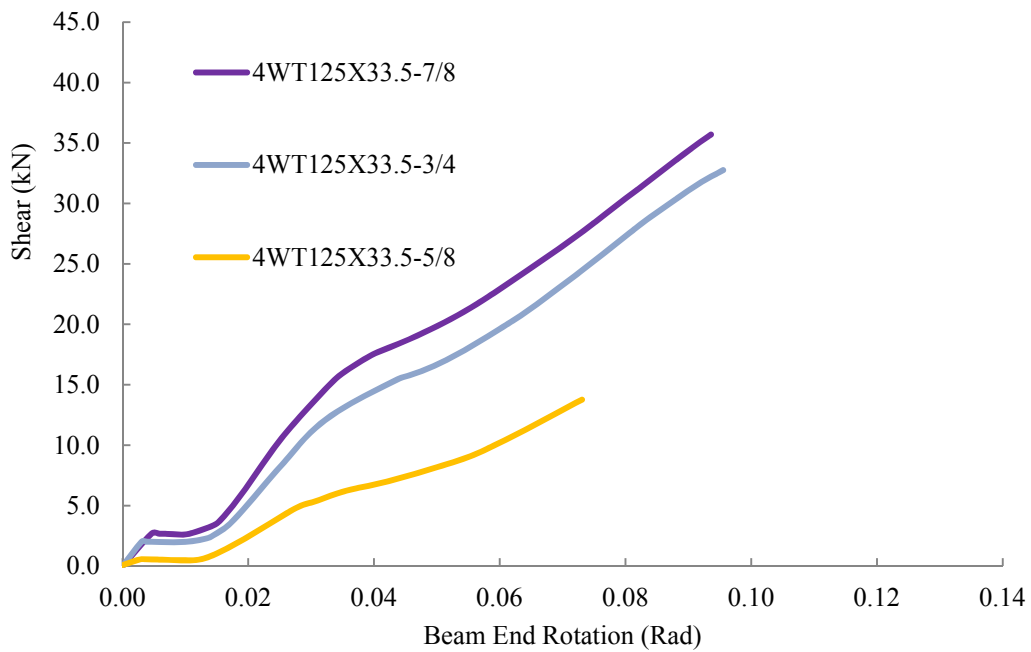


Figure 6.50: Comparison of shear response of 4WT connections with different bolt sizes

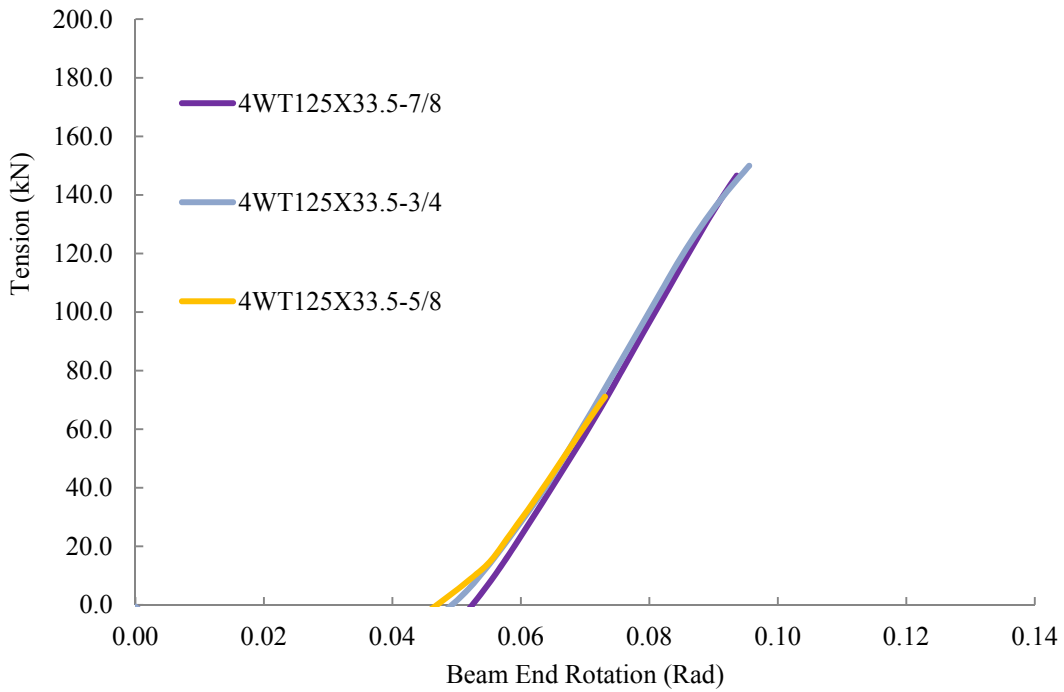


Figure 6.51: Comparison of tensile response of 4WT connections with different bolt sizes

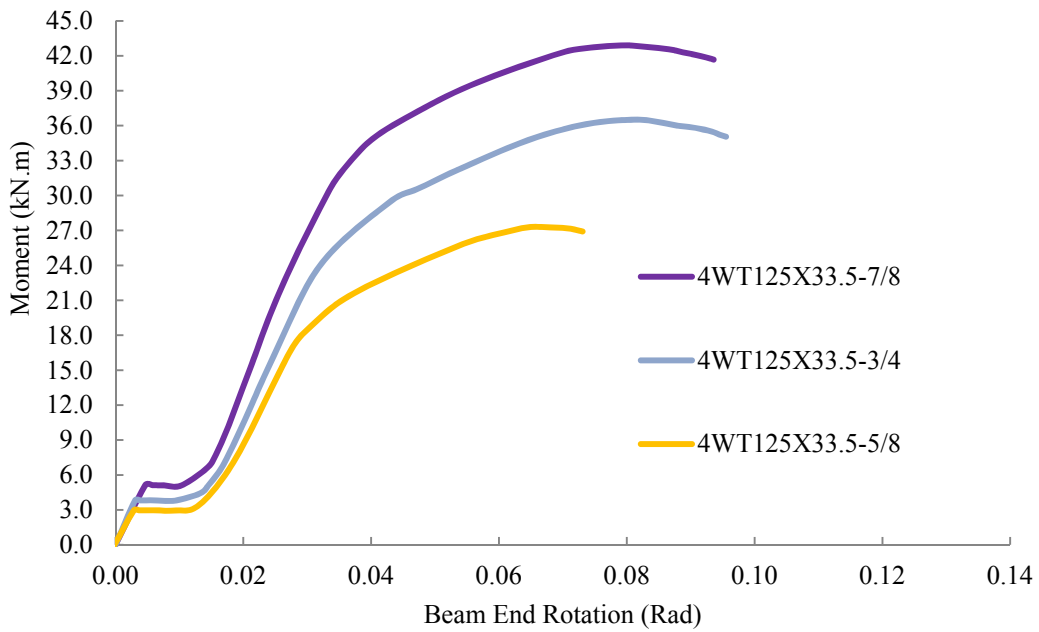


Figure 6.52: Comparison of flexural response of 4WT connections with different bolt sizes

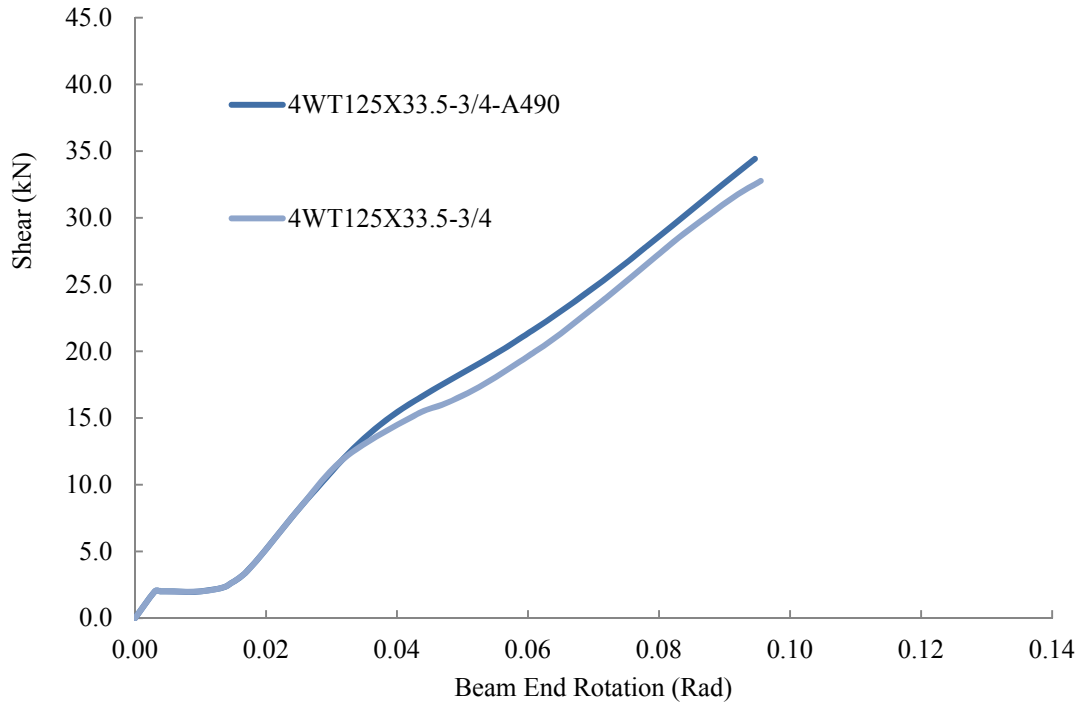


Figure 6.53: Comparison of shear response of 4WT connections with different bolt types

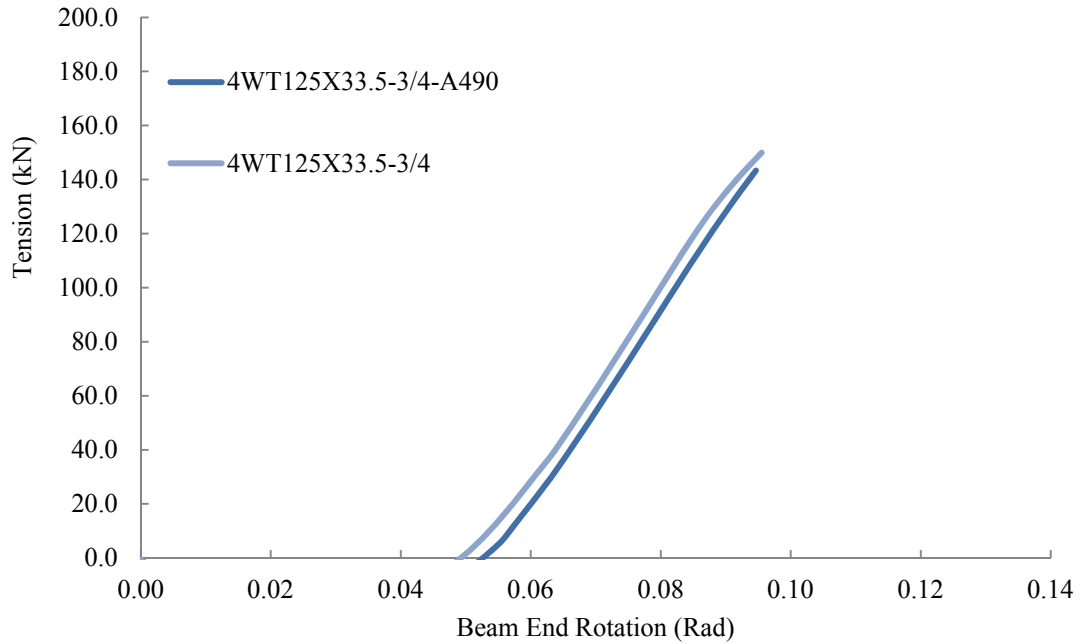


Figure 6.54: Comparison of tensile response of 4WT connections with different bolt types

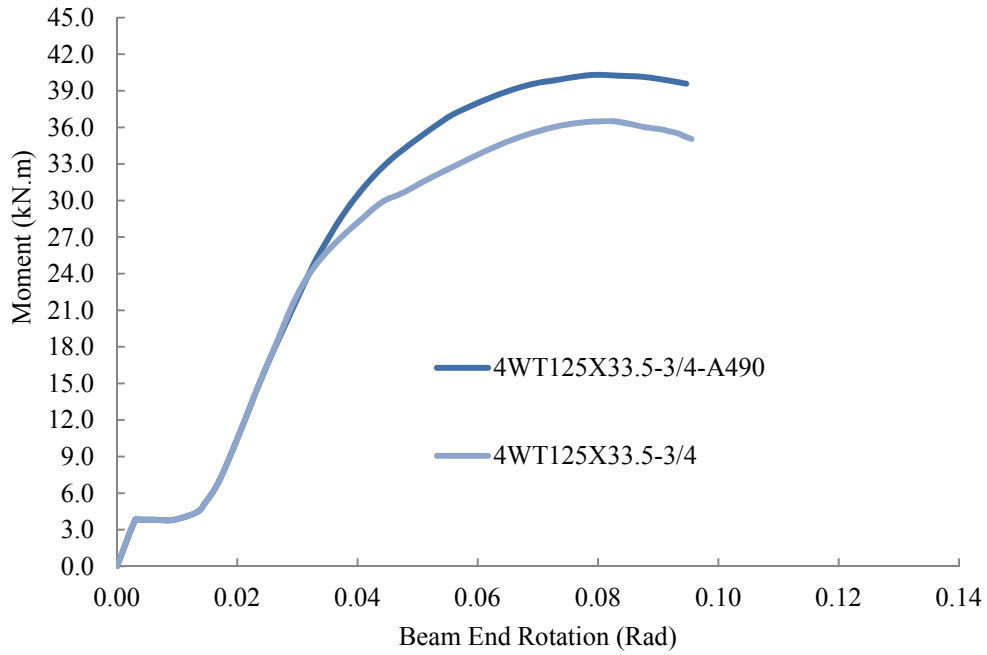


Figure 6.55: Comparison of flexural response of 4WT connections with different bolt types

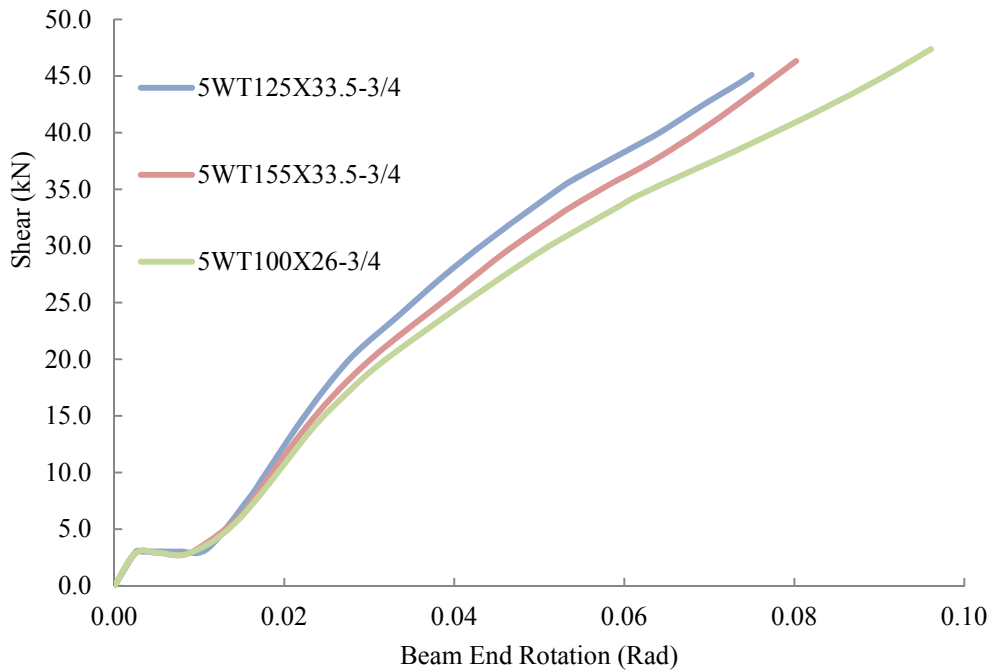


Figure 6.56: Comparison of shear response of 5WT connections with different WT sections

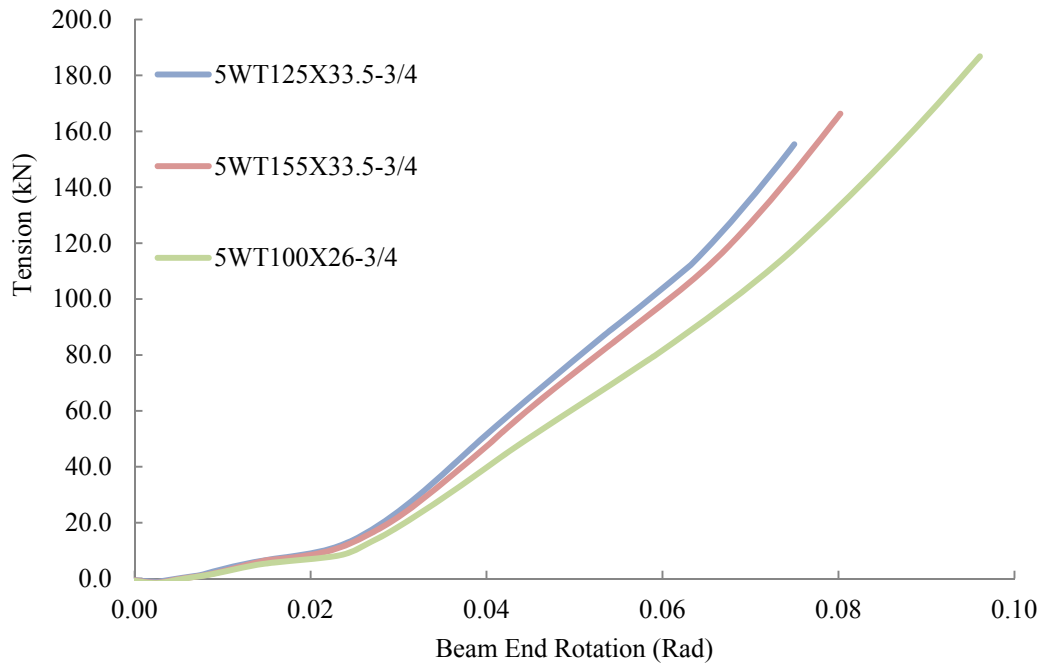


Figure 6.57: Comparison of tensile response of 5WT connections with different WT sections

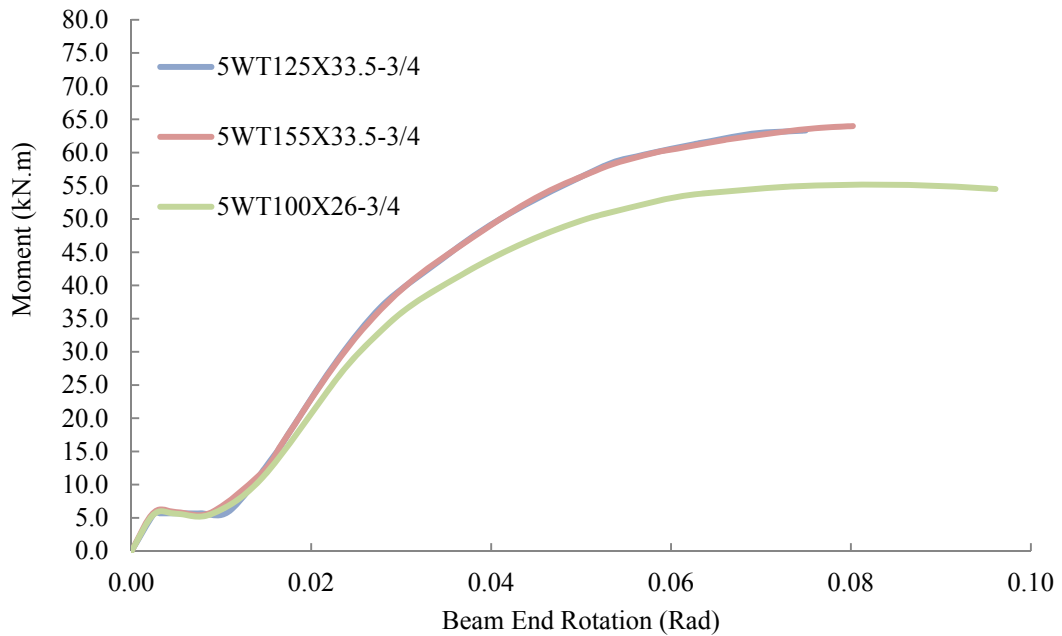


Figure 6.58: Comparison of flexural response of 5WT connections with different WT sections

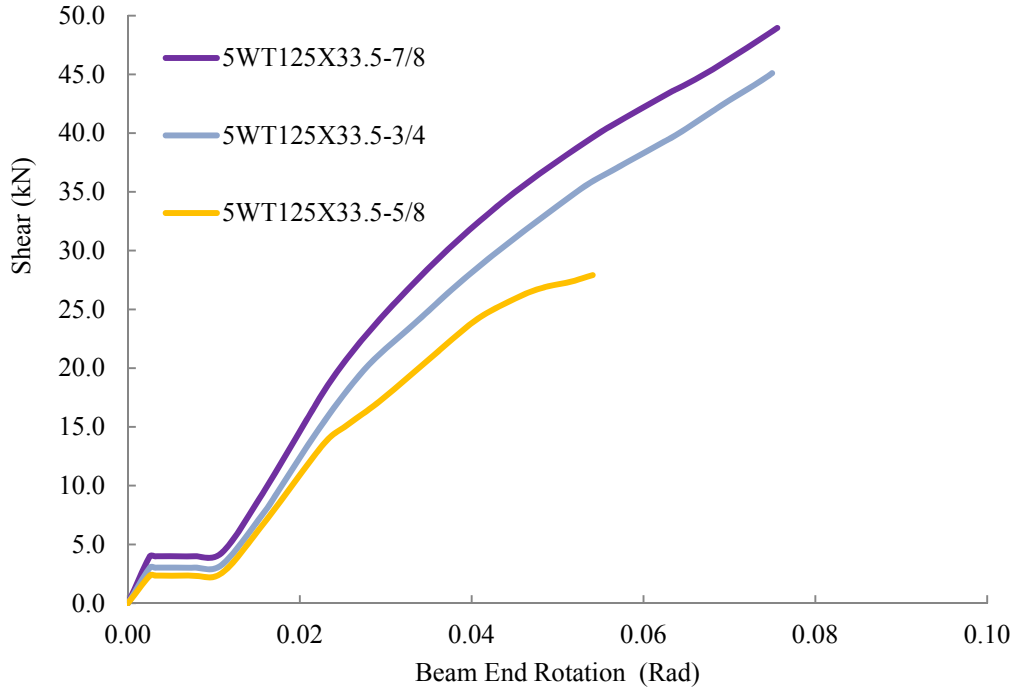


Figure 6.59: Comparison of shear response of 5WT connections with different bolt sizes

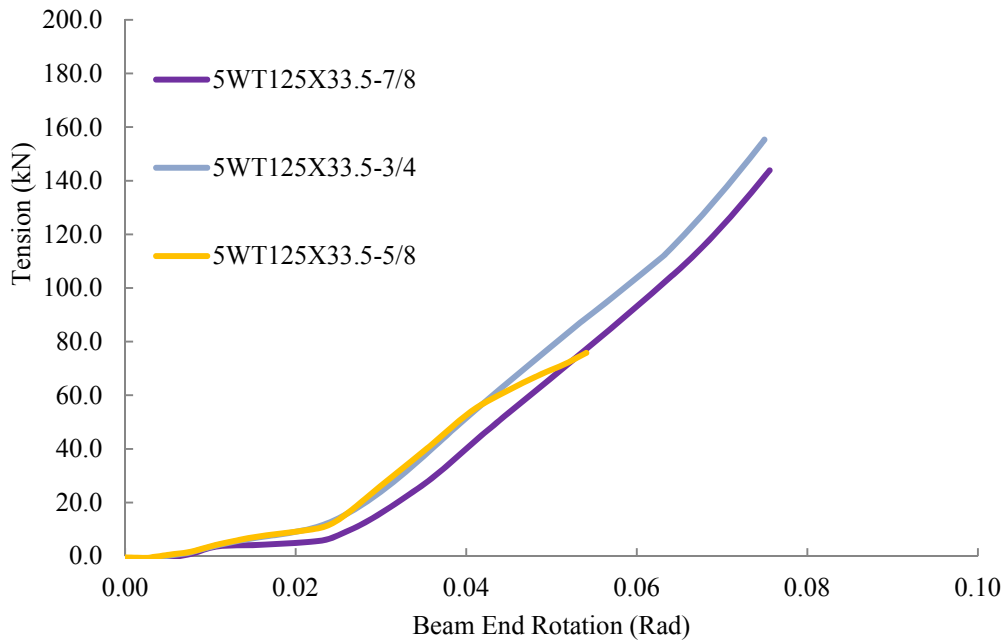


Figure 6.60: Comparison of tensile response of 5WT connections with different bolt sizes

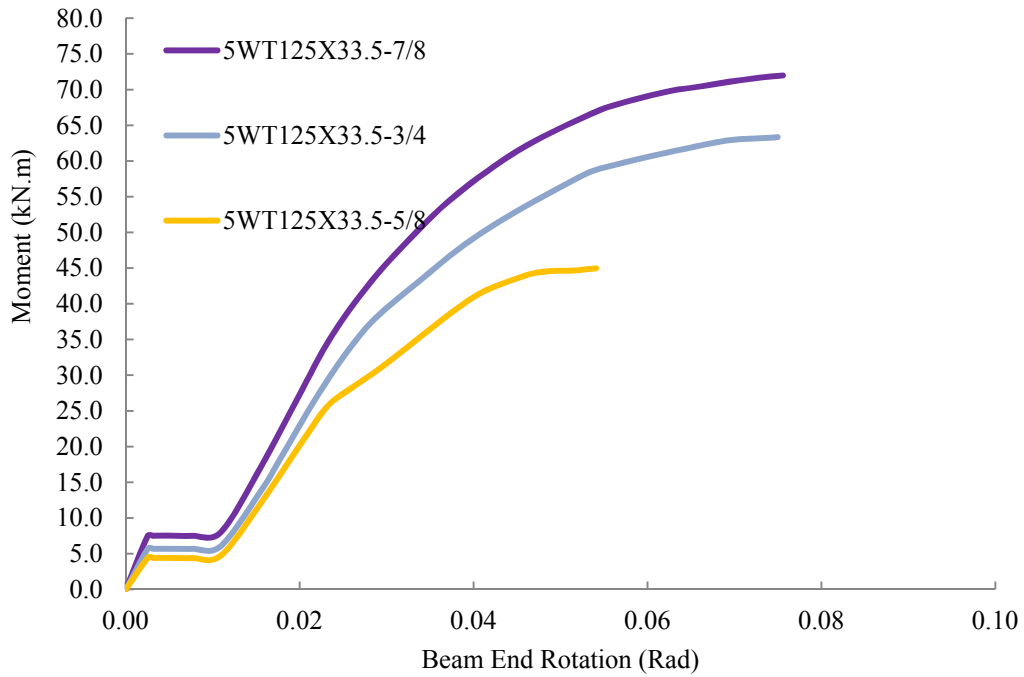


Figure 6.61: Comparison of flexural response of 5WT connections with different bolt sizes

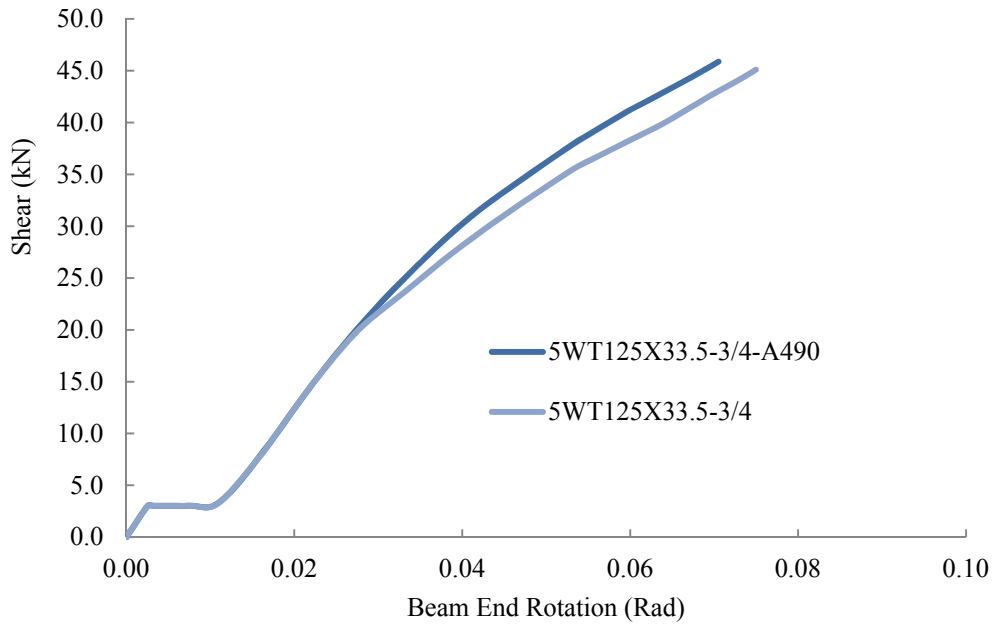


Figure 6.62: Comparison of shear response of 5WT connections with different bolt types

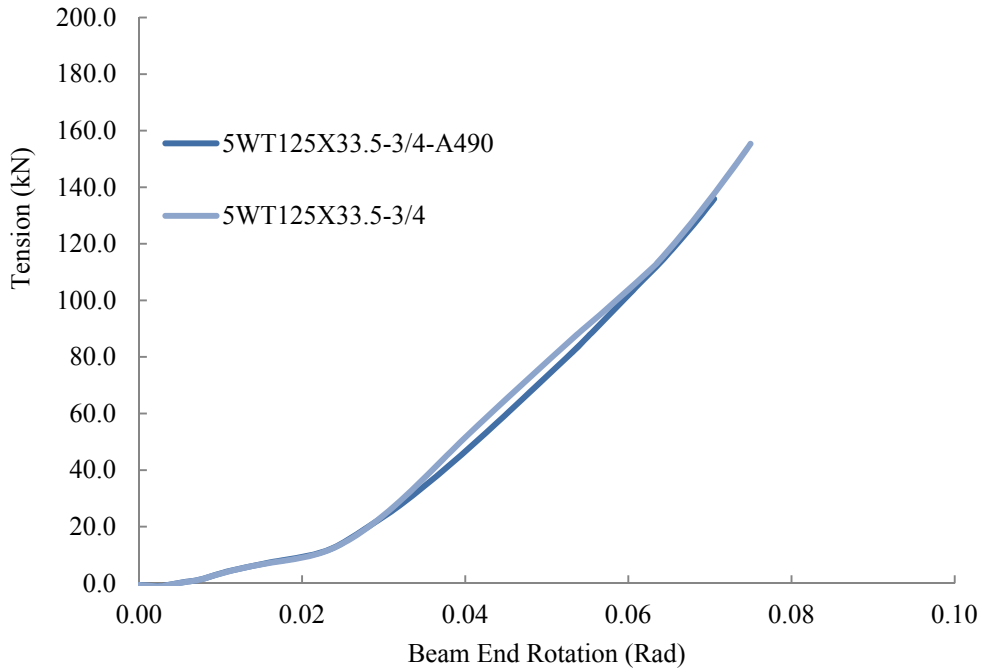


Figure 6.63: Comparison of tensile response of 5WT connections with different bolt types

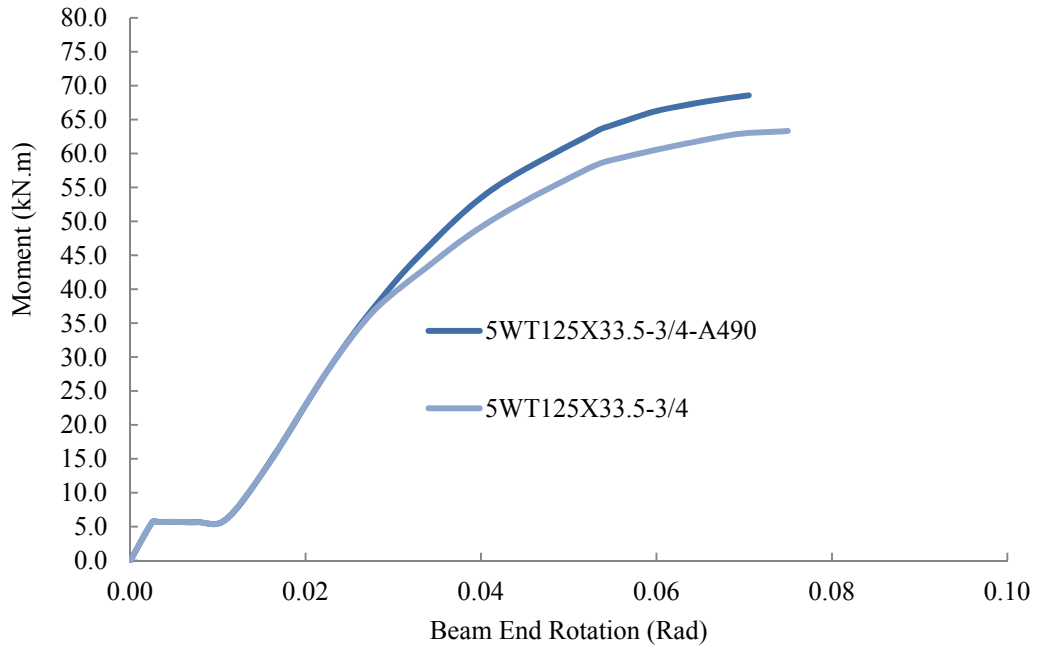


Figure 6.64: Comparison of flexural response of 5WT connections with different bolt types

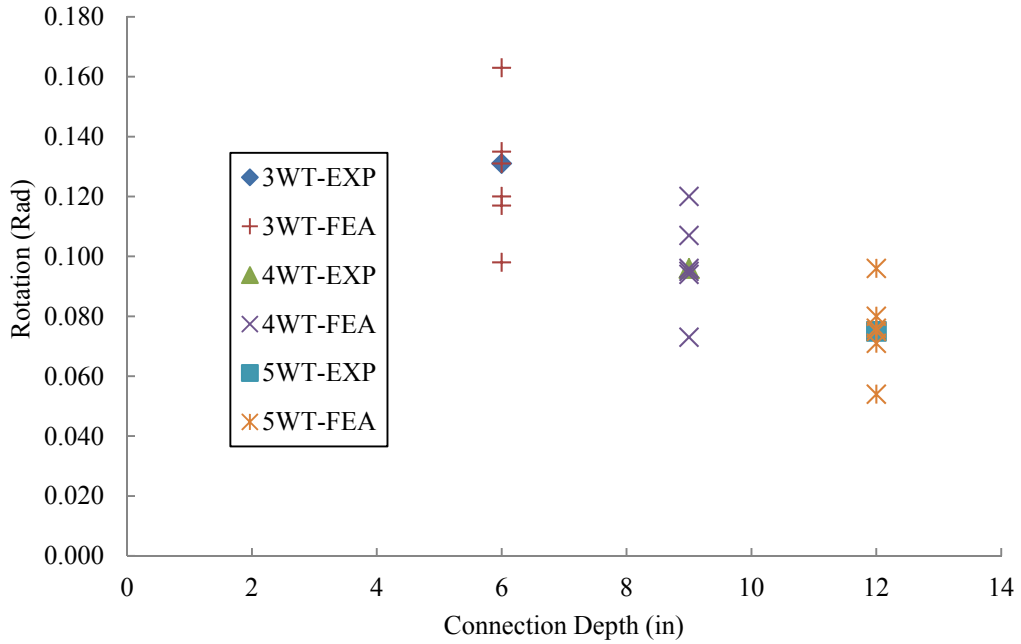


Figure 6.65: WT connection total rotation capacities versus connection depth

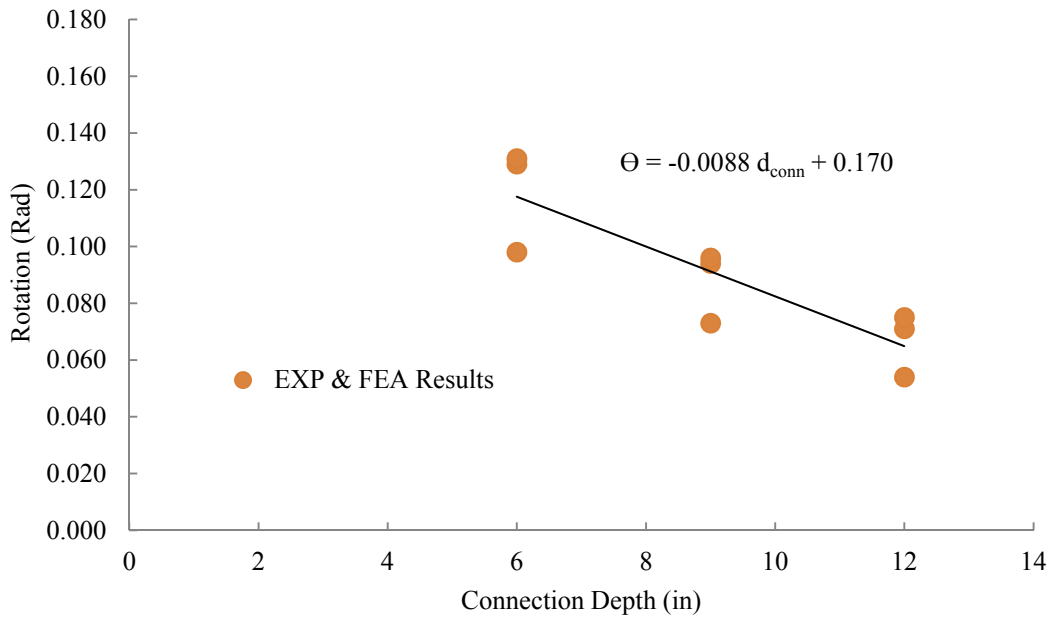


Figure 6.66: Proposed equation for WT connection total rotation capacities versus connection depth – Bolt shear rupture limit state

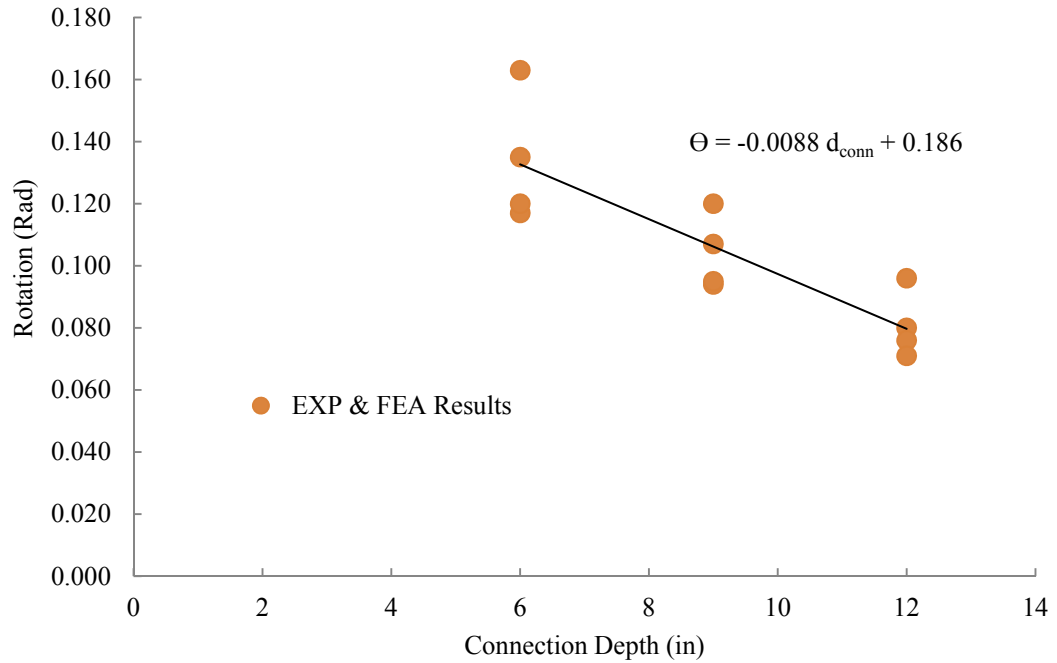


Figure 6.67: Proposed equation for WT connection total rotation capacities versus connection depth – WT rupture limit state

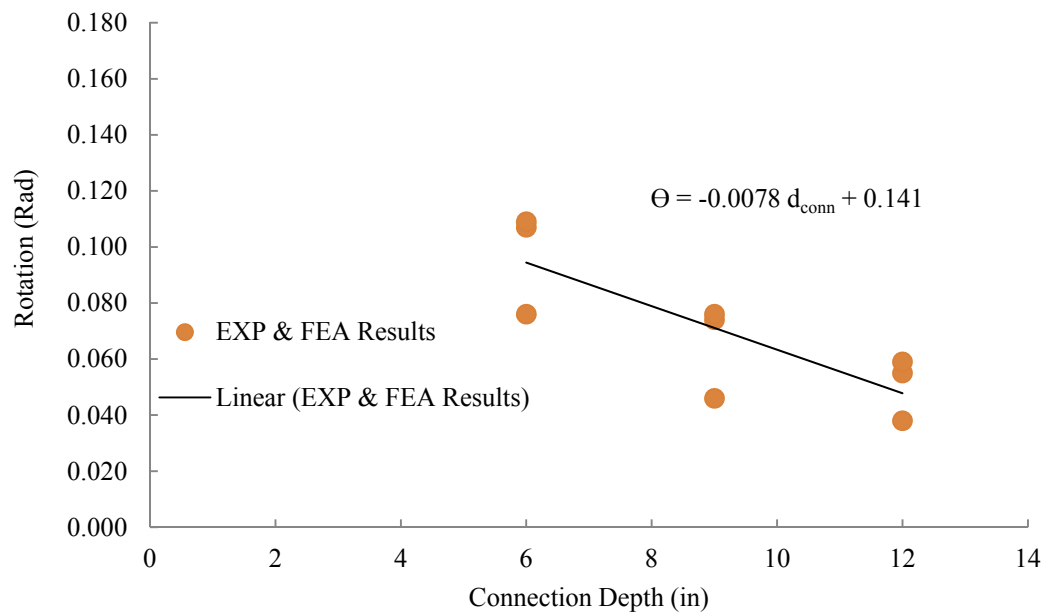


Figure 6.68: Proposed equation for WT connection plastic rotation capacities versus connection depth – Bolt shear rupture limit state

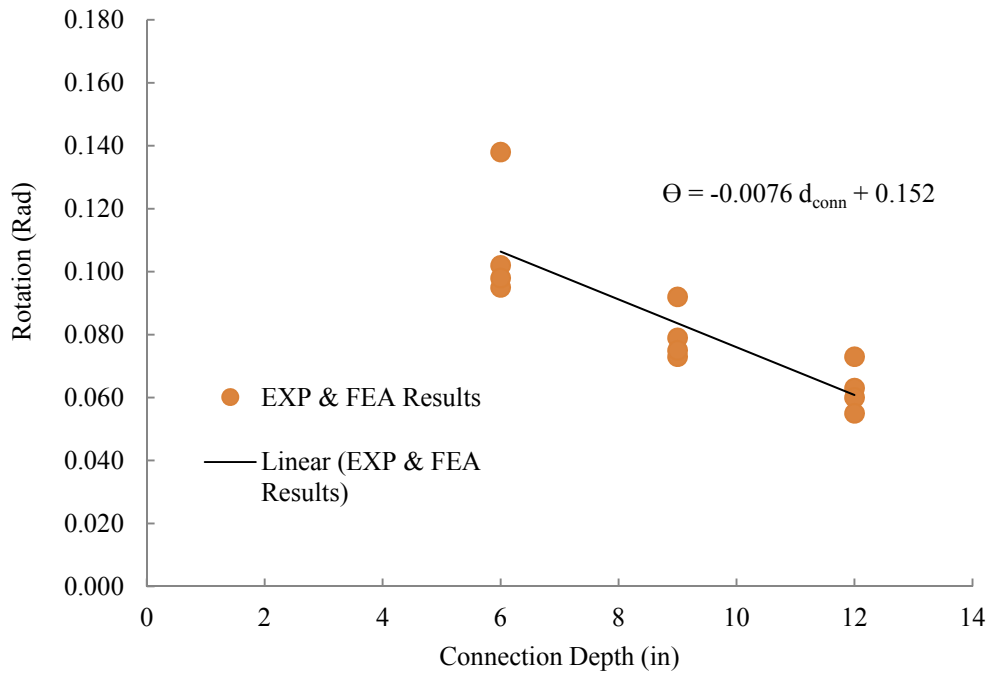


Figure 6.69: Proposed equation for WT connection plastic rotation capacities versus connection depth – WT rupture limit state

7 Behaviour of Single Angle Connections under Column Removal Scenario

7.1 Introduction

Single angle connections are one of the common single-sided shear connections used in steel construction. They are more economical than double angle connections due to reduction in both material and labour. They are also more favorable to fabricators due to ease of fabrication and beam installation. The main advantages and disadvantages of single angle connections compared with other types of single-sided connections are summarized in Table 7.1. The angle can either be bolted or welded to the beam web and bolted or welded to the column flange, as shown in . The leg that is bolted or welded to the supporting member is called the “outstanding leg”; meanwhile, the other leg that is connected to the supported beam is called the “web-framing” leg (CISC 2006). Common types of material used in single angle connections are stated in Table 7.2. Similar to shear tab and WT types of shear connections, single angles in beam-to-column connections are conventionally designed to transfer shear forces, while the rotation is not restrained. As a result, there is no substantial moment transfer.

Research on the strength and ductility of single angle connections in conventional design is limited. Besides, its response to the column removal scenario is also relatively unknown. For example, the DoD (2009) guideline provides a table that includes models for rotational ductility of shear tab and double angle connections, but not single angles. As a result, more research is required to establish the characteristic features of such connections in order to improve the current modelling definitions of shear connections in the column loss event. The actual load path, stress distributions, sources of ductility, and failure modes should be well-researched to propose modelling parameters in the column removal scenario.

In this chapter, numerical methods are applied to simulate the response of single angle connections when a column is compromised. The finite element models are verified by available experimental data following the same loading regime. Verified models are utilized to expand the database of the connection models. Shear, tension, and moment versus chord rotation diagrams are presented for numerical results and conclusions are made. The results are utilized to develop the modelling parameter that can predict the rotational behaviour of single angle connections in the new scenario.

7.2 Objectives and scope

This chapter is focused on the behaviour of single angle shear connections under simultaneous presence of shear, tension, and moment. The finite element models proposed in this chapter can shed more light on the performance and the sources of ductility in single angle connections. The results can be used to select suitable connection modelling parameters for progressive collapse evaluations of steel frames with similar single angle shear connections. The focus of the research is on bolted-bolted single angle shear connections, shown in Figure 7.1(d). Connection depth, angle thickness, bolt size and type are the main variables in the numerical models discussed herein. Equations, based on the connection depth, are proposed to predict the rotational ductility of single angle connections.

7.3 Selected previous research

Lipson (1968) appears to have initiated the investigations on single angle shear connections by performing several tests. He attempted to establish characteristic features of these connections, including the behaviour of the connection under working loads and their rotational capacities. The main purpose of Lipson's research was to determine if single angle connections can qualify as "flexible" connections. Three types of connections were well-researched, including "bolted-

bolted" and "welded-bolted" single angles. All angles were ASTM A36 type and the bolts were ASTM A325 with a 19.1 mm (3/4 inch) diameter. The welding was made with E60 electrodes. He tested the specimens under pure bending moment and also under a combination of shear and moment with or without rotation. He observed that the magnitude of the slip value for the bolts varied substantially for single angle specimens. Besides, the effect of changing the gauge distance in either leg of the bolted-bolted angles on the slip value is minimal. His experiments could not develop the full plastic moment of the connection because of the small beam rotation. (Lipson 1968).

Lipson's studies also questioned the assumed flexibility of shear connections due to the observed restraining moment developed. He attempted to ease the restraint through modifying the connection details, such as using slotted holes or different weld patterns. He concluded that the connections with short-slotted holes were as reliable as connections with round holes but with lower moment developed at the bolts. Lipson's connections were designed to transfer shear only. The connections were able to reach an ultimate rotation of 0.022 radians (Lipson and Antonio 1980). He also proposed an equation for determining the maximum moment at the bolt line based on the results for connections with round holes.

Kishi and Chen (1990) proposed a power model relationship for moment-rotation response of semi-rigid steel beam-to-column connections, including single angles. They utilized the model shown in Equation (7-1) to define the moment-rotation ($M - \theta_r$) curve:

$$M = \frac{R_1 \theta_r}{\left(1 + \left(\frac{\theta_r}{\theta_0}\right)^n\right)^{1/n}} + R_{kp} \theta_r \quad (7-1)$$

where R_{kp} is the plastic connection stiffness; θ_0 is a reference plastic rotation; n is a shape parameter; and R_1 is defined in Equation (7-2):

$$R_1 = R_{ki} - R_{kp} \quad (7-2)$$

in which R_{ki} is the initial connection stiffness.

In order to simplify the moment–rotation curve, they assumed that the curve flattens close to ultimate strength of the connection. As a result, R_{kp} becomes zero and Equation (7-1) can be re-written as Equation (7-3):

$$M = \frac{R_{ki} \theta_r}{\left(1 + \left(\frac{\theta_r}{\theta_0}\right)^n\right)^{1/n}} \quad (7-3)$$

where θ_0 is defined in Equation (7-4):

$$\theta_0 = \frac{M_u}{R_{ki}} \quad (7-4)$$

where M_u is the ultimate moment capacity of the connection.

Figure 7.2 shows the shape of the moment–rotation curve based on Equation (7-3). They calculated the shape parameter, n , by applying the method of least squares to the differences between the predicted and experimental moments. As observed, a power relationship is one method to quantify the rotational behaviour of the connections. However, in this research, the methodology adopted by current seismic and progressive collapse codes is applied, as discussed in chapter 2.

The general deformation pattern of the single angle connection shown in Figure 7.3 was based on the following assumptions: (1) the shear force has a negligible effect on connection deformation, (2) the segment of the angle connected to the column and beam behave linearly elastic and as a rigid body, respectively; (3) the segment of the angle attached to the column flange behaves as a fairly thick plate and, as a result, the fastener-nut edge is assumed to be fixed, as shown in Figure 7.4; (4) the concentrated torsional moment and connection moment applied at the free edge are in equilibrium (Figure 7.4). Applying bending-torsion theory and using the mentioned assumptions, the initial stiffness, R_{ki} , for the single angle connections is determined. Gong (2009) reported the results of tests on 19 full-

scale all-bolted single angle shear connections under the combined effects of shear and rotation, in order to determine the shear strength of the two bolt groups on two legs of the connection angles. In all the tests, the bolts were 19 mm diameter ASTM A325 bolts and the angle was L102X102X9.5, keeping the angle length as the main varying parameter. He determined the moment capacity of the connection with reasonable accuracy based on yield line theory, similar to what Thornton (1996) did for the WT connections. Figure 7.5 illustrates the concept of yield line theory applied to the single angle connection (Gong 2009).

Gong (2009) also acknowledged the major effect of lateral-torsional restraints of the connection on the ultimate strength of the beam. Based on the test results, he also observed that lateral support can reduce the load eccentricity and, hence, increase the strength of the connection.

Little experimental data is available on single angle connections subjected to simultaneous presence of shear, tension, and moment. Guravich and Dawe (2006) investigated the behaviour of simple beam-to-column connections subjected to simultaneous application of shear and tension by conducting an experimental program on different types, including single angle welded-bolted configurations. They tested two angles with different thicknesses: 7.9 and 9.5mm. Rotations of 0.03 radians were applied while maintaining a constant shear between zero and the design shear resistance. After that, tensile force was applied to the connections up to the failure point. As the tension force increased, the framing leg of the angle yielded in bearing next to the bolts. There was also the effect of shear yielding of the framing leg between the bolts, but to a lesser degree. The dominant failure mode was shear fracture of the angle at the tension zone bolt hole of the web-framing leg, which was followed by shear yielding of the compression zone for the 7.9 mm thick angle. The 9.5 mm thick ones failed due to bolt shear. The main sources of ductility were bearing around the bolt holes and bending of the legs of the angles. It was observed that single angle connections can sustain significant amounts of tension accompanied by the design shear capacity of the connection.

The thinner angle can provide slightly higher tensile resistance due to higher ductility (Guravich and Dawe 2006).

7.4 Numerical study method

The behaviour of single angle connections subjected to simultaneous shear, moment, and tension is investigated using high-fidelity finite element models. All stages of simulation, including pre- and post-processing procedures, were performed by Abaqus/CAE, with Abaqus/standard used as the analysis engine (Dassault Systèmes 2009).

7.4.1 Selected experimental program

Unpublished experiments performed by Johnson (2009) were used to verify the results of the numerical models. The same test setup used by (Thompson 2009) and Friedman (2009), discussed in chapters 5 and 6, was utilized for this suite of experiments as well. A true pin condition was applied to both far ends of the beams and the middle stub column was pushed down in order to simulate the column loss event. Due to the limited information available, the results of three bolt connections are utilized to verify the finite element models.

7.4.2 Finite element model description

Three-dimensional solid elements were used for all components of the finite element models. The models consist of the central column stub and the adjacent beams, as well as the connections with complete detailing, as shown in Figure 7.6(a). Three, four, and five bolt single angle connections were modelled, as illustrated in Figure 7.6(b) to Figure 7.6(d). The single angle connections are bolted to both the column flange and beam web. The central column stub is pushed down, while the connection performance is monitored. Since the

connection is the point of interest, all characteristic features of the connections are included in the models. Strain-based fracture criteria have been established and verified for both the angle material and the bolts in order to predict the failure modes, discussed in chapter 3. All other characteristic features of the models, including bolt pre-tensioning, material properties, contact calibration and element types are also discussed in chapter 3. The complete list of connections numerically studied, including characteristic features, is summarized in Table 7.3. The models are labelled based on the following method: first the number of bolts in a vertical line, then SA, which is the abbreviation for single angle connections utilized in this research, then the angle thickness and the bolt diameter, in imperial units. For example, 3SA-3/8-3/4 refers to the single angle connection with three bolts, 3/8 in (9.5mm) angle thickness, and 3/4 in (19.1 mm) diameter bolts. The bolts are all ASTM A325, unless at the end of the label “A490” is added. Material properties for all the angles correspond to ASTM A36.

A sample deformed shape of a connection assembly, as a typical result of the finite element analyses, is shown in Figure 7.7. Figure 7.8 to Figure 7.10 illustrate the typical deformed shape of single angle connections with different connection depths, correspondent to models 3SA-3/8-3/4, 4SA-3/8-3/4, and 5SA-3/8-3/4, respectively, accompanied by front and back views of the angles and the bolts at the time of failure. More discussion on these issues is available in section 7.6.

7.5 Verification results

Although based on the validated benchmark example provided in chapter 2, the verification process is still performed specifically for a single angle connection with three bolts. To ensure that single angle connections will survive the column removal scenario, they should be capable of carrying the combined effects of shear, moment, and tension at large rotations. These internal forces at the bolt line versus the chord rotation of connection assembly 3SA-3/8-3/4 are shown in

Figure 7.11 to Figure 7.13 to illustrate the shear, tension, and flexural responses. The dashed and solid lines represent the results of the experiments and simulations, respectively. The shear responses of the connections, demonstrated in Figure 7.11, tensile curve in Figure 7.12, and the moment response, in Figure 7.13, serve to verify the models based on acceptable correlation with the associated experimental results. The agreement between the experiment and numerical results is deemed to be satisfactory, considering the differences between the nominally identical test connections themselves.

7.6 Parametric study results

A parametric study is performed using the verified model to investigate the effects of different design parameters, such as angle thickness, bolt size and type, and also connection depth, according to Table 7.3. This investigation is discussed in sections 7.6.1 to 7.6.3.

7.6.1 Three bolt single angle connections (3SA)

to show the interactions of shear, tension, and moment for the single angle connections with three bolts (3SA). shows the behaviour of 3SA-3/8-3/4 without the test curves. The maximum moment happens at the approximate rotation of 0.08 radians. At this point, the couple force action is distinguished by compressive force at the top hole in the web-framing leg and tensile action at the bottom hole of the outstanding leg. There is some local yielding at the top of the web-framing leg due to the compressive force, which reduces the flexural resistance after the peak. As labelled in the figure, the point that the flexural phase domination ends and catenary force begins to provide the major resistance is named the “devolution point”, similar to what was discussed for shear tab and WT connections. For the 3SA-3/8-3/4 connection, the devolution point is located at the rotation of 0.12 radians, when the flexural resistance of the connection has

already reduced significantly. The main reason for this is the fact that in 3-bolt connections, the top bolt resists the moment demand through bearing resistance of the bolt–hole interaction; meanwhile, the bottom part of the section resists moment through combined effects of bending action of the outstanding leg and through tension force in the bottom bolt of the outstanding leg. As soon as localized yielding happens around the contact surface at the top of the web framing leg, the flexural resistance starts to vanish and the connection finds another load path to take more load. The failure will be in the catenary phase. The same phenomenon is observed in the 4SA and 5SA connection assemblies. Unlike the WT connection bolts, the bolts of the web framing leg remain almost elastic, although there is some plastic elongation in the two bottom bolts of the outstanding leg due to tension. The connection can sustain a large amount of rotation (0.22 radians) by providing ductility through yielding of web-framing leg and also out-of-plane deformation of the outstanding leg. The connection eventually fails because of excessive plastic deformation at the bottom hole of the outstanding leg. The deformed shape of the connection at the time of failure is shown in Figure 7.8.

shows the interaction of internal forces at the bolt line for the model 3SA-1/4-3/4. In this model, the failure is initiated in the single angle bottom hole region in the outstanding leg. A slight increase in the ductility of the connection is observed in comparison with 3SA-3/8-3/4 due to the thinner angle thickness and, consequently, more out-of-plane deformation of the outstanding leg. There are no significant plastic shear deformations observed in the bolts—even the bottom bolt of the outstanding leg—since most of the deformation happens in the thin angle. The tensile force starts to come into existence at the point of almost zero moment, which signifies the complete separation of the flexural phase from the catenary action. Although the shear response of the connection is small in comparison with the tensile forces, a “snap-through” kind of behaviour is observable. The shear force of connection 3SA-1/4-3/4 increases almost linearly up to the point of almost 0.04 radians, then it starts to reduce until 0.1 radians of rotation. After that,

it increases almost linearly, interacting with tension, at high rotations. The reason for such behaviour is that at the rotation of 0.04 radians, the heel of the angle starts to yield, which causes a reduction in the shear resistance of the connection. However, after the rotation of 0.1 radians, bearing of the bolts in the outstanding leg begins to play a role, and the shear force increases subsequently. This phenomenon is observed in 4SA and 5SA connections with thin angles (6 mm or $\frac{1}{4}$ in) as well.

shows the interaction of internal forces at the bolt line for the model 3SA-1/2-3/4. No difference is observed in the failure mode of this connection compared to other models with different angle thicknesses. The ductility of the connection is not changed either, in comparison with 3SA-3/8-3/4 and 3SA-1/4-3/4. There is tensile plastic deformation in the bolts of the outstanding leg, although the other bolts remained nearly elastic. The tensile force starts to come into existence after the point of maximum moment. This could be attributed to the thicker angle size that still possesses additional flexural resistance when tensile catenary force starts to develop. The share of out-of-plane deformation of the outstanding leg in providing the ductility of the connection is quite substantial. Similar to the other two angle connections (3SA-3/8-3/4 and 3SA-1/4-3/4), although the connection failed due to initiation of rupture at the outstanding leg bottom hole region, heel rupture is also possible due to an excessive amount of plastic deformation.

and show the interaction of internal forces at the bolt line for the models 3SA-3/8-5/8 and 3ST-3/8-7/8, respectively. There is a small amount of plastic strain observed at the top 5/8 in (15.9 mm) bolt of web framing leg, which is not observed in the 7/8 in (22.2 mm) bolts. The other characteristic features of the connection are similar to 3ST-3/8-3/4. The tensile force starts to come into existence at some point on the descending branch of flexural response, which is an indication of a flexural-phase to catenary-phase transition point. The connections can accommodate large rotations up to 0.21 radians prior to failure.

The behaviour of model 3SA-3/8-3/4-A490 is very similar to 3SA-3/8-3/4 with ASTM A325 bolts. The dominant limit state of the connection is similar, as expected. 3SA-3/8-3/4 was slightly more ductile due to a higher inherent ductility of ASTM A325 bolts. As observed, substituting the ASTM A325 bolts with ASTM A490 bolts has little effect on the connection performance.

Generally, in 3SA connections, regardless of the angle thickness, bolt size and type, as the flexural stiffness of the connection becomes zero and subsequently negative and then ramps down to zero, the tensile catenary forces increase rapidly until the failure of the connection. Tensile catenary resistance starts to grow at the approximate chord rotation angle of 0.12 radians, where the maximum flexural strength is already been reached. Basically, the connections do not have considerable flexural resistance at the time of failure. Therefore, it can be inferred that the 3SA connections fail because of catenary action. The dominant failure mode of 3SA connections is outstanding leg rupture at the bottom bolt hole region, although heel rupture is also possible due to high plastic deformation. The average rotational capacity of the 3SA connections studied in this research is about 0.22 radians, which is significantly higher than three bolt shear tab and WT connections.

7.6.2 Four bolt single angle connections (4SA)

to show the interactions of shear, tension, and moment for the single angle connections with four bolts (4SA). shows the interaction curves of the model 4SA-3/8-3/4. A point might be distinguished as a devolution point after the maximum moment occurs, as shown in , while the moment is degrading. For the 4SA connections this point is the onset of the catenary phase. There is a change in the slope of the tensile response at the approximate rotation of 0.17 radians. At this point, another yield line starts to develop at the angle heel in the outstanding leg, labelled as secondary yield line in Figure 7.9. Similar to the 3SA connections, the primary yield lines are the main sources of ductility, shown in as well.

shows the interaction of internal forces at the bolt line for the model 4SA-1/4-3/4. The general behaviour of 4SA-1/4-3/4 is similar to the 3SA-1/4-3/4 model due to the same geometric and mechanical properties. The failure is initiated in the angle bottom hole region in the outstanding leg. The ductility of the connection is similar to 4SA-3/8-3/4. No significant plastic shear deformation is observed in the bolts—even the bottom one—since most of the bearing deformations happen in the thin angle. The tensile force starts to grow at the rotation of 0.12 radians, when the resisting moment is diminishing gradually.

shows the interaction of internal forces at the bolt line for the model 4SA-1/2-3/4. The rotational ductility of the connection is comparable with 4SA-1/4-3/4 and 4SA-3/8-3/4. Most of the bolts remain elastic except the two bottom bolts at the outstanding leg. The bottom bolt at the web-framing leg also experienced some plastic deformation. The devolution to the catenary phase happens at the approximate rotation of 0.10 radians in this connection assembly.

shows the interaction of internal forces at the bolt line for the model 4SA-3/8-5/8. In this model, the failure initiated at the outstanding leg of the bottom hole. A small amount of plastic deformation happens in the bolt shank of the bottom three bolts at the column face, accompanied by slight plastic strains appearing at the bottom and top bolts in the web framing leg before failure. The ductility of the connection is almost the same as for the 4SA-3/8-3/4 model. The tensile force starts to become significant at the approximate chord rotation of 0.11 radians. At this rotation angle, the flexural behaviour keeps reducing, indicating the switch from flexural behaviour to the catenary phase.

shows the interaction of internal forces at the bolt line for the model 4SA-3/8-7/8. In this model, the failure mode is similar to other four bolt angle connections. A very slight amount of plastic deformation developed in the bolt shanks. There are significant plastic deformations along the yield lines similar to the 4SA-3/8-3/4 connection model. The devolution from flexural behaviour to the catenary phase occurs at the rotation of about 0.11 radians.

As observed in the 4SA connections, a point is distinguished as a devolution point in which the tensile force appears as an alternative load path in the connection internal force interaction curve. After this point, the tensile catenary force increases rapidly until the failure of the connection, in the presence of shear and moment. Tensile catenary resistance starts to grow at the approximate chord rotation angle of 0.11 radians, at which point the flexural response continues to degrade. Basically, the amount of moment at the failure is negligible in most of the cases. Therefore, it can be inferred that the 4SA connections fail mainly because of catenary actions. The dominant failure mode of 4SA connections is outstanding leg rupture, initiated at the bottom hole region.

7.6.3 Five bolt single angle connections (5SA)

to depict the simultaneous presence of shear, tension, and moment for the single angle connections with five bolts (5SA). The interaction of internal forces of 5SA-3/8-3/4 is demonstrated in . Similar to 4SA and 3SA connections, the “devolution” point in this connection is located on the degrading branch of flexural curve. A point is distinguished as a devolution point in which the connection cross-section goes to catenary action. After that, tensile force and moment interact until the connection failure. In this connection, all the bolts remain elastic except the three bottom bolts at the column face. Three yield lines are distinguished in the angle at the time of failure, as indicated in Figure 7.10. Local bearing yielding at the top and bottom hole of web framing web is also distinguishable; however, its magnitude is negligible in comparison with the yielding at the bolt line outstanding leg and also the heel of the angle.

shows the interaction of internal forces at the bolt line for the model 5SA-1/4-3/4. Its behaviour is similar to the 4SA-1/4-3/4 and 3SA-1/4-3/4 models due to the same geometric and mechanical properties. The failure is initiated in the bottom hole region of the outstanding leg, similarly. A slight increase in the ductility of the connection is observed in comparison with the 5SA-3/8-3/4 model because of

the more ductile behaviour of the thinner plate. There is no significant plastic shear deformation observed in the bolts—even the bottom bolts—since most of the bearing deformations happen in the thin angle. In this five bolt connection, the tensile force comes to play at the rotation of about 0.11 radians. After that, an increase in the tensile force continues until failure, while the flexural strength degrades. At the approximate rotation of 0.16, a reduction in the slope of the tensile response is observed, which was discussed in the section 7.6.2. As a result, the devolution of this connection is distinguished as flexural to the catenary phase.

shows the interaction of internal forces at the bolt line for model 5SA-1/2-3/4, with similar behaviour as 3SA-1/2-3/4 and 4SA-1/2-3/4 connections. There is a slight increase in the rotational ductility of the connection in comparison with 5SA-3/8-3/4 and 5SA-3/8-3/4. There are also plastic strains in the bottom three bolts at the column face and the bottom one at the web-framing leg prior to failure. The other bolts remained essentially elastic. The devolution from flexural behaviour to the catenary phase is obvious in this connection assembly at the rotation of 0.08 radians. This chord rotation corresponds to the maximum moment as well, after which a reduction in the flexural strength of the connection happens.

shows the interaction of internal forces at the bolt line for the model 5SA-3/8-5/8. In this model, despite the usage of smaller bolts, still the failure happens in the angle, similar to the 4SA-3/8-5/8 and 3SA-3/8-5/8 connection models. A substantial amount of plastic deformation was happening in the bolt shank, accompanied by considerable bearing deformation at the bottom hole. The ductility of the connection is almost the same as for the 5SA-3/8-3/4 model. The tensile catenary force comes to play a role at the rotation of 0.10 radians, which is deemed to be the devolution point to the tensile behaviour from the flexural phase. The amount of plastic strain in the bolts is more substantial in the 5SA-3/8-5/8 connection compared to the other five bolt single angle connections.

shows the interaction of shear, tension, and moment at the bolt line for the model 5SA-3/8-7/8, with the same failure mode as other types of five bolt connections

studied in this research. A very slight amount of plastic deformation happened in the bolt shank. There are significant plastic deformations around the bottom bolt hole area in the outstanding leg. The devolution from flexural behaviour to the catenary phase occurs at the rotation of about 0.10 radians. After 0.10 radians, although the decrease in moment strength happens continuously, there is still a substantial moment at the connection prior to failure; however, since the increase in tension is accompanied by a decrease in the moment resistance, the connection fails mainly in tension.

The behaviour of model 5SA-3/8-3/4-A490 is very similar to that of 5SA-3/8-3/4 with ASTM A325 bolts. The dominant limit state of the connection is plate failure, as expected. However, unlike the similar model with A325 bolts, no substantial shear deformation in the bottom bolt shank was observed. The ductility of the 5SA-3/8-3/4 connection is slightly more than the similar one with ASTM A490 bolts.

Generally, similar to the 3SA and 4SA connections, the “devolution point” in 5SA connections happens almost at or after the rotation at which the maximum rotation happens. A point is distinguished as a devolution point where a tensile force comes to play a role. The tensile catenary forces increased rapidly, interacting with moment, until the failure of the connection. Tensile catenary resistance starts to grow after the approximate chord rotation angle of 0.08 radians when flexural response starts to decrease. Although, the amount of moment and tension at the failure is substantial, it is deemed that the connections fail mainly because of catenary action due to gradual reduction in the moment curve. The dominant failure mode of 5SA connections is angle rupture at the bottom hole area of the outstanding leg, similar to 3SA and 4SA connections.

7.7 Comparison of the results

In this section, the effect of angle thickness, bolt size, and bolt type are discussed separately for three, four, and five bolt single angle connections.

7.7.1 Three bolt single angle connections (3SA)

7.7.1.1 Plate thickness

Figure 7.29 to Figure 7.31 illustrate the shear, tensile, and flexural responses of 3SA connections with different angle thicknesses. Generally, an increase in thickness causes an increase in shear, tensile, and flexural strengths of 3SA connections. There is a flat plateau in the shear response of 3SA-3/8-3/4 until 0.10 rad, which shows up as degradation of shear response in the connection 3SA-1/4-3/4 due to formation of a second yield line at the angle web-framing leg. This phenomenon does not cause a reduction of shear in the thicker plate. In terms of axial load path response, the difference among the curves is substantial, although the ductilities of the connections are almost the same. It can be inferred that the ductility of the connection does not change significantly by altering the angle thickness.

The maximum tensile catenary force the angles can develop is highly dependent on the angle thickness. There is an abrupt change in the axial stiffness of all thicknesses, at the approximate rotation of 0.16 radians, which is related to the initiation of yielding in the bottom of the heel of the connection at the outstanding leg. The shear strength of the connection with the 6 mm (1/4 in) thickness is about 40% that of the one with the 9.5 mm (3/8 in) thick angle. In terms of axial strength, this value is reduced to even less than 35%. Model 3SA-1/4-3/4, with the thinnest angle, shows slightly higher ductility due to the higher contribution from out-of-plane deformation of the outstanding leg. The maximum moment happens at approximately the same rotation (0.08 radians) for all thicknesses. All the

flexural responses possess a descending branch after the peak moment until zero flexural resistance, as observed in Figure 7.31.

7.7.1.2 Bolt size

Figure 7.32 to Figure 7.34 illustrate the shear, tensile, and flexural responses of the 3SA connections with different bolt sizes. Unlike the effect of angle thickness, an increase in bolt diameter does not cause a significant increase in the shear and shear responses of 3SA connections; the behaviour is almost the same, as shown in Figure 7.32 and Figure 7.33, although a slight increase is observed with an increase in bolt diameter. The change in the rotational capacity of 3SA connections due to a change in bolt diameter is also very small and considered negligible. The shear and tensile strengths of the 3SA-3/8-5/8 connection are approximately 85% those of the 3SA-3/8-3/4 connection. The maximum moment happens at approximately the same rotation (0.08 radians) for all bolt sizes. All the flexural responses possess a descending branch after the peak moment and degrade to zero, as observed in Figure 7.34. In general, since the deformation capacity of bolts is relatively small compared with the ductility provided by the angles themselves, the use of larger bolts could not improve connection ductility other than if the increase served to prevent premature bolt failure.

7.7.1.3 Bolt type

The effect of the bolt grade—ASTM A325 versus ASTM A490—is also investigated for the 3SA-3/8-3/4 model. It is observed that the shear, axial, and flexural responses of the connection assembly with two different types of bolts are almost the same, with a minor difference in the rotational ductility. The connection with ASTM A325 bolts shows slightly more ductility.

7.7.2 Four bolt single angle connections (4SA)

7.7.2.1 Plate thickness

Figure 7.35 to Figure 7.37 illustrate the shear, tensile, and flexural responses of 4SA connections with different angle sizes. The effect of angle thickness is almost the same as for the 3SA connections. It can be inferred that shear and axial strength of the connection does change significantly by altering the angle thickness. The shear strength of the connection with the 6 mm (1/4 in) thickness is about 60% of the one with the 9.5 mm (3/8 in) thick angle. In terms of axial strength, this value is reduced to less than 55%. The maximum moment happens at the same approximate rotation (0.08 radians) for all the models. All the connection models possess the flexural response with a complete descending branch after the peak moment until almost zero flexural resistance, as observed in the Figure 7.37.

7.7.2.2 Bolt size

Figure 7.38 to Figure 7.40 illustrate the shear, tensile, and flexural responses of the 4SA connections with different bolt sizes. An increase in bolt diameter causes a minor increase in the axial and shear responses of 4SA connections. The rotational ductility of 4SA connections with different bolt diameters is almost the same. The maximum moment happens at the approximate same rotation (0.08 radians) for all bolt sizes. All of the flexural responses possess a descending branch after the peak moment to zero flexural resistance, as observed in Figure 7.40.

7.7.2.3 Bolt type

Similar to the explanation for the 3SA connections, the effect of different bolt type—ASTM A325 versus ASTM A490—is also investigated for the 4SA-3/8-3/4 model. The shears, axial, and flexural responses of the connection assembly with

two different types of bolts are almost the same, with only a minor difference in the rotational ductility.

7.7.3 Five bolt single angle connections (5SA)

7.7.3.1 Plate thickness

Figure 7.41 to Figure 7.43 illustrate the shear, tensile, and flexural responses of 5SA connections with different angle sizes. The effect of angle thickness is almost the same as for the 3SA and 4SA connections. Generally, an increase in angle thickness causes an increase in shear, tensile, and flexural strength of 5SA connections. The difference in the shear and flexural responses at the beginning (up to 0.02 radians) is small and as the rotation increases, the difference becomes more substantial. In terms of load path, the axial response of the connection changes significantly by altering the angle thickness. From the strength point of view, the maximum tensile catenary force they can develop is highly dependent on the angle thickness, as observed in Figure 7.42. However, the ductility of the three connections is almost the same. The models start to go through tensile catenary force at different rotations. This issue is due to a shift of the centre of rotation of the connection towards the top of the connection. This shift is more significant in the thin angle. As a result, catenary action starts to appear at the connection at higher rotation. It can be inferred that axial response of the connection changes by altering the angle thickness. The shear and tensile strength of the connections with the 6 mm (1/4 in) thick angle is about 55% of the one with the 9.5 mm (3/8 in) angle. All of the moment curves possess a descending branch after the peak value, as observed in Figure 7.43, although the connections still possess significant flexural resistance at the time of failure.

7.7.3.2 Bolt size

Figure 7.44 to Figure 7.46 illustrate the shear, tensile, and flexural responses of the 5SA connections with different bolt sizes. An increase in bolt diameter causes a minor increase in the flexural and shear responses of 5SA connections, similar to the 4SA and 3SA connection assemblies. However, in terms of axial response, the behaviour is almost the same, as shown in Figure 7.45. The rotational ductility of 5SA connections with different bolt diameters is almost the same. The shear and tensile strength of 5ST-3/8-5/8 is more than 90% of the 3ST-3/8-3/4 connection. The maximum moment happens at the approximate same rotation (0.08 radians) for all bolt sizes. All the flexural responses possess a descending branch after the peak moment, as observed in Figure 7.46. The moment at the failure is almost half of the peak moment.

7.7.3.3 Bolt type

Similar to the explanation for the 3SA and 4SA connections, the effect of different bolt types—ASTM A325 versus ASTM A490—is also investigated for 3SA-3/8-3/4 model. It is observed that the shear, axial, and flexural responses of the connection assembly with two different types of bolts are almost the same, with only a minor difference in the rotational ductility.

Table 7.4 summarizes the results of the numerical models at the initial failure of the connections.

7.8 Rotational ductility of single angle connections in column removal scenario

As observed, the rotational capacity of single angle connections is not affected greatly by variables such as angle thickness, bolt size and type. However, the number of rows of bolts (depth of the connection) does have an effect. Within the scope of what has been studied in this research, the main failure mode was rupture

of the bottom bolt hole region in the outstanding leg. Rotational capacity is estimated based on the depth of the connection in current codes and guidelines. Figure 7.47 illustrates the distribution of rotational capacity of single angle connections studied in this research versus connection depth. Validated finite element analysis (FEA) models portray eighteen points in order to produce a reasonably sufficient number of data points for conducting a regression analysis. Figure 7.48 shows the best-fit regression line considering all of the data. As a result, Equation (7-5) in imperial and Equation (7-6) in SI units are proposed to determine rotational capacities of single angle connections in the column removal scenario.

$$\theta_{tot} = -0.0086 d_{conn} + 0.271 \quad (d_{conn} \text{ in inches}) \quad (7-5)$$

$$\theta_{tot} = -0.00034 d_{conn} + 0.271 \quad (d_{conn} \text{ in millimetres}) \quad (7-6)$$

where d_{conn} is the distance between the centres of the top and bottom bolts, and θ_{tot} is the total rotational capacity of the single angle connections in radians.

θ_{tot} consists of both elastic and plastic components. The plastic rotation is the rotation that guidelines such as ASCE 41 (2006) and DoD (2009) utilize to define the connection behaviour. By aid of finite element models, plastic rotation can be separated from the elastic part and, through a regression analysis of the data for all cases considered (Figure 7.49), is reported in Equations (7-7) and (7-8):

$$\theta_p = -0.0059 d_{conn} + 0.219 \quad (d_{conn} \text{ in inches}) \quad (7-7)$$

$$\theta_p = -0.00023 d_{conn} + 0.219 \quad (d_{conn} \text{ in millimetres}) \quad (7-8)$$

Elastic rotation ends when the first sign of plastic strain starts to appear in the connection assembly. It is noted that the average elastic rotations observed in the studied three, four and five bolt single angle connections are 0.035, 0.030, and

0.020 radians, respectively. As a result, in the absence of appropriate tools to determine the elastic rotation limit for a single angle connection, the mentioned values can be used based on the depth of the connection, assuming angles made of ASTM A36 steel material.

Figure 7.50 compares the proposed equation for estimating the plastic rotational capacity of single angle connections with those suggested for shear tab (chapter 5) and WT (chapter 6) connections for two to six bolts. It is noted that the equations shown in Figure 7.50 are all based on the assumption that failure happens in the steel connection element and not in the bolts because the bolt shear failure mode should be avoided by design. As such, the equation for shear tabs is modified slightly from the one given in chapter 5 to discount the three cases that failed by bolt shear failure (i.e., cases 4, 11, and 18 in Table 5.7). As can be seen, the plastic rotational capacities of single angle connections are considerably higher than those of WT and shear tab connections of the same depth, although the slopes of all the curves are similar. The main reason for the high rotational capacities in the SA connections is the significant contribution of out-of-plane deformation of the angle outstanding leg, as discussed earlier in the chapter. Comparing the WT and shear tab connections, the shear tab possess less plastic rotational ductility than the WT connections due to out-of-plane deformation of the WT flange, although its contribution is significantly less than the one observed in the angle leg. As a result, single angle and shear tab connections are considered to be the most and least ductile connections in the column loss event, respectively, and the WT connection behaviour is somewhere in between, closer to shear tab connection.

7.9 Conclusion

In this chapter, interaction of shear, tension, and moment in single angle connections is investigated. The main source of ductility was out-of-plane

bending of the outstanding angle leg. Other sources of ductility, such as bolt hole bearing deformation, were not significant in the studied connections. The maximum rotation of single angle connections was between 0.23 and 0.16 radians for three to five bolt connections. The response curves can be used as input for single angle connection models in full-building progressive collapse analyses. Unlike the other two types of one-sided shear connections, the flexural and catenary phases of single angle connections are effectively independent from each other for all three depths of connections studied. Other conclusions that can be drawn are:

- It cannot be assumed that all of the fasteners in a line share equally in carrying the shear and tensile load. In fact, the fasteners towards the bottom of the joint carry the largest portion of the load. This unequal loading of the fasteners is accentuated as the rotation increases, similar to shear tab and WT connections.
- The point that the flexural phase domination ends and catenary force begins to provide the major resistance is named the “devolution point”. For 3SA connections, this point occurs at a large rotation and the flexural resistance of the connection is almost zero, whereas for 5SA connections, the devolution point is close to the rotation at which the peak moment occurs. The 4SA devolution point is somewhere between these two cases. The main reason for this difference in behaviour is the fact that in the 3-bolt angle connections the bottom and top bolts resist the moment through bearing resistance of the bolt–hole interaction. However, for the bottom bolt, due to the presence of out-of-plane deformation of the angle outstanding leg, the ductility demand shifts from the bolt hole regions of the web-framing leg to a combination of out-of-plane bending of the angle leg and yielding of the angle heel at the column face. Due to the inherent flexibility of the connection, it attempts to find another load path to take additional load until failure when the flexural resistance almost vanishes. In the 4SA and 5SA connections, due to the geometry of the connection the catenary action starts earlier but still during the

degrading branch of the flexural curve. After the devolution point, tension dominates the behaviour until failure occurs. Therefore, it can be inferred that the single angle connections fail mainly because of catenary action.

Table 7.1: Advantages and disadvantages of single-sided connections (Murray 2013)

Type of connection	Advantages	Disadvantages
Tee (WT)	<ul style="list-style-type: none"> • can be used in composite construction 	<ul style="list-style-type: none"> • stiffer than other types except shear tab • tee can be heavy
Shear tab	<ul style="list-style-type: none"> • simple – few parts • can be designed to resist axial force 	<ul style="list-style-type: none"> • stiffer than other types • requires careful design
Single angle	<ul style="list-style-type: none"> • eliminate erection problem¹ • fewer parts¹ 	<ul style="list-style-type: none"> • cannot resist axial load not recommended for laterally unbraced beams • larger angle and bolts required¹

¹: comparing with double angle connections.

Table 7.2: Typical material used for SA connections

Component	Material	Description
Angle	ASTM A36, 300W, 350W	-
Bolts	ASTM A325, A490	standard/slotted hole
Welds	E70XX electrode	fillet welds

Table 7.3: Summary of characteristic features of FE models of SA connections

No.	Specimen Label	Angle Type	Angle Section	Bolt Type	Bolt diameter	Remarks
1	3SA-3/8-3/4	ASTM A36	L152X89X9.5	ASTM A325	19.1 mm (3/4 in)	Used for verification
2	3SA-1/4-3/4	ASTM A36	L152X89X6.4	ASTM A325	19.1 mm (3/4 in)	-
3	3SA-1/2-3/4	ASTM A36	L152X89X13	ASTM A325	19.1 mm (3/4 in)	-
4	3SA-3/8-5/8	ASTM A36	L152X89X9.5	ASTM A325	15.9 mm (5/8 in)	-
5	3SA-3/8-7/8	ASTM A36	L152X89X9.5	ASTM A325	22.2 mm (7/8 in)	-
6	3SA-3/8-3/4-A490	ASTM A36	L152X89X9.5	ASTM A490	19.1 mm (3/4 in)	-
7	4SA-3/8-3/4	ASTM A36	L152X89X9.5	ASTM A325	19.1 mm (3/4 in)	-
8	4SA-1/4-3/4	ASTM A36	L152X89X6.4	ASTM A325	19.1 mm (3/4 in)	-
9	4SA-1/2-3/4	ASTM A36	L152X89X13	ASTM A325	19.1 mm (3/4 in)	-
10	4SA-3/8-5/8	ASTM A36	L152X89X9.5	ASTM A325	15.9 mm (5/8 in)	-
11	4SA-3/8-7/8	ASTM A36	L152X89X9.5	ASTM A325	22.2 mm (7/8 in)	-
12	4SA-3/8-3/4-A490	ASTM A36	L152X89X9.5	ASTM A490	19.1 mm (3/4 in)	-
13	5SA-3/8-3/4	ASTM A36	L152X89X9.5	ASTM A325	19.1 mm (3/4 in)	-
14	5SA-1/4-3/4	ASTM A36	L152X89X6.4	ASTM A325	19.1 mm (3/4 in)	-
15	5SA-1/2-3/4	ASTM A36	L152X89X13	ASTM A325	19.1 mm (3/4 in)	-
16	5SA-3/8-5/8	ASTM A36	L152X89X9.5	ASTM A325	15.9 mm (5/8 in)	-
17	5SA-3/8-7/8	ASTM A36	L152X89X9.5	ASTM A325	22.2 mm (7/8 in)	-
18	5SA-3/8-3/4-A490	ASTM A36	L152X89X9.5	ASTM A490	19.1 mm (3/4 in)	-

Table 7.4: Summary of numerical responses of single angle connections at initial failure

No.	Specimen/Model Label	Connection Depth (mm)	Rotation (Rad)	V (kN)	T (kN)	M (kN.m)	Failure Mode
1	3SA-3/8-3/4	152.4	0.222	32.2	151.0	Negligible	SA bottom hole rupture
2	3SA-1/4-3/4	152.4	0.230	18.7	83.1	Negligible	SA bottom hole rupture
3	3SA-1/2-3/4	152.4	0.224	44.3	244.8	Negligible	SA bottom hole rupture
4	3SA-3/8-5/8	152.4	0.215	26.9	131.9	Negligible	SA bottom hole rupture
5	3SA-3/8-7/8	152.4	0.217	33.6	159.8	Negligible	SA bottom hole rupture
6	3SA-3/8-3/4-A490	152.4	0.213	32.8	152.7	Negligible	SA bottom hole rupture
7	4SA-3/8-3/4	228.6	0.193	34.9	179.2	1.4	SA bottom hole rupture
8	4SA-1/4-3/4	228.6	0.197	20.7	97.5	1.3	SA bottom hole rupture
9	4SA-1/2-3/4	228.6	0.196	55.6	270.4	2.8	SA bottom hole rupture
10	4SA-3/8-5/8	228.6	0.193	34.1	167.2	1.2	SA bottom hole rupture
11	4SA-3/8-7/8	228.6	0.189	35.7	186.8	2.1	SA bottom hole rupture
12	4SA-3/8-3/4-A490	228.6	0.185	36.9	178.5	1.5	SA bottom hole rupture
13	5SA-3/8-3/4	304.8	0.169	39.4	184.3	16.6	SA bottom hole rupture
14	5SA-1/4-3/4	304.8	0.171	22.2	107.1	8.7	SA bottom hole rupture
15	5SA-1/2-3/4	304.8	0.177	64.9	286.4	24.2	SA bottom hole rupture
16	5SA-3/8-5/8	304.8	0.168	37.2	170.0	15.5	SA bottom hole rupture
17	5SA-3/8-7/8	304.8	0.165	43.0	196.2	17.6	SA bottom hole rupture
18	5SA-3/8-3/4-A490	304.8	0.162	41.4	183.7	16.7	SA bottom hole rupture

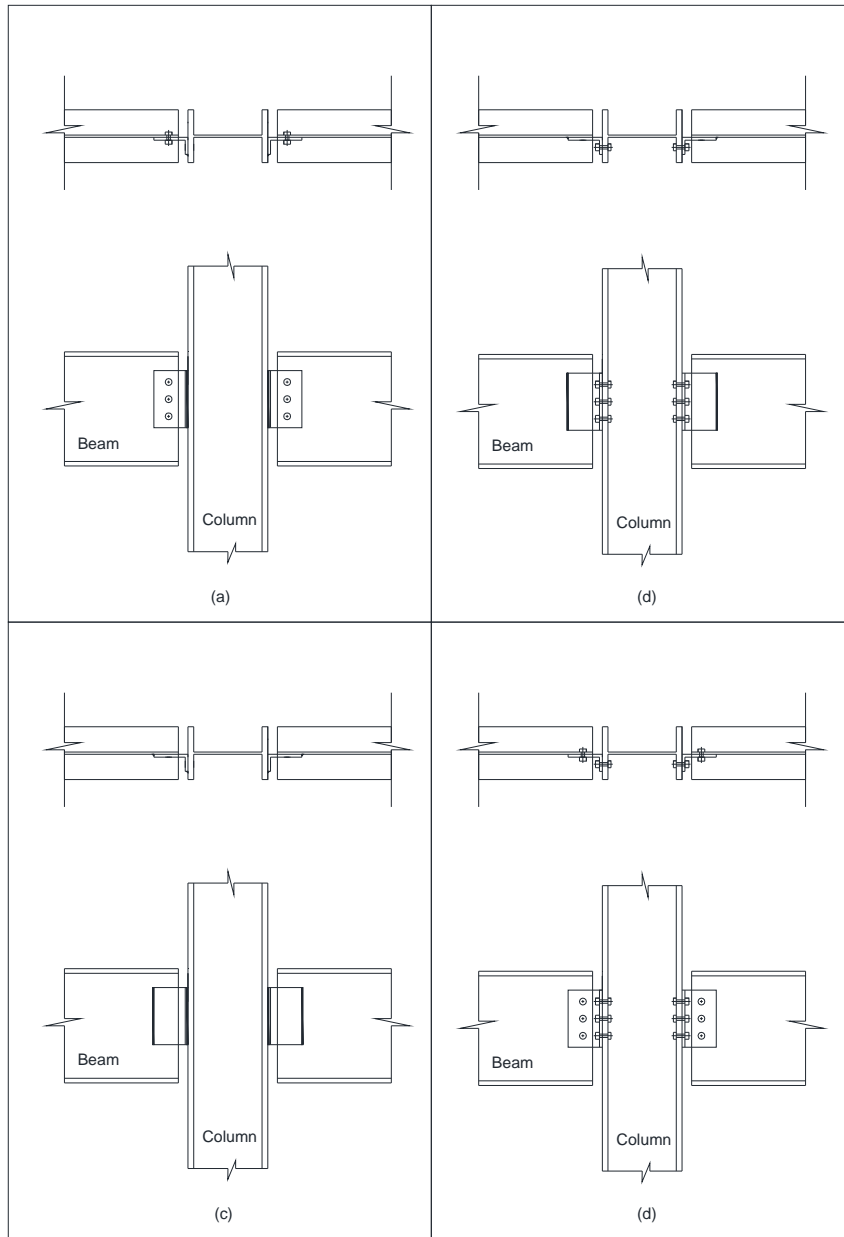


Figure 7.1: Types of SA shear connections: (a) welded-bolted (b) bolted-welded (c) welded-welded (d) bolted-bolted

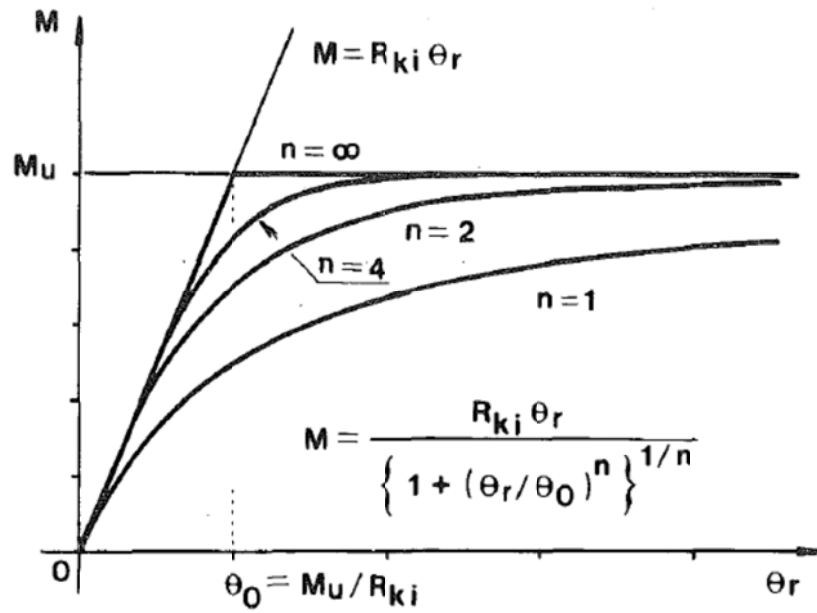


Figure 7.2: Elastic-perfectly plastic moment-rotation curves (Kishi and Chen 1990)

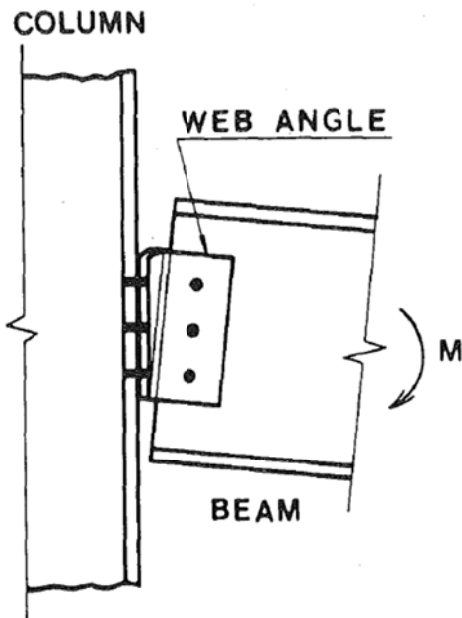


Figure 7.3: General deformation pattern of single angle connection (Kishi and Chen 1990)

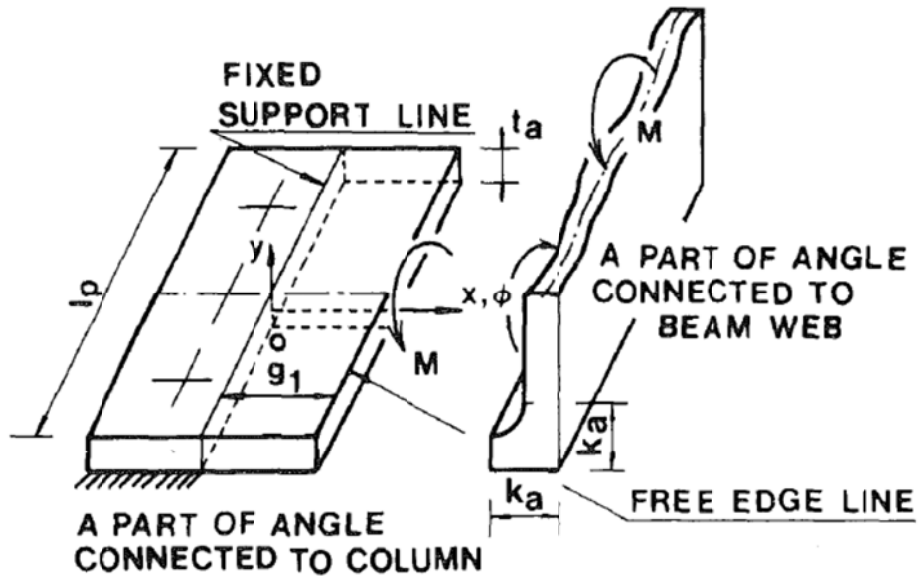


Figure 7.4: Modelling of angle performed by Kishi and Chen (1990)

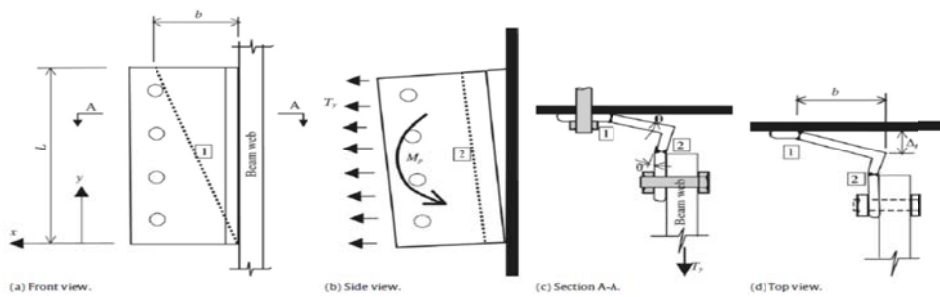


Figure 7.5: Application of yield line theory for single angle connection (Gong 2009)

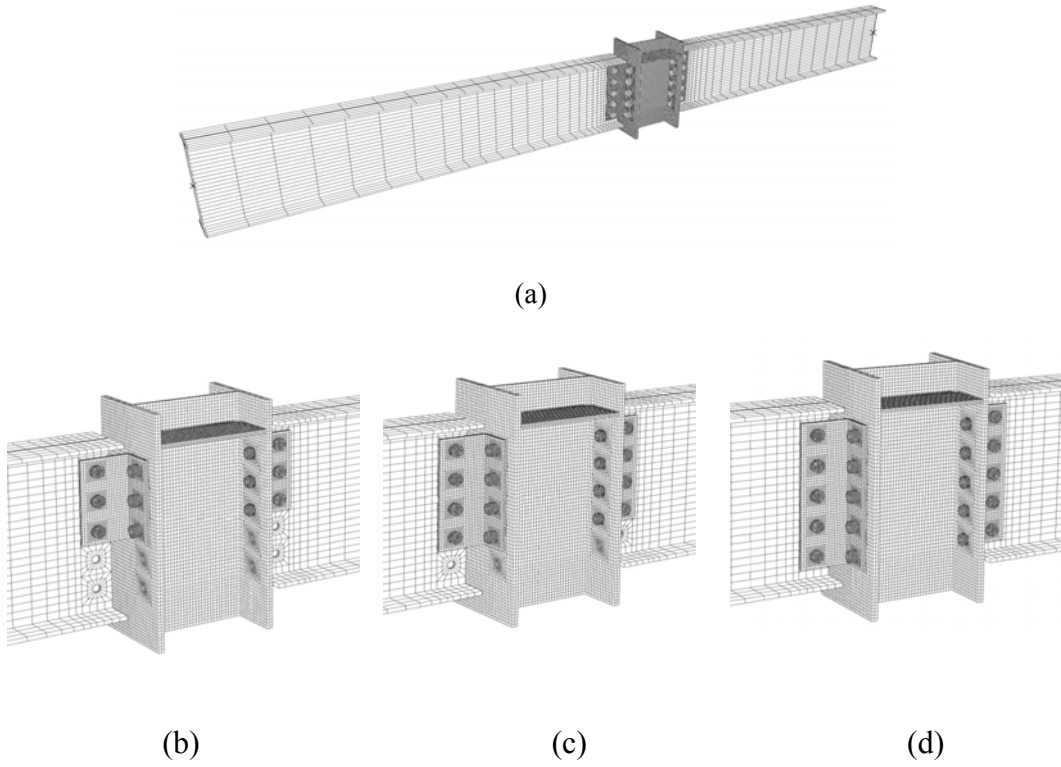


Figure 7.6: Finite element models of: (a) full connection assembly, (b) three bolt single angle connection (3SA), (c) four bolt single angle connection (4SA), (d) five bolt single angle connection (5SA)

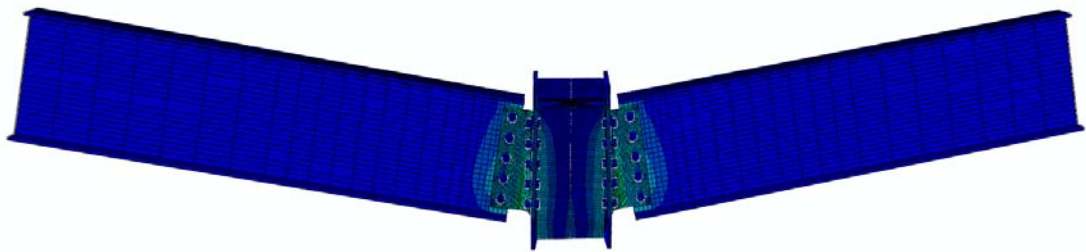


Figure 7.7: Deformed shape of finite element connection assembly

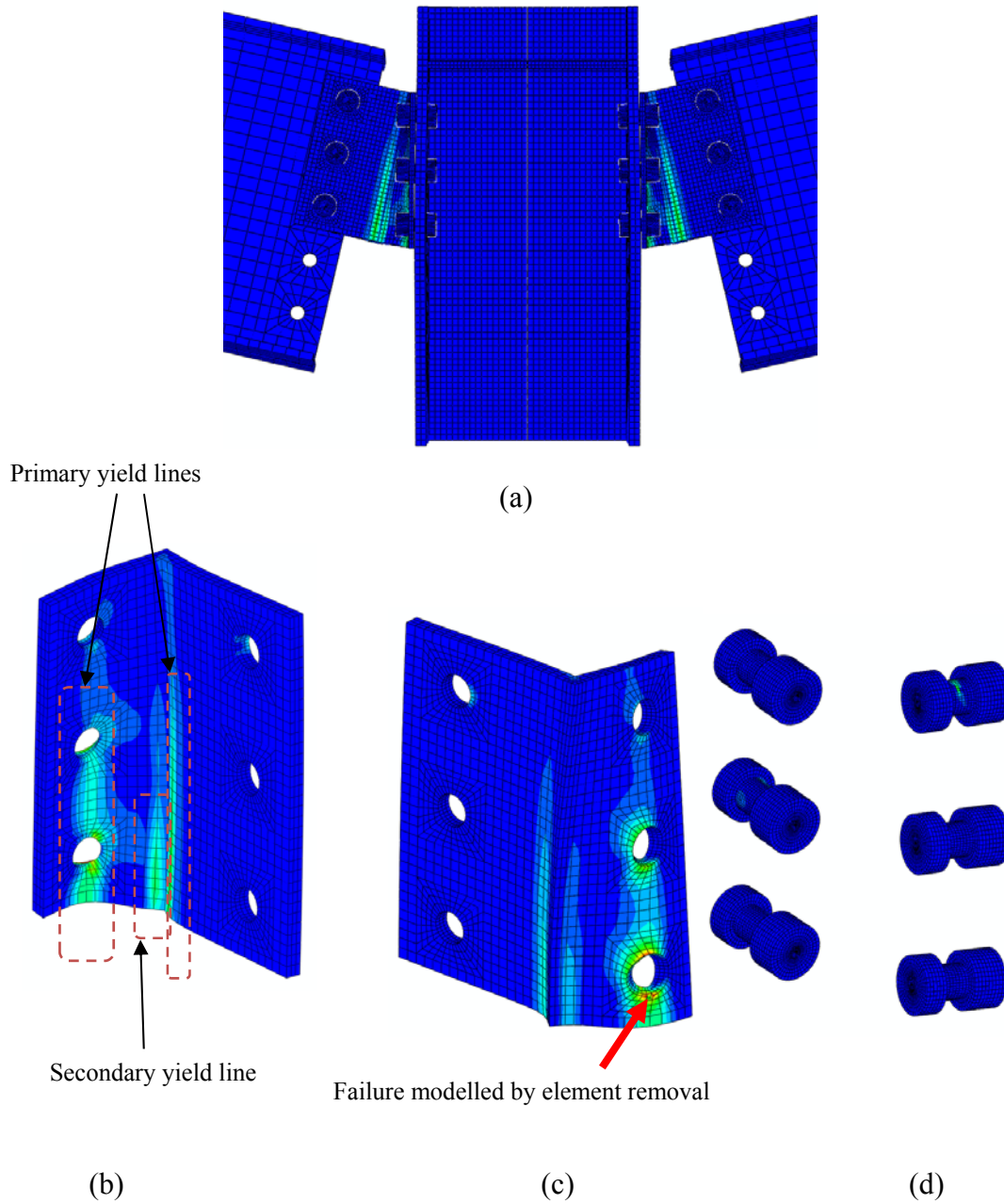


Figure 7.8: Failure of 3SA, numerical results: (a) deformed shape of connection assembly, (b) angle deformed shape – front view, (c) failure initiation – back view, (d) bolt shear deformation

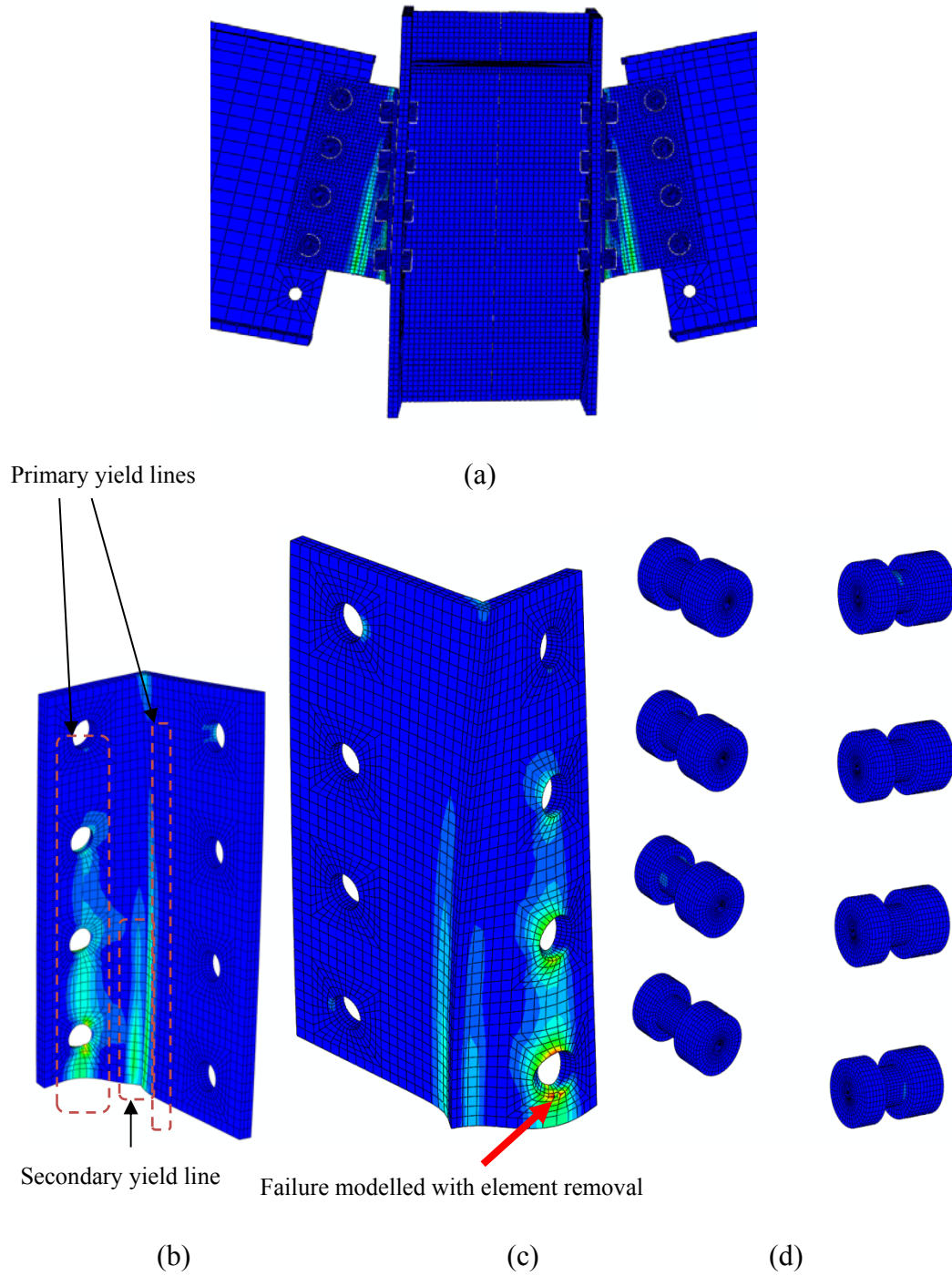


Figure 7.9: Failure of 4SA, numerical results: (a) deformed shape of connection assembly, (b) angle deformed shape – front view, (c) failure initiation – back view, (d) bolt shear deformation

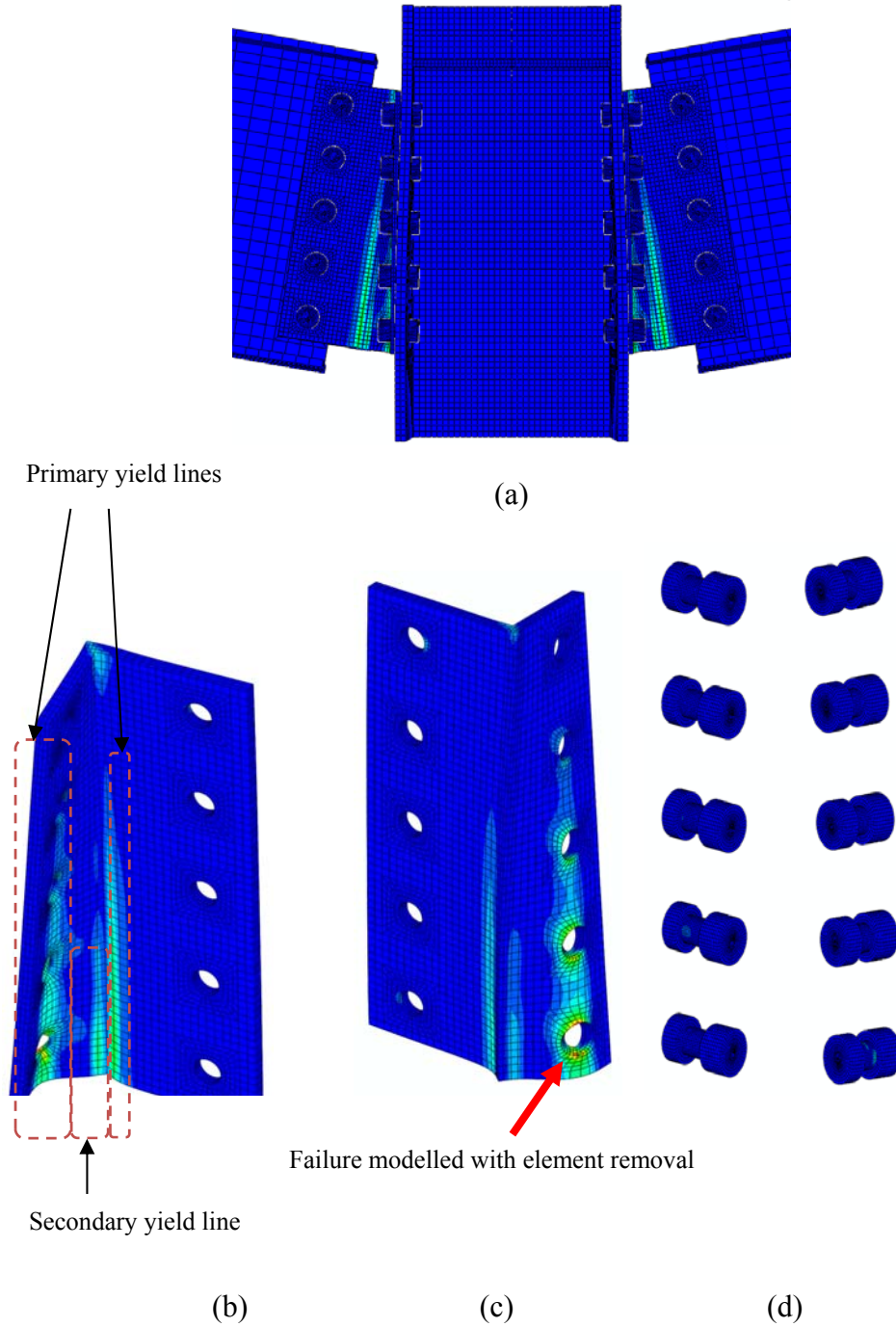


Figure 7.10: Failure of 5SA, numerical results: (a) deformed shape of connection assembly, (b) angle deformed shape – front view, (c) failure initiation – back view, (d) bolt shear deformation

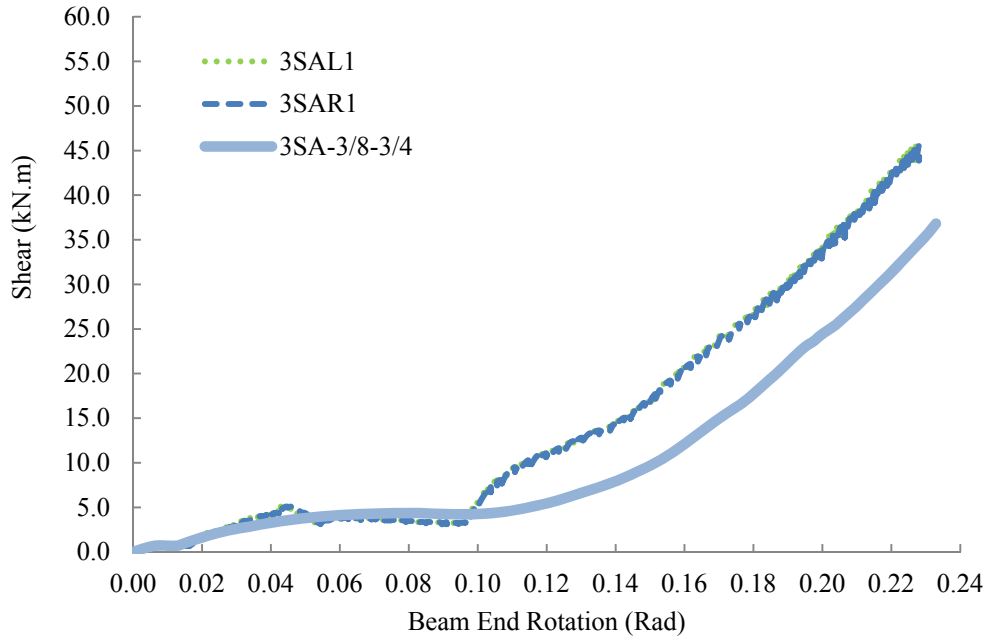


Figure 7.11: Comparison of numerical and experimental shear response of connection 3SA

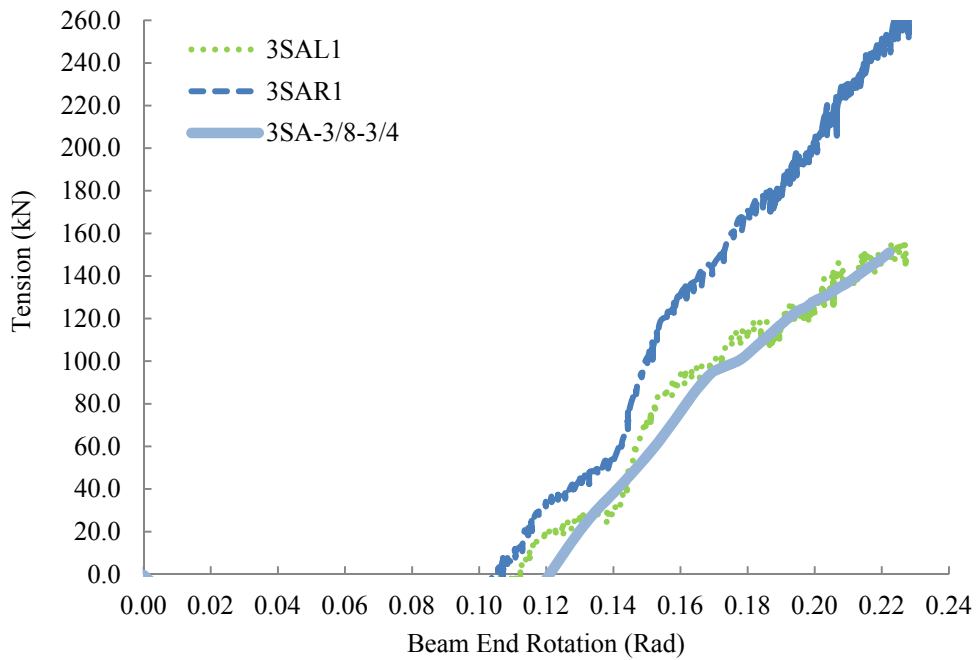


Figure 7.12: Comparison of numerical and experimental tensile response of connection 3SA

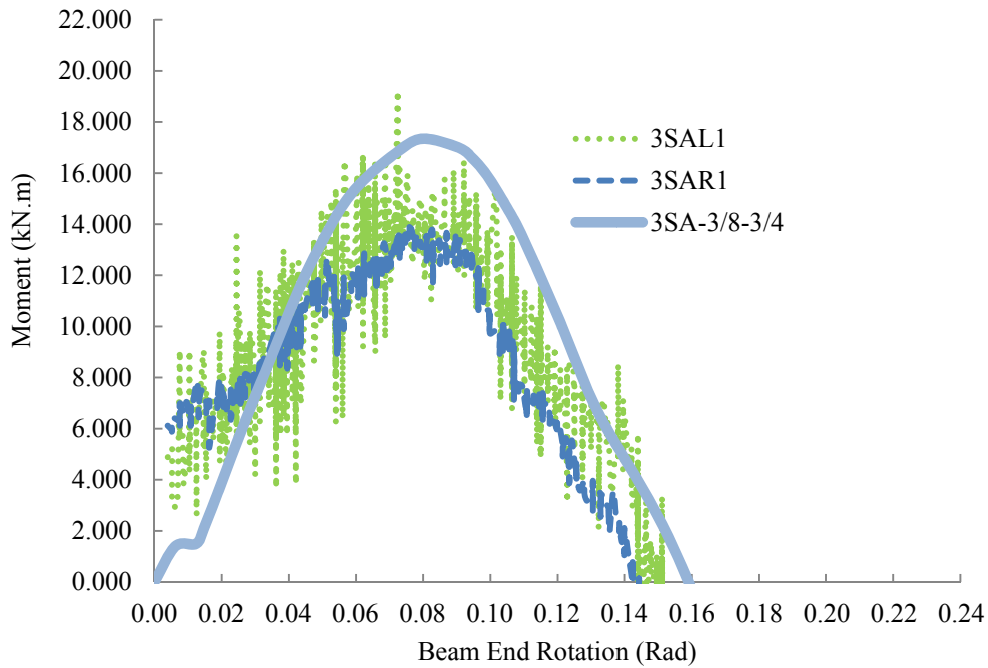


Figure 7.13: Comparison of numerical and experimental flexural response of connection 3SA

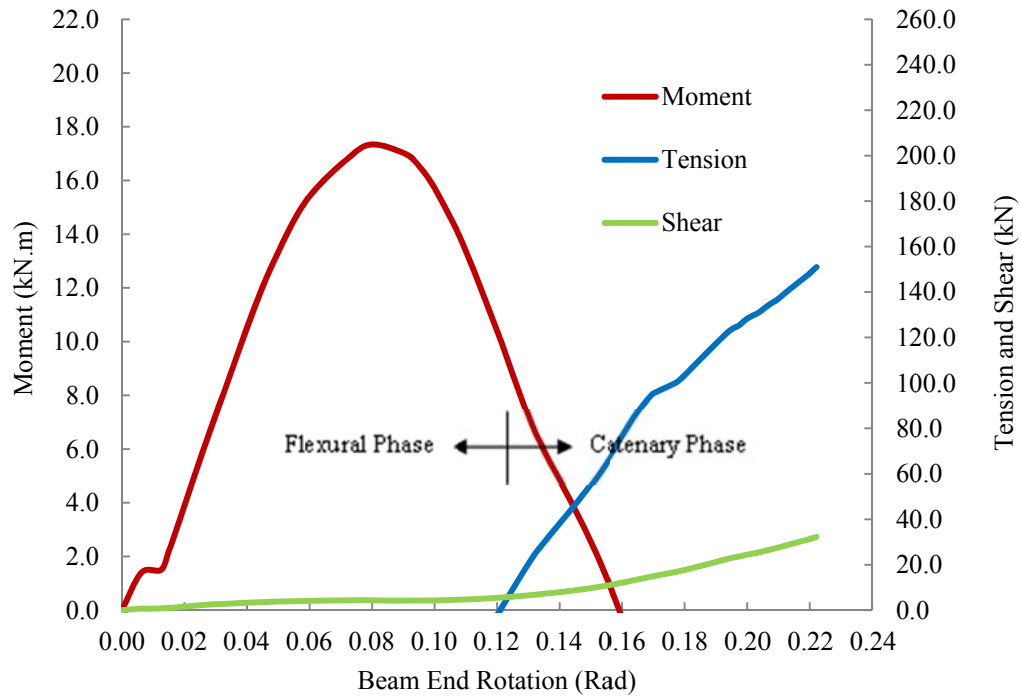


Figure 7.14: Bolt line forces versus beam end rotation – Specimen 3SA-3/8-3/4

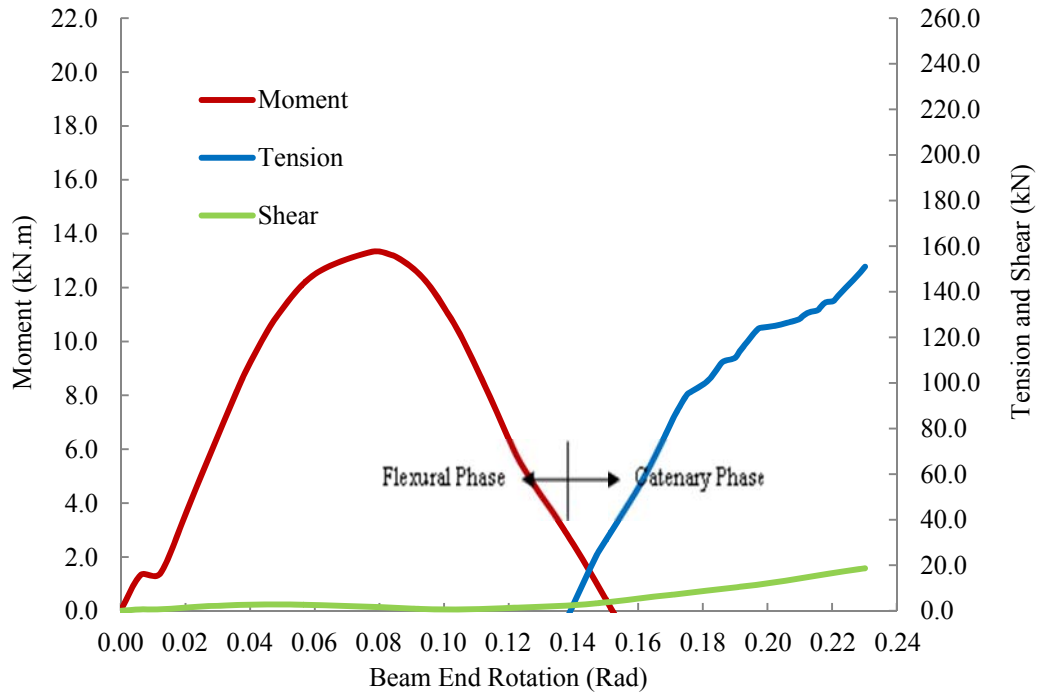


Figure 7.15: Bolt line forces versus beam end rotation – Specimen 3SA-1/4-3/4

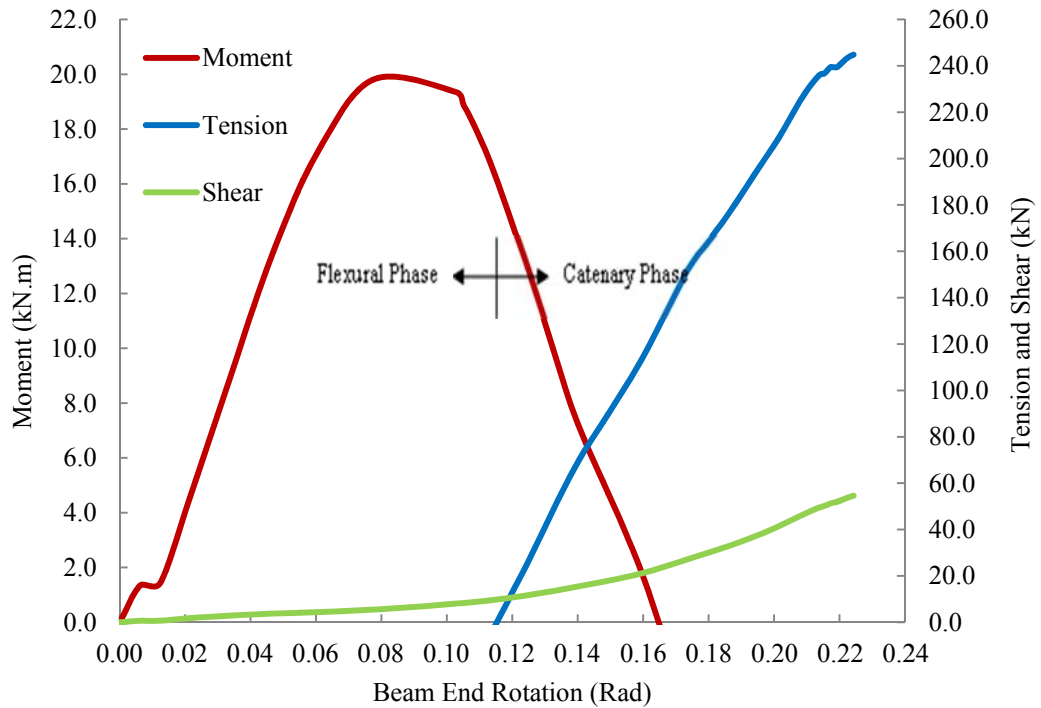


Figure 7.16: Bolt line forces versus beam end rotation – Specimen 3SA-1/2-3/4

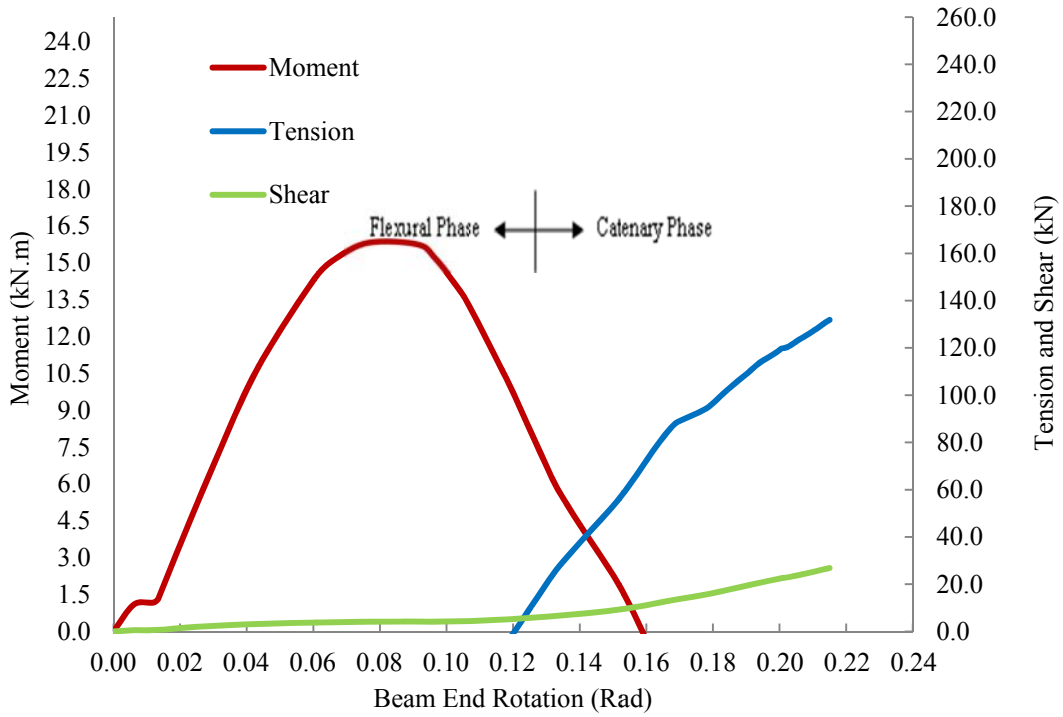


Figure 7.17: Bolt line forces versus beam end rotation – Specimen 3SA-3/8-5/8

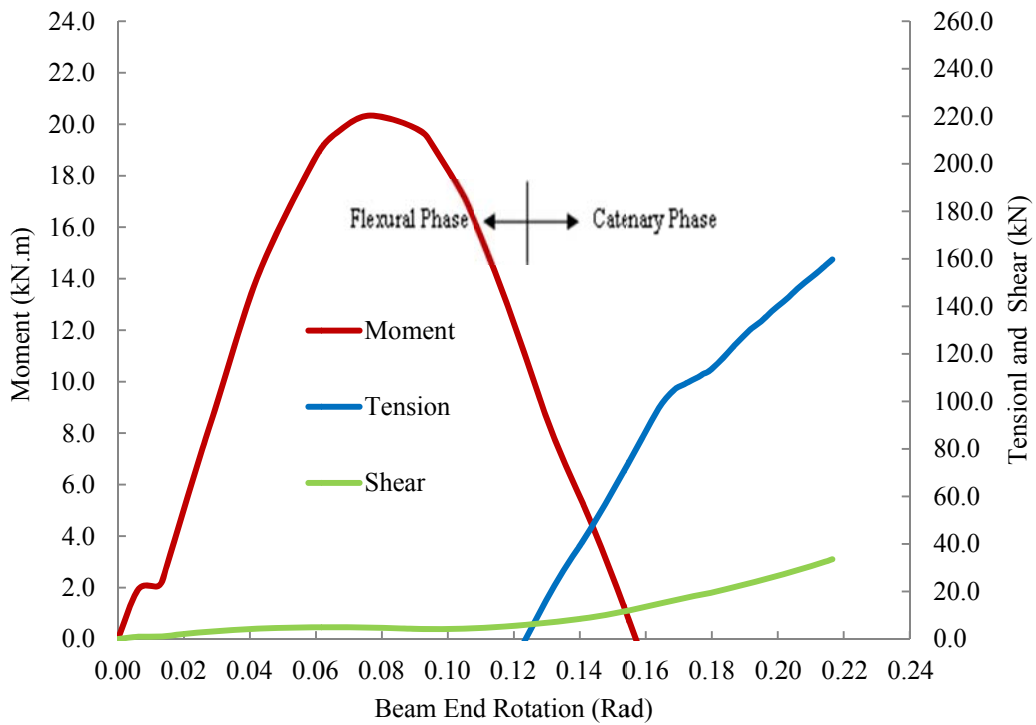


Figure 7.18: Bolt line forces versus beam end rotation – Specimen 3SA-3/8-7/8

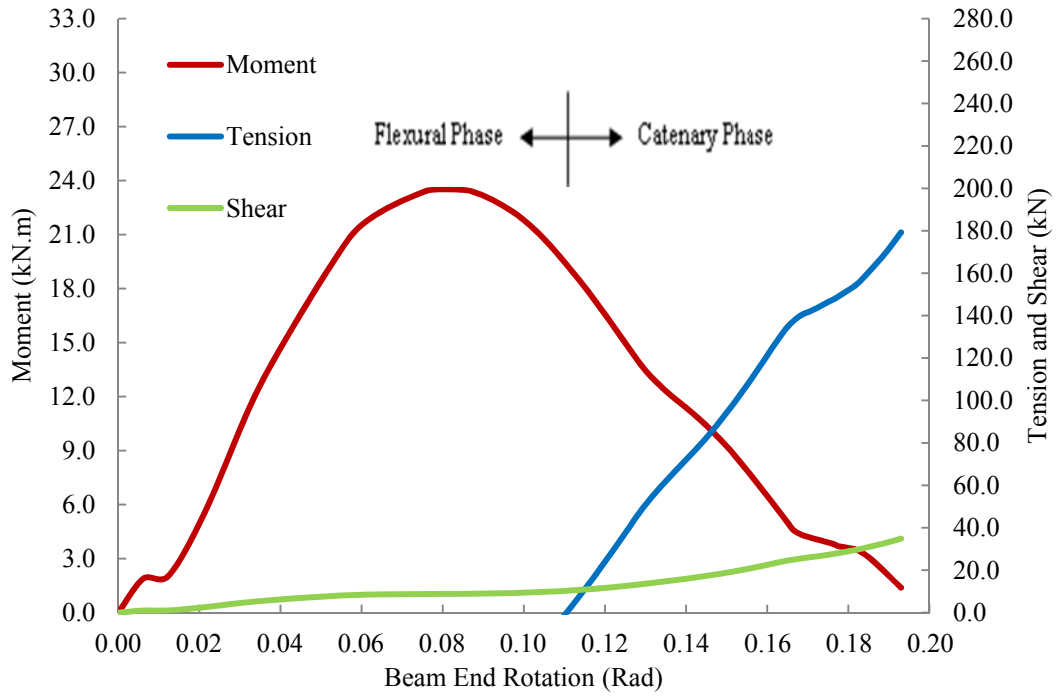


Figure 7.19: Bolt line forces versus beam end rotation – Specimen 4SA-3/8-3/4

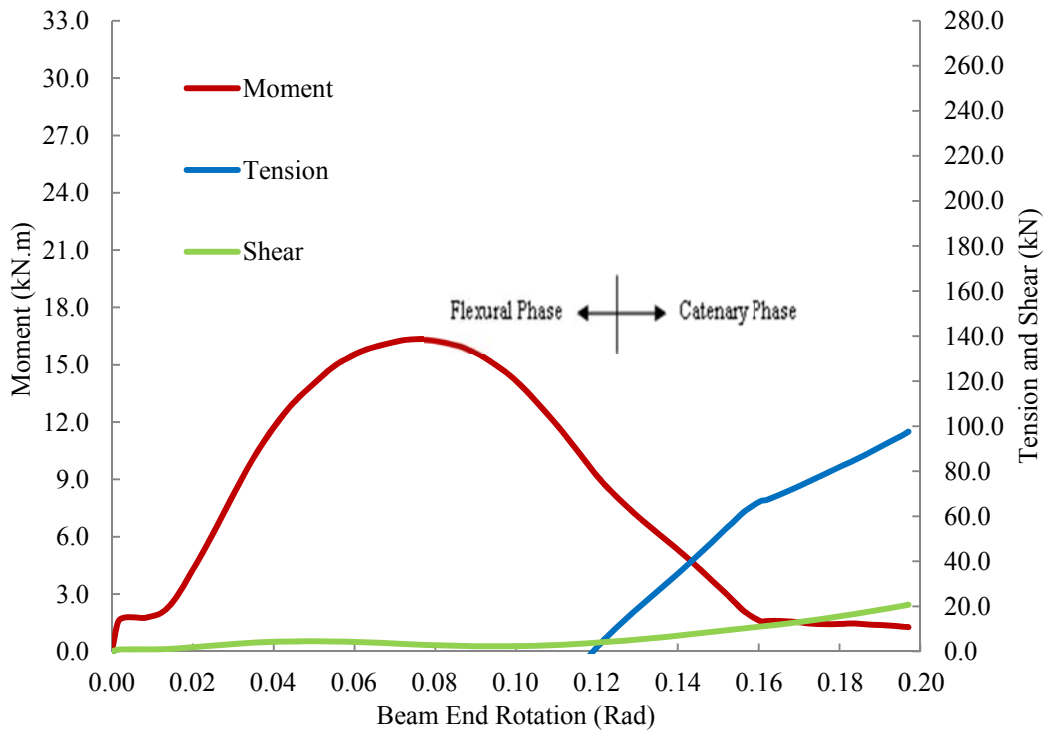


Figure 7.20: Bolt line forces versus beam end rotation – Specimen 4SA-1/4-3/4

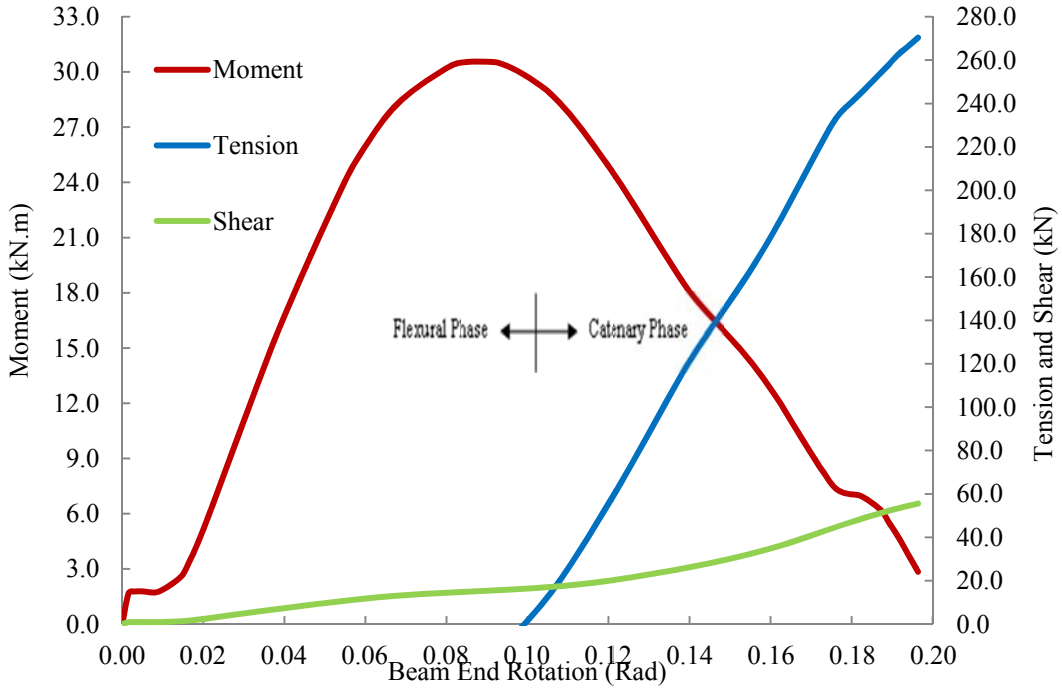


Figure 7.21: Bolt line forces versus beam end rotation – Specimen 4SA-1/2-3/4

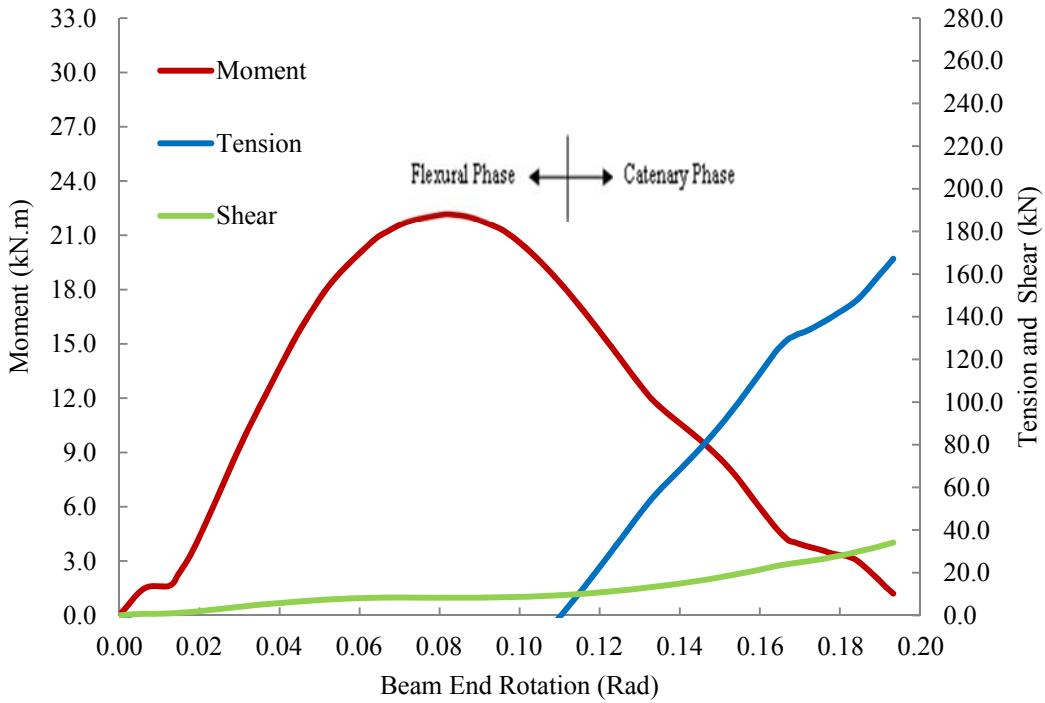


Figure 7.22: Bolt line forces versus beam end rotation – Specimen 4SA-3/8-5/8

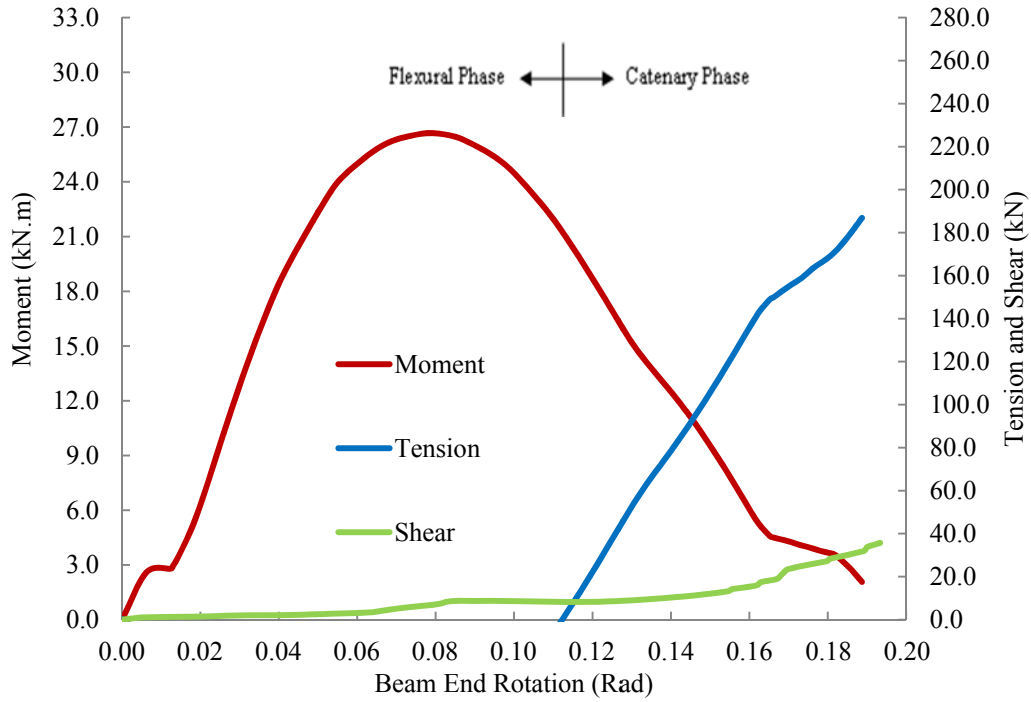


Figure 7.23: Bolt line forces versus beam end rotation – Specimen 4SA-3/8-7/8

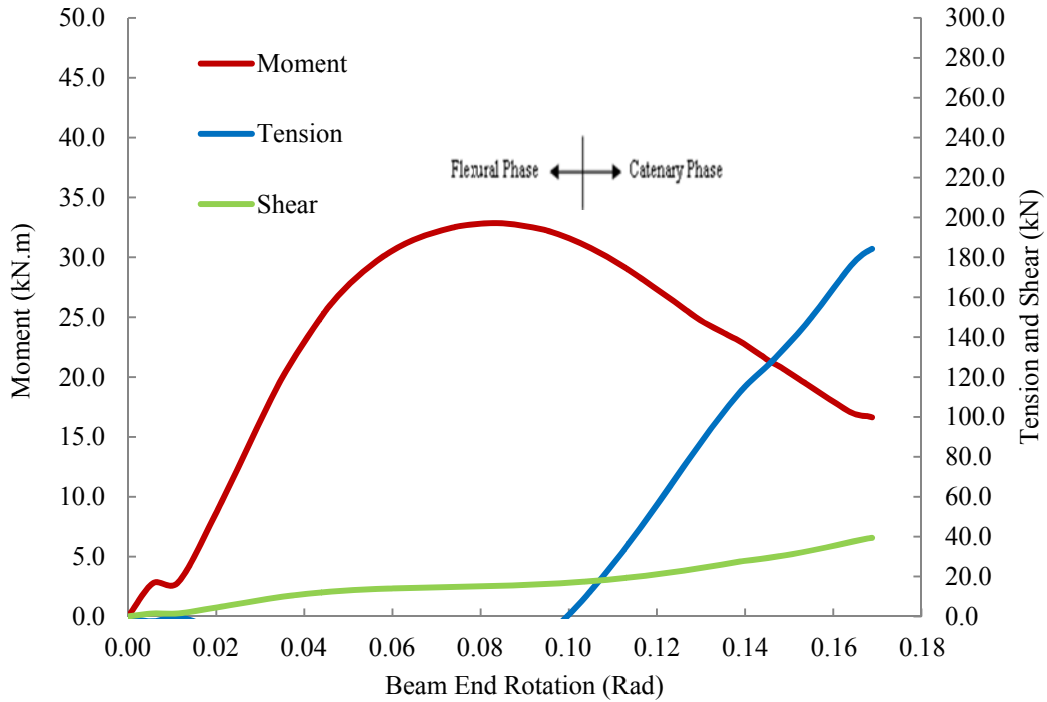


Figure 7.24: Bolt line forces versus beam end rotation – Specimen 5SA-3/8-3/4

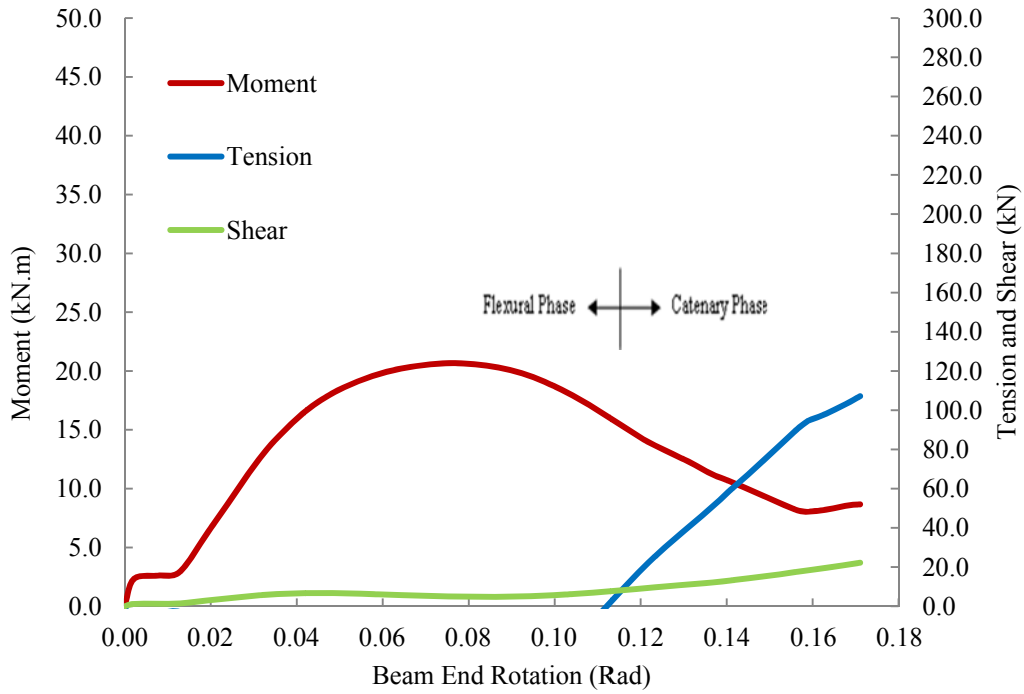


Figure 7.25: Bolt line forces versus beam end rotation – Specimen 5SA-1/4-3/4

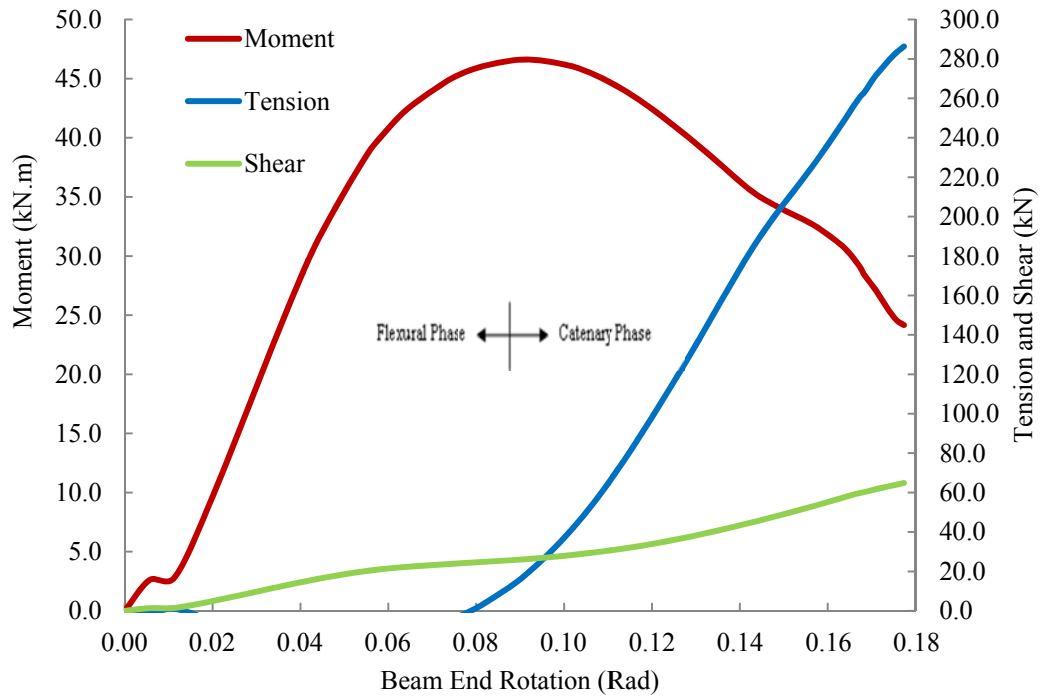


Figure 7.26: Bolt line forces versus beam end rotation – Specimen 5SA-1/2-3/4

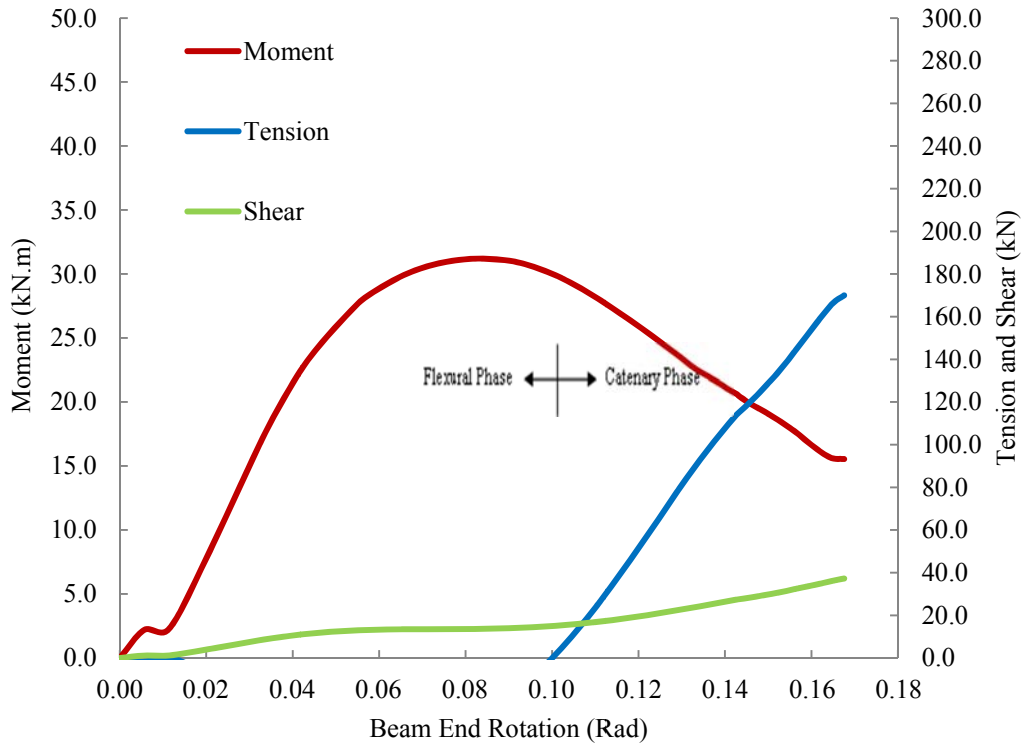


Figure 7.27: Bolt line forces versus beam end rotation – Specimen 5SA-3/8-5/8

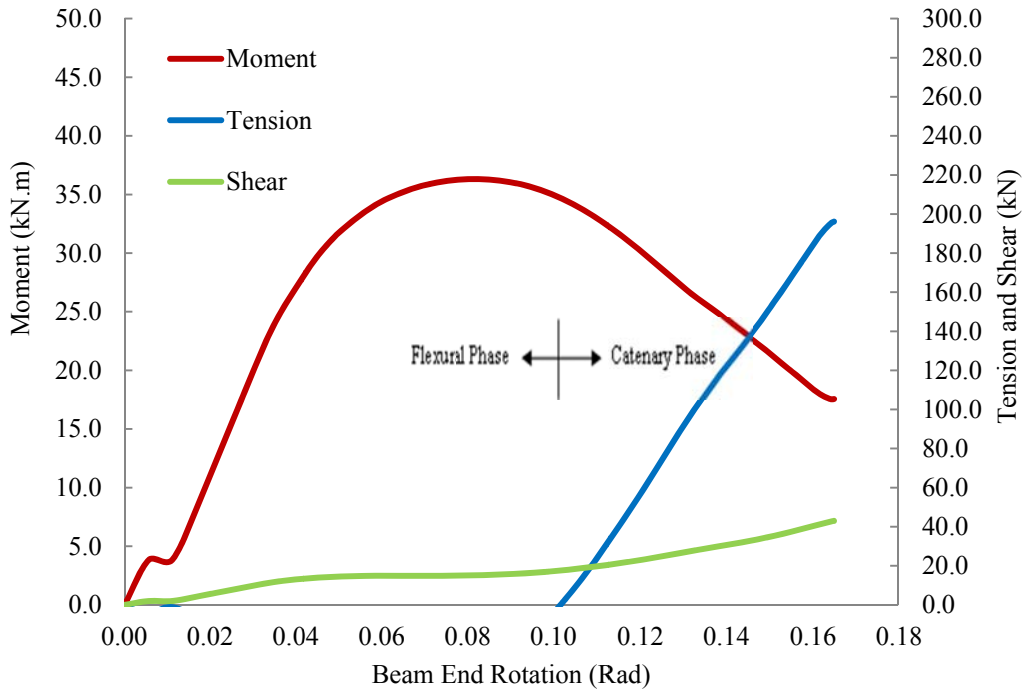


Figure 7.28: Bolt line forces versus beam end rotation – Specimen 5SA-3/8-7/8

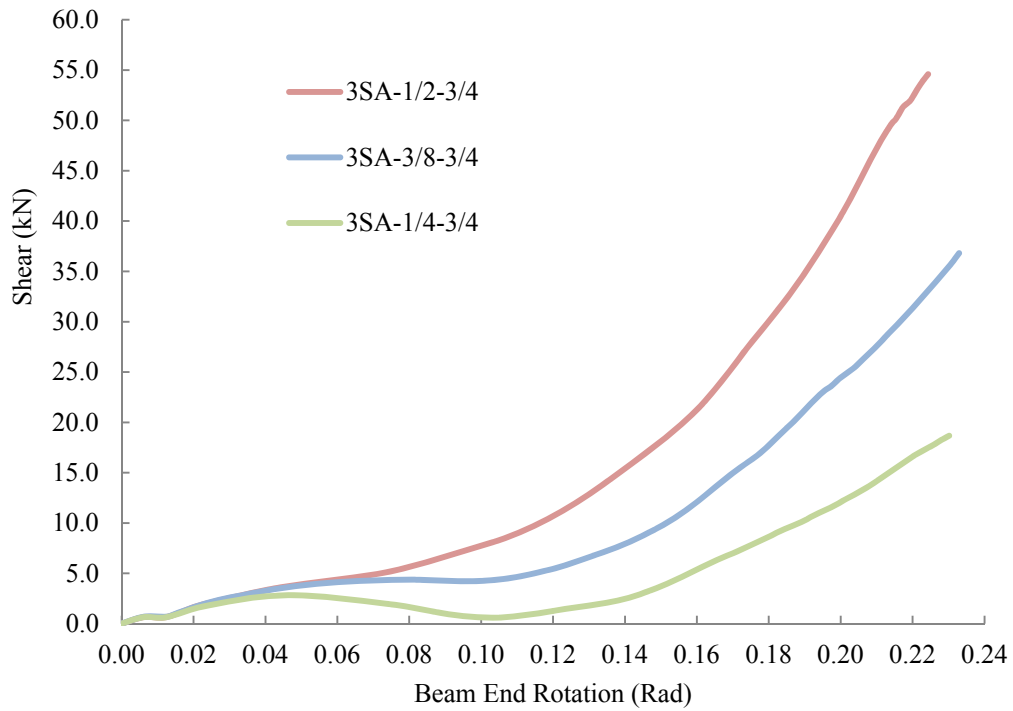


Figure 7.29: Comparison of shear response of 3SA connections with different angle thicknesses

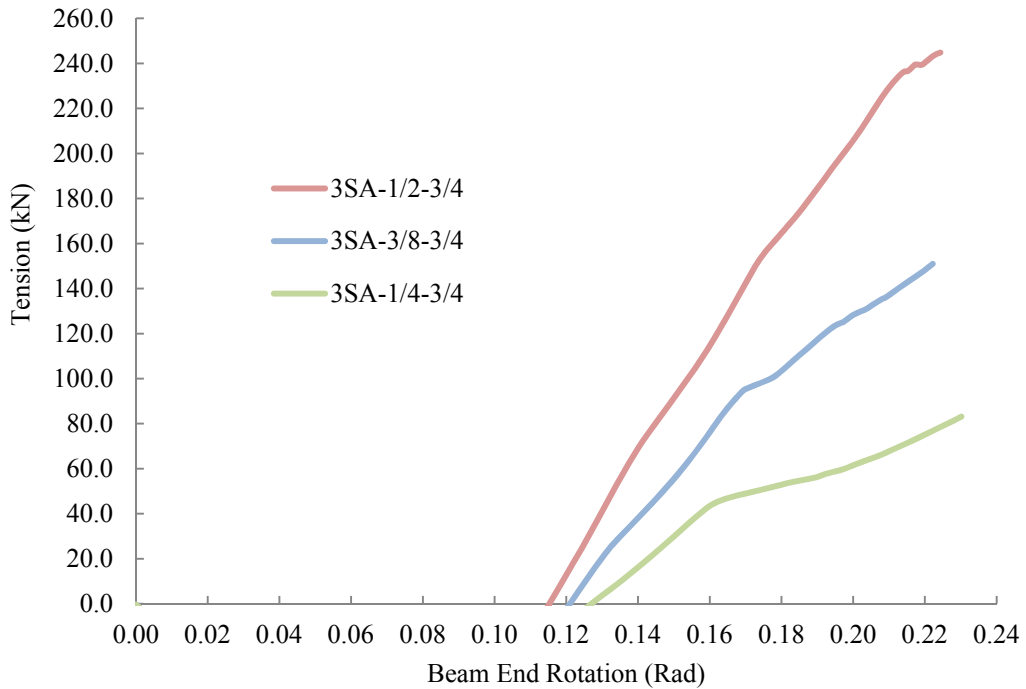


Figure 7.30: Comparison of tensile response of 3SA connections with different angle thicknesses

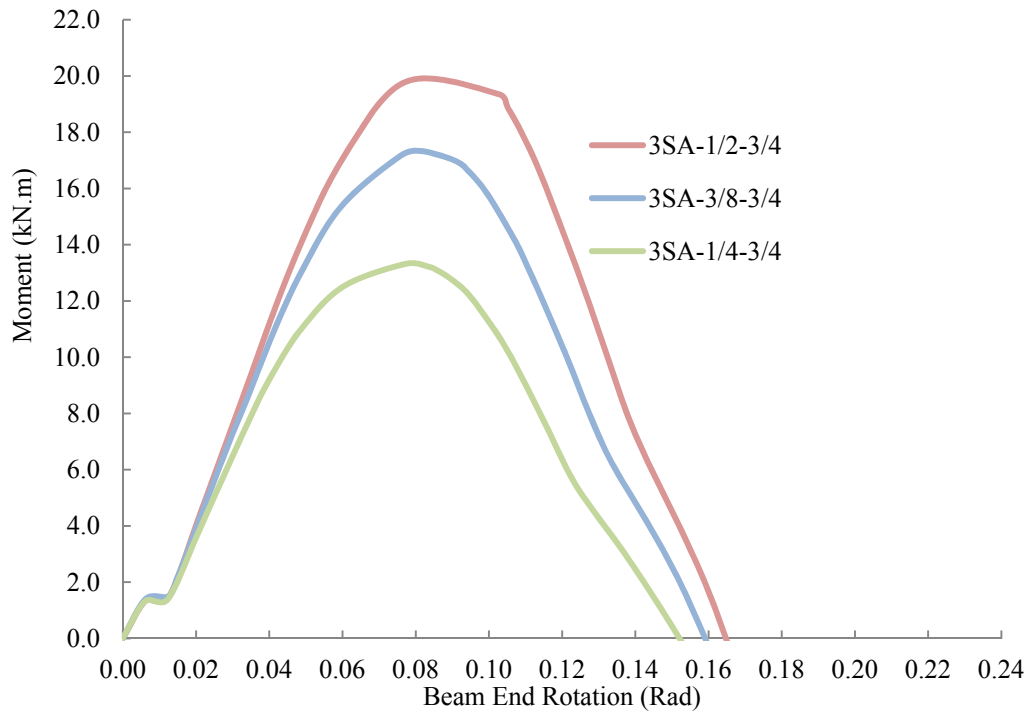


Figure 7.31: Comparison of flexural response of 3SA connections with different angle thicknesses

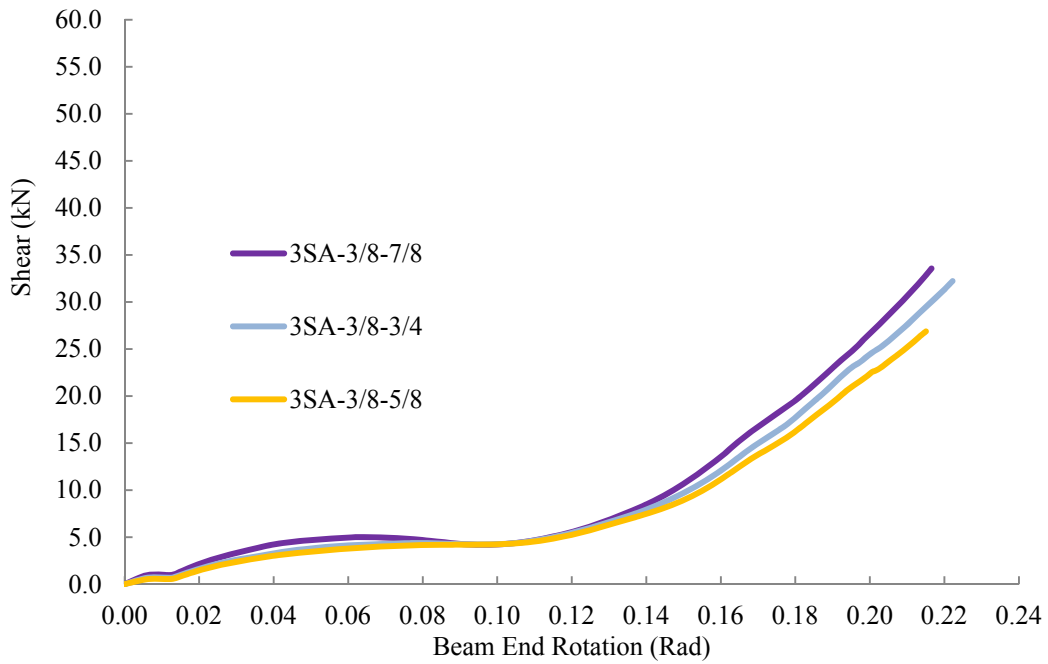


Figure 7.32: Comparison of shear response of 3SA connections with different bolt sizes

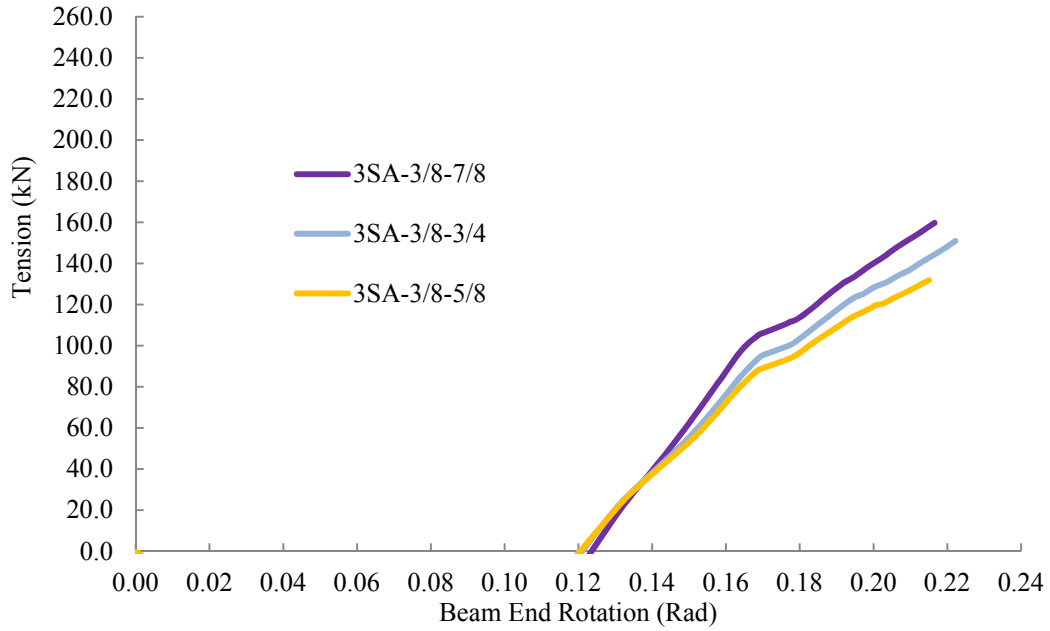


Figure 7.33: Comparison of tensile response of 3SA connections with different bolt sizes

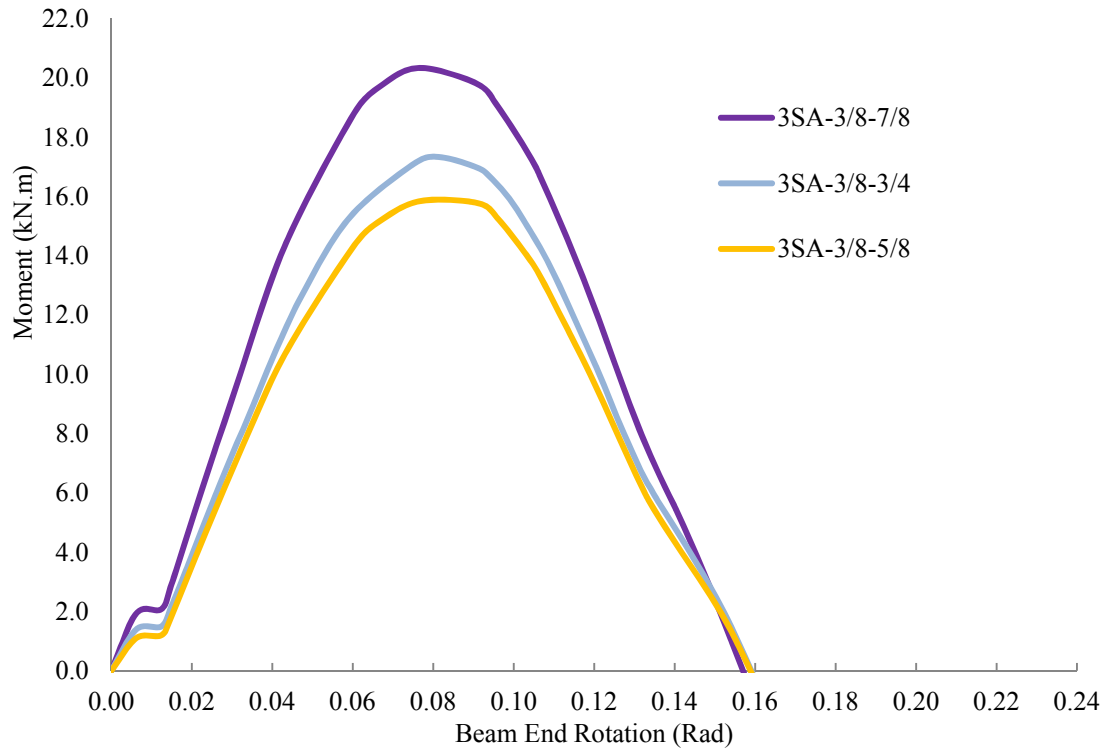


Figure 7.34: Comparison of tensile response of 3SA connections with different bolt sizes

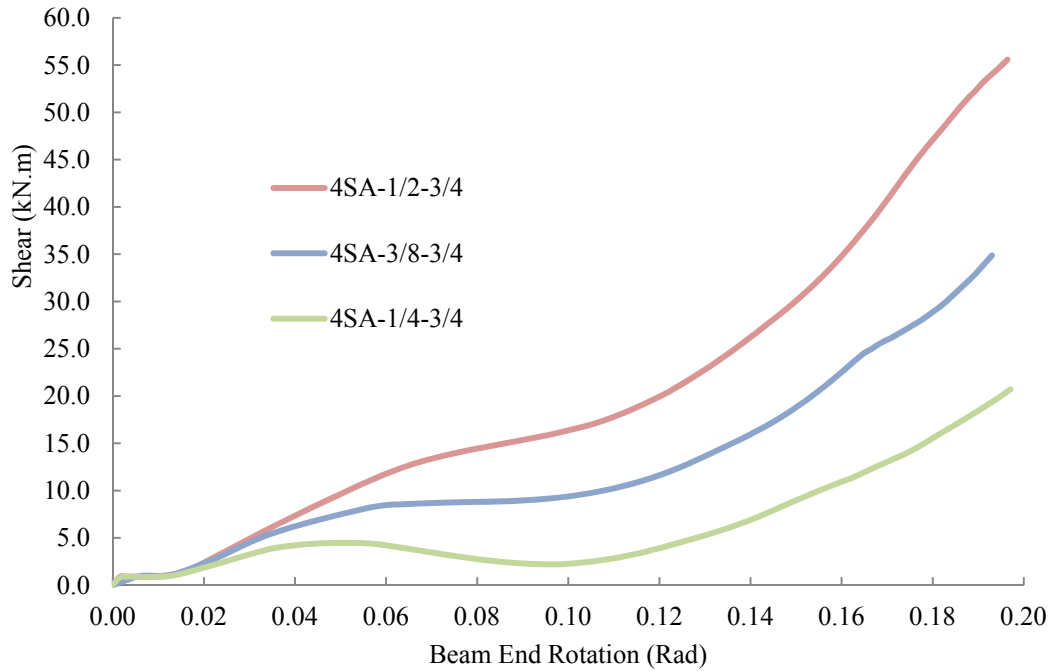


Figure 7.35: Comparison of shear response of 4SA connections with different angle thicknesses

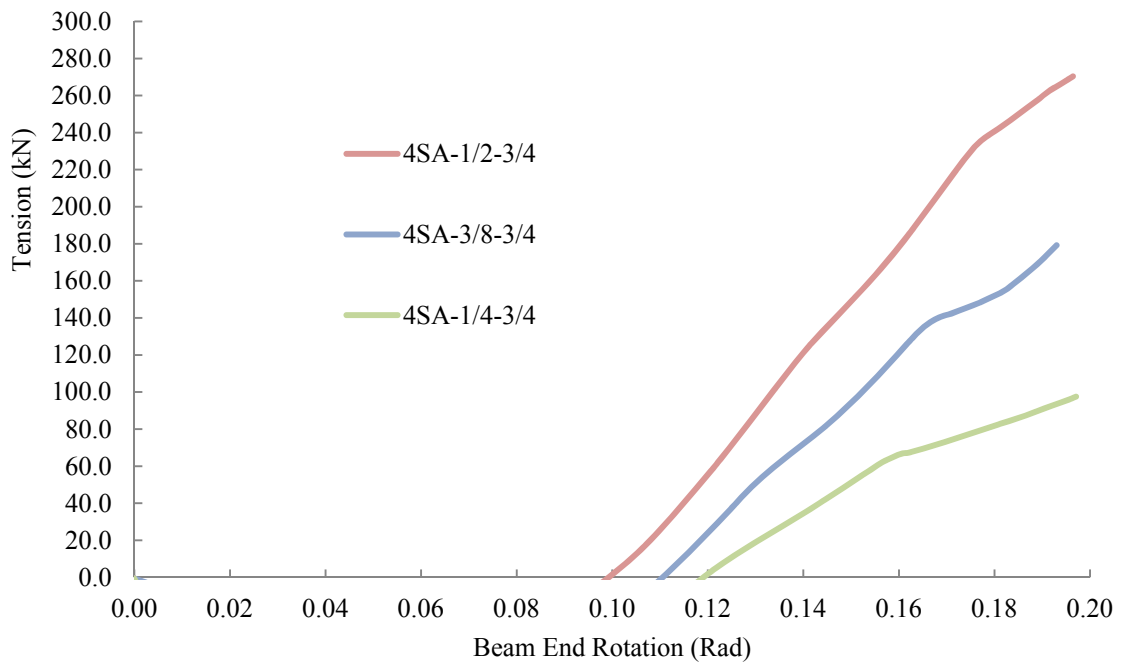


Figure 7.36: Comparison of tensile response of 4SA connections with different angle thicknesses

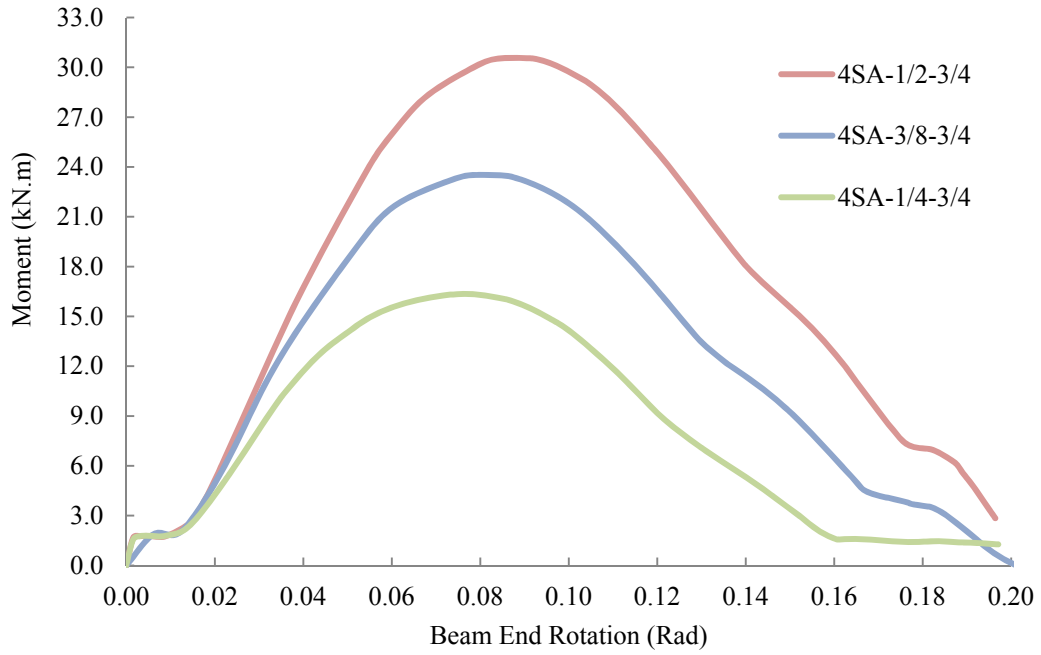


Figure 7.37: Comparison of flexural response of 4SA connections with different angle thicknesses

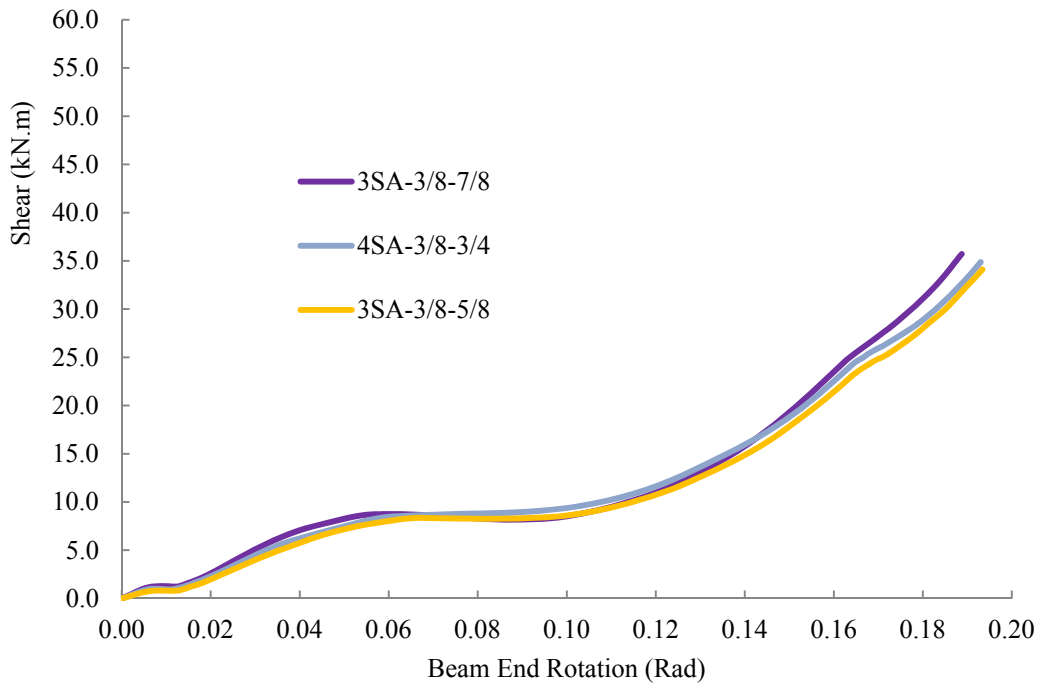


Figure 7.38: Comparison of shear response of 4SA connections with different bolt sizes

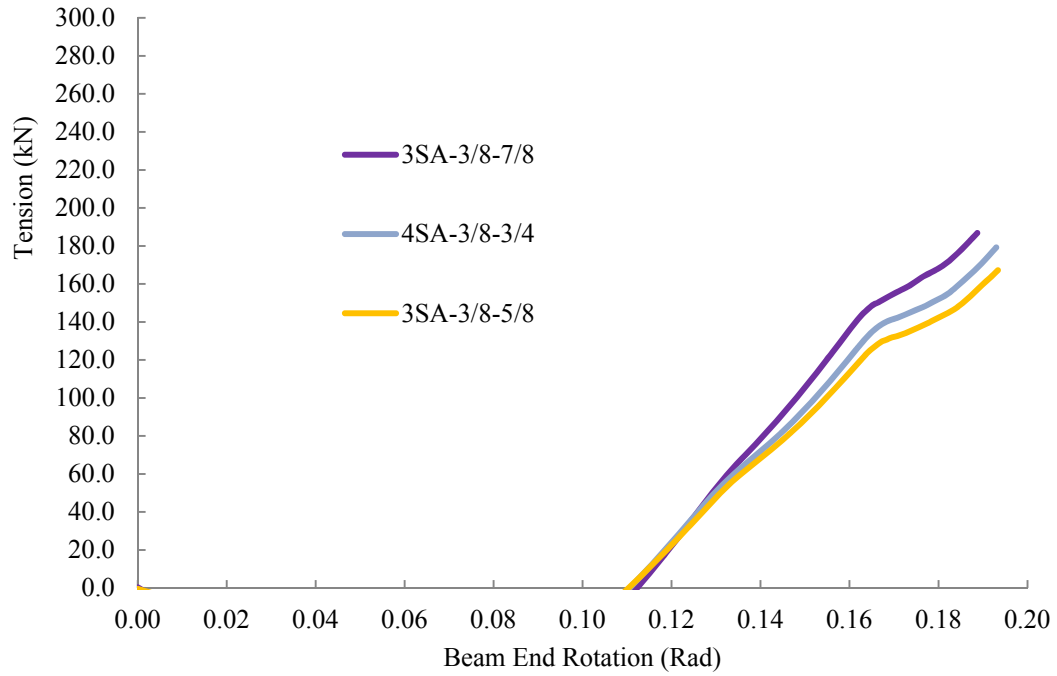


Figure 7.39: Comparison of tensile response of 4SA connections with different bolt sizes

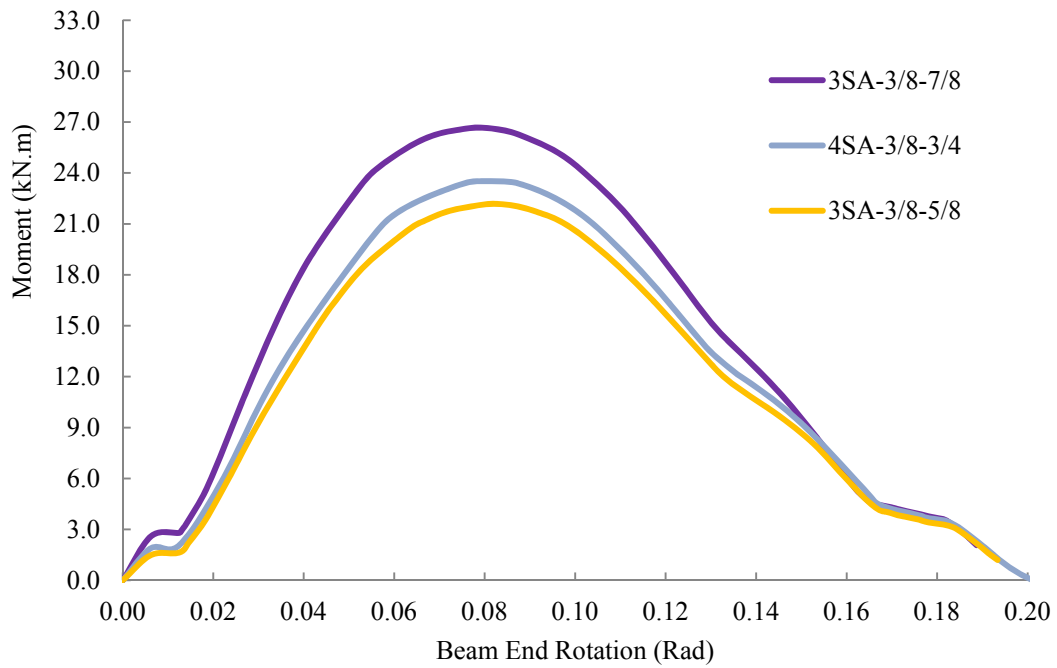


Figure 7.40: Comparison of flexural response of 4SA connections with different bolt sizes

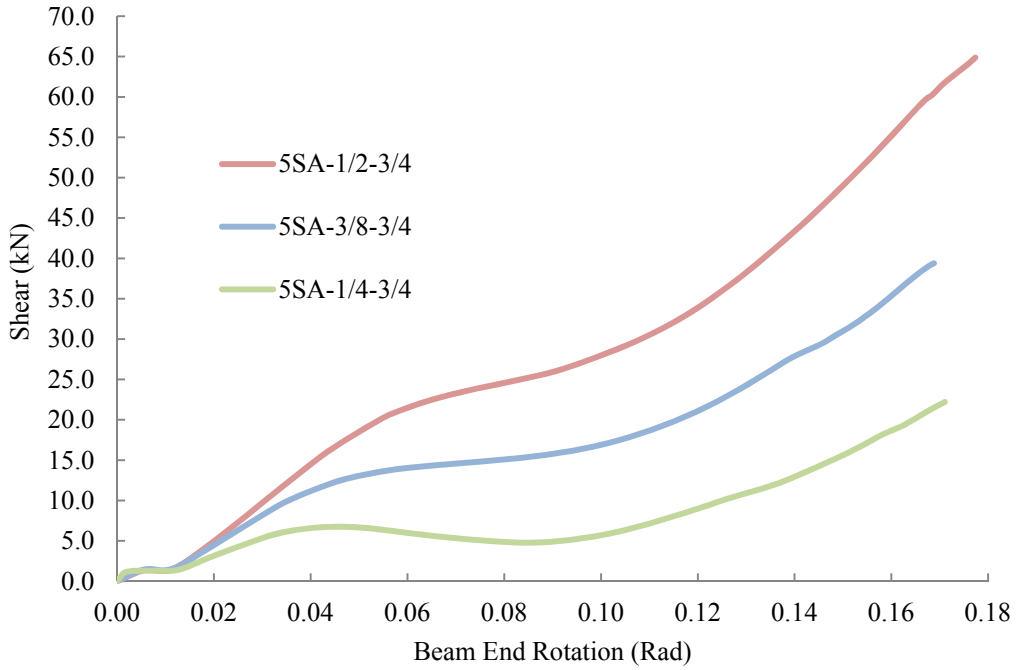


Figure 7.41: Comparison of shear response of 5SA connections with different angle thicknesses

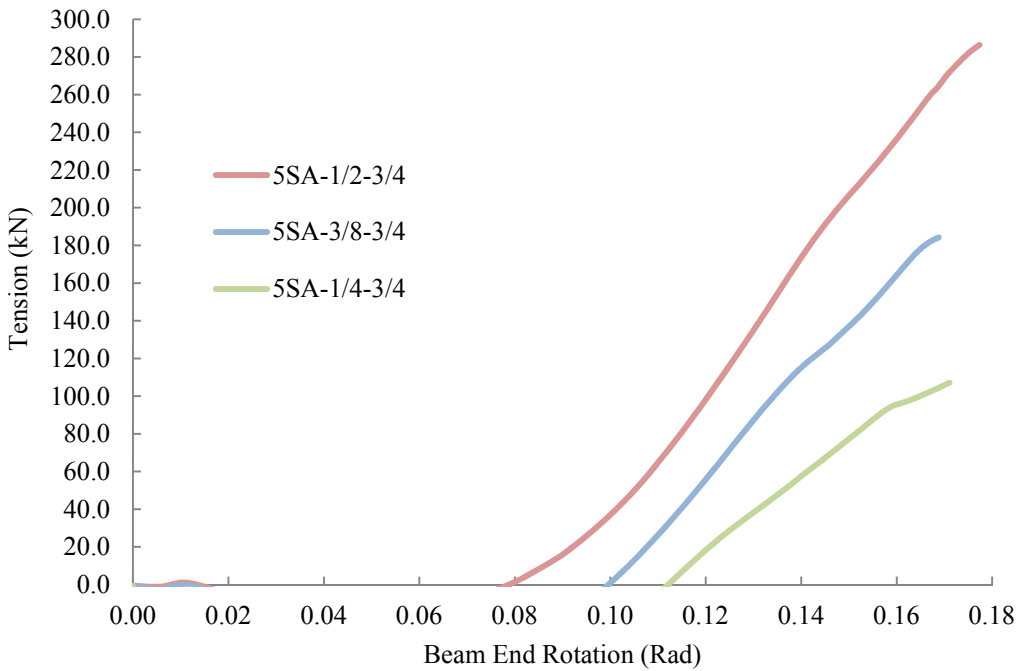


Figure 7.42: Comparison of tensile response of 5SA connections with different angle thicknesses

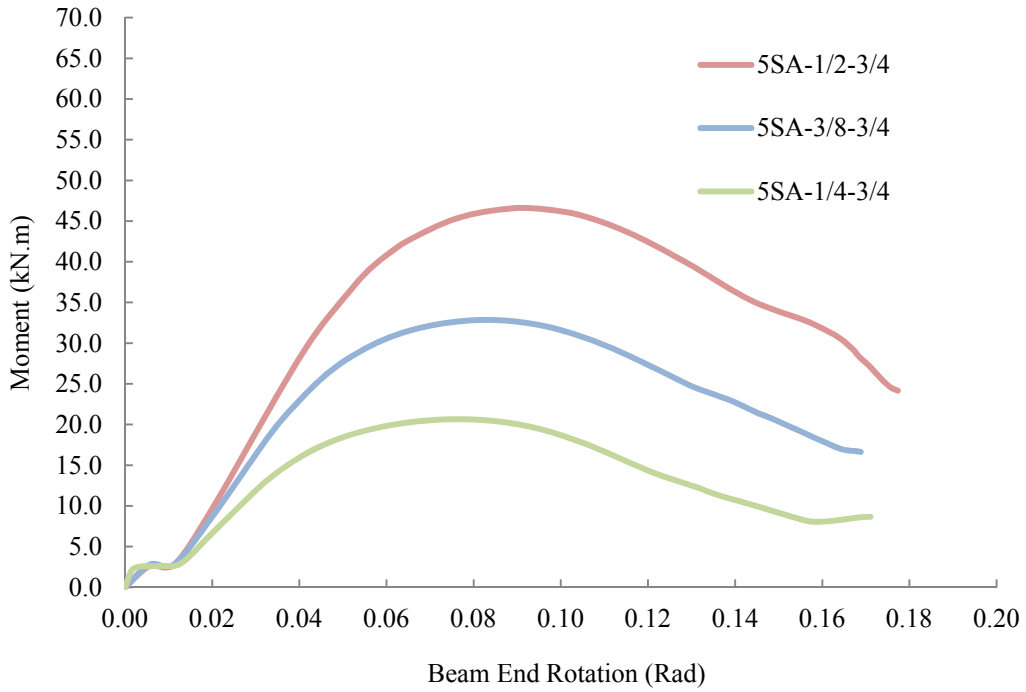


Figure 7.43: Comparison of flexural response of 5SA connections with different angle thicknesses

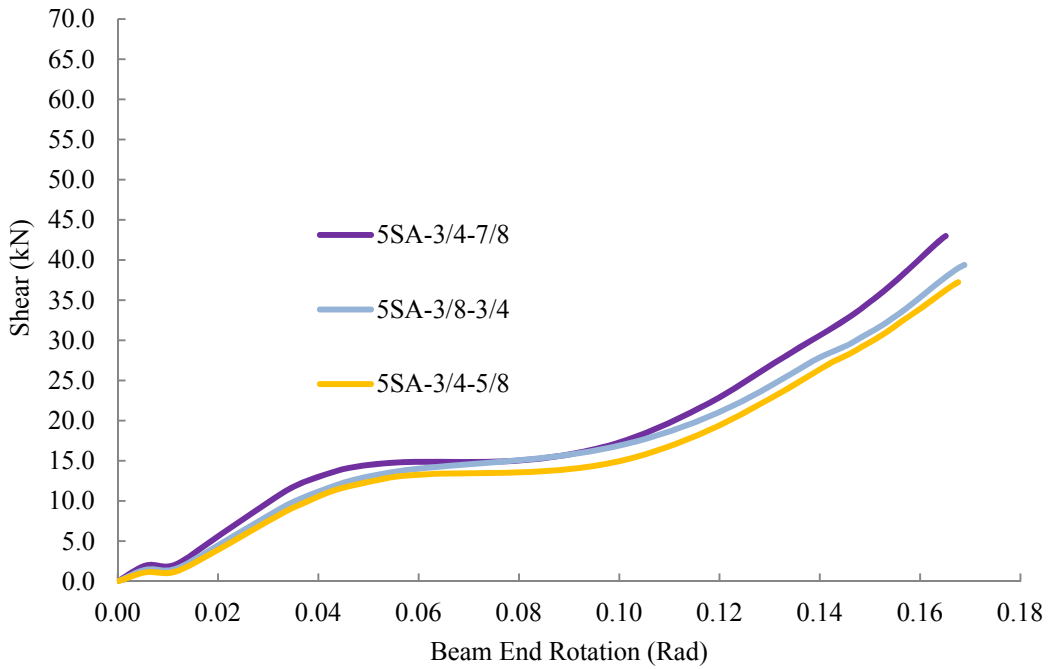


Figure 7.44: Comparison of shear response of 5SA connections with different bolt sizes

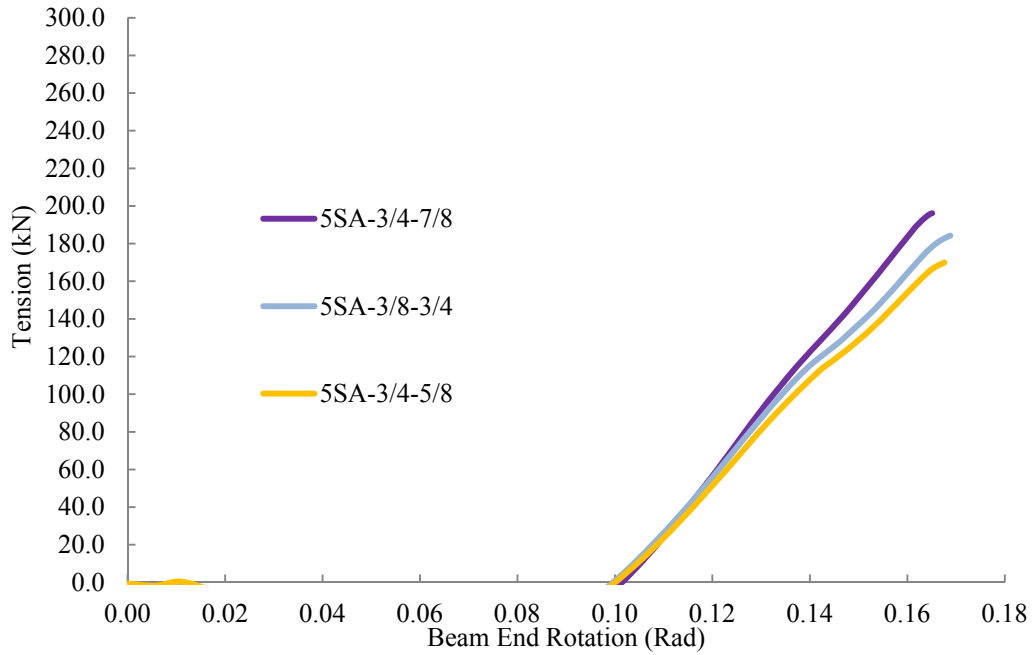


Figure 7.45: Comparison of tensile response of 5SA connections with different bolt sizes

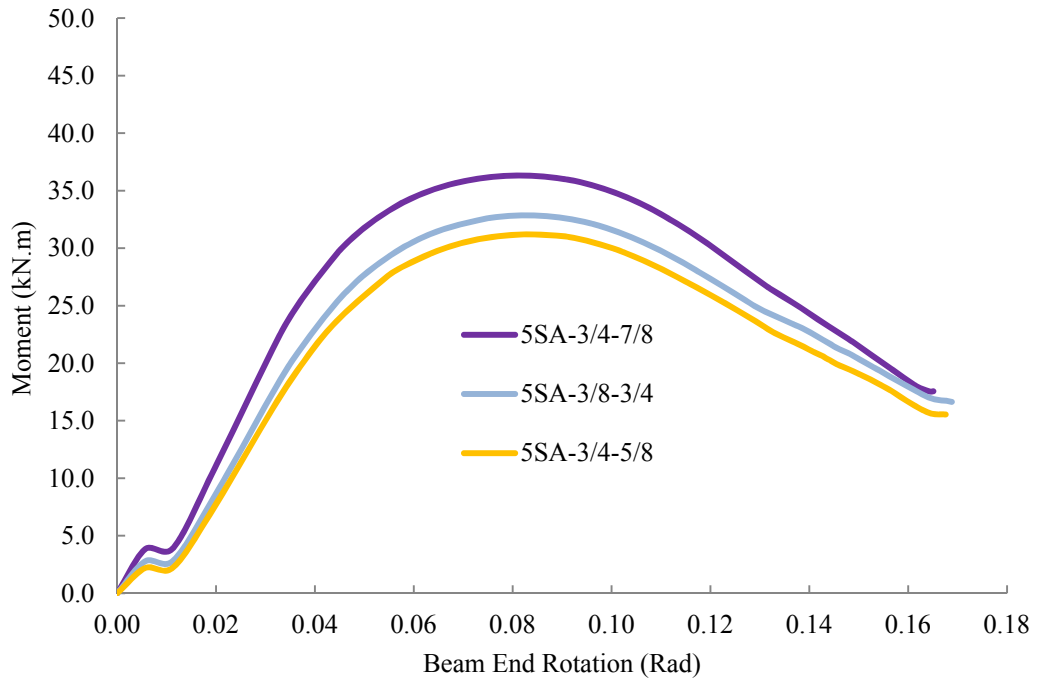


Figure 7.46: Comparison of flexural response of 5SA connections with different bolt sizes

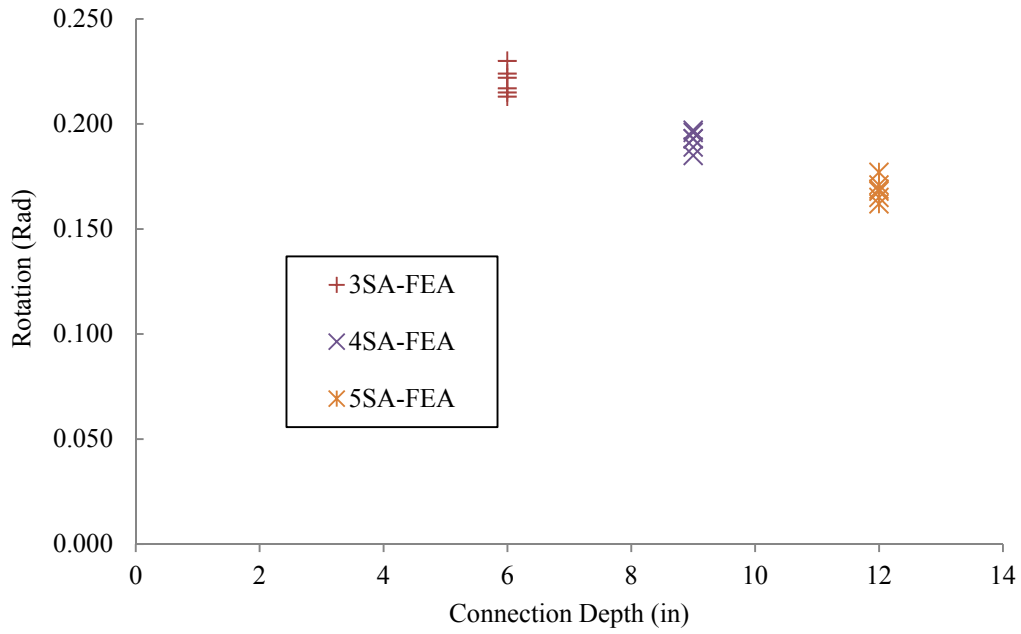


Figure 7.47: Single angle connection total rotation capacities versus connection depth

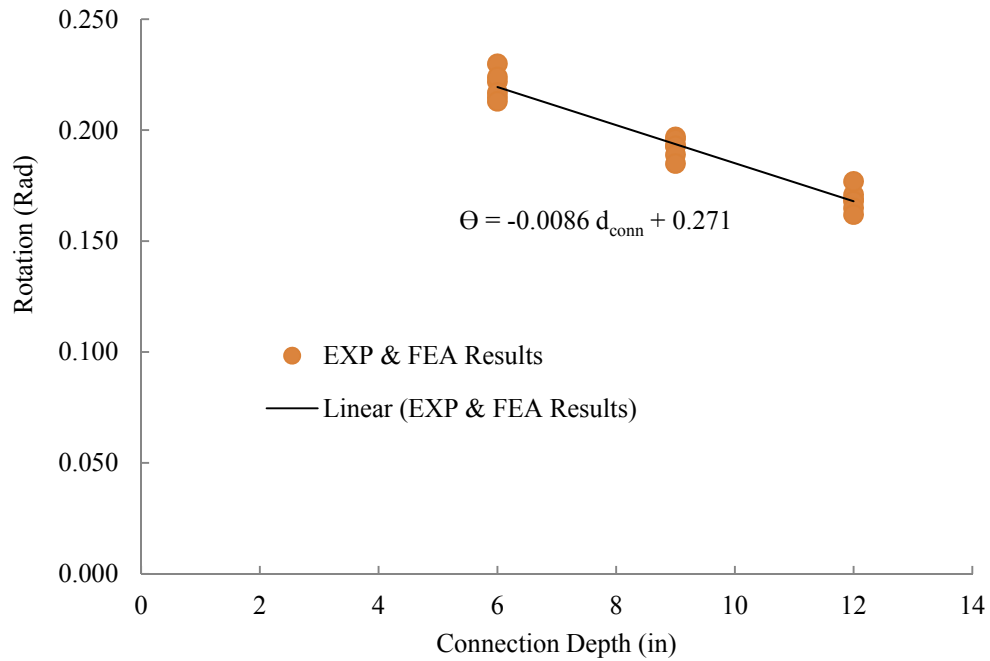


Figure 7.48: Proposed equation for single angle connection total rotation capacities versus connection depth

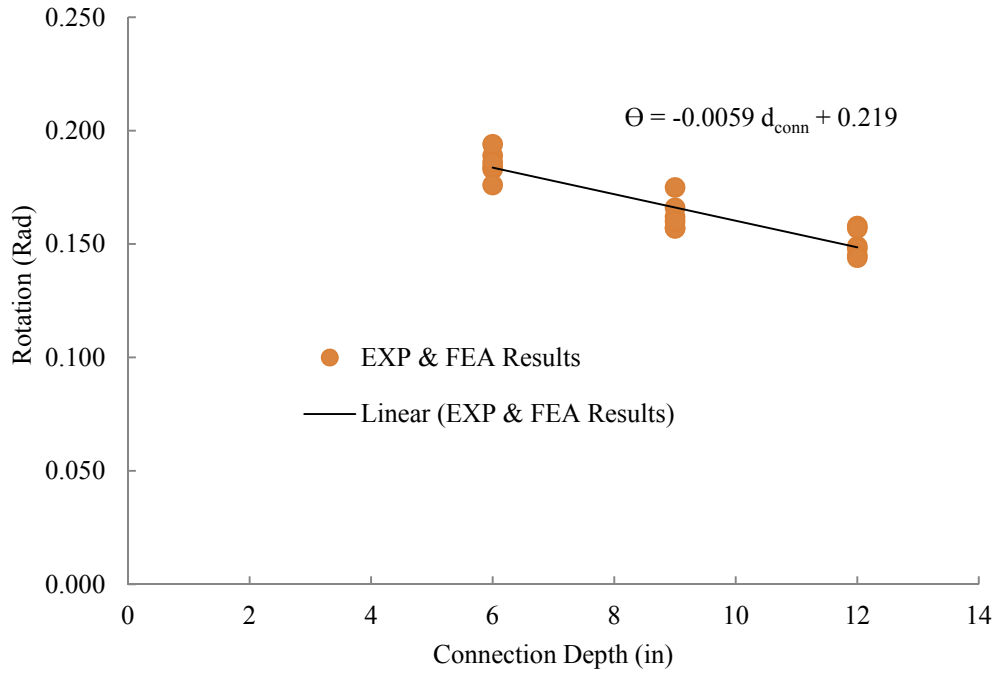


Figure 7.49: Proposed equation for single angle connection plastic rotations versus connection depth

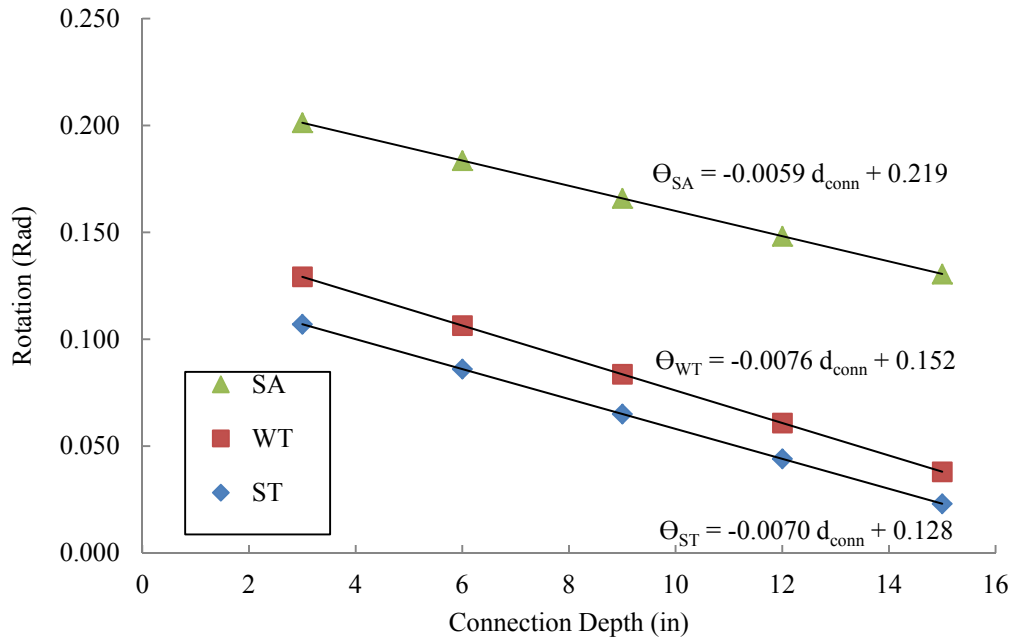


Figure 7.50: Comparison of proposed equations for plastic rotation of shear tab, single angle, and WT connections

8 Summary, Conclusions, and Recommendations for Future Research

8.1 Summary

This study is intended to quantify sources of inherent robustness of one-sided steel shear connections in order to enhance the understanding of connection robustness and, consequently, improve the analysis and design methods to mitigate the vulnerability of steel structures to a column loss event. Progressive collapse, as the main impetus for looking at steel shear connections again, is defined and discussed. The key differences between the behaviour of shear connections under conventional loading and in a double-span (column loss) event are established, including the presence of a tensile catenary force and large beam rotation. An appropriate substructure to investigate the behaviour of shear connection assemblies that can mimic the behaviour and failure modes in a progressive collapse event is selected. Subsequently, a model is developed for shear connections subjected to a column loss event and a rational approach presented to establish and calibrate a finite element model for simple shear connections. A shear tab connection model is introduced that can be used as a benchmark to validate finite element models of simple shear connections subjected to extreme loading effects such as a column removal scenario. Recommendations are provided on how to achieve a converged solution in steel shear connections using state-of-the-art simulation techniques. In a column removal scenario, considerable axial compressive force may develop via arching action before catenary action begins. This phenomenon has been simulated numerically and the results show that the vertical eccentricity between the centres of rotation of the connections at the ends of a beam is a primary parameter leading to the presence of this compressive force. Another important factor that affects the development of arching action is the stiffness of the surrounding structure.

The simultaneous presence of shear, moment and tension in shear tab, WT and single angle connections was investigated in different chapters, separately. Comparisons between the experimental and the numerical quantities emphasized the effectiveness and correctness of the proposed finite element models. It is observed that one-sided shear connections are capable of developing an alternative (catenary) load path when an adjacent column is compromised. The research also quantified the rotational capacities of the connection types studied, indicating that deeper connections possess less rotational capacity. It is observed that the rotational capacity of single angle connections is significantly higher than those of shear tab and WT types. Equations are proposed to calculate this characteristic feature of the connection and also the plastic rotational capacities based on connection depth. The effect of factors such as plate thickness, section size, bolt size and type on the connection response are also investigated. The concept of the “devolution point”, defined as the point that the flexural phase domination ends and catenary force or a combination of flexural-catenary action begins to provide the major resistance, is introduced. It is observed that shallow shear tab and WT connections and all single angle connections transfer from the flexural phase to the catenary phase at the devolution point; however, shear tab and WT connections with four and five bolts transfer from the flexural phase to a flexural-catenary phase. The results of this research project should contribute to a better understanding of the resistance of steel structures with one-sided shear connections to progressive collapse.

8.2 Conclusions

The following conclusions can be drawn from this research:

- In the finite element modelling of connections, obtaining the converged nonlinear solution is the most challenging part due to the nonlinearity definitions, including material, geometric, and boundary (contact) nonlinearities. The analyst has to decide on several issues such as mesh

discretization, element types and the solving algorithm. These selections may have significant effects on the model response and can lead to inaccurate results if not carried out properly. Satisfying the convergence issues in addition to good engineering judgment led to an accurate solution. Although experimental results are needed for model validation, it is not necessary to have them for each specific type of connection to verify the response. Following the same procedure that was previously verified can lead to “converged” (accurate) response. The example proposed in this research can be taken as a benchmark for validating the finite element modelling of shear connections in the column removal scenario.

- In a column removal scenario, considerable axial compressive force may develop via arching action before catenary action begins. This phenomenon has been simulated numerically and the results show that the vertical eccentricity between the centres of rotation of the connections at the ends of a beam is a primary parameter leading to the presence of this compressive force. Another important factor that affects the development of arching action is the stiffness of the surrounding structure. Whether the arching action forms in the connection assembly or not, the catenary resistance of the connection can act as an alternative load path in a column loss event. Since the arching action, if present, occurs at an early stage of connection response, it will not affect the ultimate capacity of the frame. Therefore, tensile catenary action is still the desired alternative load path in response to a column removal scenario, and therefore the connection must be designed to resist these tensile loads.
- Tensile catenary force, as the alternative load path mechanism in a column removal scenario, is observed interacting with flexural response at the shear tab connection location. Ductility of shear tab connections is derived largely from the local deformation of bolt holes, especially bottom holes, and to a lesser degree the bolt slippage and bolt shear deformation before failure. Tension rupture of the bottom hole was the governing failure mode in most of the cases; however, bolt shear rupture was also observed. The

maximum rotational capacity of the shear tab connections studied was between 0.06 and 0.13 radians for five to three bolts.

- The point that the flexural phase domination ends and catenary force or flexural-catenary action begins to provide the major resistance is named the “devolution point”. For shear tab connections with three bolts, this point is located at the maximum moment and the failure will be in the catenary phase. In the shear tabs with four and five bolts, a point is distinguished as a "devolution point" at which a substantial decrease in flexural stiffness happens. This decrease might be accompanied by an increase in tensile force development rate (four bolt shear tabs) or not (five bolt shear tabs). After this point, tension and moment interact until failure occurs. Therefore, it can be inferred that the four and five bolt shear tab connections fail mainly because of flexural-catenary actions.
- Tensile catenary action is acknowledged as the alternative load mechanism in a column removal scenario of the WT connections as well. Ductility of WT connections is derived largely from the local deformation in the stem adjacent to the bottom holes and the bolt slippage and deformation before failure. Out-of-plane bending of the WT flange between the bolt lines is another source; however, it was not significant in the connections with thick flanges. Based on the results of the numerical analyses, out-of-plane flange deformation is a maximum at the bottom of all three connections considered and is almost zero at the top. Either shear failure of the bottom bolt or WT-stem bottom hole rupture was the governing failure mode in all cases. The maximum rotational capacity of the WT connections studied was between 0.05 and 0.16 radians for five to three bolts.
- For three bolt WT connections, the "devolution point" happened after the maximum moment was reached and the failure was in the catenary phase. Generally, the switch between flexural behaviour and the tensile phase in WT connections with three bolts can be distinguished more accurately than for the ones with four and five bolts. In the latter cases, there is a point that can be assigned as the “devolution point”, at which the tensile

response starts to ramp up rapidly. The connection fails in the flexural-catenary phase due to the presence of a significant amount of moment and tension at the time of failure. It is noted that the WTs with five bolts go into catenary tension from the beginning. At the “devolution point”, a significant decrease in the slope of the flexural response and an increase in the tensile response are observable. Basically, the amount of moment at the failure is significant. As a result, it can be inferred that the WT connections with five bolts fail mainly because of flexural-catenary action, similar to four bolt WTs.

- Tensile catenary action is also acknowledged as the alternative load mechanism in a column removal scenario of single angle connections. The main source of ductility was out-of-plane bending of the angle. Other sources, such as bolt hole bearing deformation, were not significant in the studied connections. The maximum rotation of single angle connections was between 0.23 and 0.16 radians for three to five bolt connections.
- For three bolt single angle connections, the “devolution point” is located at a large rotation where the flexural resistance of the connection is almost zero. For single angles with five bolts, this point is close to the rotation at which the peak moment occurs. The four bolt devolution point is somewhere between these two cases. In four and five bolt single angle connections, due to the geometry of the connection, the catenary action starts earlier but still during the degrading branch of the flexural curve. After the devolution point, tension dominates the behaviour until failure occurs. Therefore, it can be inferred that all single angle connections fail mainly because of catenary action, unlike four and five bolt shear tab and WT connections. This phenomenon is related to the inherent flexibility of single angle connections in comparison with the two other types of connections.
- It cannot be assumed that all of the fasteners in a line share equally in carrying the load. In fact, the fasteners towards the bottom of the joint

carry the largest portion. This unequal loading of the fasteners is accentuated as the rotation increases.

- Different types of one-sided shear connections possess different types of failure modes. In the shear tab connections studied, the dominant mode of failure was tearing of the plate. However, in the WTs the failure mode was either bolt shear rupture or WT-stem hole tearing, depending on the bolt diameter and WT web thickness. In the single angle shear connections, the failure mode was tearing of the bottom bolt hole region of the angle leg at the column face.
- Regarding the demand on the bolts, in shear tab connections the bottom and top bolts experienced large amounts of plastic deformation. In the WT connections, bolts at the beam web had a similar response to that of the shear tab bolts. However, the bolts connecting the WT flange to the column remained mainly elastic. All bolts in the single angle connections also remained elastic, except the bottom ones at the column face that were exposed to the greatest tension as well as shear. As the inelastic bolt deformations contributed little to the overall connection ductility, as compared to bolt bearing deformations and flexure of the connection elements, bolts should be sized in design to be large enough to invoke a more ductile failure mode.
- Local yielding regions, also called local plastic hinges, are defined as the points of accumulation of plastic strain in the connecting part. These hinges are the locations where failure will initiate. It was observed that shear tab, WT and single angle connections possess different potential hinge locations. In the column removal scenario, the probable hinge locations are at the beam web bolt line for shear tabs and WTs, and the column face bolt line for single angle connections. The other potential plastic hinge locations in the single angle connections are at the angle heel in both the web-framing and outstanding legs.
- Equations are provided for determining both the total rotational capacity of the connection and the plastic rotational capacity. The plastic rotational

capacity of single angle connections is higher than that of WT and shear tabs. The main reason is the significant contribution of out-of-plane deformation of the angle outstanding leg. Comparing WT and shear tab connections, the shear tab possesses less plastic rotational ductility than the WT connections due to out-of-plane deformation of the WT flange, although its contribution is significantly less than the deformation observed in the angle leg. As a result, single angle and shear tab connections are considered to be the most and least ductile connections, respectively, in the column loss event, and the WT connection behaviour is somewhere in between, but closer to shear tab connection.

- The resulting interactive response curves can be used as input for one-sided connection models in full-building progressive collapse analyses. Continuing research in this area will result in a better understanding of connection performance and more economical design of joints with one-sided connections in the column loss event.

8.3 Recommendations for future research

- All the connections in this study possess the edge distance of 38.1 mm (1.5 in). It is recommended that other edge distances be investigated in order to determine the effects on behaviour and failure mode. Since tension rupture is one the probable modes of failure, increased edge distance might be helpful.
- The effect of different span lengths is of interest to understand the variation of demand at the location of shear connections as the span length alters.
- Numerical modelling of other types of shear connections, such as end plate and double angles, should be carried out based on the benchmark example offered in chapter 3.

- It is suggested that the effect of a floor slab be considered to determine the changes in the connection strength, rotational capacity, and also possible changes in the demands at the connections.
- Other types of shear connections with welds are of interest in the column loss event, such as welded-bolted or welded-welded WT connections. The weld can be modelled as a tie constraint—similar to the approach taken in this research—or as a discrete component with unique material properties. It is recommended that models including weld behaviour be developed with associated failure criteria.

LIST OF REFERECES

- ACI. (2010). *318-10, Building Code Requirements for Reinforced Concrete*. American Concrete Institute, Farmington Hills, MI.
- Agerskov, H. (1976). "High-strength bolted connections subject to prying." *Journal of Structural Engineering, ASCE*, 102(1), 161-175.
- AISC. (1986). *Specification for Structural Steel Buildings*. American Institute of Steel Construction, Chicago, IL.
- AISC. (2002). *Seismic Provisions for Structural Steel Buildings*. American Institute of Steel Construction, Chicago, IL.
- AISC. (2005). *Manual of Steel Construction 13th Edition*. American Institute of Steel Construction, Chicago, IL.
- AISC. (2010). *Manual of Steel Construction 14th Edition*. American Institute of Steel Construction, Chicago, IL.
- ASCE. (2006). *ASCE/SEI 41-06, Seismic Rehabilitation of Existing Buildings*. American Society of Civil Engineers, Reston, VA.
- ASCE. (2010). *ASCE/SEI7-10:Minimum Design Loads of Buildings and Other Structures*. American Society of Civil Engineers, Reston, VA.
- Ashakul, A. (2004). "Finite element analysis of single plate shear connections." *Ph.D. Thesis*, Virginia Polytechnic Institute of State University, Blacksburg, VA.
- Astaneh, A. (1989). "Demand and supply of ductility in steel shear connections." *Journal of Constructional Steel Research*, 14(1), 1-19.
- Astaneh, A., and Nader, M. N. (1989). "Design of tee framing shear connections." *AISC Engineering Journal*, First Quarter, 9-20.
- Astaneh, A., and Nader, M. N. (1990). "Experimental studies and design of steel tee shear." *Journal of Structural Engineering, ASCE*, 116(10), 2882-2902.
- Astaneh, A., Call, S. M., and McMullin, K. M. (1989). "Design of single plate shear connections." *AISC Engineering Journal*, First Quarter, 21-32.
- Astaneh, A. (2005). "Design of shear tab connections for gravity and seismic loads." *Steel TIPS*, Structural Steel Educational Council, Moraga, CA.
- Astaneh, A. (2007). "Progressive collapse prevention of steel frames with shear connections." *Steel TIPS*, Structural Steel Educational Council, Moraga, CA.

Astaneh, A., Jones, B., and Zhao, Y. (2002). "Progressive collapse resistance of steel building floors." *Steel TIPS*, Structural Steel Educational Council, Moraga, CA.

Astaneh, A., Liu, J., and McMullin, K. M. (2002). "Behavior and design of single plate shear connections." *Journal of Constructional Steel Research*, 58 , 1121-1141.

ASTM. (2008). *A 36/A 36M – 08, Standard Specification for Carbon Structural Steel*. American Society for Testing and Material, West Conshohocken, PA.

ASTM. (2009). *A 325M – 09, Standard Specification for Structural Bolts, Steel, Heat Treated 830 MPa Minimum Tensile Strength (Metric)*. American Society for Testing and Material, West Conshohocken, PA.

ASTM. (2010). *A490M – 10, Standard Specification for High-Strength Steel Bolts, Classes 10.9 and 10.9.3, for Structural Steel Joints (Metric)*. American Society for Testing and Material, West Conshohocken, PA.

ASTM. (2011). *A992/A992M – 11, Standard Specification for Structural Steel Shapes*. American Society for Testing and Material, West Conshohocken, PA.

Barth, K., Orbison, J., and Nukala, R. (2002). "Behavior of steel tension members subjected to uniaxial loading." *Journal of Constructional Steel Research*, 58, 1103-1120.

Bursi, O., and Jaspart, J. (1998). "Basic issues in the finite element simulation of extended end plate connections." *Computers & Structures*, 69, 361-382.

Bursi, O., and P., J. J. (1997). "Benchmarks for finite element modelling of bolted steel connections." *Journal of Constructional Steel Research*, 43, 17-42.

Caccavale, S. E. (1975). "Ductility of single plate framing connections." *M.Sc. Thesis*, University of Arizona, Tucson, Arizona.

CEN. (1990). *Eurocode 0-BS EN 1990:2002, Basis of structural design*, European Committee for Standardisation, Brussels, Belgium.

CISC. (2006). *Handbook of steel construction. 9th edition*. Canadian Institute of Steel Construction, Toronto, ON.

Citipitioglu, A., Haj-Ali, R., and White, D. (2002). "Refined 3D finite element modeling of partially- restrained connections including slip". *Journal of Constructional Steel Research*, 58, 995-1013.

- Crowder, B. (2005). *Progressive collapse - Historical Perspective*. Presentation by Naval Facilities Engineering Command.
- CSA. (2001). *CSA-S16-01, Limit states design of steel structures*. Canadian Standard Association, Toronto, ON.
- CSA. (2004). *CAN/CSA-A23.3-04: Design of Concrete Structures*. Canadian Standard Association, Toronto, ON.
- CSA. (2009). *CSA-S16-09:Limit states design of steel structures*. Canadian Standard Association, Toronto, ON.
- Daneshvar, H., and Driver, R. G. (2010). "Application of Seismic Steel Connection Experiments to Column Removal Scenario." *Proc., 2nd Specialty Conference on Disaster Mitigation, CSCE*, Winnipeg, MB.
- Daneshvar, H., and Driver, R. G. (2011). "Behavior of Shear Tab Connections under Column Removal Scenario." *Proc., Structures Congress, ASCE*, Las Vegas, NV.
- Daneshvar, H., Oosterhof, S. A., & Driver, R. G. (2012). "Compressive arching and tensile catenary action in steel shear connections under column removal scenario." *Proc., 3rd International Structural Specialty Conferenc, CSCE*, Edmonton, AB.
- Dassault Systèmes. (2009). "Getting started with Abaqus: Interactive Edition." *Abaqus Manual*, Dassault Systèmes Simulia Corp, Providence, RI.
- Dassault Systèmes. (2011a). "Metal Inelasticity in Abaqus." *Abaqus Course Notes*, Dassault Systèmes Simulia Corp, Providence, RI.
- Dassault Systèmes. (2011b). "Modeling contact using Abaqus/Standard.", *Abaqus Manual*, Dassault Systèmes Simulia Corp, Providence, RI.
- Dassault Systèmes. (2011c). "Obtaining a converged solution with Abaqus.", *Abaqus Manual*, Dassault Systèmes Simulia Corp, Providence, RI.
- DeStefano, J. (2006). "Detailing to prevent progressive collapse." *Structure magazine*, 66-67.
- DoD. (2009). *UFC 4-023-03, Design of buildings to resist progressive collapse*. Department of Defense, Washington, DC.
- Ellingwood, B. R., Smilowitz, R., Dusenberry, D. O., Duthinh, D., Lew, H., and Carino, N. J. (2007). "Best practices for reducing the potential for progressive

collapse in buildings.” *NISTIR 7396: National Institute of Standards and Technology, Technology Administration and Department of Commerce, U.S.*

Epstein, H., and Chamarajanagar, R. (1996). “Finite element studies for correlation with block shear tests.” *Computers and Structures*, 61(5), 967–974.

FEMA. (2000). *FEMA-356: NEHRP Guidelines for seismic rehabilitation of buildings*. Federal Emergency Management Agency, Washington, DC.

Foley, C. M., Martin, K., and Schneeman, C. (2007). “Robustness in structural steel framing systems.” *Report MU-CEEN-SE-07-01, Final report submitted to American Institute of Steel Construction*, Marquette University, Milwaukee, WI.

Friedman, A. D. (2009). “Axial, shear and moment interaction of WT connections.” *M.Sc. Thesis*, Milwaukee School of Engineering, Milwaukee, WI.

Girhammar, U. A. (1980). “Behaviour of bolted beam-to connections under catenary action in damaged steel structures.” *Swedish council for building research*, Lulea, Sweden.

Gong, Y. (2009). “Single-angle all-bolted shear connections.” *Journal of Constructional Steel Research*, 65, 1337-1345.

Goodrich, W. (2005). “Behavior of extended shear tabs in stiffened beam-to-column web connection.” *M.Sc Thesis*; Vanderbilt University, Nashville, TN.

Griffiths, H. P. (1968). “Report of the inquiry into the collapse of flats at Ronan Point, Canning Town.” *Ministry of Housing and Local Government*, London, UK.

GSA. (2003). “Progressive collapse analysis and design guidelines for new federal office buildings and major modernization projects.” U.S. General Services Administration, Washington, DC.

Guravich, S. J., and Dawe, J. L. (2006). “Simple beam connections in combined shear and tension.” *Canadian journal of civil engineering*, 33(4), 357-372.

Hornby, D. E., Richard, R. M., and Kriegh, J. D. (1984). “Single-Plate Framing Connections with Grade-50 Steel and Composite Construction.” *AISC Engineering Journal*, Third Quarter, 125-138.

Huns, B. B., Grondin, G. Y., and Driver, R. G. (2002). “Block shear behaviour of bolted gusset plates.” *Structural Engineering Report 248*, University of Alberta, Edmonton, AB.

Iwankiw, N., and Griffis, L. G. (2004). "Comparison of structural performance of multi-story buildings under extreme events." *American Institute of Steel Construction*, Chicago, IL.

Izzuddin, B., Vlassis, A., Elghazouli, A., and Nethercot, D. (2008a). "Progressive collapse of multi-storey buildings due to sudden column loss — Part I: Simplified assessment framework." *Engineering Structures*, 30(5), 1308-1318.

Izzuddin, B., Vlassis, A., Elghazouli, A., and Nethercot, D. (2008b). "Progressive collapse of multi-storey buildings due to sudden column loss—Part II: Application." *Engineering Structures*, 30(5), 1424-1438.

Johnson, M. (2009). "Axial, shear and moment interaction of single angle connections." *Unpublished M.Sc. Thesis*, Milwaukee, WI.

Ju, S. -H., Fan, C. -Y., and Wu, G. H. (2004). "Three-dimensional finite elements of steel bolted connections." *Engineering Structures*, 26(3), 403-413.

Kameshki, E., and Saka, M. (2003). "Genetic algorithm based optimum design of nonlinear planar steel frames with various semi-rigid connections." *Journal of Constructional Steel Research*, 59(1), 109-134.

Kanvinde, A., and Deierlein, G. (2004). "Prediction of ductile fracture in steel moment connections during earthquakes using micromechanical fracture models." *Proc. 13th World Conference on Earthquake Engineering 13 WCEE*. (Paper No. 297), Vancouver, B.C.

Khoo, H., Cheng, J., and Hruday, T. (2002). "Determine steel properties for large strain from a standard tension test." *Proc. Second Material Specialty Conference of the Canadian Society for Civil Engineering*, Toronto, ON.

Kishi, N., and Chen, W. F. (1990). "Moment-Rotation Relations of Semirigid Connections With Angles." *Journal of Structural Engineering*, ASCE, 116(7), 1813-1834.

Krishnamurthy, N. (1980). "Modelling and prediction of steel bolted connection behavior." *Computers & Structures*, 11(1-2), 75-82.

Krishnamurthy, N., and Graddy, D. E. (1976). "Correlation between 2- and 3-dimensional finite element analysis of steel bolted end-plate connections." *Computers & Structures*, 6(4-5), 381-389.

Kukreti, A., Murray, T., and Abolmaali, A. (1987). "End-Plate Connection Moment-Rotation relationship." *Journal of Constructional Steel Research*, 8, 137-157.

- Kulak, G. L., Fisher, J. W., and Struik, J. H. (2001). *Guide to Design Criteria for Bolted and Riveted Joints*. John Wiley & Sons Inc, Chicago, IL.
- Lim, J And Krauthammer, T. (2006). "Progressive collapse analyses of 2D steel-framed structures with different connection models." *AISC Engineering Journal*, Third Quarter, 201-215.
- Lipson, S. (1968). "Single-angle and single-plate beam framing connections." *Proc. of the Canadian structural engineering conference*. Canadian Steel Industries Construction Council. Toronto, ON, 141-162.
- Lipson, S. L., and Antonio, M. E. (1980). "Single-angle welded-bolted beam connections." *Canadian Journal of Civil Engineering*, 7(2), 315-324.
- Marchand, K. (2008). "Guidance for progressive collapse analysis: recommended performance levels for alternate path analysis of blast-damaged steel connections." *Proc. Structures Congress/North American Steel Construction Conference (NASCC)*, Nashville, TN.
- Marchand, K. A., and Alfawakhiri, F. (2004). "Facts for Steel Buildings: Blast and progressive collapse." *American Institute of Steel Construction*. Chicago, IL.
- Mlakar, P. F., Dusenberry, D. O., Harris, J. R., Haynes, G., and Phan, L. T. (2003a). "Findings and Recommendations from the Pentagon Crash." *Third Forensic Engineering Congress. American Society of Civil Engineers*, San Diego, CA, 43-45.
- Mlakar, P. F., Dusenberry, D. O., Harris, J. R., Haynes, G., & Phan, L. T. (2003b). "Structural Analysis of the Damaged Structure at the Pentagon." *Third Forensic Engineering Congress. American Society of Civil Engineers*, San Diego, CA, 21-30.
- Mlakar, P. F., Dusenberry, D. O., Harris, J. R., Haynes, G., & Phan, L. T. (2003c). "Structural Damage Induced by a Terrorist Attack on the Pentagon." *Third Forensic Engineering Congress. American Society of Civil Engineers*, San Diego, CA, 9-20.
- Murray, T. (2013). "AISC Night School: Fundamentals of Connection Design." *Professor Emeritus; Virginia Tech: American Institute of Steel Construction*. Chicago, IL.
- Nair, R. S. (2003). "Progressive collapse basics. Steel Building Symposium: Blast and Progressive Collapse Resistance." *Blast and Progressive Collapse*

Symposium, American Institute of Steel Construction and the Steel Institute of New York, New York, NY.

NIST. (2005). "Final report on the collapse of world trade center towers." *NIST NCSTAR 1: National institute of standards and technology*. Gaithersburg, MD.

NIST. (2007). "Best Practices for Reducing the Potential for Progressive Collapse in Buildings." *National Institute of Standards and Technology*. Gaithersburg, MD.

NIST. (2008). "Final report on the collapse of world trade center building 7." *National Institute of Standards and Technology*. Gaithersburg, MD.

NIST. (2010). "An Experimental and Computational Study of Steel Moment Connections under a Column Removal Scenario." *National Institute of Standards and Technology: NIST Technical Note 1669*. Gaithersburg, MD.

Oosterhof, S., and Driver, R. (2012). "Performance of Steel Shear Connections under Combined ." *Proc. 2012 Structures Congress., ASCE, Chicago, Illinois*.

Powell, G. (2005). "Progressive collapse: case studies using nonlinear analysis." *Proc. 2005 Structures Congress and the 2005 Forensic Engineering Symposium*. American Society of Civil Engineers. New York, NY.

Richard, R. M., Gillett, P. E., Kriegh, J. D., & Lewis, B. A. (1980). "The Analysis and Design of Single Plate Framing Connections." *AISC Engineering Journal*, Second Quarter, 38-52.

Riks, E. (1979). "An incremental approach to the solution of snapping and buckling problems." *Journal of Solids and Structures*, 15(7) 529-551.

Selamet, S., and Garlock, M. (2010). "Guidelines for modeling three dimensional structural connection models using finite element methods." *International Symposium "Steel Structures: Culture & Sustainability, (Paper No: 14)*. Istanbul, Turkey.

Sherman, D. R., and Ghorbanpour, A. (2002). "Design of extended shear tabs.", *Final report submitted to American institute of steel construction*, University of Wisconsin-Milwaukee, Wisconsin, WI.

Song, B., and Sezen, H. (2009). "Evaluation of an existing steel frame building against progressive collapse." *Proc., 41th Structural Conference, ASCE, Austin, TX, 1878-1885*.

Taylor, D. A. (1975). "Progressive Collapse." *Canadian Journal of Civil Engineering*, 2(4) ,517 , 517-529.

Thompson, S. L. (2009). "Axial, shear and moment interaction of single plate shear tab connections." *M.Sc. Thesis*, Milwaukee School of Engineering, Milwaukee, WI.

Thornton, W. A. (1996). "A rational approach to design of tee shear connections." *AISC Engineering Journal*, First Quarter, 34-37.

Thornton, W. A. (1997). "Load, Strength and ductility requirements for simple shear connections with shear and axial." *AISC Conference Proceedings*, 38-1 – 38-17.

Timoshenko. (1955). *Strength of Materials.*, Van Nostrand Company, New York, NY.

Weigand, J., Meissner, J., Francisco, T., Berman, J., Fahnestock, L., and Liu, J. (2012). "Overview of AISC/NSF Structural Integrity Research and Preliminary Results." *Proc. of the 2012 Structures Congress.*, ASCE, Chicago, IL.

William, M. (1988). "Introduction into steel beam-to-column building connection." Elsevier Science Publishers Ltd, New York, NY.

Yang, J.-G., Murray, T., and Plaut, R. (2000). "Three-dimensional finite element analysis of double angle connections under tension and shear." *Journal of Constructional Steel Research*, 54, 227-244.

Young, N. W., and Disque, R. O. (1981). "Design Aids for Single Plate Framing Connections." *AISC Engineering Journal*, Fourth Quarter, 129-148.

APPENDIX A

Material Properties

No material tests were performed on the test specimen used for verification in this research. Therefore, generic material properties have been used for all types of steel including the hot rolled sections, plates and bolts. There are totally four types of steel utilized, including ASTM A36 (ASTM 2008) and ASTM A992 (ASTM 2011) for plates and sections and ASTM A325 (ASTM 2009) and ASTM A490 (ASTM 2010) for bolts. Table A.1 and Table A.2 summarize the required material properties for the mentioned types of steel based on ASTM standards. It is assumed that all types of steel materials that have been considered have satisfied the requirements of their respective standards. The yield and tensile strengths define the minimum and maximum strengths that the material could have possibly possessed, which are called as “minimum nominal strength” (MINS) and “maximum nominal strength” (MANS), respectively. Table A.1 and Table A.2 are used for extracting the MINSs and MANSs for all types of steel utilized in this research.

Variability of steel material properties is much less than other construction material such as concrete. Therefore, in some circumstances, testing of steel material is not necessary. In lieu of material test data, the default nominal strength values, MINS and MANS, are commonly used for numerical modeling of the material. Although the nominal values are conservative and therefore, appropriate for design purposes, they are not necessarily representative of the probable behaviour of the material. Accordingly, available codes introduce "expected-strength" (EPS) of the material, most commonly used in seismic design, which basically anticipates the actual properties of the material more accurately. Basically, EPS is determined by multiplying the lower-bound strength (LBS) values by an appropriate translation factor (TF), as shown in Equation (A-1).

$$\text{EPS} = \text{LBS} * \text{TF} \tag{A-1}$$

Lower bound strength values are typically approximately minus one standard deviation from the statistical data, as reported in Table A.3. Applicable TFs for the types of steel utilized in this research are summarized in Table A.4. All

mentioned definitions, including MINS, MANS, LBS and EPS, should be converted to true stress using Equations (A-2) and (A-3) in order to be applicable as Abaqus input. These equations are just valid before the occurrence of localized necking. The schematic diagram of all the above definitions is shown in Figure A.1 (ASCE 2007).

$$\bar{\sigma}_{\text{true}} = \bar{\sigma}_{\text{eng}} (1 + \bar{\epsilon}_{\text{eng}}) \quad (\text{A-2})$$

$$\epsilon_{\text{true}} = \ln (1 + \epsilon_{\text{eng}}) \quad (\text{A-3})$$

ASTM A36:

For ASTM A36 (2008) material type, engineering and true MINS, MANS, LBS and EPS are calculated as shown Table A.5 and Table A.6 for shear tabs and Table A.8 and Table A.9 for single angle connections. The difference between the assumed material properties for the shear tab and angle come from the fact that TF of the yield strength for the plates and sections are not the same, as shown in Table A.4. Figure A.2 to Figure A.5 show the mentioned definitions compared with a sample steel material reported by Kulak et al. (2001). Table A.7 and Table A.10 show the Abaqus input data for the material ASTM A36 (2008) based on Table A.6 for the shear tab and Table A.9 for the angle.

ASTM A992:

For ASTM A992 (2011) material type, engineering and true MINS, MANS, LBS and EPS are calculated as shown in Table A.11 and Table A.12. Figure A.6 and Figure A.7 show the mentioned definitions compared with a sample steel ASTM A992 (2011) material reported by Kulak et al. (2001). Table A.13 shows the input data for the material ASTM A992 (2011) based on Table A.12.

Beams, stub columns and WT sections are made from ASTM A992 (2011) steel material. Based on the test report on shear tab (Thompson 2009) and WT

(Friedman 2009) shear connections, to ensure that bolt bearing deformations were minimized at the beam test specimen bolt hole locations, and hence to prevent damage to the beam during the test, a ASTM A36 (2008) web doubler plate was welded to the side of the beam web opposite that of the connection element. The thickness of the plate is, respectively, 3/8 and 1/2 inch in shear tab and WT shear connection. For the single angle connection, same plate thickness as shear tab connections is assumed. In order to avoid complexity of the geometry of the connection by adding an additional plate, the effect of additional material at the location of the connection was simulated by amplifying the yield and ultimate strength of the beam material by the factors determined in Equation (A-4).

$$\Omega = 1 + t_1 / t_2 \quad (\text{A-4})$$

in which t_1 is the thickness of the web doubler plate, and t_2 is the thickness of the beam web. Table A.12 specifies the mentioned modifications.

ASTM A325 and A490:

High strength bolts are used in structural steelwork most frequently. They are made from heat-treated steel, either carbon steel (ASTM A325 bolts (2009)) or high-strength low alloy steel (ASTM bolts A490 (2010)). The variability of bolt properties is higher than hot rolled steel sections and plates. Based on this fact, available guidelines do not provide any specific values for LBS and TF for different types of bolts. As discussed in chapter 2, in order to reach acceptable material properties for the bolts, the MINS is increased by 0%, 10%, and 20% for each specific test as shown in Table A.14 to Table A.16. Similar data have been re-produced for ATSM A490 bolts in Table A.18 to Table A.20. The assembly with the bolts that can capture the failure modes observed in the test setup was chosen as the bolt's EPS. Since there is no test result for ASTM A490 (2010) bolts, the selection of the EPS for this type was based on the ASTM A325 (2009) bolts. In other words, whatever TF that was selected for the ASTM A325 (2009) bolts, the same factor is applied to the ASTM A490 (2010) bolts. Figure A.8 to

Figure A.11 compare the true and engineering MINS, increased MINS by 10%, 20% and a sample bolt borrowed from Kulak et al. (1987) for ASTM A325 and ASTM A490 (2010), respectively. In Table A.17 and Table A.21, sample Abaqus input is shown for both types of bolts.

Table A.1: Steel sections and plate's material properties (ASTM 2008) (ASTM 2011)

	ASTM A992/A992M	ASTM A 36/A 36M
Tensile Strength, min (MPa)	450	400
Tensile Strength, max (MPa)	-	550
Yield point, min (MPa)	345	250
Yield point, max (MPa)	450	-
Yield to tensile ratio, max	0.85	-
Elongation in 200 mm, min	0.18	0.2
Elongation in 50 mm, min	0.21	0.23 (Plates) - 0.21 (Shapes)

Table A.2: Bolt's material properties (ASTM 2009) (ASTM 2010)

	ASTM A325/A325M	ASTM A490/A490M
Nominal Diameter, mm	M12 to M36	M12 to M36
Tensile Strength, min (MPa)	830	1040
Tensile Strength, max (MPa)	-	1210
Yield Strength, min (MPa)	660	940
Reduction in area	0.35	0.4
Elongation in 50 mm, min	0.14	0.14

Table A.3: Default lower-bound material strengths (ASCE 2007)

Date	Specification	Tensile Strength (MPa)	Yield Strength (MPa)
1990-Present	ASTM A36/A36M-04 and Dual Grade - Group 1	455.1	337.8
1998-Present	ASTM A992/A992M-04	448.2	344.7

Table A.4: Factors to translate lower-bound steel properties to expected-strength properties (ASCE 2007)

Property	Year	Specification	Factor
Yield Strength	1990-Present	ASTM A36/A36M-04 - Plates	1.10
	1990-Present	ASTM A36/A36M-04 and Dual Grade - Group 1	1.05
	1998-Present	ASTM A992/A992M-04	1.10
Tensile Strength	1990-Present	ASTM A36/A36M-04 and Dual Grade - Group 1	1.05
	1998-Present	ASTM A992/A992M-04	1.10

Table A.5: ASTM A36 - Engineering strain–stress properties - Shear Tab (ST)

ϵ_{eng}	$\sigma_{eng}(\text{MPa}) - \text{MINS}$	$\sigma_{eng}(\text{MPa}) - \text{MANS}$	$\sigma_{eng}(\text{MPa}) - \text{LB}$	TF	$\sigma_{eng}(\text{MPa}) - \text{EP}$
0	250.0	400	337.8	1.1	371.6
0.013	250.0	400	337.8	1.1	371.6
0.228	400.0	550	455.1	1.05	477.8

Table A.6: ASTM A36 - True strain–stress properties - Shear Tab (ST)

ϵ_{true}	$\sigma_{true}(\text{MPa}) - \text{MINS}$	$\sigma_{true}(\text{MPa}) - \text{MANS}$	$\sigma_{true}(\text{MPa}) - \text{LB}$	$\sigma_{true}(\text{MPa}) - \text{EP}$
0.000	250.0	400.0	337.8	371.6
0.013	253.3	405.2	342.2	376.5
0.205	491.2	675.4	558.8	586.7

Table A.7: ASTM A36 - Abaqus input file - ST

σ_{true}	$\sigma_{true}(\text{MPa})$
0.000	371.6
0.013	376.5
0.205	586.7

Table A.8: ASTM A36 - Engineering strain–stress properties - SA

ϵ_{eng}	$\sigma_{eng}(\text{MPa}) - \text{MINS}$	$\sigma_{eng}(\text{MPa}) - \text{MANS}$	$\sigma_{eng}(\text{MPa}) - \text{LB}$	TF	$\sigma_{eng}(\text{MPa}) - \text{EP}$
0	250.0	400	337.8	1.05	354.7
0.013	250.0	400	337.8	1.05	354.7
0.228	400.0	550	455.1	1.05	477.8

Table A.9: ASTM A36 - True strain–stress properties - SA

ϵ_{true}	$\sigma_{true}(\text{MPa})$ - MINS	$\sigma_{true}(\text{MPa})$ - MANS	$\sigma_{true}(\text{MPa})$ - LB	$\sigma_{true}(\text{MPa})$ - EP
0.000	250.0	400.0	337.8	354.7
0.013	253.3	405.2	342.2	359.3
0.205	491.2	675.4	558.8	586.7

Table A.10: ASTM A36 - Abaqus input file - SA

ϵ_{true}	$\sigma_{true}(\text{MPa})$
0.000	354.7
0.013	359.3
0.205	586.7

Table A.11: ASTM A992 - Engineering strain–stress properties

ϵ_{eng}	$\sigma_{eng}(\text{MPa})$ - MINS	$\sigma_{eng}(\text{MPa})$ - MANS	$\sigma_{eng}(\text{MPa})$ - LB	TF	$\sigma_{eng}(\text{MPa})$ - EP
0	345.0	450	345.0	1.1	379.2
0.013	345.0	450	345.0	1.1	379.2
0.208	450.0	555	450.0	1.1	493.0

Table A.12: ASTM A992 - True strain–stress properties

ϵ_{true}	$\sigma_{true}(\text{MPa})$ - MINS	$\sigma_{true}(\text{MPa})$ - MANS	$\sigma_{true}(\text{MPa})$ - LB	$\sigma_{true}(\text{MPa})$ - EP	$\sigma_{true}(\text{MPa})$ - EP - Increased for ST and SA Beam	$\sigma_{true}(\text{MPa})$ - EP - Increased for WT Beam
0.000	345.0	450.0	345.0	379.2	713.7	825.136
0.013	349.5	455.9	349.5	384.1	722.9	835.863
0.189	543.6	670.4	543.6	595.5	1120.7	1295.794

Table A.13: ASTM A992 - Abaqus input file

ϵ_{true}	$\sigma_{true}(MPa)$ -	$\sigma_{true}(MPa)$ - ST & SA Beam	$\sigma_{true}(MPa)$ - WT Beam
0.000	379.2	713.7	825.1
0.013	384.1	722.9	835.9
0.189	595.5	1120.7	1295.8

Table A.14: ASTM A325 - Engineering and true strain–stress properties –
Translate factor = 1

ϵ_{eng}	$\sigma_{eng}(MPa)$ - MINS	TF	$\sigma_{eng}(MPa)$ - EPS	ϵ_{true}	$\sigma_{true}(MPa)$ - MINS	$\sigma_{true}(MPa)$ - EPS
0	660	1	660	0.000	660.0	660.0
0.138	830	1	830	0.129	944.5	944.5

Table A.15: ASTM A325 - Engineering and true strain–stress properties –
Translate factor = 1.1

ϵ_{eng}	$\sigma_{eng}(MPa)$ - MINS	TF	$\sigma_{eng}(MPa)$ - EPS	ϵ_{true}	$\sigma_{true}(MPa)$ - MINS	$\sigma_{true}(MPa)$ - EPS
0	660	1.1	726	0.000	660.0	726.0
0.138	830	1.1	913	0.129	944.5	1039.0

Table A.16: ASTM A325 - Engineering and true strain–stress properties –
Translate factor = 1.2

ϵ_{eng}	$\sigma_{eng}(MPa)$ - MINS	TF	$\sigma_{eng}(MPa)$ - EPS	ϵ_{true}	$\sigma_{true}(MPa)$ - MINS	$\sigma_{true}(MPa)$ - EPS
0	660	1.2	792	0.000	660.0	792.0
0.138	830	1.2	996	0.129	944.5	1133.4

Table A.17: ASTM A325 – Sample Abaqus input file

ϵ_{true}	$\sigma_{true}(MPa)$
0.000	660.0
0.129	944.5

Table A.18: ASTM A490 - Engineering and true strain–stress properties –
Translate factor = 1

ϵ_{eng}	$\sigma_{eng}(\text{MPa})$ - MINS	TF	$\sigma_{eng}(\text{MPa})$ - EPS	ϵ_{true}	$\sigma_{true}(\text{MPa})$ - MINS	$\sigma_{true}(\text{MPa})$ - EPS
0	940	1	940	0.000	940.0	940.0
0.138	1040	1	1040	0.129	1183.5	1183.5

Table A.19: ASTM A490 - Engineering and true strain–stress properties –
Translate factor = 1.1

ϵ_{eng}	$\sigma_{eng}(\text{MPa})$ - MINS	TF	$\sigma_{eng}(\text{MPa})$ - EPS	ϵ_{true}	$\sigma_{true}(\text{MPa})$ - MINS	$\sigma_{true}(\text{MPa})$ - EPS
0	940	1.1	1034	0.000	940.0	1034.0
0.138	1040	1.1	1144	0.129	1183.5	1301.9

Table A.20: ASTM A490 - Engineering and true strain–stress properties –
Translate factor = 1.2

ϵ_{eng}	$\sigma_{eng}(\text{MPa})$ - MINS	TF	$\sigma_{eng}(\text{MPa})$ - EPS	ϵ_{true}	$\sigma_{true}(\text{MPa})$ - MINS	$\sigma_{true}(\text{MPa})$ - EPS
0	940	1.2	1128	0.000	940.0	1128.0
0.138	1040	1.2	1248	0.129	1183.5	1420.2

Table A.21: ASTM A490 – Sample Abaqus input file

ϵ_{true}	$\sigma_{true}(\text{MPa})$
0.000	940.0
0.129	1183.5

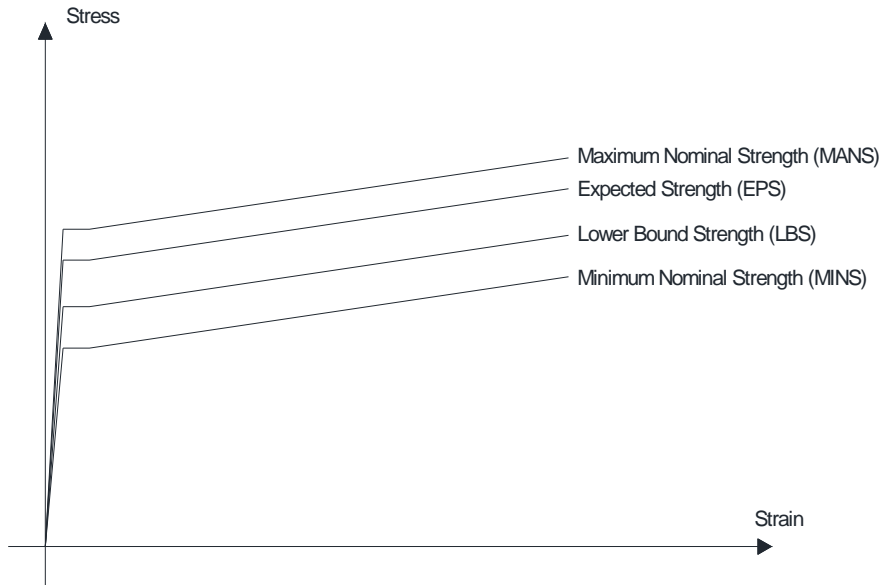


Figure A.1: Schematic material properties of steel

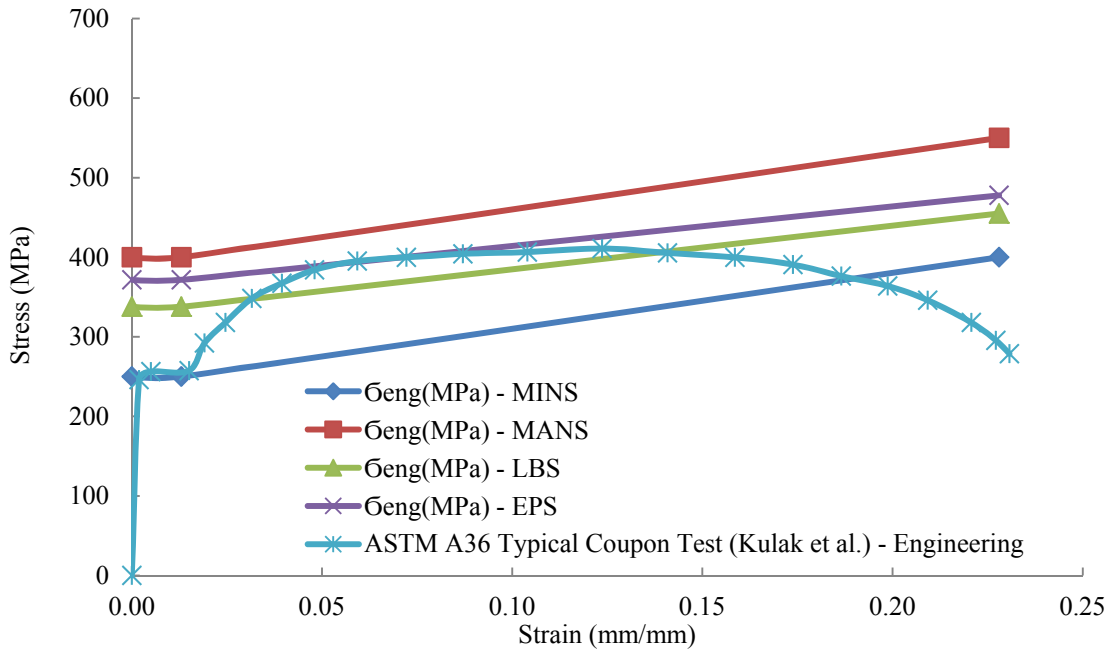


Figure A.2: ASTM A36 - Engineering Stress-Strain Behaviour - ST

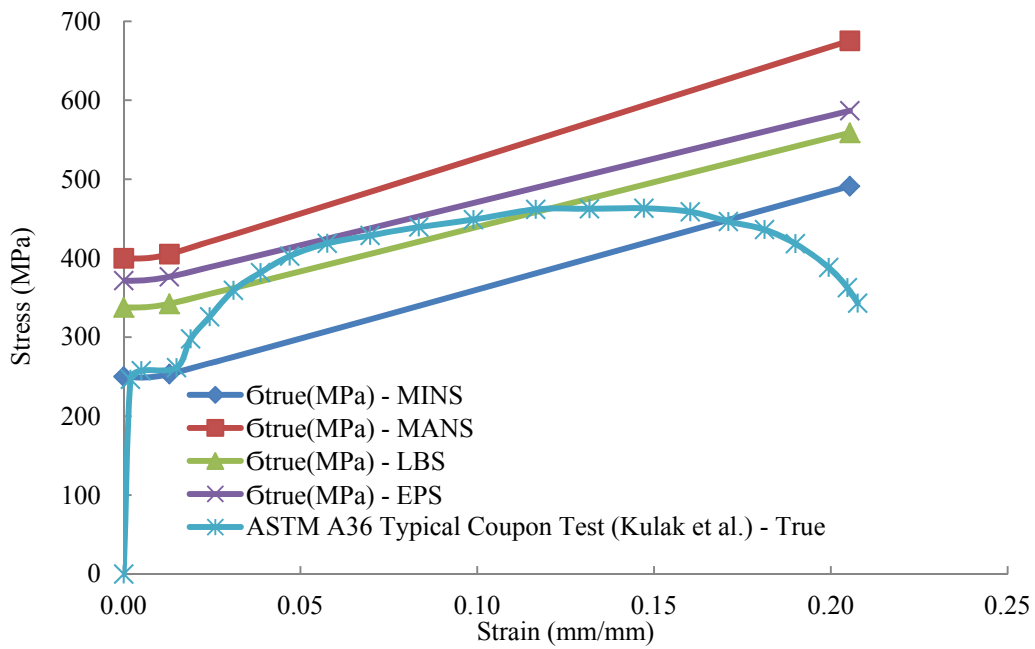


Figure A.3: ASTM A36 - True Stress–Strain Behaviour – ST

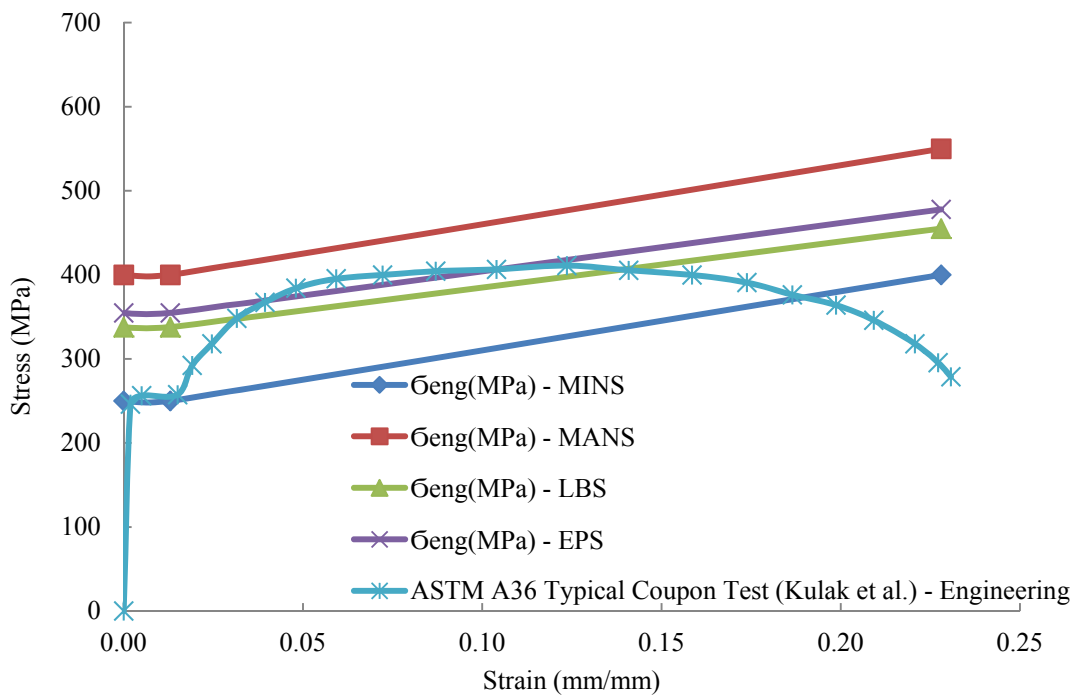


Figure A.4: ASTM A36 - Engineering Stress–Strain Behaviour - SA

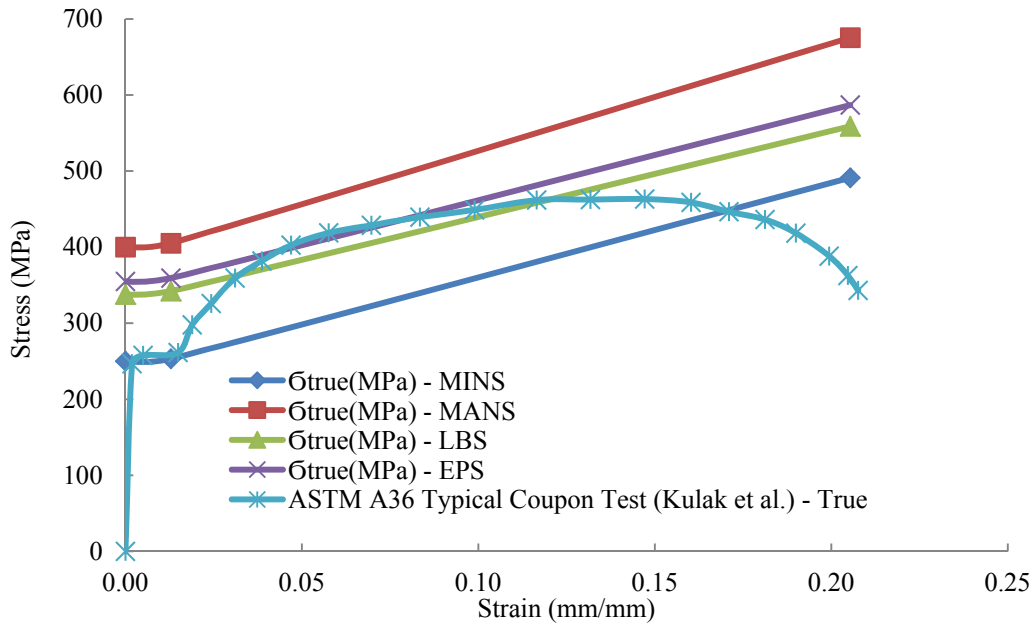


Figure A.5: ASTM A36 - True Stress–Strain Behaviour – SA

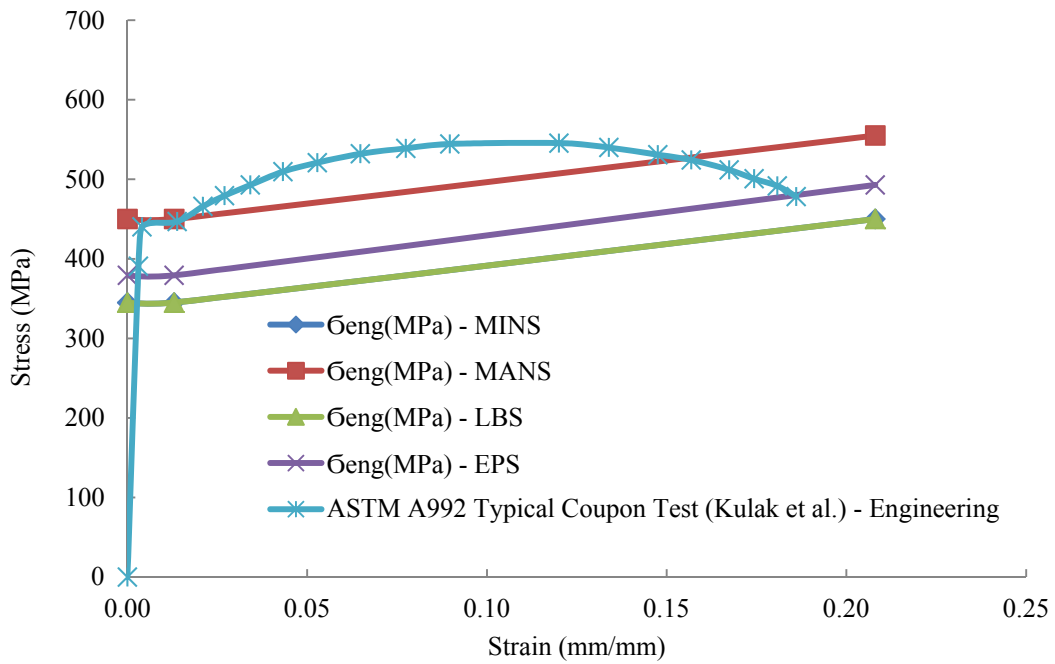


Figure A.6: ASTM A992 - Engineering Stress–Strain Behaviour

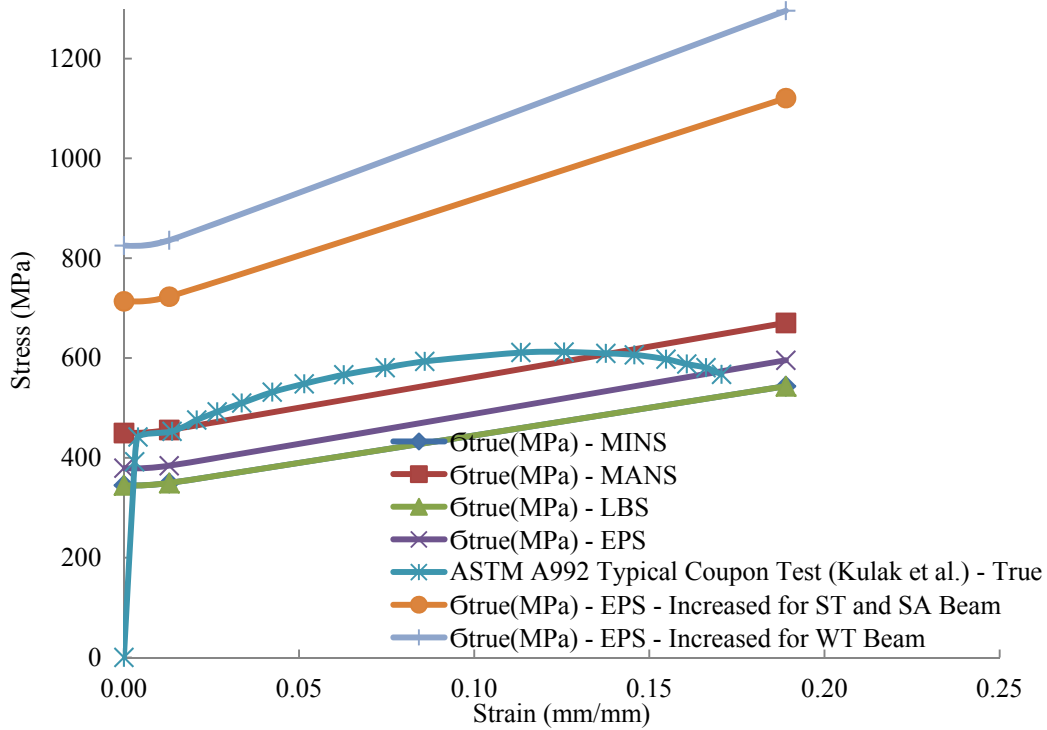


Figure A.7: ASTM A992 - True Stress–Strain Behaviour

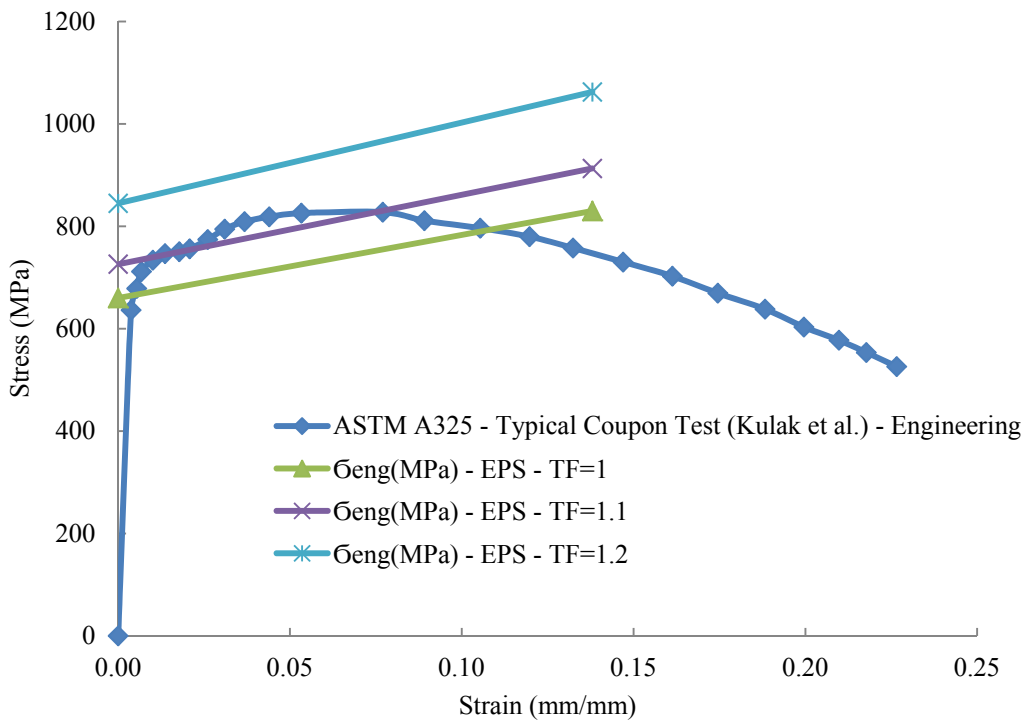


Figure A.8: ASTM A325 - Engineering Stress–Strain Behaviour

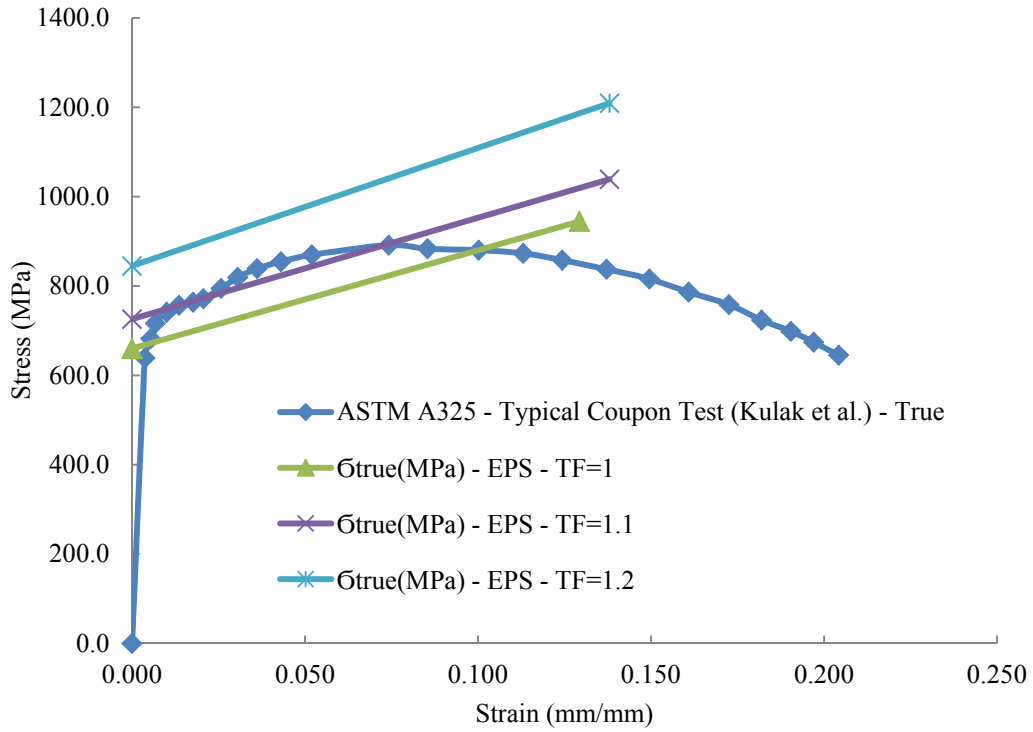


Figure A.9: ASTM A325 - True Stress-Strain Behaviour

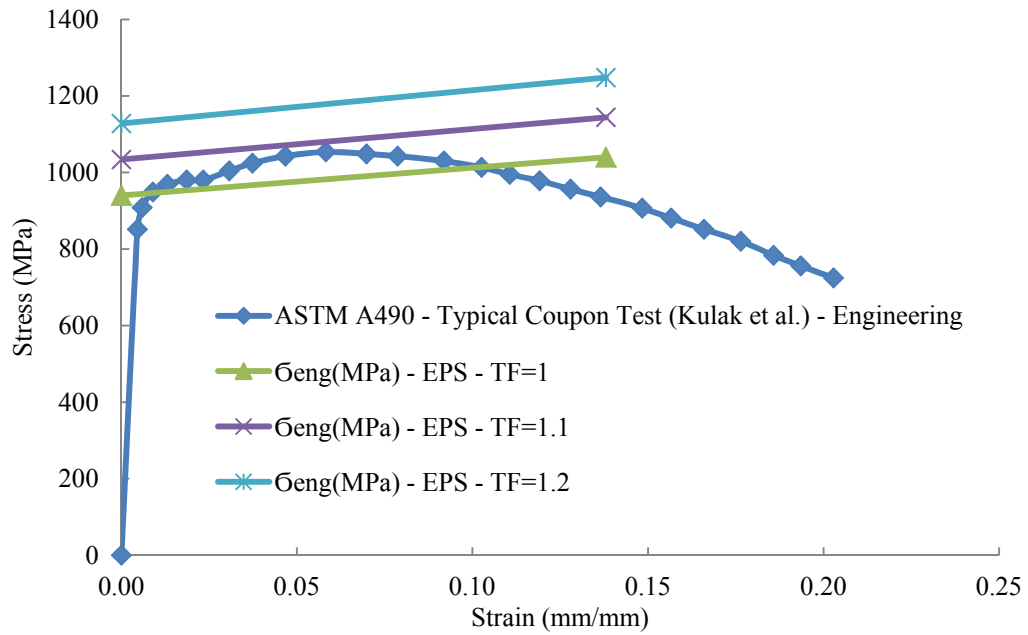


Figure A.10: ASTM A490 - Engineering Stress-Strain Behaviour

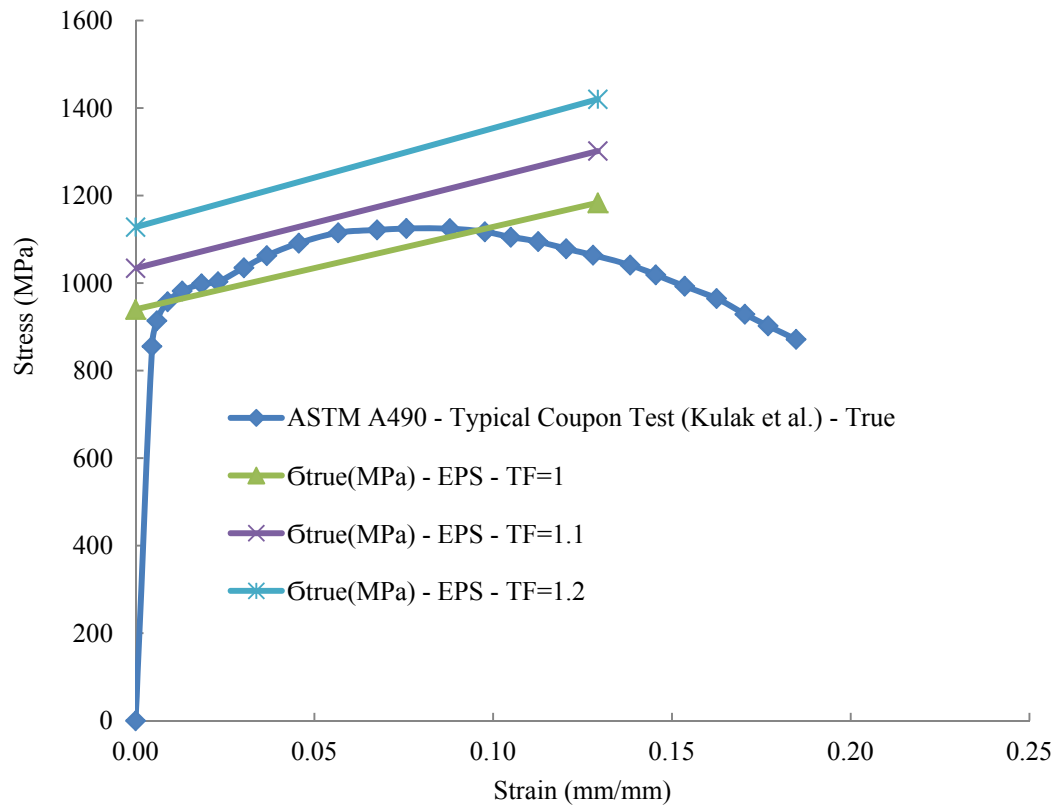


Figure A.11: ASTM A490 - True Stress–Strain Behaviour